The Multibody Systems Approach to Vehicle Dynamics

Mike Blundell and Damian Harty

Multibody Systems Approach to Vehicle Dynamics

This page intentionally left blank

Multibody Systems Approach to Vehicle Dynamics

Michael Blundell
Damian Harty

ELSEVIER
BUTTERWORTH
HEINEMANN

AMSTERDAM BOSTON HEIDELBERG LONDON NEW YORK OXFORD
PARIS SAN DIEGO SAN FRANCISCO SINGAPORE SYDNEY TOKYO

Elsevier Butterworth-Heinemann
Linacre House, Jordan Hill, Oxford OX2 8DP
200 Wheeler Road, Burlington, MA 01803

First published 2004

British Library Cataloguing in Publication Data
A catalogue record for this book is available from the British Library

ISBN 0 7506 5112 1

For information on all Elsevier Butterworth-Heinemann publications visit our website at http://books.elsevier.com

Composition by Charon Tec Pvt. Ltd, Chennai, India
Printed and bound in Maple-Vail, Kirkwood, New York, USA

Contents

This page intentionally left blank

Preface

This book is intended to bridge a gap between the subject of classical vehicle dynamics and the general-purpose computer-based discipline known as multibody systems analysis (MBS). While there are several textbooks that focus entirely on the subject, and mathematical foundations, of vehicle dynamics and other more recent texts dealing with MBS, there are none yet that link the two subjects in a comprehensive manner. A book in this area is timely. The computer-based analysis methodology (MBS) became established as a tool for engineering designers during the 1980s in a similar manner to the growth in Finite Element Analysis (FEA) technology during the previous decade. A number of computer programs were developed and marketed to the engineering industry, the most well known being MSC.ADAMS™ (Automatic Dynamic Analysis of Mechanical Systems) which will form the basis for the examples provided here. During the 1990s MBS became firmly established as part of the vehicle design and development process. It is inevitable that the engineer working on problems involving vehicle ride and handling in a modern automotive environment will be required to interface with the use of MBS to simulate vehicle motion.

The book is aimed at a wide audience including not only undergraduate, postgraduate and research students working in this area, but also practising engineers in industry requiring a reference text dealing with the major relevant areas within the discipline.

The book was originally planned as an individual effort on the part of Mike Blundell, drawing on past experience consulting on and researching into the application of MBS to solve a class of problems in the area of vehicle dynamics. From the start it was clear that a major challenge in preparing a book on this subject would be to provide meaningful comment on not only the modelling techniques but also the vast range of simulation outputs and responses that can be generated. Deciding whether a vehicle has good or bad handling characteristics is often a matter of human judgement based on the response or feel of the vehicle, or how easy the vehicle is to drive through certain manoeuvres. To a large extent automotive manufacturers still rely on track measurements and the instincts of experienced test engineers as to whether the design has produced a vehicle with the required handling qualities. To address this problem the book has been co-authored by Damian Harty who is the Chief Engineer, Dynamics at Prodrive. With experience not only in the area of computer simulation but also in the practical development and testing of vehicles on the proving ground, Damian has been able to help in documenting the realistic application of MBS in vehicle development.

Chapter 1 is intended to document the emergence of MBS and provide an overview of its role in vehicle design and development. Previous work by contributors including Olley, Segel, Milliken, Crolla and Sharp is identified providing a historical perspective on the subject during the latter part of the twentieth century.

Chapter 2 is included for completeness and covers the underlying formulations in kinematics and dynamics required for a good understanding of multibody systems formulations. A three-dimensional vector approach is used to develop the theory, this being the most suitable method for developing the rigid body equations of motion and constraint formulations described later.

Chapter 3 covers the modelling, analysis and post-processing capabilities of a typical simulation software. There are many commercial programs to choose from including not only MSC.ADAMS but also other software packages such as DADS and SIMPACK. The descriptions provided in Chapter 3 are based on MSC.ADAMS; the main reason for this choice being that the two authors have between them 25 years of experience working with the software. The fact that the software is also well established in automotive companies and academic institutions worldwide is also a factor. It is not intended in Chapter 3 to provide an MSC.ADAMS primer. There is extensive user documentation and training material available in this area from the program vendors MSC.Software. The information included in Chapter 3 is therefore limited to that needed to introduce a new reader to the subject and to provide a supporting reference for the vehicle modelling and analysis methodologies described in the following chapters.

Existing users of MSC.ADAMS will note that the modelling examples provided in Chapter 3 are based on a text-based format of model inputs, known in MSC.ADAMS as solver data sets. This was the original method used to develop MSC.ADAMS models and has subsequently been replaced by a powerful graphical user interface (GUI) known as ADAMS/View™ that allows model parameterization and design optimization studies. The ADAMS/View environment is also the basis for customized versions of MSC.ADAMS such as ADAMS/Car™ that are becoming established in industry and are also discussed in Chapter 3. The use of text-based data sets has been adopted here for a number of reasons. The first of these is that the GUI of a modern simulation program such as MSC.ADAMS is subject to extensive and ongoing development. Any attempt to describe such a facility in a textbook such as this would become outdated after a short time. As mentioned the software developers provide their own user documentation covering this in any case. It is also clear that the text-based formulations translate more readily to book format and are also useful for demonstrating the underlying techniques in planning a model, preparing model schematics and establishing the degrees of freedom in a system model. These techniques are needed to interpret the models and data sets that are described in later chapters and appendices. It is also hoped that by treating the software at this fundamental level the dependence of the book on any one software package is reduced and that the methods and principles will be adaptable for practitioners using alternative software. Examples of the later ADAMS/View command file format are included in Chapters 6 and 8 for completeness.

Chapter 4 addresses the modelling and analysis of the suspension system. An attempt has been made to bridge the gap between the textbook treatment of suspension systems and the multibody systems approach to building and simulating suspension models. As such a number of case studies have been included to demonstrate the application of the models and their use in the

vehicle design process. The chapter concludes with an extensive case study comparing a full set of analytical calculations, using the vector-based methods introduced in Chapter 2, with the output produced from MSC.ADAMS. It is intended that this exercise will demonstrate to readers the underlying computations in process when running an MBS simulation.

Chapter 5 addresses the tyre force and moment generating characteristics and the subsequent modelling of these in an MBS simulation. Examples are provided of tyre test data and the derived parameters for established tyre models. The chapter concludes with a case study using an MBS virtual tyre test machine to interrogate and compare tyre models and data sets.

Chapter 6 describes the modelling and assembly of the rest of the vehicle, including the anti-roll bars and steering systems. Near the beginning a range of simplified suspension modelling strategies for the full vehicle is described. This forms the basis for subsequent discussion involving the representation of the road springs and steering system in simple models that do not include a model of the suspension linkages. The chapter includes a consideration of modelling driver inputs to the steering system using several control methodologies and concludes with a case study comparing the performance of several full vehicle modelling strategies for a vehicle handling manoeuvre.

Chapter 7 deals with the simulation output and interpretation of results. An overview of vehicle dynamics for travel on a curved path is included. The classical treatment of understeer/oversteer based on steady state cornering is presented followed by an alternative treatment that considers yaw rate and lateral acceleration gains The subjective/objective problem is discussed with consideration of steering feel and roll angle as subjective modifiers. The chapter concludes with a consideration of the use of analytical models with a signal-to noise approach.

Chapter 8 concludes with a review of the use of active systems to modify the dynamics in modern passenger cars. The use of electronic control in systems such as active suspension and variable damping, brake-based systems, active steering systems, active camber systems and active torque distribution is described. A final summary matches the application of these systems with driving styles described as normal, spirited or the execution of emergency manoeuvres.

Appendix A contains a full set of vehicle model schematics and a complete set of vehicle data that can be used to build suspension models and full vehicle models of varying complexity. The data provided in Appendix A was used for many of the case studies presented throughout the book.

Appendix B contains example Fortran Tire subroutines to supplement the description of the tyre modelling process given in Chapter 5. A subroutine is included that uses a general interpolation approach using a cubic spline fit through measured tyre test data. The second subroutine is based on version 3 of the ‘Magic Formula’ and has an embedded set of tyre parameters based on the tyre data described in Chapter 5. A final subroutine ‘The Harty model’ was developed by Damian at Prodrive and is provided for readers who would like to experiment with a new tyre model that uses a reduced set of model parameters and can represent combined slip in the tyre contact patch.

In conclusion it seems to the authors there are two camps for addressing the vehicle dynamics problem. In one is the practical ride and handling expert. The second camp contains theoretical vehicle dynamics experts. This book is aimed at the reader who, like the authors, seeks to live between the two camps and move forward the process of vehicle design, taking full advantage of the widespread availability of convenient digital computing.

There is, however, an enormous difficulty in achieving this end. Lewis Carroll, in *Alice Through the Looking Glass*, describes an encounter between Alice and a certain Mr H. Dumpty:

> *'When* I *use a word', Humtpy Dumpty said, in rather a scornful tone, 'it means just what I choose it to mean – neither more nor less.'*
> *'The question is', said Alice, 'whether you* can *make words mean so many different things.'*

There is a similar difficulty between practical and theoretical vehicle dynamicists and even between different individuals of the same persuasion. The same word is used, often without definition, to mean just what the speaker chooses. There is no universal solution to the problem save for a thoughtful and attentive style of discussion and enquiry, taking pains to establish the meanings of even apparently obvious terms such as 'camber' – motorcycles do not have any camber by some definitions (vehicle-body-referenced) and yet to zero the camber forces in a motorcycle tyre is clearly folly. A glossary is included in Appendix C, not as some declaration of correctness but as an illumination for the text.

Mike Blundell and Damian Harty
February 2004

Acknowledgements

Mike Blundell
In developing my sections of this book I am indebted to my colleagues and students at Coventry University who have provided encouragement and material that I have been able to use. In particular I thank Barry Bolland and Peter Griffiths for their input to Chapter 2 and Bryan Phillips for his help with Chapter 5. I am also grateful to many within the vehicle dynamics community who have made a contribution including David Crolla, Roger Williams, Jim Forbes, Adrian Griffiths, Colin Lucas, John Janevic and Grahame Walter. Finally I thank the staff at Elsevier Science for their patience and help throughout the years it has taken to bring this book to print.

Damian Harty
Mike's gracious invitation to join him and infectious enthusiasm for both the topic and this project has kept me buoyed. Robin Sharp, Doug and Bill Milliken keep me grounded and rigorous when it is tempting just to play in cars and jump to conclusions. David Crolla has been an ever-present voice of reason keeping this text focused on its *raison d'être* – the useful fusion of practical and theoretical vehicle dynamics. Professional colleagues who have used banter, barracking and sometimes even rational discussion to help me progress my thinking are too numerous to mention – apart from Duncan Riding, whom I have to single out as being exceptionally encouraging. I hope I show my gratitude in person and on a regular basis to all of them and invite them to kick me if I don't. Someone who must be mentioned is Isaac Newton; his original and definitive brilliance at describing my world amazes me every day. As Mike, I thank the staff at Elsevier Science for their saintly patience.

I owe the most thanks to the management of Prodrive. Their skill at allowing me to thrive defies any succinct description but I am deeply and continuously both aware of and grateful for it.

And finally, I'd just like to say I'm very sorry for all the cars I've damaged while 'testing' them. I really am.

Nomenclature

$\{a_I\}_1$	Unit vector at marker I resolved parallel to frame 1 (GRF)
$\{a_J\}_1$	Unit vector at marker J resolved parallel to frame 1 (GRF)
a_x	Longitudinal acceleration (Wenzel model)
a_y	Lateral acceleration (Wenzel model)
b	Longitudinal distance of body mass centre from front axle
c	Damping coefficient
c	Longitudinal distance of body mass centre from rear axle
c	Specific heat capacity of brake rotor
$\{d_{IJ}\}_1$	Position vector of marker I relative to J resolved parallel to frame 1 (GRF)
f	Natural frequency (Hz)
h	Brake rotor convection coefficient
h	Height of body mass centre above roll axis
k	Path curvature
k	Radius of gyration
k	Stiffness
k_s	Spring stiffness
k_w	Stiffness of equivalent spring at the wheel centre
m	Mass of a body
$m\{g\}_1$	Weight force vector for a part resolved parallel to frame 1 (GRF)
m_t	Mass of tyre
n	Number of friction surfaces (pads)
p	Brake pressure
q_j	Set of part generalized co-ordinates
r	Yaw rate
r_1,r_2,r_3	Coupler constraint rotations
$\{r_I\}_1$	Position vector of marker I relative to frame i resolved parallel to frame 1 (GRF)
$\{r_J\}_1$	Position vector of marker J relative to frame j resolved parallel to frame 1 (GRF)
s_1,s_2,s_3	Coupler constraint scale factors
t_f	Front track
t_r	Rear track
v_{cog}	Centre of gravity (Wenzel model)
v_x	Longitudinal velocity (Wenzel model)
v_y	Lateral velocity (Wenzel model)
$\{x_I\}_1$	Unit vector along x-axis of marker I resolved parallel to frame 1 (GRF)
$\{y_I\}_1$	Unit vector along y-axis of marker I resolved parallel to frame 1 (GRF)
$\{x_J\}_1$	Unit vector along x-axis of marker J resolved parallel to frame 1 (GRF)
$\{y_J\}_1$	Unit vector along y-axis of marker J resolved parallel to frame 1 (GRF)
y_s	Asymptotic value at large slip (‘Magic Formula’)

$\{z_I\}_1$	Unit vector along z-axis of marker I resolved parallel to frame 1 (GRF)
$\{z_J\}_1$	Unit vector along z-axis of marker J resolved parallel to frame 1 (GRF)
A	Area
A_c	Convective area of brake disc
$[A_{1n}]$	Euler matrix for part n
$\{A_n\}_1$	Acceleration vector for part n resolved parallel to frame 1 (GRF)
A^p	Centripetal acceleration
$\{A^p_{PQ}\}_1$	Centripetal acceleration vector P relative to Q referred to frame 1 (GRF)
$\{A^t_{PQ}\}_1$	Transverse acceleration vector P relative to Q referred to frame 1 (GRF)
$\{A^c_{PQ}\}_1$	Coriolis acceleration vector P relative to Q referred to frame 1 (GRF)
$\{A^s_{PQ}\}_1$	Sliding acceleration vector P relative to Q referred to frame 1 (GRF)
AyG	Lateral acceleration gain
B	Stiffness factor ('Magic Formula')
$[B]$	Transformation matrix from frame O_e to O_n
$BKid$	Bottom Kingpin Marker
BM	Bump Movement
B_T	Brake torque
C	Shape factor ('Magic Formula')
$[C]$	Compliance matrix
C_F	Front axle cornering stiffness
C_r	Rolling resistance moment coefficient
C_R	Rear axle cornering stiffness
C_S	Tyre longitudinal stiffness
C_p	Process capability
CP	Centre of pressure
C_α	Tyre lateral stiffness due to slip angle
C_γ	Tyre lateral stiffness due to camber angle
D	Peak value ('Magic Formula')
DM(I,J)	Magnitude of displacement of I marker relative to J marker
DX(I,J)	Displacement in X direction of I marker relative to J marker parallel to GRF
DY(I,J)	Displacement in Y direction of I marker relative to J marker parallel to GRF
DZ(I,J)	Displacement in Z direction of I marker relative to J marker parallel to GRF
E	Young's modulus of elasticity
E	Curvature factor ('Magic Formula')
$\{F_{nA}\}_1$	Applied force vector on part n resolved parallel to frame 1 (GRF)
$\{F_{nC}\}_1$	Constraint force vector on part n resolved parallel to frame 1 (GRF)
F_{FRC}	Lateral force reacted by front roll centre
F_{RRC}	Lateral force reacted by rear roll centre
F_x	Longitudinal tractive or braking tyre force
F_y	Lateral tyre force
F_z	Vertical tyre force

F_{zc}	Vertical tyre force due to damping
F_{zk}	Vertical tyre force due to stiffness
$\{F_A\}_1\{F_B\}_1\ldots$	Applied force vectors at points A, B, … resolved parallel to frame 1 (GRF)
$[F_E]$	Elastic compliance matrix (Concept suspension)
F_D	Drag force
FG	Fixed Ground Marker
G	Shear modulus
GC	Gravitational constant
GO	Ground Level Offset
GRF	Ground Reference Frame
$\{H\}_1$	Angular momentum vector for a body
$H(\omega)$	Transfer function
HTC	Half Track Change
I	Mass moment of inertia
I	Second moment of area
ICY	Y Co-ordinate of Instant Centre
ICZ	Z Co-ordinate of Instant Centre
$[I_n]$	Inertia tensor for a part
J	Polar second moment of area
Jz	Vehicle body yaw inertia (Wenzel model)
K	Drive torque controller constant
K	Spring stiffness
K	Stability factor
K	Understeer gradient
K_z	Tyre radial stiffness
K_T	Torsional stiffness
K_{Ts}	Roll stiffness due to springs
K_{Tr}	Roll stiffness due to anti-roll bar
L	Length
L	Wheelbase
$\{L\}_1$	Linear momentum vector for a particle or body
LPRF	Local Part Reference Frame
L_R	Tyre relaxation length
M_{FRC}	Moment reacted by front roll centre
$\{M_{nA}\}_e$	Applied moment vector on part n resolved parallel to frame e
$\{M_{nC}\}_e$	Constraint moment vector on part n resolved parallel to frame e
M_s	Equivalent roll moment due to springs
M_x	Tyre overturning moment
M_y	Tyre rolling resistance moment
M_z	Tyre self-aligning moment
MRF	Marker Reference Frame
M_{RRC}	Moment reacted by rear roll centre
N_r	Vehicle yaw moment with respect to yaw rate
$[N_t]$	Norsieck vector
N_{vy}	Vehicle yaw moment with respect to lateral velocity
O_1	Frame 1 (GRF)
O_e	Euler axis frame
Oi	Reference frame for part i
Oj	Reference frame for part j

O_n	Frame for part n
$\{P_{nr}\}_1$	Rotational momenta vector for part n resolved parallel to frame 1 (GRF)
$\{P_{nt}\}_1$	Translational momenta vector for part n resolved parallel to frame 1 (GRF)
Pt	Constant power acceleration
QP	Position vector of a marker relative to the LPRF
QG	Position vector of a marker relative to the GRF
R	Radius of turn
R_1	Unloaded tyre radius
R_2	Tyre carcass radius
R_d	Radius to centre of brake pad
R_e	Effective rolling radius
$\{R_i\}_1$	Position vector of frame i on part i resolved parallel to frame 1 (GRF)
$\{R_j\}_1$	Position vector of frame j on part j resolved parallel to frame 1 (GRF)
R_1	Loaded tyre radius
$\{R_n\}_1$	Position vector for part n resolved parallel to frame 1 (GRF)
$\{R_p\}_1$	Position vector of tyre contact point P relative to frame 1, referenced to frame 1
R_u	Unloaded tyre radius
$\{R_w\}_1$	Position vector of wheel centre relative to frame 1, referenced to frame 1
$\{R_{AG}\}_n$	Position vector of point A relative to mass centre G resolved parallel to frame n
$\{R_{BG}\}_n$	Position vector of point B relative to mass centre G resolved parallel to frame n
RC_{front}	Front roll centre
RC_{rear}	Rear roll centre
RCY	Y Co-ordinate of Roll Centre
RCZ	Z Co-ordinate of Roll Centre
S_e	Error variation
Sh	Horizontal shift ('Magic Formula')
Sv	Vertical shift ('Magic Formula')
SA	Spindle Axis reference point
S_L	Longitudinal slip ratio
S_L*	Critical value of longitudinal slip
SN	Signal-to-noise ratio
S_T	Total variation
S_α	Lateral slip ratio
$S_{L\alpha}$	Comprehensive slip ratio
S_α*	Critical slip angle
S_κ	Variation due to linear effect
T	Kinetic energy for a part
T	Temperature
T	Torque
T_{env}	Environmental temperature
T_0	Initial brake rotor temperature
$\{T_A\}_1\{T_B\}_1\ldots$	Applied torque vectors at points A, B, … resolved parallel to frame 1 (GRF)

TK	Top Kingpin Marker
TR	Suspension Trail
$\{U_r\}$	Unit vector normal to road surface at tyre contact point
$\{U_s\}$	Unit vector acting along spin axis of tyre
UCF	Units Consistency Factor
US	Understeer
V	Forward velocity
V_a	Actual forward velocity
V_e	Error variance
V_g	Ground plane velocity
V_{lowlimit}	Limiting velocity
$\{V_n\}_1$	Velocity vector for part n resolved parallel to frame 1 (GRF)
$\{V_p\}_1$	Velocity vector of tyre contact point P referenced to frame 1
V_s	Desired simulation velocity
V_{xc}	Longitudinal slip velocity of tyre contact point
Vy	Lateral slip velocity of tyre contact point
Vz	Vertical velocity of tyre contact point
VR(I,J)	Radial line of sight velocity of I marker relative to J marker
WB	Wheel Base Marker
WC	Wheel Centre Marker
WF	Wheel Front Marker
WR	Wheel Recession
XP	Position vector of a point in a marker xz plane
$\{X_{\text{SAE}}\}_1$	Unit vector acting at tyre contact point in X_{SAE} direction referenced to frame 1
Y_r	Vehicle side force with respect to yaw rate
Y_{vy}	Vehicle side force with respect to lateral velocity
YRG	Yaw rate gain
$\{Y_{\text{SAE}}\}_1$	Unit vector acting at tyre contact point in Y_{SAE} direction referenced to frame 1
$\{Z_{\text{SAE}}\}_1$	Unit vector acting at tyre contact point in Z_{SAE} direction referenced to frame 1
ZP	Position vector of a point on a marker z-axis
α	Tyre slip angle
$\{\alpha_n\}_1$	Angular acceleration vector for part n resolved parallel to frame 1 (GRF)
α_f	Front axle slip angle
α_r	Rear axle slip angle
β	Side slip angle
$\dot{\beta}$	Rate of change of side slip angle (beta dot)
δ	Steer or toe angle
δ_o	Steer angle of outer wheel
δ_i	Steer angle of inner wheel
δ_{mean}	Average steer angle of inner and outer wheels
γ	Camber angle
$\{\gamma_n\}_e$	Set of Euler angles for part n
ζ	Damping ratio
κ	Longitudinal slip (Pacjeka)
κ	Sensitivity of process
θ	2nd Euler angle rotation
$\{\lambda\}_1$	Reaction force vector resolved parallel to frame 1 (GRF)
λ_d	Magnitude of reaction force for constraint d

λ_p	Magnitude of reaction force for constraint p
λ_α	Magnitude of reaction force for constraint α
μ	Friction coefficient
μ_0	Tyre to road coefficient of static friction
μ_1	Tyre to road coefficient of sliding friction
η	Signal-to-noise ratio
ρ	Density
σ	Standard deviation
σ_d	Standard deviation of attribute d
ϕ	3rd Euler angle rotation
ψ	1st Euler angle rotation
$\dot{\psi}$	Yaw rate (Wenzel model)
ω	Yaw rate
ω_d	Damped-natural frequency
ω_d	Demanded yaw rate
ω_{err}	Yaw rate error
ω_{fns}	Front axle no-slip yaw rate
ω_{friction}	Yaw rate from limiting friction
ω_{geom}	Yaw rate from geometry
ω_n	Undamped natural frequency
$\{\omega_e\}_1$	Angular velocity vector for part n resolved parallel to frame e
$\{\omega_n\}_1$	Angular velocity vector for part n resolved parallel to frame 1 (GRF)
ω_0	Angular velocity of free rolling wheel
ω_D	Angular velocity of driven wheel
Δ_d	Allowable range for attribute d
Δx	Change in longitudinal position of wheel (Concept suspension)
Δy	Change in lateral position (half/track) of wheel (Concept suspension)
$\Delta\varepsilon$	Change in steer angle (toe in/out) of wheel (Concept suspension)
$\Delta\gamma$	Change in camber angle of wheel (Concept suspension)
$\{\Phi_a\}_1$	Vector constraint equation resolved parallel to frame 1 (GRF)
Φ_d	Scalar constraint expression for constraint d
Φ_p	Scalar constraint expression for constraint p
Φ_α	Scalar constraint expression for constraint α

This page intentionally left blank

1 Introduction

The most cost-effective analysis activity is accurately recalling and comprehending what has gone before.

1.1 Overview

In 1969, man travelled to the moon and back, using maths invented by Kepler, Newton and Einstein to calculate trajectories hundreds of thousands of miles long and spacecraft with less on-board computing power than today's pocket calculator. With today's computing power and the mathematical frameworks handed down to us by Newton and Lagrange, it is scarcely credible that the motor car, itself over 100 years old, can exercise so many minds and still show scope for improvement. Yet we are still repeating errors in the dynamic design of our vehicles that were made in the 1960s. Some recent car designs, not named for legal reasons, exist that reproduce with distressing familiarity the abrupt rearward transfer of roll moment prototyped by the early Triumph Vitesse and Chevrolet Corvair.

Vehicle manufacturers are not currently forced by legislation to achieve a measurable standard of vehicle handling and stability. International standards exist that outline procedures for proving ground tests with new vehicles but these are nothing more than recommendations. Vehicle manufacturers make use of many of the tests but in the main will develop and test vehicles using in-company experience and knowledge to define the test programme.

In the absence of legislated standards, vehicle manufacturers are driven by market forces. Journalists report favourably on vehicles they enjoy driving – whether or not these are safe in the hands of the general public – and the legal profession seeks every opportunity to blur the distinction between bad driving and poor vehicle design. Matters are further complicated by market pressures driving vehicle designs to be too tall for their width – city cars and sport-utility vehicles have this disadvantage in common.

The growth in media attention and reporting to the public is undoubtedly significant. In recent years the most well-publicized example of this was the reported rollover of the Mercedes A-Class during testing by the motoring press (Figure 1.1). The test involves a slalom type manoeuvre and became popularly known as the 'elk test'. Criticisms of the manoeuvre being overly severe were addressed by suggesting that it represents a panic swerve around a fictional elk on Scandinavian roads.

The media attention was little short of disastrous for Mercedes as the car was already in production and thousands were recalled and modified. The fact that following modification the car passed the test and that Mercedes were also able to demonstrate that competitive vehicles in that class also failed the test was barely noticed. By that stage the damage had already been done.

It seems to the authors there are two camps for addressing the vehicle dynamics problem. In one is the practical ride and handling expert. Skilled at the driving task and able to project themselves into the minds of a variety of different possible purchasers of the vehicle, they are able to quickly take an established vehicle design and adjust its character to make it acceptable for the market into which it will be launched. Rarely, though, are experts from this camp called upon to work in advance on the concept or detail of the vehicle design.

The second camp contains theoretical vehicle dynamics experts. They are skilled academics in the mould of Leonard Segel who in 1956 published his 'Theoretical prediction and experimental substantiation of the responses of the automobile to steering control' (Segel, 1956). Typical of the vehicles available at that time is the Chevrolet Bel-Air convertible shown in Figure 1.2. They were rarely commended for their dynamic qualities.

Segel's work, and that of others from this era including the earlier work 'Road manners of the modern motor car' (Olley, 1945), made way for all

Fig. 1.1 Rollover of the Mercedes A-Class (courtesy of *Auto Motor und Sport*)

Fig. 1.2 1957 Chevrolet Bel-Air convertible

subsequent 'classical' vehicle dynamic analysis and forms a firm foundation upon which to build. It is rare for an expert from this camp to be part of the downstream vehicle development process.

1.2 What is vehicle dynamics?

The field known as vehicle dynamics is concerned with two aspects of the behaviour of the machine. The first is isolation and the second is control. Figure 1.3 is the authors' subjective illustration of the intricacy and interconnection of the tasks to be approached; it is not claimed to be authoritative or complete but is rather intended as a thought-starter for the interested reader.

Isolation is about separating the driver from disturbances occurring as a result of the vehicle operation. This, too, breaks into two topics: disturbances the vehicle generates itself (engine vibration and noise, for example) and those imposed upon it by the outside world. The former category is captured by the umbrella term 'refinement'. The disturbances in the latter category are primarily road undulations and aerodynamic interaction of the vehicle with its surroundings – crosswinds, wakes of structures and wakes of other vehicles. The behaviour of the vehicle in response to road undulations is referred to as 'ride' and could conceivably be grouped with refinement, though it rarely is in practice.

There is some substantial crossover in aerodynamic behaviour between isolation and control, since control implies the rejection of disturbances

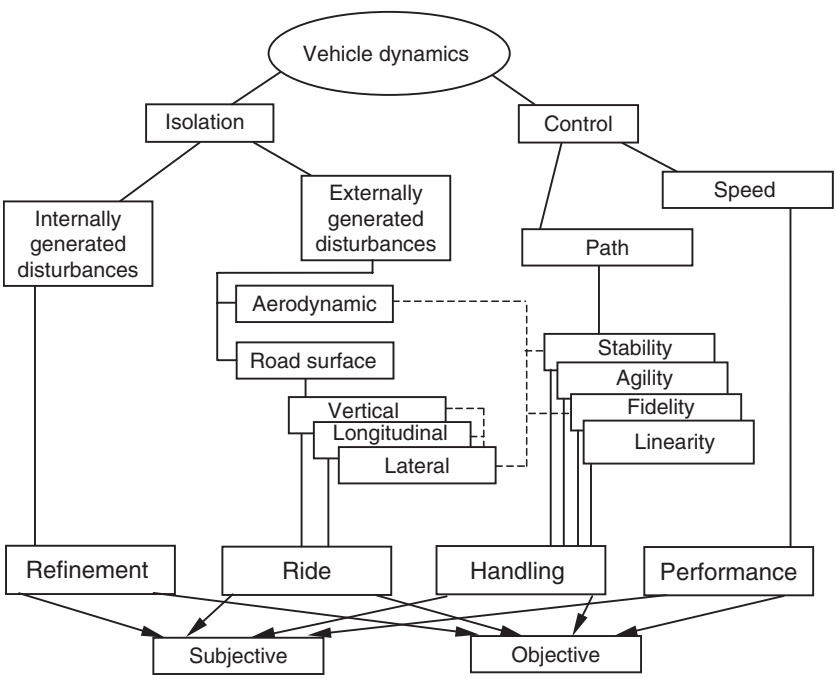

Fig. 1.3 Vehicle dynamics interactions

('fidelity') and an absence of their amplification ('stability'). Similarly, one response to road disturbances is a change in the vertical load supported by the tyre; this has a strong influence on the lateral force the tyre is generating at any given instant in time and is thus crucial for both fidelity and stability. It can be seen with some little reflection that one of the difficulties of vehicle dynamics work is not the complexity of the individual effects being considered but rather the complexity of their interactions.

Control is concerned largely with the behaviour of the vehicle in response to driver demands. The driver continuously varies both path curvature and speed, subject to the limits of the vehicle capabilities, in order to follow an arbitrary course.

Speed variation is governed by vehicle mass and tractive power availability at all but the lowest speed, and is easily understood. Within the performance task, issues such as unintended driveline oscillations and tractive force variation with driver demand may interact strongly with the path of the vehicle.

The adjustment of path curvature at a given speed is altogether more interesting. In a passenger car, the driver has a steering wheel, which for clarity will be referred to as a *handwheel*[1] throughout the book. The handwheel is a 'yaw rate' demand – a demand for rotational velocity of the vehicle when viewed from above. The combination of a yaw rate and a forward velocity vector that rotates with the vehicle gives rise to a curved path. There is a maximum path curvature available in normal driving, which is the turning circle, available only at the lowest speeds.

In normal circumstances (that is to say in day-to-day road use) the driver moves the handwheel slowly and is well within the limits of the vehicle capability. The vehicle has no difficulty responding to the demanded yaw rate. If the driver increases yaw rate demand slightly then the vehicle will increase its yaw rate by an appropriate amount. This property is referred to as 'linearity'; the vehicle is described as 'linear' (Figure 1.4). For the driver, the behaviour of the vehicle is quite instinctive. A discussion of the analysis and interpretation of vehicle linearity and departure from linearity is given in Chapter 7.

In the linear region, the behaviour of the vehicle can be represented as a connected series of 'steady state' events. Steady state is the condition in which, if the handwheel remains stationary, all the vehicle states – speed, yaw rate, path curvature and so on – remain constant and is more fully defined in Chapter 7. The steady state condition is easy to represent using an equilibrium analogy, constructed with the help of so-called 'centrifugal force'. It should be noted that this fictitious force is invented solely for convenience of calculation of an analogous equilibrium state, or the calculation of forces in an accelerating frame of reference. When a vehicle is travelling on a curved path it is not in equilibrium.

The curved path of the vehicle requires some lateral acceleration. Correctly, the lateral acceleration on a cornering vehicle is a centripetal

[1] 'Steering wheel' could mean a roadwheel which is steered, or a wheel held by the driver. In generic discussions including vehicles other than four-wheeled passenger cars (motorcycles, tilting tricycles, etc.) then 'steering wheel' contains too much ambiguity; therefore, 'handwheel' is preferred since it adds precision.

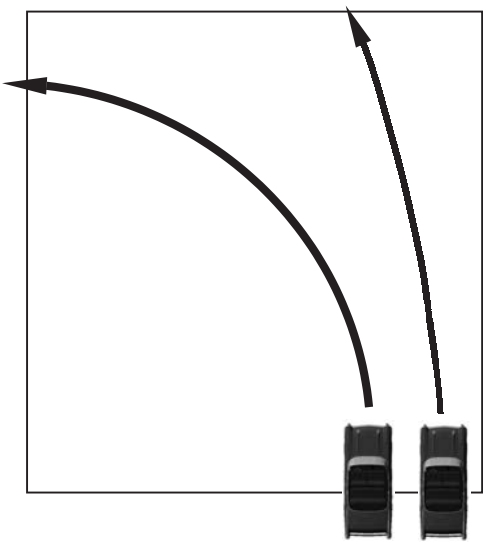

Fig. 1.4 Linearity: more handwheel input results in proportionally more yaw rate (vehicle on left)

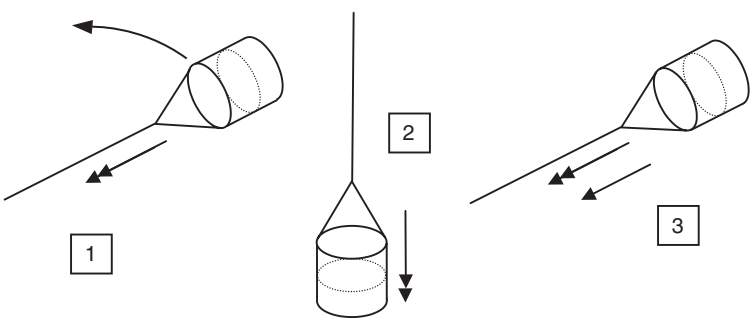

Fig. 1.5 A thought experiment comparing centripetal acceleration with linear acceleration

acceleration – 'centre seeking'. Note that speed is not the same as velocity; travelling in a curved path with a constant speed implies a changing direction and therefore a changing velocity. The centripetal acceleration definition causes some problems since everyone 'knows' that they are flung to the outside of a car if unrestrained and so there is much lax talk of centrifugal forces – 'centre fleeing'. To clarify this issue, a brief thought experiment is required (Figure 1.5). Imagine a bucket of water on a rope being swung around by a subject. If the subject looks at the bucket then the water is apparently pressed into the bucket by the mythical 'centrifugal force' (presuming the bucket is being swung fast enough). If the swinging is halted and the bucket simply suspended by the rope then the water is held in the bucket by the downward gravitational field of the earth – the weight of the water pulls it into the bucket. Imagine now a different scenario in which the bucket (on a frictionless plane) is pulled horizontally towards the observer at a constant acceleration in a linear fashion. It's best not to

complicate the experiment by worrying about what will happen when the bucket reaches the subject. It is this third scenario and not the second that is useful in constructing the cornering case. If both the first and third cases are imagined in a zero gravity environment, they still work – the water will stay in the bucket. Note that for the third scenario – what we might call the 'inertial' case as against the gravitational case in the second scenario – the acceleration is towards the open end of the bucket. This is also true for the first scenario, in which the bucket is swung; the acceleration is towards the open end of the bucket and is towards the subject – i.e. it is centripetal. That the water stays in the bucket is simply a consequence of the way the bucket applies the centripetal force to the water. Thus the tyres on a car exert a force towards the centre of a turn and the body mass is accelerated by those forces centripetally – in a curved path.

An accelerometer in the car is effectively a load cell that would be between the bucket and the water in the scenarios here and so it measures the centripetal force applied between the calibrated mass within the accelerometer (the water) and its support in the casing (the bucket). The so-called centrifugal force is one half of an action–reaction pair within the system but a free-body diagram of the bucket and rope in all three cases shows tension in the rope as an externally applied force when considering the rope as a separate free body. Only in case 2 is the bucket actually in equilibrium, with the addition of the gravitational force on the bucket and water. Therefore an accelerometer (or an observer) in the vehicle apparently senses a centrifugal force while theoretical vehicle dynamicists talk always of centripetal acceleration. Changing the sign on the inertial force, so that it is now a d'Alembert force, appears to solve the apparent confusion. This can be misleading as we now have the impression that the analysis of the cornering vehicle is a static equilibrium problem. The water is not in equilibrium when travelling in a curved path, and neither is a car.

Centripetal forces accelerate the vehicle towards the centre of the turn. This acceleration, perpendicular to the forward velocity vector, is often referred to as 'lateral' acceleration, since the vehicle generally points in the direction of the forward velocity vector (see Chapter 7 for a more precise description of the body attitude). It can be seen that the relationship between centripetal acceleration, A^p, yaw rate, ω, forward velocity, V, and radius of turn, R, is given by:

$$A^p = V^2/R = \omega V = \omega^2 R \tag{1.1}$$

The absolute limit for lateral acceleration, and hence yaw rate, is the friction available between the tyres and the road surface. Competition tyres ('racing slicks') have a coefficient of friction substantially in excess of unity and, together with large aerodynamic downforces, allow a lateral acceleration in the region of 30 m/s^2, with yaw rates correspondingly over 40 deg/s for a speed of 40 m/s (90 mph). For more typical road vehicles, limit lateral accelerations rarely exceed 9 m/s^2, with yaw rates correspondingly down at around 12 deg/s at the same speed. However, for the tyre behaviour to remain substantially linear, for a road car the lateral accelerations must be generally less than about 3 m/s^2, so yaw rates are down to a mere 4 deg/s at the same speed.

While apparently a small fraction of the capability of the vehicle, there is much evidence to suggest that the driving population as a whole rarely exceed the linearity limits of the vehicle at speed and only the most confident exceed them at lower speeds (Lechmer and Perrin, 1993). Accident investigators rarely presume a lateral acceleration of greater than 4 m/s^2 when reconstructing road traffic accidents even on dry roads unless there is strong evidence from the witness marks on the road surface.

When racing or during emergency manoeuvres on the road – typically attempting to avoid an accident – the vehicle becomes strongly 'non-linear'. The handwheel is moved rapidly and the vehicle generally has difficulty in responding accurately to the handwheel. This is the arena called 'transient handling' and is correctly the object of many studies during the product design process. In contrast to the steady state condition, all the vehicle states fluctuate rapidly and the expressions above are modified. Steady state and transient behaviour are connected. While good steady state behaviour is connected with good transient behaviour, it is not in itself sufficient (Sharp, 2000).

Transient handling studies concentrate on capturing, analysing and understanding the yaw moments applied to the vehicle and its response to them. Those moments are dominated by the lateral and longitudinal forces from the tyres. For road cars, additional aerodynamic contributions are a small modifier but for racing the aerodynamic behaviour rises in importance.

The generation of tyre forces is frequently the biggest source of confusion in vehicle dynamics, since both lateral and longitudinal mechanisms are neither obvious nor intuitive. Tyres are dealt with in some depth by Pacejka (2002) in a companion volume in this series and also have some further coverage in Chapter 5.

The tyres generate lateral forces by two mechanisms, 'camber' and 'slip angle'. Camber is the angle at which the tyre is presented to the road when viewed from the front. There exists some confusion when referring to and measuring camber angle; for clarity within this text camber angle is measured with respect to the road unless explicitly defined as being relative to the vehicle body. It is the angle with respect to the road that generates a side force. Thus a motorcycle runs a large camber angle when cornering but runs no camber angle with respect to the vehicle body.

Slip angle is the angle at which the moving tyre is presented to the road when viewed in plan. It is important to note that slip angle only exists when the vehicle is in motion. At a standstill (and at speeds under about 10 mph) the lateral stiffness of the tyres generates the forces that constrain the vehicle to its intended path. As speed rises above walking pace, the tyres have a falling static lateral stiffness until above about 5 m/s (12 mph) they have effectively none; an applied lateral force, such as a wind load, will move the vehicle sideways from its intended path. It is important to note that the presence of a slip angle does not necessarily imply sliding behaviour at the contact patch.

Slip angle forces are typically more than 20 times camber forces for a particular angle, and are thus the more important aspect for vehicle dynamics.

The lateral forces induced by the angles are strongly modified by the vertical loads on the tyres at each moment.

The tyres generate longitudinal forces by spinning at a speed different to their 'free-rolling' speed. The free-rolling speed is the speed at which the wheel and tyre would spin if no brake or drive forces are applied to them. The difference in speed is described as 'slip ratio', which is unfortunate since it is confusingly similar to slip angle. It is expressed as a percentage, so, for example, a tyre turning with a 5% slip ratio will perform 105 revolutions to travel the same distance as a free-rolling tyre performing 100 revolutions. In doing so it will impart a tractive force to the vehicle. A -5% slip ratio would imply 95 revolutions of the same wheel and the presence of a braking force.

Managing lateral tyre forces by controlling slip and camber angles is the work of the suspension linkage. For the front wheels, the driver has the ability to vary the slip angle using the handwheel. Managing the vertical loads on the tyres is the function of the suspension 'calibration' (springs, dampers and any active devices which may be present). Chapter 4 deals with suspension analysis in some detail. Management of longitudinal forces is the role of the vehicle driveline and braking system, including ABS or brake intervention systems.

A vehicle travelling in a straight line has a yaw velocity of zero and a centripetal acceleration of zero. When travelling in a steady curve, the centripetal acceleration is not zero and the yaw rate is not zero; both are constant and are related as described in equation (1.1). In performing the transition from straight running to a curved path there must be a period of yaw acceleration in order to acquire the yaw velocity that matches the centripetal acceleration. The yaw acceleration is induced and controlled by yaw moments acting on the vehicle yaw inertia.

Transient handling therefore implies the variation of yaw moments applied to the vehicle. Those moments are applied by aerodynamic behaviour and the force-generating qualities of the tyres at a distance from the vehicle centre of mass. No other mechanisms exist for generating a meaningful yaw moment on the vehicle; while gyroscopic torques exist associated with camber changes, they are small. For road vehicles, the aerodynamic modifications are generally small. Multibody system methods allow the convenient exploration of aspects of the vehicle design that influence those qualities of the tyres. Chapter 5 addresses different methods of modelling those aspects of the vehicle and their relative merits.

In order to progress from travelling in a straight line to travelling in a curved path, the following sequence of events is suggested:

1. The driver turns the handwheel, applying a slip angle at the front wheels.

2. After a delay associated with the front tyre relaxation lengths, side force is applied at the front of the vehicle. Lateral and yaw accelerations exist.

3. The body yaws (rotates in plan), applying a slip angle at the rear wheels.
4. After a delay associated with the rear tyre relaxation lengths, side force is applied at the rear of the vehicle. Lateral acceleration is increased, yaw acceleration is reduced to zero.

In the real world, the driver intervenes and the events run into one another rather than being discrete as suggested here, but it is a useful sequence for discussion purposes. A similar sequence of events describes the return to straight-line travel. Any yaw rate adjustments made by the driver follow similar sequences, too.

During the period of yaw acceleration (stages 2 and 3 above) there exists the need for an excess of lateral forces from the front tyres when compared to the rear in order to deliver the required yaw moment. At the end of this period, that excess must disappear. Side force requirements for the rear tyre are thus increasing while those for the front tyres are steady or decreasing. To understand the significance of this fact, some further understanding of tyre behaviour is necessary.

To a first approximation, camber forces may be neglected from tyre behaviour for vehicles that do not roll (lean) freely. Slip angle is the dominant side force generation mechanism. It is important to note that a tyre will adjust its slip angle to support the required side force, and not the other way around. This is a frequent source of difficulty in comprehending vehicle dynamic behaviour. All tyres display a slip angle at which the maximum side force is generated, referred to as the 'critical slip angle'. If a force is required which is greater than that which can be generated at the critical slip angle, the tyre will run up to and then beyond the critical slip angle. Beyond the critical slip angle the side force falls off with slip angle, and so an increasing amount of lateral force is available to accelerate the growth of slip angle once the critical slip angle is passed.

Returning to the vehicle, the side force requirement for the rear tyres is increasing while that for the front tyres is steady or decreasing. The rear tyres will be experiencing a growing slip angle, while the front tyres experience a steady or reducing one. If at this time the rear tyres exceed their critical slip angle, their ability to remove yaw moment is lost. The only possible way for yaw moment to be removed is by a reduction in the front tyre forces. If the yaw moment persists then yaw acceleration persists. With increasing yaw velocity, the slip angle at the front axle is reduced while that at the rear axle is increased further, further removing the rear tyres' ability to remove yaw moment from the vehicle. If the front tyres are past their critical slip angle, too, the normal stabilization mechanism is reversed. The result is an accelerating spin that departs rapidly from the driver's control. The modelling and interpretation of such events is dealt with in Chapter 7.

The behaviour of the driver is important to the system performance as a whole. The driver is called on to act as a yaw rate manager, acting on the vehicle controls as part of a closed-loop feedback system to impart the yaw moments required to control the yaw rate of the vehicle. At critical times, the workload of the driver may exceed his or her capability, resulting in a loss of control.

The goal of vehicle dynamics work is to maintain the vehicle behaviour within the bounds that can be comprehended by and controlled by the driver.

1.3 Why analyse?

In any real product-engineering programme, particularly in the ground vehicle industry, there are always time constraints. The need to introduce a new product to retain market share or to preserve competitive advantage drives increasingly tight timetabling for product engineering tasks. In the western world, and to a growing extent in the developing world, tastes are becoming ever more refined such that the demand for both quality of design and quality of construction is increasing all the while. Unlike a few decades ago, there are few genuinely bad products available.

It seems, therefore, that demands for better products are at odds with demands for compressed engineering timetables. This is true; the resolution of this conflict lies in improving the efficiency of the engineering process. It is here that predictive methods hold out some promise.

Predictive methods notionally allow several good things:

- Improved comprehension and ranking of design variables
- Rapid experimentation with design configurations
- Genuine optimization of numerical response variables

Therefore the use of predictive methods is crucial for staying 'ahead of the game' in vehicle engineering.

1.4 Classical methods

These methods are taught formally in universities as part of the syllabus. While they can be daunting at first sight, they are elegant and can prove tremendously illuminating in forming a holistic framework for what can easily be a bewildering arena.

The best practitioners of the art (Crolla, Sharp, Hales, Hemingway and the Millikens to name some) recommend the use of a body-centred state–space formulation. While full of simplifications, useful insights can be gained by studying a two degree-of-freedom model for typical passenger cars. With a reasonable increase in sophistication but well worth the effort is the elaboration to three degrees of freedom (four states) to include the influence of suspension roll.

Such classical models help the analyst discern 'the wood for the trees' – they easily bring forth, for example, the influence of suspension steer derivatives on straight-line stability. In this they contrast strongly with 'literal' linkage models, in which all the problems of real vehicles (the lack of isolation of single effects) can sometimes preclude their ranking and comprehension.

Although the task of deriving the equations of motion and arranging the terms for subsequent solution is laborious and may be error-prone, the proponents of the method point quite correctly to the increased comprehension of the problem to which it leads.

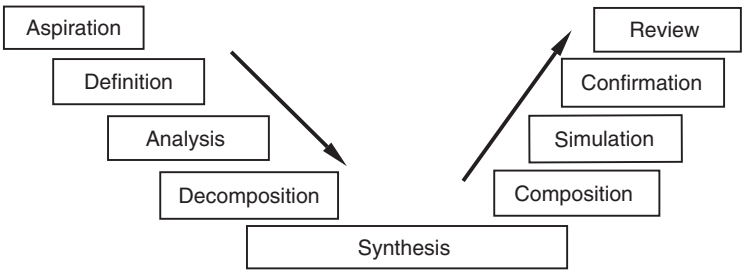

Fig. 1.6 'V' process for product design

1.5 Analytical process

It is clear that the tasks undertaken have expanded to fit the time available. Despite increases in computing power of a factor of 100 or more over the last two decades, analysis tasks are still taking as long to complete as they always have done. The increased computing power available is an irresistible temptation to add complexity to predictive models (Harty, 1999).

Complex models require more data to define them. This data takes time to acquire. More importantly, it must exist. Early in the design cycle, it is easy to fall into the 'paralysis of analysis'; nothing can be analysed accurately until it is defined to a level of accuracy matching the complexity of the modelling technique. More than the model itself, the process within which it fits must be suited to the tasks at hand.

There is nothing new in the authors' observations; Sharp (1991) comments:

> *Models do not possess intrinsic value. They are for solving problems. They should be thought of in relation to the problem or range of problems which they are intended to solve. The ideal model is that with minimum complexity which is capable of solving the problems of concern with an acceptable risk of the solution being 'wrong'. This acceptable risk is not quantifiable and it must remain a matter of judgement. However, it is clear that diminishing returns are obtained for model elaboration.*

Any method of analysis must be part of a structured process if it is to produce useful results in a timely manner. Interesting results that are too late to influence product design are of little use in modern concurrent[2] engineering practice. Rapid results that are so flawed as to produce poor engineering decisions are also of little use. The use of predictive methods within vehicle design for addressing dynamic issues with the vehicle should follow a pattern not dissimilar to that in Figure 1.6, whatever the problem or the vehicle.

[2] Concurrent = taking place at the same time. 'Concurrent engineering' was a fashionable phrase in the recent past and refers to the practice of considering functional, cost and manufacturing issues together rather than the historically derived 'sequential' approach. It was also referred to as 'simultaneous engineering' for a while, though the segmented connotations of simultaneous were considered unhelpful and so the 'concurrent' epithet was adopted.

Aspiration: The method properly starts with the recognition of the end goals. In some organizations, confusion surrounds this part of the process, with obfuscation between targets, objectives and goals; the terms are used differently between organizations and frequently with some differences between individuals in the same organization. Cutting through this confusion requires time and energy but is vital.

Definition: After definition, a clear description of 'success' and 'failure' must exist; without it the rest of the activities are, at best, wasteful dissipation. Aspirations are frequently set in terms of subjective comparisons – 'Ride comfort better than best in class'. To usefully feed these into an analytical process, they must be capable of being quantified – i.e. of having numbers associated with them. Without numbers, it is impossible to address the task using analytical methods and the analytical process should be halted. This is not to say that product development cannot continue but that to persist with a numerical process in the absence of numbers becomes folly. Analysts and development staff must be involved closely with each other and agree on the type of numerical data that defines success, how it is calculated predictively and how it is measured on a real vehicle. Commonly, some form of 'benchmarking' study – a measurement exercise to quantify the current best performers – is associated with this stage. The activity to find the benchmark is a useful shakedown for the proposed measurement processes and is generally a fruitful education for those involved.

Analysis: When success and failure have been defined for the system as a whole, the individual parts of the system must be considered. There is generally more than one way to reach a system solution by combining individual subsystems or elements. During this stage of the process, some decisions must be taken about what combination is preferred. It may be, for example, that in seeking a certain level of vehicle performance there is a choice between increasing power output and reducing weight in order to achieve a given power-to-weight ratio. That choice will be influenced by such simple things as cost (saving weight may be more expensive than simply selecting a larger engine from the corporate library) or by more abstruse notions (the need to be seen to be 'environmentally friendly', perhaps). The task of analysis is to illuminate that choice. The analysis carried out must be sufficiently accurate but not excessively so. 'Simple models smartly used' is the order of the day for analysis work. The analysis may consider many possible combinations in order to recommend a favoured combination. This activity is sometimes referred to by

the authors as 'mapping the design space' – producing guidance for those who wish to make design decisions based on wider considerations and who wish to comprehend the consequences of their decisions. The most cost-effective activity at this stage is accurately recalling and comprehending what has gone before.

Decomposition: Once the analytical stage is complete, it is time for design decisions to be made. The whole entity must be decomposed into its constituent parts, each of which has design goals associated with it – cost, performance, weight, etc. It is at this time the first real design decisions are made that shape the product. Those decisions are to be made in the light of the preceding analysis.

Synthesis: Once the design is decomposed into manageable portions, the task of synthesizing (creating) the design begins. During this phase, analytical tools are used to support individual activities and verify the conformance of the proposed design with the intended design goals. An example of this might be the use of kinematic simulation to verify that the suspension geometry characteristics are those required. Discerning the requirement itself is the function of the earlier decomposition phase.

Composition: The reassembly of the separate portions of the design, each of which by now has a high level of confidence at reaching its individual design goals.

Simulation: Might also be referred to as 'virtual prototyping'. High fidelity models that have been a long time in preparation are used to assess predictively, in some detail, the behaviour of the whole design. Models prepared during the synthesis activity are taken and reused. It is in this arena that great strides have been made in terms of processing power, model reuse and interpackage integration over the last decade. Unfortunately, in the minds of some, these super elaborate models are all that is possible and anything less is simply worthless, passé and old fashioned. These are valuable models and have a crucial part to play in the process, but without a well-shaped concept design they are unwieldy white elephants.

Also included in the simulation activity should be prototype vehicles, produced from non-representative tools and/or processes, that are physical simulations instead of mathematical ones. The increasing use of 'virtual' prototyping obviates these physical prototypes except for those where an understanding of the man/machine interaction is necessary. One of several arenas where this remains true is the dynamics task.

Confirmation: Sign-off testing is to be carried out on real vehicles. This stage should reveal no surprises, as changes at this stage are expensive.

Review: Once the design is successfully signed off, a stage that is frequently omitted is the review. What was done well? What could have been better? What technology do we wish we had then that might be available to us now? Since the most cost-effective analysis activity is to recall accurately and comprehend what has gone before, a well-documented review activity saves time and money in the next vehicle programme.

The process described is not definitive, nor is it intended to be prescriptive. It should, however, illustrate the difference between 'analysis' and 'simulation' and clearly differentiate between them.

1.6 Computational methods

Whether the equations of motion have been derived by hand or delegated to a commercial software package, the primary goal when considering vehicle dynamics is to be able to predict the time-domain solution to those equations.

Once the equations of motion have been assembled, they are integrated numerically. This is a specialized field in its own right. There are many publications in the field and it is an area rife with difficulties and pitfalls for the unwary. However, in order to successfully use the commercially available software products, some comprehension of the difficulties involved are necessary for users. This chapter deals with some of the more common difficulties with some examples for the student. By far the most dangerous type of difficulty is the 'plausible but wrong' solution. Commercial analysts must studiously guard against the 'garbage in, gospel out' mentality that pervades the engineering industry at present.

The equations can be solved in a fairly direct fashion as assembled by the commercial package pre-processor or they can be subject to further symbolic manipulation before numerical solution. So-called 'symbolic' codes, discussed later, offer some tremendous computational efficiency benefits and are being hailed by many as the future of multibody system analysis since they allow real-time computation of reasonably complex models without excessive computing power. The prospect of a real-time multibody system of the vehicle solved on-board in order to generate reference signals for the generation-after-next vehicle control systems seems genuine.

1.7 Computer-based tools

Multibody systems analysis software has become so easy to use that many users lack even a basic awareness of the methods they are using. This chapter charts the background and development to the current generation of multibody systems analysis programs. While the freedom from the purgatory of formulating one's own equations of motion is a blessing, it is partly this purgatory that aids the analyst's final understanding of the problem. Chapter 2, Kinematics and dynamics of rigid bodies, is intended as a reference and also as a 'launch pad' for the enthusiastic readers to be able to teach themselves the process of so-called 'classical' modelling.

The best multibody system codes now include, specifically for the vehicle handling task, a 'concept level' model that has no literal detail but instead a 'wheel trajectory map'. In the near future, it seems that reverse engineering tools for deducing the required wheel trajectory map will become available.

Crolla (1995) identifies the main types of computer-based tools which can be used for vehicle dynamic simulation and categorizes these as:

(i) Purpose-designed simulation codes

(ii) Multibody simulation packages that are numerical

(iii) Multibody simulation packages that are algebraic (symbolic)

(iv) Toolkits such as MATLAB

One of the major conclusions that Crolla draws is that it is still generally the case that the ride and handling performance of a vehicle will be developed and refined mainly through subjective assessments. Most importantly he suggests that in concentrating on sophistication and precision in modelling, practising vehicle dynamicists may have got the balance wrong. This is an important issue that reinforces the main approach in this book, which is to encourage the application of models that lead to positive decisions and inputs to the vehicle design process.

Crolla's paper also provides an interesting historical review that highlights an important meeting at IMechE headquarters in 1956, 'Research in automobile stability and control and tyre performance'. The author states that in the field of vehicle dynamics the papers presented at this meeting are now regarded as seminal and are referred to in the USA as simply 'The IME Papers'.

One of the authors at that meeting, Segel, can be considered to be a pioneer in the field of vehicle dynamics. His paper (Segel, 1956) is one of the first examples where classical mechanics has been applied to an automobile in the study of lateral rigid body motion resulting from steering inputs. The paper describes work carried out on a Buick vehicle for General Motors and is based on transferable experience of aircraft stability gained at the Flight Research Department, Cornell Aeronautical Laboratory (CAL). The main thrust of the project was the development of a mathematical vehicle model that included the formulation of lateral tyre forces and the experimental verification using instrumented vehicle tests. Another author at the meeting, Milliken (Milliken and Whitcomb, 1956), has also continued to make a significant contribution to the discipline.

In 1993, almost 40 years after embarking on this early work in vehicle dynamics, Segel again visited the IMechE to present a comprehensive review paper (Segel, 1993), 'An overview of developments in road vehicle dynamics: past, present and future'.

This paper provides a historical review that considers the development of vehicle dynamics theory in three distinct phases:

Period 1 – Invention of the car to early 1930s

Period 2 – Early 1930s to 1953

Period 3 – 1953 to present

In describing the start of Period 3 Segel references his early 'IME paper' (Segel, 1956). In terms of preparing a review of work in the area of vehicle dynamics there is an important point made in the paper regarding the rapid expansion in literature that makes any comprehensive summary and critique difficult. This is highlighted by the example of the 1992 FISITA Congress where a total of seventy papers were presented under the general title of 'Total Vehicle Dynamics'.

Following Segel's historical classification of the vehicle dynamics discipline to date, the authors of this text suggest that we have now entered a fourth era that may be characterized by the use of engineering analysis software as something of a 'commodity', bought and sold and often used without a great deal of formal comprehension. In these circumstances there is a need for the software to be absolutely watertight (currently not possible to guarantee) or else for a small number of experts – 'champions' – within organizations to ensure the 'commodity' users aren't drifting off the rails, to use a horribly mixed metaphor. This mode of operation is already becoming established within the analysis groups of large automotive companies where analysts make use of customized software programs such as ADAMS/Car. These programs have two distinct types of usage. At one level the software is used by an 'expert' with the experience, knowledge and skill to customize the models generated, the types of simulation to be performed and the format in which selected results will be presented. A larger group of 'standard' users are then able to use the program to carry out suspension or full vehicle simulations assuming little or no knowledge of multibody systems formulations and solution methods.

The authors in Hogg et al. (1992) give further insights into how computer models and simulation programs are used by industry in the field of road vehicle dynamics. In this case the company is Lotus. In this paper the authors describe how simulation tools can be used at various stages in the design process. This includes the manner in which MSC.ADAMS is used to 'tune' a suspension design during development to produce, for example, very low but accurately controlled levels of steer change during suspension stroke.

Hogg et al. (1992) continue to describe how for vehicle handling they used their own Simulation and Analysis Model (SAM). This functional model required a minimum of design information and used input parameters that can be obtained by measurement of suspension characteristics using a static test rig. The SAM model had 17 rigid body degrees of freedom (DOF). The paper identified that the vehicle body contributed 6 of these DOF and that each corner suspension unit had 2 DOF, one of which was the rotation of the road wheel and another that allowed vertical movement relative to the vehicle body. The suspensions were modelled to pivot about an instant centre. This is the same approach used with the swing arm full vehicle model described later in Chapter 6. The SAM model also had 3 DOF associated with steering which suggests steering torque inputs and the modelling of compliance in the steering system. The SAM model used an early version of the tyre model proposed by Pacejka and his associates (Bakker et al., 1986).

The use of MSC.ADAMS by Lotus for handling simulations is also described in this paper (Hogg et al., 1992). In this case an example output

shows good correlation between MSC.ADAMS and test measurements when comparing yaw rate for an 80 kph lane change manoeuvre. It is also stated, however, that this model had over 200 DOF and used the Pacejka tyre model that required up to 50 parameters. Pilling (1995) also gives information about the work at Lotus in the field of vehicle dynamics and simulation with an emphasis on the role of the tyre.

1.8 Commercial computer packages

General purpose programs such as MSC.ADAMS have been developed with a view to commercial gain and as such are able to address a much larger set of problems across a wide range of engineering industries. In addition to the automotive industry MSC.ADAMS is an established tool within the aerospace, large construction, electro-mechanical and the general mechanical engineering industries. The general nature of the program means that within any one industry the class of applications may develop and extend over a broad range.

The MSC.ADAMS program is typical of the range of multibody analysis programs described as numeric where the user is concerned with assembling a physical description of the problem rather than writing equations of motion. A comprehensive overview of MSC.ADAMS is provided by Ryan (1990), although since the date of that publication the development of the software has moved on considerably, particularly in the area of graphical pre- and post-processing.

Blundell (1999; 2000a,b) published a series of four IMechE papers with the aim of summarizing typical processes involved with using MSC.ADAMS to simulate full vehicle handling manoeuvres. The first paper provided an overview of the usage of multibody systems analysis in vehicle dynamics. The second paper described suspension modelling and analysis methodologies. The third paper covered tyre modelling and provided example routines used with MSC.ADAMS for different tyre models and data. The fourth and final paper brought the series together with a comparative study of full vehicle models, of varying complexity, simulating a double lane change manoeuvre. Results from the simulation models were compared with measured test data from the proving ground. The overall emphasis of the series of papers was to demonstrate the accuracy of simple efficient models based on parameters amenable to design sensitivity study variations rather than blindly modelling the vehicle ‘as is’.

Before the evolution of programs like MSC.ADAMS, engineers analysed the behaviour of mechanisms such as cam-followers and four bar linkages on the basis of pure kinematic behaviour. Graphical methods were often used to obtain solutions. Chace (1985) summarizes the early programs that led to the development of the MSC.ADAMS program. One of the first programs (Cooper et al., 1965) was KAM (Kinematic Analysis Method) capable of performing displacement, velocity and acceleration analysis and solving reaction forces for a limited set of linkages and suspension models. Another early program (Knappe, 1965) was COMMEND (Computer-Orientated Mechanical Engineering Design) which was used for planar problems.

The origin of MSC.ADAMS can be traced back to a program of research initiated by Chace at the University of Michigan in 1967. By 1969 Chace (1969, 1970) and Korybalski (Chace and Korybalski, 1970) had completed the original version of DAMN (Dynamic Analysis of Mechanical Networks). This was historically the first general program to solve time histories for systems undergoing large displacement dynamic motion. This work led in 1971 to a new program DRAM (Dynamic Response of Articulated Machinery) that was further enhanced by Angel (Chace and Angel, 1977).

The first program forming the basis of MSC.ADAMS was completed by Orlandea in 1973 and published in a series of two ASME papers (Orlandea et al., 1976a, b). This was a development of the earlier two-dimensional programs to a three-dimensional code but without some of the impact capability contained in DRAM at that time.

Blundell (1991) describes how the MSC.ADAMS software is used to study the behaviour of systems consisting of rigid or flexible parts connected by joints and undergoing large displacement motion and in particular the application of the software in vehicle dynamics. The paper also lists a number of other systems based on MSC.ADAMS that had at that time been developed specifically for automotive vehicle modelling applications. Several of the larger vehicle manufacturers have at some time integrated MSC.ADAMS into their own in-house vehicle design systems. Early examples of these were the AMIGO system at Audi (Hudi, 1988), and MOGESSA at Volkswagen (Terlinden et al., 1987). The WOODS system based on user defined worksheets was another system at that time in this case developed by German consultants for Ford in the UK (Kaminski, 1990). Ford's global vehicle modelling activities have since focused on in-house generated linear models and the ADAMS/Chassis™ (formerly known as ADAMS/Pre™) package, a layer over the top of the standard MSC.ADAMS pre- and post-processor that is strongly tailored towards productivity and consistency in vehicle analysis.

Another customized application developed by the automotive industry is described in Scapaticci et al. (1992). In this paper the authors describe how MSC.ADAMS has been integrated into a system known as SARAH (Suspension Analyses Reduced ADAMS Handling). This in-house system for the automotive industry was developed by the Fiat Research Centre Handling Group and used a suspension modelling technique that ignored suspension layout but focused on the final effects of wheel centre trajectory and orientation.

At Leeds University a vehicle-specific system was developed under the supervision of Crolla. In this case all the commonly required vehicle dynamics studies have been embodied in their own set of programs (Crolla et al., 1994) known as VDAS (Vehicle Dynamics Analysis Software). Examples of the applications incorporated in this system included ride/handling, suspensions, natural frequencies, mode shapes, frequency response and steady state handling diagrams. The system included a range of models and further new models could be added using a pre-processor.

Crolla et al. (1994) also define two fundamental types of MBS program, the first of which is that such as MSC.ADAMS where the equations are

generated in numerical format and are solved directly using numerical integration routines embedded in the package. The second and more recent type of MBS program identified formulates the equations in symbolic form and often uses an independent solver. The authors also describe toolkits as collections of routines that generate models, formulate and solve equations, and present results. The VDAS system is identified as falling into this category of computer software used for vehicle dynamics.

Other examples of more recently developed codes formulate the equations algebraically and use a symbolic approach. Examples of these programs include MESA VERDE (Wittenburg and Wolz, 1985), AUTOSIM (Sayers, 1990), and RASNA Applied Motion Software (Austin and Hollars, 1992). Crolla (Crolla et al., 1992) provides a summary comparison of the differences between numeric and symbolic code. As stated MBS programs will usually automatically formulate and solve the equations of motion although in some cases such as with the work described by Costa (1991) and Holt (Holt and Cornish, 1992; Holt, 1994) a program SDFAST has been used to formulate the equations of motion in symbolic form and another program ACSL (Automatic Continuous Simulation Language) has been used to generate a solution.

Special-purpose programs are designed and developed with the objective of solving only a specific set of problems. As such they are aimed at a specific group of problems. A typical example of this type of program would be AUTOSIM described by Sayers (1990, 1992), Sharp (1997) and Mousseau et al. (1992) which is intended for vehicle handling and has been developed as a symbolic code in order to produce very fast simulations. Programs such as this can be considered to be special purpose as they are specifically developed for a given type of simulation but do, however, allow flexibility as to the choice and complexity of the model. An extension of this is where the equations of motion for a fixed vehicle modelling approach are programmed and cannot be changed by the user such as the HVOSM (Highway-Vehicle-Object Simulation Model) developed at the University of Michigan Transport Research Institute (UMTRI) (Sayers, 1992). The program includes tyre and suspension models and can be used for impact studies in addition to the normal ride and handling simulations. Crolla et al. (1992) indicate that the University of Missouri has also developed a light vehicle dynamics simulation (LVDS) program that runs on a PC and can produce animated outputs. In the mid-1980s Systems Technology Inc. developed a program for vehicle dynamics analysis nonlinear (VDANL) simulation. This program is based on a 13 degree of freedom, lumped parameter model (Allen et al., 1987) and has been used by researchers at Ohio State University for sensitivity analysis studies (Tandy et al., 1992).

The modelling of the tyre forces and moments at the tyre to road contact patch is one of the most complex issues in vehicle handling simulation. The models used are not predictive but are used to represent the tyre force and moment curves typically found through laboratory or road-based rig testing of a tyre. Examples of tyre models used for vehicle handling discussed in this book include:

(i) A sophisticated tyre model known as the ‘Magic Formula’. This tyre model has been developed by Pacejka and his associates (Bakker et al.,

1986, 1989; Pacejka and Bakker, 1993) and is known to give an accurate representation of measured tyre characteristics. The model uses modified trigonometric functions to represent the shape of curves that plot tyre forces and moments as functions of longitudinal slip or slip angle. In recent years the work of Pacejka has become well known throughout the vehicle dynamics community. The result of this is a tyre model that is now widely used both by industry and academic institutions and is undergoing continual improvement and development. The complexity of the model does, however, mean that well over 50 or more parameters may be needed to define a tyre model and that software must be obtained or developed to derive the parameters from measured test data.

(ii) The second model considered here is known as the Fiala tyre model (Fiala, 1954) and is provided as the default tyre model in MSC.ADAMS. This is a much simpler model that also uses mathematical equations to represent the tyre force and moment characteristics. Although not so widely recognized as Pacejka's model the fact that this model is the default in MSC.ADAMS and is simpler to use led to its inclusion. The advantage of this model is that it only requires 10 parameters and that the physical significance of each of these is easy to comprehend making this a good starting point for students and newcomers to the discipline. The parameters can also be quickly and easily derived from measured test data without recourse to special software. It should also be noted, however, that this model unlike Pacejka's is not suitable for combined braking and cornering and can only be used under pure slip conditions. The Fiala formulation also has some limitations at high slip angles and is thus unsuitable for limit manoeuvres even when pure slip conditions are included.

(iii) The fourth modelling approach is to use a straightforward interpolation model. This was the original tyre modelling method used in MSC.ADAMS (Ryan, 1990). This methodology is still used by some companies but has, to a large extent, been superseded by more recent parameter-based models. The method is included here as a useful benchmark for the comparison of other tyre models in Chapter 5.

Another tyre model is provided for readers as a source listing in Appendix B. This model (Blundell, 2003) has been developed by Harty and as with the Fiala model has the advantage of requiring only a limited number of input parameters. The implementation is more complete, however, than the Fiala model and includes representation of the following:

- Comprehensive slip
- Load dependency
- Camber thrust
- Post limit

It has been found that the Harty model is robust when modelling limit behaviour including, for example, problems involving low grip or prolonged wheelspin.

1.9 Benchmarking exercises

In addition to the software discussed so far other multibody systems analysis programs such as DADS, SIMPACK, and MADYMO are commercially available and used by the engineering community. A detailed description of each of these is beyond the scope of this text and in any case the rapid development of commercial software means any such assessment here would rapidly become outdated. In broad terms DADS and SIMPACK appear to be comparable with MSC.ADAMS although at the time of writing MSC.ADAMS is the most widely used, particularly by the vehicle dynamics community. MADYMO is a program recognized as having a multibody foundation with an embedded non-linear finite element capability. This program has been developed by TNO in the Netherlands and complements their established crash test work with dummies. Recent developments in MADYMO have included the development of biofidelic humanoid models to extend the simulation of crash test dummies to 'real world' pedestrian impact scenarios.

A detailed comparison between the various codes is beyond the capability of most companies when selecting an MBS program. In many ways the use of multibody systems has followed on from the earlier use of finite element analysis, the latter being approximately 10 years more mature as applied commercial software. Finite element codes were subject to a rigorous and successful series of benchmarks under the auspices of NAFEMS (National Agency for Finite Elements and Standards) during the 1980s. The published results provided analysts with useful comparisons between major finite element programs such as NASTRAN and ANSYS. The tests performed compared results obtained for a range of analysis methods with various finite elements.

For the vehicle dynamics community Kortum et al. (1991) recognized that with the rapid growth in available multibody systems analysis programs a similar benchmarking exercise was needed. This exercise was organized through the International Association for Vehicle System Dynamics (IAVSD). In this study the various commercially available MBS programs were used to benchmark two problems. The first was to model the Iltis military vehicle and the second a five-link suspension system. A review of the exercise is provided by Sharp (1994) where some of the difficulties involved with such a wide-ranging study are discussed. An example of the problems involved would be the comparison of results. With different investigators using the various programs at widespread locations a simple problem occurred when the results were sent in plotted form using different size plots and inconsistent axes making direct comparisons between the codes extremely difficult. It was also very difficult to ensure that a consistent modelling approach was used by the various investigators so that the comparison was based strictly on the differences between the programs and not the models used. An example of this with the Iltis vehicle would be modelling a leaf spring for which in many programs there were at the time no standard elements within the main code. Although not entirely successful the exercise was useful in being the only known attempt to provide a comparison between all the main multibody programs at the time. It should also be recognized that in the period since the exercise programs such as MSC.ADAMS have been extensively developed to add a wide range of capability.

Anderson and Hanna (1989) have carried out an interesting study where they have used two vehicles to make a comparison of three different vehicle simulation methodologies. They have also made use of the Iltis, a vehicle of German design, which at that time was the current small utility vehicle used by the Canadian military. The Iltis was a vehicle that was considered to have performed well and had very different characteristics to the M-151 Jeep that was the other vehicle in this study. The authors state that the M-151 vehicle, also used by the Canadian military, had been declared unsafe due to a propensity for rolling over.

Work has been carried out at the University of Bath (Ross-Martin et al., 1992) where the authors have compared MSC.ADAMS with their own hydraulic and simulation package. The results for both programs are compared with measured vehicle test data provided in this case by Ford. The Bath model is similar to the Roll Stiffness Model described later in this book but is based on a force roll centre as described by Dixon (1987). This requires the vehicle to actually exist so that the model can use measured inputs obtained through static rig measurements, using equipment of the type described by Whitehead (1995). The roll-centre model described in this book is based on a kinematic roll centre derived using a geometric construction as described in Chapter 4, though there is little to preclude a force-based prediction by modelling the test rig on which the real vehicle is measured.

As a guide to the complexity of the models discussed in Ross-Martin et al. (1992), the Bath model required 91 pieces of information and the MSC.ADAMS model, although not described in detail, needed 380 pieces of information. It is also stated in this paper that the MSC.ADAMS model used 150 sets of non-linear data pairs that suggests detailed modelling of all the non-linear properties of individual bushes throughout the vehicle.

2 Kinematics and dynamics of rigid bodies

2.1 Introduction

The application of a modern multibody systems computer program requires a good understanding of the underlying theory involved in the formulation and solution of the equations of motion. Due to the three-dimensional nature of the problem the theory is best described using vector algebra. In this chapter the starting point will be the basic definition of a vector and an explanation of the notation that will be used throughout this text. The vector theory will be developed to demonstrate, using examples based on suspension systems, the calculation of new geometry and changes in body orientation, such as the steer change in a road wheel during vertical motion relative to the vehicle body. This will be extended to show how velocities and accelerations may be determined throughout a linked three-dimensional system of rigid bodies. The definition of forces and moments will lead through to the definition of the full dynamic formulations typically used in a multibody systems analysis code.

2.2 Theory of vectors

2.2.1 Position and relative position vectors

Consider the initial definition of the position vector that defines the location of point P in Figure 2.1.

In this case the vector that defines the position of P relative to the reference frame O_1 may be completely described in terms of its components with magnitude Px, Py and Pz. The directions of the components are defined by

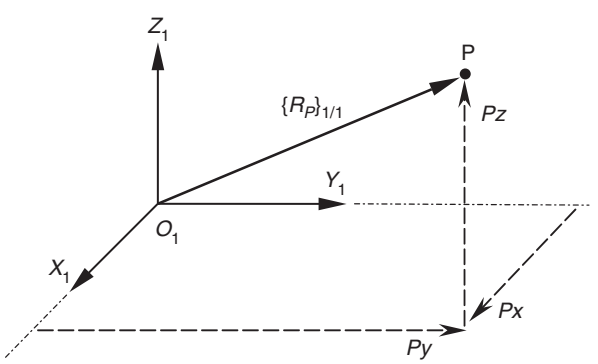

Fig. 2.1 Position vector

attaching the appropriate sign to their magnitudes:

$$\{R_P\}_{1/1} = \begin{bmatrix} Px \\ Py \\ Pz \end{bmatrix} \tag{2.1}$$

The use of brackets { } here is a shorthand representation of a column matrix and hence a vector. Note that it does not follow any quantity that can be expressed as the terms in a column matrix is also a vector.

In writing the vector $\{R_P\}_{1/1}$ the upper suffix indicates that the vector is measured relative to the axes of reference frame O_1. In order to measure a vector it is necessary to determine its magnitude and direction relative to the given axes, in this case O_1. It is then necessary to resolve it into components parallel to the axes of some reference frame that may be different from that used for measurement as shown in Figure 2.2.

In this case we would write $\{R_P\}_{1/2}$ where the lower suffix appended to $\{R_P\}_{1/2}$ indicates the frame O_2 in which the components are resolved. We can also say that in this case the vector is referred to O_2. Note that in most cases the two reference frames are the same and we would abbreviate $\{R_P\}_{1/1}$ to $\{R_P\}_1$.

It is now possible in Figure 2.3 to introduce the concept of a relative position vector $\{R_{PQ}\}_1$. The vector $\{R_{PQ}\}_1$ is the vector from Q to P. It can also be described as the vector that describes the position of P relative to Q.

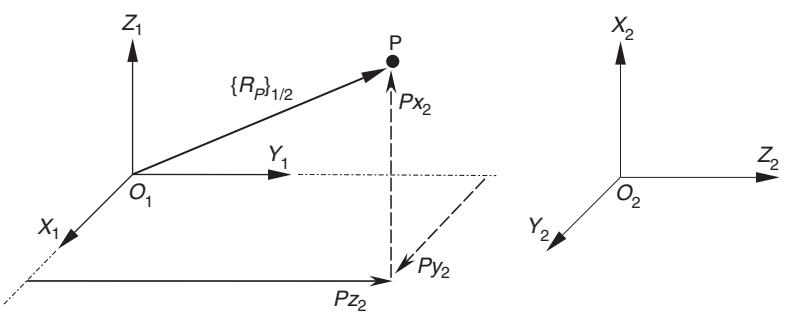

Fig. 2.2 Resolution of position vector components

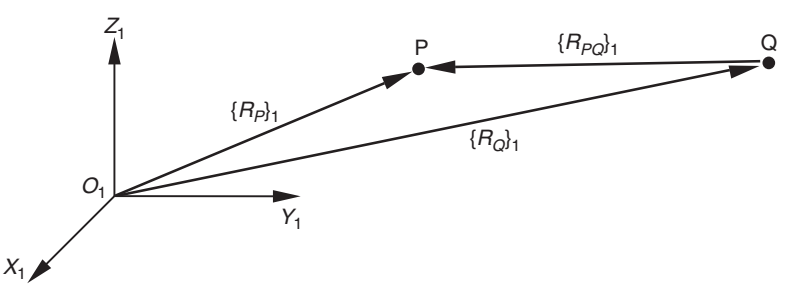

Fig. 2.3 Relative position vector

These vectors obey the triangle law for the addition and subtraction of vectors, which means that

$$\begin{aligned} \{R_{PQ}\}_1 &= \{R_P\}_1 - \{R_Q\}_1 \\ \text{or} \quad \{R_P\}_1 &= \{R_Q\}_1 + \{R_{PQ}\}_1 \end{aligned} \tag{2.2}$$

It also follows that we can write

$$\begin{aligned} \{R_{QP}\}_1 &= \{R_Q\}_1 - \{R_P\}_1 \\ \text{or} \quad \{R_Q\}_1 &= \{R_P\}_1 + \{R_{QP}\}_1 \end{aligned} \tag{2.3}$$

Application of Pythagoras' theorem will yield the magnitude $|R_P|$ of the vector $\{R_P\}_1$ as follows:

$$|R_P| = \sqrt{Px^2 + Py^2 + Px^2} \tag{2.4}$$

Similarly the magnitude $|R_{PQ}|$ of the relative position vector $\{R_{PQ}\}_1$ can be obtained using

$$|R_{PQ}| = \sqrt{(Px - Qx)^2 + (Py - Qy)^2 + (Pz - Qz)^2} \tag{2.5}$$

Consider now the angles θ_X, θ_Y and θ_Z which the vector $\{R_P\}_1$ makes with each of the X, Y and Z axes of frame O_1 as shown in Figure 2.4. This gives the direction cosines lx, ly and lz of vector $\{R_P\}_1$ where

$$\begin{aligned} lx &= \cos\theta x = \frac{Px}{|R_P|} \\ ly &= \cos\theta y = \frac{Py}{|R_P|} \\ lz &= \cos\theta z = \frac{Pz}{|R_P|} \end{aligned} \tag{2.6}$$

These direction cosines are components of the vector $\{l_P\}_1$ where

$$\{l_p\}_1 = \frac{\{R_P\}}{|R_P|} \tag{2.7}$$

It can be seen that $\{l_P\}_1$ has unit magnitude and is therefore a unit vector.

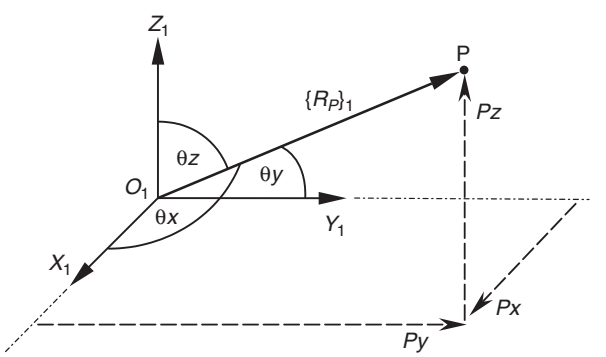

Fig. 2.4 Direction cosines

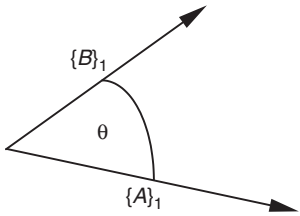

Fig. 2.5 Vector dot product

2.2.2 The dot (scalar) product

The dot, or scalar, product $\{A\}_1 \bullet \{B\}_1$ of the vectors $\{A\}_1$ and $\{B\}_1$ yields a scalar C with magnitude equal to the product of the magnitude of each vector and the cosine of the angle between them.

Thus:

$$\{A\}_1 \bullet \{B\}_1 = |C| = |A|\,|B| \cos\theta \tag{2.8}$$

The calculation of $\{A\}_1 \bullet \{B\}_1$ requires the solution of

$$\{A\}_1 \bullet \{B\}_1 = \{A\}_1^T \{B\}_1 = AxBx + AyBy + AzBz \tag{2.9}$$

$$\text{where} \qquad \{B\}_1 = \begin{bmatrix} Bx \\ By \\ Bz \end{bmatrix} \quad \text{and} \quad \{A\}_1^T = [Ax \quad Ay \quad Az] \tag{2.10}$$

The T superscript in $\{A\}_1^T$ indicates that the vector is transposed.

Clearly $\{A\}_1 \bullet \{B\}_1 = \{B\}_1 \bullet \{A\}_1$ and the dot product is a commutative operation. The physical significance of the dot product will become apparent later but at this stage it can be seen that the angle θ between two vectors $\{A\}_1$ and $\{B\}_1$ can be obtained from

$$\cos\theta = \{A\}_1 \bullet \frac{\{B\}_1}{|A|\,|B|} \tag{2.11}$$

A particular case which is useful in the formulation of constraints representing joints and the like is the situation when $\{A\}_1$ and $\{B\}_1$ are perpendicular making $\cos\theta = 0$.

As can be seen in Figure 2.6 the equation that enforces the perpendicularity of the two spindles in the universal joint can be obtained from

$$\{A\}_1 \bullet \{B\}_1 = 0 \tag{2.12}$$

2.2.3 The cross (vector) product

The cross, or vector, product of two vectors, $\{A\}_1$ and $\{B\}_1$, is another vector $\{C\}_1$ given by

$$\{C\}_1 = \{A\}_1 \times \{B\}_1 \tag{2.13}$$

The vector $\{C\}_1$ is perpendicular to the plane containing $\{A\}_1$ and $\{B\}_1$ as shown in Figure 2.7.

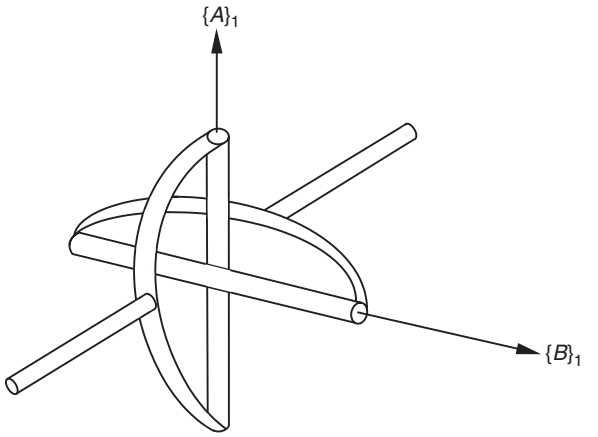

Fig. 2.6 Application of the dot product to enforce perpendicularity

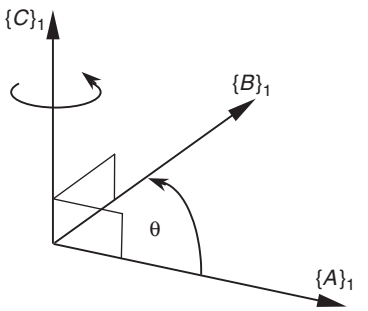

Fig. 2.7 Vector cross product

The magnitude of $\{C\}_1$ is defined as

$$|C| = |A|\,|B| \sin\theta \tag{2.14}$$

The direction of $\{C\}_1$ is defined by a positive rotation about $\{C\}_1$ rotating $\{A\}_1$ into line with $\{B\}_1$. The calculation of $\{A\}_1 \times \{B\}_1$ requires $\{A\}_1$ to be arranged in skew-symmetric form as follows:

$$\{C\}_1 = \{A\}_1 \times \{B\}_1 = [A]_1\{B\}_1 = \begin{bmatrix} 0 & -Az & Ay \\ Az & 0 & -Ax \\ -Ay & Ax & 0 \end{bmatrix} \begin{bmatrix} Bx \\ By \\ Bz \end{bmatrix} \tag{2.15}$$

Multiplying this out would give the vector $\{C\}_1$:

$$\{C\}_1 = \begin{bmatrix} -AzBy + AyBz \\ AzBx - AxBz \\ -AyBx + AxBy \end{bmatrix} \tag{2.16}$$

Exchange of $\{A\}_1$ and $\{B\}_1$ will show that the cross product operation is not commutative and that

$$\{A\}_1 \times \{B\}_1 = -\{B\}_1 \times \{A\}_1 \tag{2.17}$$

2.2.4 The scalar triple product

The scalar triple product D of the vectors $\{A\}_1$, $\{B\}_1$ and $\{C\}_1$ is defined as

$$D = \{\{A\}_1 \times \{B\}_1\} \bullet \{C\}_1 \tag{2.18}$$

2.2.5 The vector triple product

The vector triple product $\{D\}_1$ of the vectors $\{A\}_1$, $\{B\}_1$ and $\{C\}_1$ is defined as

$$\{D\}_1 = \{A\}_1 \times \{\{B\}_1 \times \{C\}_1\} \tag{2.19}$$

2.2.6 Rotation of a vector

In multibody dynamics bodies may undergo motion which involves rotation about all three axes of a given reference frame. The new components of a vector $\{A\}_1$, shown in Figure 2.8, may be determined as it rotates through an angle α about the X_1-axis, β about the Y_1-axis, and γ about the Z_1-axis of frame O_1.

Consider first the rotation α about O_1X_1. The component Ax is unchanged. The new components Ax', Ay' and Az' can be found by viewing along an X_1-axis as shown in Figure 2.9.

By inspection it is found that

$$\begin{aligned} Ax' &= Ax \\ Ay' &= Ay\cos\alpha - Az\sin\alpha \\ Az' &= Ay\sin\alpha + Az\cos\alpha \end{aligned} \tag{2.20}$$

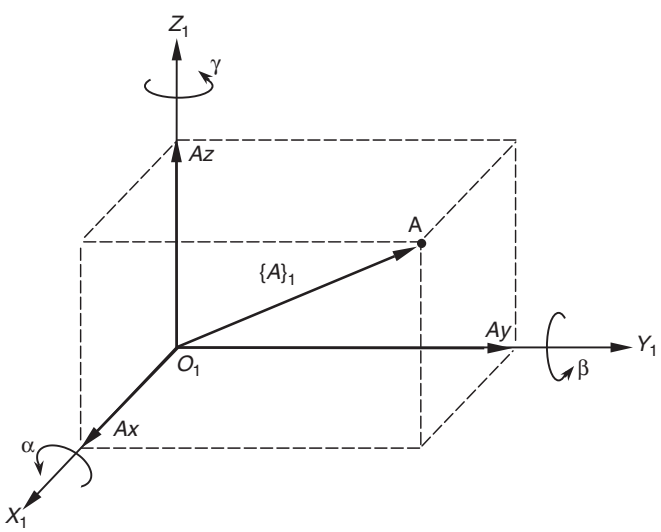

Fig. 2.8 Rotation of a vector

In matrix form this can be written:

$$\begin{bmatrix} Ax' \\ Ay' \\ Az' \end{bmatrix} = \begin{bmatrix} 1 & 0 & 0 \\ 0 & \cos\alpha & -\sin\alpha \\ 0 & \sin\alpha & \cos\alpha \end{bmatrix} \begin{bmatrix} Ax \\ Ay \\ Az \end{bmatrix} \tag{2.21}$$

In a similar manner when $\{A\}_1$ is rotated through an angle β about the Y_1-axis the components of a new vector $\{A'\}_1$ can be obtained from

$$\begin{bmatrix} Ax' \\ Ay' \\ Az' \end{bmatrix} = \begin{bmatrix} \cos\beta & 0 & \sin\beta \\ 0 & 1 & 0 \\ -\sin\beta & 0 & \cos\beta \end{bmatrix} \begin{bmatrix} Ax \\ Ay \\ Az \end{bmatrix} \tag{2.22}$$

After a final rotation of $\{A\}_1$ through an angle γ about the Z_1-axis the new components of $\{A'\}_1$ are given by

$$\begin{bmatrix} Ax' \\ Ay' \\ Az' \end{bmatrix} = \begin{bmatrix} \cos\gamma & -\sin\gamma & 0 \\ \sin\gamma & \cos\gamma & 0 \\ 0 & 0 & 1 \end{bmatrix} \begin{bmatrix} Ax \\ Ay \\ Az \end{bmatrix} \tag{2.23}$$

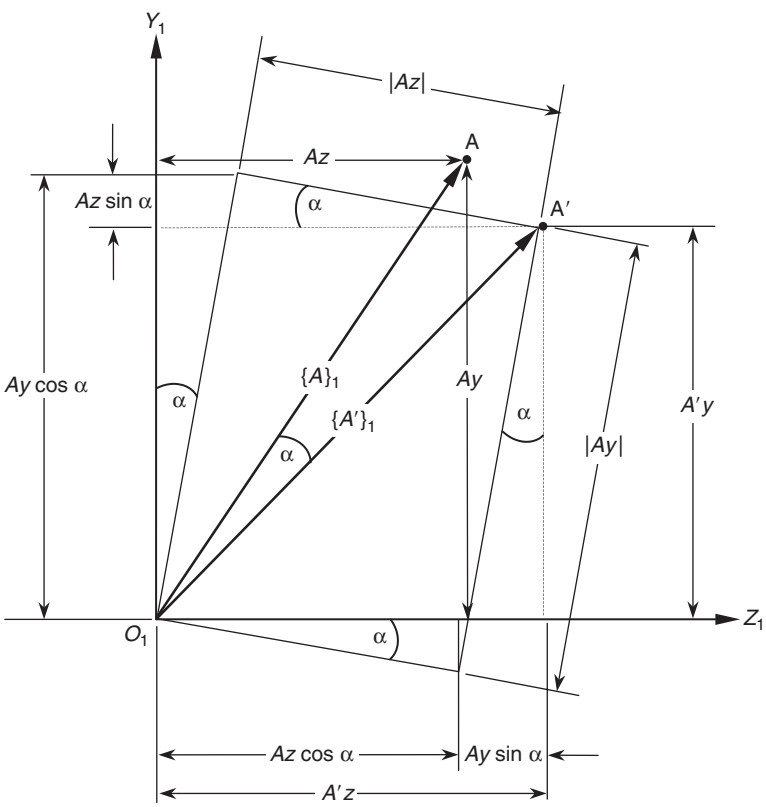

Fig. 2.9 Rotation of a vector viewed along the X_1-axis

Applying all three rotations in the sequence α, β and γ would result in the three rotation matrices being multiplied through as follows:

$$\begin{bmatrix} Ax' \\ Ay' \\ Az' \end{bmatrix} = \begin{bmatrix} \cos\gamma & -\sin\gamma & 0 \\ \sin\gamma & \cos\gamma & 0 \\ 0 & 0 & 1 \end{bmatrix} \begin{bmatrix} \cos\beta & 0 & \sin\beta \\ 0 & 1 & 0 \\ -\sin\beta & 0 & \cos\beta \end{bmatrix} \begin{bmatrix} 1 & 0 & 0 \\ 0 & \cos\alpha & -\sin\alpha \\ 0 & \sin\alpha & \cos\alpha \end{bmatrix} \begin{bmatrix} Ax \\ Ay \\ Az \end{bmatrix} \quad (2.24)$$

$$\begin{bmatrix} Ax' \\ Ay' \\ Az' \end{bmatrix} = \begin{bmatrix} \cos\gamma & -\sin\gamma & 0 \\ \sin\gamma & \cos\gamma & 0 \\ 0 & 0 & 1 \end{bmatrix} \begin{bmatrix} \cos\beta & \sin\beta\sin\alpha & \sin\beta\cos\alpha \\ 0 & \cos\alpha & -\sin\alpha \\ -\sin\beta & \cos\beta\sin\alpha & \cos\beta\cos\alpha \end{bmatrix} \begin{bmatrix} Ax \\ Ay \\ Az \end{bmatrix} \quad (2.25)$$

$$\begin{bmatrix} Ax' \\ Ay' \\ Az' \end{bmatrix} = \begin{bmatrix} \cos\gamma\cos\beta & \cos\gamma\sin\beta\sin\alpha - \sin\gamma\cos\alpha & \cos\gamma\sin\beta\cos\alpha + \sin\gamma\sin\alpha \\ \sin\gamma\cos\beta & \sin\gamma\sin\beta\sin\alpha + \cos\gamma\cos\alpha & \sin\gamma\sin\beta\cos\alpha - \cos\gamma\sin\alpha \\ -\sin\beta & \cos\beta\sin\alpha & \cos\beta\cos\alpha \end{bmatrix} \begin{bmatrix} Ax \\ Ay \\ Az \end{bmatrix} \quad (2.26)$$

It should be noted that large rotations such as these are not commutative and therefore the angles α, β and γ cannot be considered to be the components of a vector. The order in which the rotations are applied is important. As can be seen in Figure 2.10 applying equal rotations of 90° but in a different sequence will not result in the same final orientation of the vector.

An understanding that large rotations are not a vector is an important aspect of multibody systems analysis. Sets of rotations may be required as inputs to define the orientation of a rigid body or a joint. They will also form the output when the relative orientation of one body to another is requested.

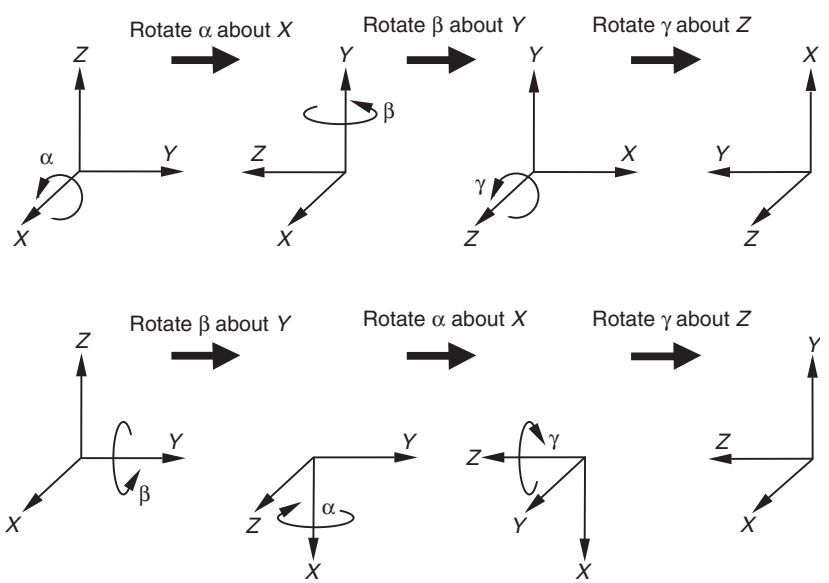

Fig. 2.10 The effect of rotation sequence on vector orientation

Note that the convention used here in Figure 2.10 is based on a set of Body (*X-Y-Z*) rotations. It will be shown later that different conventions may be used such as the Yaw-Pitch-Roll method based on a set of Body (*Z-Y-X*) rotations or the Euler angle method used in MSC.ADAMS that is based on a Body (*Z-X-Z*) combination.

2.2.7 Vector transformation

In multibody systems analysis it is often necessary to transform the components of a vector measured parallel to the axis of one reference frame to those measured parallel to a second reference frame. These operations should not be confused with vector rotation. In a transformation it is the magnitude and direction of the components that change. The direction of the vector is unchanged. Consider the transformation of a vector $\{A\}_1$, or in full definition $\{A\}_{1/1}$, from reference frame O_1 to reference frame O_2. Figure 2.11 represents a view back along the X_1-axis towards the origin O_1. The reference frame O_2 is rotated through an angle α about the X_1-axis of frame O_1.

From Figure 2.11 it can be seen that

$$\begin{aligned} Ax_2 &= Ax_1 \\ Ay_2 &= Ay_1 \cos\alpha + Az_1 \sin\alpha \\ Az_2 &= -Ay_1 \sin\alpha + Az_1 \cos\alpha \end{aligned} \tag{2.27}$$

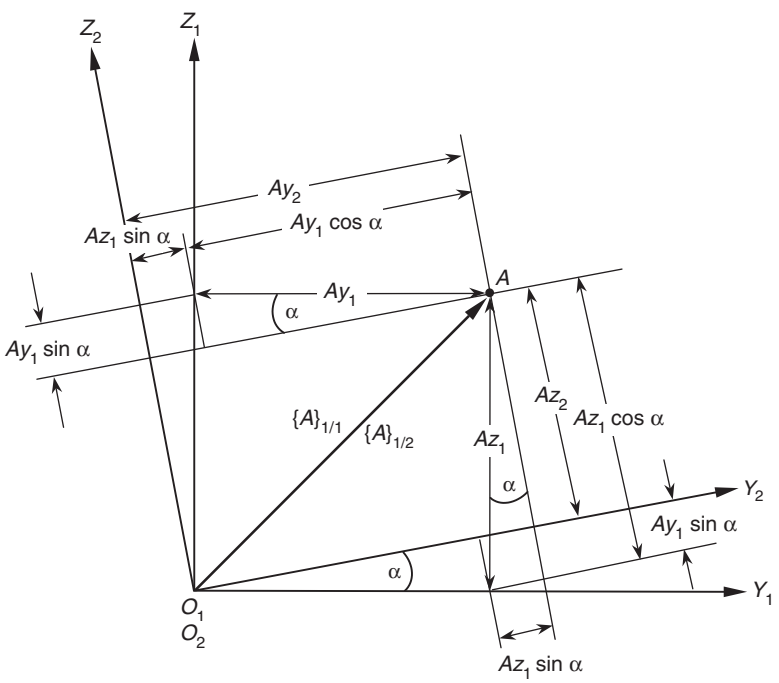

Fig. 2.11 Transformation of a vector

In matrix form this can be written:

$$\{A\}_{1/2} = \begin{bmatrix} Ax_2 \\ Ay_2 \\ Az_2 \end{bmatrix} = \begin{bmatrix} 1 & 0 & 0 \\ 0 & \cos\alpha & \sin\alpha \\ 0 & -\sin\alpha & \cos\alpha \end{bmatrix} \begin{bmatrix} Ax_1 \\ Ay_1 \\ Az_1 \end{bmatrix} \tag{2.28}$$

This equation may be expressed as

$$\{A\}_{1/2} = [T_1]_2 \{A\}_{1/1} \tag{2.29}$$

Consider next the transformation of the vector $\{A\}_{1/1}$ from reference frame O_1 to reference frame O_3. The reference frame O_3 is rotated through an angle β about the Y_1-axis of frame O_1. Following the same procedure as before we get:

$$\{A\}_{1/3} = \begin{bmatrix} Ax_3 \\ Ay_3 \\ Az_3 \end{bmatrix} = \begin{bmatrix} \cos\beta & 0 & -\sin\beta \\ 0 & 1 & 0 \\ \sin\beta & 0 & \cos\beta \end{bmatrix} \begin{bmatrix} Ax_1 \\ Ay_1 \\ Az_1 \end{bmatrix} \tag{2.30}$$

$$\{A\}_{1/3} = [T_1]_3 \{A\}_{1/1} \tag{2.31}$$

Finally consider the transformation to frame O_4 where O_4 is obtained from a rotation of γ about the Z_1-axis of frame O_1:

$$\{A\}_{1/4} = \begin{bmatrix} Ax_4 \\ Ay_4 \\ Az_4 \end{bmatrix} = \begin{bmatrix} \cos\gamma & \sin\gamma & 0 \\ -\sin\gamma & \cos\gamma & 0 \\ 0 & 0 & 1 \end{bmatrix} \begin{bmatrix} Ax_1 \\ Ay_1 \\ Az_1 \end{bmatrix} \tag{2.32}$$

$$\{A\}_{1/4} = [T_1]_4 \{A\}_{1/1} \tag{2.33}$$

The square transformation matrices $[T_1]_2$, $[T_1]_3$ and $[T_1]_4$ are the inverses of the rotation matrices developed in section 2.2.6. This is to be expected since the method here is the reverse of that shown previously where the vector, rather than the frame, was rotated. It should be noted that a transformation matrix $[T_m]_p$, which transforms a vector from frame m to frame p, has a transpose $[T_m]_p^T$ that is also its inverse $[T_m]_p^{-1}$.

In general terms the transformation of a vector from one frame m to another frame p may be written as

$$\{A\}_{n/p} = [T_m]_p \{A\}_{n/m} \tag{2.34}$$

2.2.8 Differentiation of a vector

The differentiation of a vector $\{A\}_1$ with respect to a scalar variable, such as time t, results in another vector given by

$$\frac{\mathrm{d}}{\mathrm{d}t}\{A\}_1 = \begin{bmatrix} \mathrm{d}Ax/\mathrm{d}t \\ \mathrm{d}Ay/\mathrm{d}t \\ \mathrm{d}Az/\mathrm{d}t \end{bmatrix} \tag{2.35}$$

Differentiation with respect to time is often denoted by the Newtonian dot giving

$$\{\dot{A}\}_1 = \begin{bmatrix} \dot{A}_x \\ \dot{A}_y \\ \dot{A}_z \end{bmatrix} \tag{2.36}$$

If the frames used for measurement and reference differ it is necessary to distinguish between, for example $\mathrm{d}\{A\}_{m/n}/\mathrm{d}t$ and $\{\dot{A}\}_{m/n}$ since

$$\frac{\mathrm{d}}{\mathrm{d}t}\{A\}_{m/n} \neq \{\dot{A}\}_{m/n} \tag{2.37}$$

In evaluating $\mathrm{d}\{A\}_{m/n}/\mathrm{d}t$, we measure $\{A\}$ in frame m, transform to frame n and then differentiate $\{A\}_{m/n}$ with respect to time. The notation $\{\dot{A}\}_{m/n}$, however, implies that $\{\dot{A}\}_m$ is determined first and that this vector is then transformed to frame n.

Consider the vector $\{A\}_{1/1}$ shown in Figure 2.12. The vector lies in the X_1Y_1 plane of frame O_1 and rotates at a constant speed of ω rad/s about the Z_1-axis. Frame 2 has its Z-axis coincident with Oz_1 and its X-axis is coincident with and rotates with $\{A\}_{1/1}$.

If OX_1 and OX_2 were coincident at time $t = 0$, then where A is the magnitude of $\{A\}_{1/1}$:

$$\{A\}_{1/1}^T = [A\cos\omega t \quad A\sin\omega t\, 0] \tag{2.38}$$

Transforming to frame O_2 gives

$$\{A\}_{1/2}^T = [A \quad 0 \quad 0] \tag{2.39}$$

Differentiating this with respect to time gives the following since the magnitude A does not vary with time:

$$\frac{\mathrm{d}}{\mathrm{d}t}\{A\}_{1/2}^T = [0 \quad 0 \quad 0] \tag{2.40}$$

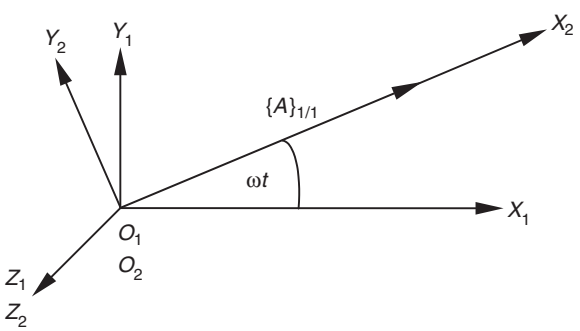

Fig. 2.12 Vector rotating with constant velocity

Now

$$\{\dot{A}\}_{1/1}^T = [-\omega A \sin \omega t \quad \omega A \cos \omega t \quad 0] \tag{2.41}$$

and

$$\{\dot{A}\}_{1/2}^T = [0 \quad \omega A \quad 0] \tag{2.42}$$

proving that

$$\frac{\mathrm{d}}{\mathrm{d}t}\{A\}_{1/2} \neq \{\dot{A}\}_{1/2} \tag{2.43}$$

2.2.9 Integration of a vector

Integration of the vector $\{A\}_1$ with respect to the scalar variable t is given by

$$\int \{A\}_1 \, \mathrm{d}t = \begin{bmatrix} \int Ax \, \mathrm{d}t \\ \int Ay \, \mathrm{d}t \\ \int Az \, \mathrm{d}t \end{bmatrix} \tag{2.44}$$

2.2.10 Differentiation of the dot product

The dot product of two vectors $\{A\}_1$ and $\{B\}_1$ is given by

$$\{A\}_1 \bullet \{B\}_1 = \{A\}_1^T\{B\}_1 = [AxBx + AyBy + AzBz] \tag{2.45}$$

Differentiation of $\{A\}_1 \bullet \{B\}_1$ with respect to time t gives

$$\frac{\mathrm{d}}{\mathrm{d}t}(\{A\}_1 \bullet \{B\}_1) = [Ax\dot{B}x + Bx\dot{A}x + Ay\dot{B}y + By\dot{A}y + Az\dot{B}z + Bz\dot{A}z] \tag{2.46}$$

or

$$\frac{\mathrm{d}}{\mathrm{d}t}(\{A\}_1 \bullet \{B\}_1) = \{A\}_1 \bullet \{\dot{B}\}_1 + \{\dot{A}\}_1 \bullet \{B\}_1 \tag{2.47}$$

The result of this is a scalar. The rule for differentiation of the dot product is similar to the differentiation of the product of two scalars u and v:

$$\frac{\mathrm{d}}{\mathrm{d}t}(uv) = u\frac{\mathrm{d}v}{\mathrm{d}t} + v\frac{\mathrm{d}u}{\mathrm{d}t} \tag{2.48}$$

2.2.11 Differentiation of the cross product

The cross product of two vectors $\{A\}_1$ and $\{B\}_1$ is given by

$$\{A\}_1 \times \{B\}_1 = \begin{bmatrix} 0 & -Az & Ay \\ Az & 0 & -Ax \\ -Ay & Ax & 0 \end{bmatrix} \begin{bmatrix} Bx \\ By \\ Bz \end{bmatrix} = \begin{bmatrix} -AzBy + AyBz \\ AzBx - AyBz \\ -AyBx + AyBy \end{bmatrix} \tag{2.49}$$

Differentiation of this vector with respect to time t gives

$$\frac{\mathrm{d}}{\mathrm{d}t}(\{A\}_1 \times \{B\}_1) = \begin{bmatrix} -Az\dot{B}y - \dot{A}zBy + Ay\dot{B}z + \dot{A}yBz \\ Az\dot{B}x + \dot{A}zBx - Ax\dot{B}z - \dot{A}yBz \\ -Ay\dot{B}x - \dot{A}yBx + Ax\dot{B}y + \dot{A}yBy \end{bmatrix} \tag{2.50}$$

or

$$\frac{\mathrm{d}}{\mathrm{d}t}(\{A\}_1 \times \{B\}_1) = \{A\}_1 \times \{\dot{B}\}_1 + \{\dot{A}\}_1 \times \{B\}_1 \tag{2.51}$$

The result of this operation is a vector. Note again that the rule for the differentiation of the cross product is similar to the rule for the differentiation of the product of two scalars.

2.2.12 Summary

1. A vector is expressed in terms of the magnitudes of its three orthogonal components listed, in natural order, as the elements of a column matrix. The brackets { } are used as a shorthand representation of a vector. Thus the vector $\{A\}_m$ with components of magnitude Ax, Ay and Az is represented by

$$\{A\}_m = \begin{bmatrix} Ax \\ Ay \\ Az \end{bmatrix} \tag{2.52}$$

2. The suffices m and n appended to the vector $\{A\}_{m/n}$ indicate that its components were measured relative to the axes of frame m but that the vector was then resolved into components parallel to the axes of frame n. We say that the vector is referred or transformed to frame n. If m is equal to n then the vector may be written as $\{A\}_m$.

3. The magnitude of the vector $\{A\}_m$ is represented by $|A|$, or simply by A when the meaning is unambiguous. This magnitude is given by

$$|A| = \sqrt{Ax^2 + Ay^2 + Az^2} \tag{2.53}$$

4. The cosines of the angles which $\{A\}_m$ makes with the X, Y and Z axes respectively of frame m are known as its direction cosines $\{l\}_m$. This vector is derived from $\{A\}_m$ as follows:

$$\{l\}_m = \frac{\{A\}_m}{|A|} \tag{2.54}$$

Since the magnitude of $\{l\}_m$ is unity, it is called a unit vector.

5. If $\{A\}_m$, $\{B\}_m$ and $\{C\}_m$ are vectors of the same dimensions and $\{C\}_m$ is the resultant of $\{A\}_m$ and $\{B\}_m$ then the equation

$$\{C\}_m = \{A\}_m + \{B\}_m \tag{2.55}$$

expresses the triangle law for the addition or subtraction of vectors. This equation is only valid if all vectors are referred to the same frame.

6. The dot product $\{A\}_m \bullet \{B\}_m$ of the vectors $\{A\}_m$ and $\{B\}_m$ is defined as a scalar whose magnitude is $|A|\,|B| \cos\theta$, θ being the angle between the vectors. The dot product is evaluated in terms of a matrix product as follows:

$$\{A\}_m \bullet \{B\}_m = \{A\}_m^T \{B\}_m \tag{2.56}$$

7. The cross product $\{A\}_m \times \{B\}_m$ of the vectors $\{A\}_m$ and $\{B\}_m$ is defined as a vector $\{C\}_m$ whose magnitude is $|A|\,|B| \sin\theta$, θ being the angle between $\{A\}_m$ and $\{B\}_m$. The vector $\{C\}_m$ is perpendicular to the plane containing the other two and its direction is the direction of advance of a right-handed screw, lying parallel to $\{C\}_m$, when subjected to a rotation which would bring $\{A\}_m$ into alignment with $\{B\}_m$ by the shortest path. The cross product is evaluated in terms of a matrix product as follows:

$$\{C\}_m = \{A\}_m \times \{B\}_m = [A]_m \{B\}_m \tag{2.57}$$

where

$$[A]_m = \begin{bmatrix} 0 & -Az & Ay \\ Az & 0 & -Ax \\ -Ay & Ax & 0 \end{bmatrix} \quad \text{and} \quad \{B\}_m = \begin{bmatrix} Bx \\ By \\ Bz \end{bmatrix} \tag{2.58}$$

$[A]_m$ is known as the skew-symmetric form of the vector $\{A\}_m$.

8. The angle θ between the vectors $\{A\}_m$ and $\{B\}_m$ may be determined from

$$\cos\theta = \frac{\{A\}_m^T \{B\}}{|A|\,|B|} \tag{2.59}$$

9. If vectors $\{A\}_m$ and $\{B\}_m$ are parallel then $\{A\}_m$ can be represented using a scalar f as follows:

$$\{A\}_m = f\{B\}_m \tag{2.60}$$

10. If vectors $\{A\}_m$ and $\{B\}_m$ are perpendicular then

$$\{A\}_m \bullet \{B\}_m = \{A\}_m^T \{B\}_m = 0 \tag{2.61}$$

11. The scalar triple product D of the vectors $\{A\}_m$, $\{B\}_m$ and $\{C\}_m$ is a scalar defined by

$$D = \{\{A\}_m \times \{B\}_m\} \bullet \{C\}_m \tag{2.62}$$

12. The vector triple product $\{D\}_m$ of the vectors $\{A\}_m$, $\{B\}_m$ and $\{C\}_m$ is a vector $\{D\}_m$ defined by

$$\{D\}_m = \{A\}_m \times \{\{B\}_m \times \{C\}_m\} \tag{2.63}$$

13. If the vector $\{A\}_m^T = [Ax\ \ Ay\ \ Az]$ is rotated through angle $+\alpha$ about the x-axis of frame m then the new vector $\{A'\}_m$ is given by

$$\{A'\}_m = \begin{bmatrix} 1 & 0 & 0 \\ 0 & \cos\alpha & -\sin\alpha \\ 0 & \sin\alpha & \cos\alpha \end{bmatrix} \begin{bmatrix} Ax \\ Ay \\ Az \end{bmatrix} \tag{2.64}$$

For rotation about $O_m Y_m$ and $O_m Z_m$, the square matrix above is replaced by those given in equations (2.22) and (2.23).

14. If the X-axes of frames m and p coincide and the Y-axis of frame p is rotated by $+\alpha$, relative to the corresponding axis of frame m, then the vector $\{A\}_{n/m}$ is transformed from frame m to frame p according to the relationship

$$\{A\}_{n/p} = [T_m]_p \{A\}_{n/m} \tag{2.65}$$

where

$$\{T\}_{m/p} = \begin{bmatrix} 1 & 0 & 0 \\ 0 & \cos\alpha & \sin\alpha \\ 0 & -\sin\alpha & \cos\alpha \end{bmatrix} \tag{2.66}$$

The other two transformations are given by equations (2.30) and (2.32).

15. The transformations of 14 above may be combined as indicated:

$$[T_m]_q = [T_p]_q [T_n]_p [T_m]_n \tag{2.67}$$

This chain of matrices is to be read from right to left.

16. Differentiation of the vector $\{A\}_m^T = [Ax\ Ay\ Az]$ with respect to the scalar variable t is defined by

$$\frac{\mathrm{d}}{\mathrm{d}t}\{A\}_m = \begin{bmatrix} \mathrm{d}Ax/\mathrm{d}t \\ \mathrm{d}Ay/\mathrm{d}t \\ \mathrm{d}Az/\mathrm{d}t \end{bmatrix} \tag{2.68}$$

The result of this operation is a vector.

17. In general,

$$\frac{\mathrm{d}}{\mathrm{d}t}\{A\}_{m/n} \neq \{\dot{A}\}_{m/n} \tag{2.69}$$

where the dot denotes differentiation with respect to time.

18. Integration of the vector $\{A\}_m^T = [Ax\ Ay\ Az]$ with respect to the scalar variable t produces another vector defined by

$$\int \{A\}_m \, \mathrm{d}t = \begin{bmatrix} \int Ax \, \mathrm{d}t \\ \int Ay \, \mathrm{d}t \\ \int Az \, \mathrm{d}t \end{bmatrix} \tag{2.70}$$

19. Differentiation of the dot product $\{A\}_m \bullet \{B\}_m$ with respect to time t is defined by

$$\frac{\mathrm{d}}{\mathrm{d}t}(\{A\}_m \bullet \{B\}_m) = \{A\}_m \bullet \{\dot{B}\}_m + \{\dot{A}\}_m \bullet \{B\}_m \tag{2.71}$$

where $\{\dot{A}\}_m = \dfrac{\mathrm{d}}{\mathrm{d}t}\{A\}_m$ and $\{\dot{B}\}_m = \dfrac{\mathrm{d}}{\mathrm{d}t}\{B\}_m$

20. Differentiation of the cross product $\{A\}_m \times \{B\}_m$ with respect to time t follows the same rule as that for the dot product. Hence,

$$\frac{\mathrm{d}}{\mathrm{d}t}(\{A\}_m \times \{B\}_m) = \{A\}_m \times \{\dot{B}\}_m + \{\dot{A}\}_m \times \{B\}_m \tag{2.72}$$

2.3 Geometry analysis

2.3.1 Three point method

In order to establish the position of any point in space, vector theory can be used to work from three points for which the co-ordinates are already established. Consider the following example, shown in Figure 2.13.

In this example the positions of A, B and C are taken to be known as the lengths *AD*, *BD* and *CD*. The position of D is unknown and must be solved. In terms of vectors this can be expressed using the following known inputs:

$\{R_A\}_1^T = [Ax \;\; Ay \;\; Az]$

$\{R_B\}_1^T = [Bx \;\; By \;\; Bz]$

$\{R_C\}_1^T = [Cx \;\; Cy \;\; Cz]$

$|R_{DA}|$

$|R_{DB}|$

$|R_{DC}|$

In order to solve the three unknowns *Dx*, *Dy* and *Dz*, which are the components of the position vector $\{R_D\}_1$, it is necessary to set up three equations as follows:

$$|R_{DA}|^2 = (Dx - Ax)^2 + (Dy - Ay)^2 + (Dz - Az)^2 \tag{2.73}$$

$$|R_{DB}|^2 = (Dx - Bx)^2 + (Dy - By)^2 + (Dz - Bz)^2 \tag{2.74}$$

$$|R_{DC}|^2 = (Dx - Cx)^2 + (Dy - Cy)^2 + (Dz - Cz)^2 \tag{2.75}$$

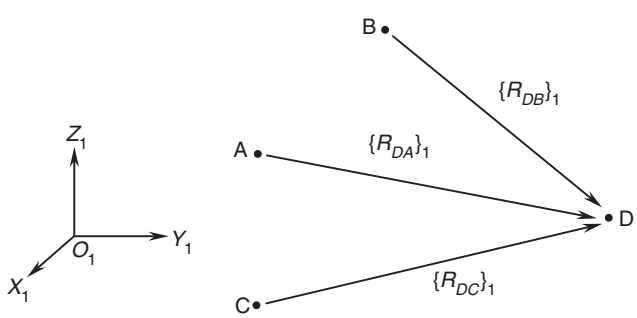

Fig. 2.13 Use of position vectors for geometry analysis

Multiplying out these three equations leads to:

$$|R_{DA}|^2 = (Dx^2 - 2DxAx + Ax^2) + (Dy^2 - 2DyAy + Ay^2) + (Dz^2 - 2DzAz + Az^2) \tag{2.76}$$

$$|R_{DB}|^2 = (Dx^2 - 2DxBx + Bx^2) + (Dy^2 - 2DyBy + By^2) + (Dz^2 - 2DzBz + Bz^2) \tag{2.77}$$

$$|R_{DC}|^2 = (Dx^2 - 2DxCx + Cx^2) + (Dy^2 - 2DyCy + Cy^2) + (Dz^2 - 2DzCz + Cz^2) \tag{2.78}$$

At this stage we need to introduce some numerical data to demonstrate how a solution can be obtained. This will also demonstrate how cumbersome the algebra will become and the need to utilize computer software to solve these problems. As an example we can take the following co-ordinates for points A, B and C:

$\{R_A\}_1 = [103 \;\; 350 \;\; 142]\,\text{mm}$

$\{R_B\}_1 = [-127 \;\; 350 \;\; 128]\,\text{mm}$

$\{R_C\}_1 = [-15 \;\; 500 \;\; 540]\,\text{mm}$

The lengths of the three rigid links can be taken as:

$|R_{DA}| = 172.064\,\text{mm}$

$|R_{DB}| = 183.527\,\text{mm}$

$|R_{DC}| = 401.103\,\text{mm}$

Substituting these numerical values into the equations above we get

$$172.064^2 = (Dx - 103)^2 + (Dy - 350)^2 + (Dz - 142)^2$$

$$183.527^2 = (Dx + 127)^2 + (Dy - 350)^2 + (Dz - 128)^2$$

$$401.103^2 = (Dx + 15)^2 + (Dy - 500)^2 + (Dz - 540)^2$$

Multiplying out gives

$$29\,606.02 = (Dx^2 - 206Dx + 10\,609) + (Dy^2 - 700Dy + 122\,500) + (Dz^2 - 284Dz + 20\,164)$$

$$33\,682.16 = (Dx^2 + 254Dx + 16\,129) + (Dy^2 - 700Dy + 122\,500) + (Dz^2 - 256Dz + 16\,384)$$

$$160\,883.617 = (Dx^2 + 30Dx + 225) + (Dy^2 - 1000Dy + 250\,000) + (Dz^2 - 1080Dz + 291600)$$

Combining the terms in these three equations leads to

$$-123\,667 = (Dx^2 - 206Dx) + (Dy^2 - 700Dy) + (Dz^2 - 284Dz) \tag{2.79}$$

$$-121\,331 = (Dx^2 - 254Dx) + (Dy^2 - 700Dy) + (Dz^2 - 256Dz) \tag{2.80}$$

$$-380\,942 = (Dx^2 + 30Dx) + (Dy^2 - 1000Dy) + (Dz^2 - 1080Dz) \tag{2.81}$$

Subtracting equation (2.79) from (2.80) gives

$$2336 = 460Dx + 28Dz$$

$$Dz = 83.43 - 16.43Dx \tag{2.82}$$

Subtracting equation (2.81) from (2.80) gives

$$259\,611 = 224Dx + 300Dy + 824Dz \tag{2.83}$$

Substituting the expression for Dz given in equation (2.82) into equation (2.83) gives

$$259\,611 = 224Dx + 300Dy + 68\,746.32 - 13\,538.32Dx$$

$$190\,864.68 = -13\,314.32Dx + 300Dy$$

This gives

$$Dy = 636.22 + 44.38Dx$$

Substituting the Dy and Dz back into equation (2.79) gives

$$\begin{aligned} -123\,667 &= (Dx^2 - 206Dx) + (636.22^2 + 1969.58Dx^2 \\ &\quad - 445\,354 - 31\,066Dx) + (83.43^2 + 269.9Dx^2 \\ &\quad - 23\,694.12 + 4666.12Dx) - 66\,355.33 \\ &= 2240.52Dx^2 + 27\,123.5Dx \end{aligned} \tag{2.84}$$

Rearranging equation (2.84) gives

$$2240.48Dx^2 + 27\,123.5Dx + 66\,355.33 = 0 \tag{2.85}$$

This is now in the familiar form of a quadratic equation $ax^2 + bx + c = 0$ for which the solution is given by

$$x = \frac{-b \pm \sqrt{b^2 - 4ac}}{2a}$$

Therefore the solution to (2.85) is obtained from

$$Dx = \frac{26\,605.88 \pm \sqrt{27\,123.5^2 - 4 \times 2240.48 \times 66\,355.33}}{2 \times 2240.48}$$

This gives two solutions:

$Dx = -3.403\,\text{mm}$ or $-8.703\,\text{mm}$

The fact that there are two possible solutions for Dx illustrates the nonlinearity of this geometric analysis. In this case inspection of the two solutions does not immediately identify which one should be eliminated. Trying each value in the equation for Dy gives

$$Dy = 636.22 + 44.38 \times (-3.403) = 485.19\,\text{mm}$$

or

$$Dy = 636.22 + 44.38 \times (-8.703) = 249.98\,\text{mm}$$

Similarly trying each value of Dx in the equation for Dz gives

$Dz = 83.43 - 16.43 \times (-3.403) = 139.34\,\text{mm}$

or

$Dz = 83.43 - 16.43 \times (-8.703) = 226.42\,\text{mm}$

Using a computer program written in BASIC to check these answers gives the following two solutions:

$Dx = -3.403\,\text{mm}$ or $-8.703\,\text{mm}$

$Dy = 485.194\,\text{mm}$ or $249.986\,\text{mm}$

$Dz = 139.338\,\text{mm}$ or $226.413\,\text{mm}$

In this case the first solution can be identified as the correct one, by inspection only, on the evidence of the Dy co-ordinate.

2.3.2 Vehicle suspension geometry analysis

The following example, based on a McPherson strut type of suspension, illustrates the steps that could be followed to determine the geometry for the suspension system shown in Figure 2.14.

The purpose of the analysis is to devise a sequence of calculations that would allow the calculation of the positions of the movable points in the suspension, $\{R_C\}_1$, $\{R_E\}_1$, $\{R_G\}_1$, $\{R_I\}_1$, $\{R_J\}_1$ and $\{R_H\}_1$, once the suspension is displaced from the co-ordinates given in Figure 2.14. In this example, the two points I and J are used to define the axis of rotation of the wheel.

The following sequence, shown in Figure 2.15, can be used to locate the movable points.

In order to impart motion to the suspension, resulting from for example hitting a bump, we can shorten the strut DG by a given amount. This will result in links DE and DC also shortening. Points C, E and G will move to

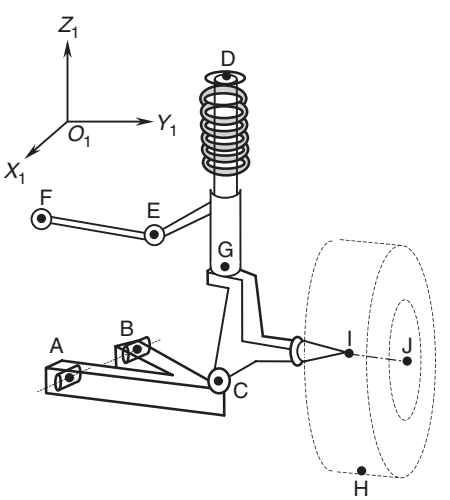

POINT	X (mm)	Y (mm)	Z (mm)
A	125	350	−80
B	−115	350	−80
C	5	625	−90
D	−15	530	545
E	155	537	250
F	25	45	270
G	−3	545	125
H	0	670	−270
I	0	65	0
J	0	730	0

Fig. 2.14 Suspension geometry data

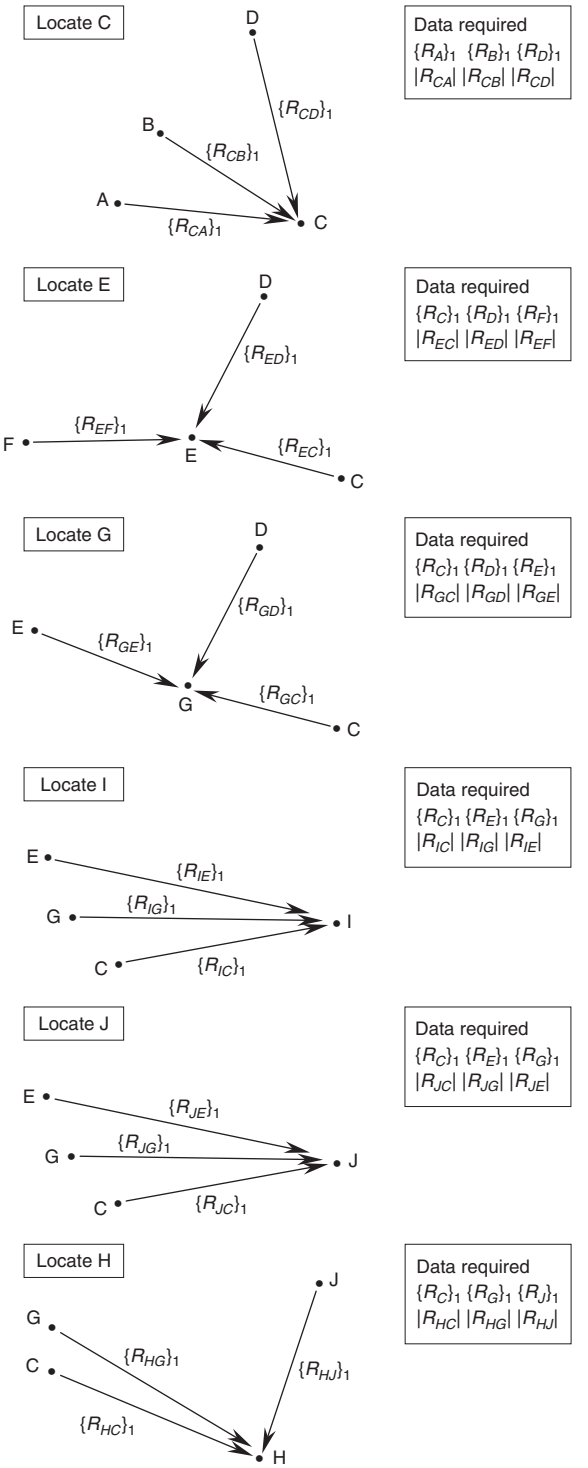

Fig. 2.15 Calculation sequence to solve suspension geometry

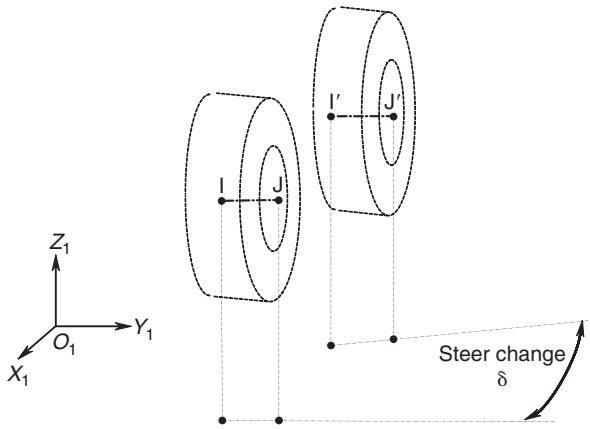

Fig. 2.16 Using vectors to determine bump steer

new positions that can be designated C′, E′ and G′. It should be noted that for the analysis using vectors here C′ and E′ are not the actual final positions but are only used to find the magnitudes of $|R_{DC'}|$ and $|R_{DE'}|$ so that the analysis may progress using the sequence shown in Figure 2.15. Having calculated the new positions of all the movable nodes the movement of the tyre contact patch, in this case taken to be point H, could be used to establish, for example, the lateral movement or half track change. The change in orientation of the wheel will also be of interest. The new positions I′ and J′ can be compared with the undisplaced positions I and J to determine the change in steer angle as shown in Figure 2.16.

The bump steer can be determined by finding the angle δ between the projection of IJ and I′J′ onto the global X_1Y_1 plane. The projection is achieved by setting the z co-ordinates of all four vectors to zero and then rearranging the vector dot product as shown in equation (2.86):

$$\cos\delta = \{R_{IJ}\}_1 \bullet \frac{\{R_{I'J'}\}}{|R_{IJ}||R_{I'J'}|} \tag{2.86}$$

2.4 Velocity analysis

Consider the rigid body, Body 2, shown in Figure 2.17. In this case we are initially only interested in motion in the X_1Y_1 plane. The body moves and rotates through an angle δγ, measured in radians, about the Z_1-axis.

The vector $\{R_{PQ}\}_1$ moves with the body to a new position $\{R_{P'Q'}\}_1$. The new vector $\{R_{P'Q'}\}_1$ is defined by the transformation

$$\{R_{P'Q'}\}_1 = [A]\{R_{PQ}\}_1 \tag{2.87}$$

where $[A]$ is the rotation matrix that rotates $\{R_{PQ}\}_1$ onto $\{R_{P'Q'}\}_1$. Expanding this gives

$$\begin{bmatrix} P'Q'x \\ P'Q'y \\ P'Q'z \end{bmatrix} = \begin{bmatrix} \cos\delta\gamma & -\sin\delta\gamma & 0 \\ \sin\delta\gamma & \cos\delta\gamma & 0 \\ 0 & 0 & 1 \end{bmatrix} \begin{bmatrix} PQx \\ PQy \\ PQz \end{bmatrix} \tag{2.88}$$

Assuming that $\delta\gamma$ is small so that we can take $\cos\delta\gamma = 1$ and $\sin\delta\gamma = \delta\gamma$ (rads) leads to

$$\begin{bmatrix} P'Q'x \\ P'Q'y \\ P'Q'z \end{bmatrix} = \begin{bmatrix} 1 & -\delta\gamma & 0 \\ \delta\gamma & 1 & 0 \\ 0 & 0 & 1 \end{bmatrix} \begin{bmatrix} PQx \\ PQy \\ PQz \end{bmatrix} \tag{2.89}$$

The change in relative position $\delta\{R_{PQ}\}_1$ is given by

$$\delta\{R_{PQ}\}_1 = \{R_{P'Q'}\}_1 - \{R_{PQ}\}_1 \tag{2.90}$$

or

$$\begin{bmatrix} \delta PQx \\ \delta PQy \\ \delta PQz \end{bmatrix} = \begin{bmatrix} 1 & -\delta\gamma & 0 \\ \delta\gamma & 1 & 0 \\ 0 & 0 & 1 \end{bmatrix} \begin{bmatrix} PQx \\ PQy \\ PQz \end{bmatrix} - \begin{bmatrix} 1 & 0 & 0 \\ 0 & 1 & 0 \\ 0 & 0 & 1 \end{bmatrix} \begin{bmatrix} PQx \\ PQy \\ PQz \end{bmatrix} \tag{2.91}$$

This gives

$$\begin{bmatrix} \delta PQx \\ \delta PQy \\ \delta PQz \end{bmatrix} = \begin{bmatrix} 0 & -\delta\gamma & 0 \\ \delta\gamma & 0 & 0 \\ 0 & 0 & 0 \end{bmatrix} \begin{bmatrix} PQx \\ PQy \\ PQz \end{bmatrix} \tag{2.92}$$

If this change takes place in time δt then

$$\frac{\delta}{\delta t} \begin{bmatrix} PQx \\ PQy \\ PQz \end{bmatrix} = \begin{bmatrix} 0 & -\delta\gamma/\delta t & 0 \\ \delta\gamma/\delta t & 0 & 0 \\ 0 & 0 & 0 \end{bmatrix} \begin{bmatrix} PQx \\ PQy \\ PQz \end{bmatrix} \tag{2.93}$$

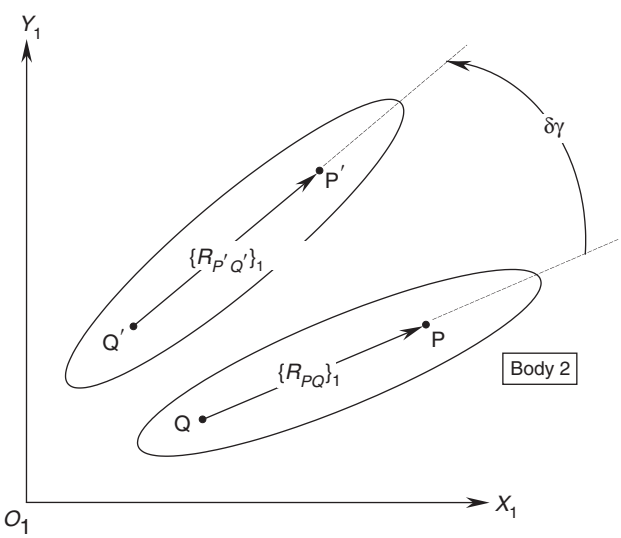

Fig. 2.17 Motion of a vector attached to a rigid body

In the limit δt approaches zero and we can write

$$\frac{\mathrm{d}}{\mathrm{d}t}\begin{bmatrix} PQx \\ PQy \\ PQz \end{bmatrix} = \begin{bmatrix} 0 & -\mathrm{d}\gamma/\mathrm{d}t & 0 \\ \mathrm{d}\gamma/\mathrm{d}t & 0 & 0 \\ 0 & 0 & 0 \end{bmatrix}\begin{bmatrix} PQx \\ PQy \\ PQz \end{bmatrix} \tag{2.94}$$

which can be written

$$\begin{bmatrix} V_{PQx} \\ V_{PQy} \\ V_{PQx} \end{bmatrix} = \begin{bmatrix} 0 & -\omega_z & 0 \\ \omega_z & 0 & 0 \\ 0 & 0 & 0 \end{bmatrix}\begin{bmatrix} PQx \\ PQy \\ PQz \end{bmatrix} \tag{2.95}$$

Note that generally rotations cannot be represented as vector quantities unless they are very small, as in finite element programs. Hence angular velocities obtained by differencing rotations over very small time intervals are in fact vector quantities.

If the rigid link also undergoes small rotations $\delta\alpha$ about the X-axis and $\delta\beta$ about the Y-axis then the full expression is

$$\begin{bmatrix} V_{PQx} \\ V_{PQy} \\ V_{PQz} \end{bmatrix} = \begin{bmatrix} 0 & -\omega_z & \omega_y \\ \omega_z & 0 & -\omega_x \\ -\omega_y & \omega_x & 0 \end{bmatrix}\begin{bmatrix} PQx \\ PQy \\ PQz \end{bmatrix} \tag{2.96}$$

Note that this matrix is the skew-symmetric form of the angular velocity vector $[\omega x \;\; \omega y \;\; \omega z]^T$. In general terms we write

$$\{V_{PQ}\}_1 = \{\omega_2\}_1 \times \{R_{PQ}\}_1 \tag{2.97}$$

The direction of the relative velocity vector $\{V_{PQ}\}_1$ is perpendicular to the line of the relative position vector $\{R_{PQ}\}_1$ as shown in Figure 2.18. The two

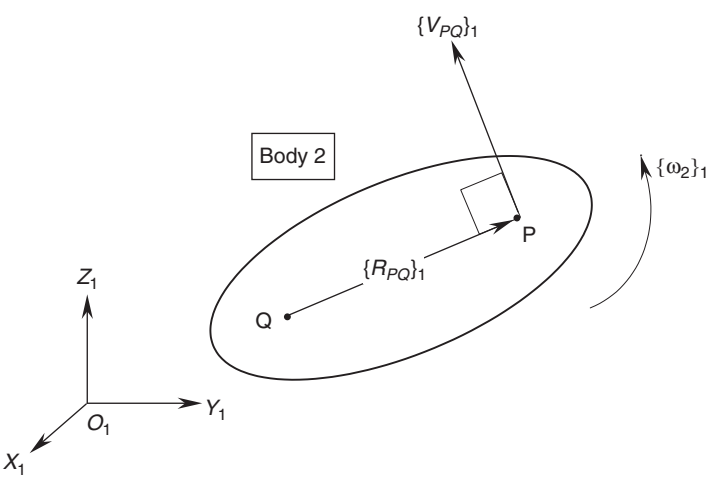

Fig. 2.18 Relative velocity vector

points P and Q are fixed in the same rigid body, Body 2. As such there can be no component of motion along the line PQ and any relative motion must therefore be perpendicular to this line.

This relationship can be expressed mathematically in two ways. The first of these uses the vector dot product to enforce perpendicularity as shown in equation (2.98):

$$\{V_{PQ}\}_1 \bullet \{R_{PQ}\}_1 = 0 \tag{2.98}$$

The second method uses the vector cross product as shown in equation (2.99):

$$\{V_{PQ}\}_1 = \{\omega_2\}_1 \times \{R_{PQ}\}_1 \tag{2.99}$$

More often than not we use the cross product as this will yield the angular velocity vector $\{\omega_2\}_1$. This may be required for a later acceleration analysis. In developing the equations to solve the velocities in a system of interconnected rigid bodies the triangle law of vector addition can also be used as shown in equation (2.100):

$$\{V_P\}_1 = \{V_Q\}_1 + \{V_{PQ}\}_1 \tag{2.100}$$

2.5 Acceleration analysis

Given that acceleration is the time rate of change of velocity we can develop the equations required for an acceleration analysis using the vectors shown in Figure 2.19.

It is possible to develop equations that would yield the relative acceleration vector $\{A_{PQ}\}_1$ using the angular velocity vector $\{\omega_2\}_1$ and the angular acceleration vector $\{\alpha_2\}_1$ as follows:

$$\{A_{PQ}\}_1 = \frac{\mathrm{d}}{\mathrm{d}t}\{V_{PQ}\}_1 \tag{2.101}$$

$$\{A_{PQ}\}_1 = \frac{\mathrm{d}}{\mathrm{d}t}\{\{\omega_2\}_1 \times \{R_{PQ}\}_1\} \tag{2.102}$$

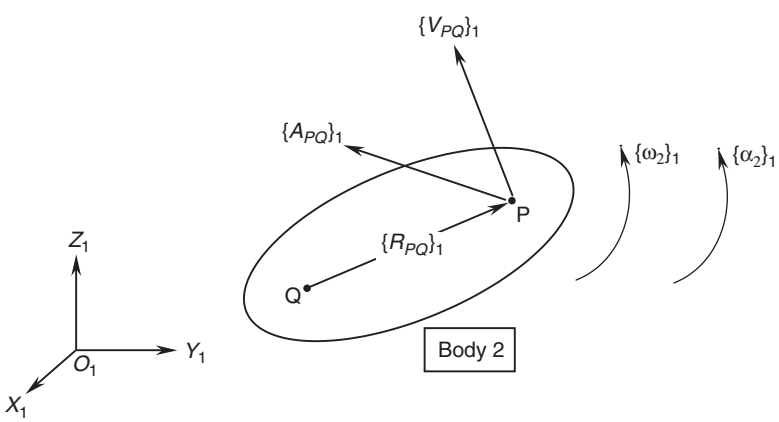

Fig. 2.19 Relative acceleration vector

$$\{A_{PQ}\}_1 = \{\omega_2\}_1 \times \frac{\mathrm{d}}{\mathrm{d}t}\{R_{PQ}\}_1 + \frac{\mathrm{d}}{\mathrm{d}t}\{\omega_2\}_1 \times \{R_{PQ}\}_1 \tag{2.103}$$

Since it is known that

$$\frac{\mathrm{d}}{\mathrm{d}t}\{R_{PQ}\}_1 = \{V_{PQ}\}_1 \tag{2.104}$$

$$\frac{\mathrm{d}}{\mathrm{d}t}\{\omega_2\}_1 = \{\alpha_2\}_1 \tag{2.105}$$

We can therefore write

$$\{A_{PQ}\}_1 = \{\omega_2\}_1 \times \{V_{PQ}\}_1 + \{\alpha_2\}_1 \times \{R_{PQ}\}_1 \tag{2.106}$$

Since it is also known that

$$\{V_{PQ}\}_1 = \{\omega_2\}_1 \times \{R_{PQ}\}_1 \tag{2.107}$$

This leads to the expression

$$\{A_{PQ}\}_1 = \{\omega_2\}_1 \times \{\{\omega_2\}_1 \times \{R_{PQ}\}_1\} + \{\alpha_2\}_1 \times \{R_{PQ}\}_1 \tag{2.108}$$

The acceleration vector $\{A_{PQ}\}_1$ can be considered to have a centripetal component $\{A^p_{PQ}\}_1$ and a transverse component $\{A^t_{PQ}\}_1$. This is illustrated in Figure 2.20 where one of the arms from a double wishbone suspension system is shown.

In this case the centripetal component of acceleration is given by

$$\{A^p_{PQ}\}_1 = \{\omega_2\}_1 \times \{\{\omega_2\}_1 \times \{R_{PQ}\}_1\} \tag{2.109}$$

Note that as the suspension arm is constrained to rotate about the axis NQ, ignoring at this stage any possible deflection due to compliance in the suspension bushes, the vectors $\{\omega_2\}_1$ for the angular velocity of Body 2 and $\{\alpha_2\}_1$ for the angular acceleration would act along the axis of rotation through NQ. The components of these vectors would adopt signs consistent with producing a positive rotation about this axis as shown in Figure 2.20.

When setting up the equations to solve a velocity or acceleration analysis it may be desirable to reduce the number of unknowns based on the knowledge that a particular body is constrained to rotate about a known axis as

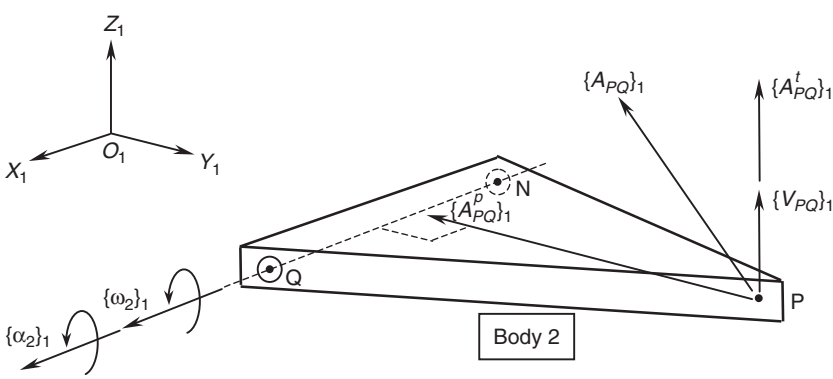

Fig. 2.20 Centripetal and transverse components of acceleration vectors

shown here. The velocity vector $\{\omega_2\}_1$ could, for example, be represented as follows:

$$\{\omega_2\}_1 = f\omega_2\{R_{QN}\}_1 \tag{2.110}$$

In this case, since $\{\omega_2\}_1$ is parallel to the relative position vector $\{R_{QN}\}_1$ a scale factor $f\omega_2$ can be introduced. This would reduce the problem from the three unknown components, ωx_2, ωy_2 and ωz_2 of the vector $\{\omega_2\}_1$ to a single unknown $f\omega_2$. A similar approach could be used for an acceleration analysis with, for example,

$$\{\alpha_2\}_1 = f\alpha_2\{R_{QN}\}_1 \tag{2.111}$$

It can also be seen from Figure 2.20 that the centripetal acceleration acts towards, and is perpendicular to the axis of rotation of the body. This relationship can be proved having found the centripetal acceleration by use of the dot product with

$$\{A^p_{PQ}\}_1 \bullet \{R_{QN}\}_1 = 0 \tag{2.112}$$

The transverse component of acceleration is given by

$$\{A^t_{PQ}\}_1 = \{\alpha_2\}_1 \times \{R_{PQ}\}_1 \tag{2.113}$$

Note that the transverse component of acceleration is also perpendicular to, in this case, the vector $\{R_{PQ}\}_1$ as defined by the dot product with

$$\{A^t_{PQ}\}_1 \bullet \{R_{PQ}\}_1 = 0 \tag{2.114}$$

Note that although the vector $\{A^t_{PQ}\}_1$ is shown to be acting in the same direction as the vector $\{V_{PQ}\}_1$ in Figure 2.20, this may not necessarily be the case. A reversal of $\{A^t_{PQ}\}_1$ would correspond to a reversal of $\{\alpha_2\}_1$. This would indicate that point P is moving in a certain direction but in fact decelerating.

The resultant acceleration vector $\{A_{PQ}\}_1$ is found to give the expression shown in equation (2.115) using the triangle law to add the centripetal and transverse components as follows:

$$\{A_{PQ}\}_1 = \{A^p_{PQ}\}_1 + \{A^t_{PQ}\}_1 \tag{2.115}$$

For the example shown here in Figure 2.20 the analysis may often focus on suspension movement only and assume the vehicle body to be fixed and not moving. This would mean that the velocity or acceleration at point Q, $\{A_Q\}_1$ would be zero. Since we can say, based on the triangle law, that

$$\{A_{PQ}\}_1 = \{A_P\}_1 - \{A_Q\}_1 \tag{2.116}$$

it therefore follows in this case that since Q is fixed:

$$\{A_P\}_1 = \{A_{PQ}\}_1 \tag{2.117}$$

Note that the same principle could be used when solving the velocities for this problem and that we could write

$$\{V_P\}_1 = \{V_{PQ}\}_1 \tag{2.118}$$

Finally it should be noted for the particular example, shown here in Figure 2.20, that we could work from either point Q or point N when solving for the velocities or accelerations and obtain the same answers for the velocity or acceleration at point P.

Combining the relative acceleration already obtained for points on a rigid body translating and rotating in space with sliding motion will introduce

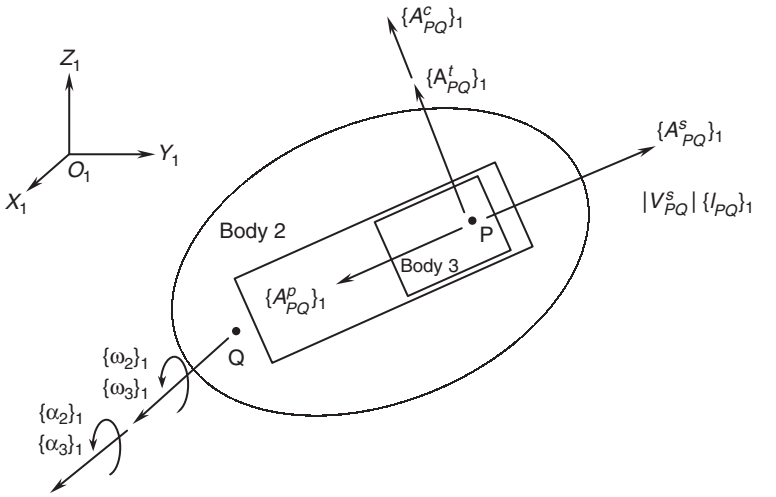

Fig. 2.21 Relative acceleration with sliding motion

two more components of relative acceleration. This is best explained by considering the situation shown in Figure 2.21 where point P is located on Body 3 and point Q is located on Body 2. In this case Body 3 is constrained to move and rotate with Body 2 but has an additional relative sliding degree of freedom that allows it to move, relative to Body 2, along a slot with an axis aligned with the two points P and Q. To simplify the understanding the two bodies are assumed to rotate, as shown, about an axis passing through point Q. Hence the relative acceleration vectors can be assumed to be acting in the directions shown, as point P moves away from point Q. The angular velocity and acceleration vectors for Body 2 and Body 3 will be the same and either may be used in the subsequent formulations.

The first of the two new components is easy to comprehend and is associated with the additional sliding motion. Since the direction of motion is known to be constrained to act along the line PQ it is possible to define the sliding acceleration, $\{A^s_{PQ}\}_1$, using the magnitude of the sliding acceleration $|A^s_{PQ}|$ factored with the unit vector $\{l_{PQ}\}_1$, acting along the line from Q to P, as follows:

$$\{A^s_{PQ}\}_1 = |A^s_{PQ}|\{l_{PQ}\}_1 \tag{2.119}$$

The second of the two new components, $\{A^c_{PQ}\}_1$, is known as the Coriolis acceleration and requires more detailed explanation. As a starting point we can assume that both bodies are rotating as shown in Figure 2.21.

In deriving the Coriolis term consider first the formulation for the velocity vector $\{V_{PQ}\}_1$. In addition to the component of velocity associated with rigid body motion that would act in a perpendicular direction to the line PQ there is an additional component of sliding velocity. This sliding component can be defined using the magnitude of the sliding velocity $|V^s_{PQ}|$ factored with the unit vector $\{l_{PQ}\}_1$, acting along the line from Q to P. The formulation of $\{V_{PQ}\}_1$ now becomes

$$\{V_{PQ}\}_1 = \{\omega_2\}_1 \times \{R_{PQ}\}_1 + |V^s_{PQ}|\{l_{PQ}\}_1 \tag{2.120}$$

Differentiating this with respect to time yields:

$$\{A_{PQ}\}_1 = \frac{\mathrm{d}}{\mathrm{d}t}\{V_{PQ}\}_1 = \frac{\mathrm{d}}{\mathrm{d}t}\{\{\omega_2\}_1 \times \{R_{PQ}\}_1 + |V^s_{PQ}|\{l_{PQ}\}_1\} \tag{2.121}$$

$$\begin{aligned}\{A_{PQ}\}_1 = {} & \{\omega_2\}_1 \times \{V_{PQ}\}_1 + \{\alpha_2\}_1 \times \{R_{PQ}\}_1 \\ & + |V^s_{PQ}| \frac{\mathrm{d}}{\mathrm{d}t}\{l_{PQ}\}_1 + |A^s_{PQ}|\{l_{PQ}\}_1\end{aligned} \tag{2.122}$$

Since

$$\frac{\mathrm{d}}{\mathrm{d}t}\{R_{PQ}\}_1 = \{V_{PQ}\}_1 = \{\omega_2\}_1 \times \{R_{PQ}\}_1 \tag{2.123}$$

it therefore follows that

$$\frac{\mathrm{d}}{\mathrm{d}t}\{l_{PQ}\}_1 = \{\omega_2\}_1 \times \{l_{PQ}\}_1 \tag{2.124}$$

and

$$|V^s_{PQ}|\{l_{PQ}\}_1 = \{V^s_{PQ}\}_1 \tag{2.125}$$

and

$$|A^s_{PQ}|\{l_{PQ}\}_1 = \{A^s_{PQ}\}_1 \tag{2.126}$$

Combining these we therefore obtain

$$\begin{aligned}\{A_{PQ}\}_1 = {} & \{\omega_2\}_1 \times \{V_{PQ}\}_1 + \{\alpha_2\}_1 \times \{R_{PQ}\}_1 + \{\omega_2\}_1 \\ & \times \{V^s_{PQ}\}_1 + \{A^s_{PQ}\}_1\end{aligned} \tag{2.127}$$

Substituting

$$\{V_{PQ}\}_1 = \{\omega_2\}_1 \times \{R_{PQ}\}_1 + \{V^s_{PQ}\}_1 \tag{2.128}$$

gives the following:

$$\begin{aligned}\{A_{PQ}\}_1 = {} & \{\omega_2\}_1 \times \{\{\omega_2\}_1 \times \{R_{PQ}\}_1 + \{V^s_{PQ}\}_1\} + \{\alpha_2\}_1 \\ & \times \{R_{PQ}\}_1 + \{\omega_2\}_1 \times \{V^s_{PQ}\}_1 + \{A^s_{PQ}\}_1\end{aligned} \tag{2.129}$$

It therefore follows that

$$\begin{aligned}\{A_{PQ}\}_1 = {} & \{\omega_2\}_1 \times \{\{\omega_2\}_1 \times \{R_{PQ}\}_1\} + \{\alpha_2\}_1 \times \{R_{PQ}\}_1 \\ & + 2\{\omega_2\}_1 \times \{V^s_{PQ}\}_1 + \{A^s_{PQ}\}_1\end{aligned} \tag{2.130}$$

In summary we can now identify all four components of acceleration associated with the combined rotation and sliding motion as the centripetal acceleration $\{A^p_{PQ}\}_1$, the transverse acceleration $\{A^t_{PQ}\}_1$, the Coriolis acceleration $\{A^c_{PQ}\}_1$ and the sliding acceleration $\{A^s_{PQ}\}_1$, where

$$\{A^p_{PQ}\}_1 = \{\omega_2\}_1 \times \{\{\omega_2\}_1 \times \{R_{PQ}\}_1\} \tag{2.131}$$

$$\{A^t_{PQ}\}_1 = \{\alpha_2\}_1 \times \{R_{PQ}\}_1 \tag{2.132}$$

$$\{A^c_{PQ}\}_1 = 2\{\omega_2\}_1 \times \{V^s_{PQ}\}_1 \tag{2.133}$$

$$\{A^s_{PQ}\}_1 = |A^s_{PQ}|\{l_{PQ}\}_1 \tag{2.134}$$

2.6 Static force and moment definition

Before progressing to the development of the equations of motion associated with large displacement rigid body dynamic motion it is necessary to examine the use of vectors for static analysis in multibody systems. In this case we define static analysis as the study of forces acting on a body or series of bodies where motion takes place in the absence of acceleration. That is a system that is either at rest or moving in a straight line with constant velocity.

In order to demonstrate the use of vectors for representation of forces consider the following example, shown in Figure 2.22, which involves a tripod structure comprising three links with ball or spherical joints at each end.

Before attempting any analysis to determine the distribution of forces it is necessary to prepare a free-body diagram and label the bodies and forces in an appropriate manner as shown in Figure 2.23.

The notation used here to describe the forces depends on whether the force is an applied external force (action-only force) or an internal force resulting from the interconnection of bodies (action–reaction force). In this example we have an applied force at point A. In order to fully define a force we must be able to specify the point of application, the line of sight and the sense of the force. In this case we can use the notation $\{F_A\}_1$ to define the force where the subscript A defines the point of application and the components of the vector F_{Ax}, F_{Ay} and F_{Az} would define both the line of sight and the sense of the force. Where the force is the result of an interaction we can use, for example, the following $\{F_{A52}\}_1$ which specifies that the force is acting at A on Body 5 due to its interaction with Body 2. Note that for this example we are assuming that A is a point that could be, for example, taken to be at the centre of a bush or spherical joint. It should also be noted that in assigning identification numbers to the bodies we are taking Body 1 to be a fixed and unmoving body that may also be referred to as a ground body. In this example the ground body is not in one place as such but can be considered to be located at the positions B, C and D where fixed anchorages are provided.

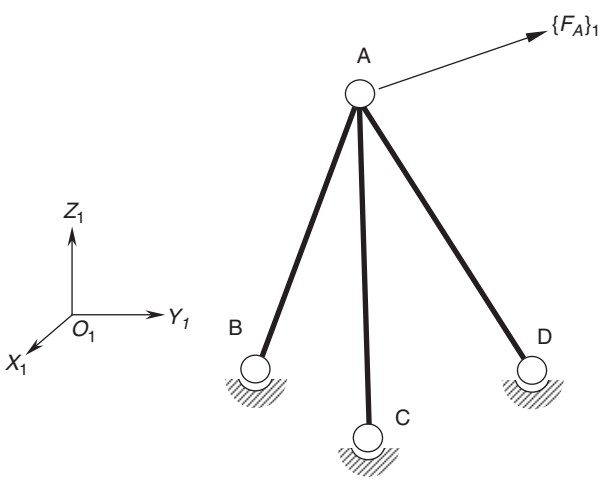

Fig. 2.22 Tripod structure

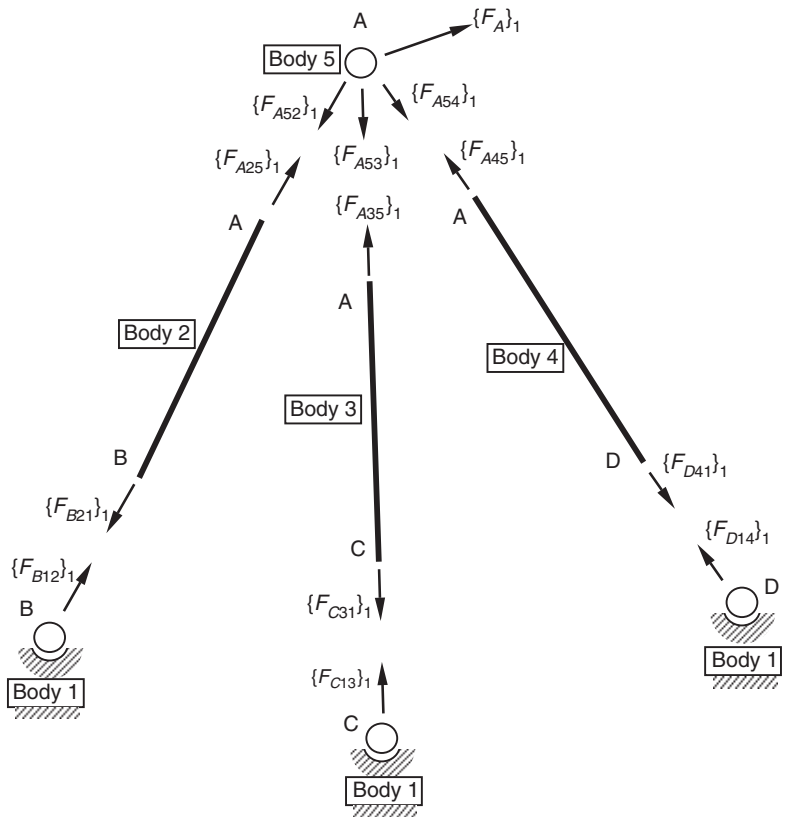

Fig. 2.23 Free-body diagram of tripod structure

For the action–reaction forces shown here Newton's third law would apply so that for the interaction of Body 5 and Body 2 we can say that $\{F_{A52}\}_1$ and $\{F_{A25}\}_1$ are equal and opposite or

$$\{F_{A52}\}_1 = -\{F_{A25}\}_1 \tag{2.135}$$

In this example we are looking at linkages that are pin-jointed, or have spherical joints at each end. An example of a similar linkage would be a tie rod in a suspension system. As both ends of the linkage are pin-jointed the force by definition must act along the linkage. In this case we could use this information to reduce the number of unknowns by using a scale factor as shown in equations (2.136) to (2.138):

$$\{F_{A25}\}_1 = f_2\{R_{AB}\}_1 \tag{2.136}$$

$$\{F_{A35}\}_1 = f_3\{R_{AC}\}_1 \tag{2.137}$$

$$\{F_{A45}\}_1 = f_4\{R_{AD}\}_1 \tag{2.138}$$

In this case the solution would be assisted as the three unknowns F_{A25x}, F_{A25y} and F_{A25z}, associated with equation (2.136) for example, would be reduced to a single unknown f_2. To maintain rigour the choice of position vector, for example $\{R_{AB}\}_1$ rather than $\{R_{BA}\}_1$, has also been used so that comparing

equation (2.136) with the forces as drawn in the free-body diagram shown in Figure 2.23 would be consistent with the scale factors having positive values. Should the solution yield negative scale factors this would simply involve a reversal of the sense of the force from that initially assumed in the free-body diagram.

In this case, since the forces act along the line of the linkages, we equate forces throughout the structure as follows:

$$\{F_{A52}\}_1 = -\{F_{A25}\}_1 = \{F_{B21}\}_1 = -\{F_{B12}\}_1 \tag{2.139}$$

$$\{F_{A53}\}_1 = -\{F_{A35}\}_1 = \{F_{C31}\}_1 = -\{F_{C13}\}_1 \tag{2.140}$$

$$\{F_{A54}\}_1 = -\{F_{A45}\}_1 = \{F_{D41}\}_1 = -\{F_{D14}\}_1 \tag{2.141}$$

Clearly by solving the unknown forces acting on the pin, Body 5, which connects to all three linkages the complete force distribution in this system will be known. Setting up the equation of equilibrium for Body 5 we get

$$\sum\{F_5\}_1 = \{0\}_1 \tag{2.142}$$

$$\{F_A\}_1 + \{F_{A52}\}_1 + \{F_{A53}\}_1 + \{F_{A54}\}_1 = \{0\}_1 \tag{2.143}$$

Using the information developed in equations (2.136) to (2.141) we can now write

$$\{F_A\}_1 + f_2\{R_{BA}\}_1 + f_3\{R_{CA}\}_1 + f_4\{R_{DA}\}_1 = \{0\}_1 \tag{2.144}$$

The direction of the position vectors as defined in equation (2.144) should be carefully noted. These have been selected to maintain the correct positive sign convention throughout the equation. Expanding equation (2.144) would lead to

$$\begin{bmatrix} F_{Ax} \\ F_{Ay} \\ F_{Az} \end{bmatrix} + f_2 \begin{bmatrix} BA_x \\ BA_y \\ BA_z \end{bmatrix} + f_3 \begin{bmatrix} CA_x \\ CA_y \\ CA_z \end{bmatrix} + f_4 \begin{bmatrix} DA_x \\ DA_y \\ DA_z \end{bmatrix} = \begin{bmatrix} 0 \\ 0 \\ 0 \end{bmatrix} \tag{2.145}$$

For a given applied force $\{F_A\}_1$, and taking the geometry of the points A, B, C and D to be known, equation (2.145) yields the three equations required to solve the three unknowns f_2, f_3 and f_4 and hence solve the force distribution in this example.

The notation that has been used to define forces in the example shown can be used where the forces represent reactions generated at a point in a multibody system. The notation needs to be altered for forces acting along the line of sight of a force element, such as a spring or damper, connecting two bodies as shown in Figure 2.24.

The vector representation of a moment is not as straightforward to interpret as the vector representation of a force. The moment $\{M_P\}_1$ shown acting about point P in Figure 2.25 is represented by a vector that is orientated along an axis about which the moment acts. The length of the vector represents the magnitude of the moment and the direction of the vector is that which is consistent with a positive rotation about the axis as shown. The components of the vector, M_{Px}, M_{Py} and M_{Pz}, are resolved parallel to a reference frame, in this case O_1. The double-headed arrows used in Figure 2.25 are intended to distinguish the moment vector from that of a force.

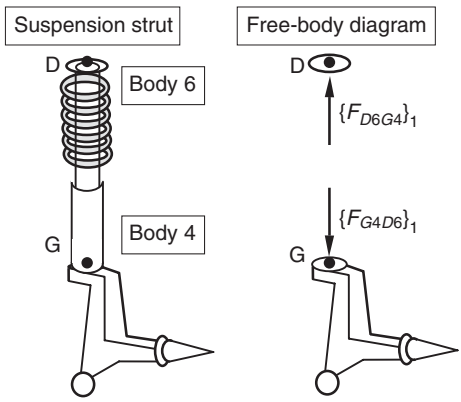

Fig. 2.24 Vector notation for line of sight forces

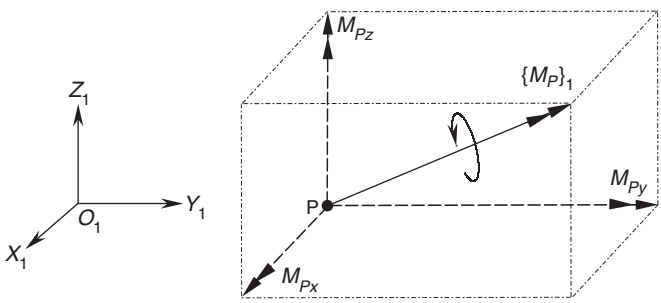

Fig. 2.25 Vector representation of a moment

Considering next the equilibrium of the body shown in Figure 2.26 it can be seen that a force acting at point P will produce a reaction moment at point Q. In order to simplify the diagram only the components of the applied force and the resulting moment are shown here. Since we are looking only at the derivation of the moment at Q the reaction force at Q is also omitted.

The moment generated at point Q, which is the point where Body 2 is fixed to the non-moving ground part Body 1, is designated as $\{M_{Q21}\}_1$. Applying the same principle as used for a force we would read this as the moment acting at point Q, on Body 2 due to its connection to Body 1, with components resolved parallel to the axes of reference frame O_1. For convenience and to assist with the interpretation of the derivation that follows the components of the force $\{F_P\}_1$, the moment $\{M_{Q21}\}_1$ and the relative position vector $\{R_{PQ}\}_1$ have all been set up in Figure 2.26 to have components that are positive.

Using the traditional approach the three equations of moment equilibrium, $\Sigma M_{Qx} = 0$, $\Sigma M_{Qy} = 0$ and $\Sigma M_{Qz} = 0$ could be transformed to produce the following three equations:

$$M_{Q21x} = -PQ_z \times F_{Py} + PQ_y \times F_{Pz} \tag{2.146}$$

$$M_{Q21y} = PQ_z \times F_{Px} - PQ_x \times F_{Pz} \tag{2.147}$$

$$M_{Q21z} = PQ_x \times F_{Py} - PQ_y \times F_{Px} \tag{2.148}$$

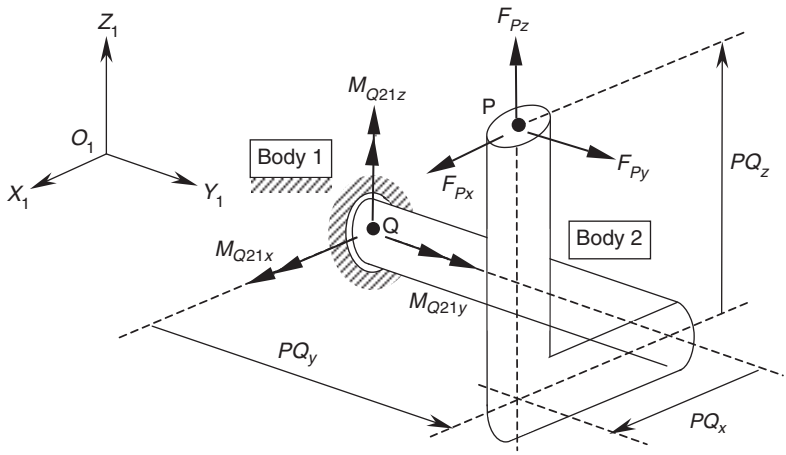

Fig. 2.26 Reaction moment between two bodies

Taking the above equations (2.146–2.148) and arranging in matrix form gives

$$\begin{bmatrix} M_{Qx} \\ M_{Qy} \\ M_{Qz} \end{bmatrix} = \begin{bmatrix} 0 & -PQ_z & PQ_y \\ PQ_z & 0 & -PQ_x \\ -PQ_y & PQ_x & 0 \end{bmatrix} \begin{bmatrix} F_{Px} \\ F_{Py} \\ F_{Pz} \end{bmatrix} \tag{2.149}$$

From (2.149) it can be seen that the moment $\{M_Q\}_1$ can be found from the cross product of the relative position vector $\{R_{PQ}\}_1$ and the force $\{F_P\}_1$:

$$\{M_Q\}_1 = \{R_{PQ}\}_1 \times \{F_P\}_1 \tag{2.150}$$

It should be noted that in using the vector cross product to compute the moment of a force about a point that the order of the operation is critical. The relative position vector is crossed with the force so that it is the relative position vector that is arranged in skew-symmetric form and not the force vector. The relative position vector must also be the vector from the point about which the moment is taken to the point of application of the force.

2.7 Dynamics of a particle

In the remaining sections of this chapter the authors have broadly followed the approach given by D'Souza and Garg (1984) to derive the equations of motion for a rigid body. The starting point is to consider the dynamics of a particle, a body for which the motion is restricted to translation without rotation. The resultant moment acting on the body is therefore zero. In the absence of rotation the velocity and acceleration will be the same at all points on the body and hence a particle may be treated as a point mass.

From Newton's second law it can be seen that the time rate of change of linear momentum $\{L\}_1$ for a particle is equal to the resultant force acting on it:

$$\sum \{F\}_1 = \frac{\mathrm{d}}{\mathrm{d}t}\{L\}_1 = \frac{\mathrm{d}}{\mathrm{d}t}(m\{V\}_1) \tag{2.151}$$

The resultant force is represented by the vector $\Sigma\{F\}_1$, m is the mass and $\{V\}_1$ is the velocity vector measured relative to an inertial reference frame O_1. The linear momentum of the body is $m\{V\}_1$. The components of the vectors in (2.151) are all resolved parallel to the axes of O_1. Taking the mass to be constant (2.151) may be written as

$$\sum\{F\}_1 = m\frac{\mathrm{d}}{\mathrm{d}t}\{V\}_1 = m\{A\}_1 \tag{2.152}$$

The accelerations in (2.152) are also measured relative to the inertial reference frame O_1. Since the velocities and accelerations used here are measured relative to a non-moving frame we refer to them as absolute. Expanding the vector equation given in (2.152) gives

$$\sum\begin{bmatrix}F_x\\F_y\\F_z\end{bmatrix} = m\begin{bmatrix}A_x\\A_y\\A_z\end{bmatrix} \tag{2.153}$$

2.8 Linear momentum of a rigid body

As a body translates and rotates in space it will have linear momentum $\{L\}_1$ associated with translation and angular momentum $\{H\}_1$ associated with rotation. For the rigid body, Body 2, shown in Figure 2.27 the mass centre is located at G_2 by the vector $\{R_{G2}\}_1$ relative to the reference frame O_2.

A small element of material with a volume δV is located at P relative to O_2 by the position vector $\{R_P\}_1$. Assuming Body 2 to be of uniform density ρ, we can say that the element of material has a mass δm given by

$$\delta m = \rho\delta V \tag{2.154}$$

and that as the element becomes infinitesimal the mass of the body m_2 is given by

$$m_2 = \rho\int_{\mathrm{vol}}\mathrm{d}V = \int_{\mathrm{vol}}\mathrm{d}m \tag{2.155}$$

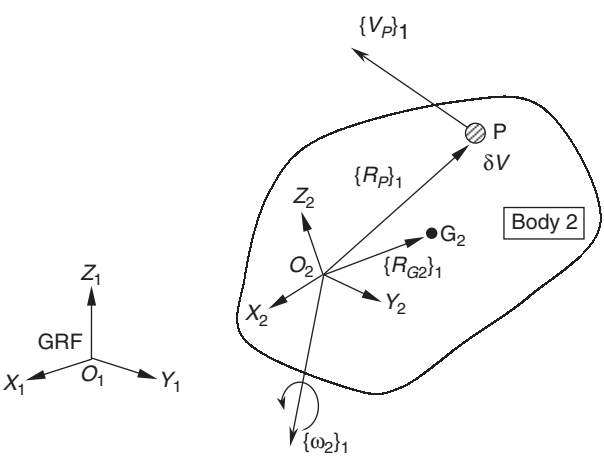

Fig. 2.27 Linear momentum of a rigid body

The position of the centre of mass $\{R_{G2}\}_1$ is then found by integrating the elemental first moments of mass about frame O_2 and dividing by the total mass m_2:

$$\{R_{G2}\}_1 = \frac{1}{m_2} \int_{\text{vol}} \{R_P\}_1 \, \mathrm{d}m \tag{2.156}$$

The linear momentum $\{L_2\}_1$ of the body is the linear momenta of the elements of mass that comprise the body. If the position of an element of mass is given by $\{R_P\}_1$ then the velocity $\{V_P\}_1$ of dm is given using the triangle law of vector addition by

$$\{V_P\}_1 = \{V_{O2}\}_1 + \{V_{PO2}\}_1$$

$$\{V_P\}_1 = \{V_{O2}\}_1 + \{\omega_2\}_1 \times \{R_P\}_1 \tag{2.157}$$

The linear momentum $\{L\}_1$ of the body is therefore found by integrating the mass particles factored by their velocity vectors $\{V_P\}_1$ over the volume of the body:

$$\{L_2\}_1 = \int_{\text{vol}} \{V_P\}_1 \, \mathrm{d}m \tag{2.158}$$

Using the expression for $\{V_P\}_1$ given in (2.157) this leads to

$$\{L_2\}_1 = \{V_{O2}\}_1 \int_{\text{vol}} \mathrm{d}m + \{\omega_2\}_1 \times \int_{\text{vol}} \{R_P\}_1 \, \mathrm{d}m \tag{2.159}$$

Using the expressions given in (2.155) and (2.156) we get an expression for the linear momentum of Body 2 in terms of the overall mass m_2 and the velocity at the mass centre $\{V_{G2}\}_1$:

$$\{L_2\}_1 = m_2\{\{V_{O2}\}_1 + \{\omega_2\}_1 \times \{R_{G2}\}_1\} = m_2\{V_{G2}\}_1 \tag{2.160}$$

It can be noted that problems are often set up in multibody dynamics so that the body frame coincides with the mass centre. In this case for Body 2, O_2 and G_2 would be coincident so that $\{RG_2\}_1$ would be zero and the linear momentum would be obtained directly from

$$\{L_2\}_1 = m_2\{V_{G2}\}_1 = m_2\{V_{O2}\}_1 \tag{2.161}$$

2.9 Angular momentum

The angular momentum $\{H_P\}_1$ of the particle of material with mass dm in Figure 2.27 can be found by taking the moment of the linear momentum of the particle about the frame O_2 as follows:

$$\{H_P\}_1 = \{R_P\}_1 \times \{\{V_{O2}\}_1 + \{\omega_2\}_1 \times \{R_P\}_1\} \, \mathrm{d}m \tag{2.162}$$

Integrating this over the volume of the body leads to the angular momentum $\{H_2\}_1$ of the rigid body about the frame O_2 as follows:

$$\begin{aligned} \{H_2\}_1 &= \int_{\text{vol}} \{R_P\}_1 \times \{\{V_{O2}\}_1 + \{\omega_2\}_1 \times \{R_P\}_1\} \, \mathrm{d}m \\ &= -\{V_{O2}\}_1 \times \int_{\text{vol}} \{R_P\}_1 \, \mathrm{d}m + \int_{\text{vol}} \{R_P\}_1 \\ &\quad \times \{\{\omega_2\}_1 \times \{R_P\}_1\} \, \mathrm{d}m \end{aligned} \tag{2.163}$$

Note that in the second line of (2.163) the vector $\{V_{O2}\}_1$ comes out of the integral and hence the order of the cross product is reversed necessitating

the reverse of sign for $\{V_{O2}\}_1$. If for Body 2 frame O_2 is positioned at either the mass centre so that $\int_{\text{vol}} \{R_P\}_1 \, \mathrm{d}m = \{0\}_1$, or at a point of attachment to the non-moving ground, where $\{V_{O2}\}_1 = \{0\}_1$, then (2.163) reduces to the more convenient form which we will assume from now on:

$$\{H_2\}_1 = \int_{\text{vol}} \{R_P\}_1 \times \{\{\omega_2\}_1 \times \{R_P\}_1\} \, \mathrm{d}m \tag{2.164}$$

If we now take the general case for any body (ignore body subscripts) and expand the vectors into their full form we get

$$\{H\}_1 = \begin{bmatrix} H_x \\ H_y \\ H_z \end{bmatrix}, \quad \{R\}_1 = \begin{bmatrix} x \\ y \\ z \end{bmatrix} \quad \text{and} \quad \{\omega\}_1 = \begin{bmatrix} \omega_x \\ \omega_y \\ \omega_z \end{bmatrix}$$

Applying the vector cross product, making use of the skew-symmetric form of a vector in the normal manner, leads to

$$\begin{aligned} \{R\}_1 \times \{\{\omega\}_1 \times \{R\}_1\} &= \begin{bmatrix} 0 & -z & y \\ z & 0 & -x \\ -y & x & 0 \end{bmatrix} \begin{bmatrix} 0 & -\omega_z & \omega_y \\ \omega_z & 0 & -\omega_x \\ -\omega_y & \omega_x & 0 \end{bmatrix} \begin{bmatrix} x \\ y \\ z \end{bmatrix} \\ &= \begin{bmatrix} 0 & -z & y \\ z & 0 & -x \\ -y & x & 0 \end{bmatrix} \begin{bmatrix} -\omega_z y + \omega_y z \\ -\omega_z x - \omega_x z \\ -\omega_y x + \omega_x y \end{bmatrix} \\ &= \begin{bmatrix} y(\omega_x y - \omega_y x) - z(\omega_z x - \omega_x z) \\ z(\omega_y z - \omega_z y) - x(\omega_x y - \omega_y x) \\ x(\omega_z x - \omega_x z) - y(\omega_y z - \omega_z y) \end{bmatrix} \end{aligned} \tag{2.165}$$

Substituting (2.165) into (2.164) gives the general expression for the angular momentum $\{H\}_1$ of a body where for simplicity the integral sign is now taken to indicate integration over the volume of the body:

$$\{H\}_1 = \int \{R\}_1 \times \{\{\omega\}_1 \times \{R\}_1\} \, \mathrm{d}m \tag{2.166}$$

$$H_x = \omega_x \int (y^2 + z^2) \, \mathrm{d}m - \omega_y \int xy \, \mathrm{d}m - \omega_z \int xz \, \mathrm{d}m \tag{2.167}$$

$$H_y = -\omega_x \int xy \, \mathrm{d}m + \omega_y \int (x^2 + z^2) \, \mathrm{d}m - \omega_z \int yz \, \mathrm{d}m \tag{2.168}$$

$$H_z = -\omega_x \int xz \, \mathrm{d}m - \omega_y \int yz \, \mathrm{d}m + \omega_z \int (x^2 + y^2) \, \mathrm{d}m \tag{2.169}$$

It is now possible to substitute into (2.167) to (2.169) the following general terms for the moments of inertia I_{xx}, I_{yy} and I_{zz} of the rigid body:

$$I_{xx} = \int (y^2 + z^2) \, \mathrm{d}m \tag{2.170}$$

$$I_{yy} = \int (x^2 + z^2) \, \mathrm{d}m \tag{2.171}$$

$$I_{zz} = \int (x^2 + y^2)\, \mathrm{d}m \tag{2.172}$$

In addition we can introduce the products of inertia I_{xy}, I_{yz} and I_{xz}:

$$I_{xy} = I_{yx} = -\int xy\, \mathrm{d}m \tag{2.173}$$

$$I_{yz} = I_{zy} = -\int yz\, \mathrm{d}m \tag{2.174}$$

$$I_{xz} = I_{zx} = -\int xz\, \mathrm{d}m \tag{2.175}$$

This allows (2.167) to (2.169) to be arranged in matrix form as follows:

$$\begin{bmatrix} H_x \\ H_y \\ H_z \end{bmatrix} = \begin{bmatrix} I_{xx} & I_{xy} & I_{xz} \\ I_{xy} & I_{yy} & I_{yz} \\ I_{xz} & I_{yz} & I_{zz} \end{bmatrix} \begin{bmatrix} \omega_x \\ \omega_y \\ \omega_z \end{bmatrix} \tag{2.176}$$

If we return to our earlier consideration of Body 2 shown in Figure 2.27 the matrix equation in (2.176) would lead to

$$\{H_2\}_{1/1} = [I_2]_{2/1}\{\omega_2\}_{1/1} \tag{2.177}$$

In writing the vectors $\{H_2\}_{1/1}\{\omega_2\}_{1/1}$ we revert to the full definition of a vector used here where the upper suffix indicates that the vector is measured relative to the axes of reference frame O_1 and the lower suffix indicates that the components of the vector are resolved parallel to the axes of frame O_1. The matrix $[I_2]_{2/1}$ is the moment of inertia matrix for Body 2 about its mass centre G_2 located at frame O_2. The use of the upper and lower suffix here indicates that the moments of inertia have been measured relative to frame O_2 but transformed to frame O_1. This is necessary so that the vector operation in (2.177) is consistent. This is only possible if the vectors and matrix are referred to the same frame, which in this case is O_1.

Note that in this form (2.177) is not practical since the orientation of frame O_2 relative to frame O_1 will change as the body rotates requiring the recomputation of $[I_2]_{2/1}$ at each time step. The matrix $[I_2]_{2/2,}$ or in simpler form $[I_2]_2$, is constant since it is measured relative to and referred to a frame that is fixed in Body 2 and hence only needs to be determined once for an undeformable body. When considering the equation for the angular momentum of a body it is preferable therefore to consider all quantities to be referred to a frame fixed in the body, in this case frame O_2:

$$\{H_2\}_{1/2} = [I_2]_{2/2}\{\omega_2\}_{1/2} \tag{2.178}$$

Before progressing to develop the equations used to describe the dynamics of rigid bodies translating and rotating in three-dimensional space the definition of the moments of inertia introduced here requires further consideration.

2.10 Moments of inertia

From our previous consideration of the angular momentum of a rigid body we see that there are three moments of inertia and three products of inertia

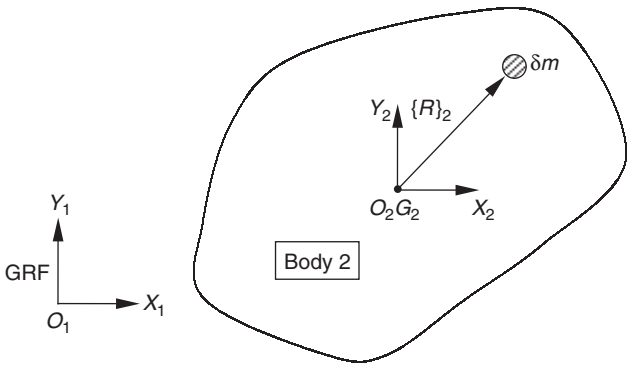

Fig. 2.28 Moment of inertia for plane motion

the values of which must be specified to analyse the rotational motion of the body. Before considering the three-dimensional situation it is useful to start with the two-dimensional inertial properties associated with plane motion.

For the Body 2 shown in Figure 2.28 we assume that a constraint has been applied that allows the body to move only in the X_1Y_1 plane of frame O_1, the ground reference frame. As such the body has three degrees of freedom, these being translation in the X_1 direction, translation in the Y_1 direction and rotation about the Z_1-axis. From the expressions given earlier for the moments of inertia it can be seen that these are in fact the second moments of the mass distribution about the chosen frame fixed in the body.

For the body shown in Figure 2.28 we are only interested in rotation about the Z_1-axis and as such only require the I_{zz} moment of inertia. To indicate that this is for Body 2 we will refer to this as I_{2zz}. Considering the particle of mass δm located by a general position vector $\{R\}_2$ at point P we see that we are not only measuring the vector with respect to frame O_2 but we are also referring the vector to frame O_2.

Ignoring the z co-ordinate as this is for plane motion in X_1Y_1 we can take the general case and say that the position of the element is given by $\{R\}_2^T = [x \;\; y \;\; 0]$. The moment of inertia I_{2zz} is found by summing the second moments of the elements of mass over the volume of the body:

$$I_{2zz} = \Sigma |R|_2^2 \, \delta m$$

$$= \Sigma (x^2 + y^2) \, \delta m \tag{2.179}$$

In the limit as the volume of the element becomes infinitesimal we can obtain an expression for the moment of inertia I_{2zz} as follows:

$$I_{2zz} = \int (x^2 + y^2) \, \mathrm{d}m \tag{2.180}$$

The moment of inertia I_{2zz} in (2.180) is therefore the integral of the mass elements each multiplied by the square of the radial distance from the z-axis. This distance is referred to as the radius of gyration, in this case k_{2zz} where this is given by

$$k_{2zz} = \sqrt{\frac{I_{2zz}}{m_2}} \tag{2.181}$$

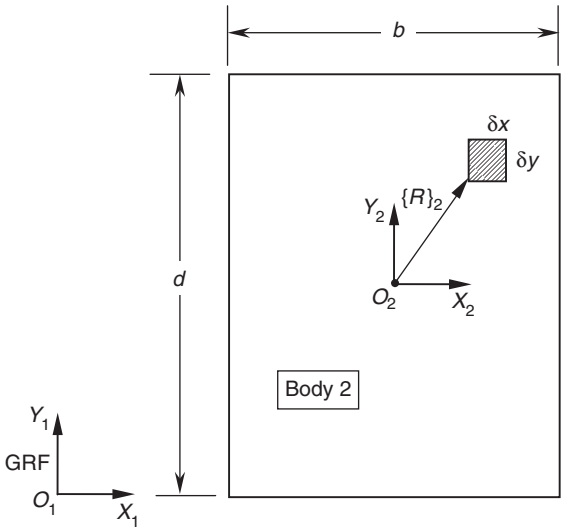

Fig. 2.29 Moment of inertia for a rectangle

From this we can use the radius of gyration to express the moment of inertia in more general terms as

$$I_{2zz} = m_2 k_{2zz}^2 \tag{2.182}$$

It is now possible to demonstrate how the moment of inertia may be derived for a standard shape. This is demonstrated in the following example where the moment of inertia is derived for the rectangle shown in Figure 2.29. This again considers the two-dimensional case for plane motion where the rectangular body, Body 2, is constrained to move only in the X_1Y_1 plane of frame O_1.

Taking this body to have a thickness of t and a density of ρ we can say that the mass δm of the small element of mass with dimensions δx and δy is given by

$$\delta m = \rho t \, \delta x \delta y \tag{2.183}$$

The moment of inertia I_{2zz} is again found by summing the second moments of the elements of mass over the volume of the body:

$$\begin{aligned} I_{2zz} &= \Sigma (x^2 + y^2) \, \delta m \\ &= \rho t \, \Sigma (x^2 + y^2) \, \delta x \delta y \end{aligned} \tag{2.184}$$

This leads to the following equation as the volume of the element becomes infinitesimal:

$$I_{2zz} = \rho t \int_{-d/2}^{d/2} \int_{-b/2}^{b/2} (x^2 + y^2) \, \mathrm{d}x \mathrm{d}y \tag{2.185}$$

Solving this double integral gives

$$I_{2zz} = \rho t \int_{-d/2}^{d/2} \left[\frac{x^3}{3} + y^2 x \right]_{-b/2}^{b/2} \mathrm{d}y$$

$$I_{2zz} = \rho t \int_{-d/2}^{d/2} \left(\frac{b^3}{24} + \frac{y^2 b}{2}\right) - \left(-\frac{b^3}{24} - \frac{y^2 b}{2}\right) \mathrm{d}y$$

$$I_{2zz} = \rho t \int_{-d/2}^{d/2} \left(\frac{b^3}{12} + y^2 b\right) \mathrm{d}y$$

$$I_{2zz} = \rho t \left[\frac{b^3 y}{12} + \frac{y^3 b}{3}\right]_{-d/2}^{d/2}$$

$$I_{2zz} = \rho t \left(\frac{b^3 d}{24} + \frac{d^3 b}{24}\right) - \left(-\frac{b^3 d}{24} - \frac{d^3 b}{24}\right)$$

$$I_{2zz} = \rho t \left(\frac{b^3 d + d^3 b}{12}\right) \tag{2.186}$$

Since the mass of the rectangle body m_2 is given by $m_2 = \rho tbd$ we can write

$$I_{2zz} = m_2 \left(\frac{b^2 + d^2}{12}\right) \tag{2.187}$$

Another example of a standard shape is the ring shown in Figure 2.30. This again considers the two-dimensional case for plane motion where the rectangular body, Body 2, is constrained to move only in the X_1Y_1 plane of frame O_1.

Taking this body to have a thickness of t and a density of ρ we can say that the mass δm of the small elemental ring of mass, at a radius $R = |R|_2$, with radial width δr, is given by

$$\delta m = \rho t 2\pi R \delta r \tag{2.188}$$

The moment of inertia I_{2zz} is again found by summing the second moments of the elements of mass over the volume of the body:

$$I_{2zz} = \Sigma R^2 \delta m$$
$$= 2\pi\rho t \, \Sigma R \cdot R^2 \delta r \tag{2.189}$$

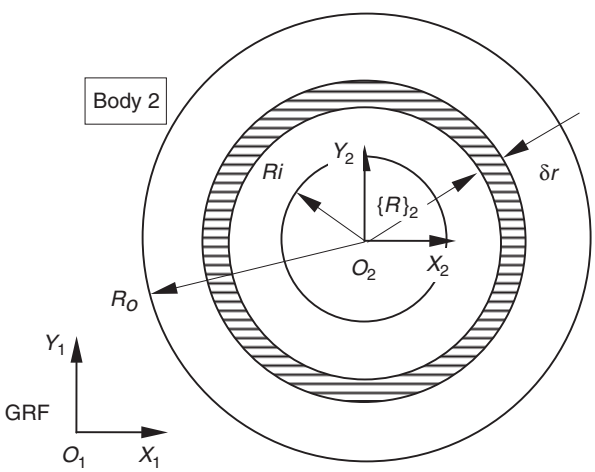

Fig. 2.30 Moment of inertia for a ring

This leads to the following equation as the volume of the element becomes infinitesimal:

$$I_{2zz} = 2\pi\rho t \int_{Ri}^{Ro} R^3 \, dr \tag{2.190}$$

Solving this integral gives

$$I_{2zz} = 2\pi\rho t \left[\frac{R^4}{4}\right]_{Ri}^{Ro}$$

$$I_{2zz} = \frac{\pi t \rho}{2} (Ro^4 - Ri^4)$$

Since the mass of the ring m_2 is given by $m_2 = \rho t \pi (Ro^2 - Ri^2)$ we can write

$$I_{2zz} = \frac{m_2}{2} \frac{(Ro^4 - Ri^4)}{(Ro^2 - Ri^2)}$$
$$I_{2zz} = \frac{m_2}{2} (Ro^2 + Ri^2) \tag{2.191}$$

2.11 Parallel axes theorem

If a rigid body comprises rigidly attached combinations of regular shapes such as those just described the overall inertial properties of the body may be found using the parallel axis theorem. Returning to the three-dimensional situation we can consider the two parallel axes systems O_2 and O_3 both fixed in Body 2 as shown in Figure 2.31.

It is now possible to show that there is an inertia matrix for Body 2 associated with frame O_2 which would be written $[I_2]_{2/2.}$ In a similar manner it is possible to determine the terms in a moment of inertia matrix $[I_2]_{3/2}$ where the use of the upper suffix here indicates that the moments of inertia have been measured relative to the origin of frame O_3 and the lower suffix indicates

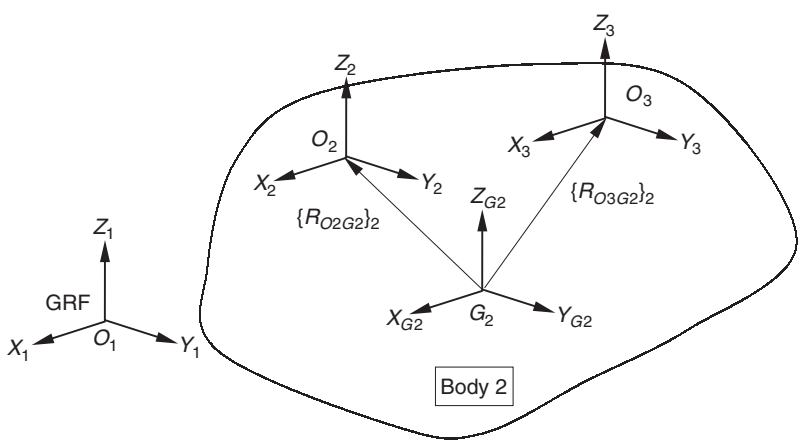

Fig. 2.31 Parallel axes theorem

that the terms in the matrix are transformed to frame O_2. Since O_2 and O_3 are parallel the matrix $[I_2]_{3/3}$ would be identical to $[I_2]_{3/2}$.

The positions of the frames O_2 and O_3 relative to G_2, the mass centre of Body 2, can be given by

$$\{R_{O2G2}\}_2 = \begin{bmatrix} x_2 \\ y_2 \\ z_2 \end{bmatrix}, \quad \{R_{O3G2}\}_2 = \begin{bmatrix} x_3 \\ y_3 \\ z_3 \end{bmatrix} \tag{2.192}$$

where according to the triangle law of vector addition if a, b and c are the components of the relative position vector $\{R_{O3O2}\}_2$ we can write

$$\{R_{O3O2}\}_2 = \begin{bmatrix} a \\ b \\ c \end{bmatrix}, \quad \{R_{O3G2}\}_2 = \begin{bmatrix} x_2 + a \\ y_2 + b \\ z_2 + c \end{bmatrix} \tag{2.193}$$

On this basis it is possible to relate a moment of inertia, for example $I_2x_3x_3$ for frame O_3 to $I_2x_2x_2$ for frame O_2:

$$\begin{aligned} I_2x_3x_3 &= \int (y_3^2 + z_3^2)\,\mathrm{d}m \\ &= \int [(y_2 + b)^2 + (z_2 + c)^2]\,\mathrm{d}m \\ &= \int [(y_2^2 + 2y_2b + b^2) + (z_2^2 + 2z_2c + c^2)]\,\mathrm{d}m \\ &= I_2x_2x_2 + 2b\int y_2\,\mathrm{d}m + 2c\int z_2\,\mathrm{d}m + (b^2 + c^2)\,m_2 \\ &= I_2x_2x_2 + 2m_2(by_2 + cz_2) + m_2(b^2 + c^2) \end{aligned} \tag{2.194}$$

If we take the situation where O_2 is coincident with G_2, the mass centre of Body 2, such that x_2, y_2 and z_2 are zero, then (2.194) can be simplified to

$$I_2x_3x_3 = I_2x_2x_2 + m_2(b^2 + c^2) \tag{2.195}$$

In a similar manner it is possible to relate a product of inertia, for example $I_2y_3z_3$ for frame O_3 to $I_2y_2z_2$ for frame O_2:

$$\begin{aligned} I_2y_3z_3 &= -\int y_3z_3\,\mathrm{d}m \\ &= -\int (y_2 + b)(z_2 + c)\,\mathrm{d}m \\ &= -\int y_2z_2 + cy_2 + bz_2 + bc\,\mathrm{d}m \\ &= I_2y_2z_2 - m_2(cy_2 + bz_2) - m_2bc \end{aligned} \tag{2.196}$$

Taking again O_2 to lie at the mass centre G_2 we can simplify (2.196) to

$$I_2y_3z_3 = I_2y_2z_2 - m_2bc \tag{2.197}$$

On the basis of the derivation of the relationships in (2.195) and (2.197) we can find in a similar manner the full relationship between $[I_2]_{3/2}$ and $[I_2]_{2/2}$ to be

$$[I_2]_{3/2} = [I_2]_{2/2} + m_2 \begin{bmatrix} b^2 + c^2 & -ab & -ac \\ -ab & c^2 + a^2 & -bc \\ -ac & -bc & a^2 + b^2 \end{bmatrix} \tag{2.198}$$

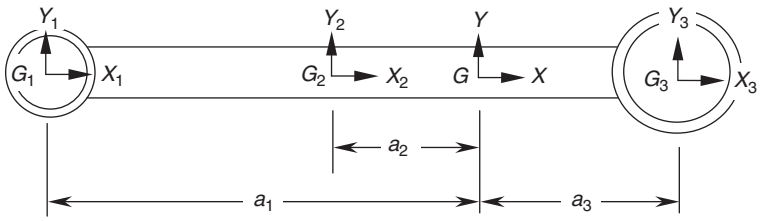

Fig. 2.32 Application of parallel axes theorem

A practical application of the parallel axes theorem given in (2.198) is provided using the simplified representation of a tie rod as shown in Figure 2.32. The body can be considered an assembly of three components with centres of mass at G_1, G_2 and G_3. The mass centre of the entire body is located at G. The components have masses m_1, m_2 and m_3 and moments of inertia about the local z-axis at each mass centre I_{G1zz}, I_{G2zz} and I_{G3zz}.

Applying the parallel axes theorem would in this case give a moment of inertia I_{Gzz} for the body using

$$I_{Gzz} = I_{G1zz} + m_1 a_1^2 + I_{G2zz} + m_2 a_2^2 + I_{G3zz} + m_3 a_3^2 \tag{2.199}$$

2.12 Principal axes

The principal axes of any rigid body are those for which the products of inertia are all zero resulting in an inertia matrix of the form

$$[I] = \begin{bmatrix} I_1 & 0 & 0 \\ 0 & I_2 & 0 \\ 0 & 0 & I_3 \end{bmatrix} \tag{2.200}$$

where in this case I_1, I_2 and I_3 are the principal moments of inertia. The three planes formed by the principal axes are referred to as the principal planes as shown in Figure 2.33. In this example the geometry chosen is a solid cylinder to demonstrate the concept.

For the cylinder the principal axes are represented by the frame O_2 positioned at the mass centre of the body. In this case each of the principal planes is a plane of symmetry for the body. As can be seen for each element of mass with positive co-ordinates there are other elements of mass, reflected in each of the principal planes, with negative co-ordinates. The result of this is that the products of inertia are all zero.

Returning to the consideration of the angular momentum of a body given in (2.178) this can now be written as shown in equation (2.201) where I_1, I_2 and I_3 are the principal moments of inertia for Body 2 taken about the origin of frame O_2. The moment of inertia matrix is referred to the principal axes, again frame O_2 and the products of inertia are zero:

$$\{H_2\}_{1/2} = [I_2]_{2/2}\{\omega_2\}_{1/2}$$

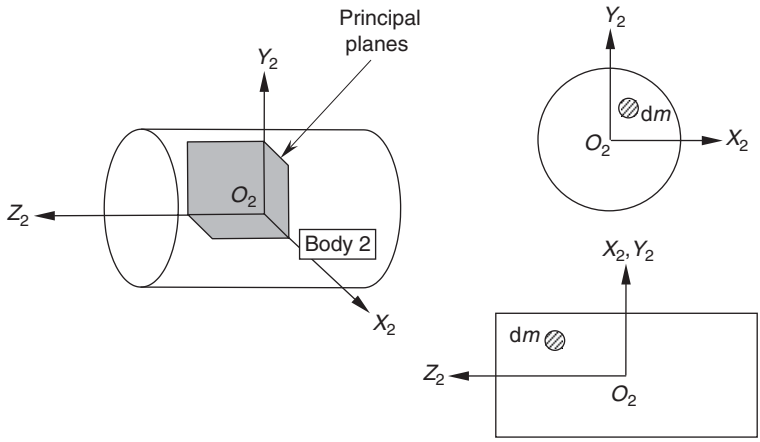

Fig. 2.33 Principal axes for a body

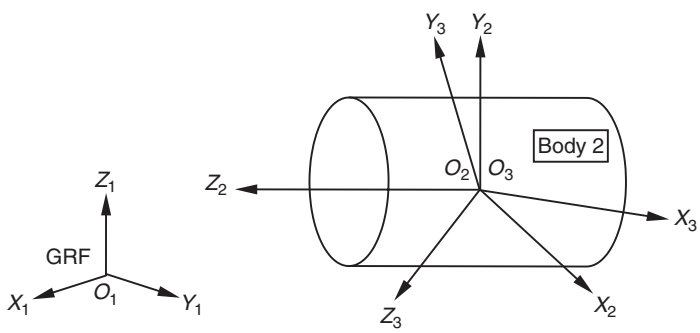

Fig. 2.34 Transformation to principal axes

$$\begin{bmatrix} H_{2x} \\ H_{2y} \\ H_{2z} \end{bmatrix} = \begin{bmatrix} I_1 & 0 & 0 \\ 0 & I_2 & 0 \\ 0 & 0 & I_3 \end{bmatrix} \begin{bmatrix} \omega_{2x} \\ \omega_{2y} \\ \omega_{2z} \end{bmatrix} = \begin{bmatrix} I_1 & \omega_{2x} \\ I_2 & \omega_{2y} \\ I_3 & \omega_{2z} \end{bmatrix} \tag{2.201}$$

The principal axes and the principal moments of inertia may be obtained by considering the two frames O_3 and O_2 both located at the mass centre in Body 2 as shown in Figure 2.34. The axes associated with frame O_2 are again taken to be the principal axes of the body. The angular momentum $\{H_2\}_{1/2}$ referred to O_2 can be transformed from the angular momentum $\{H_2\}_{1/3}$ referred to O_3 using the rotational transformation matrix $[T_3]_2$ as described in section 2.2.7:

$$\{H_2\}_{1/2} = [T_3]_2 \{H_2\}_{1/3} \tag{2.202}$$

Since $\{H_2\}_{1/2} = [I_2]_{2/2}\{\omega_2\}_{1/2}$ and $\{H_2\}_{1/3} = [I_2]_{2/3}\{\omega_2\}_{1/3}$ it follows from (2.202) that

$$[I_2]_{2/2}\{\omega_2\}_{1/2} = [T_3]_2 [I_2]_{2/3}\{\omega_2\}_{1/3} \tag{2.203}$$

If we pre-multiply a transformation matrix $[T]$ by its transpose $[T]^T$ a property of these matrices is that we produce an identity matrix:

$$[T]^T[T] = \begin{bmatrix} 1 & 0 & 0 \\ 0 & 1 & 0 \\ 0 & 0 & 1 \end{bmatrix} \tag{2.204}$$

This allows us to further develop (2.203) to give

$$[I_2]_{2/2}\{\omega_2\}_{1/2} = [T_3]_2[I_2]_{2/3}[T_3]_2^T[T_3]_2\{\omega_2\}_{1/3} \tag{2.205}$$

Since we also know that $\{\omega_2\}_{1/2} = [T_3]_2\{\omega_2\}_{1/3}$ we can therefore write

$$[I_2]_{2/2} = [T_3]_2[I_2]_{2/3}[T_3]_2^T \tag{2.206}$$

In this case we require a transformation matrix $[T_3]_2$ which is orthogonal and will lead to a diagonal matrix $[I_2]_{2/2}$. If we now take (2.206) and pre-multiply by $[T_3]_2^T$ we get

$$[T_3]_2^T[I_2]_{2/2} = [I_2]_{2/3}[T_3]_2^T$$

$$\begin{bmatrix} T_{11} & T_{21} & T_{31} \\ T_{12} & T_{22} & T_{32} \\ T_{13} & T_{23} & T_{33} \end{bmatrix}\begin{bmatrix} I_1 & 0 & 0 \\ 0 & I_2 & 0 \\ 0 & 0 & I_3 \end{bmatrix} = \begin{bmatrix} I_{xx} & I_{xy} & I_{xz} \\ I_{xy} & I_{yy} & I_{yz} \\ I_{xz} & I_{yz} & I_{zz} \end{bmatrix}\begin{bmatrix} T_{11} & T_{21} & T_{31} \\ T_{12} & T_{22} & T_{32} \\ T_{13} & T_{23} & T_{33} \end{bmatrix}$$

$$\begin{bmatrix} T_{11}I_1 & T_{21}I_2 & T_{31}I_3 \\ T_{12}I_1 & T_{22}I_2 & T_{32}I_3 \\ T_{13}I_1 & T_{23}I_2 & T_{33}I_3 \end{bmatrix}$$

$$= \begin{bmatrix} I_{xx}T_{11} + I_{xy}T_{12} + I_{xz}T_{13} & I_{xx}T_{21} + I_{xy}T_{22} + I_{xz}T_{23} & I_{xx}T_{31} + I_{xy}T_{32} + I_{xz}T_{33} \\ I_{xy}T_{11} + I_{yy}T_{12} + I_{xz}T_{13} & I_{xy}T_{21} + I_{yy}T_{22} + I_{yz}T_{23} & I_{xy}T_{31} + I_{yy}T_{32} + I_{yz}T_{33} \\ I_{xz}T_{11} + I_{yz}T_{12} + I_{zz}T_{13} & I_{xz}T_{21} + I_{yz}T_{22} + I_{zz}T_{23} & I_{xz}T_{31} + I_{yz}T_{32} + I_{zz}T_{33} \end{bmatrix} \tag{2.207}$$

Equating the first columns from the matrices on either side of (2.207) leads to the eigenvalue equation in (2.208):

$$I_1\begin{bmatrix} T_{11} \\ T_{12} \\ T_{13} \end{bmatrix} = \begin{bmatrix} I_{xx} & I_{xy} & I_{xz} \\ I_{xy} & I_{yy} & I_{yz} \\ I_{xz} & I_{yz} & I_{zz} \end{bmatrix}\begin{bmatrix} T_{11} \\ T_{12} \\ T_{13} \end{bmatrix} \tag{2.208}$$

This equation can be rearranged to give

$$\begin{bmatrix} I_{xx} - I_1 & I_{xy} & I_{xz} \\ I_{xy} & I_{yy} - I_1 & I_{yz} \\ I_{xz} & I_{yz} & I_{zz} - I_1 \end{bmatrix}\begin{bmatrix} T_{11} \\ T_{12} \\ T_{13} \end{bmatrix} = \begin{bmatrix} 0 \\ 0 \\ 0 \end{bmatrix} \tag{2.209}$$

For a non-trivial solution to (2.209) we require the determinant of the square matrix containing I_1 to be zero leading to the characteristic equation:

$$\begin{vmatrix} I_{xx} - I_1 & I_{xy} & I_{xz} \\ I_{xy} & I_{yy} - I_1 & I_{yz} \\ I_{xz} & I_{yz} & I_{zz} - I_1 \end{vmatrix} = 0 \tag{2.210}$$

The process used to find the determinant is documented in standard texts dealing with the mathematical manipulation of matrices but for a general three by three square matrix may be summarized as follows:

$$\begin{vmatrix} A & B & C \\ D & E & F \\ G & H & I \end{vmatrix} = A(EI - HF) - B(DI - GF) + C(DH - GE) \tag{2.211}$$

The solution of (2.210) leads to a cubic equation in I_1 with three positive real roots, these being the three principal moments of inertia I_1, I_2 and I_3. If each of these is substituted in turn into equations that equate all three columns on either side of (2.207) we get

$$I_1 \begin{bmatrix} T_{11} \\ T_{12} \\ T_{13} \end{bmatrix} = \begin{bmatrix} I_{xx} & I_{xy} & I_{xz} \\ I_{xy} & I_{yy} & I_{yz} \\ I_{xz} & I_{yz} & I_{zz} \end{bmatrix} \begin{bmatrix} T_{11} \\ T_{12} \\ T_{13} \end{bmatrix} \tag{2.212}$$

$$I_2 \begin{bmatrix} T_{21} \\ T_{22} \\ T_{23} \end{bmatrix} = \begin{bmatrix} I_{xx} & I_{xy} & I_{xz} \\ I_{xy} & I_{yy} & I_{yz} \\ I_{xz} & I_{yz} & I_{zz} \end{bmatrix} \begin{bmatrix} T_{21} \\ T_{22} \\ T_{23} \end{bmatrix} \tag{2.213}$$

$$I_3 \begin{bmatrix} T_{31} \\ T_{32} \\ T_{33} \end{bmatrix} = \begin{bmatrix} I_{xx} & I_{xy} & I_{xz} \\ I_{xy} & I_{yy} & I_{yz} \\ I_{xz} & I_{yz} & I_{zz} \end{bmatrix} \begin{bmatrix} T_{31} \\ T_{32} \\ T_{33} \end{bmatrix} \tag{2.214}$$

The solution of (2.212) to (2.214) thus yields all the terms in $[T_3]_2$, the transformation matrix from frame O_3 to O_2. In summary I_1, I_2 and I_3 are the eigenvalues of the inertia matrix $[I_2]_{2/3}$ and are also the principal moments of inertia for Body 2, these being the diagonal terms in the matrix $[I_2]_{2/2}$. The three column matrices in (2.212) to (2.214) are the eigenvectors of $[I_2]_{2/3}$:

$$\begin{bmatrix} T_{11} \\ T_{12} \\ T_{13} \end{bmatrix} \quad \begin{bmatrix} T_{21} \\ T_{22} \\ T_{23} \end{bmatrix} \quad \begin{bmatrix} T_{31} \\ T_{32} \\ T_{33} \end{bmatrix}$$

If each vector is now normalized so that the length of the vector is unity, we get the direction cosines between each of the axes of O_2, the principal axes of Body 2, and O_3.

We can now consider a practical application of this with regard to vehicle dynamics where the body of a vehicle will generally be the largest and most significant mass in the model. For the vehicle body, Body 2, shown in Figure 2.35 we can take frame O_3 to be positioned at the mass centre and orientated so that the x-axis is along the centre line and pointing to the rear of the vehicle and the z-axis is vertical. The X_3Z_3 plane is thus a plane of symmetry. It should be noted that in reality this assumption involves some approximation due to the asymmetry of the masses that may be lumped with the vehicle body such as the engine, battery, exhaust system and fuel

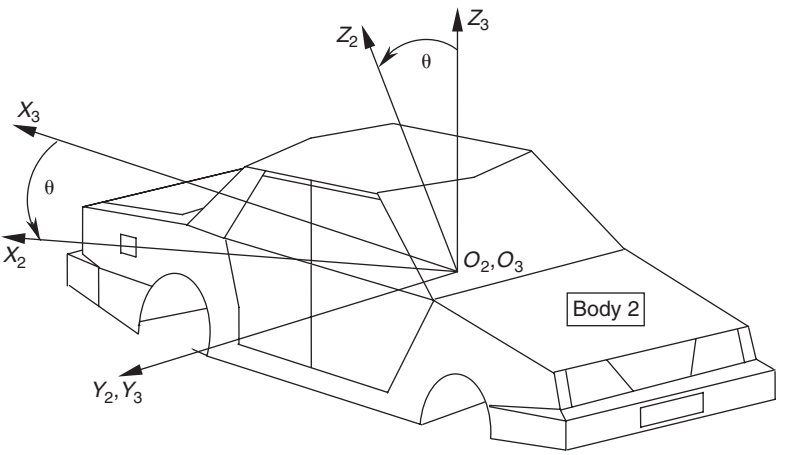

Fig. 2.35 Vehicle body co-ordinate system

tank. The frame O_2 shown in Figure 2.35 is also positioned at the mass centre and has its Y_2-axis coincident with the Y_3-axis of frame O_3. The frame O_2 represents the principal axes of the vehicle body and is obtained by a transformation from O_3 represented by the rotation through an angle θ about the Y_2- and Y_3-axes.

In determining the products of inertia for this body it can be seen that for every element of mass with a positive y co-ordinate there exists an equivalent element with a negative y co-ordinate. As a result we get

$$I_{xy} = I_{yx} = -\int xy \, \mathrm{d}m = 0$$

$$I_{yz} = I_{zy} = -\int yz \, \mathrm{d}m = 0$$

The inertia matrix for Body 2 $[I_2]_{2/3}$ measured from frame O_2 and referred to O_3 is therefore

$$[I_2]_{2/3} = \begin{bmatrix} I_{xx} & 0 & I_{xz} \\ 0 & I_2 & 0 \\ I_{xz} & 0 & I_{zz} \end{bmatrix} \tag{2.215}$$

From this it can be seen that the y-axis is a principal axis and is normal to the plane of symmetry. The principal moment of inertia I_2 is therefore equal to I_{yy}. From section 2.2.7 we can see that the matrix $[T_3]_2$ that transforms from frame O_3 to O_2 is given by

$$[T_3]_2 = \begin{bmatrix} \cos\theta & 0 & -\sin\theta \\ 0 & 1 & 0 \\ \sin\theta & 0 & \cos\theta \end{bmatrix} \tag{2.216}$$

From (2.206) we can see that using the transformation matrix $[T_3]_2$ given for this particular case will lead to

$$[I_2]_{2/2} = [T_3]_2 [I_2]_{2/3} [T_3]_2^T$$

$$\begin{bmatrix} I_1 & 0 & 0 \\ 0 & I_2 & 0 \\ 0 & 0 & I_3 \end{bmatrix} = \begin{bmatrix} \cos\theta & 0 & -\sin\theta \\ 0 & 1 & 0 \\ \sin\theta & 0 & \cos\theta \end{bmatrix} \begin{bmatrix} I_{xx} & 0 & I_{xz} \\ 0 & I_2 & 0 \\ I_{xz} & 0 & I_{zz} \end{bmatrix} \begin{bmatrix} \cos\theta & 0 & \sin\theta \\ 0 & 1 & 0 \\ -\sin\theta & 0 & \cos\theta \end{bmatrix}$$

$$\begin{bmatrix} I_1 & 0 & 0 \\ 0 & I_2 & 0 \\ 0 & 0 & I_3 \end{bmatrix} = \begin{bmatrix} \cos\theta & 0 & -\sin\theta \\ 0 & 1 & 0 \\ \sin\theta & 0 & \cos\theta \end{bmatrix} \begin{bmatrix} I_{xx}\cos\theta - I_{xz}\sin\theta & 0 & I_{xx}\sin\theta + I_{xz}\cos\theta \\ 0 & I_2 & 0 \\ I_{xz}\cos\theta - I_{zz}\sin\theta & 0 & I_{xz}\sin\theta + I_{zz}\cos\theta \end{bmatrix}$$

$$\begin{bmatrix} I_1 & 0 & 0 \\ 0 & I_2 & 0 \\ 0 & 0 & I_3 \end{bmatrix} = \begin{bmatrix} I_{xx}\cos^2\theta - 2I_{xz}\sin\theta\cos\theta + I_{zz}\sin^2\theta & 0 & I_{xx}\sin\theta\cos\theta + I_{xz}\cos^2\theta - I_{xz}\sin^2\theta - I_{zz}\sin\theta\cos\theta \\ 0 & I_2 & 0 \\ I_{xx}\sin\theta\cos\theta + I_{xz}\cos^2\theta - I_{xz}\sin^2\theta - I_{zz}\sin\theta\cos\theta & 0 & I_{xx}\sin^2\theta - 2I_{xz}\sin\theta\cos\theta + I_{zz}\cos^2\theta \end{bmatrix} \tag{2.217}$$

Multiplying out the matrix equation in (2.217) leads to the following expressions for the principal moments of inertia I_1 and I_3:

$$I_1 = I_{xx}\cos^2\theta - 2I_{xz}\sin\theta\cos\theta + I_{zz}\sin^2\theta \tag{2.218}$$

$$I_3 = I_{xx}\sin\theta\cos\theta + I_{xz}\cos^2\theta + I_{xz}\sin^2\theta - I_{zz}\sin\theta\cos\theta \tag{2.219}$$

Equating now the zero elements on the left-hand side of (2.217) with the terms in either row 1 column 3 or column 1 row 3 gives

$$0 = I_{xx}\sin\theta\cos\theta - I_{xz}\sin^2\theta + I_{xz}\cos^2\theta - I_{zz}\sin\theta\cos\theta \tag{2.220}$$

This can be rearranged to give

$$0 = I_{xz}(\cos^2\theta - \sin^2\theta) + (I_{xx} - I_{zz})\sin\theta\cos\theta \tag{2.221}$$

From trigonometric addition formulae we can make use of

$$\cos 2\theta = \cos^2\theta - \sin^2\theta \quad \text{and} \quad \sin 2\theta = 2\sin\theta\cos\theta$$

which leads to

$$0 = I_{xz}\cos 2\theta + \frac{1}{2}(I_{xx} - I_{zz})\sin 2\theta \tag{2.222}$$

Rearranging (2.222) leads to an expression from which we can determine a value for θ using the known values for I_{xx}, I_{zz} and I_{xz}:

$$\tan 2\theta = \frac{I_{xz}}{\frac{1}{2}(I_{zz} - I_{xx})} \tag{2.223}$$

Using the value obtained for θ in (2.223) it is now possible to substitute this back into (2.218) and (2.219) and obtain values for the two unknown principal moments of inertia I_1 and I_3.

2.13 Equations of motions

If we consider the rigid body, Body 2, shown in Figure 2.36 we can formulate six equations of motion corresponding with the six degrees of freedom resulting from unconstrained motion.

From our earlier consideration of linear momentum given in (2.161) we can write

$$\Sigma\{F_2\}_1 = \frac{\mathrm{d}}{\mathrm{d}t}\{L_2\}_1 = m_2 \frac{\mathrm{d}}{\mathrm{d}t}\{V_{G2}\}_1 \tag{2.224}$$

Expressing this in the familiar form of Newton's second law we get

$$\Sigma\{F_2\}_1 = m_2\{A_{G2}\}_1 \tag{2.225}$$

The vector equation given in (2.225) will thus yield the three equations associated with the translational motion of the body. It may be noted that for these equations the vectors in (2.225) may be conveniently referred to the fixed ground reference frame O_1.

In the same way that a resultant force acting on the body produces a change in linear momentum, a resultant moment will produce a change in angular momentum. If we consider the expression for angular momentum given in (2.178) we can obtain the equations of motion associated with rotational motion. For the rotational equations it is convenient to refer the vectors to the reference frame O_2 fixed in and rotating with Body 2:

$$\Sigma\{M_{G2}\}_{1/2} = \frac{\mathrm{d}}{\mathrm{d}t}\{H_2\}_{1/2} = \frac{\mathrm{d}}{\mathrm{d}t}[I_2]\{\omega_2\}_{1/2} \tag{2.226}$$

It can also be shown that

$$\frac{\mathrm{d}}{\mathrm{d}t}\{H_2\}_{1/1} = \frac{\mathrm{d}}{\mathrm{d}t}\{H_2\}_{1/2} + \{\omega_2\}_{1/2} \times \{H_2\}_{1/2} \tag{2.227}$$

$$\{M_{G2}\}_{1/2} = [I_2]_{2/2}\{\alpha_2\}_{1/2} + \{\omega_2\}_{1/2} \times \{H_2\}_{1/2} \tag{2.228}$$

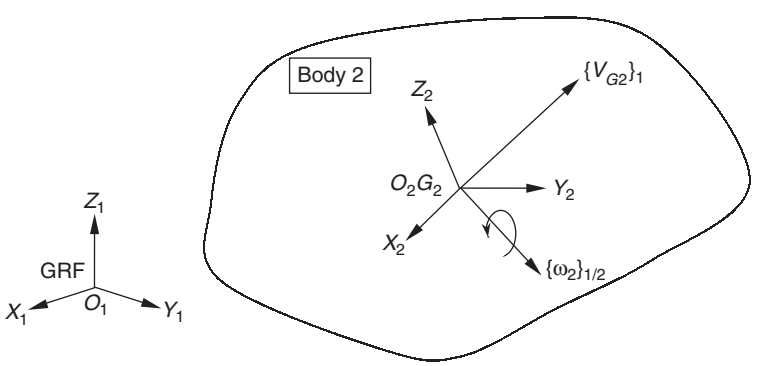

Fig. 2.36 Rigid body motion

Expanding (2.228) gives

$$\begin{bmatrix} M_x \\ M_y \\ M_z \end{bmatrix} = \begin{bmatrix} I_{xx} & I_{xy} & I_{xz} \\ I_{xy} & I_{yy} & I_{yz} \\ I_{xz} & I_{yz} & I_{zz} \end{bmatrix} \begin{bmatrix} \alpha_{2x} \\ \alpha_{2y} \\ \alpha_{2z} \end{bmatrix} + \begin{bmatrix} 0 & -\omega_{2z} & \omega_{2y} \\ \omega_{2z} & 0 & -\omega_{2x} \\ -\omega_{2y} & \omega_{2x} & 0 \end{bmatrix} \begin{bmatrix} \mathrm{H}_{2x} \\ \mathrm{H}_{2y} \\ \mathrm{H}_{2z} \end{bmatrix} \tag{2.229}$$

Substituting in terms for H_{2x}, H_{2y} and H_{2z} now leads to the equations given in (2.230) to (2.231). For convenience we can drop the subscript for Body 2:

$$\begin{aligned} M_x = {} & I_{xx}\alpha_x + I_{xy}(\alpha_y - \omega_x\omega_z) + I_{xz}(\alpha_z + \omega_x\omega_y) \\ & + (I_{zz} - I_{yy})\omega_y\omega_z + I_{yz}(\omega_y^2 - \omega_z^2) \end{aligned} \tag{2.230}$$

$$\begin{aligned} M_y = {} & I_{xy}(\alpha_x - \omega_y\omega_z) + I_{yy}\alpha_y + I_{yz}(\alpha_z - \omega_x\omega_y) \\ & + (I_{xx} - I_{zz})\omega_x\omega_z + I_{xz}(\omega_z^2 - \omega_x^2) \end{aligned} \tag{2.231}$$

$$\begin{aligned} M_z = {} & I_{xz}(\alpha_x - \omega_y\omega_z) + I_{yz}(\alpha_y - \omega_x\omega_z) \\ & + I_{zz}\alpha_z + (I_{yy} - I_{xx})\omega_x\omega_y + I_{xy}(\omega_x^2 - \omega_y^2) \end{aligned} \tag{2.232}$$

In summary the rotational equations of motion for Body 2 may be written in vector form as

$$\Sigma\{M_{G2}\}_{1/2} = [I_2]_{2/2}\{\alpha_2\}_{1/2} + [\omega_2]_{1/2}[I_2]_{2/2}\{\omega_2\}_{1/2} \tag{2.233}$$

Hence we can see that in setting up the equations of motion for any rigid body the translational equations for all bodies in a system may conveniently be referred to a single fixed inertial frame O_1. The rotational equations, however, are better referred to a body centred frame, in this case O_2. A considerable simplification in these equations will result if frame O_2 is selected such that its axes are the principal axes of the body ($I_1 = I_{xx}$, $I_2 = I_{yy}$, $I_3 = I_{zz}$) and the products of inertia are zero. The equations that result are known as Euler's equations of motion:

$$M_x = I_1\alpha_x + (I_3 - I_2)\omega_y\omega_z \tag{2.234}$$

$$M_y = I_2\alpha_y + (I_1 - I_3)\omega_x\omega_z \tag{2.235}$$

$$M_z = I_3\alpha_z + (I_2 - I_1)\omega_x\omega_y \tag{2.236}$$

The equations given in (2.234) to (2.236) become even simpler when the motion of a body is constrained so that rotation takes place in one plane only. If, for example, rotation about the x- and y-axes are prevented then equation (2.236) reduces to the more familiar form associated with two-dimensional motion:

$$M_z = I_3\alpha_z \tag{2.237}$$

The following example also demonstrates how gyroscopic effects associated with three-dimensional motion may be identified. If we consider the swing arm suspension system shown in Figure 2.37 we can take the suspension arm Body 2 to be constrained by a revolute joint to rotate with a constant angular velocity of 10 rad/s about the axis of the joint as shown. While this motion is in progress the road wheel, Body 3, is also rotating

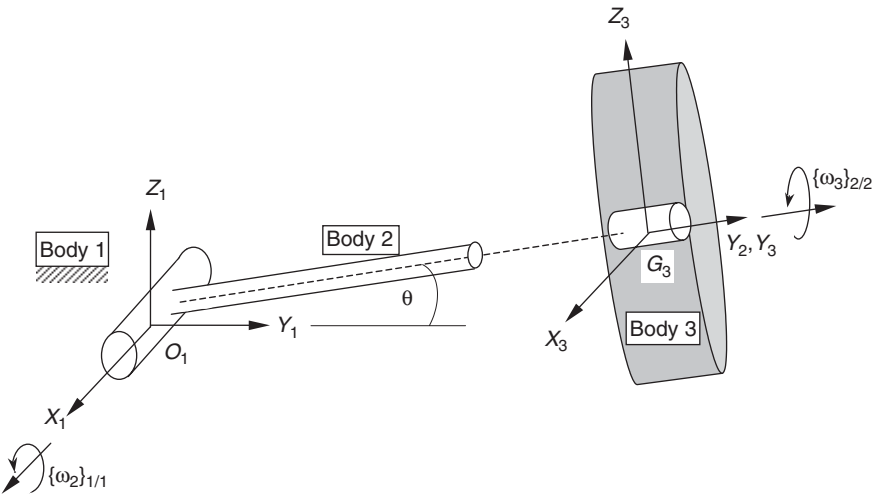

Fig. 2.37 Swing arm suspension dynamics

with a constant angular velocity of 100 rad/s about the axis of the revolute joint representing the wheel bearing.

The following data may be used to represent the mass properties of the road wheel:

$m_3 = 16\,\text{kg}$

$I_{31} = I_{3xx} = 0.5\,\text{kg m}^2$

$I_{32} = I_{3yy} = 1.0\,\text{kg m}^2$

$I_{33} = I_{3zz} = 0.5\,\text{kg m}^2$

In order to determine the reaction torque on the wheel bearing when the axle is still in a horizontal position, $\theta = 0$, we can use the following to give us the required angular velocity vector $\{\omega_3\}_{1/3}$:

$$\{\omega_2\}_{1/2} = \begin{bmatrix} 10 \\ 0 \\ 0 \end{bmatrix} \text{rad/s} \quad \{\omega_3\}_{2/3} = \begin{bmatrix} 0 \\ 100 \\ 0 \end{bmatrix} \text{rad/s} \quad \{\omega_3\}_{1/3} = \begin{bmatrix} 10 \\ 100 \\ 0 \end{bmatrix} \text{rad/s}$$

In the absence of angular acceleration equation (2.233) can be adapted to give for this problem

$$\Sigma\{M_3\}_{1/3} = [\omega_3]_{1/3}[I_3]_{1/3}\{\omega_3\}_{1/3} \tag{2.238}$$

Expanding this gives

$$\sum \begin{bmatrix} M_{3x} \\ M_{3y} \\ M_{3z} \end{bmatrix}_{1/3} = \begin{bmatrix} 0 & -\omega_{3z} & \omega_{3y} \\ \omega_{3z} & 0 & -\omega_{3x} \\ -\omega_{3y} & \omega_{3x} & 0 \end{bmatrix}_{1/3} \begin{bmatrix} I_{3xx} & 0 & 0 \\ 0 & I_{3yy} & 0 \\ 0 & 0 & I_{3zz} \end{bmatrix}_{3/3} \begin{bmatrix} \omega_{3x} \\ \omega_{3y} \\ \omega_{3z} \end{bmatrix}_{1/3} \tag{2.239}$$

Substituting in the numerical data for this problem gives

$$\sum \begin{bmatrix} M_{3x} \\ M_{3y} \\ M_{3z} \end{bmatrix}_{1/3} = \begin{bmatrix} 0 & 0 & 100 \\ 0 & 0 & -10 \\ -100 & 10 & 0 \end{bmatrix} \begin{bmatrix} 0.5 & 0 & 0 \\ 0 & 1.0 & 0 \\ 0 & 0 & 0.5 \end{bmatrix} \begin{bmatrix} 10 \\ 100 \\ 0 \end{bmatrix} \text{Nm}$$

$$\sum \begin{bmatrix} M_{3x} \\ M_{3y} \\ M_{3z} \end{bmatrix}_{1/3} = \begin{bmatrix} 0 & 0 & 100 \\ 0 & 0 & -10 \\ -100 & 10 & 0 \end{bmatrix} \begin{bmatrix} 5.0 \\ 100 \\ 0 \end{bmatrix} \text{Nm}$$

$$\sum \begin{bmatrix} M_{3x} \\ M_{3y} \\ M_{3z} \end{bmatrix}_{1/3} = \begin{bmatrix} 0 \\ 0 \\ 500 \end{bmatrix} \text{Nm} \tag{2.240}$$

As can be seen from the result in (2.240) the reaction torque on the wheel bearing is about the z-axis and is due to gyroscopic effects as the wheel spins about the y-axis and rotates about the x-axis.

It should be noted that in addition to the derivation of the equations of motion based on the direct application of Newton's laws, variational methods, including, for example, Lagranges equations, provide an elegant alternative and are often employed in MBS formulations. Many texts on classical dynamics such as D'Souza and Garg (1984) include a thorough treatment of these methods.

Variational methods are attractive for a number of reasons. Equations are formulated using kinetic energy and work resulting in scalar rather than vector terms. Solutions can also be more efficient since constraint forces that do not perform work can be omitted. Variational methods also make use of generalized rather than physical co-ordinates reducing the number of equations required.

The theory and methods described in this chapter form a basis for the multibody systems formulations covered in the next chapter. The vector notation used here will be used to describe the part equations and the constraint equations required to represent joints constraining relative motion between interconnected bodies. In Chapter 4 the vector-based methods described here will be used to carry out a range of analyses from first principles on a double wishbone suspension system and to compare the calculated results with those found using MSC.ADAMS.

3 Multibody systems simulation software

3.1 Overview

There exists a range of commercial computer packages that can be used to solve problems in multibody systems analysis. In addition to the commercial packages that may be licensed there are also programs developed by academic institutions that may be available, albeit without the level of development and support that would be expected when buying the software from an established program developer. The features described in this chapter are from MSC.ADAMS but in principle will equip the reader to understand the capabilities of other multibody systems analysis programs used in vehicle dynamics.

General-purpose MBS programs are able to address a large set of problems across a wide range of engineering industries and are not restricted to the applications in vehicle dynamics discussed here. The main use of MSC. ADAMS within the automotive industry is to simulate the performance of subsystems and full vehicles. Models are increasingly being used for large amplitude non-linear vibration problems such as powertrain isolation and driveline oscillations. The analyst will often wish to validate the performance of a suspension model over a range of displacements between full bump to rebound before the assembly of a full vehicle model that may be used for ride, handling and durability studies. A detailed model may include representations of the body, subframes, suspension arms, struts, anti-roll bars, steering system, engine, drivetrain and tyres.

The main analysis code consists of a number of integrated programs that perform three-dimensional kinematic, static, quasi-static or dynamic analysis of mechanical systems. These programs may be thought of as the core solver. In addition there are a number of auxiliary programs, which can be supplied to link with the core solver. These programs can be used to model vehicle tyre characteristics, automatically generate vehicle suspensions and full vehicle models, or model the human body. Once a model has been defined the core solver will assemble the equations of motion and solve them automatically. It is also possible to include differential equations directly in the solution, which allows the modelling of a variety of control systems.

The software can link or interface with CAD systems, finite element programs, software used for advanced visualization or additional software modules such as those used for tyre modelling. The combined use of these systems can lead to the development of what may be referred to as virtual prototypes, that is computer models that can simulate the tests and conditions that a real prototype would be subject to during the development of a new engineering product. The extent of these interfaces involving MSC.ADAMS is illustrated in Ryan (1993) and reproduced here in Figure 3.1.

Note that although the software has been continually developed since this publication Figure 3.1 is still a useful illustration of the integration of MBS software in a CAE environment.

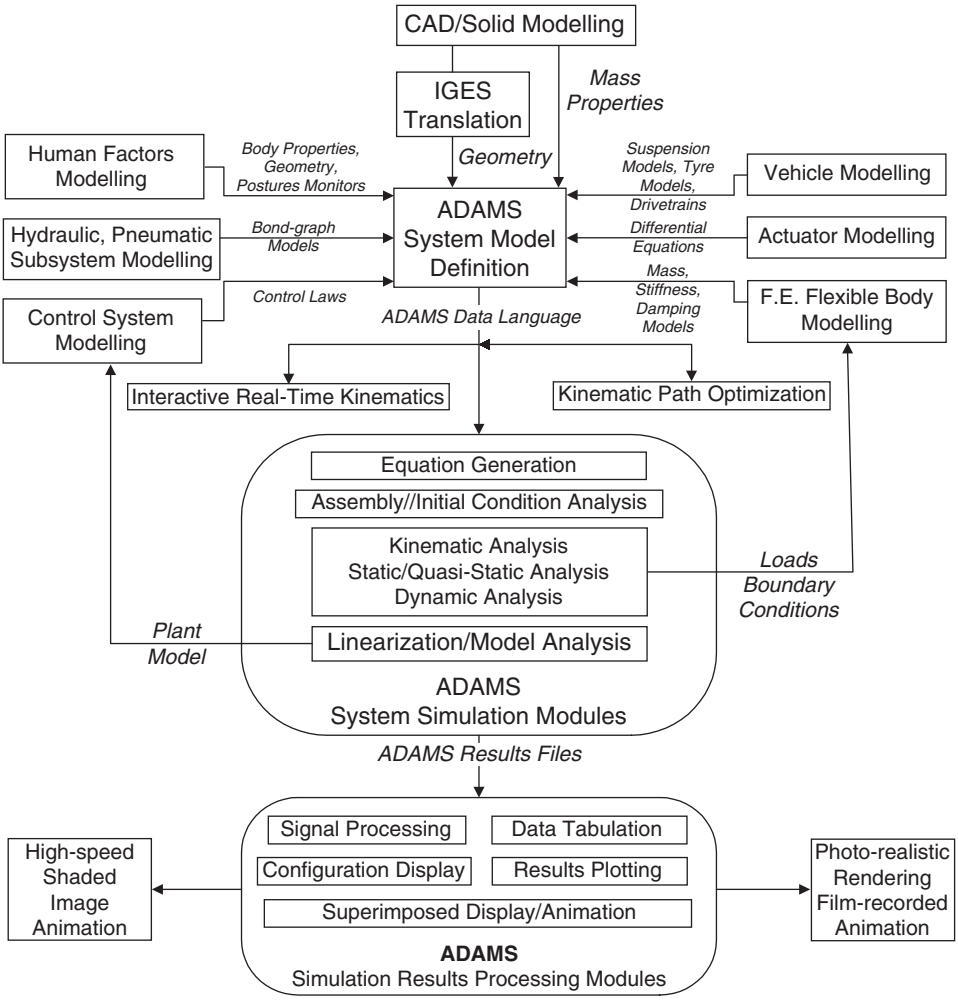

Fig. 3.1 Integration of MSC.ADAMS with CAE software

The first step in any simulation is to prepare a data set, which will define the system being modelled. This will include a description of the rigid parts, connecting joints, motion generators, forces and compliances. With most codes the data set is user friendly in that the data statements are easily understood with few restrictions on format. For advanced applications users can often prepare their own user-written subroutines in languages such as FORTRAN 90 or ANSI 'C' that can be linked with the main code.

For each rigid body in the system it is necessary to define the mass, centre of mass location, and mass moments of inertia. Each body will possess a set of co-ordinates, which can be defined in global or local co-ordinate systems and are considered to move with the part during the simulation. These points are used to define centre of mass locations, joint locations and orientations, force locations and directions. The relative motion between different parts in the system can usually be constrained using joints, joint primitives, couplers, gears and user-defined constraints.

The next step in building the model would typically be the definition of external forces and internal force elements. External forces can be constant, time histories or functionally dependent on any state variable. These forces can also be defined to be translational or rotational. They can act in the global system or can act in the local system of the body so that they effectively 'follow' the part during the simulation.

Users can also set up internal force elements acting between two parts to represent springs, dampers, cables or rubber mounts. Internal force elements will always act along the line of sight between the points the force element connects on the two parts. These force elements are often referred to as action–reaction forces as they always produce equal and opposite forces on the two parts connected by the force element. The elements can also be defined to act in only tension or compression and may be linear or non-linear.

It is also useful if the multibody systems analysis program allows the definition of elaborate mathematical equations within the data set. This enables the user to formulate an expression involving user-defined constants, system constants, system variables, arithmetic IFs, FORTRAN 90 or ANSI 'C' library functions, standard mathematical functions or 'off-the-shelf' functions supplied with the main code to represent events such as impacts. The access to system variables can be a powerful modelling tool. The user can effectively access any displacement, velocity, acceleration or other force in the system when defining the force equation. Forces can also be defined as a function of time to vary or switch on and off as the simulation progresses. Caution is needed to ensure formulations are continuous in the time domain to avoid problems during the numerical solution of the resulting equations. Recent versions of the software also include a general contact force model between geometries associated with the rigid bodies.

Enforced displacement input can be defined at certain joints to be either constant or time dependent. When a motion is defined at a joint it may be translational or rotational. The motion effectively provides another constraint so that the degree of freedom at that joint is lost to the motion. Motion expressions can be defined using all the functions available as for force definitions except that the only system variable that can be accessed is time.

A multibody systems analysis program will often provide a number of elements with the capability to model flexibility of bodies and elastic connections between parts. These may include features for modelling beam elements, rubber bushings or mounts, plus a general stiffness and damping field element. At various positions in a model rigid parts can be elastically connected together in preference to using a rigid constraint element such as a joint or joint primitive. Vehicle suspension bushes can be represented by a set of six action–reaction forces, which will hold the two parts together. The equations of force are linear and uncoupled. The user is only required to provide the six diagonal coefficients of stiffness and damping. For more complicated cases a general-purpose statement can be used to provide a linear or non-linear representation of a flexible body or connection.

Using recent advances in software techniques to allow the combination of component mode synthesis representations for the stiff, small amplitude, linear dynamic behaviour of structural elements, one or more of the major

structural parts of the system may be represented in modal form to study the influence of its flexibility on the behaviour of the system as a whole. A disadvantage of this method of working is the opportunity to consume large amounts of computing resources solving these models if care is not taken to ensure the flexibility is germane to the task at hand. Where a full representation of the flexibility of the structure is unnecessary, a simpler representation is possible using joints, 'hinges' and an associated stiffness at keypoints in the structure. This is the authors' preferred compromise between accuracy and computational efficiency. This level of abstraction requires a high degree of understanding of the structural behaviour of elements of the system and can easily lead to poorly conditioned numerical problems if carelessly performed, raising solution times drastically. Worse still, it can lead to 'plausible but wrong' answers, particularly if mass properties are poorly distributed.

Using component mode synthesis, a complete set of modal components can be used with a full vehicle comprehensive model. This approach confuses accuracy with usefulness in a manner that is becoming increasingly common. The use of such models works against volatility of design, and such models cannot be effectively used with an emerging design but belong to a new generation of mathematical prototypes for use in a later vehicle program. The notion that too much complexity is a bad thing has already been discussed in Chapter 1.

For full vehicle applications it is important to obtain an accurate model for the tyres and the associated forces generated at the tyre–road surface contact patch. For each tyre on the vehicle model the program will calculate the three orthogonal forces and three orthogonal torques acting at the wheel centre as a result of the conditions at the tyre–road surface contact patch. In order to perform these calculations it is necessary to continuously update the tyre model regarding the position, velocity and orientation of the wheel centre marker and any changes in the topography of the road surface. Once this information has been received the tyre model must then calculate the set of forces acting at the contact patch. Once these forces have been calculated they can be resolved back to the wheel centre. The multibody systems analysis program will then integrate through time to find the new position and orientation of the vehicle and then repeat the process.

A more detailed description of the modelling features available in a typical multibody systems analysis program such as the MSC.ADAMS program follows. It should be noted that commercial software is undergoing continual development and as such the description provided here is limited to the software features required to carry out the simulations described in this text. Elements such as springs, dampers, bushes and bump stops are described in this chapter as these are considered fundamental components of an MBS modelling system.

3.2 Modelling features

3.2.1 Planning the model

Before progressing to detail the methods used to describe the typical elements of a multibody systems model it is necessary to outline some of the planning that goes into the development of the model. The first step should be to sketch out a system schematic which would typically illustrate

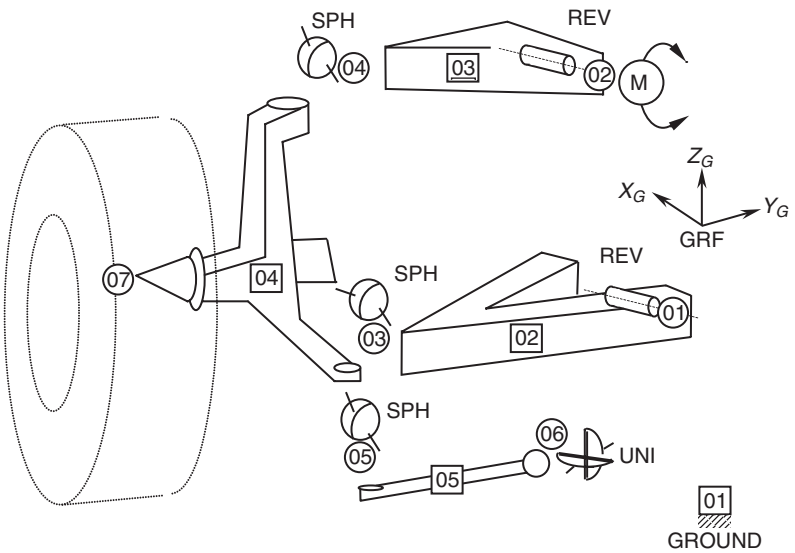

Fig. 3.2 Double wishbone suspension system schematic

items such as the parts, joints, imparted motions and applied forces. The model may well include other elements that include, for example, springs, dampers and beams. The drawing of a schematic is an important first step as it will help the user not only to plan the data that will need to be collated but more importantly to estimate the degrees of freedom in the system and develop an understanding of how the mechanism will work. The use of a modern GUI should not discourage this process. Figure 3.2 provides an example of a system schematic for a double wishbone suspension system. Users may develop their own style when drawing a schematic but the symbols shown in Figure 3.3 are provided as a suggested starting point for the sketching of the various elements of a model.

3.2.2 Reference frames

The three-dimensional description of a multibody system requires the use of reference frames, not only to set up the configuration and physical properties of the model, but also to describe the calculated outputs such as the displacements, velocities and accelerations. There are three types of right-handed Cartesian co-ordinate systems that will be used in this text:

(i) The Ground Reference Frame (GRF). This is by definition the single inertial reference frame that is considered to be fixed or at 'absolute' rest. Any point defined to belong to this reference frame has zero velocity and acceleration. The ground reference frame is taken to be fixed on a body or part known as the ground part, the physical significance of which may vary from model to model. For a single suspension model the ground part may be taken to encompass the points on the vehicle body or subframe to which the suspension linkages attach. For a full vehicle model the ground part would relate to the surface of the road used to formulate the contact forces and moments in the tyre model. In addition to providing the single inertial reference frame the ground reference frame can be considered to be the origin of

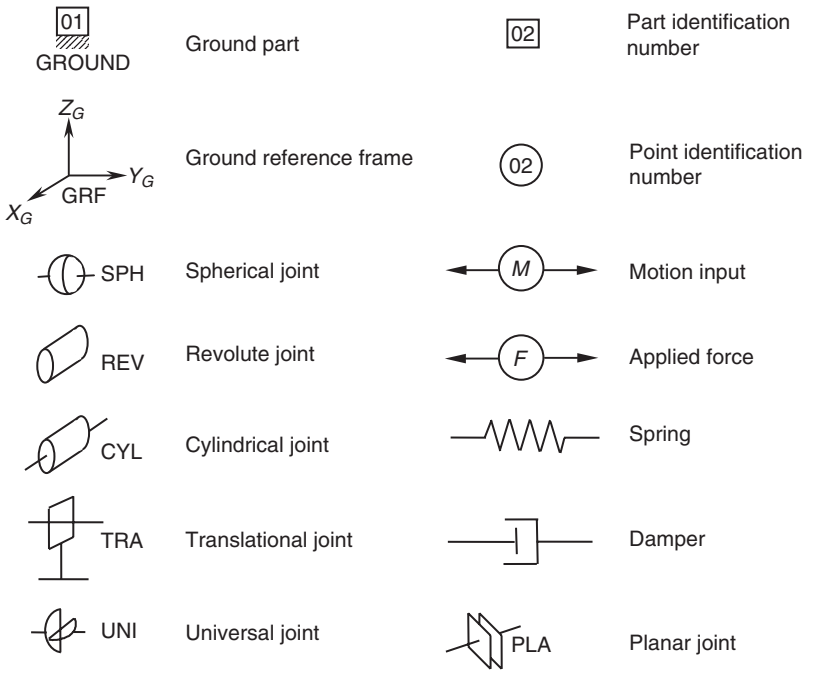

Fig. 3.3 Suggested symbols for elements of system schematic

the entire model. As such the absolute co-ordinates and orientations of all other reference frames and points in the model are measured relative to the ground reference frame. Throughout this text the ground part is taken to be the first part in the model and the ground reference frame to be the first frame O_1. Practitioners may also describe this frame as a 'global' system. The exact terminology may vary with different multibody system programs but the notion is identical between them.

(ii) The Local Part Reference Frame (LPRF). Each body or part in the system can be considered to have a local part reference frame that moves and changes orientation with the part. This is referred to in MSC.ADAMS as a body co-ordinate system (BCS). The position and orientation of the local part reference frame is defined relative to the ground reference frame. The use of a local axis system on the part may be desirable to facilitate the definition of points on the body by perhaps exploiting the symmetry of the body where the axes of symmetry, at the model definition stage, are not parallel to the axes of the ground reference frame. The use of a local part reference frame is optional and if omitted the local part reference frame can be considered to be coincident with and parallel to the ground reference frame at the model definition stage.

(iii) Markers. Markers, in MSC.ADAMS terminology, are the points located throughout the model to define, for example, mass centres, the positions of joints, the ends of springs and the graphical representation of the bodies used for subsequent animations. Markers may belong to the ground part or any moving part in the system, in which case the marker will move and rotate with the part. In some cases a marker is only required to define the

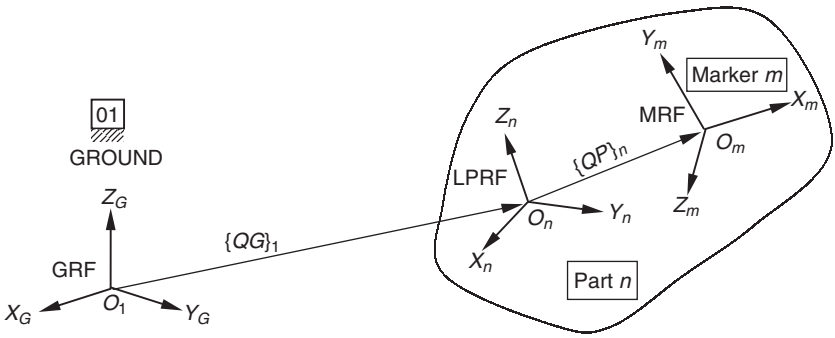

Fig. 3.4 Relative position definition of the LPRF and MRF

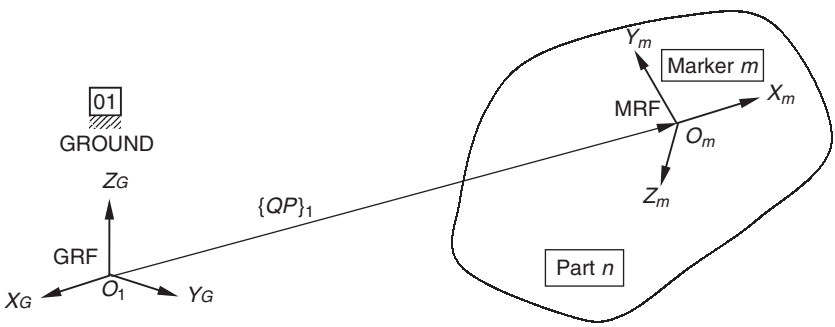

Fig. 3.5 Relative position definition of the MRF in the absence of the LPRF

co-ordinates of a point, such as the end of a spring, where a local definition of the orientation is not important. In other instances the orientation of the marker does require definition. An example of this would be the definition of revolute joints for which the axis of rotation must be specified. A marker has therefore an associated reference frame, the Marker Reference Frame (MRF), and is defined relative to the local part reference frame.

The relationship between the three reference frames, in terms of position, is illustrated in Figure 3.4. The position of the local part reference frame O_n for any body, in this case part n, is defined using, in MSC.ADAMS terminology, a position vector $\{QG\}_1$. The position of any markers belonging to part n, for example marker m with marker reference frame O_m, is defined relative to O_n, using a relative position vector $\{QP\}_n$. Note that the x, y and z components of $\{QP\}_n$ are resolved parallel to O_n.

As mentioned earlier the definition of the local part reference frame is optional and if omitted the local part reference frame is taken to be coincident with and parallel to the ground reference frame when setting up the model. The position of the marker reference frame O_m is then defined relative to the ground reference frame by the position vector $\{QP\}_1$ as illustrated in Figure 3.5. Note that the x, y and z components of $\{QP\}_1$ are now resolved parallel to the ground reference frame O_1.

There are a number of different methods by which the orientation of one reference frame to another may be established when defining a model.

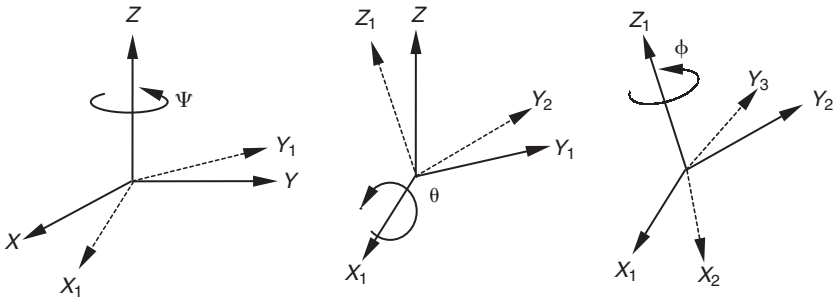

Fig. 3.6 Orientation of a frame by the Euler angle method. (This material has been reproduced from the Proceedings of the Institution of Mechanical Engineers, K2 Vol. 213 'The modelling and simulation of vehicle handling. Part 1: analysis methods', M.V. Blundell, page 110, by permission of the Council of the Institution of Mechanical Engineers)

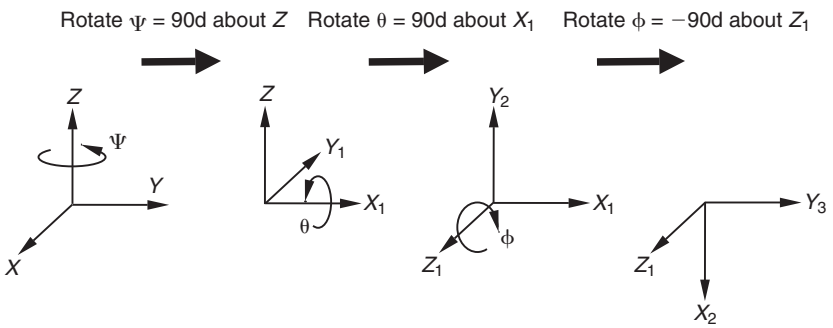

Fig. 3.7 Example application of the Euler angle method to orientate a frame

The two most commonly used methods in MSC.ADAMS are presented here and will be similar to methods used in alternative multibody systems programs. The first of these methods is a body-fixed 3-1-3 sequence of rotations as shown in Figure 3.6. This Euler angle method involves the definition of three sequential rotations ψ, θ, and ϕ. The first rotation ψ acts about the z-axis (Z) of the initial frame (X, Y, Z). The second rotation θ is about the new x-axis (X_1) of the rotated frame (X_1, Y_1, Z). The final rotation ϕ is about the z-axis (Z_1) of the second rotated frame (X_1, Y_2, Z_1).

The orientation of the positioned frame is thus the result of the three cumulative rotations and as such these will generally be difficult to envisage. In some cases the required rotations may be generated as output from a CAD package which will alleviate the problem. In other cases the Euler angles may be straightforward to derive as the positioned frame can be defined, for example, by combinations of 90 degree rotations.

The Euler angle method can be used for orientating both the local part reference frame relative to the ground reference frame and the marker reference frame relative to the local part reference frame. An example of the use of Euler angles is shown in Figure 3.7 where the (ψ, θ, ϕ) sequence is (90d, 90d, −90d), the letter d being used here to denote the use of degrees rather than radians.

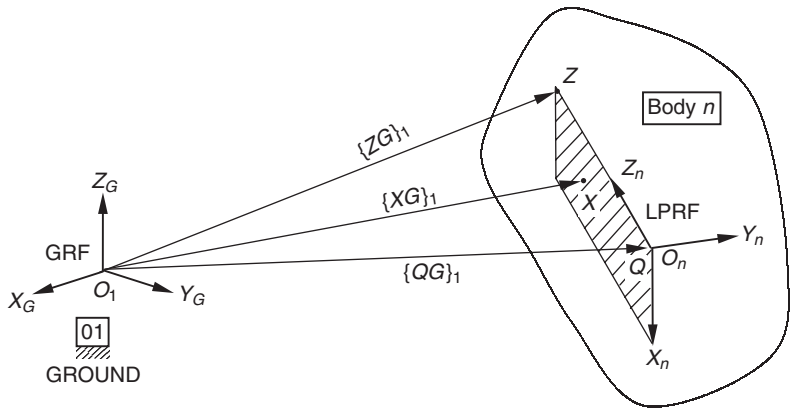

Fig. 3.8 Orientation of the local part reference frame using the *X*-point-*Z*-point method

An alternative method of orientating a reference frame is referred to as the *X*-point-*Z*-point method and involves defining the co-ordinates of a point that lies on the *Z*-axis of the positioned frame and another point that lies in the *XZ* plane of the positioned frame. This is illustrated in Figure 3.8 where this method is used to orientate the local part reference frame relative to the ground reference frame. The position of the local part reference frame, O_n, is defined, as stated earlier, by the vector $\{QG\}_1$. The point Q is coincident with O_n. The position of Z is defined to by $\{ZG\}_1$. The distance of Z from G along the Z-axis of O_n is arbitrary. The position of X is defined by $\{XG\}_1$ and may lie anywhere in the XZ plane other than on the Z-axis of O_n.

In order to determine the exact orientation of the positioned frame the vector cross product can be applied to first obtain the new Y-axis. The vector cross product of the new Y-axis and the new Z-axis can then be used to find the new X-axis. It will be seen later that if only either the X- or Z-axis is important then it is only necessary to specify either $\{XG\}_1$ or $\{ZG\}_1$.

The *X*-point-*Z*-point method can also be used to orientate a marker reference frame relative to a local part reference frame as illustrated in Figure 3.9. The notation is changed using QP, XP, ZP instead of the QG, XG, ZG used to orientate the local part reference frame. It should also be noted that as with $\{QP\}_n$ the components of $\{XP\}_n$ and $\{ZP\}_n$ would be resolved parallel to the axes of the local part reference frame O_n.

As discussed earlier if the definition of the local part reference frame is omitted the local part reference frame is taken to be coincident with and parallel to the ground reference frame when setting up the model. The orientation of the marker reference frame O_m is then defined relative to the ground reference frame. As shown in Figure 3.9 the position vector $\{QP\}_1$ would define the position of the marker reference frame and similarly $\{XP\}_1$ and $\{ZP\}_1$ would now be used to define the orientation. As with $\{QP\}_1$ the x, y and z components of $\{XP\}_1$ and $\{ZP\}_1$ are now resolved parallel to the ground reference frame O_1. It should be noted that the methods described here have been extended and are more general including the capabilty to implement parameter-based reference frames.

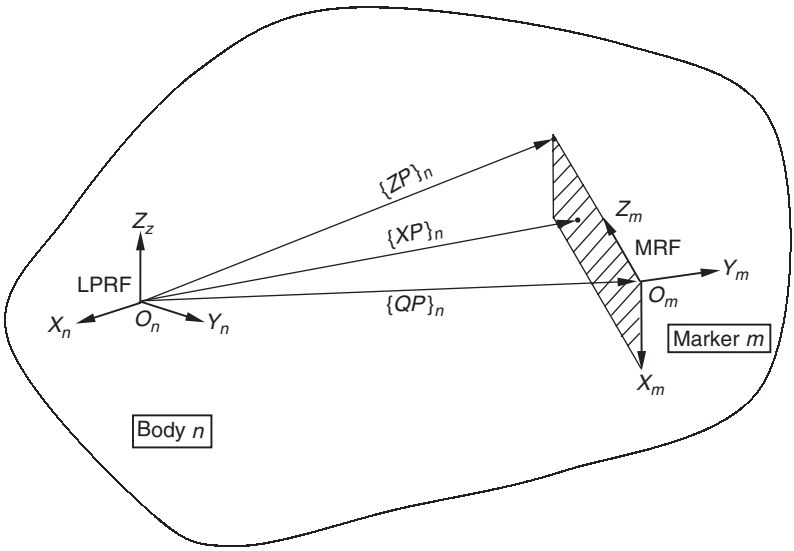

Fig. 3.9 Orientation of the marker reference frame using the *X*-point-*Z*-point method

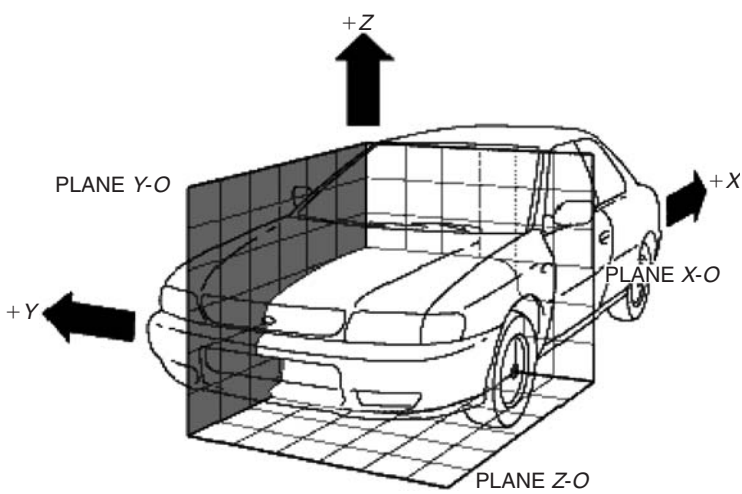

Fig. 3.10 Ground reference frame for full vehicle models

For the vehicle models described later in this text a consistent approach will be used for the ground reference frame, as shown in Figure 3.10, where the *X*-axis points back along the vehicle, the *Y*-axis points to the right of the vehicle and the *Z*-axis is up. The *XZ* plane will always be taken to be coincident with the centre line of the vehicle so as to exploit symmetry when defining, for example, the *Y* co-ordinates of left and right suspension systems.

3.2.3 Basic model components

When developing the data set for a model in a multibody systems analysis program such as MSC.ADAMS the following can be considered to be basic model components:

(i) Rigid bodies (parts)
(ii) Geometry (markers)
(iii) Constraints (joints, gears, couplers, …)
(iv) Forces (applied, spring forces, damping forces, …)
(v) User-defined algebraic and differential equations

3.2.4 Parts and markers

An example of a marker statement used to define the position and orientation of a geometric point on a part is given below.

MARKER/0200,PART=02,QP=103.0,57.5,247.2,REU=90D,90D,0D

In this example marker 0200 is defined to belong to part 02 and to be located relative to the local part reference frame of part 02 by the co-ordinates specified through the QP argument. The orientation of the axes of marker 0200 relative to the local part reference frame is specified by the Euler angle rotations, in degrees, specified by the REU argument.

The part statement can be used to define any rigid body or lumped mass. For a vehicle suspension system components such as the control arms and wheel knuckle would typically be modelled as rigid bodies. The type of analysis being performed will dictate the amount of data that must be defined for the body. For a dynamic analysis a full definition will be required to include the mass, centre of mass position, the mass moments of inertia, the orientation of the axes about which the mass moments of inertia are measured and any initial translational and angular velocities to be applied to the body. As mentioned earlier it is also possible to define a local part reference frame to which any markers belonging to the part can be referenced. Every input deck will also include a ground part. The following are two examples of a part statement:

```
PART/01,GROUND
PART/02,MASS=10.5,CM=0200,IP=3.8E3,0.02E3,3.8E3,
  VX=−25000,WZ=90.2
```

The first of these defines the ground part. Using the system of units used throughout this text the second statement defines a part with a mass of 10.5 kg with a mass centre located at the position of marker 0200. The IP argument specifies three sequential mass moments of inertia, these being the mass moments of inertia in kg mm^2 about the x-axis, y-axis and z-axis. It is possible to specify another marker belonging to the part about which these are measured but in the absence of this the mass moments of inertia are taken to be measured about the axes of marker 0200 defining the centre of mass. Since the definition does not continue to include the cross product moments of inertia it follows that the orientation of the centre of mass marker 0200 is aligned with the principal axes of the body. In this case the part has also been given a translational velocity of 25 000 mm/s. This is measured parallel to the axes of the ground reference frame. In this case the body is

moving parallel to the x-axis and in the negative direction. An angular velocity of 90.2 rad/s has also been defined. It is important to note that this is resolved using the axes of the centre of mass marker and in this case involves a positive angular velocity about the z-axis of marker 0200.

3.2.5 Equations of motion for a part

The following sections describe the formulation of the rigid body equations of motion, constraint equations and solution methods used in a general purpose MBS program such as MSC.ADAMS. The formulations are based on those given by Wielenga (1987) and are presented here using the vector methods described in Chapter 2. Although the solvers have been subject to continual development since 1987 the following will serve as an introduction to the typical calculations performed by the software. As a starting point it can be shown that kinematic variables are required to represent the location and orientation of a part with respect to the ground reference frame (GRF) as shown in Figure 3.11. Note that here we are using the general form of the position vector $\{Rn\}_1$ to locate the part rather than the equivalent $\{QG\}_1$ used in MSC.ADAMS terminology.

The location of any part is specified by a position vector $\{Rn\}_1$ from the GRF to the centre of mass, G, of the part. In this case the part is labelled as the nth part in the system and the GRF is taken to be the first frame O_1. The components of the vector $\{Rn\}_1$ are resolved parallel to the axes of the GRF as indicated by the subscript 1. The velocity is obtained using

$$\{Vn\}_1 = \frac{\mathrm{d}}{\mathrm{d}t}\{Rn\}_1 \tag{3.1}$$

The orientation of the part reference frame is specified by a set of Euler angles (ψ, ϕ, θ). Note that the Euler angles are stored in an order that differs from the sequence (ψ, θ, ϕ) used to change the orientation of a reference frame shown in Figure 3.6.

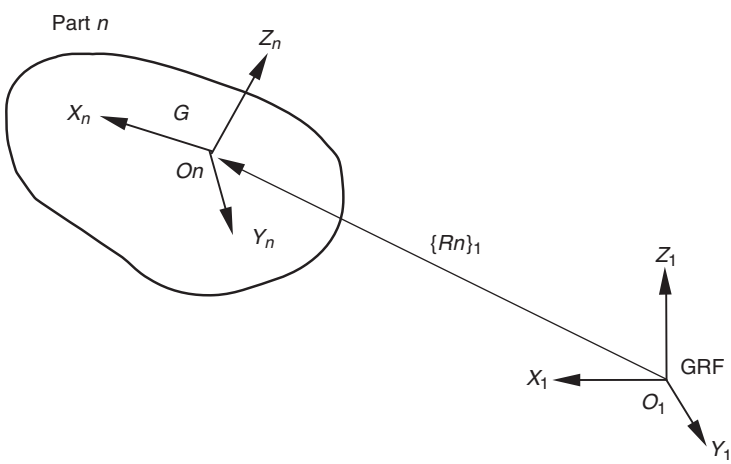

Fig. 3.11 The location and orientation of a part. (This material has been reproduced from the Proceedings of the Institution of Mechanical Engineers, K2 Vol. 213 'The modelling and simulation of vehicle handling. Part 1: analysis methods', M.V. Blundell, page 110, by permission of the Council of the Institution of Mechanical Engineers)

There are three frames of interest during the transformation. The first is the GRF (X, Y, Z) which is also frame O_1. The second is a frame made up of the axes about which each of the rotations takes place. This is known as the Euler-axis frame (Z, X_1, Z_1) and will be referred to as frame O_e. Note that this is not a reference frame in the true sense as the three axes are not perpendicular to one another. The third frame is the resulting part frame (X_2, Y_3, Z_1). For the nth part in a system this would be the part frame O_n. The matrix $[A_{1n}]$ is the Euler matrix for part n and performs the transformation from the part frame O_n to the GRF O_1:

$$[A_{1n}] = \begin{bmatrix} \cos\psi\cos\phi - \sin\psi\cos\theta\sin\phi & -\cos\psi\sin\phi - \sin\psi\cos\theta\cos\phi & \sin\psi\sin\theta \\ \sin\psi\cos\phi + \cos\psi\cos\theta\sin\phi & -\sin\psi\sin\phi + \cos\psi\cos\theta\cos\phi & -\cos\psi\sin\theta \\ \sin\theta\sin\theta & \sin\theta\cos\phi & \cos\theta \end{bmatrix} \tag{3.2}$$

Note that the inverse of this matrix $[A_{n1}]$ is simply the transpose and performs the transformation from the GRF to the part frame. Another matrix $[B]$ performs the transformation from the Euler-axis frame $O_e(Z, X_1, Z_1)$ to the part frame $O_n(X_2, Y_3, Z_1)$:

$$[B] = \begin{bmatrix} \sin\theta\sin\phi & 0 & \cos\phi \\ \sin\theta\cos\phi & 0 & -\sin\phi \\ \cos\theta & 1 & 0 \end{bmatrix} \tag{3.3}$$

Note that this matrix becomes singular when $\sin\theta = 0$. This corresponds to the situation where Z and Z_1 are parallel and point in the same direction ($\theta = 0$), or parallel and point in the opposite direction ($\theta = 180$ degrees). When this occurs an internal adjustment is used to set up a new part frame where the Z_1-axis is rotated through 90 degrees. Note also that the $[B]$ matrix corresponds with an internal reordering of the Euler angles to (Z, Z_1, X_1).

For large rotations the set of Euler angles for the nth part $\{\gamma n\}_e = [\psi n\ \phi n\ \theta n]^T$ cannot actually be represented by a vector as indicated here although they can be considered to make up a set of kinematic orientation variables for the nth part. An infinitesimal change in orientation in the part frame O_n can, however, be represented by a vector which will be denoted $\{\delta\gamma n\}_n$. In a similar manner an infinitesimal change in the Euler angles can be represented by a vector $\{\delta\gamma n\}_e$. The angular velocity vector for the part in the local part frame can also be specified by $\{\omega n\}_n$. MSC.ADAMS also requires the components of these vectors in the Euler-axis frame O_e. The angular velocity in the Euler-axis frame is simply the time derivative of the Euler angles:

$$\{\omega n\}_e = \frac{\mathrm{d}}{\mathrm{d}t}\{\gamma n\}_e \tag{3.4}$$

The transformation between the part frame and the Euler-axis frame is established using the $[B]$ matrix:

$$\{\delta\gamma n\}_n = [B]\{\delta\gamma n\}_e \tag{3.5}$$

$$\{\omega n\}_n = [B]\{\omega n\}_e \tag{3.6}$$

In summary there are now a set of kinematic position and velocity variables for the *n*th part with components measured in the GRF and also a set of orientation and angular velocity variables measured about the Euler-axis frame:

$$\{Rn\}_1 = [Rnx\ Rny\ Rnz]^T \tag{3.7}$$

$$\{Vn\}_1 = [Vnx\ Vny\ Vnz]^T \tag{3.8}$$

$$\{\gamma n\}_e = [\psi n\ \phi n\ \theta n]^T \tag{3.9}$$

$$\{\omega n\}_e = [\omega n\psi\ \omega n\phi\ \omega n\theta]^T \tag{3.10}$$

There is also a set of kinematic equations associated with the part which may be simply stated as:

$$\{Vn\}_1 = \frac{\mathrm{d}}{\mathrm{d}t}\{Rn\}_1 \tag{3.11}$$

$$\{\omega n\}_e = \frac{\mathrm{d}}{\mathrm{d}t}\{\gamma n\}_e \tag{3.12}$$

The remaining part variables and equations are those obtained by considering the equations of motion for a rigid body. Each part can be considered to have a set of six generalized co-ordinates given by

$$q_j = [Rnx, Rny, Rnz, \psi n, \theta n, \phi n] \tag{3.13}$$

The translational co-ordinates are the translation of the centre of mass measured parallel to the axes of the ground reference frame while the rotational co-ordinates are provided by the Euler angles for that part. For any part the translational forces are therefore summed in the X, Y and Z directions of the GRF while the summation of moments takes place at the centre of mass and about each of the axes of the Euler-axis frame. Using a form of the Lagrange equations this can be shown as:

$$\frac{\mathrm{d}}{\mathrm{d}t}\left(\frac{\partial T}{\partial \dot{q}_j}\right) - \frac{\partial T}{\partial q_j} - Q_j + \sum_{i=1}^{n}\frac{\partial \Phi_i}{\partial q_j}\lambda_i = 0 \tag{3.14}$$

The kinetic energy T is expressed in terms of the generalized co-ordinates q_j and is given by

$$T = \frac{1}{2}\{Vn\}_1^T m\{Vn\}_1 + \frac{1}{2}\{\omega n\}_e^T [B]^T [I_n][B]\{\omega n\}_e \tag{3.15}$$

The mass properties are specified by m which is the mass of the part and $[I_n]$ which is the mass moment of inertia tensor for the part and given by

$$[I_n] = \begin{bmatrix} I_{xx} & I_{xy} & I_{xz} \\ I_{yx} & I_{yy} & I_{yz} \\ I_{zx} & I_{zy} & I_{zz} \end{bmatrix} \tag{3.16}$$

The terms Φ and λ represent the reaction force components acting in the direction of the generalized co-ordinate q_j. The term Q_j represents the sum of the applied force components acting on the part and in the direction of the generalized co-ordinate q_j. The equation can be simplified by introducing

a term for the momenta P_j associated with motion in the q_j direction, and a term C_j to represent the constraints:

$$P_j = \frac{\partial T}{\partial \dot{q}_j} \tag{3.17}$$

$$C_j = \sum_{i=1}^{n} \frac{\partial \Phi_i}{\partial q_j} \lambda_i \tag{3.18}$$

This results in the equation:

$$\dot{P}_j - \frac{\partial T}{\partial q_j} - Q_j + C_j = 0 \tag{3.19}$$

By way of example consider first the equations associated with the translational co-ordinates. The generalized translational momenta $\{Pn_t\}_1$ for the part can be obtained from:

$$\{An\}_1 = \frac{\mathrm{d}}{\mathrm{d}t}\{Vn\}_1 \tag{3.20}$$

$$\{Pn_t\}_1 = \partial T/\partial\{Vn\}_1 = m\{Vn\}_1 \tag{3.21}$$

$$\frac{\mathrm{d}}{\mathrm{d}t}\{Pn_t\}_1 = m\{An\}_1 \tag{3.22}$$

This results in $\{An\}_1$ as the acceleration of the centre of mass for that part. It should also be noted that the kinetic energy is dependent on the velocity but not the position of the centre of mass, $\partial T/\partial\{Rn\}_1$ is equal to zero. We can now write the equation associated with translational motion in the familiar form:

$$m\{An\}_1 - \Sigma\{Fn_A\}_1 + \Sigma\{Fn_C\}_1 = 0 \tag{3.23}$$

where $\{Fn_A\}_1$ and $\{Fn_C\}_1$ are the individual applied and constraint reaction forces acting on the body. The rotational momenta $\{Pn_r\}_e$ for the part can be obtained from:

$$\{Pn_r\}_e = \partial T/\partial\{\omega n\}_e = [B]^T[I_n][B]\{\omega n\}_e \tag{3.24}$$

We can now write the equations associated with rotational motion in the form:

$$\{Pn_r\}_e - \partial T/\partial\{\gamma n\}_e - \Sigma\{Mn_A\}_e + \Sigma\{Mn_C\}_e = 0 \tag{3.25}$$

$$\{Pn_r\}_e = [B]^T[I_n][B]\{\omega n\}_e \tag{3.26}$$

In this case $\{Mn_A\}_e$ and $\{Mn_C\}_e$ are the individual applied and constraint reaction moments acting about the Euler-axis frame at the centre of mass of the body. Introducing the equation above for the rotational momenta introduces an extra three variables and equations for each part.

The 15 variables for each part are:

$$\{Rn\}_1 = [Rnx\ Rny\ Rnz]^T \tag{3.27}$$

$$\{Vn\}_1 = [Vnx\ Vny\ Vnz]^T \tag{3.28}$$

$$\{\gamma n\}_e = [\psi n\ \phi n\ \theta n]^T \tag{3.29}$$

$$\{\omega n\}_e = [\omega\psi n\ \omega\phi n\ \omega\theta n]^T \tag{3.30}$$

$$\{Pn_r\}_e = [P\psi n\ P\phi n\ P\theta n]^T \tag{3.31}$$

The 15 equations for each part are:

$$\{Vn\}_1 = \frac{\mathrm{d}}{\mathrm{d}t}\{Rn\}_1 \tag{3.32}$$

$$\{\omega n\}_e = \frac{\mathrm{d}}{\mathrm{d}t}\{\gamma n\}_e \tag{3.33}$$

$$\{Pn_r\}_e = [B]^T[I_n][B]\{\omega n\}_e \tag{3.34}$$

$$m\{An\}_1 - \Sigma\{Fn_A\}_1 + \Sigma\{Fn_C\}_1 = 0 \tag{3.35}$$

$$\{Pn_r\}_e - \partial T/\partial\{\gamma n\}_e - \Sigma\{Mn_A\}_e + \Sigma\{Mn_C\}_e = 0 \tag{3.36}$$

3.2.6 Basic constraints

Constraints are used to restrict the motion of parts. There are a number of modelling elements that can be used to do this and the constraint may restrict the absolute motion of a body relative to the ground or the relative motion between interconnected parts. Constraints can be considered to be of two types:

(i) Holonomic constraints are those which are dependent on restricting displacement and result in algebraic equations.

(ii) Non-holonomic constraints are those where a velocity dependent motion is enforced and result in differential equations.

There are a wide range of constraint elements available ranging from joint primitives that can constrain combinations of individual degrees of freedom between bodies through mechanical type joints and gear elements to higher pair constraints such as those constraining a point to lie on a curve. The examples shown here are restricted to those that are used to support the examples used in this text.

A typical example of a joint primitive is the use of an inplane type of constraint that restricts the motion of a point on one body to remain in a plane on another body. A typical example of this is given later when the vertical motion of individual suspension models is controlled by using a jack to impart motion to the wheel centre as shown in Figure 3.12.

In this example the I marker is defined to belong to the wheel knuckle and is located at the wheel centre. The J marker is defined to belong to the jack part and will move vertically with that part according to other constraints that control its motion. The orientation of the J marker must be defined in this case so that the *x*- and *y*-axes define the surface plane of the jack in which the I marker will be constrained to remain. For simplicity the jack in Figure 3.12 is shown below the wheel but in actual fact it would be defined to locate the *xy* plane of J at the wheel centre. The orientation of the I marker is not important but the J marker must be defined as shown. In this case the *z* direction of the J marker is parallel to the *z*-axis of the ground reference frame

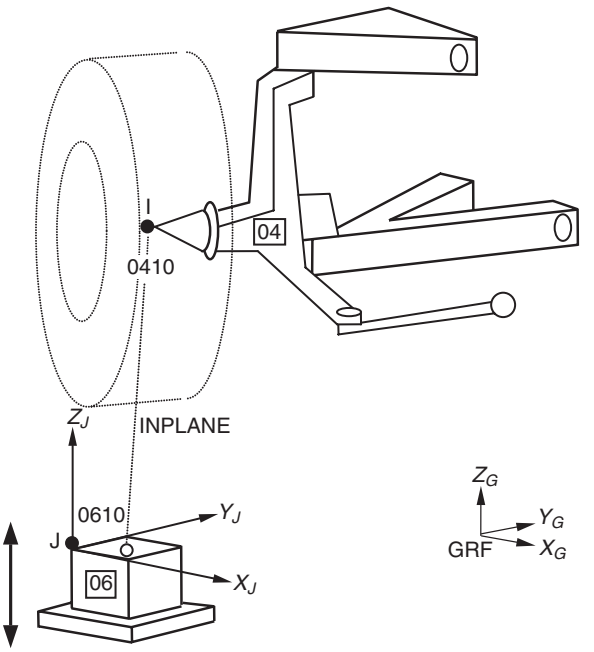

Fig. 3.12 Application of inplane joint primitive

so no further definition is required to change the orientation of the J marker. If this was not the case the *ZP* method is often the most convenient method to orientate the *z*-axis of the J marker normal to the surface of the plane.

An example of the statement used to generate the inplane joint primitive in this example is shown below:

JPRIM/10,I=0410,J=0610,INPLANE

In this case the I marker on the wheel is identified as 0410 and the J marker on the jack is defined as 0610. This joint primitive would constrain the single translational degree of freedom between the I marker and the J marker in the direction normal to the *xy* plane of the jack. In other words the I marker has five degrees of freedom relative to the top surface of the jack defined by the *xy* plane of the J marker. The I marker can translate in the J marker *X* and *Y* directions and is free to rotate about all axes. There are further types of joint primitive in addition to the inplane type introduced here. Others, for example, can constrain a marker on one body to follow a line defined on another body or can constrain the orientation of two markers on different bodies to remain parallel wherever those markers may be in the system model.

The various joints and joint primitives can be developed using combinations of four basic constraint elements. For each constraint the resulting forces and moments need to be added into the force and moment balance for a part. Consider first the basic *atpoint* constraint element shown in Figure 3.13 which constrains a point I on one part to remain at the same location in space as a point J on another part, but does not prevent any relative rotation between the two points.

This constraint can be represented by a vector constraint equation working in co-ordinates parallel to the axes of the GRF:

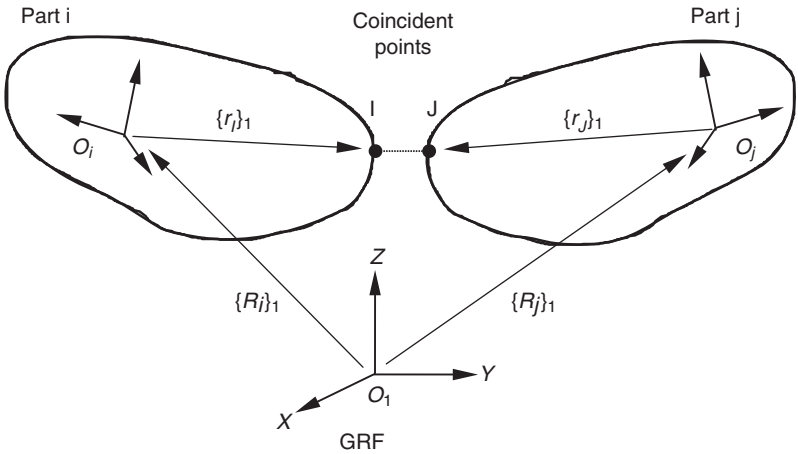

Fig. 3.13 Atpoint constraint element. (This material has been reproduced from the Proceedings of the Institution of Mechanical Engineers, K2 Vol. 213 'The modelling and simulation of vehicle handling. Part 1: analysis methods', M.V. Blundell, page 114, by permission of the Council of the Institution of Mechanical Engineers)

$$\{\Phi_a\}_1 = (\{R_i\}_1 + \{r_I\}_1) - (\{R_j\}_1 + \{r_J\}_1) = \{0\} \tag{3.37}$$

This expression may be simplified by introducing a vector term $\{d_{IJ}\}_1$ to represent the constrained displacement between the I and the J marker:

$$\{d_{IJ}\}_1 = (\{R_i\}_1 + \{r_I\}_1) - (\{R_j\}_1 + \{r_J\}_1) \tag{3.38}$$

The reaction force on part i can be represented by the vector $\{\lambda\}_1$ with a moment given by $\{r_I\}_1 \times \{\lambda\}_1$. Applying Newton's third law the reaction force on part j can be represented by the vector $-\{\lambda\}_1$ with a moment given by $-\{\lambda\}_1 \times \{r_J\}_1$. In order to complete the calculation the contribution to the term $\Sigma\{Mn_C\}_e$ in equation (3.36) a transformation of the moments into the co-ordinates of the part Euler-axis frame is required. For part i this would be achieved using $[B_i]^T\{r_I\}_i \times [A_{i1}]\{\lambda\}_1$. For part j this would be achieved using $-[B_j]^T\{r_J\}_i \times [A_{j1}]\{\lambda\}_1$.

The second basic constraint element constrains a point on one part to remain fixed within a plane on another part and is known as the *inplane* constraint or joint primitive an application of which was shown earlier in Figure 3.12. As such it removes one degree of freedom out of the plane as shown in Figure 3.14.

The plane is defined by a unit vector $\{a_J\}_1$ fixed in part j and perpendicular to the plane. The I marker belonging to part i is constrained to remain in the plane using the vector dot (scalar) product to enforce perpendicularity:

$$\{d_{IJ}\}_1 \bullet \{a_J\}_1 = 0 \tag{3.39}$$

Expanding this using the definition given for $\{d_{IJ}\}_1$ in equation (3.38) gives the full expression for the constraint Φ_d:

$$\Phi_d = [(\{R_i\}_1 + \{r_I\}_1) - (\{R_j\}_1 + \{r_J\}_1)] \bullet \{a_J\}_1 = 0 \tag{3.40}$$

This constraint can be represented by a vector constraint equation working in co-ordinates parallel to the axes of the GRF. The magnitude of the reaction

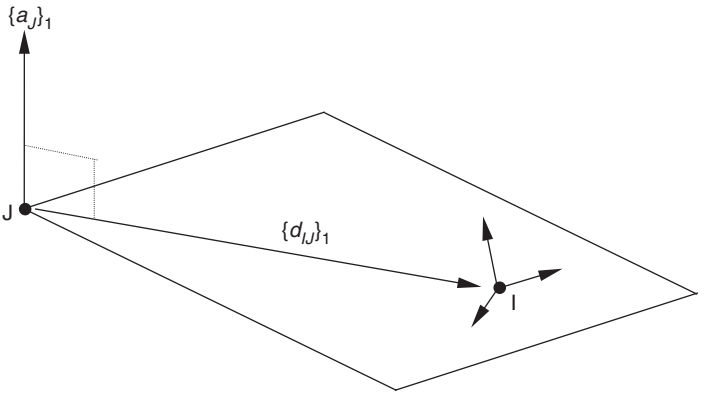

Fig. 3.14 Inplane constraint element. (This material has been reproduced from the Proceedings of the Institution of Mechanical Engineers, K2 Vol. 213 'The modelling and simulation of vehicle handling. Part 1: analysis methods', M.V. Blundell, page 114, by permission of the Council of the Institution of Mechanical Engineers)

force corresponding to this constraint can be represented by a scalar term λ_d. The reaction force on part i can be represented by the vector $\{a_J\}_1\lambda_d$ with a moment given by $\{r_I\}_1 \times \{a_J\}_1\lambda_d$. Applying Newton's third law again the reaction force on part j can be represented by the vector $-\{a_J\}_1\lambda_d$. The moment contribution to part j is given by $-(\{r_J\}_1 + \{d_{IJ}\}_1) \times \{a_J\}_1\lambda_d$.

Expanding this again using the definition given for $\{d_{IJ}\}_1$ in equation (3.38) gives $-(\{R_i\}_1 + \{r_I\}_1 - \{R_j\}_1) \times \{a_J\}_1\lambda_d$. In order to complete the calculation the contribution to the term $\Sigma\{Mn_C\}_e$ in equation (3.36) a transformation of the moments into the co-ordinates of the part Euler-axis frame is needed.

For part i this would be achieved using $[B_i]^T\{r_I\}_i \times [A_{ij}]\{a_J\}_1\lambda_d$.

For part j this would be achieved using $[B_j]^T\{a_J\}_j \times [A_{j1}](\{R_i\}_1 + [A_{1i}]\{r_I\}_i - \{R_j\}_1)\lambda_d$.

The third basic constraint element constrains a unit vector fixed in one part to remain perpendicular to a unit vector located in another part and is known as the *perpendicular* constraint. The constraint shown in Figure 3.15 is defined using a unit vector $\{a_J\}_1$ located at the J marker in part j and a unit vector $\{a_I\}_1$ located at the I marker belonging to part i.

The vector dot (scalar) product is used to enforce perpendicularity as shown in equation (3.41):

$$\Phi_p = \{a_I\}_1 \bullet \{a_J\}_1 = 0 \tag{3.41}$$

The constraint can be considered to be enforced by equal and opposite moments acting on part i and part j. The constraint does not contribute any forces to the part equations but does include the scalar term λ_p in the formulation of the moments. The moment acting on part i is given by $\{a_I\}_1 \times \{a_J\}_1\lambda_p$ Applying Newton's third law the moment acting on part j is given by $-\{a_I\}_1 \times \{a_J\}_1\lambda_p$. The moments must be transformed into the co-ordinates of the part Euler-axis frame.

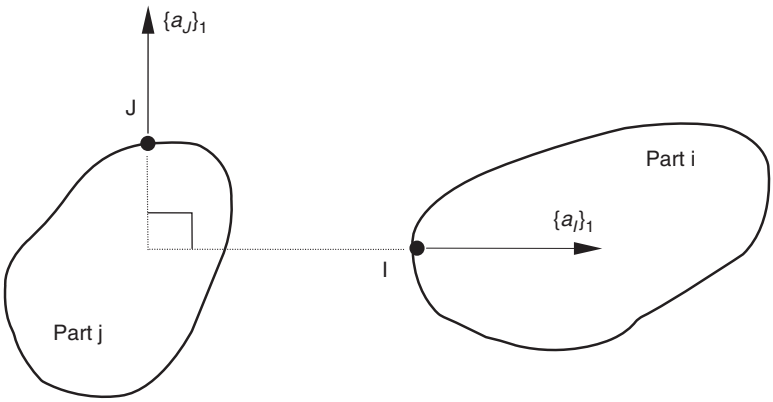

Fig. 3.15 Perpendicular constraint element. (This material has been reproduced from the Proceedings of the Institution of Mechanical Engineers, K2 Vol. 213 'The modelling and simulation of vehicle handling. Part 1: analysis methods', M.V. Blundell, page 115, by permission of the Council of the Institution of Mechanical Engineers)

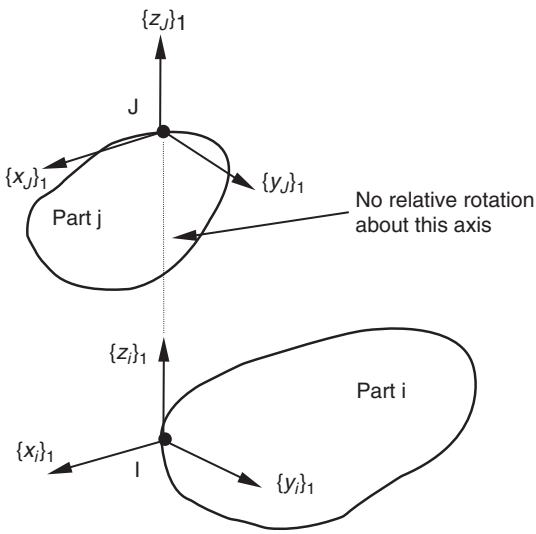

Fig. 3.16 Angular constraint element. (This material has been reproduced from the Proceedings of the Institution of Mechanical Engineers, K2 Vol. 213 'The modelling and simulation of vehicle handling. Part 1: analysis methods', M.V. Blundell, page 115, by permission of the Council of the Institution of Mechanical Engineers)

For part i this would be achieved using $[B_i]^T\{a_I\}_i \times [A_{ij}]\{a_J\}_j\lambda_p$.

For part j this would be achieved using $[B_j]^T\{a_J\}_j \times [A_{ji}]\{a_I\}_i\lambda_p$.

The fourth and final basic constraint element is the *angular* constraint which prevents the relative rotation of two parts about a common axis. The constraint equation is:

$$\Phi_\alpha = \arctan\left(\{x_i\}_1 \bullet \{y_j\}_1 / \{x_i\}_1 \bullet \{x_j\}_1\right) = 0 \tag{3.42}$$

Table 3.1 Basic constraint element equations

Constraint	Full equation	Abbreviated form
Atpoint	$\{\Phi_a\}_1 = (\{R_i\}_1 + \{r_I\}_1) - (\{R_j\}_1 + \{r_J\}_1)$	$\{d_{IJ}\}_1$
Inplane	$\Phi_d = [(\{R_i\}_1 + \{r_I\}_1) - (\{R_j\}_1 + \{r_J\}_1)] \bullet \{a_J\}_1$	$\{d_{IJ}\}_1 \bullet \{a_J\}_1$
Perpendicular	$\Phi_p = \{a_I\}_1 \bullet \{a_J\}_1$	$\{a_I\}_1 \bullet \{a_J\}_1$
Angular	$\Phi_\alpha = \arctan(\{x_i\}_1 \bullet \{y_j\}_1 / \{x_i\}_1 \bullet \{x_j\}_1)$	α_{IJ}

Table 3.2 Force contributions for basic constraint elements

Constraint	Part i force	Part j force
Atpoint	$\{\lambda\}$	$-\{\lambda\}$
Inplane	$[A_{1_j}]\{a_J\}_j\lambda_d$	$-[A_{1_j}]\{a_J\}_j\lambda_d$
Perpendicular	0	0
Angular	0	0

Table 3.3 Moment contributions for basic constraint elements

Constraint	Part i moment	Part j moment
Atpoint	$[B_i]^T\{r_I\}_i \times [A_{i1}]\lambda$	$[B_j]^T\{r_J\}_i \times [A_{j1}]\lambda$
Inplane	$[B_i]^T\{r_I\}_i \times [A_{ij}]\{a_J\}_j\lambda_d$	$[B_j]^T\{a_J\}_j \times [A_{j1}](\{R_i\}_1 + [A_{1i}]\{r_I\}_i - \{R_j\}_1)\lambda_d$
Perpendicular	$[B_i]^T\{a_I\}_i \times [A_{ij}]\{a_J\}_j\lambda_p$	$[B_j]^T\{a_J\}_j \times [A_{ji}]\{a_I\}_i\lambda_p$
Angular	$[B_i]^T\{z_i\}_i\lambda_\alpha$	$-[B_j]^T\{z_j\}_j\lambda_\alpha$

In applying this constraint it is assumed that other system constraints will maintain the z-axes of the two parts to remain parallel as shown in Figure 3.16.

The moment acting on part i is given by $\{z_i\}_1\lambda_\alpha$ and on part j by $-\{z_j\}_1\lambda_\alpha$. Transforming into the Euler axis system for each part gives a moment in the co-ordinate system for part i equal to $[B_i]^T\{z_i\}_i\lambda_\alpha$ and on part j by $-[B_j]^T\{z_j\}_j\lambda_\alpha$.

The equations associated with each of the four basic constraint elements are summarized in Table 3.1.

The force and moment contributions to each part in the generalized co-ordinates are summarized in Table 3.2 and Table 3.3.

3.2.7 Standard joints

As stated there are a number of mechanical type joints that may be used to constrain the motion of bodies. Examples of some of the most commonly used joints are shown in Figure 3.17.

Of the joints shown in Figure 3.17 the spherical, revolute, translational, cylindrical and universal will figure most prominently in this text, particularly with regard to the modelling of suspension systems. The concept of an I marker on one part connecting to a J marker on another part is used again for joint elements. An example of the syntax used to define a joint in MSC.ADAMS is shown below:

JOINT/02,I=0602,J=0902,SPH

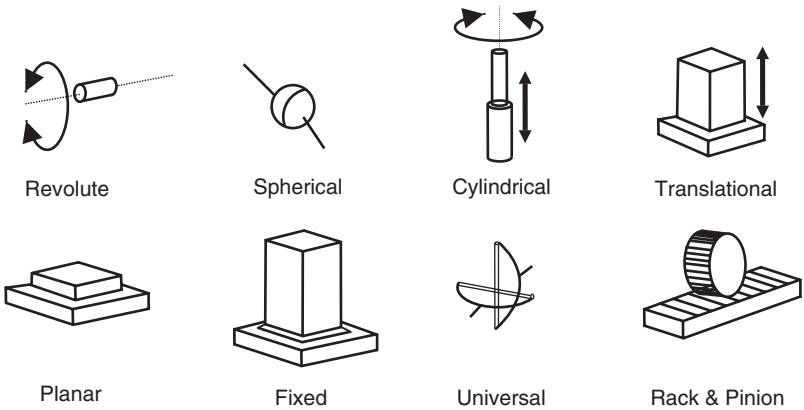

Fig. 3.17 Examples of commonly used joint constraints. (This material has been reproduced from the Proceedings of the Institution of Mechanical Engineers, K2 Vol. 213 'The modelling and simulation of vehicle handling. Part 1: analysis methods', M.V. Blundell, page 108, by permission of the Council of the Institution of Mechanical Engineers)

Table 3.4 Joint constraints in MSC.ADAMS

Joint type	Constraints			Abbreviated equation
	Trans'	Rot'	Total	
Spherical	3	0	3	$\{d_{IJ}\}_1 = 0$
Planar	1	2	3	$\{z_I\}_i \bullet \{x_J\}_j = 0, \{z_I\}_i \bullet \{y_J\}_j = 0, \{d_{IJ}\}_1 \bullet \{z_J\}_j = 0$
Universal	3	1	4	$\{d_{IJ}\}_1 = 0, \{z_I\}_i \bullet \{z_J\}_j = 0$
Cylindrical	2	2	4	$\{z_I\}_i \bullet \{x_J\}_j = 0, \{z_I\}_i \bullet \{y_J\}_j = 0, \{d_{IJ}\}_1 \bullet \{x_J\}_j = 0, \{d_{IJ}\}_1 \bullet \{y_J\}_j = 0$
Revolute	3	2	5	$\{d_{IJ}\}_1 = 0, \{z_I\}_i \bullet \{x_J\}_j = 0, \{z_I\}_i \bullet \{y_J\}_j = 0$

For a spherical joint the I marker and J marker are defined to be coincident at the centre of the joint but the orientation of the markers is irrelevant. For other joints such as the revolute, cylindrical and translational it is necessary not only to position the joint through the co-ordinates of the I and J marker but also to define the orientation of the axis associated with the mechanical characteristics, rotation and/or translation, of the joint. The method used in MSC.ADAMS is to use the local z-axis of the markers to define the axis, the most convenient method of doing this often being to define a *ZP* parameter for each marker. For the universal joint the axes of the spindles need to be defined perpendicular to one another. For this joint the I and J marker are defined to be coincident with the z-axis of each orientated to suit the axis of the spindle on the side of the joint associated with the body to which the marker belongs.

The vector equations that have been derived earlier for the basic constraints can be applied in a similar manner to generate constraint equations for the standard joints. A spherical joint, for example, fulfils exactly the same function as an atpoint joint primitive. Examples of constraint equations for some commonly used joints are shown in Table 3.4.

It is also possible to define initial conditions associated with a joint such as a revolute, translational or cylindrical. These are defined to be translational or rotational according to the characteristics of the associated joint. An example is shown below for a cylindrical joint that is defined to have an initial translational velocity of zero but a starting displacement of 100 mm. At this stage it is important to note that the ordering and direction of the z-axes of the markers are important. For the example below this would in physical terms define a 100 mm translation of the I marker 0703 relative to the J marker 0403 in the direction defined by the positive z-axis of both markers:

JOINT/03,I=0703,J=0403,CYL,ICTRAN=0,100

The initial condition is enforced at the start of analysis but released once the simulation commences, in other words after time equals zero. For translational, revolute and cylindrical joints it is also possible to constrain the movement of the joint during the simulation using a motion statement of the type shown below:

MOTION/04,JOINT=04,ROT,FUNCTION=360D*TIME

For the joint referenced it is necessary to define a functional equation, normally only dependent on time, that controls the movement of the I marker relative to the J marker at the associated joint. In the example shown here the function is defining a rotation of 360 degrees, or one revolution, for every second of time taken and as positive when rotating about the z-axes of the markers. It will be seen later that the functional equation can be extended to encompass more complex formulations using a library of off-the-shelf mathematical functions and expressions of the type associated with engineering or scientific programming software. Newcomers to multibody systems analysis often find the concept of a defined motion being a constraint difficult to grasp as the modelling element involves movement. The motion statement here constrains the associated degree of freedom at the joint. The movement defined by the function is enforced and cannot be altered by, for example, changes to the mass properties of the bodies or the introduction of external forces. It should also be noted that where a motion is applied to a joint it would be inconsistent to specify initial conditions for the degree of freedom associated with the motion at the joint.

Another constraint element that will be used in this text is referred to as a coupler and is used to constrain, or couple, the movement of two or three joints by applying scale factors. The main application of a coupler in this text is to represent the mechanical behaviour of a steering box and so define the ratio between the rotation of the steering column and the rack. A more detailed description of the modelling issues for this is given later in Chapter 6. An example of a coupler statement is given below:

COUPLER/0305,JOINTS=03,04,TYPE=T:R,SCALES=22D,-5

Care is needed with the syntax and ordering of this statement as can be seen when we develop the algebraic equation that it represents. The coupler defined here relates the translational motion at joint 03 with the rotational motion at joint 04. The scale factors provided define the relationship as

$$22\mathrm{D} \times q4 - 5 \times q3 = 0 \quad \text{or} \quad 22\mathrm{D} \times q6 = 5 \times q3 \tag{3.43}$$

In this case $q3$ is the translational motion at joint 03 and $q4$ is the rotational motion at joint 04. So for every 22 degrees of rotation at joint 04 there is a

corresponding 5 mm of travel at joint 03. Note again that the ordering and orientation of the markers defining the coupled joints is critical if the correct physical representation of the system is to be obtained. At joint 03 the motion is that of the I marker relative to the J marker in the positive direction of the z-axes of the markers. At joint 04 the motion is taken to be a positive rotation of the I marker relative to the J marker about the z-axes of the markers. The coupler does not take into account mechanical features such as play in the joints or backlash and as such does not model the reaction forces within the real mechanism. The coupler also does not consider one joint to drive the other. This will be a function of other forces defined elsewhere in the system model. As with the motion statement a degree of freedom is lost to the system as the coupler has enforced a kinematic relationship between the motion at joints that cannot be changed by external forces.

3.2.8 Degrees of freedom

Having introduced the modelling of rigid bodies and constraints it is now possible to describe the determination of the degrees of freedom (DOF) in a mechanical system. The starting point for this is to consider that any free-floating rigid body in three-dimensional space will have six degrees of freedom as shown in Figure 3.18. For the vehicle body shown here and for the handling simulations that will be discussed later the body will have no direct constraint connecting it to the ground part. The only contact will be through the forces and moments generated by a tyre model. For the axis system shown here the vehicle will have degrees of freedom associated with translational motion in the longitudinal direction X, the lateral direction Y and the vertical direction Z. The rotational motions will involve roll about the x-axis, pitch about the y-axis and yaw about the z-axis. For vehicles such as ships and aircraft the terms surge, sway and heave are used to describe the translational motions but these are not commonly used in vehicle dynamics. It should also be noted that for the examples in this text the x-axis is taken to point towards the rear of the vehicle where in other texts discussing vehicle motion this is often forward to be consistent with the normal direction of travel.

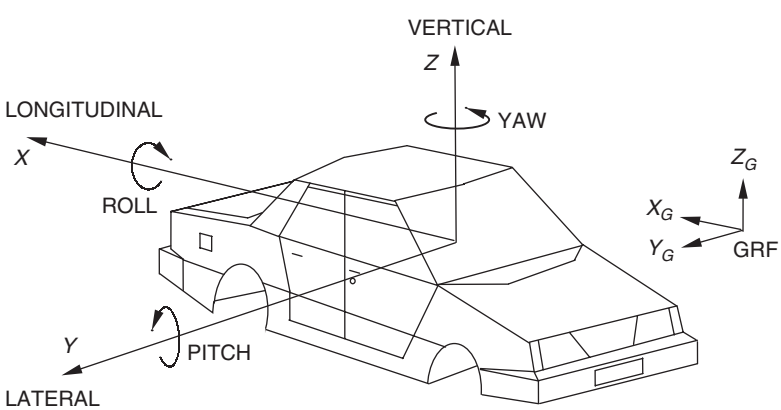

Fig. 3.18 Degrees of freedom associated with an unconstrained rigid body

For any multibody systems model it is important that the analyst can determine and understand the total degrees of freedom in the system. This can be achieved by using the Gruebler equation:

$$\textit{Total DOF} = 6 \times (\textit{Number of parts} - 1) - (\textit{Number of constraints}) \quad (3.44)$$

The parts count in (3.44) is reduced by one to account for the fact that the non-moving ground is counted as a part in the system. The degrees of freedom removed by typical constraint elements are summarized in Table 3.5 and may be used to complete the calculation.

At this stage it is necessary to introduce the subject of redundant constraints and overconstraint checking. As a starting point consider a typical application in a suspension that involves the modelling of the mounts attaching a control arm or wishbone to the body or chassis. This is illustrated in Figure 3.19

Table 3.5 Degrees of freedom removed by constraint elements

Constraint element	Translational constraints	Rotational constraints	Coupled constraints	Total constraints
Cylindrical joint	2	2	0	4
Fixed joint	3	3	0	6
Planar joint	1	2	0	3
Rack-and-pinion joint	0	0	1	1
Revolute joint	3	2	0	5
Spherical joint	3	0	0	3
Translational joint	2	3	0	5
Universal joint	3	1	0	4
Atpoint joint primitive	3	0	0	3
Inline joint primitive	2	0	0	2
Inplane joint primitive	1	0	0	1
Orientation joint primitive	0	3	0	3
Parallel joint primitive	0	2	0	2
Perpendicular joint primitive	0	1	0	1
Motion (translational)	1	0	0	1
Motion (rotational)	0	1	0	1
Coupler	0	0	1	1

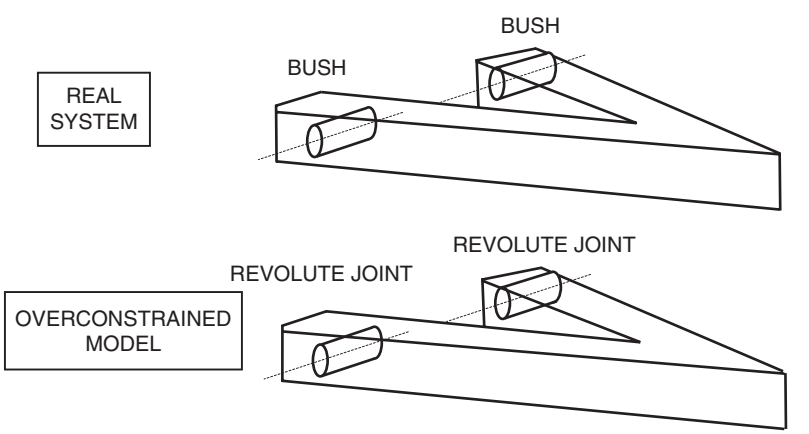

Fig. 3.19 Redundant constraints in a suspension model

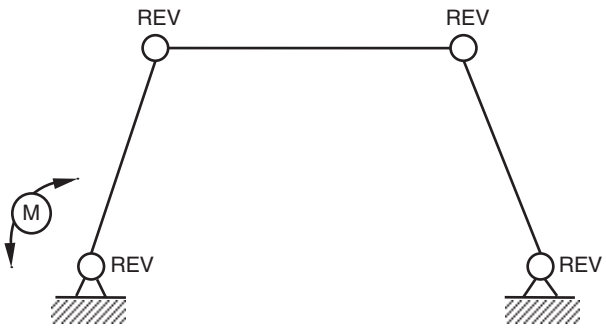

Fig. 3.20 Overconstrained four-bar linkage problem

where in the real system the suspension arm is attached by two rubber bush mounts. As such the suspension arm is elastically mounted and if modelled in this way loses none of its six degrees of freedom to the mounts. The geometry and alignment of the bushes might suggest that the rigid body modelling approach might utilize a revolute joint at each bush location. This in fact would introduce redundant constraints. A single revolute joint would fix the suspension arm and only allow it to rotate about the axis of the revolute joint. Introducing the second revolute joint only replicates the function of the first and would introduce in this case five redundant constraints.

Taking this a step further, consider the classical four-bar linkage problem shown in Figure 3.20. The mechanism forms a single loop comprising three moving parts and the fixed ground part. Revolute joints are used to constrain two of the parts to the ground and a motion is applied at one of these to impart movement to the system. An initial modelling attempt might consider all four joints as revolute joints as the likelihood is that in the real mechanism they would all appear similar.

On the basis of this modelling approach it is possible to apply the Greubler equation given in (3.44) and obtain the total degrees of freedom in the system based on the calculation tabulated below:

$$\begin{aligned} \text{Parts } 6 \times (4 - 1) &= 18 \\ \text{Revolutes } -5 \times 4 &= -20 \\ \text{Motion } -1 \times 1 &= -1 \\ \hline \text{Total DOF} &= -3 \end{aligned}$$

The total sum of the degrees of freedom for this system is negative, which is physically impossible but has resulted through the selection of the joints and the introduction of redundant constraints. General-purpose programs such as MSC.ADAMS will usually identify the redundant constraints and remove them automatically allowing the analysis to proceed. It is, however, preferable for the analyst to set the model up in such a way that it is not overconstrained and the degrees of freedom in the system are fully understood.

As a first step in rectifying the problem shown in Figure 3.20 it might seem possible to overcome the problem by adding in extra bodies and constraints that result in an overall balance for the system as shown in Figure 3.21.

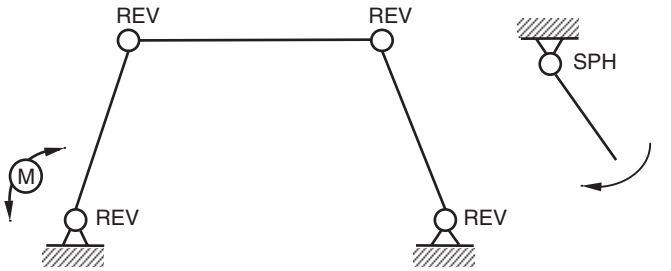

Fig. 3.21 Overconstrained loop in a system model

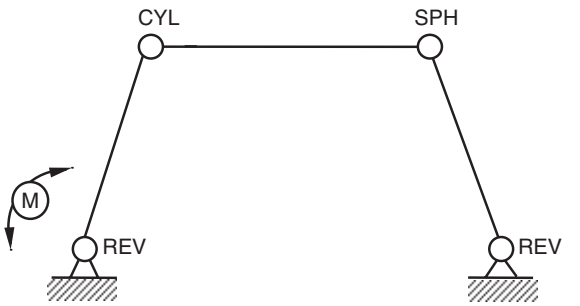

Fig. 3.22 Zero degree of freedom four-bar linkage model

The addition of an extra body attached to the ground by a spherical joint appears to add the extra 3 degrees of freedom needed to at least obtain a zero degree of freedom model that would be used for a kinematic analysis as tabulated below:

Parts $6 \times (5 - 1)$	=	24
Revolutes -5×4	=	-20
Spherical -3×1	=	-3
Motion -1×1	=	-1
Total DOF	=	0

Although it appears the problem has been solved there are still redundant constraints in the system. In balancing the degrees of freedom in the model it is necessary that not only is the overall system not overconstrained but also any individual loops within the model. A possible solution in this case is to select the joints shown in Figure 3.22.

For the joints selected now the result is a zero degree of freedom model that would be used for a kinematic analysis. The degree of freedom balance is tabulated below:

Parts $6 \times (4 - 1)$	=	18
Revolutes -5×2	=	-10
Spherical -3×1	=	-3
Cylindrical -4×1	=	-4
Motion -1×1	=	-1
Total DOF	=	0

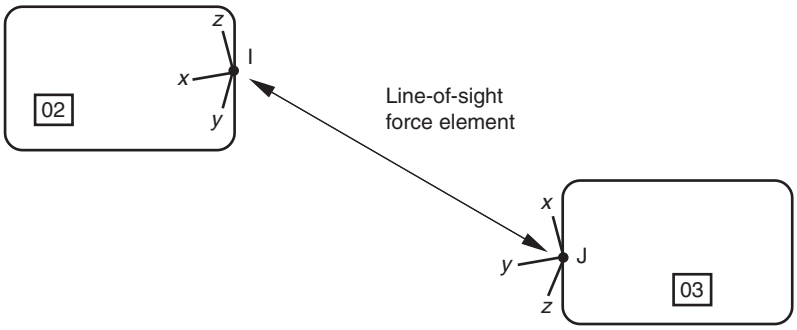

Fig. 3.23 Line-of-sight force element

The cylindrical joint is used to prevent an unwanted degree of freedom that would result in the central link spinning about its own axis.

3.2.9 Force elements

There are two fundamental types of force element that may be defined in a multibody systems model. The first of these are force elements that can be considered internal to the system model and involve the effects of compliance between bodies. Examples of these include springs, dampers, rubber bushes and roll bars. As such these forces involve a connection between two bodies and due to the principle of Newton's third law are often referred to as action–reaction forces. For the translational class of force elements used to define springs and dampers the force will act along the line between two markers that define the ends of the element and as such this form of definition is referred to as the line-of-sight method.

The second type of force is one that is external and applied to the model. Examples of these include gravitational forces, aerodynamic forces and any other external force applied to the model where the reaction on another body is not required. As such they may be referred to as action-only forces. The forces generated by a tyre model and input through the wheel centres into a full vehicle model can also be considered to be this type of force. These forces may be translational or rotational and as they require the definition of a magnitude, line of action and sense the method of definition is referred to as the component method.

The definition of line-of-sight forces is illustrated in Figure 3.23 which shows a force acting along the line of sight between two points, an I and a J marker, on two separate parts. The forces acting on the I and the J marker are equal and opposite. As the line of the force is defined entirely by the location of the I and the J marker the orientation of these is not relevant when defining the force.

The component method applies to translational action-only forces where the direction and sense of the force must be defined and to rotational forces where the axis about which the torque acts is required. In MSC.ADAMS it is the z-axis of the J marker that is used to define the direction and sense of a translational action-only force. The force acts on the I marker as shown in Figure 3.24 and there is no reaction on the J marker.

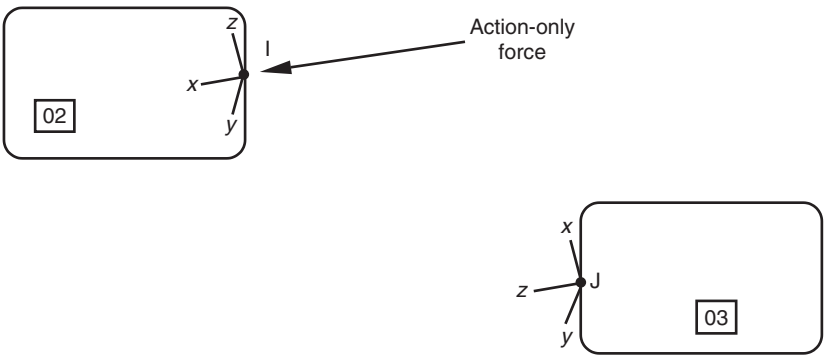

Fig. 3.24 Action-only force

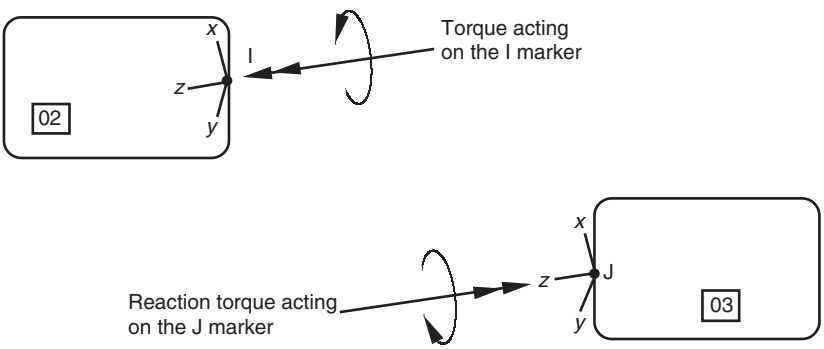

Fig. 3.25 Action–reaction torque

Rotational forces may be defined to be action–reaction or action-only. In either case the torque produced is assumed to act on the I marker. For an action-only torque it is again the z-axis of the J marker that is used, in this case to define the axis of rotation. If the torque is action–reaction the z-axes of the I and J marker must be parallel and point in the same direction as shown in Figure 3.25.

Considering next the definition of translational spring elements we can start with a definition that is linear and introduce the use of system variables for the formulation of a force. As can be seen in Figure 3.26 the formulation of the spring force will be dependent on the length of the spring. This is made available through a system variable defined here as $DM(I, J)$ which represents the scalar magnitude of the displacement between the I and the J marker at any point in time during the simulation. The spring force F_S is initially defined here to be linear using

$$F_S = k(DM(I, J) - L) \tag{3.45}$$

where k is the spring stiffness and L is the free length of the spring, at zero force.

The equation used in (3.45) to determine F_S follows the required convention that the scalar value of force produced is positive when the spring is in compression, zero when it is at its free length and negative when it is in tension.

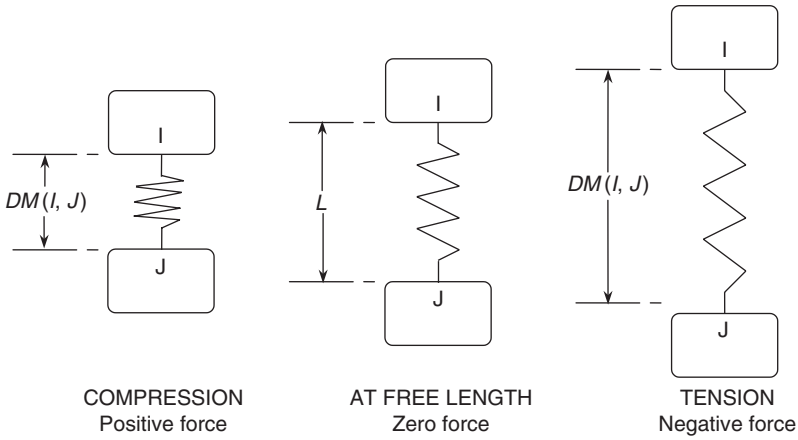

Fig. 3.26 Spring in compression, at free length and in tension

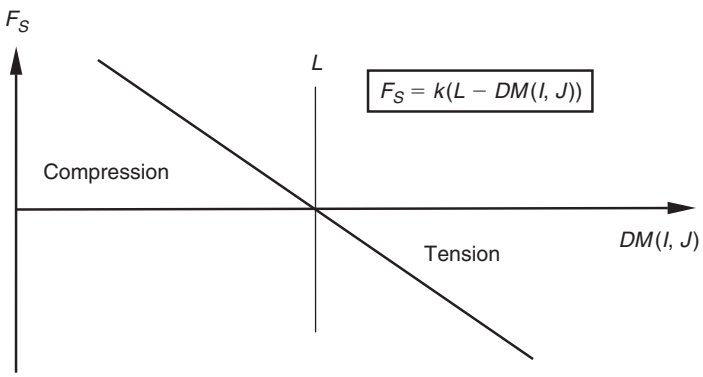

Fig. 3.27 Formulation of a linear spring force

This should not be confused with the components of any reaction force recovered at the I or the J marker. The sign of these will be dependent not only on the state of the spring but also on the orientation of the spring force line of action and the reference frame in which the components are being resolved. The formulation of the spring force F_S is shown graphically in Figure 3.27.

Note that the formulation used here produces a force that is positive in compression and negative in tension. This is opposite to the convention used for stresses in stress analysis and finite element programs. An example of the syntax that could be used to formulate this using a SFORCE statement, would be

```
SFORCE/0509,I=0205,J=0409,TRANS,FUNCTION
  =40*(250-DM(0205,0409))
```

where using the units that are consistent throughout this text we would have:

FUNCTION = the spring force F_S(N)
The spring stiffness $k = 40$ N/mm
The free length $L = 250$ mm
DM(0205,0409) = the magnitude of the displacement between I and J (mm)

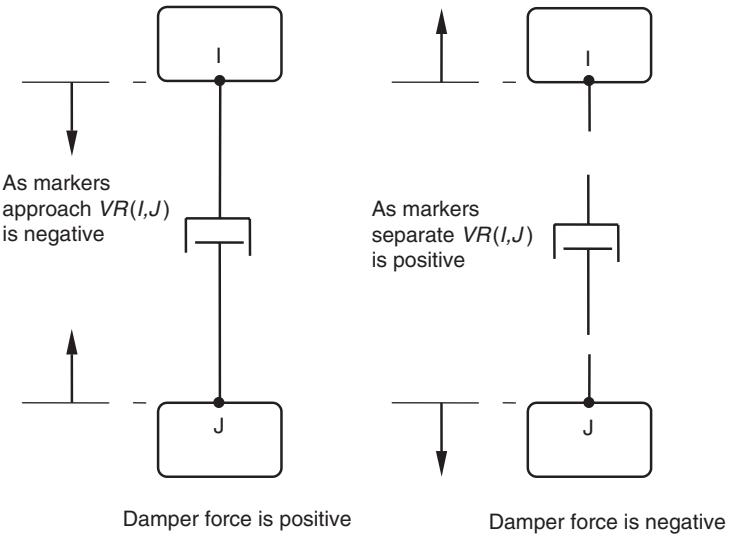

Fig. 3.28 Sign convention for damper forces and velocities

An alternative form of definition that could be used with MSC.ADAMS involves the use of the SPRINGDAMPER statement. In this case this would have exactly the same effect as the SFORCE statement above:

SPRING/0509,I=0205,J=0409,TRANS,K=40,L=250

In a similar manner to the definition of a spring force the representation of a damper force will involve using the line-of-sight method to formulate an action–reaction force between an I marker on one part and a J marker on another part. We will again start with the linear case where we formulate a damper force F_D using

$$F_D = -c \bullet VR(I, J) \tag{3.46}$$

where

$VR(I, J)$ = radial line of sight velocity between I and J marker
c = damping coefficient

Since the force generated in a damper is related to the sliding velocity acting along the axis of the damper we introduce another system variable $VR(I, J)$ that will take a positive sign when the markers are separating, as in suspension rebound, and a negative sign when the markers are approaching, as when a suspension moves upwards relative to the body in bump. The formulation of the damper force F_D in (3.46) is such that the damper forces are consistent with those of a spring. The force generated is positive in a repelling mode and negative in an attracting mode as illustrated in Figure 3.28.

The formulation of the damper force F_D is shown graphically in Figure 3.29.

An example of the syntax that could be used to formulate this in MSC.ADAMS, using an SFORCE statement, would be

```
SFORCE/0509,I=0205,J=0409,TRANS,FUNCTION=
  -5*VR(0205,0409)
```

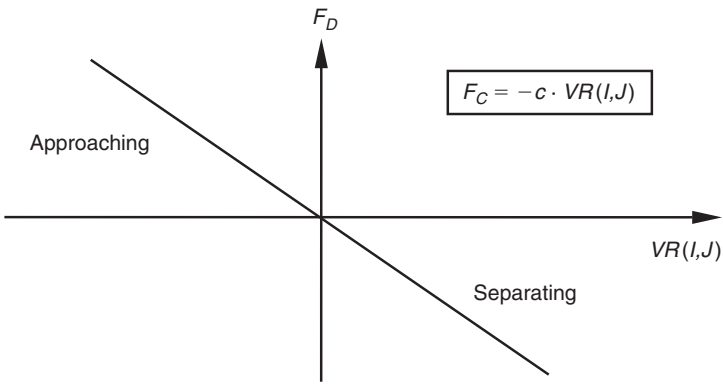

Fig. 3.29 Formulation of a linear damper force

where using the units that are consistent throughout this text we would have:

FUNCTION = the damper force F_D(N)
The damping coefficient $C = 5$ Ns/mm
VR(0205,0409) = the radial line of sight velocity between I and J (mm/s)

An alternative form of definition that could be used with MSC.ADAMS involves the use of the SPRINGDAMPER statement. In this case this would have exactly the same effect as the SFORCE statement above:

SPRINGDAMPER/0509,I=0205,J=0409,TRANS,C=5

The definitions of spring and damper forces so far has been based on the assumption that the force element can be modelled as linear. This can be extended to consider the modelling of a non-linear element. The example used will be based on the front and rear dampers for a typical road vehicle.

The non-linear damper forces are defined in MSC.ADAMS using *xy* data sets where the *x* values represent the velocity in the damper, *VR*(*I*, *J*), and the *y* values are the force. During the analysis the force values are extracted using a cubic spline fit. The damper forces are not only non-linear but are also asymmetric, having different properties in bump and rebound. The curves for the front and rear dampers are shown in Figure 3.30.

An example of the syntax that could be used to formulate the non-linear characteristics of the front damper force in MSC.ADAMS, using an SFORCE statement, would be

SFORCE/2728,I=1627,J=1728,TRANS,FUNCTION=
CUBSPL(VR(1627,1728),0,1)

The function formulation used here, CUBSPL, is based on a cubic curve fitting method (Forsythe et al., 1977). Note that although the function is used here to fit values to *xy* pairs of data it is also possible to use the function to fit values to three-dimensional *xyz* data sets of the type used for carpet plots. In these cases MSC.ADAMS uses a cubic interpolation method to interpolate with respect to the *x* independent variables and then uses linear interpolation between curves of the second *z* independent variables. This will be covered in more detail in Chapter 5 when the interpolation method

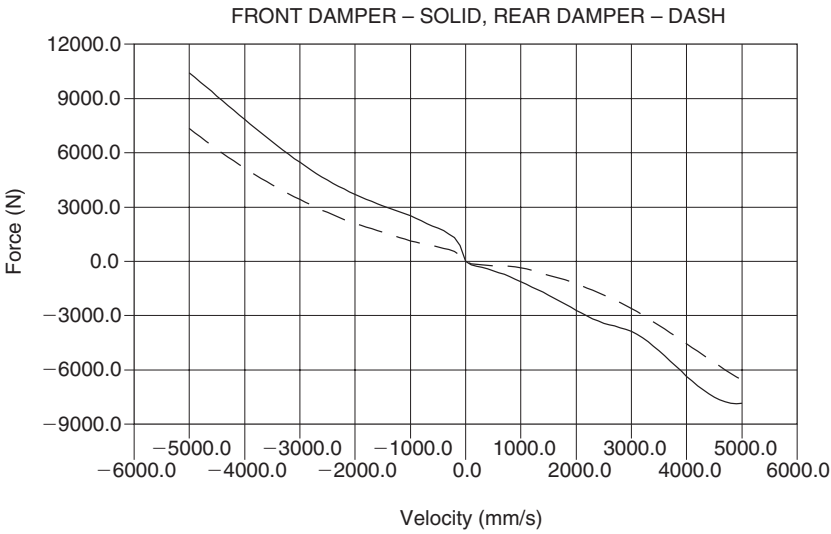

Fig. 3.30 Non-linear force characteristics for front and rear dampers

is described for use with tyre models. The format for this function expression used here is

FUNCTION = CUBSPL(x, z, id)

where
x = the independent variable on the *x*-axis, in this case *VR*(1627,1728)
z = is set to zero to indicate that the data set is two dimensional
id = the id of the spline data set, in this case spline number 1

An example of the spline data set used here to represent the non-linear damper force follows. In this case the velocities are defined in mm/s on the *x*-axis and the values of force (N) are returned on the *y*-axis. It is important that the data set has sufficient range at both the top and bottom end to encompass the conditions during the simulation. Should the independent variable used on the *x*-axis reach values outside of the range of the spline data then the program will have to extrapolate values that can lead to unreliable results.

SPLINE/1
,X = −5000, −3150, −2870, −2450, −2205, −1925, −1610, −1260
,−910, −630, −470, −400, −350, −300, −250, −230, −200, −190
,−160, −120, −80, −55, −40, −20, −10, −1, −0.1, 0, 0.3, 3, 30, 40,
60,80, 100, 200, 250, 400, 490, 770, 1050, 1330, 1820, 2060, 2485, 2590
,2730, 2835, 2940, 3080, 5000

,Y = 10 425, 5800, 5200, 4400, 4000, 3600, 3200, 2800, 2400, 2000, 1800
,1700, 1600, 1500, 1400, 1350, 1310, 1290, 1200, 1000, 700, 400, 210, 80
,40, 4, 0.4, 0, −1, −10, −100, −123, −150, −182, −200, −260, −300
,−400, −500, −800, −1200, −1600, −2400, −2800, −3400, −3500
,−3600, −3700, −3800, −4000, −7840

Although the method of modelling a non-linear force element has been demonstrated here using a damper the method is equally applicable to other

force elements such as springs and rubber bushes. For road springs it is usually sufficient to model these as linear but should a non-linear formulation be required the same approach is used with the magnitude of the displacement in the spring, $DM(I, J)$, being the independent x variable. The modelling of non-linear bush characteristics is dealt with later in this chapter.

Before moving on from the subject of springs and dampers it should be noted that it is also possible to define, in addition to applied torques, rotational springs and dampers. This will be dealt with in Chapter 6 where a rotational spring damper is used to idealize the characteristics of a suspension system in a full vehicle model based on axles that rotate, relative to the vehicle body, about the roll centres of the suspension systems.

Certain types of analysis may also require a suspension model to include the force characteristics of bump and rebound stops. For simulations, such as a vehicle traversing off-road terrain, or the road wheel striking a pothole, the bump and rebound stops will need to be modelled. This may be particularly relevant when the vehicle or suspension model is being used to predict the distribution of force as inputs to finite element models.

If we consider the case of a bump stop, as illustrated in Figure 3.31, it can be seen that we face a new modelling problem. The force element needs now to represent the non-linear problem of a gap which closes so that the force must not only include the non-linear characteristics of the rubber on contact but also be able to switch on and off as the gap closes and opens. The approach used to model the bump or rebound stop will depend on its location. The approach used here might need modification for a rebound stop built into a suspension strut.

In this example the J marker is taken to belong to the vehicle body or subframe and the I marker is located at a point on the suspension that would strike the face of the bump stop. The point at which contact is established can be found here by comparing the z component of the displacement of

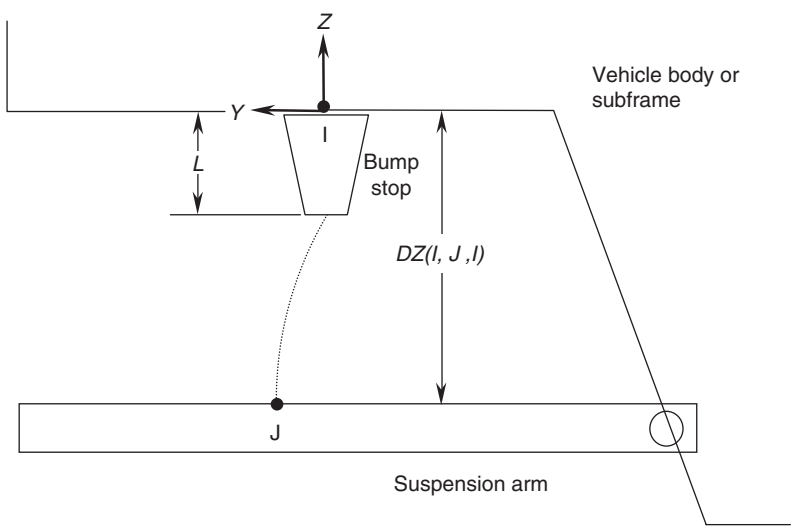

Fig. 3.31 Modelling a bump stop contact force

the I marker from the J marker resolved parallel to the axes of the I marker or *DZ*(*I*, *J*, *I*). Note that the third marker in brackets has been added to the system variable *DZ* to indicate that the component of displacement is resolved using this frame rather than by default the ground reference frame.

A first attempt at modelling this force could be achieved with the following SFORCE statement. In this example 0206 is the I marker, 0307 is the J marker, the length of the bump stop is 50 mm and a linear stiffness for the bump stop of 300 N/mm is used.

```
SFORCE/0607,I=0206,J=0307,TRANS,
FUNCTION=IF(DZ(0206,0307,0206)-50:300*(50-DZ
  (0206,0307,0206)),0,0)
```

This example has introduced an arithmetic IF that allows us to conditionally program the value of the FUNCTION and hence the force returned by this statement. The format used here is

IF (expression 1: expression 2, expression 3, expression 4)

Expression 1 is evaluated and the value obtained is used to determine which expression is used to evaluate the FUNCTION as follows:

IF expression 1 $<$ 0 then the FUNCTION = expression 2
IF expression 1 = 0 then the FUNCTION = expression 3
IF expression 1 $>$ 0 then the FUNCTION = expression 4

In this case expression 1 is DZ(0206,0307,0206)-50. Clearly when this is greater than zero the gap is open and so the calculated force from expression 4 is zero. When expression 1 is equal to zero the I marker is just making contact with the face of the bump stop but no deformation has taken place and so the force is still zero. When expression 1 is less than zero then the contact force is generated using 300*(50-DZ(0206,0307,0206)). Note that this has been programmed to ensure that a positive value is generated for the bump stop as it compresses.

Although the method introduced here might work it is possible that it will cause problems during the numerical integration of the solution. This is because the arithmetic IF causes the force to switch on and off instantaneously about the point of contact. Such modelling is usually undesirable and some method is needed to improve the formulation by 'smoothing' the transition as contact occurs. This could be achieved by introducing another feature known as a STEP FUNCTION as follows:

```
SFORCE/0607,I=0206,J=0307,TRANS,
  FUNCTION=STEP(VARVAL(1),0,0,0.5,1)*(300*(50-DZ
  (0206,0307,0206)))
VARIABLE/1,FUNCTION=50-DZ(0206,0307,0206)
```

Although referred to here as a step users of similar multibody systems software packages may also think of it as a ramp since the change in value returned by the function is not an instantaneous step change. The STEP function used here uses a cubic polynomial to smooth the transition from one state to another as shown in Figure 3.32.

This example also introduces the use of VARIABLES that can be used to program equations and substitute the returned value, VARVAL(id), into

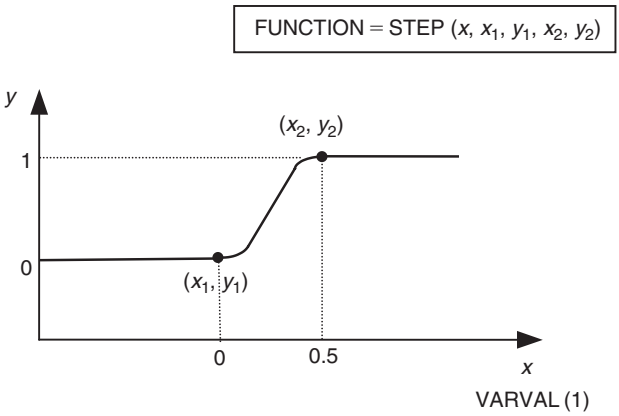

Fig. 3.32 Step function for a bump stop force

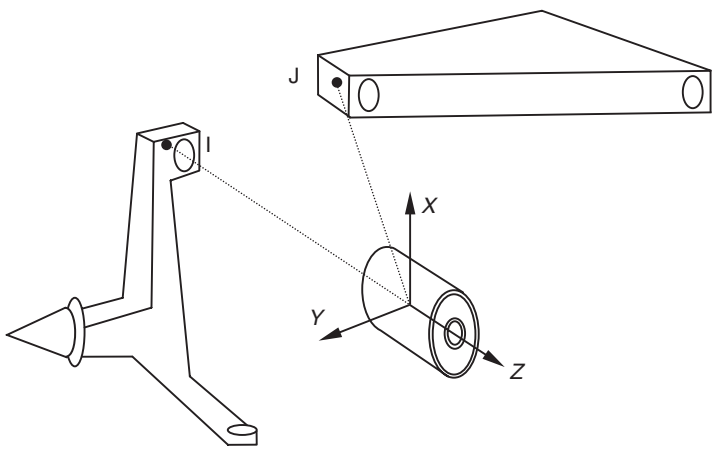

Fig. 3.33 Modelling of suspension bushes

another FUNCTION. In this case VARIABLE/1,FUNCTION = 50-DZ (0206,0307,0206) is used to program the deformation of the bump stop. The value of this, VARVAL(1) is used to define the variable on the *x*-axis that is used to step from one state to another. In this the step function is used to smooth the formulation of the contact force between 0 and 0.5 mm of bump stop deformation.

Additional functions exist, such as an IMPACT function which might be used to switch on a contact force or to extend the material model from the initial linear one used here to a non-linear model. Another consideration here is that the force formulation takes no account of the possibility that the solution could find a point where the I marker actually moves through the bump stop and past the J marker into the vehicle body. Although this makes no sense physically there is nothing in the formulation to take account of this and should it happen the force would actually reverse direction leading to a probable failure of the solution. Clever programming can take this into account. In addition to improving the material model this could include, for

example, building a sensor into the model to stop the simulation should this be about to occur allowing the analyst to investigate the problem further.

The various elastic bushes or mounts used throughout a suspension system to isolate vibration may be represented initially by six linear uncoupled equations based on stiffness and damping. As with a joint a bush connects two parts using an I marker on one body and a J marker on another body. These markers are normally taken to be coincident when setting up the model but it will be seen from the formulation presented here that any initial offset, either translational or rotational, would result in an initial preforce or torque in the bush. This would be in addition to any initial value for these that the user may care to define.

The general form of the equation for the forces and torques generated in the bush is given in (3.47):

$$\{F_{ij}\}_j = -[k]\{d_{ij}\}_j - [c]\{v_{ij}\}_j + \{f_{ij}\}_j \tag{3.47}$$

where
$\{F_{ij}\}_j$ is a column matrix containing the components of the force and torque acting on the I marker from the J marker
$[k]$ is a square stiffness matrix where all off diagonal terms are zero
$\{d_{ij}\}_j$ is a column matrix containing the components of the displacement and rotation of the I marker relative to the J marker
$[c]$ is a square damping matrix where all off diagonal terms are zero
$\{v_{ij}\}_j$ is a column matrix of time derivatives of the terms in the $\{d_{ij}\}$ matrix
$\{f_{ij}\}_j$ is a column matrix containing the components of the preforce and pretorque applied to the I marker

Expanding equation (3.47) leads to the following set of uncoupled equations presented in matrix form as

$$\begin{bmatrix} F_x \\ F_y \\ F_z \\ T_x \\ T_y \\ T_z \end{bmatrix} = -\begin{bmatrix} k_x & 0 & 0 & 0 & 0 & 0 \\ 0 & k_y & 0 & 0 & 0 & 0 \\ 0 & 0 & k_z & 0 & 0 & 0 \\ 0 & 0 & 0 & k_{tx} & 0 & 0 \\ 0 & 0 & 0 & 0 & k_{ty} & 0 \\ 0 & 0 & 0 & 0 & 0 & k_{tz} \end{bmatrix} \begin{bmatrix} d_x \\ d_y \\ d_z \\ r_x \\ r_y \\ r_z \end{bmatrix} - \begin{bmatrix} c_x & 0 & 0 & 0 & 0 & 0 \\ 0 & c_y & 0 & 0 & 0 & 0 \\ 0 & 0 & c_z & 0 & 0 & 0 \\ 0 & 0 & 0 & c_{tx} & 0 & 0 \\ 0 & 0 & 0 & 0 & c_{ty} & 0 \\ 0 & 0 & 0 & 0 & 0 & c_{tz} \end{bmatrix} \begin{bmatrix} v_x \\ v_y \\ v_z \\ \omega_x \\ \omega_y \\ \omega_z \end{bmatrix} + \begin{bmatrix} f_x \\ f_y \\ f_z \\ t_x \\ t_y \\ t_z \end{bmatrix} \tag{3.48}$$

It should be noted that all the terms in (3.47) and (3.48) are referenced to the J marker reference frame and that the equilibriating force and torque acting on the J marker is determined from

$$\{F_{ji}\}_j = -\{F_{ij}\}_j \tag{3.49}$$

$$\{T_{ji}\}_j = -\{T_{ij}\}_j - \{d_{ij}\}_j \times \{F_{ij}\}_j \tag{3.50}$$

The shape and construction of the bush will dictate the manner in which the I marker and J marker are set up and orientated. This is illustrated in Figure 3.34 where it can be seen that for the cylindrical bush where there are no voids the radial stiffness is constant circumferentially. For this bush it is only necessary to ensure the z-axes of the I and J markers are aligned with

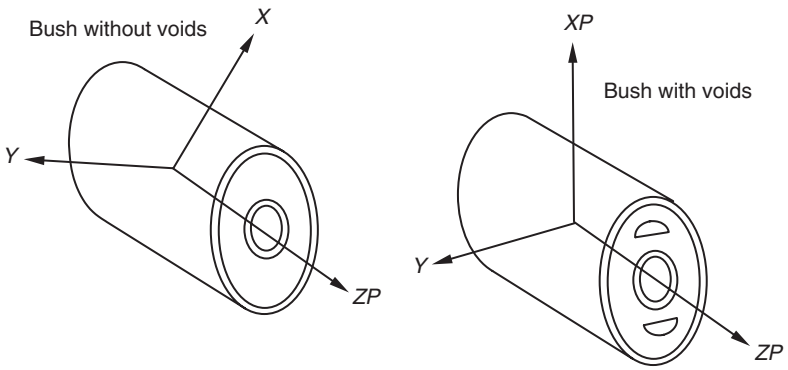

Fig. 3.34 Orientation of bush axis system

the axis of the bush. For the bush with voids the radial stiffness will require definition in both the x and y directions as shown.

An example of the command used to define a massless bush with linear stiffness and damping properties is:

```
BUSH/03,I=0203,J=0503,
,K=7825,7825,944,KT=2.5E6,2.5E6,944
,C=35,35,480,CT=61E3,61E3,40
```

It is also possible to extend the definition of bushes from linear to non-linear. Examples of this will be given in the next chapter. The most advanced examples of the modelling of force elements extend to the incorporation of finite element type representations of beams and flexible bodies into the multibody systems model. In modelling a vehicle the most likely use of a beam type element is going to be in modelling the roll bars or possibly if considered relevant an appropriate suspension member such as a tie rod.

The beam element in MSC.ADAMS requires the definition of an I marker on one body and a J marker on another body to represent the ends of the beam with length L as shown in Figure 3.35. The beam element transmits forces and moments between the two markers, has a constant cross-section and obeys Timoshenko beam theory.

The beam centroidal axis is defined by the x-axis of the J marker and when the beam is in an undeflected state, the I marker lies on the x-axis of the J marker and has the same orientation. The forces and moments shown in Figure 3.35 are:

Axial forces F_{Ix} and F_{Jx}

Shear forces F_{Iy}, F_{Iz}, F_{Jy} and F_{Jz}

Twisting moments M_{Ix} and M_{Jx}

Bending moments M_{Iy}, M_{Iz}, M_{Iy} and M_{Jz}

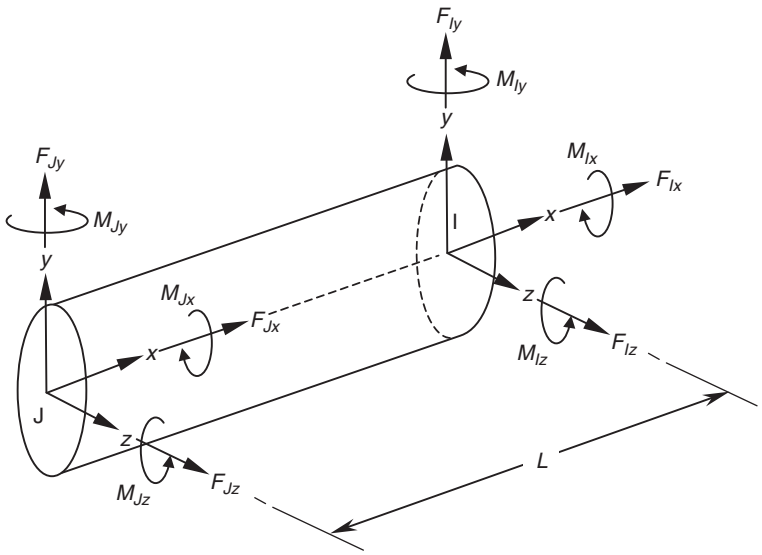

Fig. 3.35 Massless beam element

The forces and moments applied to the I marker are related to the displacements and velocities in the beam using the beam theory equations presented in matrix form as:

$$\begin{bmatrix} F_{Ix} \\ F_{Iy} \\ F_{Iz} \\ M_{Ix} \\ M_{Iy} \\ M_{Iz} \end{bmatrix} = -\begin{bmatrix} k_{11} & 0 & 0 & 0 & 0 & 0 \\ 0 & k_{22} & 0 & 0 & 0 & k_{26} \\ 0 & 0 & k_{33} & 0 & k_{35} & 0 \\ 0 & 0 & 0 & k_{44} & 0 & 0 \\ 0 & 0 & k_{35} & 0 & k_{55} & 0 \\ 0 & k_{26} & 0 & 0 & 0 & k_{66} \end{bmatrix} \begin{bmatrix} d_x - \mathrm{L} \\ d_y \\ d_z \\ r_x \\ r_y \\ r_z \end{bmatrix} - \begin{bmatrix} c_{11} & c_{21} & c_{31} & c_{41} & c_{51} & c_{61} \\ c_{21} & c_{22} & c_{32} & c_{42} & c_{52} & c_{62} \\ c_{31} & c_{32} & c_{33} & c_{43} & c_{53} & c_{63} \\ c_{41} & c_{42} & c_{42} & c_{44} & c_{54} & c_{64} \\ c_{51} & c_{52} & c_{52} & c_{53} & c_{55} & c_{65} \\ c_{61} & c_{62} & c_{63} & c_{64} & c_{65} & c_{66} \end{bmatrix} \begin{bmatrix} v_x \\ v_y \\ v_z \\ \omega_x \\ \omega_y \\ \omega_z \end{bmatrix} \tag{3.51}$$

The terms d_x, d_y and d_z in (3.51) are the x, y and z displacements of the I marker relative to the J marker measured in the J marker reference frame. The terms r_x, r_y and r_z are the relative rotations of the I marker with respect to the J marker measured about the x-axis, y-axis and z-axis of the J marker. It should be noted here that the rotations in the beam are assumed to be small and that large angular deflections are not commutative. In these cases, typically when deflections in the beam approach 10% of the undeformed length the theory does not correctly define the behaviour of the beam. The terms V_x, V_y, V_z, ω_x, ω_y and ω_z are the velocities in the beam obtained as time derivatives of the translational and rotational displacements.

The stiffness and damping matrices are symmetric. The terms in the stiffness matrix are given by:

$$K_{11} = \frac{EA}{L} \quad K_{22} = \frac{12EI_{zz}}{L^3(1+P_y)} \quad K_{26} = \frac{-6EI_{zz}}{L^2(1+P_y)} \quad K_{33} = \frac{12EI_{yy}}{L^3(1+P_z)}$$

$$K_{35} = \frac{6EI_{yy}}{L^2(1+P_z)} \quad K_{44} = \frac{GI_{xx}}{L} \quad K_{55} = \frac{4+P_zEI_{yy}}{L(1+P_z)} \quad K_{66} = \frac{4+P_yEI_{zz}}{L(1+P_y)}$$

where $P_y = 12EI_{zz}A_{SY}/(GAL^2)$ and $P_z = 12EI_{yy}A_{SZ}/(GAL^2)$. Young's modulus of elasticity for the beam is given by E and the shear modulus is given by G. The cross-sectional area of the beam is given by A. The terms I_{yy} and I_{zz} are the second moments of area about the neutral axes of the beam cross-section. For a solid circular section with diameter D these would, for example, be given by $I_{yy} = I_{zz} = \pi D^4/64 \cdot I_{xx}$ is the polar second moment of area. Again for a solid circular section this is given by $I_{xx} = \pi D^4/32$.

The final part of the definition of the terms in the stiffness matrix is the correction factors for shear deflection in the y and z directions for Timoshenko beams. These are given in the y direction by $A_{sy} = A/I_{yy}^2 \int_A (Q_y/l_z)^2 \, dA$ and in the z direction by $A_{sy} = A/I_{zz}^2 \int_A (Q_z/l_y)^2 \, dA$. The terms Q_y and Q_z are the first moments of area about the beam section y- and z-axes respectively. The terms l_y and l_z are the dimensions of the beam cross-section in the y and z directions of the cross-section axes.

The structural damping terms c_{11} through to c_{66} in (3.51) may be input directly or by using a ratio to factor the terms in the stiffness matrix. In a similar manner to the dampers and bushes discussed earlier it is possible to define a beam with non-linear properties using more advanced elements that allow the definition of general force fields.

As with the bush elements the beam will produce an equilibriating force and moment acting on the J marker using

$$\{F_{ji}\}_j = -\{F_{ij}\}_j \tag{3.52}$$

$$\{M_{ji}\}_j = -\{M_{ij}\}_j - \{d_{ij}\}_j \times \{F_{ij}\}_j \tag{3.53}$$

where $\{d_{ij}\}_j$ is the position vector of the I marker relative to the J marker referenced to the J marker axis system. An example of the command used to define a massless beam is

```
BEAM/0304,I=0203,J=0504,
,LENGTH=250,A=315,IXX=4021240,IYY=2010620,
  IZZ=2010620
,EMOD=200E3,GMOD=70E3,ASY=1.33,ASZ=1.33,
  CRATIO=0
```

3.2.10 Summation of forces and moments

Having considered the definition of force elements in terms of model definition we may conclude by considering the formulation of the equations for the forces and moments acting on a body. An applied force or moment can be defined using an equation to specify the magnitude, which may be functionally dependent on displacements, velocities, other applied forces and time. Using the example in Figure 3.36 there is an applied force $\{F_A\}_1$ acting at point A, the weight of the body $m\{g\}_1$ acting at the centre of mass G, a force $\{F_B\}_1$ and a torque $\{T_B\}_1$ due to an element such as a bush or beam connection to another part. In addition there is an applied torque $\{T_C\}_1$ acting at point C. Note that at this stage all the force and torque vectors are assumed to be resolved parallel to the GRF and that $\{g\}_1$ is the vector of acceleration due to gravity and is again measured in the GRF.

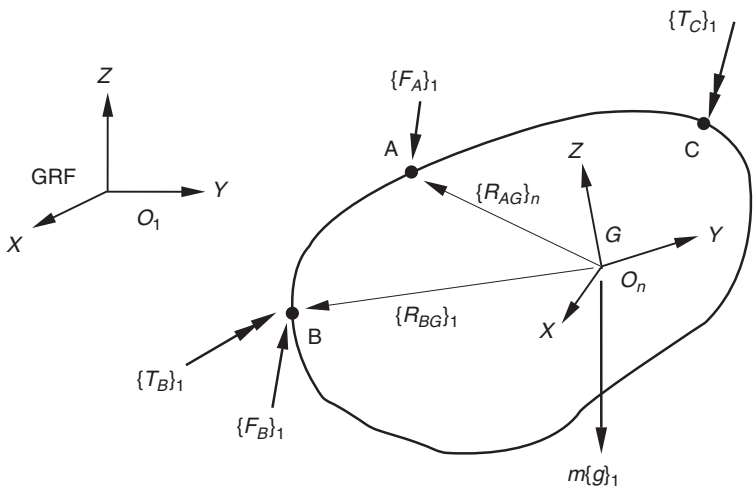

Fig. 3.36 Applied forces and torques on a body

The summation of applied forces resolved in the GRF as required in equation (3.54) is obtained in this example by:

$$\Sigma\{Fn_A\}_1 = \{F_A\}_1 + \{F_B\}_1 + m\{g\}_1 \tag{3.54}$$

The summation of moments about G is not so straightforward. MSC.ADAMS performs the moment calculations about the axes of the Euler-axis frame. It is therefore necessary to use the transformation matrix $[A_{n1}]$ to transform forces and torques to the part frame O_n and to use $[B_n]^T$ to transform from the part frame to the Euler-axis frame:

$$\{F_A\}_n = [A_{n1}]\{F_A\}_1 \tag{3.55}$$

$$\{F_B\}_n = [A_{n1}]\{F_B\}_1 \tag{3.56}$$

$$\{T_B\}_n = [A_{n1}]\{T_B\}_1 \tag{3.57}$$

$$\{T_C\}_n = [A_{n1}]\{T_C\}_1 \tag{3.58}$$

It is now possible to calculate the moments at G due to the forces at A and B working in the part frame:

$$\{M_A\}_n = \{R_{AG}\}_n \times \{F_A\}_n \tag{3.59}$$

$$\{M_B\}_n = \{R_{BG}\}_n \times \{F_B\}_n \tag{3.60}$$

The next step is to transform the moments and torques to the Euler-axis frame and to summate as required in equation (3.61):

$$\Sigma\{Mn\}_e = [B_n]^T\{M_A\}_n + [B_n]^T\{M_B\}_n + [B_n]^T\{T_B\}_n + [B_n]^T\{T_C\}_n \tag{3.61}$$

3.3 Analysis capabilities

3.3.1 Overview

Once the model has been assembled the main code may be used to carry out kinematic, static, quasi-static or dynamic analyses. Kinematic analysis is applicable to systems possessing zero rigid body degrees of freedom.

Any movement in this type of system will be due to prescribed motions at joints. The program uncouples the equations of motion and force and then solves separately and algebraically for displacements, velocities, accelerations, and forces.

For static analysis the velocities and accelerations are set to zero and the applied loads are balanced against the reaction forces until an equilibrium position is found. This may involve the system moving through large displacements between the initial definition and the equilibrium position and therefore requires a number of iterations before convergence on the solution closest to the initial configuration. Static analysis is often performed as a preliminary to a dynamic analysis. An example would be to perform a static analysis on a full vehicle model before a dynamic handling simulation. This establishes the configuration of the vehicle at 'kerb height' before the vehicle moves forward during the dynamic phase of the simulation. Quasi-static analysis is a series of static equilibrium solutions at selected time steps. Although the system can be considered to be moving the dynamic response is not required. An example would be to perform a quasi-static analysis on a vehicle mounted on a tilting surface. As the surface rotates to different angles with time the static equilibrium of the vehicle can be calculated at selected angles.

Dynamic analysis is performed on systems with one or more degrees of freedom. The differential equations representing the system are automatically formulated and then numerically integrated to provide the position, velocities, accelerations and forces at successively later times. Although the user will select output at various points in time the program will often compute solutions at many intermediate points in time. The interval between each of these solution points is known as an integration time step. The size of the integration time step is constantly adjusted using internal logic although the user may override the system defaults if so desired. Before considering the implementation of these analysis methods in more detail we must consider the fundamental methods used to solve linear and non-linear equations. An additional modal analysis capability may be used to linearize the non-linear equations of motion about a selected operating point and then find the natural frequencies and mode shapes associated with the system. It is also possible to extract the linearized state–space plant model in a format suitable for input to a control system design package.

3.3.2 Solving linear equations

Multibody systems programs solve both linear and non-linear equations during the analysis phase. Linear equations can be assembled in matrix form as shown in (3.62):

$$[A][x] = [b] \tag{3.62}$$

where

$[A]$ is a square matrix of constants
$[x]$ is a column matrix of unknowns
$[b]$ is a column matrix of constants

The formulations in a multibody systems program generally lead to a matrix $[A]$ where most of the elements are zero. As such the matrix is

referred to as sparse and the ratio of non-zero terms to the total number of matrix elements is referred to as the sparsity of the matrix. In a program such as MSC.ADAMS the sparsity of the matrix is typically in the range of 2 to 5% (Wielenga, 1987). The computer solvers that are developed in multibody systems to solve linear equations can be designed to exploit the sparsity of the [A] matrix leading to relatively fast solution times. This is one of the reasons, apart from improvements in computer hardware, that multibody systems programs can appear to solve quite complex engineering problems in seconds or minutes. These solution speeds can be quite notable when compared with other computer software such as finite elements or computational fluid dynamics programs.

The solution of (3.62) follows an established approach that initially involves decomposing or factorizing the [A] matrix into the product of a lower triangular and an upper triangular matrix:

$$[A] = [L][U] \tag{3.63}$$

For the lower triangular matrix [L] all the elements above the diagonal are set to zero. For the upper triangular matrix [U] all the elements on and below the diagonal are set to zero. In the following step a new set of unknowns [y] is substituted into (3.63) leading to

$$[L][U][x] = [b] \tag{3.64}$$

$$[U][x] = [y] \tag{3.65}$$

$$[L][y] = [b] \tag{3.66}$$

The terms in the [L] and [U] matrices may be obtained by progressive operations on the [A] matrix where the terms in one row are all factored and then added or subtracted to the terms in another row. This process can be demonstrated by considering the expanded [A], [L] and [U] matrices as shown in (3.67) where to demonstrate the influence of sparsity some of the terms in the [A] matrix are initially set to zero:

$$\begin{bmatrix} L_{11} & 0 & 0 & 0 \\ L_{21} & L_{22} & 0 & 0 \\ L_{31} & L_{32} & L_{33} & 0 \\ L_{41} & L_{42} & L_{43} & L_{44} \end{bmatrix} \begin{bmatrix} 1 & U_{12} & U_{13} & U_{14} \\ 0 & 1 & U_{23} & U_{24} \\ 0 & 0 & 1 & U_{34} \\ 0 & 0 & 0 & 1 \end{bmatrix} = \begin{bmatrix} A_{11} & A_{12} & 0 & A_{14} \\ A_{21} & 0 & 0 & A_{24} \\ A_{31} & 0 & A_{33} & 0 \\ A_{41} & 0 & A_{43} & A_{44} \end{bmatrix} \tag{3.67}$$

The fact that the [A] matrix is sparse leads to the [L] and [U] matrices also being sparse with subsequent savings in computer simulation time and memory storage. If we start by multiplying the rows in [L] into the first column of [U] we can begin to obtain the constants in the [L] and [U] matrices from those in the [A] matrix:

$$L_{11} = A_{11}$$

$$L_{21} = A_{21}$$

$$L_{31} = A_{31}$$

$$L_{41} = A_{41}$$

In a similar manner for the second column of $[U]$ we get:

$$\begin{aligned}
L_{11}U_{12} &= A_{12} && \text{therefore} && U_{12} = A_{12}/A_{11}\\
L_{21}U_{12} + L_{22} &= 0 && \text{therefore} && L_{22} = -A_{21}A_{12}/A_{11}\\
L_{31}U_{12} + L_{32} &= 0 && \text{therefore} && L_{32} = -A_{31}A_{12}/A_{11}\\
L_{41}U_{12} + L_{42} &= 0 && \text{therefore} && L_{42} = -A_{41}A_{12}/A_{11}
\end{aligned}$$

Moving on to the third column of $[U]$ gives:

$$\begin{aligned}
L_{11}U_{13} &= 0 && \text{therefore} && U_{13} = 0\\
L_{21}U_{13} + L_{22}U_{23} &= 0 && \text{therefore} && U_{23} = 0\\
L_{31}U_{13} + L_{32}U_{23} + L_{33} &= A_{33} && \text{therefore} && L_{33} = A_{33}\\
L_{41}U_{13} + L_{42}U_{23} + L_{43} &= A_{43} && \text{therefore} && L_{43} = A_{43}
\end{aligned}$$

Finishing with the multiplication of the rows in $[L]$ into the fourth column of $[U]$ gives:

$$\begin{aligned}
&L_{11}U_{14} = A_{14}\\
&L_{21}U_{14} + L_{22}U_{24} = A_{24}\\
&L_{31}U_{14} + L_{32}U_{24} + L_{33}U_{34} = 0\\
&L_{41}U_{14} + L_{42}U_{24} + L_{43}U_{34} + L_{44} = A_{44}
\end{aligned}$$

therefore

$$\begin{aligned}
U_{14} &= A_{14}/A_{11}\\
U_{24} &= -(A_{24} - A_{21}A_{14}/A_{11})/(A_{21}A_{12}/A_{11})\\
U_{34} &= (-(A_{31}A_{14}/A_{11}) - (A_{31}A_{12}/A_{11})(A_{24} - A_{21}A_{14}/A_{11})/(A_{21}A_{12}/A_{11}))/A_{33}\\
L_{44} &= A_{44} - A_{41}A_{14}/A_{11} - (A_{41}A_{12}/A_{11})(A_{24} - A_{21}A_{14}/A_{11})/(A_{21}A_{12}/A_{11})\\
&\quad -A_{43}(-(A_{31}A_{14}/A_{11}) - (A_{31}A_{12}/A_{11})(A_{24} - A_{21}A_{14}/A_{11})/\\
&\quad (A_{21}A_{12}/A_{11}))/A_{13}
\end{aligned}$$

From the preceding manipulations we can see that for this example some of the terms in the $[L]$ and $[U]$ matrices come to zero. Using this we can update (3.67) to give

$$\begin{bmatrix} L_{11} & 0 & 0 & 0\\ L_{21} & L_{22} & 0 & 0\\ L_{31} & L_{32} & L_{33} & 0\\ L_{41} & L_{42} & L_{43} & L_{44} \end{bmatrix} \begin{bmatrix} 1 & U_{12} & 0 & U_{14}\\ 0 & 1 & 0 & U_{24}\\ 0 & 0 & 1 & U_{34}\\ 0 & 0 & 0 & 1 \end{bmatrix} = \begin{bmatrix} A_{11} & A_{12} & 0 & A_{14}\\ A_{21} & 0 & 0 & A_{24}\\ A_{31} & 0 & A_{33} & 0\\ A_{41} & 0 & A_{43} & A_{44} \end{bmatrix} \tag{3.68}$$

Consideration of (3.68) reveals that some elements in the factors $[L]$ and $[U]$ are non-zero where the corresponding elements in $[A]$ are zero. Such elements, for example L_{22}, L_{32}, and L_{42} here, are referred to as 'fills'. Having completed the decomposition process of factorizing the $[A]$ matrix into the $[L]$ and $[U]$ matrices the next step, forward–backward substitution, can commence.

The first step is a forward substitution, utilizing the now known terms in the $[L]$ matrix to find the terms in $[y]$. For this example if we expand

$[L][y] = [b]$ as given in (3.66) we get

$$\begin{bmatrix} L_{11} & 0 & 0 & 0 \\ L_{21} & L_{22} & 0 & 0 \\ L_{31} & L_{32} & L_{33} & 0 \\ L_{41} & L_{42} & L_{43} & L_{44} \end{bmatrix} \begin{bmatrix} y_1 \\ y_2 \\ y_3 \\ y_4 \end{bmatrix} = \begin{bmatrix} b_1 \\ b_2 \\ b_3 \\ b_4 \end{bmatrix} \tag{3.69}$$

therefore

$y_1 = b_1/L_{11}$

$y_2 = (b_2 - L_{21}y_1)/L_{22}$

$y_3 = (b_3 - L_{31}y_1 - L_{32}y_2)/L_{33}$

$y_4 = (b_4 - L_{41}y_1 - L_{42}y_2 - L_{43}y_3)/L_{44}$

The next step is a back substitution, utilizing the terms found in the $[U]$ matrix to find the overall solution for the terms in $[x]$. For this example if we expand $[U][x] = [y]$ as given in (3.65) we get

$$\begin{bmatrix} 1 & U_{12} & 0 & U_{14} \\ 0 & 1 & 0 & U_{24} \\ 0 & 0 & 1 & U_{34} \\ 0 & 0 & 0 & 1 \end{bmatrix} \begin{bmatrix} x_1 \\ x_2 \\ x_3 \\ x_4 \end{bmatrix} = \begin{bmatrix} y_1 \\ y_2 \\ y_3 \\ y_4 \end{bmatrix} \tag{3.70}$$

therefore

$x_4 = y_4$

$x_3 = (y_3 - U_{34}x_4)$

$x_2 = (y_2 - U_{24}x_4)$

$x_1 = (y_1 - U_{12}x_2 - U_{14}x_4)$

It can be seen that in the solution of (3.69) it is necessary to divide by the diagonal terms in $[L]$. These are referred to as 'pivots' and must be non-zero to avoid a singular matrix and failure in solution. There will also be problems if the pivots are so small that they approach a zero value. In these circumstances the condition of the matrices is said to be poor. The answer to this is to rearrange the order of the equations, referred to as pivot selection, until the best set of pivots is available. This process is also called refactorization. The mathematics has been developed so that the process will also attempt to minimize the number of fills to assist with a faster solution. The sequence of operations can be stored to speed solution as the simulation progresses unless the physical configuration of the system changes to a point where the matrix changes sufficiently to justify the reselection of a set of pivots. It should be noted that in general solution of these equations will involve much larger matrices than the four by four example shown here and the sparsity of the matrix will be more apparent for these larger problems.

3.3.3 Non-linear equations

In the case of non-linear equations an iterative approach must be undertaken in order to obtain a solution. A set of non-linear equations may be described in matrix form using

$$[G][x] = 0 \tag{3.71}$$

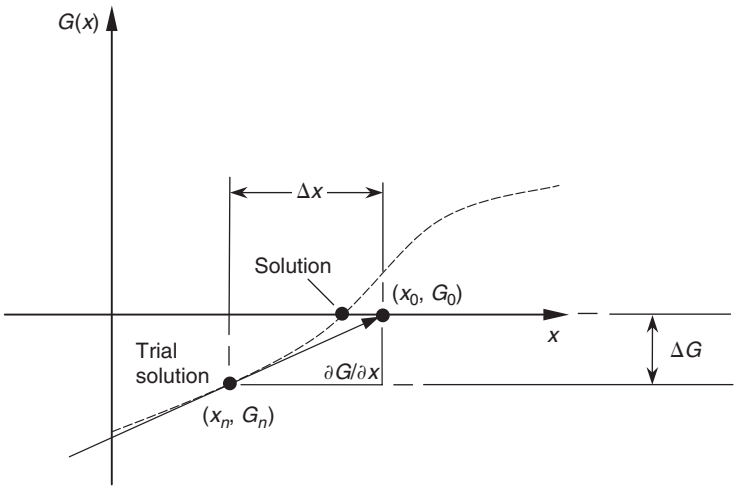

Fig. 3.37 Application of Newton–Raphson iteration

where
$[x]$ is a set of unknown variables
$[G]$ is a set of implicit functions dependent on $[x]$

Consider the solution of a single non-linear equation $G(x) = 0$, where G is an implicit function dependent on x. If we plot a graph of $G(x)$ against x the solution is the value of x where the curve intersects the x-axis as shown in Figure 3.37.

The solution may be obtained using Newton–Raphson iteration based on the assumption that very close to the solution the curve may be approximated to a straight line where it crosses the x-axis. This is illustrated in Figure 3.37 where the line is determined by a trial solution, for say the nth iteration, located at (x_n, G_n) and the slope or derivative of the curve $(\partial G/\partial x)$ at this point.

If we take the point (x_0, G_0) to be that at which the straight line crosses the x-axis then the gradient $\partial G/\partial x$ is given by

$$\frac{\partial G}{\partial x} = \frac{G_0 - G_n}{x_0 - x_n} = \frac{\Delta G}{\Delta x} \tag{3.72}$$

Rearranging this we can write

$$(\partial G/\partial x)\,\Delta x = \Delta G \tag{3.73}$$

We can now extend this to demonstrate how the method can be used to iterate and close in on the solution. This is shown graphically in Figure 3.38.

Extending the single equation $G(x)$ to a set of simultaneous non-linear equations we can write

$$\left[\frac{\partial G}{\partial x}\right][\Delta x] = [\Delta G] \tag{3.74}$$

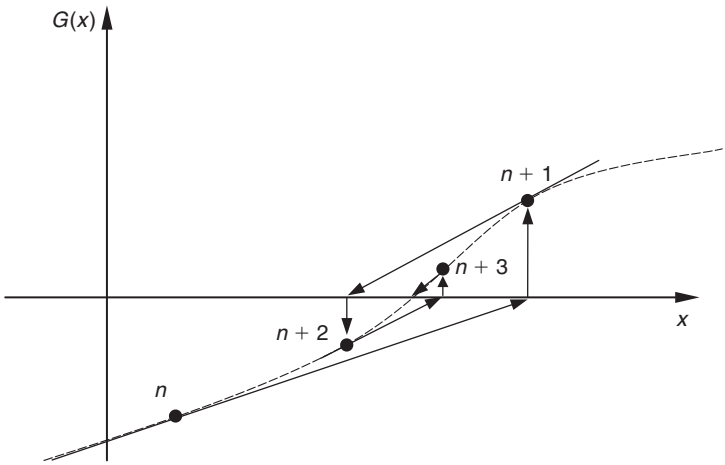

Fig. 3.38 Convergence of Newton–Raphson iteration

where $[\partial G/\partial x]$ is a matrix of partial derivatives representing the slopes of straight lines used in the solution. This is usually referred to as the Jacobian matrix. $[\Delta x]$ is a column matrix of updates to the values of x for each equation and $[\Delta G]$ is a column matrix of terms representing the current error in each equation.

Once all the terms in $[\Delta G]$ approach zero a solution has been achieved. In practice since this method involves the programming of a numerical approximation a small error tolerance is used to determine that the terms in $[\Delta G]$ have converged. For example, if we were to use an error tolerance equal to 10^{-4} then we could say that convergence has been achieved when for each equation in the system

$$-10^{-4} \leqslant \Delta G \leqslant 10^{-4} \tag{3.75}$$

The iterative process used here can be illustrated using the flow chart shown in Figure 3.39.

The Newton–Raphson method can be modified to speed up the solution process by not performing Step 3 and Step 4 in Figure 3.39. These two steps are the most computationally intensive and a more rapid solution may be achieved by calculating the Jacobian matrix, for example, on every second or third iteration. The graphical illustration of the process in Figure 3.38 shows how the use of the slope $\partial G/\partial x$ from the previous iteration may often be an acceptable modification to the solution process.

3.3.4 Integration methods

The solution of non-linear equations for dynamic systems with one or more degrees of freedom is a fundamental component of the application of multibody systems analysis to engineering problems. A number of methods have been developed and the process is commonly referred to as integration. The example here is based on the description given by Wielenga (1987) of a Backwards Differentiation Formula (BDF) method. The method described here can be considered to have two phases. The first of these is the use of a polynomial fit through past values of a given equation to predict a value

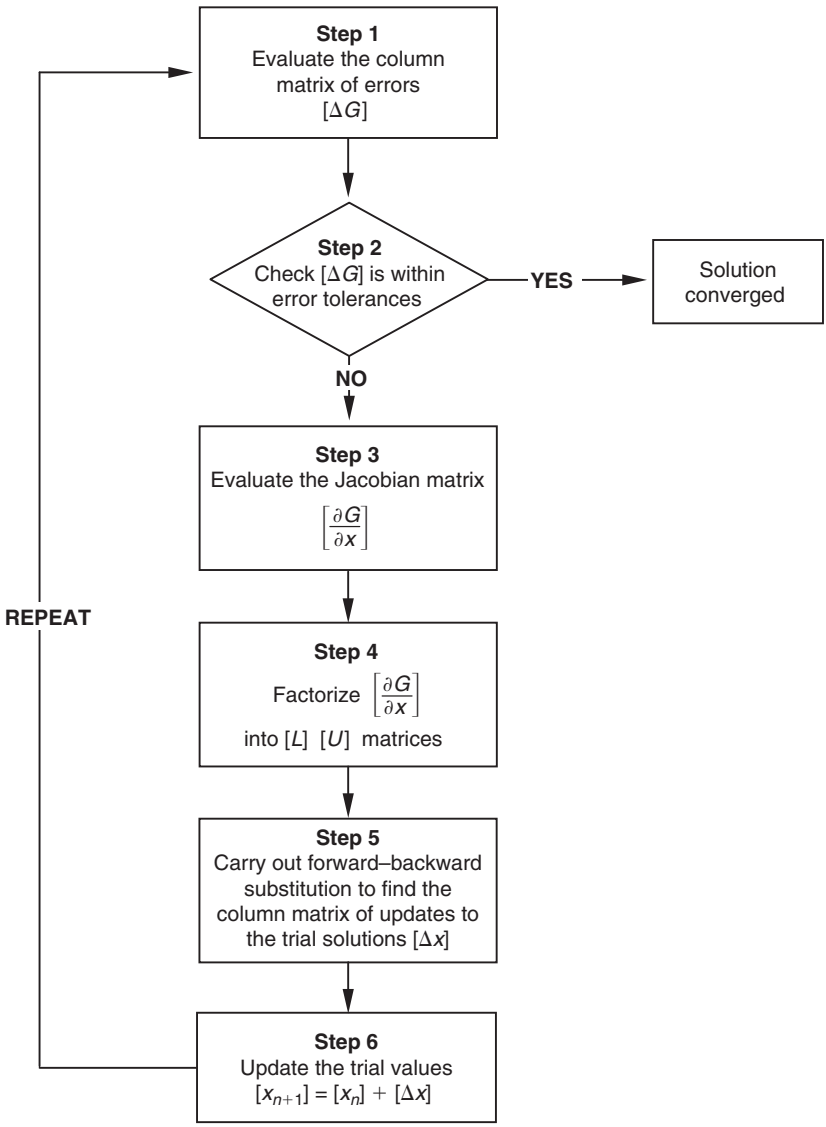

Fig. 3.39 Flow chart illustrating solution of non-linear equations

at the next integration time step (solution point). The second step is to use the Newton–Raphson method described in the previous section to correct the prediction and achieve convergence. As such this method may also be described as a predictor–corrector approach. The equations being solved are first order differential equations and are also referred to as state equations. The state equations are implicit and have the general formulation $G(x, \dot{x}, t) = 0$.

Clearly most dynamic problems such as the unforced vibration of the simple one degree of freedom system shown in Figure 3.40 involve acceleration and have an equation of motion that is second order as shown in (3.76):

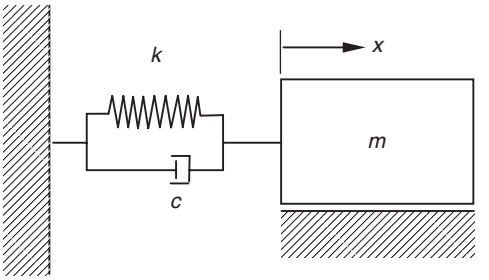

Fig. 3.40 Simple 1 degree-of-freedom mass, spring, damper system

$$m\frac{\mathrm{d}^2x}{\mathrm{d}t^2} + c\frac{\mathrm{d}x}{\mathrm{d}t} + kx = 0 \tag{3.76}$$

The implementation of this as first order differential equations is simply a matter of introducing a new variable, for example z, for the velocity and writing (3.76) as two implicit first order differential equations:

$$z - \frac{\mathrm{d}x}{\mathrm{d}t} = 0 \tag{3.77}$$

$$m\frac{\mathrm{d}z}{\mathrm{d}t} + cz + kx = 0 \tag{3.78}$$

The predictor phase of the solution can be explained with the help of the plot of the value of the state variable x as a function of time t as shown in Figure 3.41. The current solution point, or nth integration time step, is shown to be occurring at time t_n. Previous successful solutions have been computed at times t_{n-1}, t_{n-2}, t_{n-3}, …, t_{n-k}. The next value to be predicted x_{n+1} will occur at time t_{n+1}. The time between each solution point is the integration time step h. Note that this should not be confused with output steps that are generally defined before the analysis and are used to fix the time interval at which results will be calculated for printing and plotting. The integration time step must be at least as small as the output time step to compute solutions but will generally be smaller in order to obtain a solution. In some programs the integration time steps may be fixed but usually, as with programs like MSC.ADAMS, they will be variable and will use programmed logic to determine the optimum step size for the problem in hand.

For the solution at the next time step to lie on the polynomial both the value of the state variable x_{n+1} and the derivative $\mathrm{d}x_{n+1}/\mathrm{d}t$ must satisfy the polynomial.

The derivative $\mathrm{d}x_{n+1}/\mathrm{d}t$ at the next time step t_{n+1} can be related to the unknown future value x_{n+1} and the past computed values using

$$\frac{\mathrm{d}x_{n+1}}{\mathrm{d}t} = Pn\left(x_{n+1},\, x_n,\, x_{n-1},\, x_{n-2},\, x_{n-3},\, \ldots,\, x_{n-k}\right) \tag{3.79}$$

For the solution at the next time step to lie on the polynomial both the value of the state variable x_{n+1} and the derivative must satisfy the polynomial.

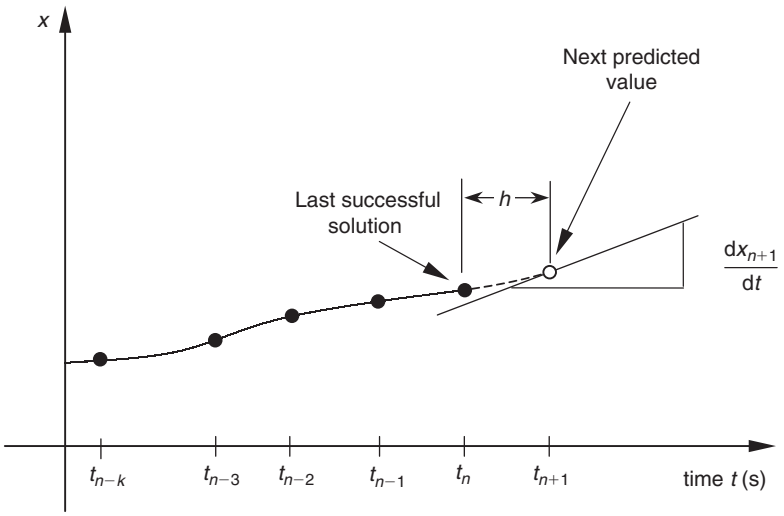

Fig. 3.41 Use of predictor to fit a polynomial through past values

For successful computation of the next solution at time = t_{n+1} there are therefore two unknowns, x_{n+1} and dx_{n+1}/dt, that must be found. This requires two equations, the first being the polynomial in (3.79) and the second being the state equation $G(x, \dot{x}, t) = 0$. Using the Newton–Raphson approach described in the previous section the solution takes the form in (3.80):

$$\frac{\partial G}{\partial \dot{x}}\,\Delta\dot{x}_{n+1} + \frac{\partial G}{\partial x}\,\Delta x_{n+1} = -G\left(\dot{x}_{n+1},\, x_{n+1},\, t\right) \tag{3.80}$$

If we substitute a term β that represents the ratio $\Delta\dot{x}_{n+1} = \beta\Delta x_{n+1}$ we end up with the following two equations on which the solution is based:

$$\left[\beta\frac{\partial G}{\partial \dot{x}} + \frac{\partial G}{\partial x}\right]\Delta x_{n+1} = -G\left(\dot{x}_{n+1},\, x_{n+1},\, t\right) \tag{3.81}$$

$$\Delta\dot{x}_{n+1} = \beta\Delta x_{n+1} \tag{3.82}$$

The integration process can be thought of as having two distinct phases. The first of these is the predictor phase that results in values of x_{n+1} and $\dot{x}_{n+1}$ that satisfy a polynomial fit through past values. The second is the corrector phase that iterates using the process shown in Figure 3.39 until the error is within tolerance and the solution can progress to the next time step. Parameters can be set that control the solution process. Examples of these are the initial, maximum and minimum integration step sizes to be used and the order of the polynomial fit. Parameters used during the corrector phase include the acceptable error tolerance, the maximum number of iterations and the pattern or sequence to be used in updating the Jacobian matrix during the iterations. In general these will default to values programmed into the software but with experience users will find the most suitable settings for the analysis in hand.

The integration step size is variable and if a solution is not achieved at the next prediction point the solver can reduce the integration time step and alter the order of the polynomial to attempt another solution. This typically occurs when there is a sudden change in an equation associated with a physical event such as an impact or clash of parts. A general rule in modelling is never to program an equation that instantly changes value at a certain time. Problems will be avoided by using, for example, a function that allows a smooth transition from one value to another over a physically small time interval.

Consideration of the predictor–corrector approach will indicate that at the start of a transient solution the solver may step forward and backward initially as it establishes a suitable scheme to progress the solution. Experienced users will again be aware of this and avoid programming important events to occur immediately after the start. For example, the simulation of a 5 second lane change manoeuvre may be best accomplished by an initial static analysis followed by the transient simulation for, say, 1 second of straight line driving before any steering inputs are made.

Advanced applications may also involve the incorporation of control algorithms based on a discreet time step. An example discussed later in this book will include the modelling of an Antilock Braking System (ABS) using a fixed time cycle. A possible solution here is to fix the integration minimum and maximum step size to ensure the solver computes solutions at the fixed time steps of the ABS algorithm. This may of course result in inefficient computation at some stages of the simulation. On the other hand the fixed step scheme must be refined enough to deal with any sudden non-linear events during the analysis.

Commercial multibody systems codes often have a range of integrators available that will adopt variations on the solution process discussed here. The most commonly used in MSC.ADAMS is referred to as the Gstiff integrator (Gear, 1971). Rather than storing past values of the polynomial a Taylor expansion (3.83) is used to store the polynomial in a form using the current value of the state variable x and the integration step size h. This is known as a Nordsieck vector. At a current time t the Nordsieck vector $[N_t]$ has the form

$$[N_t]^T = \left[x \quad h\frac{\mathrm{d}x}{\mathrm{d}t} \quad \frac{h^2}{2}\frac{\mathrm{d}^2x}{\mathrm{d}t^2} \quad \frac{h^3}{3!}\frac{\mathrm{d}^3x}{\mathrm{d}t^3} \quad \cdots \quad \frac{h^k}{k!}\frac{\mathrm{d}^kx}{\mathrm{d}t^k} \right] \tag{3.83}$$

The components of $[N_t]$ are added together to predict the next value of x at a time step h forward to a new time $t + h$. As the simulation progresses the Nordsieck vector is updated by pre-multiplying by the Pascal triangle matrix to give a new vector $[N_{t+h}]$. An example of this is shown for a polynomial with an order k equal to 5 in (3.84):

$$[N_{t+h}] = \begin{bmatrix} 1 & 1 & 1 & 1 & 1 & 1 \\ 0 & 1 & 2 & 3 & 4 & 5 \\ 0 & 0 & 1 & 3 & 4 & 5 \\ 0 & 0 & 0 & 1 & 4 & 5 \\ 0 & 0 & 0 & 0 & 1 & 5 \\ 0 & 0 & 0 & 0 & 0 & 1 \end{bmatrix} [N_t] \tag{3.84}$$

The predicted values in $[N_{t+h}]$ lie on the polynomial described by $[N_t]$ but are subject to further change as the state equations have not yet been corrected using the process shown in Figure 3.39. During the corrector phase the starting values of x and $(\mathrm{d}x/\mathrm{d}t)$ are taken from $[N_{t+h}]$. As the value of x changes during the Newton–Raphson iteration process the components of the Nordsieck vector are updated by $[\Delta N]$ where

$$[\Delta N] = [c][\Delta x] \tag{3.85}$$

and

$$[c]^T = [c_0\ c_1\ c_2\ c_3\ \ldots\ c_k] \tag{3.86}$$

The matrix $[c]$ contains constants with values dependent on the polynomial order k (Orlandea, 1973).

3.4 Systems of units

As with all engineering analysis it is important that consistent units are used throughout any calculation or simulation exercise. For static analysis the choice of a system of units can be quite forgiving as long as consistency is observed. For dynamic analysis more care is required. At a basic level if we consider the application of Newton's second law to a body n with mass m_n and acceleration $\{A_{Gn}\}_1$ at the mass centre G_n we have with the vector convention used here:

$$\Sigma\{F_n\}_1 = m_n\{A_{Gn}\}_1 \tag{3.87}$$

It is important to note that equation (3.87) is only valid for certain systems of units. For a metric system of SI units (force = N, mass = kg, acceleration = m/s^2) equation (3.87) can be used as it stands. The system of units used mainly in this text, and popular in Europe, is to use mm as the unit of choice for length. Clearly equation (3.87) would produce incorrect forces unless the right-hand side of (3.87) was divided by a constant, in this case 1000, to ensure consistency.

Early users of programs such as MSC.ADAMS needed to define such a constant when defining gravitational forces, even for dynamic models operating in a zero gravity environment. As such users were reminded of some of the basic fundamentals of dynamics when using such software. More modern programs require the users to define only a set of units and apply the correction internally. The following table is provided to show the required corrections to various systems of units. Although for most users of MBS this will be for reference only, advanced users developing subroutines that link with MBS may still be required to implement a constant to ensure consistency. An early term used to define the constant was the 'gravitational constant' although a more recent and applicable definition is the 'units consistency factor' or *UCF* where for any system of units the following equation is valid for the given units consistency factor in Table 3.6:

$$\Sigma\{F_n\}_1 = \frac{m_n\{A_{Gn}\}_1}{UCF} \tag{3.88}$$

In the following table the units consistency factor is for the systems of units common to both metric and imperial systems.

Table 3.6 Units consistency

Measurement	SI	Metric	Metric	Metric	FPS	FPS	IPS
Length	m	mm	cm	m	ft	ft	in
Velocity	m/s	mm/s	cm/s	m/s	ft/s	ft/s	in/s
Acceleration	m/s^2	mm/s^2	cm/s^2	m/s^2	ft/s^2	ft/s^2	in/s^2
Mass	kg	kg	kg	kg	slug	lbm	lbm
Force	N	N	kgf	kgf	lbf	lbf	lbf
Inertia	$kg\,m^2$	$kg\,mm^2$	$kg\,cm^2$	$kg\,m^2$	$slug\,ft^2$	$lbm\,ft^2$	$lbm\,in^2$
Gravity	$9.81\,m/s^2$	$9807\,mm/s^2$	$981\,cm/s^2$	$9.81\,m/s^2$	$32.2\,ft/s^2$	$32.2\,ft/s^2$	$386.1\,in/s^2$
UCF	1.0	1000	981	9.81	1.0	32.2	386.1

3.5 Pre- and post-processing

Most general-purpose multibody systems analysis programs offer a pre- and post-processor that allows users to define models and evaluate results using the same graphical environment often referred to as a Graphical User Interface (GUI). In recent years the graphical capability of programs such as ADAMS/View has advanced considerably allowing users to build geometries, calculate mass and inertial properties and parameterize models for design studies. The capability to set up Design of Experiments (DOE) studies is another powerful tool that may be exploited during the design phase. Post-processors have the capability to output results in tabular format, *x*–*y* plots and continuous graphic animation. The graphical functionality of some programs also allows important results to be plotted and models to be animated as the equations are solved. A typical example of vehicle graphic representation is shown in Figure 3.42.

An early customization of MSC.ADAMS for automotive applications was the ADAMS/Vehicle program originally developed as a commercially available product which has been used by engineers from the Newman/Hass Indy Car racing team (Trungle, 1991). The program allowed a suspension model to be created, carry out an analysis and post-process the results without specialist knowledge of MSC.ADAMS. The program could also be used to automatically generate a full vehicle model, hence the title. The pre-processor included a number of established suspension configurations where the data was input via screen templates using familiar suspension terminology. This has been subsequently replaced by updated products specifically aimed at the automotive areas of suspension and full vehicle modelling. At the time of writing there are two MSC.ADAMS related vehicle products in use, ADAMS/Car and ADAMS/Chassis. A detailed description will not be provided here. Such is the pace of development in these areas that any description will rapidly become outdated.

ADAMS/Car has been developed working with a consortium of major vehicle manufacturers including Audi, BMW, Renault and Volvo. The vehicle manufacturers' involvement included developing the specification for the functionality of the software. This included, for example, determining the suspension systems that would be included, the manoeuvres to be simulated and the outputs and their manner of presentation. An example of the ADAMS/Car graphical interface is shown in Figure 3.43.

Fig. 3.42 MSC.ADAMS vehicle graphical representation (provided courtesy of Prodrive)

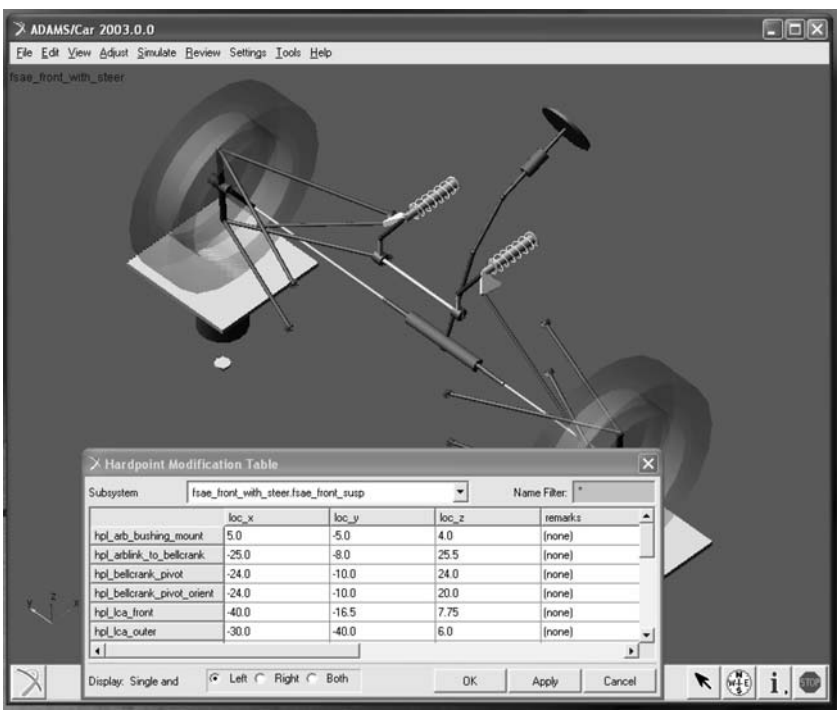

Fig. 3.43 ADAMS/Car graphical user interface (provided courtesy of MSC.Software)

The user interface has been developed from the ADAMS/View environment and includes two basic modes of operation:

(i) The Expert User mode is intended for experienced users who have access to the fundamental software modelling elements. As such they are able, for example, to create or modify system model templates of suspensions and steering systems. They would also be able to modify or create test procedures to be simulated.

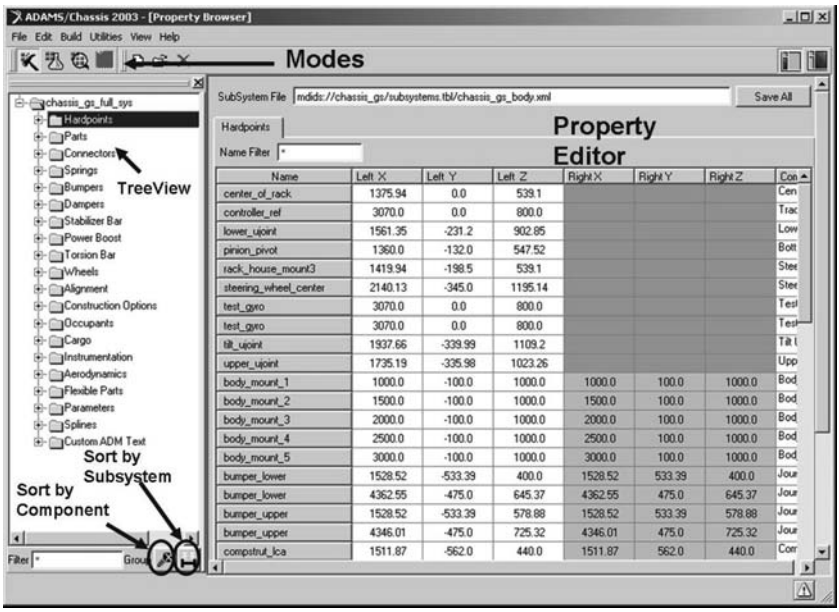

Fig. 3.44 ADAMS/Chassis user interface (provided courtesy of MSC.Software)

(ii) The Standard User mode is intended for design, test and development engineers in addition to analysts. These users would not necessarily be MSC.ADAMS experts but would be able to use the existing templates to enter data and create models using familiar terminology.

In parallel to ADAMS/Car the ADAMS/Chassis system is also used for vehicle work and offers similar capability. The ADAMS/Chassis program was originally developed in-house by Ford in the late 1980s. The program was originally called ADAMS/Pre and as the name suggests the early implementation was a pre-processor that automatically formatted ADAMS data sets. In its current form it has additional capability to run customized simulations and has its own post-processor. Ford allowed the program to be taken on and developed by another company before the product was acquired by the developers of MSC.ADAMS. Due to its origin ADAMS/Chassis appears on the surface unlike any of the other customized MSC.ADAMS programs. The program uses a graphical interface based more on data forms to enter the data. An example is shown in Figure 3.44.

The program also requires a high level of programming skill on the part of any expert user who is going to customize or develop the way models are generated, simulations are run or results are plotted and reported. In addition to vehicle dynamics knowledge the ADAMS/Chassis expert would need a working knowledge of ADAMS/Solver language, C++ and FORTRAN in order to perform any meaningful customization. It is perhaps fortuitous that the program offers a good range of suspension systems in the current implementation.

Once the full vehicle is assembled there exists a range of pre-programmed manoeuvres that may be selected and simulated. Examples are listed here in Table 3.7 using the terminology particular to ADAMS/Chassis to name the manoeuvres.

Table 3.7 Full vehicle manoeuvres implemented in ADAMS/Chassis

- Brake-in-turn
- Brake drift
- Constant radius
- Cross wind
- Frequency response
- J-turn
- Lane change
- On center handling
- Parking effort
- Steady state drift
- User defined event
- Straight line acceleration
- Straight line deceleration
- Straight line drive
- Step steer
- Static vehicle characteristics (SVC)
- Swept steer
- Low G swept steer
- Throttle-off-in-turn
- Throttle-on-in-turn
- Tire wear

Table 3.8 ADAMS/Car calculated suspension outputs

- Ackerman
- Ackerman angle
- Ackerman error
- Percent Ackerman
- Anti-dive
- Anti-lift
- Camber angle
- Camber compliance
- Caster angle
- Caster moment arm
- Caster moment arm
- Dive
- Fore-aft stiffness
- Front swing-arm angle
- Front swing-arm length
- Ideal steer angle
- King pin inclination angle
- Lateral camber compliance
- Lateral deflection compliance
- Lateral steer compliance
- Lift
- Outside turn diameter
- Ride rate
- Ride steer
- Roll angle
- Roll camber coefficient
- Roll center height
- Roll steer
- Scrub radius
- Side angle
- Side swing-arm angle
- Side swing-arm length
- Spindle vector
- Steer angle
- Suspension roll rate
- Toe angle
- Total roll rate
- Turn radius
- Wheel load
- Wheel rate
- Wheel travel

Both ADAMS/Car and ADAMS/Chassis include a substantial list of pre-programmed suspension outputs that can be automatically calculated and reported to the user. Examples are provided in Table 3.8.

It is perhaps in the calculation of outputs such as these that the customized software offers a significant benefit to the analyst. The next chapter will consider some of the more significant outputs listed in Table 3.8. Examples will be provided showing how, for example, a geometric roll centre can be located programming equations from first principles.

4 Modelling and analysis of suspension systems

In this chapter, the basic role of the suspension system is discussed from a functional, analytical perspective. Several types of suspension are introduced and methods of their analysis are described in a typical commercial multibody systems analysis package. One of the best known suspension types is shown in Figure 4.1, this being a suspension system referred to in Europe as a double wishbone system. In the USA the practice is to call the same system a short–long arm (SLA) suspension system. We will be considering the modelling and analysis of suspension systems as separate units, a practice sometimes referred to as quarter vehicle modelling. The discussion in this chapter will be restricted to passive systems and will not address active suspension systems.

It is also intended in this chapter to demonstrate the manner in which the vector-based methods described in Chapter 2 can be applied to carry out three-dimensional kinematic, static and dynamic force analyses of a double wishbone suspension system. The model geometry has also been analysed using an equivalent MBS model in MSC.ADAMS allowing a comparison of results from theory and MBS and providing readers with an insight into the computational processes involved.

The traditional treatment of suspension systems, dealing usually with a projection in one plane, is used here only where useful to explain standard terms that the student or developing practitioner should be aware of.

The concept of a roll centre is one that has been used extensively by vehicle designers in order to relate suspension layout to vehicle handling performance, particularly when considering understeer or oversteer. The roll

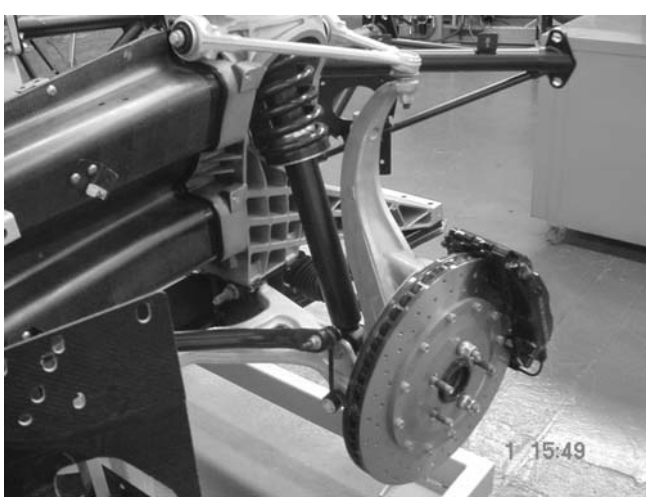

Fig. 4.1 Aston Martin Vanquish double wishbone front suspension system

centre is introduced in this chapter using a classical treatment together with a description of the typical process used in MBS for computation.

Before progressing to a detailed treatment of the modelling and analysis issues it is important to fully describe the function of a suspension system and the needs that must be addressed. The initial sections of this chapter identify these needs in a systematic manner providing a checklist against which suspension performance may be evaluated during the vehicle design process. The follow-on treatment of modelling and simulation can then be related back to the various needs now described.

4.1 The need for suspension

The term suspension seems an odd one when considering the function in a modern vehicle, as the vehicle body appears to sit on rather than be suspended from the mechanism. Some authors have noted that the name relates back to the days of the stagecoach where an attempt was made to improve the abominable ride comfort over very long journeys by suspending the coach body on leather straps from corner posts attached to the chassis frame. Hence the concept of a suspension system took early form.

In its simplest form, a modern road vehicle suspension may be thought of as a linkage to allow the wheel to move relative to the body and some elastic element to support loads while allowing that motion. As suspensions become more complex, the need for well-controlled damping forces and multi-directional compliance emerges. Multibody systems analysis can help quantify an existing design in terms of these parameters or help to synthesize a new design from a set of target parameters.

Most practical vehicles have some form of suspension, particularly when there are four or more wheels. The suspension system addresses two basic needs:

- Reduction of vertical wheel load variations
- Isolation of road inputs from the body

However, the introduction of a suspension system introduces some tasks of its own; each additional interface and component brings with it some structural compliance. This may lead to a delay in transmitting loads to the body, with a possible degradation to the vehicle handling task. It also offers the opportunity (or risk) of modifying the way the wheel is presented to the road. The new components must themselves be capable of surviving the design life when the vehicle is used as intended. Therefore, as a consequence of its existence the suspension generates four more needs:

- Control of transmission of handling loads to body
- Control of wheel plane geometry due to compliant effects
- Control of wheel plane geometry due to kinematic effects
- Comprehension of component load environment

Modern multibody systems analysis tools offer the opportunity to evaluate each of the six needs listed, either to investigate design strategies for whole

Table 4.1 Suspension design process activities

	Wheel load variation	Body isolation	Handling load control	Compliant wheel plane control	Kinematic wheel plane control	Component loading environment
Investigate	✔	✔	✔	✔	✔	✔
Set targets	✔	✔	✔	✔	✔	✔
Verify	✔	✔	✔	✔	✔	✔

systems, set design targets for components or to verify the performance of proposed designs. Any rigorous design process must therefore be able to quantify matters in these 18 different ways as shown in Table 4.1.

It is easy to focus on one small subset of the task above but to do so fails to deliver the full range of benefits possible from multibody systems analysis software. The software is generally expensive and the skilled personnel to operate it are hard to come by and so such a focus represents a lost opportunity for the organization.

4.1.1 Wheel load variation

Since a vehicle with four wheels is statically indeterminate with respect to the calculation of reaction forces, only with some elastic behaviour ('compliance') in the suspension can a determinate solution be formulated unless some presumption of symmetry is made; otherwise, the 'wobbly table' case exists where there are at least three possible load distributions (Figure 4.2). This leads to abrupt fluctuations in load of a type barely tolerable in restaurants and unconscionable for road vehicle behaviour. For the problem shown we have one system and three possible reaction load solutions. These include being balanced on the two longest legs (left in Figure 4.2) – unlikely in practice but a solution in theory – or being balanced on three

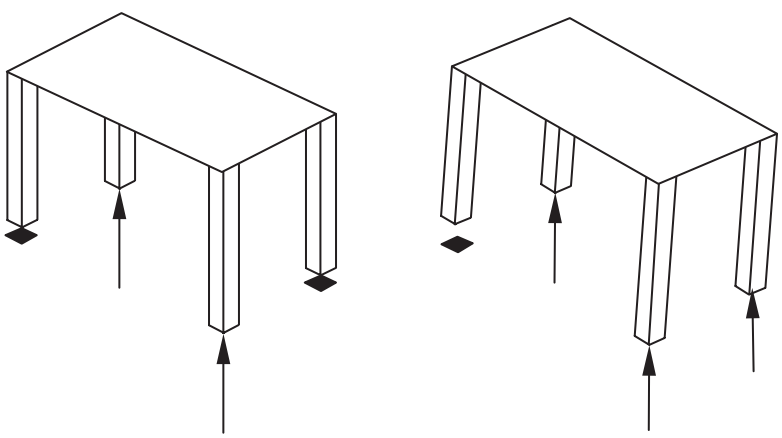

Fig. 4.2 A classic case of static indeterminancy

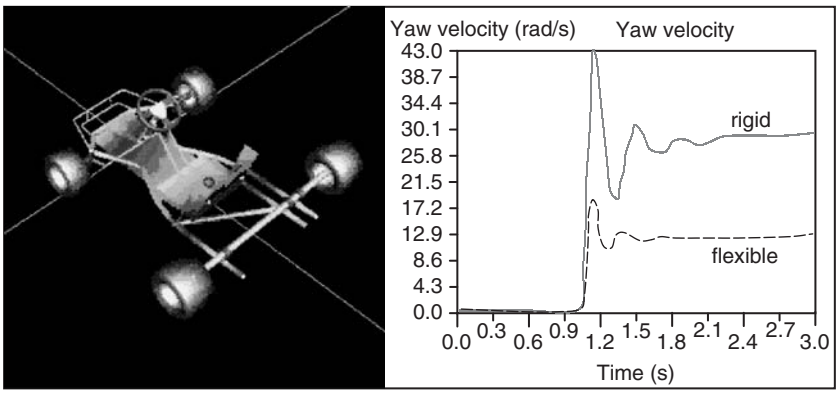

Fig. 4.3 The influence of racing kart frame flexibility (provided courtesy of MSC.Software)

legs (right in Figure 4.2) in one of two stable states. This system represents a classic case of static indeterminacy.

Consideration of a shopping trolley, a notionally rigid vehicle with four wheels that displays many irksome traits, shows that even on the most well-prepared supermarket floor the absence of suspension causes problems with load distribution between the four wheels due to inconsistent manufacture. The least loaded wheel is prone to shimmy and the uneven wheel load distribution can emphasize frictional asymmetry in the castoring joints with even the most fastidious grocery-packing practices, giving the familiar 'mind of its own' sensation.

Less infuriating 'rigid' vehicles include some agricultural equipment that uses compliant behaviour in the tyre sidewalls to accommodate uneven terrain, and racing karts that use a significant amount of compliance in the frame structure of the vehicle to modify vertical wheel loads. An example of this is shown in Figure 4.3 where the inclusion of the racing kart frame flexibility clearly influences the yaw rate response for a simulated manoeuvre.

More formally, the problem may be posed as a rigid platform, Body 2, of total weight $m_2\{g\}_1$, with reactions acting at wheel locations A, B, C and D as shown in Figure 4.4.

Consider first the equations that would be needed for equilibrium of forces. Note that for rigour we are continuing with the vector notation established in Chapter 2:

$$\sum\{F_2\}_1 = \{0\}_1 \tag{4.1}$$

$$\{F_A\}_1 + \{F_B\}_1 + \{F_C\}_1 + \{F_D\}_1 - m_2\{g\}_1 = \{0\}_1 \tag{4.2}$$

$$\begin{bmatrix} 0 \\ 0 \\ F_{Az} \end{bmatrix} + \begin{bmatrix} 0 \\ 0 \\ F_{Bz} \end{bmatrix} + \begin{bmatrix} 0 \\ 0 \\ F_{Cz} \end{bmatrix} + \begin{bmatrix} 0 \\ 0 \\ F_{Dz} \end{bmatrix} - m_2 \begin{bmatrix} 0 \\ 0 \\ g \end{bmatrix} = \begin{bmatrix} 0 \\ 0 \\ 0 \end{bmatrix} \tag{4.3}$$

From (4.3) we now get the expression in (4.4) that we would normally get quickly by inspection:

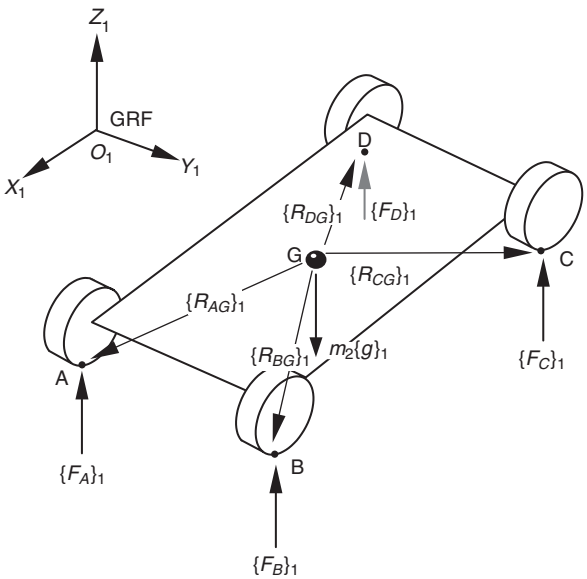

Fig. 4.4 The wheel load reaction problem

$$F_{Az} + F_{Bz} + F_{Cz} + F_{Dz} - m_2 g = 0 \tag{4.4}$$

If we continue now to take moments about the mass centre G of Body 2 we have

$$\sum\{M_G\}_1 = \{0\}_1 \tag{4.5}$$

$$\{R_{AG}\} \times \{F_A\}_1 + \{R_{BG}\}_1 \times \{F_B\}_1 + \{R_{CG}\}_1 \times \{F_C\}_1 + \{R_{DG}\}_1 \times \{F_D\}_1 = \{0\}_1 \tag{4.6}$$

If we expand the vector moment terms for the force acting at A only we get

$$\begin{bmatrix} 0 & -AG_z & AG_y \\ AG_z & 0 & -AG_x \\ -AG_y & AG_x & 0 \end{bmatrix} \begin{bmatrix} 0 \\ 0 \\ F_{Az} \end{bmatrix} = \begin{bmatrix} AG_y F_{Az} \\ -AG_x F_{Az} \\ 0 \end{bmatrix} \tag{4.7}$$

From (4.7) it is clear that we can now write equation (4.6) as

$$AG_y F_{Az} + BG_y F_{Bz} + CG_y F_{Cz} + DG_y F_{Dz} = 0 \tag{4.8}$$

$$-AG_x F_{Az} - BG_x F_{ABz} - CG_x F_{Cz} - DG_x F_{Dz} = 0 \tag{4.9}$$

It can now be seen that we have the classical case of an indeterminate problem where there are insufficient equations available to solve for the unknowns. The four unknowns here are F_{Az}, F_{Bz}, F_{Cz} and F_{Dz}. There are, however, only the three equations (4.4), (4.8) and (4.9) available to effect a solution. Trying to arrange the equations in matrix form for solution demonstrates the futility of the problem.

$$\begin{bmatrix} 1 & 1 & 1 & 1 \\ AG_y & BG_y & CG_y & DG_y \\ -AG_x & -BG_x & -CG_x & -DG_x \\ ? & ? & ? & ? \end{bmatrix} \begin{bmatrix} F_{Az} \\ F_{Bz} \\ F_{Cz} \\ F_{Dz} \end{bmatrix} = \begin{bmatrix} m_2 g \\ 0 \\ 0 \\ ? \end{bmatrix} \tag{4.10}$$

If a modified formulation is adopted, the problem can be posed more completely. If the rigid platform is presumed to be sprung in the manner of a normal road vehicle with an effective wheel rate, k_A, k_B, k_C and k_D, at A, B, C and D then a new formulation is possible. Writing A_{2z}, B_{2z}, C_{2z} and D_{2z} for the height of corners A, B, C and D on Body 2 and A_{1z}, B_{1z}, C_{1z} and D_{1z} for the ground height corners at A, B, C and D we can then define a preload Fp_A, Fp_B, Fp_C and Fp_D on each spring such that if the z co-ordinates of Body 2 at the corner are equal to the z co-ordinates of the ground, Body 1, at each corner then the spring load is equal to the preload. This leads to the following equations for the spring force at each corner:

$$F_{Az} = k_A(A_{2z} - A_{1z}) + Fp_A \tag{4.11}$$

$$F_{Bz} = k_B(B_{2z} - B_{1z}) + Fp_B \tag{4.12}$$

$$F_{Cz} = k_C(C_{2z} - C_{1z}) + Fp_C \tag{4.13}$$

$$F_{Dz} = k_D(D_{2z} - D_{1z}) + Fp_D \tag{4.14}$$

At first sight it would appear this is simply a more elaborate formulation of the previous problem; there are still four unknown quantities (the corner heights of Body 2) and three equations (4.4), (4.8) and (4.9). However, consideration of the rigid platform yields a fourth relationship:

$$D_{2z} = C_{2z} + (B_{2z} - A_{2z}) \tag{4.15}$$

This leads to, after some manipulation of (4.10) substituting in the spring equations (4.11–4.13) for F_{Az}, F_{Bz}, F_{Cz} and relying on (4.15) to solve for F_{Dz}, the equations in (4.16):

$$\begin{bmatrix} k_A - k_D & k_B + k_D & k_C + k_D \\ k_A AG_y - k_D DG_y & k_B BG_y + k_D DG_y & k_C CG_y + k_D DG_y \\ k_A AG_x - k_D DG_x & k_B BG_x + k_D DG_x & k_C CG_x + k_D DG_x \end{bmatrix} \begin{bmatrix} A_{2z} \\ B_{2z} \\ C_{2z} \end{bmatrix} = \begin{bmatrix} \lambda_1 \\ \lambda_2 \\ \lambda_3 \end{bmatrix} \tag{4.16}$$

where

$$\lambda_1 = m_2 g + k_A A_{1z} - Fp_A + k_B B_{1z} - Fp_B + k_C C_{1z} - Fp_C + k_D D_{1z} - Fp_D \tag{4.17}$$

$$\lambda_2 = (k_A A_{1z} - Fp_A)AG_y + (k_B B_{1z} - Fp_B)BG_y + (k_C C_{1z} - Fp_C)CG_y + (k_D D_{1z} - Fp_D)DG_y \tag{4.18}$$

$$\lambda_3 = (k_A A_{1z} - Fp_A)AG_x + (k_B B_{1z} - Fp_B)BG_x + (k_C C_{1z} - Fp_C)CG_x + (k_D D_{1z} - Fp_D)DG_x \tag{4.19}$$

The equations in (4.16) may be solved by Gaussian elimination and substitution. It can be seen that preloads (Fp_A, Fp_B, Fp_C and Fp_D), the ground

heights (A_{1z}, B_{1z}, C_{1z} and D_{1z}), and the corner stiffness (k_A, k_B, k_C and k_D), and wheel locations are the inputs to the calculations. The unknowns that are found from (4.16) are the body heights at three corners (A_{2z}, B_{2z} and C_{2z}). These are used to find D_{2z} from (4.15) leading to the force solution in each corner from equations (4.11–4.14). Thus, the presence of an elastic suspension for the roadwheels allows a solution to the 'wobbly table' problem for vehicles with four or more wheels even when traversing terrain that is not smooth.

4.1.2 Body isolation

The interaction of a single wheel with terrain of varying height is frequently idealized as shown in Figure 4.5. This is a so-called 'quarter vehicle' model and is widely used to illustrate the behaviour of suspension systems. It may be thought of as a stationary system under which a ground profile passes to give a time-varying ground input, z_g. Note that at this point we are assuming the tyre to be rigid. Whether classical models or 'literal' multibody system models are used, the methods used to comprehend body isolation are the same.

Classically, the system may be formulated as a single second order differential equation:

$$m\ddot{z} + c(\dot{z} - \dot{z}_g) + k_s(z - z_g) = 0 \tag{4.20}$$

In order to more fully understand the isolation behaviour of the suspension, a fully developed (steady state) harmonic solution of the equation above may be presumed to apply. 'Harmonic' simply means that both input and output may be described with sine functions and that the phase relationships are fixed. This may be conveniently expressed in the form

$$z = A \cdot e^{(j\omega t + \phi)} \tag{4.21}$$

where j is the imaginary square root of -1. Thus for the two derivatives of z it may be written:

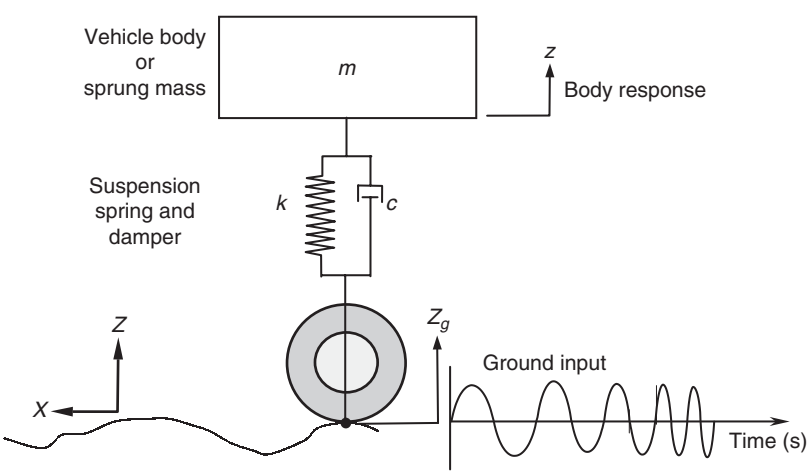

Fig. 4.5 A classical quarter vehicle ride model

$$\dot{z} = j\omega A e^{(j\omega t+\phi)} = j\omega z \tag{4.22}$$

and

$$\ddot{z} = -\omega^2 A e^{(j\omega t+\phi)} = -\omega^2 z \tag{4.23}$$

The original equation (4.20) can then be written:

$$-m\omega^2 z + jc\omega(z - z_g) + k(z - z_g) = 0 \tag{4.24}$$

Rearranging this in the form of a transfer function gives

$$H(\omega) = \frac{(k) + j(c\omega)}{(k - m\omega^2) + j(c\omega)} \tag{4.25}$$

This expression relates the amplitude and phase of ground movements to the amplitude and phase of the body movements and is commonly reproduced in many vibration theory books and courses.

Considering the transfer function, several behaviours may be observed. At frequencies of zero and close to zero, the transfer function is unity. This may reasonably be expected; if the ground is moved very slowly the entire system translates with it, substantially undistorted. The behaviour of the system may be described as 'static' where its position is governed only by the preload in the spring and the mass carried by the spring; dynamic effects are absent.

At one particular frequency where $\omega = \sqrt{k/m}$, the real part of the denominator becomes zero and the transfer function is given by

$$H(\omega) = \frac{(k) + j(c\omega)}{j(c\omega)} = \frac{-jk}{j(c\omega)} + 1 \tag{4.26}$$

At this frequency, the behaviour of the system is called 'resonant'. Examination of the transfer function shows it is at its maximum value. Since k, c and ω are all positive real numbers, the transfer function shows that ground inputs are amplified at this frequency. If c is zero, i.e. there is no damping present in the system, then the transfer function is infinite. If c is very large, the transfer function has an amplitude of unity. For typical values of c, the amplitude of the transfer function is greater than unity.

At substantially higher frequencies where $\omega \gg \sqrt{k/m}$, the transfer function is dominated by the term $-m\omega^2$ in the denominator and tends towards

$$H(\omega) = \frac{1}{-m\omega^2} \tag{4.27}$$

At these higher frequencies, the amplitude of the transfer function falls away rapidly.

It may therefore be noted that if it is desired to have the body isolated from the road inputs, the system must operate in the latter region where $\omega \gg \sqrt{k/m}$. In fact this is a general conclusion for any dynamic system; for isolation to occur it must operate above its resonant frequency. Given that the mass of the vehicle body is a function of things beyond the suspension designer's control, it is generally true that the only variables available

to the designer are spring and damper calibration. Therefore the preceding analysis would suggest that the softest springs possible, to position the resonant frequency as low as possible, are preferred.

In a purely technical sense this is indeed true; however, our vehicles are to have as their primary purpose the transport of people. People in general have a susceptibility to motion sickness for very low frequency motions; this places a practical lower limit on our resonant frequency of something around 0.5 Hz, or 3 rad/s. Given that the human frame is primarily engineered for walking, a more typical value for the resonant frequency of the body mass on the road springs is just over 1 Hz, this being the frequency at which we walk for the majority of the time. This is one of several reasons why babies may be readily nursed to sleep in cars; the motion of the vehicle gives an acceleration environment not unlike being held in the arms of a walking adult.

Our real vehicle systems are rarely so straightforward to address as this, however. Real vehicle suspensions have vertical and longitudinal compliance behaviour. Suspension components rotate as well as translate and the sprung mass has rotational as well as translational freedoms. Modern multibody system analysis software allows us to describe the individual components of the system and will automatically calculate the contribution of, for example, sprung mass pitch inertia to the acceleration solution for the body. The software also allows the linearization of the system about an operating point and the calculation of modes of vibration of the system. For example, the longitudinal compliance typically snubs out under hard braking and the fore–aft isolation suffers; proprietary software will allow the calculation of fore–aft resonant frequencies under cruise and braking conditions and their comparison by an intelligent user will explain (and perhaps generate solutions for) harsh behaviour over small obstacles while braking.

At no stage with added complexity do the basic rules for dynamic systems break down; there remains a subresonant, stiffness-dominated regime, a resonant, damping-dominated regime and a post-resonant, mass-dominated regime. The software user who keeps a grasp of these basic concepts, while allowing the software to undertake the task of assembling the equations of motion and solving them, is productive within an engineering organization.

4.1.3 Handling load control

The simplest possible representation for a vehicle, Body 2, manoeuvring in the ground plane is shown in Figure 4.6. If we break from the full 3D vector notation the following pair of differential equations describes it fully:

$$\sum M_{2z} = I_{zz}\dot{\omega}_{2z} \tag{4.28}$$

$$\sum F_{2y} = m_2(\dot{V}_{2y} + V_{2x}\omega_{2z}) \tag{4.29}$$

These equations, their significance and a more formal derivation are well described in the seminal IME paper (Segel, 1956). The formulation states that yaw acceleration is the applied yaw moments divided by the yaw inertia of the vehicle, and that lateral acceleration is the applied lateral forces

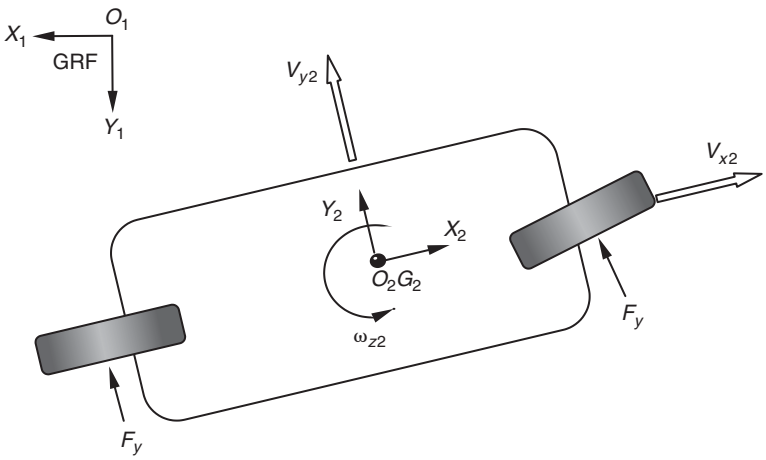

Fig. 4.6 The simplest possible representation of a vehicle manoeuvring in the ground plane

divided by the mass of the vehicle. The additional term in the lateral force expression reflects a body-centred formulation, which is more convenient when the model is expanded to more than the 2 degrees of freedom shown.

The two equations are correctly referred to as a 2-degree-of-freedom ('2 DOF') model; they are sometimes referred to as a 'bicycle' model but the authors dislike this description since it implies that the description may be suitable for two-wheeled vehicles, which it most certainly is not.

Even with this simplest possible representation, it can be seen that the vehicle may be thought of as a free-floating 'puck' (as used in ice hockey), to which forces are applied by the tyres in order to manipulate its heading and direction. To many casual observers it appears that the vehicle runs on little 'rails' provided by the tyres and that the function of the tyres is simply to provide a cushion of air beneath the steel wheel rims. This is simply not so, and examination of the behaviour of rally cars in the hands of skilled drivers reveals behaviour which visually resembles that of a hovercraft. All vehicles on pneumatic tyres behave as the rally cars behave, adopting a sideslip angle to negotiate even the slightest curve. Since this angle is typically less than a degree it is not always apparent to the untrained observer; it may, however, be seen on high speed, steady corners such as motorway interchanges if vehicles are observed attentively.

The generation of the forces necessary to initiate the turn, to constrain the vehicle at the correct sideslip angle and to return it to the straight-running condition is the role of the tyres. In order to successfully control the vehicle, however, those loads must be transmitted to the sprung mass. This is a key role for the vehicle suspension system.

Close examination of the vehicle behaviour described by the equations above can demonstrate the slight phasing of the forces necessary to allow the vehicle to accelerate in yaw and be constrained to the desired yaw

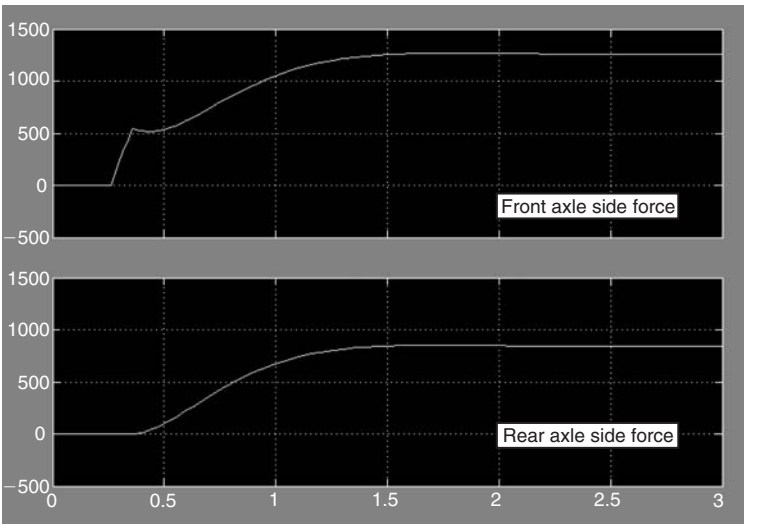

Fig. 4.7 Side forces calculated for a 0.1 rad/s ramped input to 0.01 rad beginning at 0.3 s

velocity (Figure 4.7). Errors in that phasing generated by flexibility (compliance) on one axle or the other can lead to an error in the vehicle behaviour as perceived by the driver. This error may take the form of a disconcerting delay in response to the steering if the front axle has more compliance than the rear, or a rather more serious delay in the action of the rear axle in constraining the body slip angle to its required value. In the latter case, particularly for aggressive transient manoeuvres (i.e. accident avoidance) then the rear tyre slip angle may exceed its critical value, leading to a divergent behaviour of the vehicle – that is to say a spin.

Since for modern vehicles the isolation of road inputs is a high priority, there is always a desire to introduce some elastomeric elements into the vehicle between the suspension elements and the vehicle body. Multibody system analysis tools allow the study of handling degradation due to the introduction of such elastomers and allow the ride/refinement compromise to be quantified before excessive experimentation is carried out on the vehicle. MBS analysis in the right hands allows an understanding of those design parameters that dominate refinement performance and those that dominate handling performance. The understanding so gained allows better conceptual design of suspension systems in order to separate clearly the refinement and handling functionality for elastomeric elements. Modern multi-link rear suspensions are a good example of such well-separated systems and are a significant part of the simultaneous improvement in both ride and handling, traditionally areas of mutual exclusivity that have befallen modern road cars.

Even for a suspension with no elastomers, such as may be used on a competition vehicle, some structural compliance is always present. MBS analysis allows this compliance to be optimized and matched front to rear in order to avoid onerous design constraints using conservative stiffness targets, which would almost certainly incur some sort of weight disadvantage.

A final, important element of the study of handling load transfer is one that allows a single, unified treatment but rarely receives it. The notions of anti-dive/squat and 'roll centre' are rarely discussed together and yet their influence on vehicle handling loads is via the same mechanism; they lend themselves to the consistent rational treatment given here. The so-called 'roll centre' concept has to be one of the most non-intuitive and misunderstood modifiers of vehicle behaviour since empirically observed in racing circles in the 1920s. The understanding developed then is most applicable to beam axles and adds more difficulty than clarity for independent suspensions. The authors prefer the concept of 'sprung' and 'unsprung' load-paths to the vehicle body.

Figure 4.8 shows a single wheel of an independently suspended vehicle viewed from the side. A braking load is applied at the contact patch, reflecting the fitment of outboard brakes as is common practice. Were the brakes inboard or were this a tractive case, the load would be applied at the wheel hub height and the diagrams would be redrawn appropriately. In this case the suspension is of a leading arm type. Since all independent suspensions may be represented as some form of equivalent length virtual swinging arm (although the length and pivot location vary with some types more than others) this is a useful notion.

Three different orientations for the swinging arm are shown. The first has the swinging arm pivot on a direct line between the contact patch and the

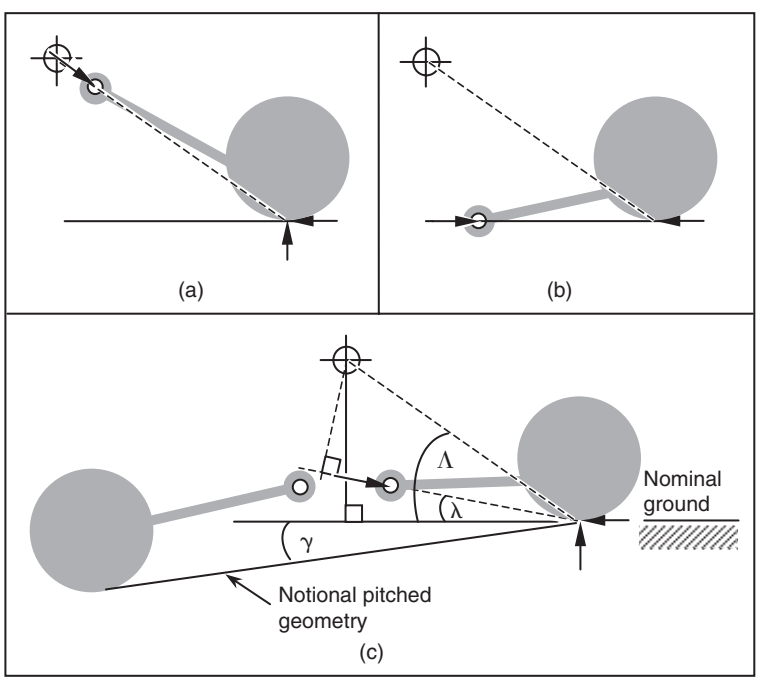

Fig. 4.8 (a) No-dive suspension – pitch moment transfer solely via an unsprung loadpath. (b) Pitch moment transfer solely via a sprung loadpath. (c) Typical arrangement; pitch moment carried by a combination of sprung and unsprung loadpaths

mass centre. Considering the wheel and arm together as a single entity and noting the ability of the pivot to support no moments, we may draw the reaction force at the pivot as being on a line between the contact patch and the pivot. The horizontal magnitude is the same as the applied longitudinal force at the wheel, giving a full solution for the force at the inboard pivot. The reaction on the sprung mass is equal and opposite to the force on the pivot, with a line of action passing directly through the mass centre. This is widely recognized as a 'no-dive' (no pitch) type of suspension. Although there is no body pitch, this does not mean there is no load transfer between rear and front wheels. We may therefore conclude that the braking load is carried to the vehicle mass centre entirely through the suspension linkage components and that none is carried in the suspension springs – i.e. via an 'unsprung' loadpath.

The second diagram has the swinging arm pivot at ground level. Using similar logic as before, the force at the pivot may be drawn as purely lateral, equal and opposite to that at the wheel. This in turn means the horizontal force is applied to the body at ground level, giving a pitch moment. That pitch moment cannot be reacted until the suspension has deformed sufficiently to give an equal and opposite moment on the sprung mass. In this case, the load transfer between rear and front axles is performed entirely by the suspension springing and none is carried in the suspension linkage components – i.e. via a 'sprung' loadpath.

The third diagram shows a more typical situation, with some of the pitch moment carried by an unsprung loadpath and most carried by a sprung loadpath. Some fraction that is a function of the two angles λ and Λ may be calculated and expressed as an 'anti-dive' fraction or percentage, or alternatively the anti-pitch angle λ may be quoted separately. The authors prefer

$$\textit{Anti-dive}\ \% = 100(\lambda + \gamma)/(\Lambda + \gamma) \tag{4.30}$$

Other texts give differing descriptions and definitions. What matters is not the definition, although it is important to be certain how the quantities in use are defined if they are to be compared one with another, but the significance of the sprung and unsprung load transfers themselves:

- Unsprung load transfer occurs via the stiff metallic elements in the system and is thus very rapid. It is limited in speed by the frequency of the wheel hop mode, a mode of vibration in which the unsprung mass oscillates on the tyre stiffness somewhere of the order of 15 Hz.
- Sprung load transfer occurs via the elastic elements of the system and is limited in speed by the frequency of the primary suspension mode. This is of the order of 1.5 Hz.

It may be seen then that unsprung load transfer is some 10 times faster than sprung load transfer. Herein lies the key to understanding some of the most important effects of the so-called 'roll centre'. Figure 4.9 is very similar to Figure 4.8 except that it shows the vehicle from the front instead of the side. Otherwise, the diagrams are identical. Figure 4.9(a) shows a 'no-roll' suspension with load transfer entirely by an unsprung loadpath. Figure 4.9(b) shows a suspension that transmits load entirely via a sprung loadpath.

The point frequently but ambiguously referred to as the 'roll centre' is where the line of action of the unsprung loadpath crosses the vehicle centre line.

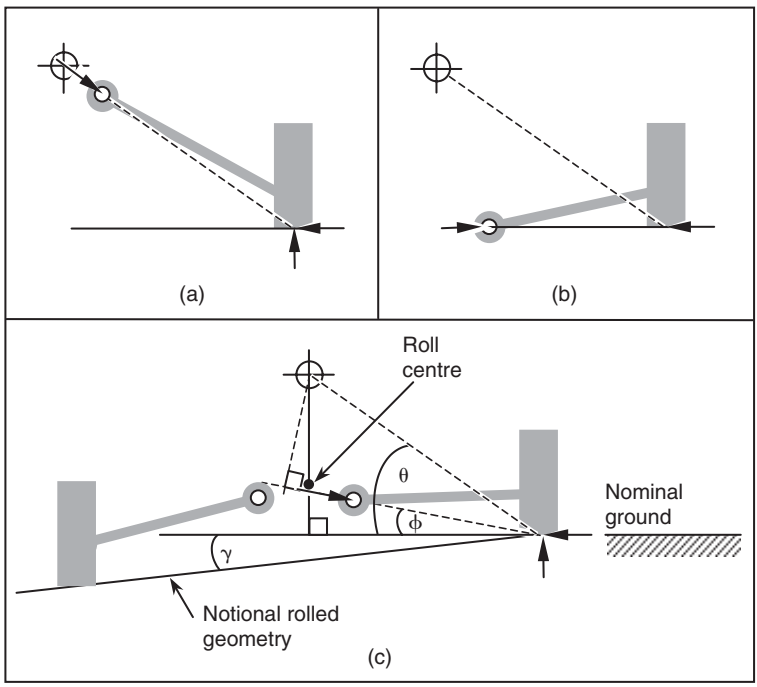

Fig. 4.9 (a) No-roll suspension – roll moment transfer solely via an unsprung loadpath. (b) Roll moment transfer solely via a sprung loadpath. (c) Typical arrangement; roll moment carried by a combination of sprung and unsprung loadpaths

As with the anti-pitch behaviour, the absolute height is of less importance than the distribution of loads between sprung and unsprung loadpaths. It is not any kind of centre of motion.

Again as with the anti-pitch behaviour, some fraction that is a function of the two angles ϕ and θ may be calculated and expressed as an 'anti-roll' fraction or percentage, or alternatively the anti-roll angle, ϕ, may be quoted separately. Alternatively, an anti-roll fraction or percentage could be quoted based on the fraction of the 'roll centre height' compared to the mass centre height. The authors prefer to use a ratio of the two angles ϕ and θ to express the anti-roll fraction similarly to before:

$$\textit{Anti-roll } \% = 100(\phi + \gamma)/(\theta + \gamma) \tag{4.31}$$

For lateral handling loads, the same ideas of relative speed between unsprung and sprung loadpaths apply. This has a particular importance when considered in the light of the phasing of front and rear axle forces in order to manipulate the yaw moments on the body. For a vehicle in yaw, the rate of load transfer may thus be set differently at different ends of the vehicle in order to modify the transient behaviour as compared to the steady state behaviour. For example, it is typical for vehicles to run around 20% rear anti-roll and only around 6% front anti-roll. This means that as a manoeuvre develops, load transfer from the outside rear tyre may briefly outpace load transfer from the front tyre. The resulting yaw moment acts to stabilize the

Fig. 4.10 The combination of anti-roll geometry to give a single 'roll centre' between left and right wheels is clearly nonsensical when the loading is strongly asymmetric – even when the asymmetry is less extreme than the racing Ford Falcon shown here.

vehicle and mitigates sudden, aggressive steer inputs. Vehicles that do not have this type of geometry, notably those with trailing arm rear suspensions, are unable to benefit from these effects.

For both longitudinal and lateral load transfers there is no conceptual reason why either the anti-pitch angle or anti-roll angle may not be negative. Motorcycles, for example, have a negative anti-pitch angle equal to the steer axis rake when they are fitted with conventional telescopic forks. This has the disadvantage of requiring extra performance from the suspension springs since they must carry more than the straightforward load transfer one might instinctively expect.

Some practitioners attempt to calculate combined measures for both suspensions on the same axle or indeed all the suspensions on the vehicle. For beam axles there is some logic in combining the characteristics since the wheels are physically joined but for independent suspensions, calculating some combined metric is of questionable value. For example, attempting to combine anti-roll angles across one axle in a purely geometric manner, when their relative importance is determined by wheel loading, is clearly nonsensical, as shown in Figure 4.10.

Multibody systems analysis allows both an understanding of the load transfers in a rig-based environment, such as may be measured on the MIRA Kinematics & Compliance rig (Whitehead, 1995) and also during real driving manoeuvres. In both situations, the ability of an MBS model to retrieve forces in each suspension member in convenient frames of reference while working with quarter, half or full vehicle models is a powerful tool to unscramble some of these less-than-intuitive effects with vehicle designs.

4.1.4 Compliant wheel plane control

Hand-in-glove with an understanding of the load transmission paths and time delays associated with the activity manoeuvring the vehicle in the ground plane comes an understanding of the resulting motion of the wheel plane with respect to the ground. From the treatment of tyres that follows in Chapter 5, and as described briefly in the introductory chapter, it is clear that the angles at which the tyres are presented to the road are of crucial importance in modifying the forces generated by the tyres and hence the resulting motion of the vehicle.

There are some subtle and intricate effects present in real vehicle systems that defy simplistic comprehension and evaluation. For example, the deformation of anti-roll bars reorients the links with which they are connected to the moving suspension members and may introduce forces that 'steer' the wheel plane with respect to the vehicle. This may not have been considered at the time the suspension was schemed conceptually but yet may modify the behaviour of the vehicle in practice.

Multibody systems analysis allows the reconstruction of rig-based measurements for such wheel plane compliant behaviour before prototype vehicles exist. It also allows a systematic and well-controlled comparison of behaviour with different levels of compliance in order to establish the influences of the different aspects of wheel plane compliance on vehicle behaviour. Typically such studies carry across several revisions of a model within a market segment and are thus of some strategic benefit.

4.1.5 Kinematic wheel plane control

Suspension arrangements typically consist of some connection of linkages to a device for holding the bearings in which the wheel actually turns. The interaction of those individual elements comprising the linkage means that the wheel plane typically undergoes some sort of translation and rotation as the suspension articulates.

This motion of the wheel plane is traditionally defined with respect to the vehicle body, although for a moving vehicle it is the angles and velocities with respect to the road that are of import. However, using the vehicle body gives a convenient frame of reference and so the following descriptions will do so:

(i) Toe change (steer) with suspension articulation gives a lateral force and yaw moment by directly adding to or subtracting from the tyre slip angle and is readily understood. Some care is needed when discussing this characteristic since there are a number of possibilities for definition; steer may be defined as a right-hand positive rotation about the vehicle vertical axis or it may be defined as a handed rotation, different on left and right sides of the vehicle ('toe-out') or even as a term relating the behaviour to the yaw moment it induces on the vehicle ('roll understeer').

(ii) Camber change acts to mitigate the angle with which the tyre is presented to the road due to the roll of the body with respect to road surface. For typical passenger vehicles, the vehicles roll 'out' of turns, with the inside edge of the vehicle platform being further away from the road than

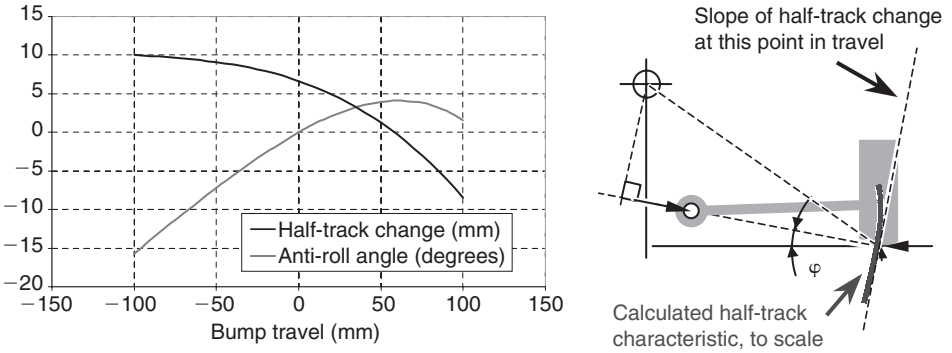

Fig. 4.11 Relationship between calculated half-track change and anti-roll angle

the outside. Were the wheels to remain perpendicular to the vehicle platform at all times, they would be presented to the road with a camber angle equal to the vehicle roll angle. For most independent suspension types, the wheels camber somewhat with respect to the body such that they are presented to the road at something less than the vehicle roll angle. This is referred to as 'camber compensation'. Were the wheels to remain upright with respect to the road, this would be 100% or 'full' camber compensation. As the wheel is presented to the road progressively more and more upright, the tyre is loaded more and more evenly across its width and lasts longer. This is of primary concern for competition vehicles. Camber angles also generate forces in their own right and the tendency of a tyre leaned 'out' of the turn is to reduce the cornering forces generated by tyre slip angles; therefore by balancing camber compensations front to rear some influence may be exerted on the overall handling balance of the vehicle.

(iii) It is typical for independent suspensions to move the contact patch of the tyre laterally as they articulate. Although less intuitively direct than the toe change mechanism, half-track change (lateral displacement) influences the lateral velocity of the tyre contact patch via roll rate. Hence the slip angle of the tyre is affected, since the angle is defined as the arctangent of lateral and longitudinal velocities; an increase in lateral velocity directly increases slip angle. If the track change is plotted against bump travel, with both measured at the contact patch, a direct indication of the anti-roll angle is obtained with no need for knowledge of construction methods for any particular type of suspension, as shown in Fig. 4.11.

Equally, there is often a desire to calculate some of these measures, particularly camber values and anti-roll elements, with respect to the ground. Unfortunately the location and orientation of the ground cannot reliably be determined using only a quarter vehicle model. Non-linear force-deflection characteristics are typical for the suspension elements and so the frequently used 'symmetric roll' presumption is often flawed. The amount of roll generated for a particular lateral loading varies with suspension calibration and the amount of roll moment carried on a particular axle varies with suspension calibration. Thus the boundary conditions cannot be known for a quarter vehicle model with any useful degree of certainty except for symmetric

events. It is strongly suggested that the simplest interpretations of the vehicle kinematic measures be used and comparisons drawn between these simple measures. For comprehending the effects on a full vehicle, a full vehicle model is recommended.

4.1.6 Component loading environment

Multibody systems models of the quarter vehicle type are often used to distribute design loads through the different suspension members with a view to sizing them intelligently in the first instance. A distinction needs to be drawn between design loads and service loads when discussing multibody systems analyses for this purpose. Design loads are calculated by postulating notional extremes for possible loads that may be induced in reality. An example of this might be the case where a car has been parked between two kerbs, between which it is a snug fit, and the driver then applies maximum effort to the handwheel. The exact philosophy for the selection and implementation of design loads is typically historical; they have been empirically defined and honed over many years of development experience. In practice they often correspond to events described as 'extreme service loads' or 'abuse loads'. They are events that the vehicle must survive but may need some attention immediately following it; in the steering example given, the steering alignment may be distorted by events but the vehicle would probably be required to remain capable of being driven. In industry many companies have standard cases such as the 3*g* bump case where the static wheel load is factored up to represent dynamic abuse situations such as striking a road hump at speed. The specification of abuse loads can be traced back to a publication in the *Automobile Engineer* by Garrett (1953) where a range of recommended wheel loads were proposed for the design of vehicles of that period. Design loads are frequently viewed as 'one-off' events in the life of the vehicle.

In contrast to design loads, there is another category of loads to which the vehicle is exposed. These are the service loads. This is the loading environment to which the vehicle is subject during its durability sign-off testing. Durability sign-off criteria vary widely but they typically consist of a specified number of repetitions of different events at prescribed speeds and loading conditions. They induce a large number of repetitions of events that are probably more commonplace in the life of a vehicle – driving up kerbs, for example. In contrast to the design events, the vehicle is expected to emerge largely undamaged from the durability sign-off procedure – although no expectation of remaining service life is usually associated with durability sign-off. The relationship between durability sign-off criteria and actual usage of the vehicle is another question entirely; durability sign-off procedures themselves are often compiled in the light of historical warranty costs and other such influences.

There is, then, a key difference between design and service events. The design events are slightly fictitious and are usually analysed using a static or quasi-static procedure. While of questionable 'accuracy' they are of tremendous value. They may be calculated with the scarcest data about the vehicle and allow the early intelligent sizing of many different components, once applied to the wheel of a quarter vehicle model and distributed about

a conceptual suspension layout. The resulting loading environment for each component may be used by designers to sketch a meaningful first-sight design. This can avoid packaging difficulties induced by ill-informed sketching of components and the subsequent 'stealing' of space needed for section modulus in key components.

Service loads are altogether more detailed. They are typically well-defined events where road profiles and speeds are well known. Once a reasonably representative geometry and suspension setting data set is available, the description of events may be combined with some form of enveloping tyre model in order to predict load–time histories for each component in the suspension. This in turn may be passed to finite element-based fatigue calculation methods in order to evaluate the number of times a component may be subject to this event before failure. Hypotheses such as the linear damage accumulation hypothesis (Miner's rule) may be used to sum up the contribution of different events to the life of the component. Interested readers are referred to the *SAE Fatigue Design Handbook* (Rice, 1997) for more information on component fatigue analysis.

With the calculation of service loads, instead of a single set of peak loads as produced from the design loads there is a vast amount of time-domain data. Typical data rates for service load events are around 200 points per second and service load events last of the order of 10 seconds. With a repertoire of up to 20 events describing a typical durability sign-off, it may be seen that the calculation of service loads results in an increase in the quantity of results data of the order of five orders of magnitude. Calculation and subsequent processing times rise too, though not quite by the same amount since linear static FE calculation times are a significant proportion of the overall elapsed time following design load calculations. However, as an overall process time amplification the expectation should be between two and three orders of magnitude for the calculation and use of service loads as compared to design loads. For some simple components, the use of a previously verified and correlated rig test may prove less onerous to the organization.

4.2 Types of suspension system

There are various suspension systems used on cars and trucks and as described in Chapter 3 specialized versions of MBS programs such as the ADAMS/Chassis and ADAMS/Car programs provide templates with preprogrammed configurations of suspension systems commonly used by automotive manufacturers. Many established textbooks on vehicle dynamics and some that focus on suspensions provide a detailed treatment of the various types of suspension system and their function. The coverage here will be to briefly mention some of the most common systems and then to direct our attention to the MBS modelling and simulation environment. The double wishbone and McPherson strut systems are very common and will provide the basis for the ensuing discussion.

At the time of writing the following configurations, shown graphically in Figure 4.12, are those, for example, provided with the ADAMS/Chassis program to model vehicle front suspension systems. Note that the software follows its roots and uses the Short–Long Arm naming convention used

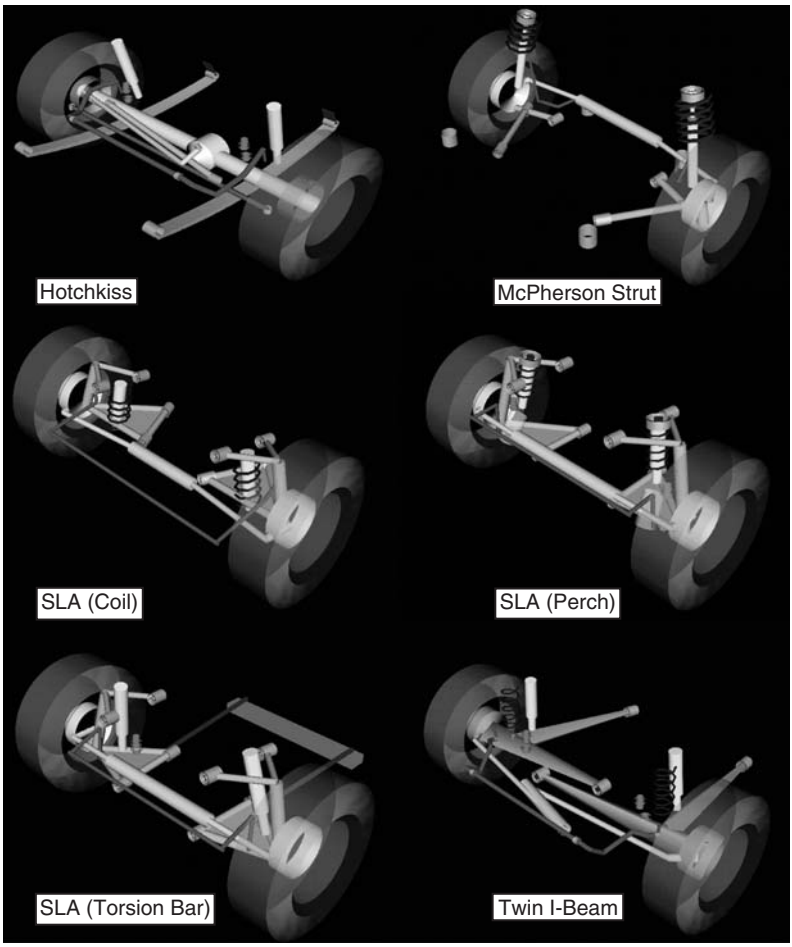

Fig. 4.12 Graphical representation of front suspension configurations in ADAMS/Chassis (provided courtesy of MSC.Software)

in the USA for a double wishbone suspension system. The systems are also shown as 'half vehicle' models, the approach being to model both left and right sides of the system. The systems shown include:

(i) Hotchkiss (3 Link or Beam Leaf model)

(ii) McPherson Strut

(iii) Short–Long Arm (Coil, Perch or Torsion Bar)

(iv) Twin I-Beam

For the rear suspension the following examples shown in Figure 4.13 are some of the suspensions, in addition to the Hotchkiss suspension already shown in Figure 4.12 for the front, that are provided in ADAMS/Chassis:

(i) 4 Link Panhard

(ii) 4 Link Watts

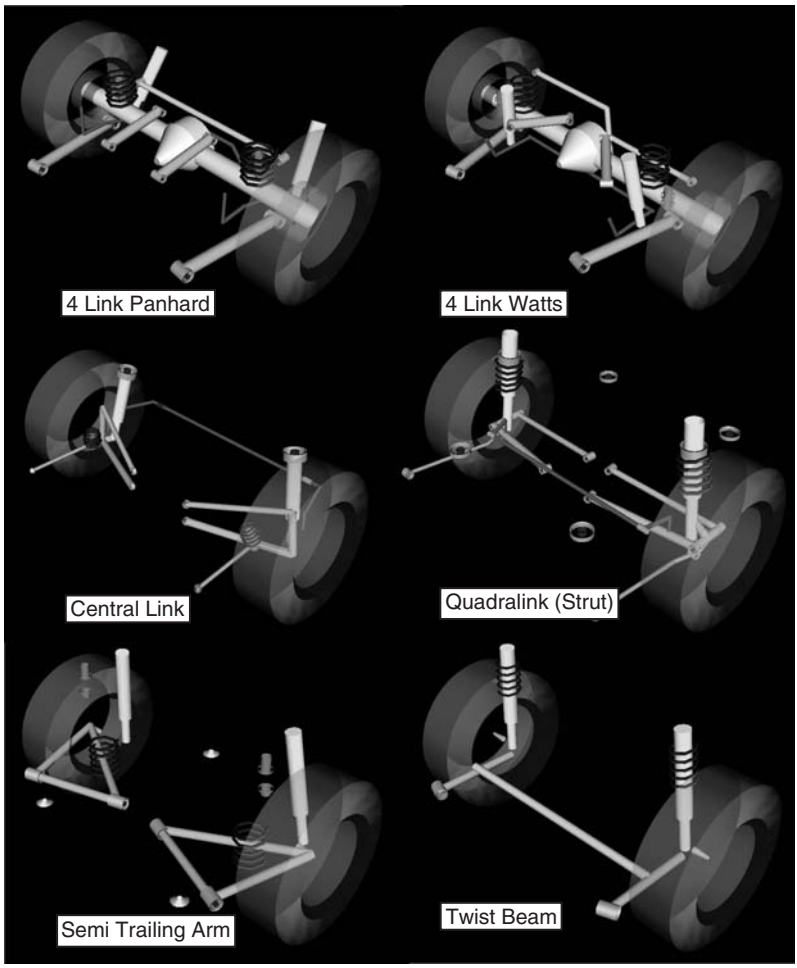

Fig. 4.13 Graphical representation of rear suspension configurations in ADAMS/Chassis (provided courtesy of MSC.Software)

(iii) Central Link

(iv) Quadralink (Strut)

(v) Semi Trailing Arm

(vi) Twist Beam

As stated the double wishbone suspension system will form the basis of much of the following discussion in this chapter. For readers new to the subject area and unfamiliar with the system the main components are indicated in Figure 4.14.

Figure 4.14 shows the main components, the modelling of which will be dependent on the type of analysis to be performed and the outputs that must be produced. If the model is to be used only for the prediction of suspension characteristics such as camber angle or half-track change with bump movement then an accurate definition of the mass and inertial properties of

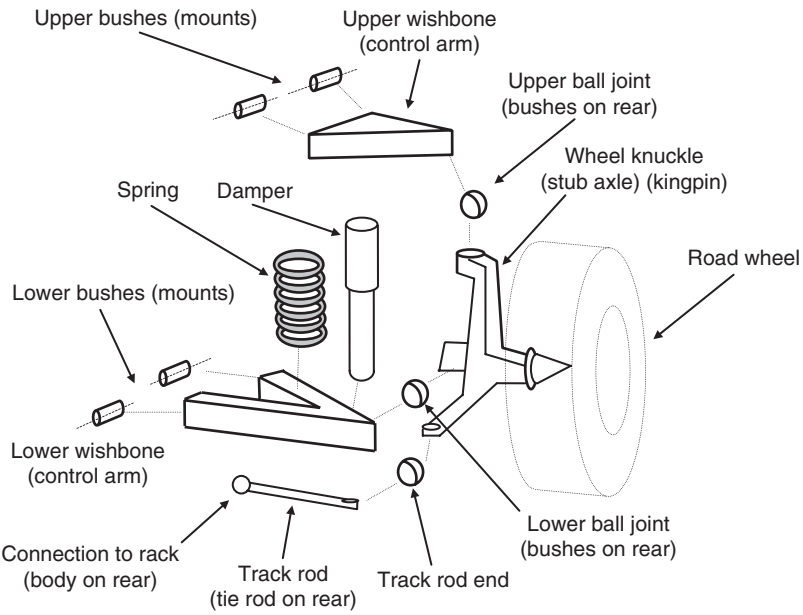

Fig. 4.14 Double wishbone suspension system

the rigid bodies will not be required. This information would be required, however, if the model is to be used for a dynamic analysis predicting the response of the suspension to inputs at the tyre contact patch.

The modelling of the connections between the suspension links will also depend on the type of vehicle and whether the suspension is for the front or rear of the vehicle. On the front of the vehicle the connections between the control arms and the wheel knuckle would be modelled using spherical joints to represent the ball joints used here. On the rear these connections are more likely to include the compliance effects of rubber bushes. On a racing car where ride comfort is not an issue the suspension model is likely to be rigidly jointed throughout. Not shown in Figure 4.14 are the bump and rebound stops that would need to be included when considering situations where the wheel loads are severe enough to generate contact with these force elements.

The other type of suspension system that is very common on road vehicles is the McPherson strut system as illustrated in Figure 4.15. The main difference between this system and the double wishbone system is the absence of an upper control arm and the combination of the spring and the damper into a single main strut, the body of which is the major component in the system.

4.3 Quarter vehicle modelling approaches

One of the earliest documented applications of the MSC.ADAMS program by the automotive industry (Orlandea and Chace, 1977) was the use of the software to analyse suspension geometry. This approach is now well

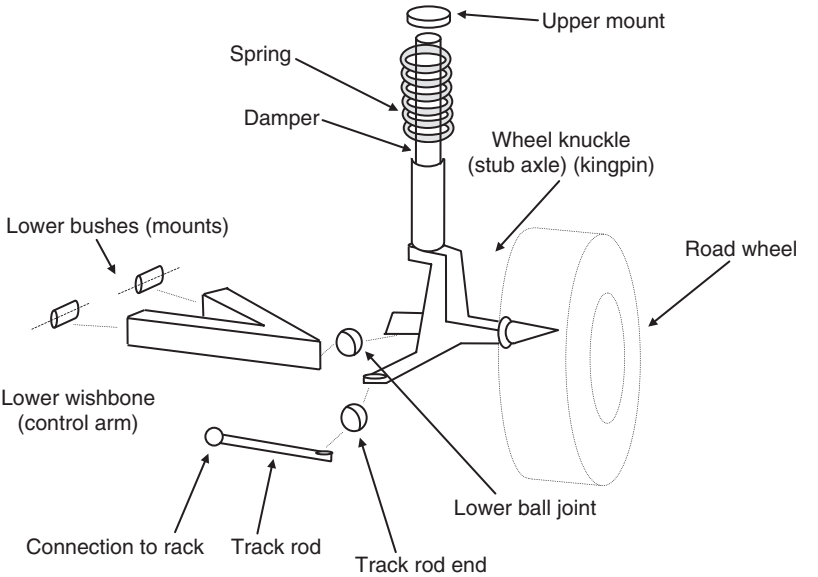

Fig. 4.15 McPherson strut suspension system

established and will be discussed further in the next section of this chapter. The output from this type of analysis is mainly geometric and allows results such as camber angle or roll centre position to be plotted graphically against vertical wheel movement.

The inclusion of bush compliance in the model at this stage will depend on whether the bushes have significant influence on geometric changes in the suspension and road wheel as the wheel moves vertically relative to the vehicle body. With the development of multi-link type suspensions, such as the rear suspension on the Mercedes Model W201 (von der Ohe, 1983), it would appear difficult to develop a model of the linkages that did not include the compliance in the bushes. This type of suspension was used as a benchmark during the IAVSD exercise (Kortum and Sharp, 1993) mentioned in Chapter 1 comparing the application of multibody systems analysis programs in vehicle dynamics.

This modelling issue is best explained by an example using the established double wishbone suspension system. The modelling of the suspension using bushes to connect the upper and lower arms to the vehicle body is shown in Figure 4.16. Vertical motion is imparted to the suspension using a jack part connected to the ground part by a translational joint. A translational motion is applied at this joint to move the jack over a range of vertical movement equivalent to moving between the full bump and full rebound positions. Although the jack is shown below the wheel in Figure 4.16 the jack is connected to the wheel using an inplane joint primitive acting at either the wheel base or the wheel centre as described in Chapter 3.

The joint primitive constrains the wheel centre or wheel base to remain in the plane at the top of the jack but does not constrain the wheel to change

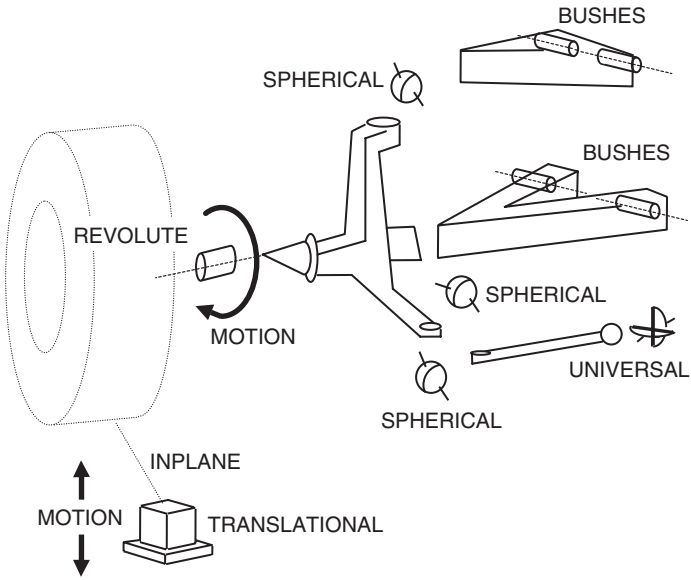

Fig. 4.16 Double wishbone suspension modelled with bushes. (This material has been reproduced from the Proceedings of the Institution of Mechanical Engineers, K2 Vol. 213 'The modelling and simulation of vehicle handling. Part 2: vehicle modelling', M.V. Blundell, page 121, by permission of the Council of the Institution of Mechanical Engineers)

Table 4.2 Degree-of-freedom calculation for suspension system with bushes

Component	Number	DOF	ΣDOF
Parts	6	6	36
Translationals	1	−5	−5
Revolutes	1	−5	−5
Universals	1	−4	−4
Sphericals	3	−3	−9
Inplanes	1	−1	−1
Motions	2	−1	−2
			ΣDOF for system = 10

orientation or to move in the lateral or longitudinal directions. A zero motion input is applied at the revolute joint connecting the wheel to the wheel knuckle in order to constrain the spin freedom of the wheel. For the suspension modelled in this manner it is possible to calculate the degrees of freedom for the system as shown in Table 4.2.

The double wishbone suspension model shown in Figure 4.16 can be simplified to represent the bushes connecting the upper arm and the lower arm to the vehicle body by revolute joints as shown in Figure 4.17.

For the suspension modelled in this manner it is possible to calculate the degrees of freedom for the system as shown in Table 4.3.

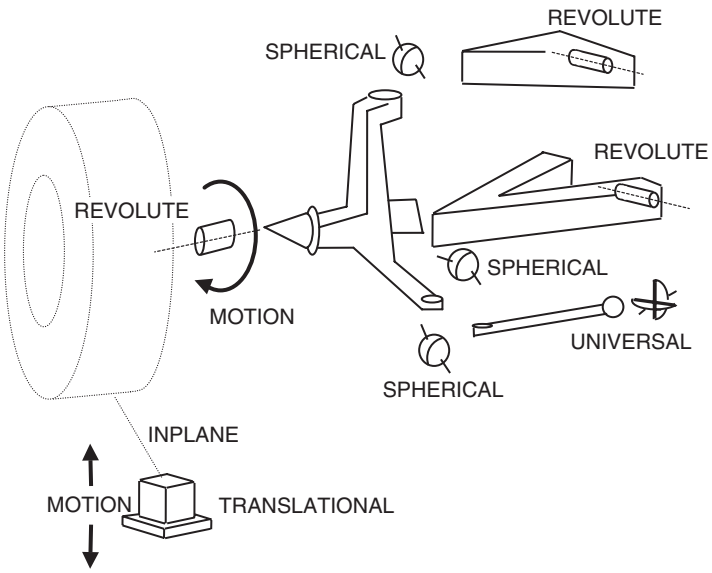

Fig. 4.17 Double wishbone suspension modelled with joints. (This material has been reproduced from the Proceedings of the Institution of Mechanical Engineers, K2 Vol. 213 'The modelling and simulation of vehicle handling. Part 2: vehicle modelling', M.V. Blundell, page 122, by permission of the Council of the Institution of Mechanical Engineers)

Table 4.3 Degree-of-freedom calculation for suspension system without bushes

Component	Number	DOF	ΣDOF
Parts	6	6	36
Translationals	1	−5	−5
Revolutes	3	−5	−15
Universals	1	−4	−4
Sphericals	3	−3	−9
Inplanes	1	−1	−1
Motions	2	−1	−2
			ΣDOF for system = 0

This generates a model that has zero degrees of freedom and allows a kinematic analysis to be performed. The fact that at least one of the degrees of freedom constrained in this model is due to a time dependent motion, input at a joint, means that the model will move and operate as a mechanism rather than 'lock' as a structure.

The modelling of the bushes will also have a significant impact on the collation of data and the effort required to input and check the values. This is illustrated in Table 4.4 where the typical MSC.ADAMS inputs required to model a connection as a rigid joint, linear bush and non-linear bush are compared. It should be noted that while this provides an indication using a textual format of the relative data requirements, the modern graphical user interface in a program such as MSC.ADAMS provides useful spline editing

Table 4.4 MSC.ADAMS statements for a joint, linear bush and non-linear bush

NON-LINEAR BUSH	LINEAR BUSH	JOINT
BUSH/16,I=1216	BUSH/16,I=1216	JO/16,REV,I=1216
,J=0116	,J=0116	,J=0116
,K=0,0,0	,K=7825,7825,944	
,KT=0,0,500	,KT=2.5E6,2.5E6,500	
,C=35,35,480	,C=35,35,480	
,CT=61000,61000,40	,CT=61000,61000,40	

```
GFORCE/16,I=1216
,FLOAT=011600,RM=1216
,FX=CUBSPL(DX(1216,0116,1216),0,161)\
,FY=CUBSPL(DY(1216,0116,1216),0,161)\
,FZ=CUBSPL(DZ(1216,0116,1216),0,162)\
,TX=CUBSPL(AX(1216,0116),0,163)\
,TY=CUBSPL(AY(1216,0116),0,163)\
,TZ=0.0\
SPLINE/161,
,X=-1.8,-1.5,-1.4,-1.22,-1.123,-1.0,-0.75,-0.5,-0.25,0,0.25,0.5
,0.75,1.0,1.123,1.22,1.4,1.5,1.8
,Y=15350,10850,9840,6716,5910,5059,3761,2507,1253,0,-1253,-2507
,-3761,-5059,-5910,-6716,-9840,-10850,-15350
SPLINE/162,
,X=-5,-4,-3,-2.91,-2.75,-2.5,-2,-1.5,-1,-0.5,0,0.5,1,1.5,2,2.5
,2.75,2.91,3,4,5
,Y=7925,3925,1925,1790,1626,1450,1136,830,552,276,0,-276,-552,-830
,-1136,-1450,-1626,-1790,-1925,-3925,-7925
SPLINE/163,
,X=-0.22682,-0.20939,-0.19196,-0.17453,-0.1571,-0.13963,-0.10472
,-0.06981,-0.03491,0,0.03491,0.06981,0.10472,0.13963,0.1571,0.17453
,0.19196,0.20939,0.22682
,Y=241940,198364,160018,125158,93387,75415,52951,35702,18453,0
,-18453,-35702,-52951,-75415,-93387,-125158,-160018,-198364,-241940
```

and plotting capabilities that considerably ease the modelling and inclusion of non-linear elements, such as the bushes described here.

There are three main types of analysis that individual suspension models are likely to be used for during the design and development of a vehicle. The quantity and type of data will vary from vehicle to vehicle and the type of analysis to be performed. A summary of the typical modelling data is provided for guidance in Table 4.5. Note that for some suspensions, such as a twist beam type, the modelling of structural compliance will also need to be included.

Before leaving the subject of quarter vehicle suspension models it is worth considering the typical implementation of a spring damper unit in a race car. The advent of inter-university competitions where students design, build and race a vehicle has become popular on automotive courses in recent years. An example of such a vehicle is the Formula Student car built by students at Coventry University shown in Figure 4.18.

The modelling of part of the suspension system is shown in Figure 4.19. The push rod connects the suspension arm to the bell crank and uses a

Table 4.5 Indicative data requirements for individual suspension analyses

Kinematic or quasi-static vertical rebound to bump analysis
Co-ordinates of suspension linkage connections
Bush stiffnesses (if this affects the movement)
Spring stiffness (if suspension wheel rate is to be calculated)
Static or quasi-static durability analysis
Co-ordinates of suspension linkage connections
Bush stiffnesses
Spring stiffness
Bump and rebound stops
Component flexibility (some suspensions)
Dynamic durability or vibration analysis
Co-ordinates of suspension linkage connections
Mass and inertial properties
Bush stiffnesses
Bush damping coefficients
Spring stiffness
Damper properties
Bump and rebound stops
Component flexibility (some suspensions)

Fig. 4.18 Coventry University Formula Student car

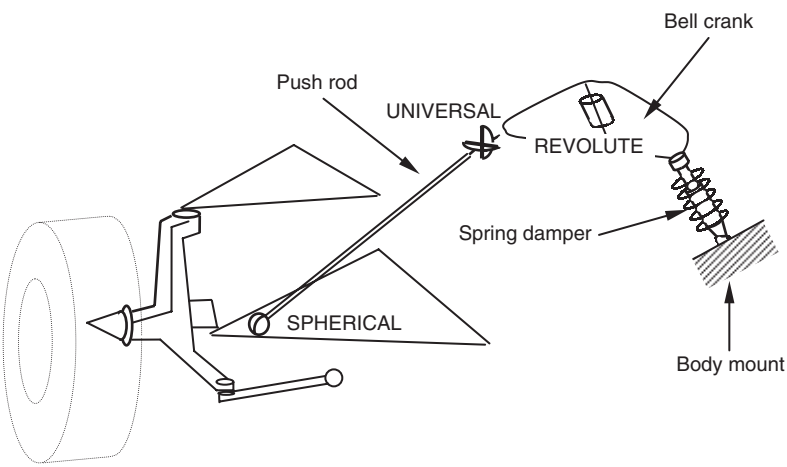

Fig. 4.19 Modelling of push rod and bell crank mechanism in student race car

spherical joint at one end and a universal joint at the other end to constrain unwanted spin of the push rod about its own axis. The bell crank is attached to the chassis with a revolute joint, the rotation about which is resisted by the spring damper unit. It can be noted that it is not really necessary to model the spring damper as rigid bodies. The definition of the forces generated will be sufficient to simulate the handling of the full vehicle.

4.4 Determination of suspension system characteristics

The suspension design process discussed at the beginning of this chapter has been summarized in Table 4.1 by six areas in which the suspension performance can be assessed. Ultimately the quality of the design will be judged on the performance of the full vehicle, but an early assessment of the suspension design as an individual unit is essential. In order to quantify the performance of the suspension system a range of characteristics may be determined through simulation of a single suspension system or quarter vehicle model. During this chapter it will be shown that a single suspension system can be analysed in a number of ways that will provide information to support the six suspension design activities that have been identified.

It should also be noted, however, that while the emphasis in this book is to explain the function and modelling of suspension systems using quarter models, customized software such as ADAMS/Car and ADAMS/Chassis extend the modelling as stated to a half vehicle model analysed using a virtual test rig, an example of which is shown in Figure 4.20.

Such a system also allows the additional incorporation of roll bars and a steering system to investigate the cross coupling of left and right suspension systems through roll bar compliance and the effects of steering inputs in isolation or in combination with suspension movement.

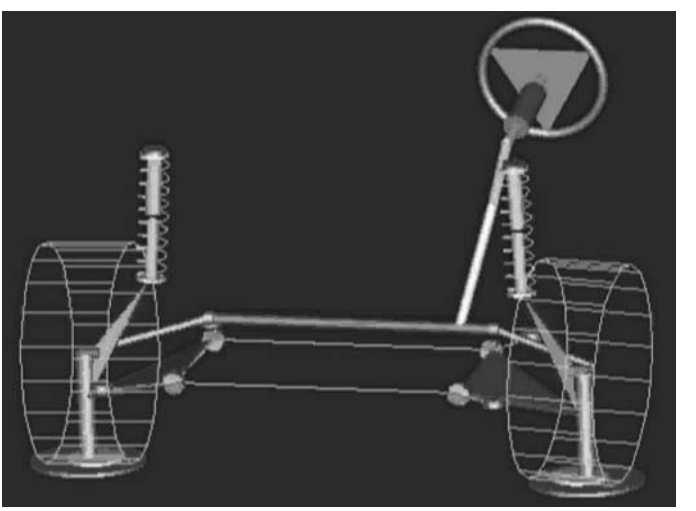

Fig. 4.20 Use of virtual test rig to analyse a half vehicle suspension model (provided courtesy of MSC.Software)

A more detailed discussion of suspension analysis methods, such as those used to investigate body isolation issues, will follow later in this chapter but using a virtual rig such as this the following are typical of some of the analyses performed:

(i) The wheels may be moved vertically relative to the vehicle body through a defined bump–rebound travel distance. For the half model shown in Figure 4.20 the vertical movement may involve single, opposite or parallel wheel travel representing ride or roll motions for the vehicle. The measured outputs allow the analyst to consider, depending on the model used, aspects of kinematic and compliant wheel plane control.

(ii) Lateral force and aligning torque may be applied at the tyre contact path allowing measurement, for example, of the resulting toe angle change and lateral deflection of the wheel (compliant wheel plane control).

In addition to the above basic types of analysis it is also possible to use an MBS suspension model to consider wheel envelopes where under the full range of suspension travel and steering inputs an envelope mapped by the outer surface of the tyre can be developed allowing the clearance with surrounding vehicle structure to be checked.

In practice this has been achieved by using the wheel centre position, orientation and tyre geometry from the MBS simulation as input to a CAD system where the clearances can be checked. An example of the graphic visualization of a wheel envelope, for vertical wheel travel only, using superimposed animation frames is shown in Figure 4.21.

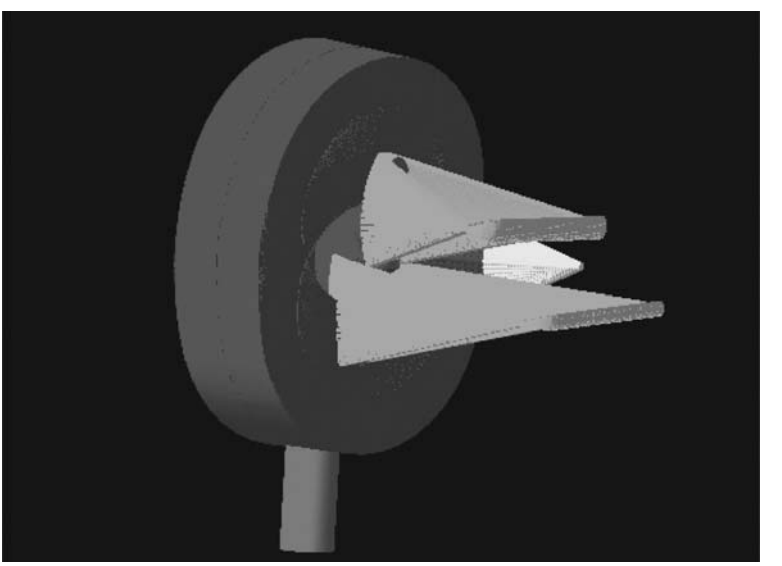

Fig. 4.21 Superimposed animation frames giving visual indication of wheel envelope

4.5 Suspension calculations

4.5.1 Measured outputs

A glossary of terms providing a formal specification of various suspension characteristics has been provided by the Society of Automotive Engineers (1976). In the past variations in formulations and terminology have been provided by researchers, authors and also practising engineers following corporate methodologies. The concept of a roll centre has also been subject to a number of definitions (Dixon, 1987).

As discussed in Chapter 3 programs such as ADAMS/Car and ADAMS/Chassis offer a range of pre-computed outputs for suspension characteristics. The user documentation provided with those software systems includes an extensive description of each output and need not be repeated here. For completeness those outputs considered to be most common in their usage and most relevant only to the following discussion in this textbook will be described in this chapter.

As discussed in the previous sections, one of the main uses of a multibody systems model of a suspension system is to establish during the design process geometric position and orientation as a function of vertical movement between the rebound and bump positions. As the output required does not include dynamic response it is suitable to use a kinematic or quasi-static analysis to simulate the motion. It should be noted that this information could also be obtained using a CAD package or a program developed solely for this purpose. The fact that a multibody systems program is used is often associated with the stages of model development described in Chapter 1 that lead through from the individual suspension model to a model of the full vehicle.

A large number of parameters can be measured on an existing suspension system and laboratory rigs such as the Kinematics and Compliance measurement facility (or K&C Rig) described by Whitehead (1995) have been developed specifically for this purpose. The descriptions provided here will be limited to the most commonly calculated outputs, these being:

- Bump movement (spindle rise)
- Wheel recession
- Half track change
- Steer (toe) angle
- Camber angle
- Castor angle
- Steer axis inclination
- Suspension trail
- Ground level offset
- Wheel rate
- Roll centre height

In each case the parameters are presented as *XY* plots with the bump movement as the independent variable usually on the *x*-axis. The calculation of these outputs can be programmed to create a variable that is derived directly from measured system variables or is based on a trigonometric or algebraic derivation. It should be noted that parameters such as the camber angle determined here are measured relative to the vehicle body which is assumed to be fixed and should not be confused with the camber angle measured between the tyre and the road surface discussed later in Chapter 5.

The vertical motion is imparted to the wheel using a body to represent a jack with the wheel centre constrained to remain in the plane of the jack using an inplane joint primitive as described in Chapter 3 and shown in Figure 4.22. The motion applied to the translational joint between the jack and the ground will be that needed to move the wheel between the rebound and bump positions. If, as is usual, the model is defined in a position midway between these it is often the practice to define the motion as sinusoidal with a cycle of 1 second. This would provide results in the bump position at 0.25 second the rebound position at 0.75 second and allow for presentation purposes smooth animation of continuous cycles. Running the analysis for 1 second with, say, 80 output steps would ensure that output is calculated in the full bump and rebound positions.

The motion statement applied to the translational joint that would accomplish this for a suspension where the total movement between the rebound and bump is 200 mm would be

```
MOTION/04, JOINT = 04, TRANS, FUNCTION
  = 100 * SIN(TIME * 360D)
```

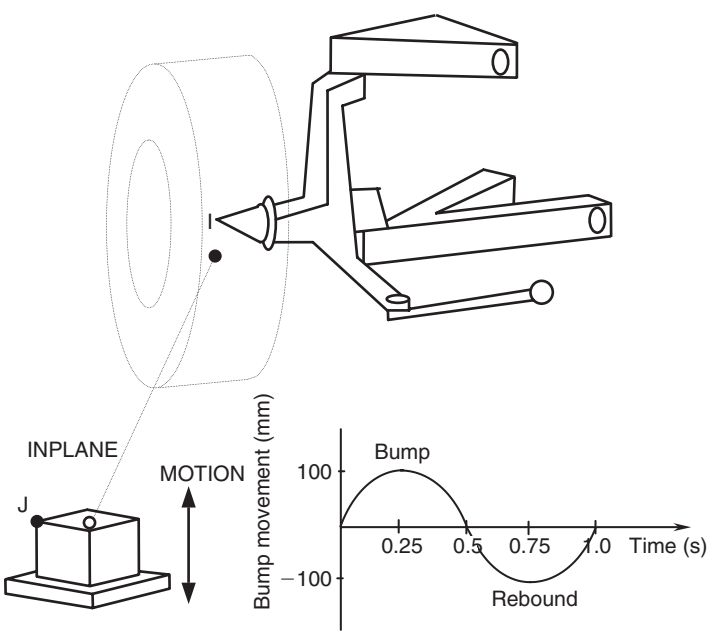

Fig. 4.22 Input of vertical motion at the wheel centre

Note that the TIME variable is in seconds and is converted to degrees within the function to represent one cycle over 1 second of simulation time.

It should also be noted that if the movement is not symmetric, that is to say that the distance moved in bump is different to that moved in rebound, a more complicated function will be needed for the motion input. In the following example the suspension is required to move 110 mm into the bump position and 90 mm into the rebound position. It is still desirable to have an overall sinusoidal motion for animation purposes and so an arithmetic IF is used in the function to switch the amplitude at the half cycle position of 0.5 second as follows:

```
MOTION/04, JOINT = 04, TRANS
  ,FUNCTION = IF(TIME−0.5: 110*SIN(TIME*360D), 0.0
  ,90 * SIN(TIME * 360D))
```

4.5.2 Suspension steer axes

Suspension characteristics, such as castor angle, suspension trail and the steering axis inclination, require an initial computation of the suspension system steer axis. Generally the concept of a steer axis is straightforward when considering, for example, the double wishbone system described earlier. In such a case it is easy to see that the wheel will steer about an axis passing through the lower and upper ball joints.

For a McPherson strut suspension system, the steer axis may be defined to pass through a point located at the lower ball joint and a point located where the upper part of the strut is mounted to the vehicle body. Note that this line is not necessarily parallel to the sliding axis of the upper part of the strut.

For some suspensions, such as a multi-link system, the location of the steer axis is not immediately evident from the suspension geometry. In these cases it is necessary that the software be programmed to calculate the steer axis as the instant axis of rotation of the wheel carrier parts.

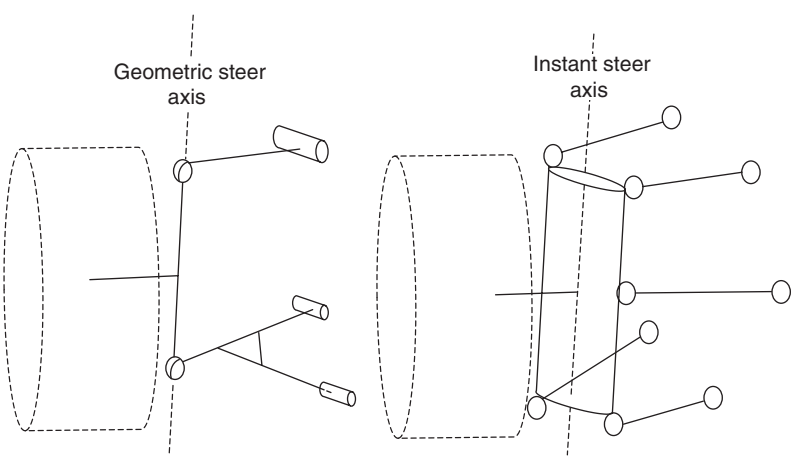

Fig. 4.23 Geometric and instant steer axes of a suspension system

Using the instant axes method the left and right steer axes can be computed from the suspension's compliance matrix. The process involves locking the spring to prevent wheel rise and applying an incremental steering torque or force. The resulting translation and rotation of the wheel carrier parts can then be used to compute the instant axis, and hence steer axis of rotation for each wheel carrier.

Note that the formulations of suspension output that follow are for a quarter vehicle suspension model located on the right side of the vehicle using the general vehicle co-ordinate system in this text with the x-axis pointing to the rear, the y-axis to the side and the z-axis upwards. Needless to say users must ensure the formulations are consistent with the vehicle co-ordinate system and the side of the vehicle being considered to ensure the correct sign for the calculated outputs. For each of the suspension characteristics discussed a typical system variable calculation is provided. This will assist users of MBS programs who need to develop their own calculations without access to the automated outputs in a program such as ADAMS/Car.

4.5.3 Bump movement, wheel recession and half track change

As stated earlier it can be the practice to impart vertical motion to a suspension system at either the wheel centre or wheel base. In the following example the displacements at the wheel centre are used to determine the suspension movement. The displacements at the wheel base would be corrected for camber, steer and castor angle changes and dependent on the suspension geometry. On the real vehicle the displacements of the tyre contact patch relative to the road wheel would also result due to the effects of tyre distortion. This is discussed later in Chapter 5.

Bump movement (BM) is the independent variable and is taken as positive as the wheel moves upwards in the positive z direction relative to the vehicle body. Similarly wheel recession (WR) and half track change (HTC) are taken as positive as the wheel moves back and outwards in the positive x and y directions respectively.

The displacements are obtained simply by comparing the movement of a marker at the wheel centre (WC) relative to an initially coincident fixed marker on the ground (FG). The displacements are shown in Figure 4.24 where the MSC.ADAMS system variable format is used to describe the outputs.

4.5.4 Camber and steer angle

Camber angle, γ, is defined as the angle measured in the front elevation between the wheel plane and the vertical. Camber angle is measured in degrees and taken as positive if the top of the wheel leans outwards relative to the vehicle body as shown in Figure 4.25.

The steer or toe angle, δ, is defined as the angle measured in the top elevation between the longitudinal axis of the vehicle and the line of intersection of the wheel plane and road surface. Steer angle is taken here as positive if the front of the wheel toes towards the vehicle.

Both camber and steer angle can be calculated using two markers located on the wheel spindle axis. In this case a marker is used at the wheel centre

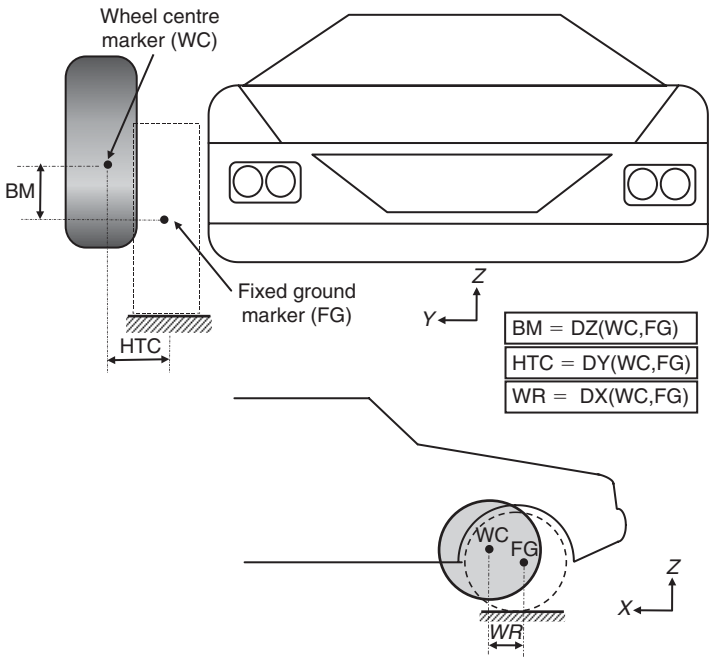

Fig. 4.24 Bump movement, wheel recession and half track change

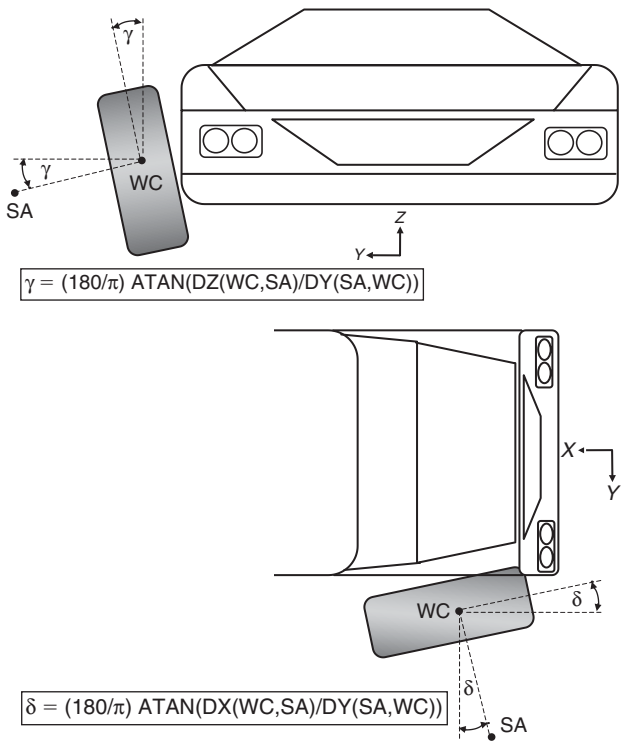

Fig. 4.25 Calculation of camber angle and steer angle

(WC) and another on the spindle axis (SA), taken in this example to be outboard of the wheel centre. The calculation of camber and steer angle is converted from radians to degrees by the factor (180/π).

4.5.5 Castor angle and suspension trail

Castor angle, ϕ, is defined as the angle measured in the side elevation between the steering (kingpin) axis and the vertical. Castor angle is measured in degrees and taken as positive if the top of the steering axis leans towards the rear as shown in Figure 4.26.

Suspension trail (TR) is the longitudinal distance in the *x* direction between the wheel base and the intersection between the steering axis and the ground. The suspension trail generates a measure of stability providing a moment arm for lateral tyre forces that will cause the road wheels to 'centre'. The suspension trail combines with tyre pneumatic trail, discussed in Chapter 5, and contributes to the steering 'feel'.

4.5.6 Steering axis inclination and ground level offset

The steering axis inclination, θ, is defined as the angle measured in the front elevation between the steering (kingpin) axis and the vertical. The angle is measured in degrees and taken as positive if the top of the steering axis leans inwards as shown in Figure 4.27.

Ground level offset (GO) is the lateral distance in the *y* direction between the wheel base and the intersection between the steering axis and the ground. The ground level offset is often referred to as the scrub radius as the amount of 'scrub' in the tyre as it steers will depend on the magnitude of the ground level offset.

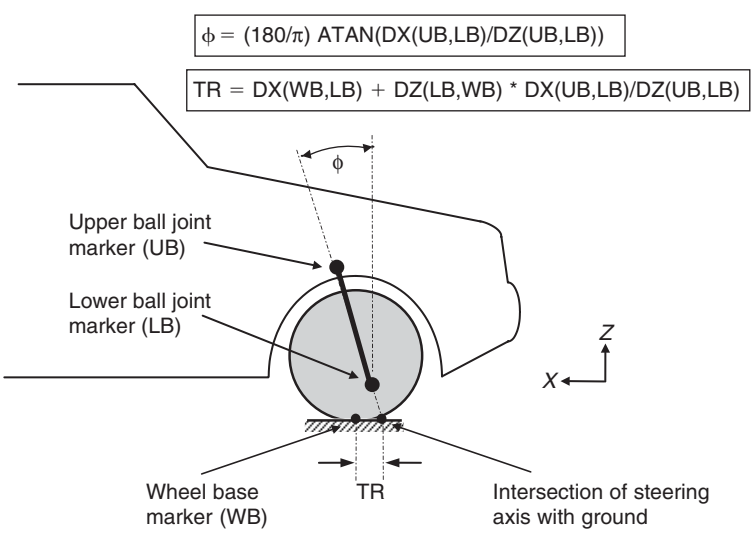

Fig. 4.26 Calculation of castor angle and suspension trail

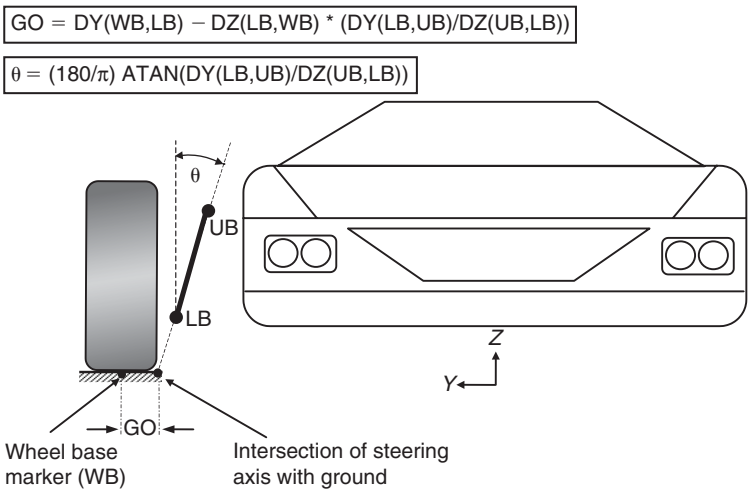

Fig. 4.27 Calculation of steering axis inclination and ground level offset

4.5.7 Instant centre and roll centre positions

The determination of the instant centre and the roll centre position is more complicated than the previous calculations described here and the following is included to demonstrate the approach that is used with MBS software to establish these positions.

The methods used here are based on the traditional graphical (kinematic) type of construction as described by Gillespie (1992). The approach used to program the computations will require the definition of algebraic equations that calculate the gradients and intersection points of the lines used in the construction. For the MSC.ADAMS program, there are two methods that may be used to achieve this in the absence of a dedicated program such as ADAMS/Car:

(i) Programming in the input deck using the VARIABLE statement.

(ii) Preparing a user-written FORTRAN subroutine and linking with MSC.ADAMS.

The methods used to formulate the construction will be dependent on the type of suspension system being considered. Examples are provided here for a double wishbone and a McPherson strut suspension system. For a double wishbone suspension the methods used to determine the instant centre and roll centre position for the front suspension are based on the construction shown in Figure 4.28.

The instant centre is found by intersecting two lines projected along the upper and lower arms. The instant centre is the instantaneous centre of rotation for the complete suspension system. The suspension system can be thought of as an equivalent swing arm that pivots about the instant centre. As such the instant centre is also sometimes referred to as the effective swing arm pivot. The roll centre is found by projecting a line between the wheel base and the instant centre. The point at which this line intersects the centre line of the vehicle is taken to be the roll centre.

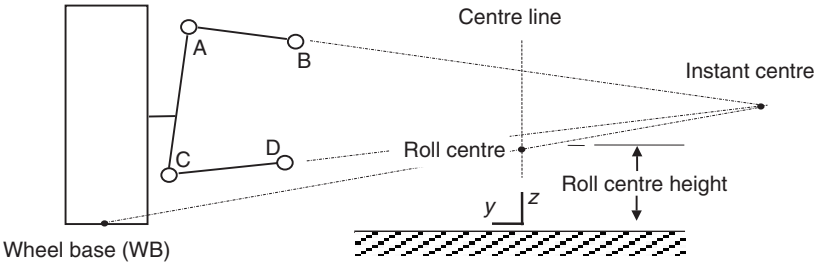

Fig. 4.28 Instant centre and roll centre positions for a double wishbone suspension. (This material has been reproduced from the Proceedings of the Institution of Mechanical Engineers, K2 Vol. 213 'The modelling and simulation of vehicle handling. Part 2: vehicle modelling', M.V. Blundell, page 123, by permission of the Council of the Institution of Mechanical Engineers)

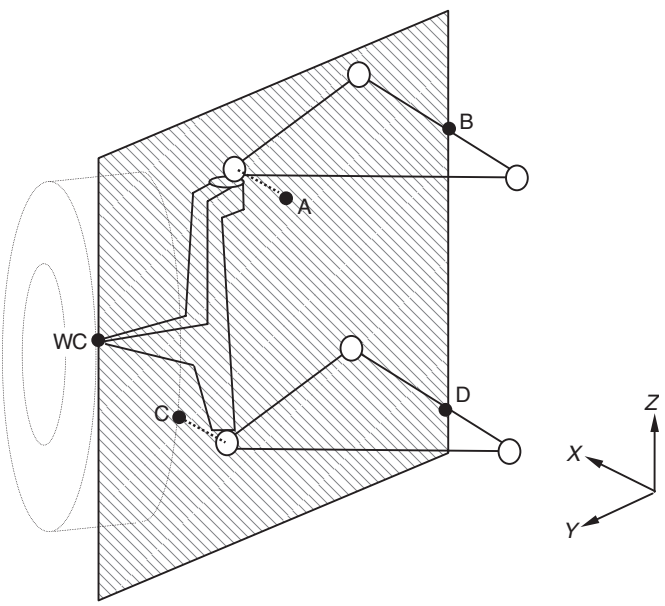

Fig. 4.29 Position of instant centre construction points on wheel centre *YZ* plane

It should be noted that the two-dimensional representation shown in Figure 4.28 is a simplification of the three-dimensional system and the graphical construction that takes place in a *YZ* plane passing through the wheel centre as shown in Figure 4.29.

Since it cannot be assumed that the axes through the wishbone mount points are parallel to the *x*-axis the positions of points B and D will need to be obtained by interpolation to the *YZ* plane passing through the wheel centre. Positions A and C are found simply by projecting the upper and lower ball joints on to the same plane.

In order to program this construction algebraically the first step is to set up expressions for the gradients *GR*1 and *GR*2 of the upper and lower arms:

$$GR1 = (BZ - AZ)/(BY - AY) \tag{4.32}$$

$$GR2 = (DZ - CZ)/(DY - CY) \tag{4.33}$$

where AY, AZ, BY, BZ, CY, CZ, DY, DZ are the y and z co-ordinates of points A, B, C and D.

The co-ordinates of the instant centre ICY and ICZ, can be established from two simultaneous equations based on the upper and lower arms:

$$ICZ = AZ + GR1 \times (ICY - AY) \tag{4.34}$$

$$ICZ = CZ + GR2 \times (ICY - CY) \tag{4.35}$$

Rearranging these two equations gives:

$$AZ + GR1 \times ICY - GR1 \times AY = CZ + GR2 \times ICY - GR2 \times CY \tag{4.36}$$

$$ICY \times (GR1 - GR2) = GR1 \times AY - GR2 \times CY + CZ - AZ \tag{4.37}$$

which allows the instant centre to be located using:

$$ICY = (GR1 \times AY - GR2 \times CY + CZ - AZ)/(GR1 - GR2) \tag{4.38}$$

$$ICZ = AZ + GR1 \times (ICY - AY) \tag{4.39}$$

The gradient of the line joining the wheel base to the instant centre $GR3$, can be expressed as

$$GR3 = (ICZ - WBZ)/(ICY - WBY) \tag{4.40}$$

where WBY and WBZ are the y and z co-ordinates of the wheel base.

This allows the roll centre to be located using:

$$RCY = 0.0 \tag{4.41}$$

$$RCZ = WBZ + GR3 \times (RCY - WBY) \tag{4.42}$$

The roll centre height RCH, can now be defined by

$$RCH = RCZ - RZ \tag{4.43}$$

where RZ is the z co-ordinate of the road.

The methods used to determine the instant centre and roll centre position for a McPherson strut suspension are based on the construction shown in Figure 4.30.

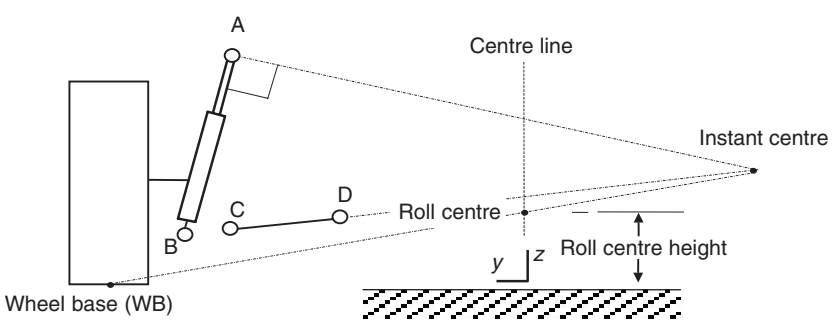

Fig. 4.30 Instant centre and roll centre positions for a McPherson strut suspension

The instant centre is found by intersecting lines projected along the transverse arm and perpendicular to the axis of the strut. The roll centre is found by projecting a line between the wheel base and the instant centre. The point at which this line intersects the centre line of the vehicle is taken to be the roll centre. All calculations are assumed to take place in the same *YZ* plane as the wheel centre. The first step is again to set up expressions for the gradients *GR*1 for the line perpendicular to the strut and *GR*2 for the line projected along the transverse arm:

$$GR1 = (BY - AY)/(AZ - BZ) \tag{4.44}$$

$$GR2 = (DZ - CZ)/(DY - CY) \tag{4.45}$$

where *AY*, *AZ*, *BY*, *BZ*, *CY*, *CZ*, *DY*, *DZ* are the y and z co-ordinates of points A, B, C and D.

The co-ordinates of the instant centre *ICY* and *ICZ*, can be established from two simultaneous equations based on the upper and lower arms:

$$ICZ = AZ + GR1 \times (ICY - AY) \tag{4.46}$$

$$ICZ = CZ + GR2 \times (ICY - CY) \tag{4.47}$$

Rearranging these two equations gives:

$$AZ + GR1 \times ICY - GR1 \times AY = CZ + GR2 \times ICY - GR2 \times CY \tag{4.48}$$

$$ICY \times (GR1 - GR2) = GR1 \times AY - GR2 \times CY + CZ - AZ \tag{4.49}$$

This allows the instant centre to be located using:

$$ICY = (GR1 \times AY - GR2 \times CY + CZ - AZ)/(GR1 - GR2) \tag{4.50}$$

$$ICZ = AZ + GR1 \times (ICY - AY) \tag{4.51}$$

The gradient of the line joining the wheel base to the instant centre *GR*3, can be expressed as

$$GR3 = (ICZ - WBZ)/(ICY - WBY) \tag{4.52}$$

where *WBY* and *WBZ* are the y and z co-ordinates of the wheel base.

This allows the roll centre to be located using:

$$RCY = 0.0 \tag{4.53}$$

$$RCZ = WBZ + GR3 \times (RCY - WBY) \tag{4.54}$$

The roll centre height *RCH*, can be defined by:

$$RCH = RCZ - RZ \tag{4.55}$$

where *RZ* is the z co-ordinate of the road.

As stated earlier the calculation of the instant centre and roll centre position can be implemented either by programming in the input deck with the VARIABLE statement or by preparing a user-written FORTRAN subroutine. By way of example these methods are demonstrated for a front suspension system only. Using the VARIABLE statement it is possible to program the equations laid out for the double wishbone system as shown in Table 4.6.

Table 4.6 Calculation of roll centre height using the VARIABLE statement

```
VAR/14,IC=1,FU=DZ(1414,1411)/(DY(1414,1411)+1E-6)                    !GR1
VAR/15,IC=1,FU=DZ(1216,1213)/(DY(1216,1213)+1E-6)                    !GR2
VAR/16,IC=1,FU=((VARVAL(14)*DY(1411))                                !ICY
,-(VARVAL(15)*DY(1213))+DZ(1213)
,-DZ(1411))/(VARVAL(14)-VARVAL(15)+1E-6)
VAR/17,FU=DZ(1411)+VARVAL(14)*(VARVAL(16)-DY(1411))                  !ICZ
VAR/18,FU=(VARVAL(17)*DZ(1029))/(VARVAL(16)-DY(1029)+1E-6)           !GR3
VAR/19,FU=DZ(1029)+VARVAL(18)*(0.0-DY(1029))                         !RCZ
VAR/20,FU=VARVAL(19)+152.6                                           !RCH
REQ/1,F2=VARVAL(16)\F3=VARVAL(17)\F4=VARVAL(20)\
,TITLE=NULL:ICY:ICZ:RCH:NULL:NULL:NULL:NULL
```

Table 4.7 FORTRAN subroutine to calculate roll centre height

```
SUBROUTINE REQSUB(ID,TIME,PAR,NPAR
,IFLAG,RESULT)
C M Blundell Coventry University
  Nov 1994
C Calculation of Roll Centre Height
  and Instant
C Centre Position -ROVER front
  suspension.
C
C Definition of Parameters:
C PAR(1)  Subroutine id. Must be 1
C PAR(2)  WC marker
C PAR(3)  WB marker
C PAR(4)  Marker at point A
C PAR(5)  Marker at point B
C PAR(6)  Marker at point C
C PAR(7)  Marker at point D
C PAR(8)  Radius of wheel
C PAR(9)  RZ Height of Road in global Z
C
C Results passed back to MSC.ADAMS as
  follows:
C Note that the AView does not use
C RESULT(1) or RESULT(5)
C
C RESULT(2) Roll Centre Height above
  ground
C RESULT(3) Roll Centre Z coordinate
C RESULT(6) ICY coordinate
C RESULT(7) ICZ coordinate
C
IMPLICIT DOUBLE PRECISION (A-H,O-Z)
DIMENSION PAR(*),RESULT(8)
LOGICAL IFLAG
DIMENSION DATA(6)
LOGICAL ERRFLG
C
IDWC=PAR(2)
IDWB=PAR(3)
IDA=PAR(4)
IDB=PAR(5)
IDC=PAR(6)
IDD=PAR(7)
RADIUS=PAR(7)
RZ=PAR(8)
CALL INFO ('DISP',IDWC,0,0,DATA,ERRFLG)
CALL ERRMES(ERRFLG,'WC ID',ID,'STOP')
WCX=DATA(1)
WCY=DATA(2)
WCZ=DATA(3)
CALL INFO('DISP',IDWB,0,0,DATA,ERRFLG)
CALL ERRMES(ERRFLG,'WB ID',ID,'STOP')
WBY=DATA(2)
WBZ=DATA(3)
CALL INFO('DISP',IDA,0,0,DATA,ERRFLG)
CALL ERRMES(ERRFLG,'IDA',ID,'STOP')
AY=DATA(2)
AZ=DATA(3)
CALL INFO('DISP',IDB,0,0,DATA,ERRFLG)
CALL ERRMES(ERRFLG,'IDB',ID,'STOP')
BY=DATA(2)
BZ=DATA(3)
CALL INFO('DISP',IDC,0,0,DATA,ERRFLG)
CALL ERRMES(ERRFLG,'IDC',ID,'STOP')
CY=DATA(2)
CZ=DATA(3)
CALL INFO('DISP',IDD,0,0,DATA,ERRFLG)
CALL ERRMES(ERRFLG,'IDD',ID,'STOP')
DY=DATA(2)
DZ=DATA(3)
GR1=(BZ-AZ)/(BY-AY)
GR2=(DZ-CZ)/(DY-CY)
RICY=((GR1*AY)-(GR2*CY)+CZ-AZ))
,/(GR1-GR2)
RICZ=AZ+GR1*(RICY-AY)
RCY=0.0
GR3=(RICZ-WBZ)/(RICY-WBY)
RCZ=WBZ+GR3*(RCY-WBY)
RCH=RCZ-RZ
RESULT(2)=RCH
RESULT(3)=RCZ
RESULT(6)=RICY
RESULT(7)=RICZ
RETURN
END
```

Variables such as BZ-AZ are defined using system variables which measure components of displacements between markers, such as DZ(1414,1411). The REQUEST statement REQ/1 demonstrates how to access the information calculated by the VARIABLE statements.

The alternative method of writing a FORTRAN subroutine is demonstrated in Table 4.7 by the listing of a user-written REQSUB developed specifically for a double wishbone suspension. The subroutine would be called from the main data set as follows:

```
REQUEST/id,FUNCTION=USER(1,par1,par2,par3,par4,par5,par6,
   par7,par8,par9)
```

where the parameters par1, par2, …, par9 are the various items of data outlined in the subroutine.

4.5.8 Calculation of wheel rate

The wheel rate for a suspension system can be thought of as the stiffness of an 'equivalent' spring acting between the wheel centre and the vehicle body as shown in Figure 4.31. This is the definition most useful for developing basic full vehicle MBS models where the wheel will be modelled as rigid with a separate tyre model. This differs slightly from other definitions sometimes used for wheel (or suspension rate) where the force displacement curve is measured at the centre of the tyre contact patch. In a quarter vehicle MBS model this would simply involve moving the point of jack contact with the wheel from the wheel centre to the tyre contact patch.

The wheel rate should also not be confused with the term ride rate. This is associated with the force displacement relationship between the vehicle body, or sprung mass, and the ground. To derive this with a quarter vehicle model it would be necessary to model an additional spring, representing

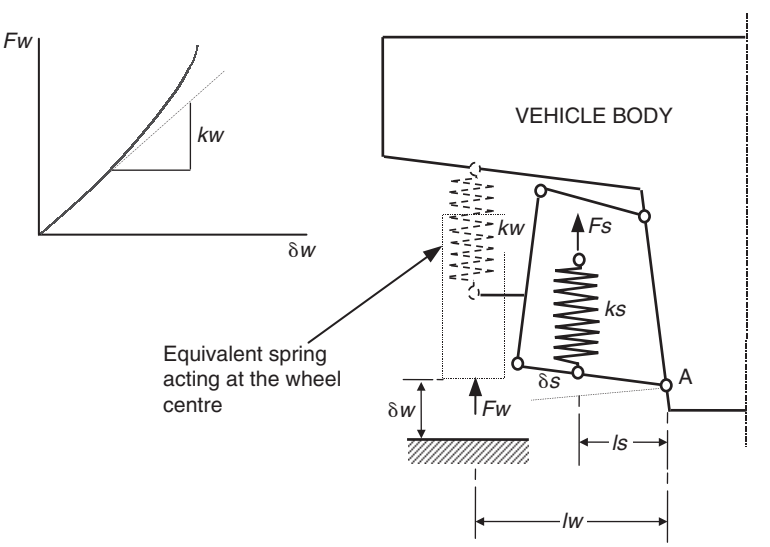

Fig. 4.31 Equivalent spring acting at the wheel centre

the stiffness of the tyre, acting between the wheel centre and the jack with contact at the centre of the tyre contact patch.

The suspension outputs discussed until this point have been based on the suspension geometry and as such have not required the inclusion of the road spring in the model. By including the road spring and plotting the force against the displacement in the jack translational joint, the wheel rate may be obtained from the slope of the curve at the origin.

An estimate of the wheel rate may also be made as follows. Treating the road spring as linear gives the basic force displacement relationship

$$Fs = ks \cdot \delta s \tag{4.56}$$

For the equivalent spring we also have

$$Fw = kw \cdot \delta w \tag{4.57}$$

Taking moments about point A gives

$$Fw = (Ls/Lw)Fs \tag{4.58}$$

From the suspension geometry we can approximate the displacement in the road spring from

$$\delta s = (Ls/Lw)\delta w \tag{4.59}$$

This allows an estimate of the wheel rate, kw, based on the road spring stiffness and suspension geometry from

$$kw = Fw/\delta w = (Ls/Lw)Fs/(Lw/Ls)\delta s = (Ls/Lw)^2 ks \tag{4.60}$$

The introduction of a square function in the ratio can be considered a combination of two effects:

(i) The extra mechanical advantage in moving the road spring to the wheel centre.

(ii) The extra spring compression at the wheel centre.

4.6 The compliance matrix approach

The use of a compliance matrix, in programs such as ADAMS/Car, is a method not commonly described in standard texts on vehicle dynamics but is well suited to an automated computer MBS analysis particularly when the influence of compliance requires consideration. The suspension compliance matrix relates incremental movements of the suspension to incremental forces applied at the wheel centres. The suspension compliance matrix is computed at each solution position as the suspension moves through its range of travel. Characteristics such as suspension ride rate and aligning torque camber compliance are computed based on the compliance matrix.

The compliance matrix for a suspension system, $[C]$, is defined as the partial derivatives of displacements with respect to applied forces

$$[C] = [\partial \Delta / \partial F] \tag{4.61}$$

If a system is assumed to be linear, the compliance matrix can be used to predict the system movement due to force inputs

$$\{\Delta\} = [C]\{F\} \tag{4.62}$$

Expanding equation (4.62) leads to a 12×12 matrix relating the motion of the left and right wheel centres to unit forces and torques applied to the wheel centres. From this perspective, matrix element $C_{i,j}$ is the displacement of system degree of freedom i due to a unit force at degree of freedom j where the degrees of freedom are the three displacements Δx, Δy and Δz and the three rotations Ax, Ay and Az at each of the left and right wheel centres.

$$\begin{bmatrix} \Delta x_{LW} \\ \Delta y_{LW} \\ \Delta z_{LW} \\ Ax_{LW} \\ Ay_{LW} \\ Az_{LW} \\ \Delta x_{RW} \\ \Delta y_{RW} \\ \Delta z_{RW} \\ Ax_{RW} \\ Ay_{RW} \\ Az_{RW} \end{bmatrix} = \begin{bmatrix} C_{1,1} & C_{1,2} & C_{1,3} & C_{1,4} & C_{1,5} & C_{1,6} & C_{1,7} & C_{1,8} & C_{1,9} & C_{1,10} & C_{1,11} & C_{1,12} \\ C_{2,1} & C_{2,2} & C_{2,3} & C_{2,4} & C_{2,5} & C_{2,6} & C_{2,7} & C_{2,8} & C_{2,9} & C_{2,10} & C_{2,11} & C_{2,12} \\ C_{3,1} & C_{3,2} & C_{3,3} & C_{3,4} & C_{3,5} & C_{3,6} & C_{3,7} & C_{3,8} & C_{3,9} & C_{3,10} & C_{3,11} & C_{3,12} \\ C_{4,1} & C_{4,2} & C_{4,3} & C_{4,4} & C_{4,5} & C_{4,6} & C_{4,7} & C_{4,8} & C_{4,9} & C_{4,10} & C_{4,11} & C_{4,12} \\ C_{5,1} & C_{5,2} & C_{5,3} & C_{5,4} & C_{5,5} & C_{5,6} & C_{5,7} & C_{5,8} & C_{5,9} & C_{5,10} & C_{5,11} & C_{5,12} \\ C_{6,1} & C_{6,2} & C_{6,3} & C_{6,4} & C_{6,5} & C_{6,6} & C_{6,7} & C_{6,8} & C_{6,9} & C_{6,10} & C_{6,11} & C_{6,12} \\ C_{7,1} & C_{7,2} & C_{7,3} & C_{7,4} & C_{7,5} & C_{7,6} & C_{7,7} & C_{7,8} & C_{7,9} & C_{7,10} & C_{7,11} & C_{7,12} \\ C_{8,1} & C_{8,2} & C_{8,3} & C_{8,4} & C_{8,5} & C_{8,6} & C_{8,7} & C_{8,8} & C_{8,9} & C_{8,10} & C_{8,11} & C_{8,12} \\ C_{9,1} & C_{9,2} & C_{9,3} & C_{9,4} & C_{9,5} & C_{9,6} & C_{9,7} & C_{9,8} & C_{9,9} & C_{9,10} & C_{9,11} & C_{9,12} \\ C_{10,1} & C_{10,2} & C_{10,3} & C_{10,4} & C_{10,5} & C_{10,6} & C_{10,7} & C_{10,8} & C_{10,9} & C_{10,10} & C_{10,11} & C_{10,12} \\ C_{11,1} & C_{11,2} & C_{11,3} & C_{11,4} & C_{11,5} & C_{11,6} & C_{11,7} & C_{11,8} & C_{11,9} & C_{11,10} & C_{11,11} & C_{11,12} \\ C_{12,1} & C_{12,2} & C_{12,3} & C_{12,4} & C_{12,5} & C_{12,6} & C_{12,7} & C_{12,8} & C_{12,9} & C_{12,10} & C_{12,11} & C_{12,12} \end{bmatrix} \begin{bmatrix} Fx_{LW} \\ Fy_{LW} \\ Fz_{LW} \\ Tx_{LW} \\ Ty_{LW} \\ Tz_{LW} \\ Fx_{RW} \\ Fy_{RW} \\ Fz_{RW} \\ Tx_{RW} \\ Ty_{RW} \\ Tz_{RW} \end{bmatrix} \tag{4.63}$$

From equation (4.63) it can be seen that the coefficients on the leading diagonal of matrix $[C]$ directly relate the displacement or rotation to the associated force or torque applied at that degree of freedom. For example, in the absence of any other forces or torques, the vertical motion of the left wheel centre due to a unit vertical force applied at the left wheel centre is given by $\Delta z_{LW} = C_{3,3} Fz_{LW}$. Figure 4.32 illustrates this for another example where the vertical motion of the left wheel centre due to the application only of a unit vertical force applied at the right wheel centre given by $\Delta z_{LW} = C_{3,9} Fz_{RW}$. From Figure 4.32 it can be seen that for an independent

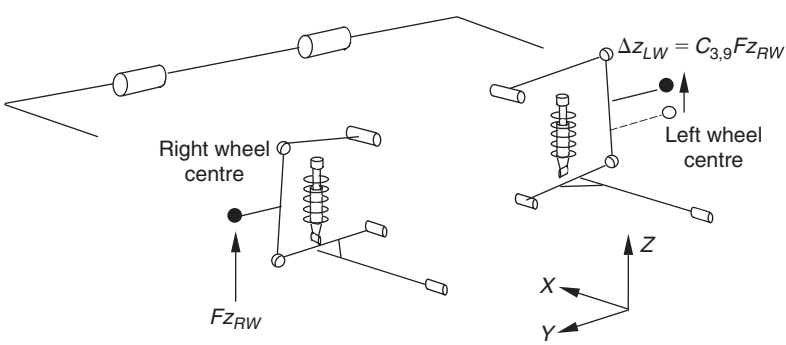

Fig. 4.32 Application of compliance matrix to suspension system vehicle half model

suspension without a roll bar $C_{3,9}$ would be zero in the absence of any mechanical coupling between the left and right suspension systems. The other elements of the compliance matrix are defined similarly.

As stated the compliance matrix approach is well suited to investigate the effects of suspension movement due to compliance. By way of further example consider the definition used in ADAMS/Car for the calculation of Aligning torque − Steer and camber compliance.

The aligning torque steer compliance is the change in steer angle due to unit aligning torques applied through the wheel centres. Similarly the aligning torque camber compliance is the change in camber angle due to unit aligning torques acting through the wheel centres.

Figure 4.33 illustrates the determination of steer angle resulting at the right wheel due to unit aligning torques acting through both the left and right wheel centres. Note that the usual symbol for steer angle is δ. For the

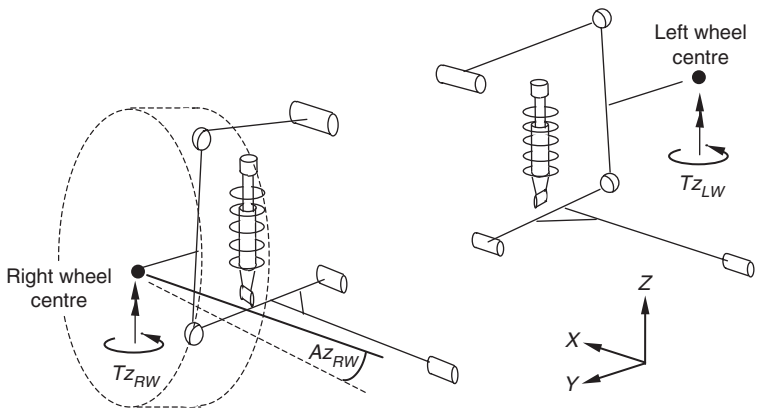

Fig. 4.33 Steer angle at right wheel due to aligning torques at left and right wheels

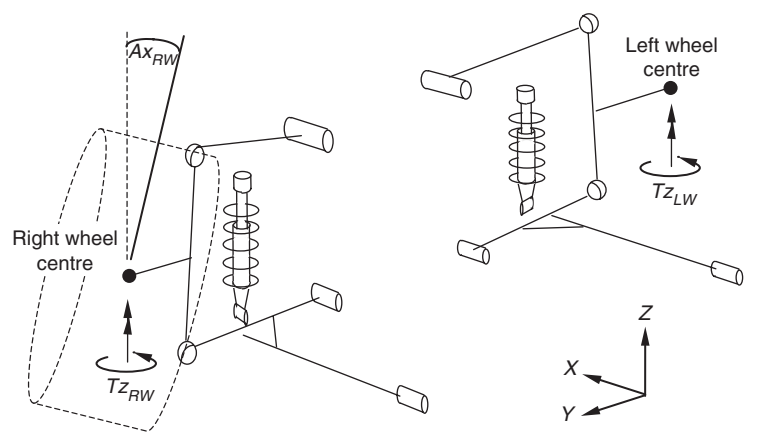

Fig. 4.34 Camber angle at right wheel due to aligning torques at left and right wheels

matrix approach used here, however, this is given by Az_{RW}. In this system a positive steer angle results when the wheel turns to the left, which in Figure 4.33 is consistent with a positive rotation Az_{RW} about the z-axis for the right wheel. In this case for the right wheel the steer angle would be given by $Az_{RW} = C_{12,6}Tz_{LW} + C_{12,12}Tz_{RW}$.

Similarly Figure 4.34 illustrates the determination of camber angle, Ax_{RW}, resulting at the right wheel due to unit aligning torques acting through both the left and right wheel centres.

In this system a positive camber angle results when the top of the wheel tilts away from the body, which in Figure 4.34 would actually be a negative rotation Ax_{RW} about the x-axis for the right wheel. In this case for the right wheel the camber angle would be given by $Ax_{RW} = C_{10,12}Tz_{RW} - C_{10,6}Tz_{LW}$.

Needless to say the sign convention used to define positive steer and camber angles always requires careful consideration particularly when considering the definitions given here using a compliance matrix approach to measure movement of the road wheels relative to the vehicle body.

4.7 Case study 1 – Suspension kinematics

The following case study is provided to illustrate the application of the methodology described in the previous sections to calculate the suspension characteristics as the suspension moves between the bump and rebound positions. Examples of the plotted outputs described here are shown in Figures 4.38 to 4.43. These plots were from a study based on the front suspension of a passenger car, considering the suspension connections to be joints, linear or non-linear bushes. The assembly of parts used to make up the front suspension system is shown schematically in Figure 4.35. Example data sets for this model are provided in Appendix A together with more detailed system schematics.

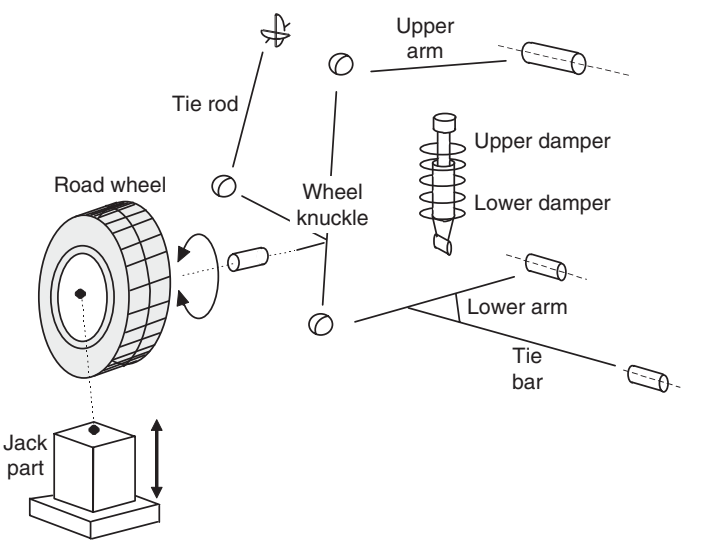

Fig. 4.35 Assembly of parts in the front suspension system example

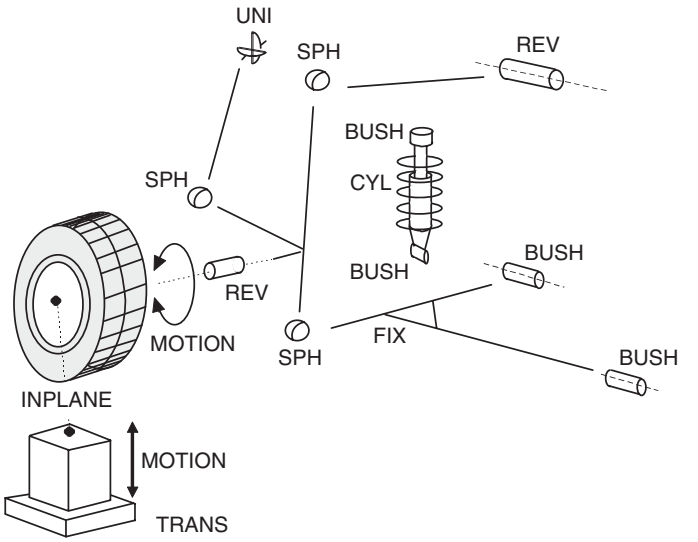

Fig. 4.36 Modelling the front suspension example using bushes

The modelling of the suspension system using bushes is shown in Figure 4.36. The upper link is attached to the body using a connection that is rigid enough to be modelled as a revolute joint. Bushes are used to model the connection of the lower arm and the tie bar to the vehicle body.

Bushes are also used to model the connections at the top and bottom of the damper unit. Where the tie bar is bolted to the lower arm a fix joint has been used to rigidly connect the two parts together. This joint removes all six relative degrees of freedom between the two parts creating in effect a single lower control arm.

The modelling issue raised here is that rotation will take place about an axis through these two bushes where the bushes are not aligned with this axis. As rotation takes place the bushes must distort in order to accommodate this. The modelling of these connections as non-linear, linear or as a rigid joint was therefore investigated to establish the effects on suspension geometry changes during vertical movement. For the suspension modelled in this manner it is possible to calculate the degrees of freedom for the system as follows:

Parts	9×6	$=$	54
Fix	1×-6	$=$	-6
Trans	1×-5	$=$	-5
Rev	2×-5	$=$	-10
Uni	1×-4	$=$	-4
Cyl	1×-4	$=$	-4
Sphs	3×-3	$=$	-9
Inplane	1×-1	$=$	-1
Motion	2×-1	$=$	-2
	ΣDOF	$=$	13

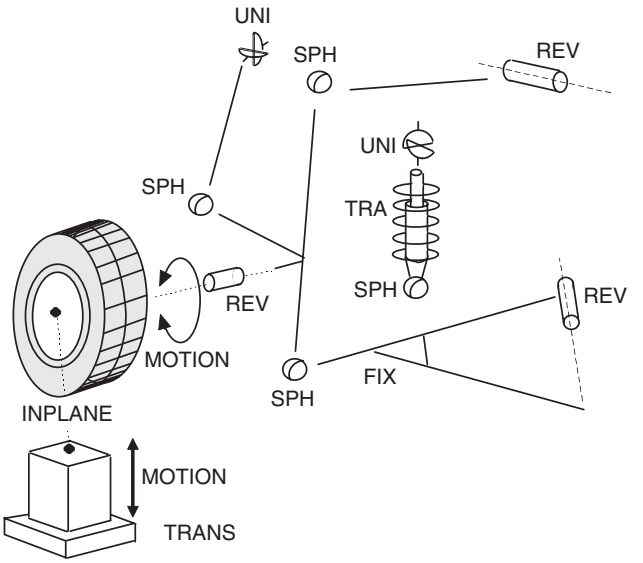

Fig. 4.37 Modelling the front suspension example using rigid joints

In order to produce a zero-degree-of-freedom model for this suspension the bushes at the top and bottom of the strut have been replaced by a universal and a spherical joint.

The bushes that were used to connect the lower arm and the tie rod assembly to the vehicle body were replaced in this study by a revolute joint. The axis of this joint was aligned between the two bushes as shown in Figure 4.37. For the suspension modelled in this manner using rigid joints it is possible to calculate the degrees of freedom for the system as follows:

Parts	9×6	$=$	54
Fix	1×-6	$=$	-6
Trans	2×-5	$=$	-10
Rev	3×-5	$=$	-15
Uni	2×-4	$=$	-8
Sphs	4×-3	$=$	-12
Inplane	1×-1	$=$	-1
Motion	2×-1	$=$	-2
	ΣDOF	$=$	0

For this suspension it was possible to compare the simulation results with measured suspension rig test data provided by the vehicle manufacturer for the variation of:

(i) Camber angle (deg) with bump movement (mm)

(ii) Steer angle (deg) with bump movement (mm)

(iii) Vertical force (N) with bump movement (mm)

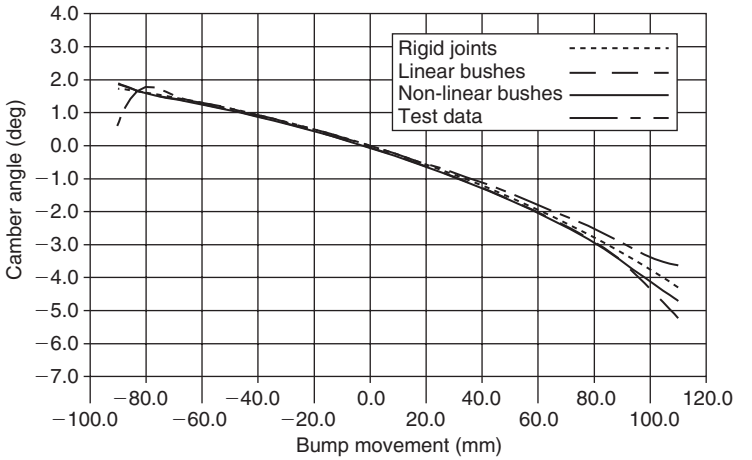

Fig. 4.38 Front suspension – camber angle with bump movement

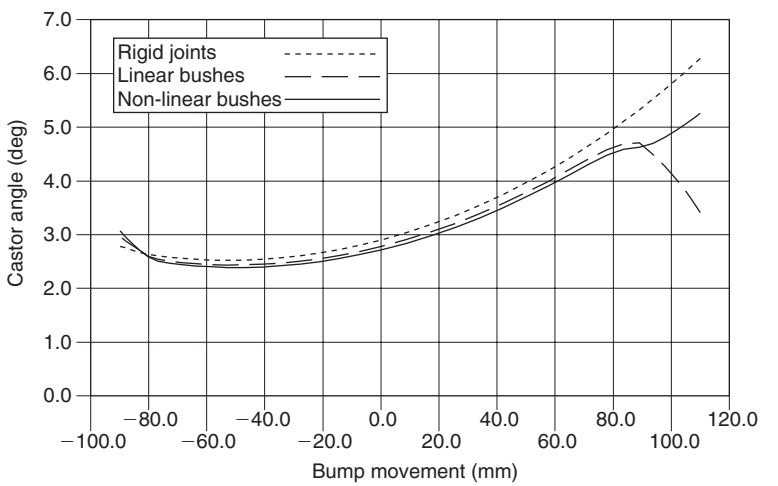

Fig. 4.39 Front suspension – castor angle with bump movement

Examination of the results shown here indicate that despite the alignment of the bushes on the lower arm assembly the calculated suspension characteristics agree well for models using rigid joints, linear bushes or non-linear bushes. It is noticeable with the front suspension that the plots begin to deviate when approaching the full bump or full rebound positions. This is due to contact with the bump stop or rebound stop generating forces that are then reacted back through the suspension to the bushes. The reaction forces at the bushes leads to distortions that produce the changes in suspension geometry as shown in the plots. This effect is not present in the models using rigid joints that have zero degrees of freedom. Geometry changes are entirely dependent on the position and orientation of the joints.

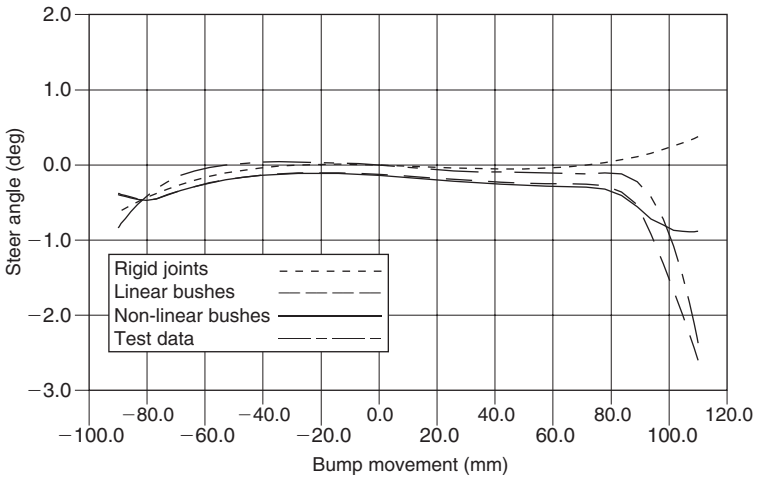

Fig. 4.40 Front suspension – steer angle with bump movement

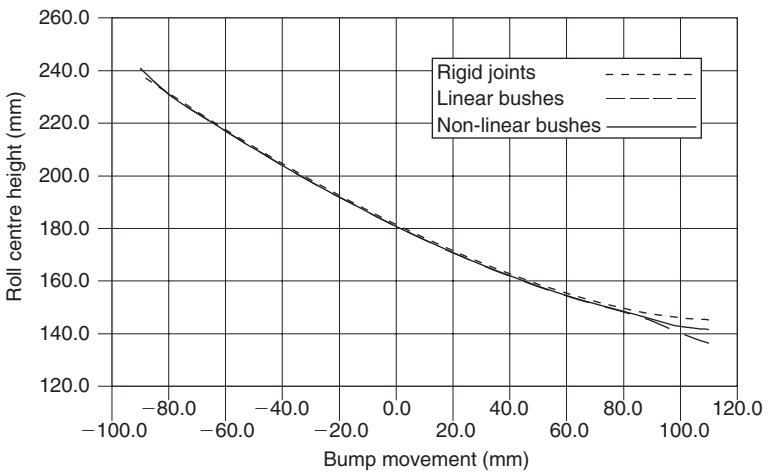

Fig. 4.41 Front suspension – roll centre height with bump movement. (This material has been reproduced from the Proceedings of the Institution of Mechanical Engineers, K2 Vol. 213 'The modelling and simulation of vehicle handling. Part 2: vehicle modelling', M.V. Blundell, page 125, by permission of the Council of the Institution of Mechanical Engineers)

Considering the merits of each modelling approach it appears from the curves plotted that for the range of vertical movement expected of a handling model there is little difference between models using rigid joints, linear bushes or non-linear bushes. The use of the non-linear model will significantly increase the effort required to model the vehicle. This is evident from Table 4.4 which compares the data inputs required to model the connection of the front suspension lower arm to the vehicle body.

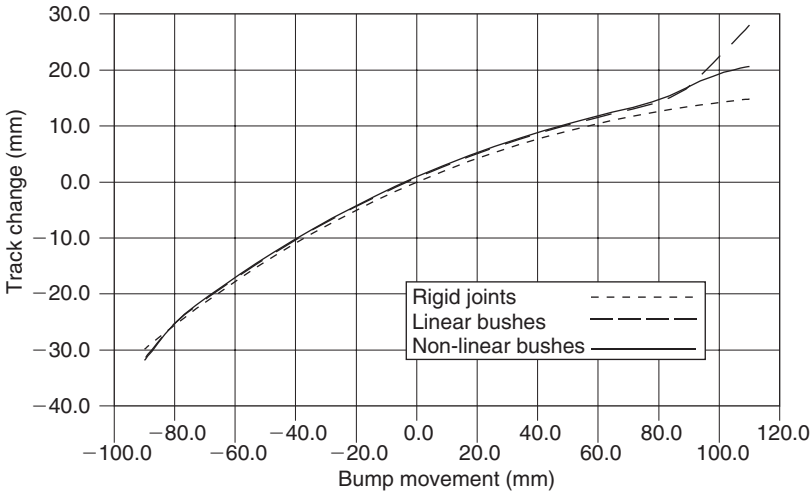

Fig. 4.42 Front suspension – half track change with bump movement

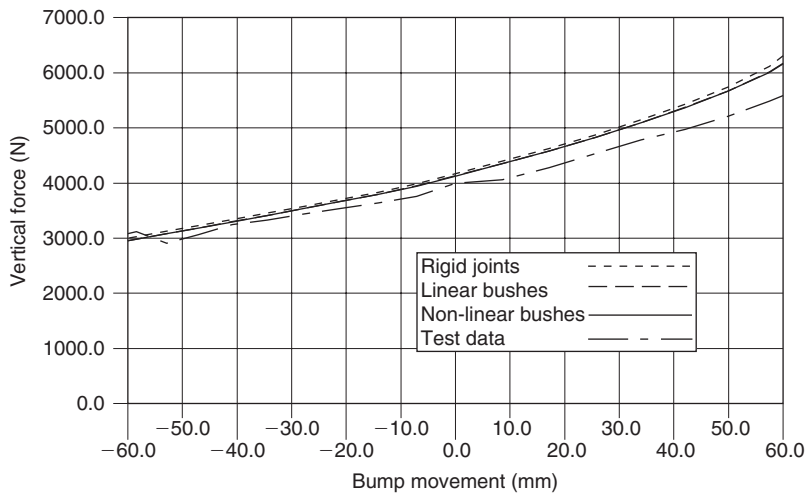

Fig. 4.43 Front suspension – vertical force with bump movement

4.8 Durability studies (component loading)

4.8.1 Overview

Multibody systems programs can often be used to determine the loads acting on suspension components and the body pickup points as inputs to finite element models of the components or vehicle structure. These simulations are aimed to match the series of tests that a vehicle manufacturer would perform on the proving ground to test the durability of the vehicle and chassis components. Different manufacturers will implement their own

Fig. 4.44 Vehicle durability testing on cobbled road surface (provided courtesy of Jaguar Cars Ltd)

Table 4.8 Typical suspension loadcases

Loadcase	Fx(N)	Fy(N)	Fz(N)
3g bump			11 180
2g rebound			−7 460
0.75g cornering (outer wheel)		4 290	5 880
0.75g cornering (inner wheel)		−1 180	1 620
1g braking	5 530		5 530
0.35g reverse braking	−2 150		3 330
Kerb impact		9 270	4 120
Pothole braking	15 900		12 360

procedures but typically these will involve establishing road loads resulting, for example, from accelerating, braking, cornering, striking potholes and driving on rough surfaces such as that shown in Figure 4.44.

The loads that are applied to the suspension may be considered to act at the tyre contact patch or at the wheel centre depending on the type of loadcase. The loads shown in Table 4.8 are typical of those that might be used for a static analysis on a vehicle of the type for which data is provided in this textbook. In this example, the loads are defined in the x, y and z directions for a co-ordinate system located at the centre of the tyre contact patch as shown in Figure 4.45.

For the loads shown in Table 4.8 it is possible to calculate values for cases such as cornering and braking using traditional vehicle dynamics and the principles of weight transfer. For cases involving impacts with kerbs and bumps it may be necessary to obtain instrumented road load measurements on the proving ground. A particularly severe case involves braking while

driving through a pothole. To simulate this sort of case the input loads at the contact patch may be set to produce forces, say acting along a tie rod, that are consistent with measured strains on the actual component during the proving ground tests.

The purpose of the multibody systems model of the suspension in this case is to obtain the distribution of the load through the suspension. This is illustrated in Figure 4.45 where it is indicated that for a given set of loads at the tyre contact patch it is possible to predict the forces and moments that would, for example, act through the bushes mounting the suspension arm to the body of the vehicle.

These forces and moments can then be used as boundary conditions for finite element models of vehicle structure or of suspension components. A typical finite element model of a suspension arm is shown in Figure 4.46.

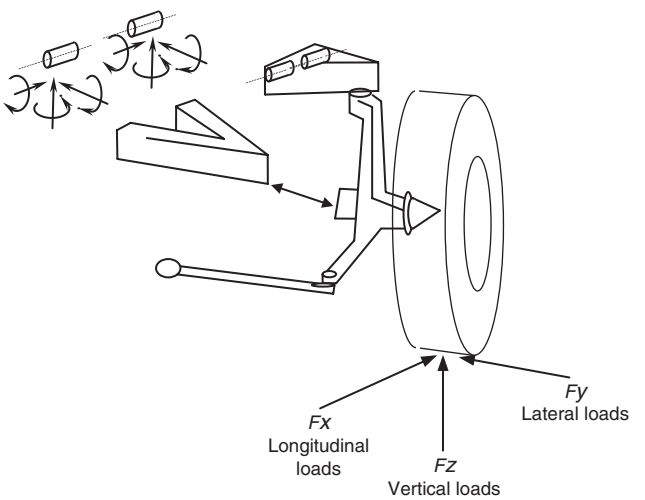

Fig. 4.45 Application of road loads at the tyre contact patch

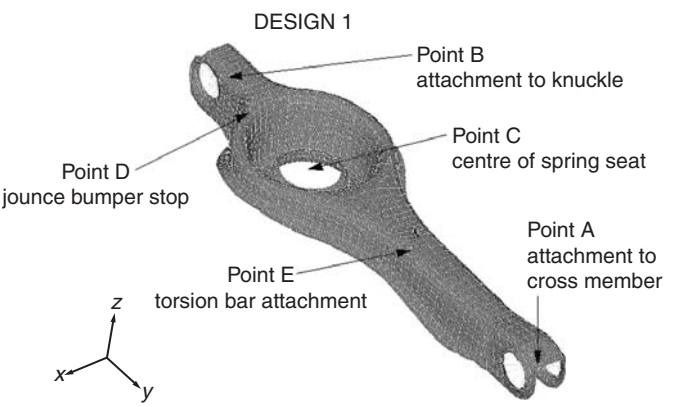

Fig. 4.46 Finite element model of suspension arm (provided courtesy of Jaguar Cars Ltd)

Once generated the suspension model may be used in two ways. One of these is to apply the load and carry out a static analysis. This may result in the suspension system moving through relatively large displacement to obtain a static equilibrium position for the given load. The static reactions in joints, bushes and spring seats can then be extracted. It is also possible to make the load a function of time and then to apply a quasi-static analysis. This has the advantage that the graphical post-processor can be used to animate the simulation to demonstrate how the suspension moves under the given load. An example of this for the 3G bump case would be to apply the 1G load for an initial static analysis at time equal to zero and then to apply the remaining 2G of the load over, say, 1 second of simulation time.

The use of equivalent static loads to represent real dynamic effects has been used by the automotive industry for some time. The derivation of design loads similar to those shown in Table 4.8 can be traced back to a publication in the early 1950s (Garrett, 1953) in the *Automobile Engineer*. The disadvantage of the static analysis is that any velocity dependent forces will not be transmitted through the damper without the inclusion of some static equivalent.

The extension of this is to carry out a dynamic simulation if possible. The model used may be a quarter suspension model or even a simulation of the complete vehicle. An example of this would be the simulation of a sports-utility type vehicle in off-road conditions. An early example of this (Rai and Soloman, 1982) was the use of MSC.ADAMS to carry out dynamic simulation of suspension abuse tests. The problem for the analyst with the dynamic approach is the amount of reaction force time history output generated at bush and joint positions.

The input loads used to represent braking and cornering may be obtained using basic vehicle data and weight transfer analysis. As an example consider the free-body diagram shown in Figure 4.47 where the wheel loads are obtained for a vehicle braking case. Note that in this example we are ignoring the effects of rolling resistance in the tyre, discussed later in Chapter 5, and the vehicle is on flat road with no incline.

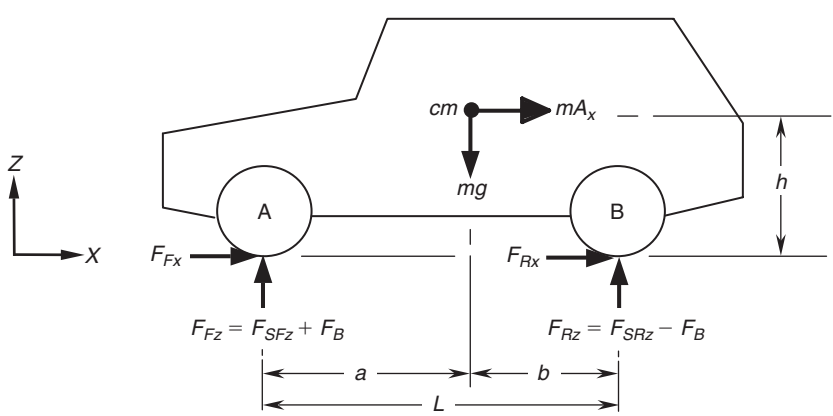

Fig. 4.47 Forward braking free-body diagram

The vertical forces acting on the front and rear tyres when the vehicle is at rest can be found by the simple application of static equilibrium. These forces, F_{SFz} for the front wheel and F_{SRz} for the rear wheel, are given by

$$F_{SFz} = \frac{mgb}{2L} \qquad F_{SRz} = \frac{mga}{2L} \tag{4.63a}$$

It can be noted that the division of the loads by 2 in (4.63a) is simply to reflect that we are dealing with a symmetric case so that half of the mass is supported by the wheels on each side of the vehicle. In this analysis the vehicle will brake with a deceleration A_x as shown in Figure 4.47. During braking weight transfer will arise, resulting in an increase in load on the front tyres by an additional load F_B and a corresponding reduction in load F_B on the rear tyres. This can be obtained by taking moments about either wheel, for mA_x only and not mg, to give

$$F_B = \frac{mA_x h}{2L} \tag{4.64}$$

Note that in determining the longitudinal braking forces F_{Fx} and F_{Rx} we have a case of indeterminancy with four unknown forces and only three equations of static equilibrium. The solution is found using another relationship to represent the relationship between the braking and vertical loads. At this stage we will assume that the braking system has been designed to proportion the braking effort so that the coefficient of friction μ is the same at the front and rear tyres. The generation of longitudinal braking force in the tyre is generally not this straightforward and will be covered in the next chapter. We can now combine the static and dynamic forces acting vertically on the wheels to give the full set of forces:

$$F_{Fz} = F_{SFz} + F_B = \frac{mgb}{2L} + \frac{mA_x h}{2L} \tag{4.65}$$

$$F_{Rz} = F_{RFz} - F_B = \frac{mga}{2L} - \frac{mA_x h}{2L} \tag{4.66}$$

$$F_{Fx} + F_{Rx} = mA_x \tag{4.67}$$

$$\frac{F_{Fx}}{F_{Fz}} = \frac{F_{Rx}}{F_{Rz}} = \mu \tag{4.68}$$

4.8.2 Case study 2 – Static durability loadcase

In order to demonstrate the application of road input loads to the suspension model a case study is presented here based on the same front suspension system described in section 4.7 for Case study 1. The loading to be applied is for the pothole braking case outlined in Table 4.8. Due to the severity of the loading, the suspension model used here is one that includes the full non-linear definition of all the bushes, the bump stop (spring aid) and a rebound stop. The model also includes a definition of the dampers and the damping terms in the bushes. These will be required later for an analysis

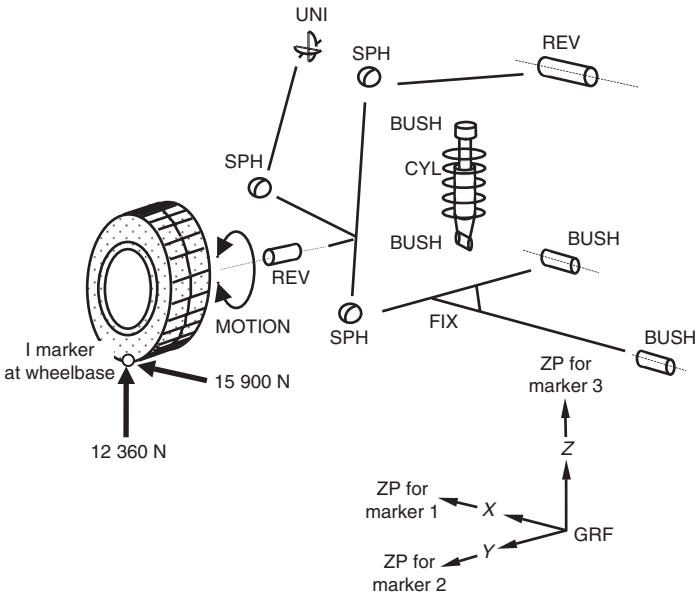

Fig. 4.48 Application of pothole braking loads to suspension model

that demonstrates the dynamic input of a road load but are not used for the initial phase where the load is applied quasi-statically. A schematic for the model is shown in Figure 4.48 where it can be seen that the jack that was used earlier to move the suspension between the rebound and bump positions has been replaced by applied forces acting on a marker located at the bottom of the road wheel.

The loads are applied as action-only single forces acting on the I marker at the contact patch. In this example we are treating the wheel as a single rigid body and ignoring any compliance in the tyre. The I marker is in this case located at an undeformed radius directly below the wheel centre. The motion statement associated with the road wheel revolute joint has a function set to zero to effectively lock the rotation of the wheel. The loads are applied parallel to the axes of the Ground Reference Frame (GRF) at the start and remain parallel to the GRF during the simulation. They do not rotate with the wheel as the suspension deforms under the loading.

For an action-only force it was shown in Chapter 3 that the point of application for the force is given as the I marker and the line of action and direction of the force is given by the z-axis of the J marker. A convenient way to create a set of J markers that may be used for each loadcase is to define three markers that are used for this purpose alone as follows:

```
PART/01, GROUND
MARKER/01, ZP = 1, 0, 0    ! Global x direction
MARKER/02, ZP = 0, 1, 0    ! Global y direction
MARKER/03, ZP = 0, 0, 1    ! Global z direction
```

Note that in this case the QP vectors have been omitted so that by default all three markers are located at the GRF on the ground part. The ZP vectors

orientate the markers so that each z-axis aligns with one of the axes of the GRF. The ZP definition on Marker/03 is included for completeness although if this were left out Marker/03 would by default still be parallel to the GRF.

It is now possible to include a set of three single forces to define the pothole braking case. To allow the use of animation the loads will be applied as an initial static analysis where only the vertical static tyre load is applied followed by a quasi-static analysis where the additional loads are applied as a function of time. As the analysis is quasi-static the time taken to ramp on the loads is arbitrary. In this example a period of 1 second is used by way of example. The following SFORCE statements may be used to implement this:

SFORCE/01, I = 1029, J = 1, TRANS, ACTION
,FUNCTION = 15900 * TIME
SFORCE/02, I = 1029, J = 2, TRANS, ACTION, FUNCTION = 0
SFORCE/03, I = 1029, J = 3, TRANS, ACTION
,FUNCTION = 3727 + 8633 * TIME

From this it can be seen that for the pothole braking case a longitudinal load in the x direction and a vertical load in the z direction are applied. The lateral load in the y direction is set to zero. The functions are set for this example so that for the initial static analysis a vertical load of 3727 N is applied with the additional components due to pothole braking being added over 1 second. It can be seen from this that the functions used to define the forces can be quickly changed to correspond with each of the loadcases given in Table 4.8.

The graphics showing the suspension deformed under full load are shown in Figure 4.49 with additional graphics showing the force components at the contact patch. An *XY* plot showing the development of force magnitude in the spring is shown in Figure 4.50. Examination of the numerical values associated with the components of this force at full load, after 1 second, would provide the inputs for any subsequent finite element models.

It should be noted that with the quasi-static example used here there is no velocity dependent load transmission through the damper. To increase the validity of the results it would be necessary to estimate an equivalent load and apply this as an additional static force. An alternative would be to develop the analysis of the suspension to apply the force as a function of time and carry out a dynamic simulation as described next.

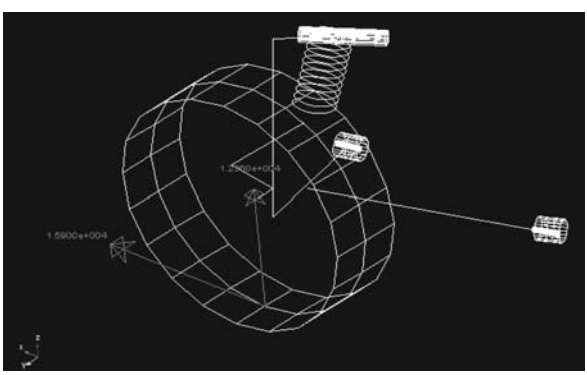

Fig. 4.49 MSC.ADAMS graphics of suspension at maximum pothole braking case load

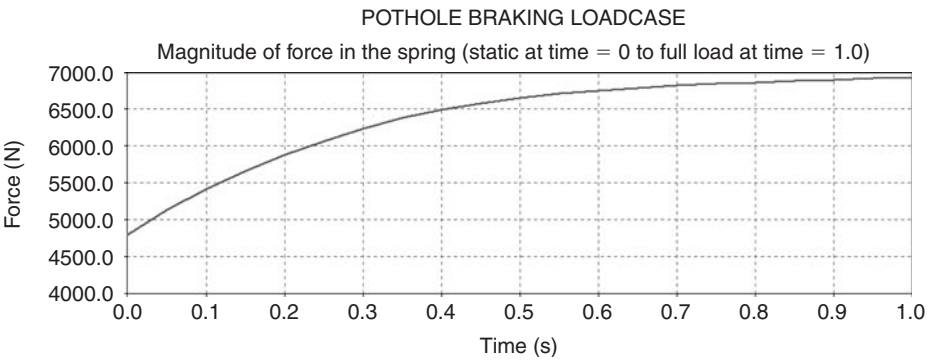

Fig. 4.50 MSC.ADAMS plot of spring load for pothole braking case

4.8.3 Case study 3 – Dynamic durability loadcase

In this case study we extend the model of the single suspension system to include an additional part representing the corner of the vehicle body, quarter model, to which the suspension linkages attach as shown in Figure 4.51.

The vehicle body is attached to the ground part by a translational joint that allows the body to move vertically in response to the loads transmitted through the suspension system. A jack part is reintroduced to reproduce vertical motion inputs representative of road conditions. An additional complexity in the model is the introduction of stiffness and damping terms

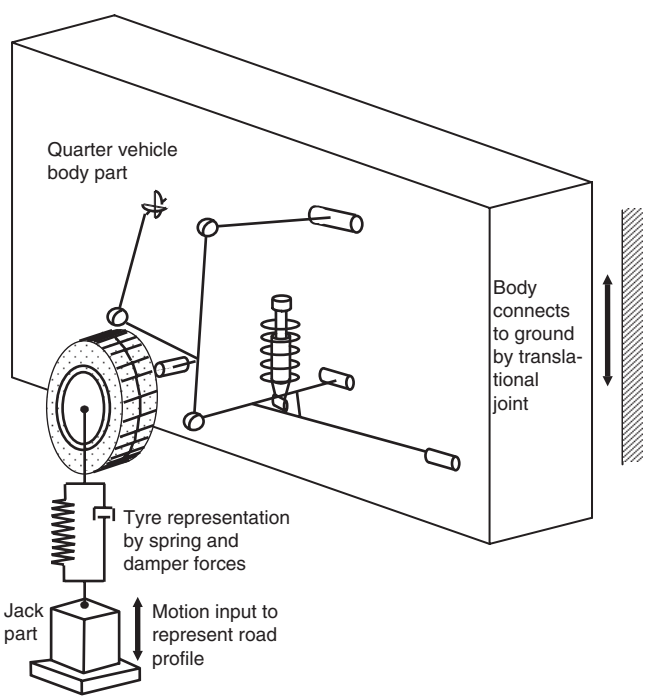

Fig. 4.51 Quarter vehicle body and suspension model

in a force element that represents the behaviour of the tyre. The force element acts between the centre of the wheel and a point on the jack coincident with the centre of the tyre contact patch. In this case this is assumed to be directly below the wheel centre. It is important that the force element for the tyre acts only in compression and allows the tyre to lift off the top of the jack if the input is severe enough.

The tyre is taken to have linear radial stiffness of 160 N/mm and a damping coefficient of 0.5 Ns/mm. The undeformed radius of the tyre, equivalent to the free length of the tyre spring, is taken here to be 318 mm. A step function can also be used to zero the tyre force if contact with the jack is lost. The full definition can be accomplished using the following SFORCE statement that is taken to act between Marker 1010 at the wheel centre and Marker 2029 on the jack part:

```
SFORCE/1029, I=1010, J=2029, TRANS
,FU=STEP(318-DM(1010,2029),0,0,0.1,160*(318-DM(1010,2029))
   -0.5*VR(1010,2029))
```

The next step is to define the motion imparted to the jack part to represent the input from the road surface. This is illustrated in Figure 4.52 where the profile for a 'sleeping policeman' road obstacle is given. The profile is defined as a set of *xy* pairs. Note here that the *xy* values are local to the definition of the obstacle profile and not associated with the *X*- and *Y*-axes of the ground reference frame. The vehicle is assumed to be moving with a forward speed of 10 m/s so that the *x* values associated with distance can be converted to time.

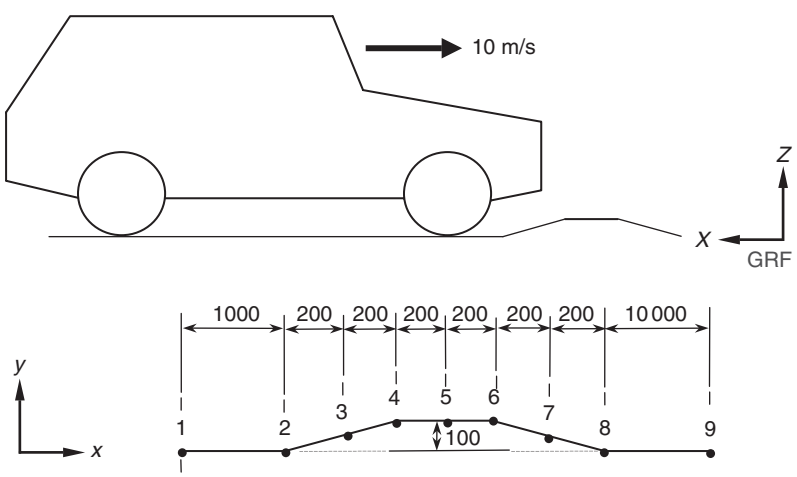

Point	1	2	3	4	5	6	7	8	9
Distance *x* (mm)	0	1000	1200	1400	1600	1800	2000	2200	12 200
Time *x* (s)	0	0.10	0.12	0.14	0.16	0.18	0.20	0.22	1.22
Height *y* (mm)	0	0	50	100	100	100	50	0	0

Fig. 4.52 Road profile for 'sleeping policeman' speed bump

One method that could be used to input a motion associated with the profile of the road surface would be to use a SPLINE statement as follows:

```
MOTION/20, JOINT=20, TRANS, FUNCTION=CUBSPL(TIME, 0, 10)
SPLINE/10
,X = 0, 0.10, 0.12, 0.14, 0.16, 0.18, 0.20, 0.22, 1.22
,Y = 0,   0,    50,   100,  100,  100,   50,    0,    0
```

Caution is needed here, however, for although the data points may be sufficient to capture the profile of the bump there may not be enough to ensure a good spline fit. A more elegant but elaborate method might be to forgo the use of interpolation and use a combination of arithmetic IF and step functions. This method requires care in formatting but may be applied as follows:

```
MOTION/20, JOINT = 20, TRANS
,FU=IF(TIME−0.14: STEP(TIME, 0.1, 0, 0.14, 100), 100
,STEP(TIME, 0.16, 100, 0.22, 0))
```

The MSC.ADAMS graphics showing the suspension deflecting on the jack and the subsequent departure of the tyre from the road surface are shown in Figure 4.53. A plot showing the time histories for the vehicle body and road wheel vertical displacement is shown in Figure 4.54. The force in the

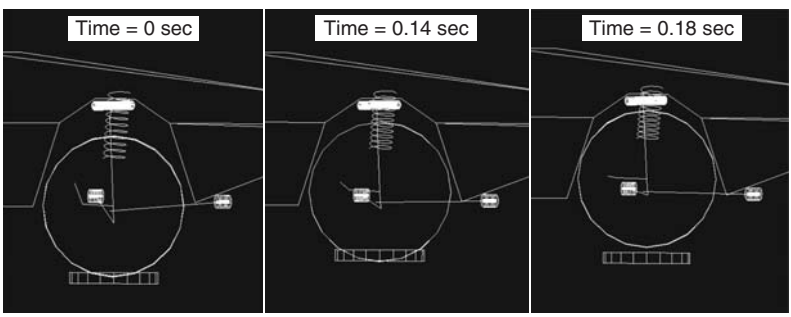

Fig. 4.53 MSC.ADAMS graphics of suspension deflecting on a speed bump

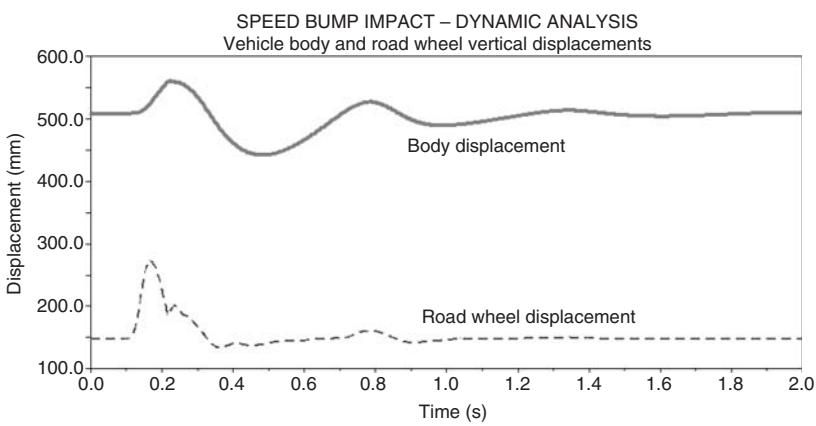

Fig. 4.54 MSC.ADAMS plot vehicle body and road wheel displacements for speed bump strike

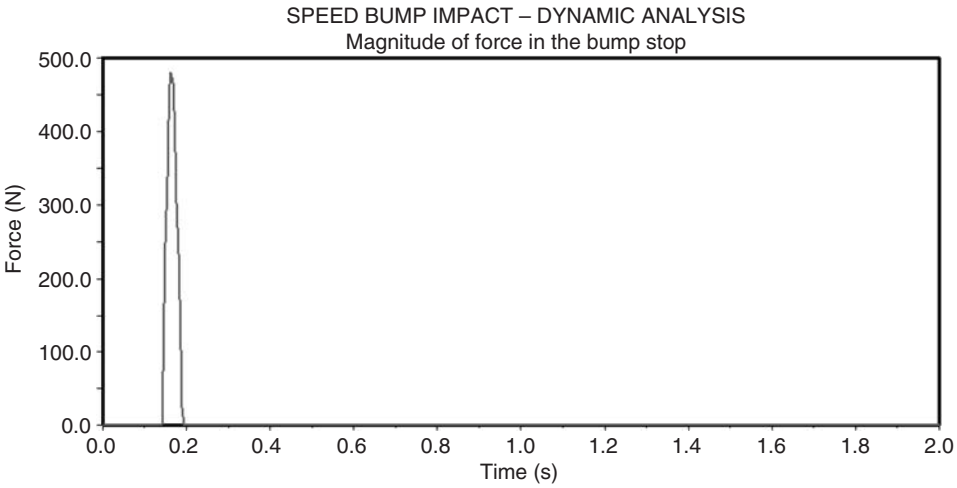

Fig. 4.55 MSC.ADAMS plot of bump stop force time history for speed bump strike

bump stop is provided by way of example (Figure 4.55). It should be noted that at this stage the analysis only represents vertical force input and not longitudinal force input from the road surface.

4.9 Ride studies (body isolation)

The determination of vehicle 'ride' quality is associated with the extent to which the occupants of the vehicle are affected by vehicle motion. Automotive companies will often have departments concerned with ride and handling where multibody systems analysis will be deployed to support design and analysis work. Another area of activity is referred to as Noise Vibration and Harshness (NVH). In general vibrations with frequencies up to 25 Hz are generally said to be associated with ride. These modes of vibration are usually amenable to analysis with the multibody techniques described in this textbook.

Vibrations with frequencies above 25 Hz are usually referred to as noise. The analysis of these modes and other acoustic type problems is more in the domain of advanced finite element analysis and as such is not covered here. Vehicles should be thought of as dynamic systems, a mixture of masses, springs and dampers, where vibration is exhibited in response to excitation. The source of excitation may be due to out-of-balance loads from rotating bodies such as the road wheel or from other sources in the vehicle including the engine and driveline. The other main source of vibration will be associated with the profile of the road surface. At this stage it is easy to envisage that the excitation of vehicle pitch may be in response to a road with an undulating type profile of relatively long wavelength whereas the excitation of a smaller mass such as the road wheel will occur at higher frequencies. This might, for example, occur while driving on a cobbled type of road surface.

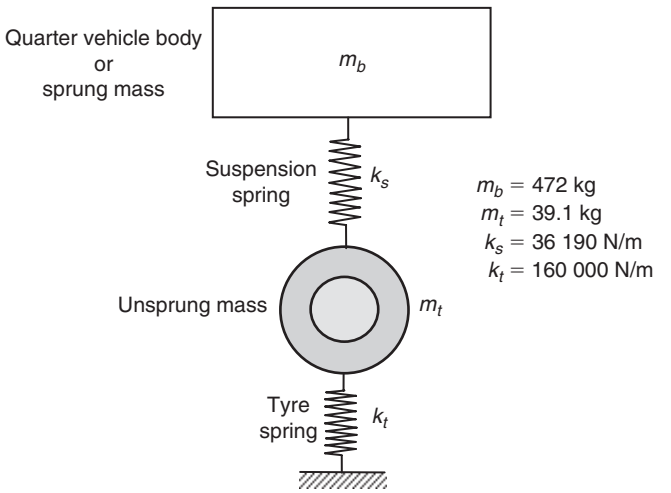

Fig. 4.56 Two degree of freedom quarter vehicle model

4.9.1 Case study 4 – Dynamic ride analysis

In this case study we adapt the quarter vehicle model shown in Figure 4.51 for a ride analysis. Before considering the output from the simulation simple manual calculations can be performed to check and confirm the MSC.ADAMS results. These calculations can find the natural frequencies for the body on the suspension and for the unsprung mass between the road spring and the tyre spring. Figure 4.56 shows a two degree of freedom quarter vehicle model with the data used to support the calculations.

The undamped natural frequencies for the body, f_b, and unsprung mass, f_t, can be estimated using the following equations. Note that for the body we determine an equivalent stiffness k_{eqv} to represent the combined contribution of the road and tyre springs:

$$k_{\text{eqv}} = \frac{k_s k_t}{k_s + k_t} \tag{4.69}$$

$$f_b = \frac{1}{2\pi}\sqrt{\frac{k_{\text{eqv}}}{m_b}} \tag{4.70}$$

$$f_t = \frac{1}{2\pi}\sqrt{\frac{k_s + k_t}{m_t}} \tag{4.71}$$

Performing the calculations using the data given results in values as follows:

$k_{\text{eqv}} = 26\,639\,\text{N/mm}$

$f_b = 1.196\,\text{Hz}$

$f_t = 11.15\,\text{Hz}$

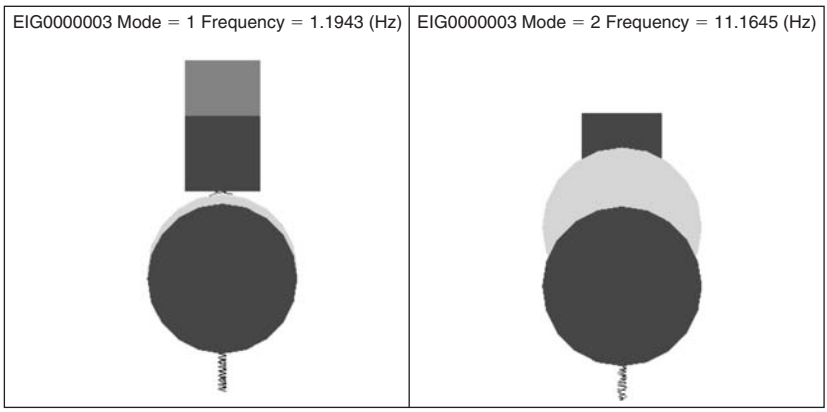

Fig. 4.57 MSC.ADAMS prediction of the modes of vibration of the simplified quarter vehicle model

An MSC.ADAMS model consisting exactly of the model as sketched above can be used to calculate undamped linear modes in a more exact fashion, giving two modes of vibration as might be expected but slightly differing numerical results.

The modal solution uses the ADAMS/Linear™ product, which in turn uses numerical perturbation methods to estimate mass and stiffness matrices about an operating point before solving for eigenvalues in the normal fashion. For purely mechanical systems such as the one modelled it can be relied upon to give good quality results. However, for systems where forces are time dependent and are modelled in specific ways (e.g. as differential equations for modelling turbocharger behaviour as described in Chapter 6, or tyre relaxation length modelling) then the results are not necessarily reliable at the time of writing and must be examined on an individual basis before confidence is placed in them. MSC.ADAMS and other software packages are subject to ongoing modification and development and so functionality of this nature should be evaluated periodically; such evaluations should be part of the software commissioning process within individual organizations, particularly if critical decisions are to be based on software output.

The estimates given above are a simplification of the real analytical solution to the system. Such a solution is obtained using the equations of motion taking x_b and x_t in this example to represent the vertical displacements of the body and tyre respectively. The equations are written by inspection thus:

$$m_t\ddot{x}_t = k_t(-x_t) + k_b(x_b - x_t) \tag{4.72}$$

$$m_b\ddot{x}_b = k_b(x_t - x_b) \tag{4.73}$$

These can be arranged more conveniently as:

$$m_t\ddot{x}_t = x_t(-k_t - k_b) + x_b(k_b) \tag{4.74}$$

$$m_b\ddot{x}_b = x_t(k_b) + x_b(-k_b) \tag{4.75}$$

If a solution is assumed of the form

$$x_i = X_i \, e^{\lambda t} \tag{4.76}$$

then

$$\ddot{x}_i = \lambda^2 X_i \, e^{\lambda t} = \lambda^2 x_i \tag{4.77}$$

thus

$$m_t \lambda^2 x_t = x_t(-k_t - k_b) + x_b(k_b) \tag{4.78}$$

$$m_b \lambda^2 x_b = x_t(k_b) + x_b(-k_b) \tag{4.79}$$

which may be rearranged into the familiar eigenvalue problem:

$$\begin{bmatrix} -k_t - k_b - m_t\lambda^2 & k_b \\ k_b & -k_b - m_b\lambda^2 \end{bmatrix} \begin{bmatrix} x_t \\ x_b \end{bmatrix} = 0 \tag{4.80}$$

in which the determinant of the matrix can be used to find the eigensolution when set to zero:

$$(-k_t - k_b - m_t\lambda^2)(-k_b - m_b\lambda^2) - k_b^2 = 0 \tag{4.81}$$

$$(m_t m_b)\lambda^4 + (k_b m_t + (k_t + k_b)m_b)\lambda^2 + k_t k_b + k_b^2 - k_b^2 = 0 \tag{4.82}$$

which may be recognized as a quadratic in λ^2 and solved in the normal manner:

$$\lambda^2 = \frac{-b \pm \sqrt{b^2 - 4ac}}{2a} \tag{4.83}$$

$$a = m_t m_b \tag{4.84}$$

$$b = k_b m_t + (k_t + k_b)m_b \tag{4.85}$$

$$c = k_t k_b + k_b^2 - k_b^2 = k_t k_b \tag{4.86}$$

The calculated roots using this method are

λ^2: -56.3075
-4920.87

λ: $7.50383i$
$70.1489i$

frequencies: 1.19427 Hz
11.1645 Hz

which can be seen to agree exactly with the MSC.ADAMS model. However, the differences between the exact method and the approximate method are small – less than 0.15%. Thus the approximate method is a 'good enough' check for this system. This is generically true for quarter vehicle models, where the second mode of vibration is typically an order of magnitude higher than the first. However, for particularly stiff suspensions or compliant tyres as may be used on circuit cars, the suitability of the approximate method breaks down and therefore it should be used with some care.

While the approximate method produces usefully accurate results for this simplified model, when a real suspension system is analysed in MSC.ADAMS using the same method (eigenvalues predicted by the ADAMS/Linear product) using the same data but including real wishbone and elastomer geometry, the results can be seen to be somewhat different.

The first and most obvious source of error is the use of the spring rate directly from the detailed model in the simplified 2 DOF models. In the literal model, as in the real vehicle, the motion of the wheel does not directly correspond to the motion of the spring. Using the model, the so-called 'motion ratio' can be examined between spring and wheel. It can be seen (Figure 4.59) that the spring changes length by 1.43 mm for every 1 mm of

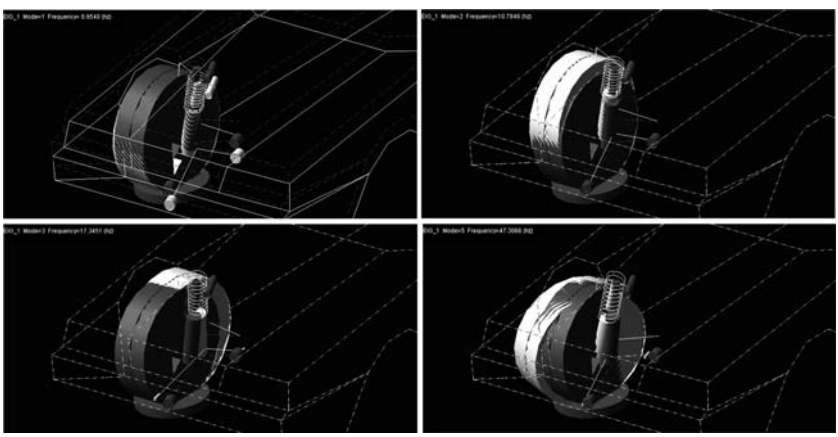

Figure 4.58 MSC.ADAMS prediction of the modes of vibration for the full linkage quarter vehicle model with elastomers and individual component mass and inertia data. Primary ride mode (top left) 0.95 Hz. Wheel hop mode (top right) 10.78 Hz. Fore–aft compliance mode (bottom left) 17.35 Hz. Unsprung mass lateral mode (bottom right) 47.31 Hz

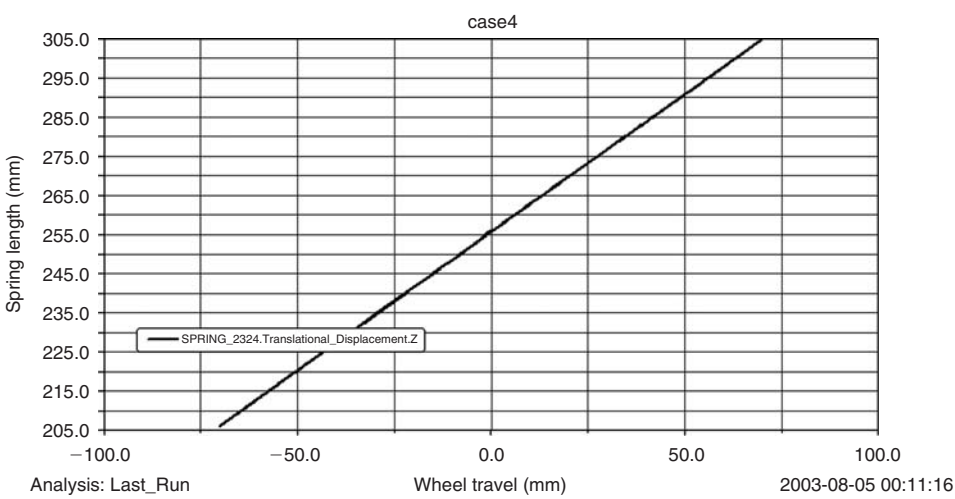

Fig. 4.59 Spring motion with respect to wheel motion from the model

wheel vertical motion. Some practitioners quote this as a motion ratio of 1.43:1 and some as 0.699:1. It is very important the definition of motion ratio as quoted is understood before the number is used since it is not always true that the spring moves less than the wheel.

Using the motion ratio, the wheel rate due to the spring can be seen to be $31.96/1.43^2 = 15.63\,\mathrm{N\,mm^{-1}}$. Reassessing the classical calculations, the estimated ride frequency is now 0.874 Hz, with a ride rate of $14.24\,\mathrm{N\,mm^{-1}}$. The estimated frequency is now less than that calculated using the full model (which was 0.954 Hz), suggesting there is some additional stiffness or reduced mass in the mode of vibration. Examining the model again, the so-called 'ride rate' (k_{eqv}) can be taken directly (Figure 4.60). In the case of this particular suspension geometry, the ride rate is $14.97\,\mathrm{N\,mm^{-1}}$. The difference between the two ride rates may be attributed to additional rates arising from the suspension bushes; these are commonly referred to as 'parasitic' rates. Although that term implies something undesirable about them, they are generally small and do not degrade the suspension behaviour unduly.

It may be noted, however, that the difference between the two results is not fully accounted for by the difference in wheel rate. For this particular example, using the analytical solution for the two-mass solution we may calculate 'effective' masses and stiffnesses for each mode of vibration. In the results from the full linkage model, these effective masses and stiffnesses are reported in the results file. They are known as 'modal' mass and stiffness values. For the model in question, these values are given as:

Primary ride mode:	$17.2232\,\mathrm{N\,mm^{-1}}$	479.355 kg
Wheel hop mode:	$177.019\,\mathrm{N\,mm^{-1}}$	38.552 kg

It is clear then that there is some other stiffness influence on the ride rate within the model that is not readily apparent to the user. Similarly, the mass is larger than the mass associated with the body alone. This acknowledges

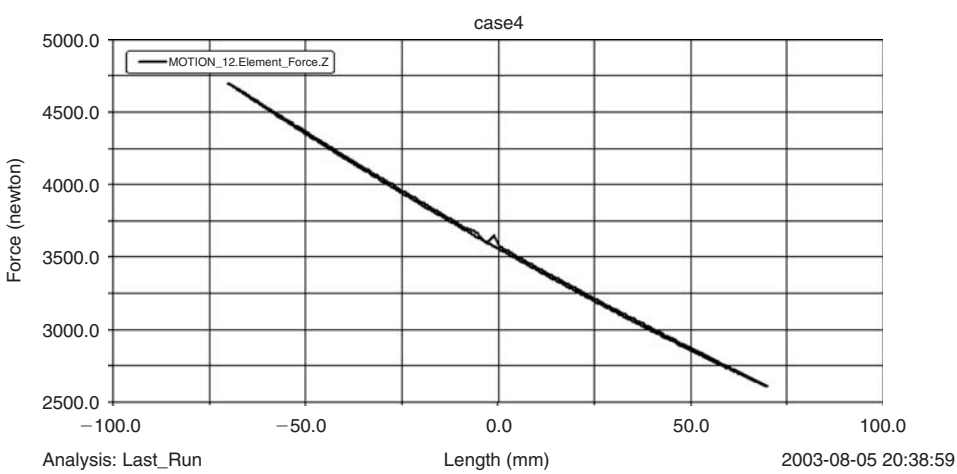

Fig. 4.60 Wheel rate measured from full linkage model

the fact that several components are in motion with different velocities when the modes of vibration are excited and thus are storing kinetic energy.

For an appreciation of these and other differences between the simplified and detailed model, the kinetic and strain energy tables calculated by MSC.ADAMS can be examined in some detail. Table 4.9 shows the output from the calculations directly. It can be seen that the kinetic energy for the primary ride mode is contained almost entirely in the body mass. However, it will be noted that 472/0.985 = 479 kg; thus the kinetic energy table shows the contributions of the other components in the model to the modal mass. The largest of the other contributors to the modal mass are the suspension arms and damper. For the strain energy results, it can be seen that the compliance in the lower arm bushes and the damper lower bush contribute significantly to strain energy storage in the primary ride mode of vibration.

Table 4.9 ADAMS/Linear output tables

```
************************
   Mode number             =  1
   Damping ratio           =  2.20914E-11
   Undamped natural freq.  =  9.54000E-01 Cycles per second
   Generalized stiffness   =  1.72232E+01 User units
   Generalized mass        =  4.79355E+02 User units
   Kinetic energy          =  2.18135E-01

              Percentage distribution of Kinetic energy
            |  X      Y     Z      RXX   RYY   RZZ    RXY    RXZ   RYZ
            +-----------------------------------------------------------
PART/20     |
PART/1      |               98.50
PART/10     |         0.06   0.04  0.02
PART/11     |         0.03   0.02
PART/12     |                0.22  0.05
PART/13     |                0.30
PART/14     |                0.34  0.03   0.01          0.01
PART/15     |                0.04  0.01
PART/16     |                0.08
PART/17     |         0.01   0.20  0.01
            +-----------------------------------------------------------

               Percentage distribution of Strain energy
            |  Total  X     Y      Z      RXX    RYY    RZZ
            +-----------------------------------------------------------
BUSH/16     |   0.01                       0.01
BUSH/17     |   0.01                       0.01
BUSH/19     |   0.14                       0.14
BUSH/21     |  16.32  0.06   2.47  13.78
SFOR/1029   |   5.35  0.01   0.55   4.79
SFOR/2728   |
SFOR/2526   |
SFOR/3233   |
SPRI/2324   |  37.71  0.19   0.25  37.27
GFOR/16     |  20.16  2.38  17.27   0.02  0.49
GFOR/17     |   2.56  0.22   1.79   0.13  0.42
            +-----------------------------------------------------------
```

The preceding results were all generated using an undamped eigensolution. However, for vehicle ride work, the influence of the dampers is critical. Moreover, the dampers are typically highly non-linear devices. Therefore, a further treatment of the existing MSC.ADAMS model is required once the modal 'positioning' (i.e. the undamped frequencies for primary ride, wheel hop and fore–aft compliance) is established.

In terms of the modelling approach the only modification here is a change in the motion applied to the jack where the function now represents a sinusoidal input with fixed amplitude but with a frequency that increases as a function of time as illustrated in Figure 4.61. The motion input is referred to as a frequency sweep, sometimes described as a 'chirp' – for reasons which are obvious if the resulting signal is audible.

The following motion statement is an example of a suitable input function where the amplitude of the road input is fixed at 10 mm and the frequency is increased using the following function from zero to 20 Hz after 80 seconds.

```
MOTION/20, JOINT = 20, TRANS
,FUNCTION = 10.0 * SIN(TIME/8 * TIME * 360D)
```

Using this simulation we can produce a time history plot showing the change in vertical acceleration of the sprung and unsprung masses of the quarter vehicle model as the simulation progresses. Examination of the response shown in Figure 4.62 reveals that excitation of a system resonance (a 'mode of vibration') occurs at two points during the simulation. The first of these corresponds with the natural frequency of the body and the second with the natural frequency of the unsprung mass.

Another interpretation of the results obtained here is to perform a Fast Fourier Transform (FFT) so that the results can be plotted in the frequency rather than the time domain as shown in the lower half of Figure 4.62. The simulation was allowed to run for 81.91 seconds with an output sample rate of 100 Hz, giving 8192 points including the zero time point. A single buffer transform was performed on the entire record for each of the signals. Although flawed, this method is adequate for identifying frequency peaks. However, for quantifying amplitude content the underlying presumption

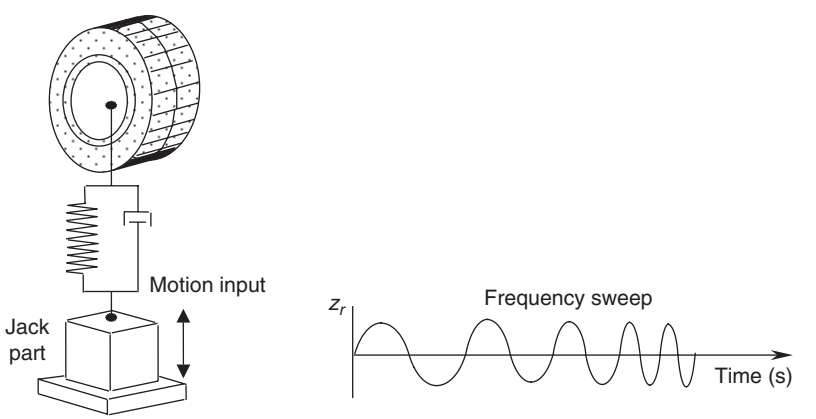

Fig. 4.61 Input of frequency sweep via jack motion

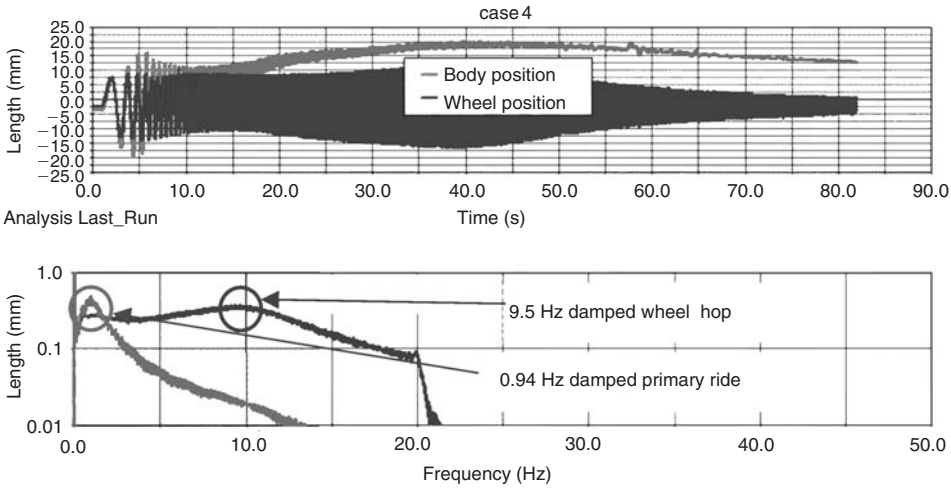

Fig. 4.62 Quarter vehicle body vertical acceleration time history

that the signal repeats itself after the end of the observation buffer is clearly in error; therefore the magnitude results of this exercise should not be used further.

From Figure 4.62 it can be seen that the damped natural frequency of the body occurs at around 0.94 Hz and that the natural frequency of the unsprung mass is about 9.5 Hz. Comparing these values with the previous values, it can be seen they are systematically low. This is to be expected since the addition of a damping ratio ζ reduces the damped natural frequency ω_d when compared with the undamped natural frequency ω_n:

$$\omega_d = \omega_n \sqrt{1 - \zeta^2} \tag{4.87}$$

The greatest reduction in frequency comes with the heavily damped wheel hop mode. Observing the change between undamped and damped frequency allows an estimate of the damping ratio to be made. For the two modes the damping ratios can be estimated as 0.07 and 0.48 for primary ride and wheel hop, respectively. The damping of the primary ride is low. However, if the exercise were to be repeated at different amplitudes of excitation, the level of damping in the primary ride is certain to vary since the damper characteristics are highly non-linear. For this reason, the time-domain method and subsequent processing are the preferred methods for evaluating ride behaviour once simplified undamped positioning calculations have been carried out.

The next question has to be 'how does one choose where to position primary ride behaviour?' In order to answer this, some knowledge of typical road surfaces is required. Road surfaces are, to a first approximation, a random process passing under the car. They can be described by the expression

$$u(\omega) = \frac{K(2\pi V)^{R-1}}{\omega^R} \tag{4.88}$$

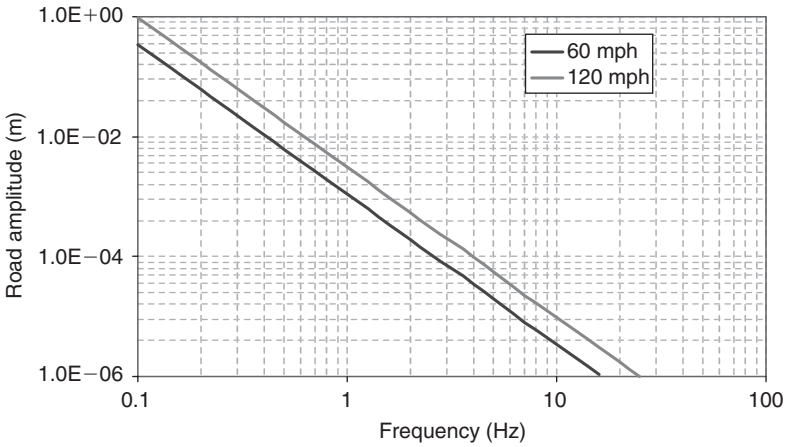

Fig. 4.63 Road surface frequency content

where R and K are constants of 2.5 and 5×10^{-5} respectively. The value of K varies with the nature of the road being studied. For novel applications or for previously unknown markets, some measurement of road profiles is desirable; for the developed western world the values given are generally appropriate. For military applications, a value of 1 for R may be appropriate. The very smoothest roads are unlikely to have R higher than 4.

It can be seen that the spectral content as seen by the car varies with vehicle speed. Gillespie (1992) gives a 'rational' argument to suggest that spectral content rises with speed squared. However, Hales (1989) gives a different view, reproduced in essence here. The road surface is a process that may be approximated by a straight line on a log–log plot and represented by

$$\log[u(n)] = \log[K] - R \cdot \log[n] \tag{4.89}$$

implying that

$$u(n) = \frac{K}{n^R} \tag{4.90}$$

This is a spatial representation of the road profile, with n defined in cycles/metre. It appears under the car at frequency of $V \cdot n$ Hz, where V is the forward speed of the car, thus

$$V \cdot n = \frac{\omega}{2\pi} \Rightarrow n = \frac{\omega}{2\pi V} \tag{4.91}$$

We can write

$$u(n) = \frac{g(n)}{n} = g(n) \cdot \frac{2\pi V}{\omega} = u(\omega) \cdot 2\pi V \tag{4.92}$$

if we acknowledge that $g(n) = g(\omega)$ – i.e. that the process is unchanged whatever we choose to express it as a function of. Hence:

$$u(\omega) = \frac{1}{2\pi V} \cdot \frac{K}{n^m} = \frac{1}{2\pi U} \cdot \frac{K}{(\omega/2\pi V)^m} = \frac{K(2\pi V)^{m-1}}{\omega^m} \tag{4.93}$$

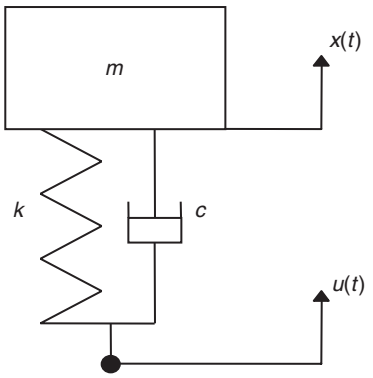

Fig. 4.64 Single-degree-of-freedom ride model

If a single degree of freedom ride model is considered (Figure 4.64) for the purposes of positioning the ride mode, then the frequency domain relationship between ground input, u, and displacement of the vehicle body, x, is given by

$$\frac{x(\omega)}{u(\omega)} = \frac{k^2 + \omega^2 c^2}{(k - \omega^2 m)^2 + \omega^2 c^2} \tag{4.94}$$

The acceleration environment is the prime concern in ride studies. Assuming harmonic solutions (i.e. made up of sine waves), we may write

$$\ddot{x}(\omega) = \frac{\ddot{x}(\omega)}{u(\omega)} \cdot u(\omega) = -\omega^2 \frac{x(\omega)}{u(\omega)} \cdot u(\omega) \tag{4.95}$$

Thus we have all that is needed to calculate a harmonic acceleration response of the car over a typical road profile. If the acceleration response is compared to the curves in ISO2631-1:1997, then some direct measure of ride comfort can be made.

Figure 4.65 shows a prediction of the same vehicle travelling at 60 and 120 mph on the same road, with threshold figures based on 1 hour exposure to the vibration environment. Considering Figure 4.65, it may be supposed that a better riding vehicle could be made by positioning the primary ride resonance at a lower frequency in order to better match the shape of the threshold curves and thus improve the aggregate ride over the frequency range of interest. Notwithstanding the difficulty in general that lower ride frequencies mean larger suspension motions, if we presume these difficulties can be overcome, another difficulty remains – the problem of motion sickness.

Figure 4.66 shows the acceleration response for a 0.2 Hz primary ride car, which has a much lower exceedance of the perception threshold. However, superimposed on the graph is a motion sickness threshold for 5% of the population at 1 hour's exposure. It can be seen that in the region substantially below resonance for the 1 Hz car, the motion sickness threshold exceedance is entirely in the region in which the vehicle does not amplify road inputs; in other words, motion sickness is induced by irregularities in

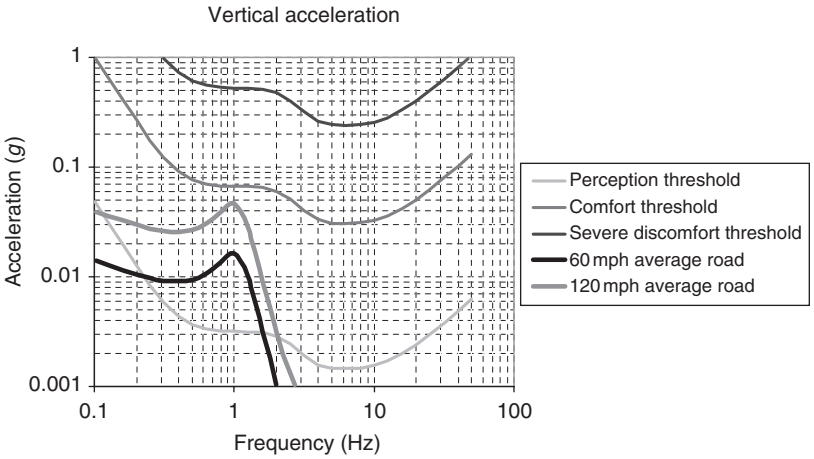

Fig. 4.65 A prediction of the harmonic response of a vehicle body in comparison with the acceleration curves laid down in ISO2631-1:1997

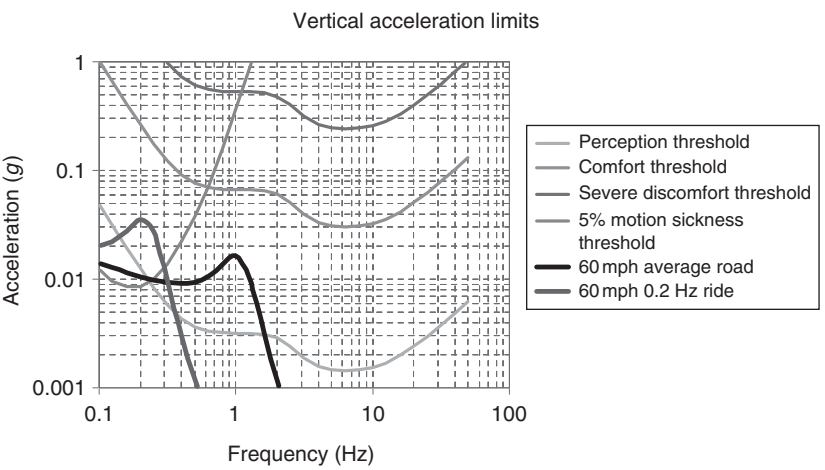

Fig. 4.66 A prediction of the harmonic response of a vehicle body in comparison with the acceleration curves laid down in ISO2631-1:1997 with the inclusion of motion sickness threshold data, comparing a 0.2 Hz vehicle with a 1 Hz vehicle

the road and not exacerbated in the vehicle. For the 0.2 Hz car, however, it can be seen that the vehicle resonance on its suspension contributes to a significant exceedance of the threshold motion sickness – the suspension will make people ill. Considering Figure 4.66 in some detail, it would seem that a practical limiting suspension frequency is where the 5% motion sickness line crosses the comfort threshold. This is around 0.65 Hz. For motorsport or military vehicles, it may be acceptable to use the severe discomfort threshold; in this case the practical lower limit for ride frequencies is around 1.25 Hz.

It should be noted that the threshold values for accelerations drop off significantly above 2 Hz. For this reason, motor vehicles rarely have primary

ride modes much above 2.5 Hz, even quite aggressively suspended ones. There is thus a 'window' in which we position the primary ride behaviour of our vehicles to make them compatible with the operators.

For autonomous vehicles that never carry humans, these restrictions are relaxed and the suspension primary ride frequency can be chosen on the basis of some other functional aspect.

4.10 Case study 5 – Suspension vector analysis comparison with MBS

4.10.1 Problem definition

The following study is intended to demonstrate the application of the vector theory outlined in Chapter 2 to a range of suspension analyses. Before the advent of computer programs to analyse the motion of suspension linkages vehicle designers resorted to graphical methods or simplified calculations often using two-dimensional representations to study the suspension in a fore–aft or transverse plane. These methods are still taught and included in many texts addressing vehicle dynamics. They can develop an understanding of suspension design, and the effect on total vehicle performance, that can be lost using the automated methods in modern computer aided analysis.

The aim of this textbook is to bridge the gap between traditional vehicle dynamics theories and the multibody systems approach. The following calculations are typical of the processes carried out using MBS software. While the methods used here do not represent exactly the internal machinations of, for example, the MSC.ADAMS software they do give an indication of the computational process involved. The example chosen here is based on a typical double wishbone suspension system. The answers obtained are compared with those running an MSC.ADAMS model using the same data. The calculations will include a series of analyses including:

- Geometry analysis
- Velocity analysis
- Acceleration analysis
- Static force analysis
- Dynamic force analysis

The geometric data required to define this problem is defined in Figure 4.67. Note that in this example the x-axis is orientated towards the front of the vehicle rather than pointing to the rear as used generally throughout this text. This is therefore the front left suspension system on the vehicle.

4.10.2 Velocity analysis

The starting point for this analysis is to establish a boundary condition, or road input, at the tyre contact patch P as the vehicle negotiates the road hump shown in Figure 4.68 with a forward speed of 15 m/s. The analysis is

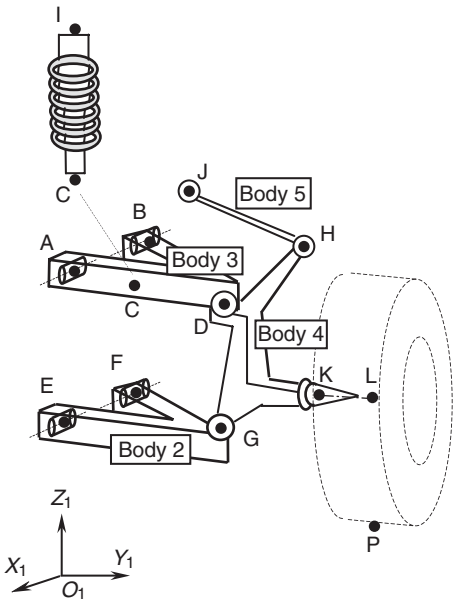

POINT	X (mm)	Y (mm)	Z (mm)
A	103	350	142
B	−127	350	128
C	−12	491	104
D	−12	589	127
E	122	345	−80
F	−108	345	−80
G	7	620	−89
H	−156	545	178
I	−15	500	540
J	−156	317	186
P	0	678	−265
K	0	600	0
L	0	678	0

Fig. 4.67 Double wishbone suspension example geometry data

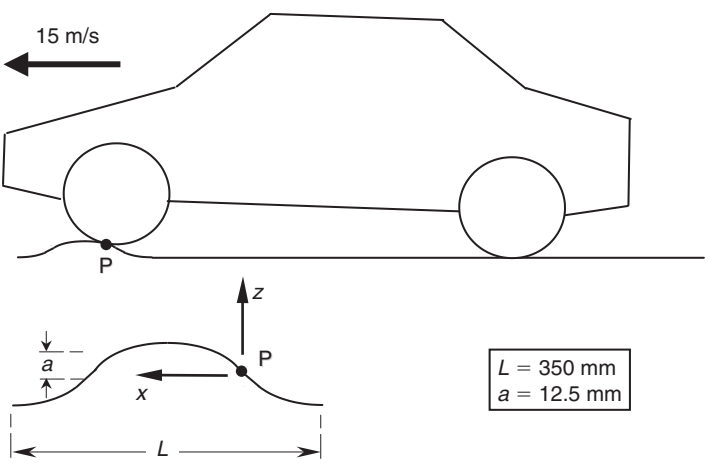

Fig. 4.68 Road input definition for velocity analysis

simplified by ignoring the compliance in the tyre and the profile of the road hump is taken as a sine function.

The local x–z axis taken to reference the geometry of the road hump is located at a point where the vertical velocity V_{Pz} of the contact point P reaches a maximum with a corresponding vertical acceleration A_{Pz} equal to zero. The profile of the road hump can be defined using

$$z = a \sin\left(\frac{2\pi x}{L}\right) \tag{4.96}$$

Working in mm and taking the wavelength L as 350 mm and the amplitude a as 12.5 mm, for a total bump height of 25 mm, gives

$$z = 12.5 \sin\left(\frac{\pi x}{175}\right) \tag{4.97}$$

We are after the vertical velocity of point P which can be expressed as:

$$\frac{\mathrm{d}z}{\mathrm{d}t} = \frac{\mathrm{d}z}{\mathrm{d}x}\frac{\mathrm{d}x}{\mathrm{d}t} \tag{4.98}$$

where

$$\frac{\mathrm{d}x}{\mathrm{d}t} = 15\,000 \text{ mm/s}$$

and

$$\frac{\mathrm{d}z}{\mathrm{d}x} = \frac{12.5\pi}{175}\cos\left(\frac{\pi x}{175}\right) \tag{4.99}$$

giving

$$\frac{\mathrm{d}z}{\mathrm{d}t} = \frac{12.5\pi}{175}\cos\left(\frac{\pi x}{175}\right) 15\,000 \tag{4.100}$$

The maximum value of $\mathrm{d}z/\mathrm{d}t$ occurs when $\cos(\pi x/175) = 1$ and occurs at values of $x = 0, 350, 700, \ldots$ giving

$$\left(\frac{\mathrm{d}z}{\mathrm{d}t}\right)_{\max} = \frac{12.5\pi}{175}\ 15\,000 = 3366 \text{ mm/s} \tag{4.101}$$

The acceleration $\mathrm{d}^2z/\mathrm{d}t^2$ is given by

$$\frac{\mathrm{d}^2z}{\mathrm{d}t^2} = -\frac{12.5\pi^2}{175^2}\sin\left(\frac{\pi x}{175}\right) 15\,000 \tag{4.102}$$

and has a value of zero at $x = 0, 350, 700, \ldots$

This provides inputs for the following velocity and acceleration analyses of

$V_{P_z} = 3366 \text{ mm/s}$
$A_{P_z} = 0 \text{ mm/s}^2$

The approach taken here is to initially ignore the spring damper assembly between points C and I shown in Figure 4.67. Solving for the rest of the suspension system will deliver the velocity $\{V_C\}_1$ of point C thus providing a boundary condition allowing a separate analysis of the spring damper to follow.

Before proceeding with the velocity analysis it is necessary to identify the unknowns that define the problem and the same number of equations as unknowns leading to a solution. The angular velocities of the rigid bodies representing suspension components can be used to find the translational

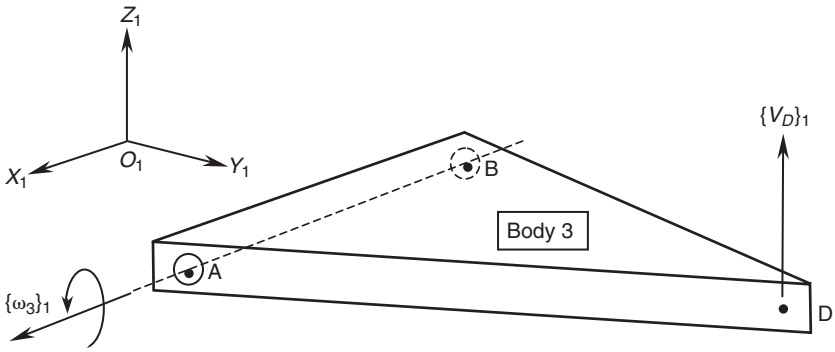

Fig. 4.69 Angular and translational velocity vectors for the upper wishbone

velocities at points within the system. An example of this is shown for the upper wishbone in Figure 4.69.

Referring back to the earlier treatment in Chapter 2 we can remind ourselves that as the suspension arm is constrained to rotate about the axis AB, ignoring at this stage any possible deflection due to compliance in the suspension bushes, the vector $\{\omega_3\}_1$ for the angular velocity of Body 3 will act along the axis of rotation through AB. The components of this vector would adopt signs consistent with producing a positive rotation about this axis as shown in Figure 4.69.

When setting up the equations to solve a velocity analysis it will be desirable to reduce the number of unknowns based on the knowledge that a particular body is constrained to rotate about a known axis as shown here. The velocity vector $\{\omega_3\}_1$ could, for example, be represented as follows:

$$\{\omega_3\}_1 = f\omega_3\{R_{AB}\}_1 \tag{4.103}$$

Since $\{\omega_3\}_1$ is parallel to the relative position vector $\{R_{AB}\}_1$ a scale factor $f\omega_3$ can be introduced. This reduces the problem from the three unknown components, ωx_3, ωy_3 and ωz_3 of the vector $\{\omega_3\}_1$, to a single unknown $f\omega_3$.

Once the angular velocities of Body 3 have been found it follows that the translational velocity of, for example, point D can be found from

$$\{V_{DA}\}_1 = \{\omega_3\}_1 \times \{R_{DA}\}_1 \tag{4.104}$$

It also follows that since point A is considered fixed with a velocity $\{V_A\}_1$ equal to zero that the absolute velocity $\{V_D\}_1$ of point D can be found from a consideration of the triangle law of vector addition giving

$$\{V_D\}_1 = \{V_{DA}\}_1 \tag{4.105}$$

A consideration of the complete problem indicates that the translational velocities throughout the suspension system can be found if the angular velocities of all the rigid bodies 2, 3, 4 and 5 are known. Clearly the same approach can be taken with the lower wishbone, Body 2, as with the upper wishbone using a single a scale factor $f\omega_2$ to replace the three unknown components, ωx_2, ωy_2 and ωz_2, of the vector $\{\omega_2\}_1$. Finally a consideration of the boundaries of this problem reveals that while points A, B, E, F and J are fixed the longitudinal velocity, V_{Px} and the lateral velocity V_{Py} at the contact point P remain as unknowns.

Thus this analysis can proceed if we can develop 10 equations to solve the 10 unknowns:

$f\omega_2, f\omega_3, \omega x_4, \omega y_4, \omega z_4, \omega x_5, \omega y_5, \omega z_5, V_{Px}, V_{Py}$

Working through the problem it will be seen that a strategy can be developed using the triangle law of vector addition to generate sets of equations. As a starting point we will develop a set of three equations using

$$\{V_{DG}\}_1 = \{V_D\}_1 - \{V_G\}_1 \tag{4.106}$$

In this form the equation (4.106) does not introduce any of the 10 unknowns listed above. It will therefore be necessary to initially define $\{V_{DG}\}_1$, $\{V_D\}_1$ and $\{V_G\}_1$ in terms of the angular velocity vectors that contain unknowns requiring solution. The first step in the analysis can therefore proceed as follows.

Determine an expression for the velocity $\{V_G\}_1$ at point G:

$$\{V_G\}_1 = \{V_{GE}\}_1 = \{\omega_2\}_1 \times \{R_{GE}\}_1 \tag{4.107}$$

$$\{\omega_2\}_1 = f\omega_2\{R_{EF}\}_1 = f\omega_2\begin{bmatrix}230\\0\\0\end{bmatrix}\text{rad/s} \tag{4.108}$$

$$\begin{bmatrix}V_{Gx}\\V_{Gy}\\V_{Gz}\end{bmatrix} = f_{\omega 2}\begin{bmatrix}0&0&0\\0&0&-230\\0&230&0\end{bmatrix}\begin{bmatrix}-115\\275\\-9\end{bmatrix} = \begin{bmatrix}0\\2070f_{\omega 2}\\63\,250f_{\omega 2}\end{bmatrix}\text{mm/s} \tag{4.109}$$

Determine an expression for the velocity $\{V_D\}_1$ at point D:

$$\{V_D\}_1 = \{V_{DA}\}_1 = \{\omega_3\}_1 \times \{R_{DA}\}_1 \tag{4.110}$$

$$\{\omega_3\}_1 = f\omega_3\{R_{AB}\}_1 = f\omega_3\begin{bmatrix}230\\0\\14\end{bmatrix}\text{rad/s} \tag{4.111}$$

$$\begin{bmatrix}V_{Dx}\\V_{Dy}\\V_{Dz}\end{bmatrix} = f_{\omega 3}\begin{bmatrix}0&-14&0\\14&0&-230\\0&230&0\end{bmatrix}\begin{bmatrix}-115\\239\\-15\end{bmatrix} = \begin{bmatrix}-3346f_{\omega 3}\\1840f_{\omega 3}\\54\,970f_{\omega 3}\end{bmatrix}\text{mm/s} \tag{4.112}$$

Determine an expression for the relative velocity $\{V_{DG}\}_1$ of point D relative to point G:

$$\{V_{DG}\}_1 = \{\omega_4\}_1 \times \{R_{DG}\}_1 \tag{4.113}$$

$$\begin{bmatrix}V_{DGx}\\V_{DGy}\\V_{DGz}\end{bmatrix} = \begin{bmatrix}0&-\omega_{4z}&\omega_{4y}\\\omega_{4z}&0&-\omega_{4x}\\-\omega_{4y}&\omega_{4x}&0\end{bmatrix}\begin{bmatrix}-19\\-31\\216\end{bmatrix} = \begin{bmatrix}31\omega_{4z}+216\omega_{4y}\\-19\omega_{4z}-216\omega_{4x}\\19\omega_{4y}-31\omega_{4x}\end{bmatrix}\text{mm/s} \tag{4.114}$$

We can now apply the triangle law of vector addition to equate the expression for $\{V_{DG}\}_1$ in equation (4.114) with $\{V_D\}_1$ in equation (4.112) and $\{V_G\}_1$ in equation (4.109):

$$\{V_{DG}\}_1 = \{V_D\}_1 - \{V_G\}_1 \tag{4.115}$$

$$\begin{bmatrix} 31\omega_{4z} + 216\omega_{4y} \\ -19\omega_{4z} - 216\omega_{4x} \\ 19\omega_{4y} - 31\omega_{4x} \end{bmatrix} = \begin{bmatrix} -3346 f_{\omega 3} \\ 1840 f_{\omega 3} \\ 54\,970 f_{\omega 3} \end{bmatrix} - \begin{bmatrix} 0 \\ 2070 f_{\omega 2} \\ 63\,250 f_{\omega 2} \end{bmatrix} \text{mm/s} \tag{4.116}$$

Rearranging (4.116) yields the first three equations required to solve the analysis:

$$\text{Equation 1} \quad 3346 f_{\omega 3} + 216_{\omega 4y} + 31_{\omega 4z} = 0 \tag{4.117}$$

$$\text{Equation 2} \quad 2070 f_{\omega 2} - 1840 f_{\omega 3} - 216\omega_{4x} - 19\omega_{4z} = 0 \tag{4.118}$$

$$\text{Equation 3} \quad 63\,250 f_{\omega 2} - 54\,970 f_{\omega 3} - 31\omega_{4x} + 19\omega_{4y} = 0 \tag{4.119}$$

We can now proceed to set up the next set of three equations working from point H to point D and using the triangle law of vector addition:

$$\{V_{DH}\}_1 = \{V_D\}_1 - \{V_H\}_1 \tag{4.120}$$

Determine an expression for the velocity $\{V_H\}_1$ at point H:

$$\{V_H\}_1 = \{V_{HJ}\}_1 = \{\omega_5\}_1 \times \{R_{HJ}\}_1 \tag{4.121}$$

$$\begin{bmatrix} V_{Hx} \\ V_{Hy} \\ V_{Hz} \end{bmatrix} = \begin{bmatrix} 0 & -\omega_{5z} & \omega_{5y} \\ \omega_{5z} & 0 & -\omega_{5x} \\ -\omega_{5y} & \omega_{5x} & 0 \end{bmatrix} \begin{bmatrix} 0 \\ 228 \\ -8 \end{bmatrix} = \begin{bmatrix} -228\omega_{5z} - 8\omega_{5y} \\ 8\omega_{5x} \\ 228\omega_{5x} \end{bmatrix} \text{mm/s} \tag{4.122}$$

We already have an expression for $\{V_D\}_1$ in equation (4.112) and can determine an expression for the relative velocity $\{V_{DH}\}_1$ of point D relative to point H using

$$\{V_{DH}\}_1 = \{\omega_4\}_1 \times \{R_{DH}\}_1 \tag{4.123}$$

$$\begin{bmatrix} V_{DHx} \\ V_{DHy} \\ V_{DHz} \end{bmatrix} = \begin{bmatrix} 0 & -\omega_{4z} & \omega_{4y} \\ \omega_{4z} & 0 & -\omega_{4x} \\ -\omega_{4y} & \omega_{4x} & 0 \end{bmatrix} \begin{bmatrix} 144 \\ 44 \\ -51 \end{bmatrix} = \begin{bmatrix} -44\omega_{4z} - 51\omega_{4y} \\ 144\omega_{4z} + 51\omega_{4x} \\ -144\omega_{4y} + 44\omega_{4x} \end{bmatrix} \text{mm/s} \tag{4.124}$$

We can now apply the triangle law of vector addition to equate the expression for $\{V_{DH}\}_1$ in equation (4.124) with $\{V_D\}_1$ in equation (4.112) and $\{V_H\}_1$ in equation (4.122):

$$\{V_{DH}\}_1 = \{V_D\}_1 - \{V_H\}_1 \tag{4.125}$$

$$\begin{bmatrix} -44\omega_{4z} - 51\omega_{4y} \\ 144\omega_{4z} + 51\omega_{4x} \\ -144\omega_{4y} + 44\omega_{4x} \end{bmatrix} = \begin{bmatrix} -3346 f_{\omega 3} \\ 1840 f_{\omega 3} \\ 54\,970 f_{\omega 3} \end{bmatrix} - \begin{bmatrix} -228\omega_{5z} - 8\omega_{5y} \\ 8\omega_{5x} \\ 228\omega_{5x} \end{bmatrix} \text{mm/s} \tag{4.126}$$

Rearranging (4.126) yields the next three equations required to solve the analysis:

$$\text{Equation 4} \quad 3346f_{\omega 3} - 51\omega_{4y} - 44\omega_{4z} - 8\omega_{5y} - 228\omega_{5z} = 0 \tag{4.127}$$

$$\text{Equation 5} \quad -1840f_{\omega 3} + 51\omega_{4x} + 144\omega_{4z} + 8\omega_{5x} = 0 \tag{4.128}$$

$$\text{Equation 6} \quad -54\,970f_{\omega 3} + 44\omega_{4x} - 144\omega_{4y} + 228\omega_{5x} = 0 \tag{4.129}$$

We can now proceed to set up the next set of three equations working from point G to point P and using the triangle law of vector addition:

$$\{V_{PG}\}_1 = \{V_P\}_1 - \{V_G\}_1 \tag{4.130}$$

Determine an expression for the relative velocity $\{V_{PG}\}_1$ of point P relative to point G:

$$\{V_{PG}\}_1 = \{\omega_4\}_1 \times \{R_{PG}\}_1 \tag{4.131}$$

$$\begin{bmatrix} V_{PGx} \\ V_{PGy} \\ V_{PGz} \end{bmatrix} = \begin{bmatrix} 0 & -\omega_{4z} & \omega_{4y} \\ \omega_{4z} & 0 & -\omega_{4x} \\ -\omega_{4y} & \omega_{4x} & 0 \end{bmatrix} = \begin{bmatrix} -7 \\ 58 \\ -176 \end{bmatrix} = \begin{bmatrix} -58\omega_{4z} - 176\omega_{4y} \\ -7\omega_{4z} + 176\omega_{4x} \\ 7\omega_{4y} + 58\omega_{4x} \end{bmatrix} \text{mm/s} \tag{4.132}$$

We already have an expression for $\{V_G\}_1$ in equation (4.109) and we can define the vector $\{V_P\}_1$ in terms of the known vertical velocity component V_{Pz} and the unknown components V_{Px} and V_{Py}:

$$\{V_P\}_1 = \begin{bmatrix} V_{Px} \\ V_{Py} \\ 3366 \end{bmatrix} \text{mm/s} \tag{4.133}$$

We can now apply the triangle law of vector addition to equate the expression for $\{V_{PG}\}_1$ in equation (4.132) with $\{V_P\}_1$ in equation (4.133) and $\{V_G\}_1$ in equation (4.109):

$$\{V_{PG}\}_1 = \{V_P\}_1 - \{V_G\}_1 \tag{4.134}$$

$$\begin{bmatrix} -58\omega_{4z} - 176\omega_{4y} \\ -7\omega_{4z} + 176\omega_{4x} \\ 7\omega_{4y} + 58\omega_{4x} \end{bmatrix} = \begin{bmatrix} V_{Px} \\ V_{Py} \\ 3366 \end{bmatrix} - \begin{bmatrix} 0 \\ 2070f_{\omega 2} \\ 63\,250f_{\omega 2} \end{bmatrix} \text{mm/s} \tag{4.135}$$

Rearranging (4.135) yields the next set of three equations required to solve the analysis:

$$\text{Equation 7} \quad 176\omega_{4y} + 58\omega_{4z} + V_{Px} = 0 \tag{4.136a}$$

$$\text{Equation 8} \quad -2070f_{\omega 2} - 176\omega_{4x} + 7\omega_{4z} + V_{Py} = 0 \tag{4.136b}$$

$$\text{Equation 9} \quad -63\,250f_{\omega 2} - 58\omega_{4x} - 7\omega_{4y} = -3366 \tag{4.136c}$$

This leaves us with nine equations and 10 unknowns. The last equation is obtained by constraining the rotation of the tie rod (Body 5) to prevent spin

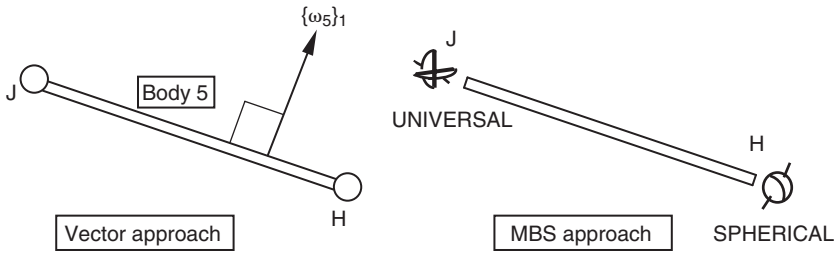

Fig. 4.70 Constraining the spin degree of freedom of the tie rod

about its own axis. This degree of freedom has no bearing on the overall kinematics of the suspension linkage. If there is to be no spin component of angular velocity parallel to the axis of the tie rod, spin, then the angular velocity vector $\{\omega_5\}_1$ must be perpendicular to the line H–J as shown in Figure 4.70. Note that this is equivalent to a common practice in MBS modelling where a universal or Hookes joint is used at one end of the link with a spherical joint at the other end. The universal joint allows the tie rod to articulate in a way that does not constrain overall suspension movement but constrains the spin freedom that would exist if a spherical joint were used at each end.

Using the vector dot product to enforce perpendicularity, as described in Chapter 2, yields the tenth and final equation required to solve this part of the problem:

$$\{\omega_5\}_1 \bullet \{R_{HJ}\}_1 = 0 \tag{4.137}$$

$$\begin{bmatrix}\omega_{5x}\omega_{5y}\omega_{5z}\end{bmatrix}\begin{bmatrix}0\\228\\-8\end{bmatrix} = 0 \text{ mm/s} \tag{4.138}$$

$$\text{Equation 10} \quad 228\omega_{5y} - 8\omega_{5z} = 0 \tag{4.139}$$

The 10 equations can now be set up in matrix form ready for solution. The solution of a 10 by 10 matrix will require access to a mathematical or spreadsheet program that offers the capability to invert the matrix.

$$\begin{bmatrix}
0 & 3346 & 0 & 216 & 31 & 0 & 0 & 0 & 0 & 0\\
2070 & -1840 & -216 & 0 & -19 & 0 & 0 & 0 & 0 & 0\\
63\,250 & -54\,970 & -31 & 19 & 0 & 0 & 0 & 0 & 0 & 0\\
0 & 3346 & 0 & -51 & -44 & 0 & -8 & -228 & 0 & 0\\
0 & -1840 & 51 & 0 & 144 & 8 & 0 & 0 & 0 & 0\\
0 & -54\,970 & 44 & -144 & 0 & 228 & 0 & 0 & 0 & 0\\
0 & 0 & 0 & 176 & 58 & 0 & 0 & 0 & 1 & 0\\
-2070 & 0 & -176 & 0 & 7 & 0 & 0 & 0 & 0 & 1\\
-63\,250 & 0 & -58 & -7 & 0 & 0 & 0 & 0 & 0 & 0\\
0 & 0 & 0 & 0 & 0 & 0 & 228 & -8 & 0 & 0
\end{bmatrix}
\begin{bmatrix}
f_{\omega 2}\\ f_{\omega 3}\\ \omega_{4x}\\ \omega_{4y}\\ \omega_{4z}\\ \omega_{5x}\\ \omega_{5y}\\ \omega_{5z}\\ V_{Px}\\ V_{Py}
\end{bmatrix}
=
\begin{bmatrix}
0\\0\\0\\0\\0\\0\\0\\0\\-3366\\0
\end{bmatrix} \tag{4.140}$$

Solving equation (4.140) yields the following answers for the 10 unknowns:

$f_{\omega 2} = 5.333 \times 10^{-2}$ rad/mm.s
$f_{\omega 3} = 6.104 \times 10^{-2}$ rad/mm.s
$\omega_{4x} = -8.774 \times 10^{-3}$ rad/s
$\omega_{4y} = -0.945$ rad/s
$\omega_{4z} = -1.446 \times 10^{-3}$ rad/s
$\omega_{5x} = 14.121$ rad/s
$\omega_{5y} = 3.881 \times 10^{-2}$ rad/s
$\omega_{5z} = 1.106$ rad/s
$V_{Px} = 166.468$ mm/s
$V_{Py} = 108.859$ mm/s

It is now possible to use the two scale factors found, $f_{\omega 2}$ and $f_{\omega 3}$, to calculate the angular velocity vectors $\{\omega_2\}_1$ and $\{\omega_3\}_1$:

$$\{\omega_2\}_1 = f_{\omega 2}\{R_{EF}\}_1 = 5.333 \times 10^{-2}\begin{bmatrix}230\\0\\0\end{bmatrix} = \begin{bmatrix}12.266\\0\\0\end{bmatrix} \text{rad/s} \tag{4.141}$$

$$\{\omega_3\}_1 = f_{\omega 3}\{R_{AB}\}_1 = 6.1041 \times 10^{-2}\begin{bmatrix}230\\0\\14\end{bmatrix} = \begin{bmatrix}14.039\\0\\0.855\end{bmatrix} \text{rad/s} \tag{4.142}$$

In summary the angular velocity vectors for the rigid bodies are as follows:

$\{\omega_2\}_1^T = [12.266 \quad 0 \quad 0]$ rad/s
$\{\omega_3\}_1^T = [14.039 \quad 0 \quad 0.855]$ rad/s
$\{\omega_4\}_1^T = [-8.774 \times 10^{-3} \quad -0.945 \quad -1.446 \times 10^{-3}]$ rad/s
$\{\omega_5\}_1^T = [14.121 \quad 3.881 \times 10^{-2} \quad 1.106]$ rad/s

We can now proceed to calculate the translational velocities at all the moving points, C, D, G, H and P, within this part of the model:

$$\{V_C\}_1 = \{V_{CA}\}_1 = \{\omega_3\}_1 \times \{R_{CA}\}_1 \tag{4.143}$$

$$\begin{bmatrix}V_{Cx}\\V_{Cy}\\V_{Cz}\end{bmatrix} = \begin{bmatrix}0 & -0.855 & 0\\0.855 & 0 & -14.039\\0 & 14.039 & 0\end{bmatrix}\begin{bmatrix}-115\\141\\-38\end{bmatrix} = \begin{bmatrix}-120.555\\435.157\\1979.499\end{bmatrix} \text{mm/s} \tag{4.144}$$

$$\{V_D\}_1 = \{V_{DA}\}_1 = \{\omega_3\}_1 \times \{R_{DA}\}_1 \tag{4.145}$$

$$\begin{bmatrix}V_{Dx}\\V_{Dy}\\V_{Dz}\end{bmatrix} = \begin{bmatrix}0 & -0.855 & 0\\0.855 & 0 & -14.039\\0 & 14.039 & 0\end{bmatrix}\begin{bmatrix}-115\\239\\-15\end{bmatrix} = \begin{bmatrix}-204.345\\112.260\\3355.321\end{bmatrix} \text{mm/s} \tag{4.146}$$

$$\{V_G\}_1 = \{V_{GE}\}_1 = \{\omega_2\}_1 \times \{R_{GE}\}_1 \tag{4.147}$$

$$\begin{bmatrix} V_{Gx} \\ V_{Gy} \\ V_{Gz} \end{bmatrix} = \begin{bmatrix} 0 & 0 & 0 \\ 0 & 0 & -12.266 \\ 0 & 12.266 & 0 \end{bmatrix} \begin{bmatrix} -115 \\ 275 \\ -9 \end{bmatrix} = \begin{bmatrix} 0 \\ 110.394 \\ 3373.150 \end{bmatrix} \text{mm/s} \tag{4.148}$$

$$\{V_H\}_1 = \{V_{HJ}\}_1 = \{\omega_5\}_1 \times \{R_{HJ}\}_1 \tag{4.149}$$

$$\begin{bmatrix} V_{Hx} \\ V_{Hy} \\ V_{Hz} \end{bmatrix} = \begin{bmatrix} 0 & -1.1062 & 3.881 \times 10^{-2} \\ 1.1062 & 0 & -14.121 \\ -3.881 \times 10^{-2} & 14.121 & 0 \end{bmatrix} \begin{bmatrix} 0 \\ 229 \\ -9 \end{bmatrix} = \begin{bmatrix} -252.524 \\ 112.968 \\ 3219.588 \end{bmatrix} \text{mm/s} \tag{4.150}$$

The velocity vector $\{V_P\}_1$ is already available. In summary the velocity vectors for the moving points are as follows:

$$\{V_C\}_1^T = [-120.555 \;\; 435.157 \;\; 1979.499] \text{ mm/s}$$

$$\{V_D\}_1^T = [-204.345 \;\; 112.260 \;\; 3355.321] \text{ mm/s}$$

$$\{V_G\}_1^T = [0.0 \;\; 110.394 \;\; 3373.150] \text{ mm/s}$$

$$\{V_H\}_1^T = [-252.524 \;\; 112.968 \;\; 3219.588] \text{ mm/s}$$

$$\{V_P\}_1^T = [166.468 \;\; 108.859 \;\; 3366.0] \text{ mm/s}$$

Having found the velocity $\{V_C\}_1$ at the bottom of the spring damper unit point C we can now proceed to carry out a separate analysis of the unit to find the sliding component of velocity acting along the axis C–I. For this phase of the analysis we introduce two new bodies, Body 6 and Body 7, to represent the upper and lower part of the damper as shown in Figure 4.71.

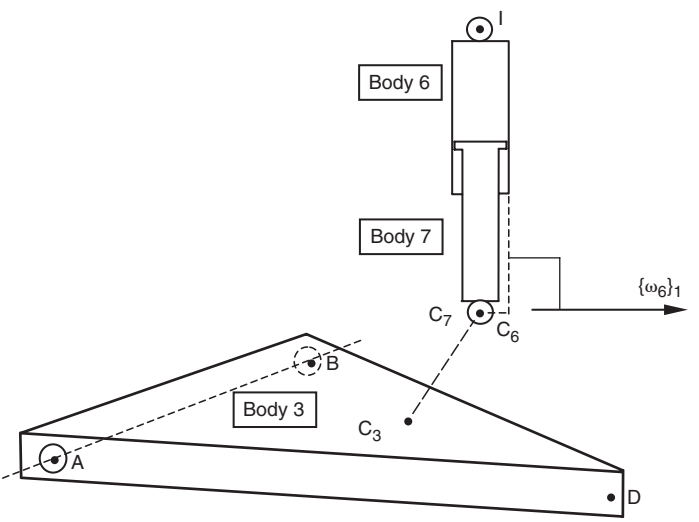

Fig. 4.71 Modelling the damper unit for a velocity analysis

This phase of the analysis can be facilitated by modelling three coincident points, C_3 on Body 3, C_6 on Body 6 and C_7 on Body 7, all located at point C. While points C_3 and C_7 can be considered physical located at point C, point C_6 is a virtual extension of the upper damper as shown in Figure 4.71. The sliding velocity in the damper can then be determined from the relative velocity $\{V_{C6C7}\}_1$ of points C_6 and C_7. Since C_6 and C_7 are coincident the relative velocity vector can only act along the direction of sliding, axis C–I, allowing us to adopt a scale factor and reduce the number of unknowns:

$$\{V_{C6C7}\}_1 = f_{vs}\{R_{CI}\}_1 \tag{4.151}$$

Since I is a fixed point and applying the triangle law of vector addition gives

$$\{V_{C6}\}_1 = \{V_{C6I}\}_1 = \{V_{C7}\}_1 + \{V_{C6C7}\}_1 \tag{4.152}$$

Note also that since points C_3 and C_7 move together and are physically located at point C we already have the velocity for this boundary condition from the preceding velocity analysis of the double wishbone linkage:

$$\{V_{C7}\}_1^T = \{V_{C3}\}_1^T = \{V_C\}_1^T = [-120.555 \quad 435.157 \quad 1979.499] \text{ mm/s} \tag{4.153}$$

Combining these last three equations to substitute (4.151) and (4.153) into equation (4.152) gives

$$\{V_{C6}\}_1 = \{V_{C6I}\}_1 = \begin{bmatrix} -120.555 \\ 435.157 \\ 1979.499 \end{bmatrix} + f_{vs}\begin{bmatrix} 3 \\ -9 \\ -436 \end{bmatrix} \text{mm/s} \tag{4.154}$$

As the suspension moves and the strut component rotates it is also clear that as the only degree of freedom between Body 6 and Body 7 is relative sliding motion then

$$\{\omega_6\}_1 = \{\omega_7\}_1 \tag{4.155}$$

The velocity vector $\{V_{C6I}\}_1$ can also be defined using

$$\{V_{C6}\}_1 = \{V_{C6I}\}_1 = \{\omega_6\}_1 \times \{R_{CI}\}_1 \tag{4.156}$$

$$\begin{bmatrix} V_{C6Ix} \\ V_{C6Iy} \\ V_{C6Iz} \end{bmatrix} = \begin{bmatrix} 0 & -\omega_{6z} & \omega_{6y} \\ \omega_{6z} & 0 & -\omega_{6x} \\ -\omega_{6y} & \omega_{6x} & 0 \end{bmatrix}\begin{bmatrix} 3 \\ -9 \\ -436 \end{bmatrix} = \begin{bmatrix} 9\omega_{6z} - 436\omega_{6y} \\ 3\omega_{6z} + 436\omega_{6x} \\ -3\omega_{6y} - 9\omega_{6x} \end{bmatrix} \text{mm/s} \tag{4.157}$$

Equating the expressions for $\{V_{C6I}\}_1$ in (4.154) and (4.157) gives

$$\begin{bmatrix} 9\omega_{6z} - 436\omega_{6y} \\ 3\omega_{6z} + 436\omega_{6x} \\ -3\omega_{6y} - 9\omega_{6x} \end{bmatrix} = \begin{bmatrix} -120.555 \\ 435.157 \\ 1979.499 \end{bmatrix} + f_{vs}\begin{bmatrix} 3 \\ -9 \\ -436 \end{bmatrix} \text{mm/s} \tag{4.158}$$

Rearranging (4.158) yields three equations that can be used to solve this part of the analysis:

$$\text{Equation 1} \qquad 3f_{vs} + 436\omega_{6y} - 9\omega_{6z} = 120.555 \tag{4.159}$$

Equation 2 $$-9f_{vs} - 436\omega_{6x} - 3\omega_{6z} = -435.157 \tag{4.160}$$

Equation 3 $$-436f_{vs} + 9\omega_{6x} + 3\omega_{6y} = -1979.499 \tag{4.161}$$

This leaves us with four unknowns, ω_{6x}, ω_{6y}, ω_{6z} and f_{vs}, but only three equations. We can use the same approach here as used with the tie rod in the preceding analysis. Since the spin degree of freedom of Body 6 about the axis C–I has no bearing on the overall solution we can again use the vector dot product to enforce perpendicularity of $\{\omega_6\}_1$ to $\{R_{CI}\}_1$ as shown in Figure 4.71. This will yield the fourth equation as follows:

$$\{\omega_6\}_1 \bullet \{R_{CI}\}_1 = 0 \tag{4.162}$$

$$[\omega_{6x}\omega_{6y}\omega_{6z}] \begin{bmatrix} 3 \\ -9 \\ -436 \end{bmatrix} = 0\,\text{mm/s} \tag{4.163}$$

Equation 4 $$3\omega_{6x} - 9\omega_{6y} - 436\omega_{6z} = 0 \tag{4.164}$$

The four equations can now be set up in matrix form ready for solution. The solution of a four by four matrix will require a lengthy calculation or access as before to a program that offers the capability to invert the matrix:

$$\begin{bmatrix} 3 & 0 & 436 & -9 \\ -9 & -436 & 0 & -3 \\ -436 & 9 & 3 & 0 \\ 0 & 3 & -9 & -436 \end{bmatrix} \begin{bmatrix} f_{vs} \\ \omega_{6x} \\ \omega_{6y} \\ \omega_{6z} \end{bmatrix} = \begin{bmatrix} 120.555 \\ -435.157 \\ -1979.499 \\ 0 \end{bmatrix} \tag{4.165}$$

Solving equation (4.165) yields the following answers for the four unknowns:

$f_{vs} = 4.561\,\text{s}^{-1}$

$\omega_{6x} = 0.904\,\text{rad/s}$

$\omega_{6y} = 0.245\,\text{rad/s}$

$\omega_{6z} = 1.159\,\text{rad/s}$

This gives us the last two angular velocity vectors upper and lower damper bodies:

$$\{\omega_6\}_1^T = [0.904 \quad 0.245 \quad 1.159]\ \text{rad/s}$$

$$\{\omega_7\}_1^T = [0.904 \quad 0.245 \quad 1.159]\ \text{rad/s}$$

From equation (4.151) we now have

$$\{V_{C6C7}\}_1 = f_{vs}\{R_{CI}\}_1 = 4.561 \begin{bmatrix} 3 \\ -9 \\ -436 \end{bmatrix} = \begin{bmatrix} 13.682 \\ -41.045 \\ -1988.378 \end{bmatrix} \text{mm/s} \tag{4.166}$$

Since the velocity vector $\{V_{C6C7}\}_1$ acts along the axis of the strut C–I the magnitude of this vector will be equal to the sliding velocity V_s:

$$V_s = |\,V_{C6C7}\,| = 1988.641\,\text{mm/s} \tag{4.167}$$

Table 4.10 Comparison of angular velocity vectors computed by theory and MSC.ADAMS

Body	Angular velocity vectors					
	Theory			MSC.ADAMS		
	ω_x (rad/s)	ω_y (rad/s)	ω_z (rad/s)	ω_x (rad/s)	ω_y (rad/s)	ω_z (rad/s)
2	12.266	0.0	0.0	12.266	0.0	0.0
3	14.039	0.0	0.855	14.040	0.0	0.855
4	-8.774×10^{-3}	−0.945	-1.446×10^{-3}	-8.774×10^{-3}	−0.945	-1.446×10^{-3}
5	14.121	3.881×10^{-2}	1.106	14.121	5.394×10^{-2}	1.106
6	0.904	0.245	1.159×10^{-3}	0.904	0.245	1.163×10^{-3}
7	0.904	0.245	1.159×10^{-3}	0.904	0245	1.163×10^{-3}

Table 4.11 Comparison of translational velocity vectors computed by theory and MSC.ADAMS

Point	Translational velocity vectors					
	Theory			MSC.ADAMS		
	V_x (mm/s)	V_y (mm/s)	V_z (mm/s)	V_x (mm/s)	V_y (mm/s)	V_z (mm/s)
C	−120.555	435.157	1979.499	−120.495	435.224	1979.570
D	−204.345	112.260	3355.321	−204.244	112.316	3355.440
G	0.0	110.394	3373.150	0.0	110.393	3373.130
H	−252.524	112.968	3219.588	−252.210	112.972	3219.588
P	166.468	108.859	3366.0	166.468	108.859	3366.0
C_6C_7	13.682	−41.045	−1988.378	13.682	−41.046	−1988.440

At this stage it can be seen that the sliding velocity V_s is realistic in magnitude. Given knowledge of the damper force–velocity relationship it would be possible to determine the damping forces produced and reacted at points I and C in the system.

A comparison of the angular velocities found from the preceding calculations and those using an equivalent MSC.ADAMS model is shown in Table 4.10.

A comparison of the translational velocities found at points within the suspension system from the preceding calculations and those found using an equivalent MSC.ADAMS model is shown in Table 4.11.

4.10.3 Acceleration analysis

As before the approach taken here is to initially ignore the damper assembly between points C and I. Solving for the rest of the suspension system will deliver the acceleration $\{A_C\}_1$ of point C thus providing a boundary condition allowing a separate analysis of the damper to follow.

Before proceeding with the acceleration analysis it is necessary to identify the unknowns that define the problem. The angular accelerations and angular velocities of the rigid bodies representing suspension components can

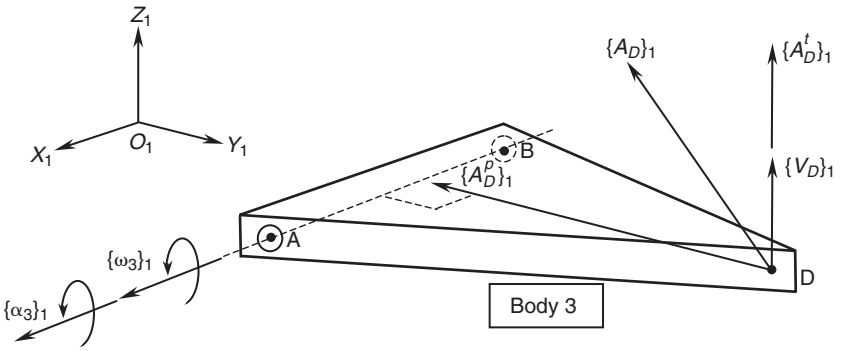

Fig. 4.72 Angular and translational acceleration and velocity vectors for the upper wishbone

be used to find the translational accelerations at points within the system. An example of this is shown for the upper wishbone in Figure 4.72.

Referring back to the earlier velocity analysis we can remind ourselves that as the suspension arm is constrained to rotate about the axis AB, ignoring at this stage any possible deflection due to compliance in the suspension bushes, the vector $\{\alpha_3\}_1$ for the angular acceleration of Body 3 will act along the axis of rotation through AB. The components of this vector would adopt signs consistent with a positive rotation about this axis as shown in Figure 4.72.

When setting up the equations to solve an acceleration analysis it will be as before desirable to reduce the number of unknowns based on the knowledge that a particular body is constrained to rotate about a known axis as shown here. The acceleration vector $\{\alpha_3\}_1$ could, for example, be represented as follows:

$$\{\alpha_3\}_1 = f\alpha_3\{R_{AB}\}_1 \tag{4.168}$$

Since $\{\alpha_3\}_1$ is parallel to the relative position vector $\{R_{AB}\}_1$ a scale factor $f\alpha_3$ can be introduced. This reduces the problem from the three unknown components, αx_3, αy_3 and αz_3 of the vector $\{\alpha_3\}_1$ to a single unknown $f\alpha_3$.

It also follows that since point A is considered fixed with an acceleration $\{A_A\}_1$ equal to zero that the absolute acceleration $\{A_D\}_1$ of point D can be found from a consideration of the triangle law of vector addition giving

$$\{A_D\}_1 = \{A_{DA}\}_1 \tag{4.169}$$

Once the angular accelerations of Body 3 have been found, together with the known angular velocities, it follows now that the translational acceleration $\{A_D\}_1$ of, for example, point D can be found from

$$\{A_D\}_1 = \{A_D^p\}_1 + \{A_D^t\}_1 \tag{4.170}$$

where the centripetal acceleration $\{A_D^p\}_1$ is given by

$$\{A_D^p\}_1 = \{\omega_3\}_1 \times \{\{\omega_3\}_1 \times \{R_{DA}\}_1\} = \{\omega_3\}_1 \times \{V_D\}_1 \tag{4.171}$$

and the transverse acceleration $\{A_D^t\}_1$ is given by

$$\{A_D^t\}_1 = \{\alpha_3\}_1 \times \{R_{DA}\}_1 \tag{4.172}$$

As with the velocity analysis clearly the same approach can be taken with the lower wishbone, Body 2, as with the upper wishbone using a single scale factor $f\alpha_2$ to replace the three unknown components, αx_2, αy_2 and αz_2 of the vector $\{\alpha_2\}_1$. Finally a consideration of the boundaries of this problem again reveals that while points A, B, E, F and J are fixed the longitudinal acceleration, A_{Px} and the lateral acceleration A_{Py} at the contact point P remain as unknowns.

Thus this analysis can proceed if we can develop 10 equations to solve the 10 unknowns:

$f\alpha_2$, $f\alpha_3$, αx_4, αy_4, αz_4, αx_5, αy_5, αz_5, A_{Px}, A_{Py}

Working through the problem it will be seen that the same strategy used in the velocity analysis can be developed using the triangle law of vector addition to generate sets of equations. As a starting point we will develop a set of three equations using

$$\{A_{DG}\}_1 = \{A_D\}_1 - \{A_G\}_1 \tag{4.173}$$

In this form the equation (4.173) does not introduce any of the 10 unknowns listed above. It will therefore be necessary to initially define $\{A_{DG}\}_1$, $\{A_D\}_1$ and $\{A_G\}_1$ in terms of the angular acceleration vectors that contain unknowns requiring solution. The first step in the analysis can therefore proceed as follows.

Determining an expression for the acceleration $\{A_G\}_1$ at point G using values for $\{\omega_2\}_1$ and $\{V_G\}_1$ found from the earlier velocity analysis gives

$$\{A_G\}_1 = \{A_{GE}\}_1 = \{\omega_2\}_1 \times \{V_G\}_1 + \{\alpha_2\}_1 \times \{R_{GE}\}_1 \tag{4.174}$$

$$\{\alpha_2\}_1 = f\alpha_2 \{R_{EF}\}_1 = f\alpha_2 \begin{bmatrix} 230 \\ 0 \\ 0 \end{bmatrix} \text{rad/s}^2 \tag{4.175}$$

$$\begin{bmatrix} A_{Gx} \\ A_{Gy} \\ A_{Gz} \end{bmatrix} = \begin{bmatrix} 0 & 0 & 0 \\ 0 & 0 & -12.266 \\ 0 & 12.266 & 0 \end{bmatrix} \begin{bmatrix} 0.0 \\ 110.394 \\ 3373.150 \end{bmatrix} + f_{\alpha 2} \begin{bmatrix} 0 & 0 & 0 \\ 0 & 0 & -230 \\ 0 & 230 & 0 \end{bmatrix} \begin{bmatrix} -115 \\ 275 \\ -9 \end{bmatrix} \text{mm/s}^2 \tag{4.176}$$

$$\begin{bmatrix} A_{Gx} \\ A_{Gy} \\ A_{Gz} \end{bmatrix} = \begin{bmatrix} 0 \\ -41\,375.058 \\ 1354.093 \end{bmatrix} + \begin{bmatrix} 0 \\ 2070 f_{\alpha 2} \\ 63\,250 f_{\alpha 2} \end{bmatrix} \text{mm/s}^2 \tag{4.177}$$

Determining an expression for the acceleration $\{A_D\}_1$ at point D using values for $\{\omega_3\}_1$ and $\{V_D\}_1$ found from the earlier velocity analysis gives

$$\{A_D\}_1 = \{A_{DA}\}_1 = \{\omega_3\}_1 \times \{V_D\}_1 + \{\alpha_3\}_1 \times \{R_{DA}\}_1 \tag{4.178}$$

$$\{\alpha_3\}_1 = f\alpha_3\{R_{AB}\}_1 = f\alpha_3 \begin{bmatrix} 230 \\ 0 \\ 14 \end{bmatrix} \text{rad/s}^2 \tag{4.179}$$

$$\begin{bmatrix} A_{Dx} \\ A_{Dy} \\ A_{Dz} \end{bmatrix} = \begin{bmatrix} 0 & -0.855 & 0 \\ 0.855 & 0 & -14.039 \\ 0 & 14.039 & 0 \end{bmatrix} \begin{bmatrix} -203.345 \\ 112.260 \\ 3355.321 \end{bmatrix} + f_{\alpha 3} \begin{bmatrix} 0 & -14 & 0 \\ 14 & 0 & -230 \\ 0 & 230 & 0 \end{bmatrix} \begin{bmatrix} -115 \\ 239 \\ -15 \end{bmatrix} \text{mm/s}^2 \tag{4.180}$$

$$\begin{bmatrix} A_{Dx} \\ A_{Dy} \\ A_{Dz} \end{bmatrix} = \begin{bmatrix} -96.030 \\ -47\,281.651 \\ 1576.804 \end{bmatrix} + \begin{bmatrix} -3346 f_{\alpha 3} \\ 1840 f_{\alpha 3} \\ 54\,970 f_{\alpha 3} \end{bmatrix} \text{mm/s}^2 \tag{4.181}$$

Determining an expression for the relative acceleration $\{A_{DG}\}_1$ of point D relative to point G using values for $\{\omega_4\}_1$ and $\{V_{DG}\}_1$ found from the earlier velocity analysis gives

$$\{A_{DG}\}_1 = \{\omega_4\}_1 \times \{V_{DG}\}_1 + \{\alpha_4\}_1 \times \{R_{DG}\}_1 \tag{4.182}$$

$$\begin{bmatrix} A_{DGx} \\ A_{DGy} \\ A_{DGz} \end{bmatrix} = \begin{bmatrix} 0 & 1.446 \times 10^{-3} & -0.945 \\ -1.446 \times 10^{-3} & 0 & 8.774 \times 10^{-3} \\ 0.945 & -8.774 \times 10^{-3} & 0 \end{bmatrix} \begin{bmatrix} -204.345 \\ 1.866 \\ -17.829 \end{bmatrix} + \begin{bmatrix} 0 & -\alpha_{4z} & \alpha_{4y} \\ \alpha_{4z} & 0 & -\alpha_{4x} \\ -\alpha_{4y} & \alpha_{4x} & 0 \end{bmatrix} \begin{bmatrix} -19 \\ -31 \\ 216 \end{bmatrix} \text{mm/s}^2 \tag{4.183}$$

$$\begin{bmatrix} A_{DGx} \\ A_{DGy} \\ A_{DGz} \end{bmatrix} = \begin{bmatrix} 16.851 \\ 0.139 \\ -193.122 \end{bmatrix} + \begin{bmatrix} 31\alpha_{4z} + 216\alpha_{4y} \\ -19\alpha_{4z} - 216\alpha_{4x} \\ 19\alpha_{4y} - 31\alpha_{4x} \end{bmatrix} \text{mm/s}^2 \tag{4.184}$$

We can now apply the triangle law of vector addition to equate the expression for $\{A_{DG}\}_1$ in equation (4.184) with $\{A_D\}_1$ in equation (4.181) and $\{A_G\}_1$ in equation (4.177):

$$\{A_{DG}\}_1 = \{A_D\}_1 - \{A_G\}_1 \tag{4.185}$$

$$\begin{bmatrix} 16.851 \\ 0.139 \\ -193.122 \end{bmatrix} + \begin{bmatrix} 31\alpha_{4z} + 216\alpha_{4y} \\ -19\alpha_{4z} - 216\alpha_{4x} \\ 19\alpha_{4y} - 31\alpha_{4x} \end{bmatrix} = \begin{bmatrix} -96.030 \\ -47\,281.651 \\ 1576.804 \end{bmatrix} + \begin{bmatrix} -3346 f_{\alpha 3} \\ 1840 f_{\alpha 3} \\ 54\,970 f_{\alpha 3} \end{bmatrix} - \begin{bmatrix} 0 \\ -41\,375.058 \\ 1354.093 \end{bmatrix} - \begin{bmatrix} 0 \\ 2070 f_{\alpha 2} \\ 63\,250 f_{\alpha 2} \end{bmatrix} \text{mm/s}^2 \tag{4.186}$$

Rearranging (4.186) yields the first three equations required to solve the analysis:

$$\text{Equation 1} \quad 3346f_{\alpha 3} + 216\alpha_{4y} + 31\alpha_{4z} = -112.881 \tag{4.187}$$

$$\text{Equation 2} \quad 2070f_{\alpha 2} - 1840f_{\alpha 3} - 216\alpha_{4x} - 19\alpha_{4z} = -5906.732 \tag{4.188}$$

$$\text{Equation 3} \quad 63\,250f_{\alpha 2} - 54\,970f_{\alpha 3} - 31\alpha_{4x} + 19\alpha_{4y} = 415.833 \tag{4.189}$$

We can now proceed to set up the next set of three equations working from point H to point D and using the triangle law of vector addition:

$$\{A_{DH}\}_1 = \{A_D\}_1 - \{A_H\}_1 \tag{4.190}$$

Determining an expression for the acceleration $\{A_H\}_1$ at point H using values for $\{\omega_5\}_1$ and $\{V_H\}_1$ found from the earlier velocity analysis gives

$$\{A_H\}_1 = \{A_{HJ}\}_1 = \{\omega_5\}_1 \times \{V_H\}_1 + \{\alpha_5\}_1 \times \{R_{HJ}\}_1 \tag{4.191}$$

$$\begin{bmatrix} A_{Hx} \\ A_{Hy} \\ A_{Hz} \end{bmatrix} = \begin{bmatrix} 0 & -1.106 & 3.881 \times 10^{-2} \\ 1.106 & 0 & -14.121 \\ -3.881 \times 10^{-2} & 14.121 & 0 \end{bmatrix} \begin{bmatrix} -252.524 \\ 112.968 \\ 3219.588 \end{bmatrix} + \begin{bmatrix} 0 & -\alpha_{5z} & \alpha_{5y} \\ \alpha_{5z} & 0 & -\alpha_{5x} \\ -\alpha_{5y} & \alpha_{5x} & 0 \end{bmatrix} \begin{bmatrix} 0 \\ 228 \\ -8 \end{bmatrix} \text{mm/s}^2 \tag{4.192}$$

$$\begin{bmatrix} A_{Hx} \\ A_{Hy} \\ A_{Hz} \end{bmatrix} = \begin{bmatrix} 9.602 \times 10^{-3} \\ -45\,743.094 \\ 1605.022 \end{bmatrix} + \begin{bmatrix} -228\alpha_{5z} - 8\alpha_{5y} \\ 8\alpha_{5x} \\ 228\alpha_{5x} \end{bmatrix} \text{mm/s}^2 \tag{4.193}$$

We already have an expression for $\{A_D\}_1$ in equation (4.181) and can determine an expression for the relative acceleration $\{A_{DH}\}_1$ of point D relative to point H using values for $\{\omega_4\}_1$ and $\{V_{DH}\}_1$ found from the earlier velocity analysis:

$$\{A_{DH}\}_1 = \{\omega_4\}_1 \times \{V_{DH}\}_1 + \{\alpha_4\}_1 \times \{R_{DH}\}_1 \tag{4.194}$$

$$\begin{bmatrix} A_{DHx} \\ A_{DHy} \\ A_{DHz} \end{bmatrix} = \begin{bmatrix} 0 & 1.446 \times 10^{-3} & -0.945 \\ -1.446 \times 10^{-3} & 0 & 8.774 \times 10^{-3} \\ 0.945 & -8.774 \times 10^{-3} & 0 \end{bmatrix} \begin{bmatrix} 48.179 \\ -0.708 \\ 135.733 \end{bmatrix} + \begin{bmatrix} 0 & -\alpha_{4z} & \alpha_{4y} \\ \alpha_{4z} & 0 & -\alpha_{4x} \\ -\alpha_{4y} & \alpha_{4x} & 0 \end{bmatrix} \begin{bmatrix} 114 \\ 44 \\ -51 \end{bmatrix} \text{mm/s}^2 \tag{4.195}$$

$$\begin{bmatrix} A_{DHx} \\ A_{DHy} \\ A_{DHz} \end{bmatrix} = \begin{bmatrix} -128.269 \\ 1.121 \\ 45.535 \end{bmatrix} + \begin{bmatrix} -44\alpha_{4z} - 51\alpha_{4y} \\ 144\alpha_{4z} + 51\alpha_{4x} \\ -144\alpha_{4y} + 44\alpha_{4x} \end{bmatrix} \text{mm/s}^2 \tag{4.196}$$

We can now apply the triangle law of vector addition to equate the expression for $\{A_{DH}\}_1$ in equation (4.196) with $\{A_D\}_1$ in equation (4.181) and $\{A_H\}_1$ in equation (4.193):

$$\{A_{DH}\}_1 = \{A_D\}_1 - \{A_H\}_1 \tag{4.197}$$

$$\begin{bmatrix} -128.269 \\ 1.121 \\ 45.535 \end{bmatrix} + \begin{bmatrix} -44\alpha_{4z} - 51\alpha_{4y} \\ 144\alpha_{4z} + 51\alpha_{4x} \\ -144\alpha_{4y} + 44\alpha_{4x} \end{bmatrix} = \begin{bmatrix} -96.030 \\ -47\,281.651 \\ 1576.804 \end{bmatrix} + \begin{bmatrix} -3346 f_{\alpha 3} \\ 1840 f_{\alpha 3} \\ 54\,970 f_{\alpha 3} \end{bmatrix} - \begin{bmatrix} 9.602 \times 10^{-3} \\ -45\,743.094 \\ 1605.022 \end{bmatrix} + \begin{bmatrix} -228\alpha_{5z} - 8\alpha_{5y} \\ 8\alpha_{5x} \\ 228\alpha_{5x} \end{bmatrix} \text{mm/s}^2 \tag{4.198}$$

Rearranging (4.198) yields the next three equations required to solve the analysis:

Equation 4 $$3346 f_{\alpha 3} - 51\alpha_{4y} - 44\alpha_{4z} - 8\alpha_{5y} - 228\alpha_{5z} = 32.229 \tag{4.199}$$

Equation 5 $$-1840 f_{\alpha 3} + 51\alpha_{4x} + 144\alpha_{4z} + 8\alpha_{5x} = -1539.678 \tag{4.200}$$

Equation 6 $$-54\,970 f_{\alpha 3} + 44\alpha_{4x} - 144\alpha_{4y} + 228\alpha_{5x} = -73.753 \tag{4.201}$$

We can now proceed to set up the next set of three equations working from point G to point P and using the triangle law of vector addition:

$$\{A_{PG}\}_1 = \{A_P\}_1 - \{A_G\}_1 \tag{4.202}$$

Determining an expression for the relative acceleration $\{A_{PG}\}_1$ of point P relative to point G using values for $\{\omega_4\}_1$ and $\{V_{PG}\}_1$ found from the earlier velocity analysis gives

$$\{A_{PG}\}_1 = \{\omega_4\}_1 \times \{V_{PG}\}_1 + \{\alpha_4\}_1 \times \{R_{PG}\}_1 \tag{4.203}$$

$$\begin{bmatrix} A_{PGx} \\ A_{PGy} \\ A_{PGz} \end{bmatrix} = \begin{bmatrix} 0 & 1.446 \times 10^{-3} & -0.945 \\ -1.446 \times 10^{-3} & 0 & 8.774 \times 10^{-3} \\ 0.945 & -8.774 \times 10^{-3} & 0 \end{bmatrix} \begin{bmatrix} 166.468 \\ -1.535 \\ -7.150 \end{bmatrix} + \begin{bmatrix} 0 & -\alpha_{4z} & \alpha_{4y} \\ \alpha_{4z} & 0 & -\alpha_{4x} \\ -\alpha_{4y} & \alpha_{4x} & 0 \end{bmatrix} \begin{bmatrix} -7 \\ 58 \\ -176 \end{bmatrix} \text{mm/s}^2 \tag{4.204}$$

$$\begin{bmatrix} A_{PGx} \\ A_{PGy} \\ A_{PGz} \end{bmatrix} = \begin{bmatrix} 6.755 \\ -0.303 \\ 157.326 \end{bmatrix} + \begin{bmatrix} -58\alpha_{4z} - 176\alpha_{4y} \\ -7\alpha_{4z} + 176\alpha_{4x} \\ 7\alpha_{4y} + 58\alpha_{4x} \end{bmatrix} \text{mm/s}^2 \tag{4.205}$$

We already have an expression for $\{A_G\}_1$ in equation (4.177) and we can define the vector $\{A_P\}_1$ in terms of the known vertical acceleration component A_{Pz} and the unknown components A_{Px} and A_{Py}:

$$\{A_P\}_1 = \begin{bmatrix} A_{Px} \\ A_{Py} \\ 0.0 \end{bmatrix} \text{mm/s}^2 \tag{4.206}$$

We can now apply the triangle law of vector addition to equate the expression for $\{A_{PG}\}_1$ in equation (4.205) with $\{A_P\}_1$ in equation (4.206) and $\{A_G\}_1$ in expression (4.177):

$$\{A_{PG}\}_1 = \{A_P\}_1 - \{A_G\}_1 \tag{4.207}$$

$$\begin{bmatrix} 6.755 \\ -0.303 \\ 157.326 \end{bmatrix} + \begin{bmatrix} -58\alpha_{4_z} - 176\alpha_{4_y} \\ -7\alpha_{4_z} + 176\alpha_{4x} \\ 7\alpha_{4_y} + 58\alpha_{4x} \end{bmatrix} = \begin{bmatrix} A_{Px} \\ A_{Py} \\ 0.0 \end{bmatrix} - \begin{bmatrix} 0 \\ -41\,375.058 \\ 1354.093 \end{bmatrix} - \begin{bmatrix} 0 \\ 2070 f_{\alpha 2} \\ 63\,250 f_{\alpha 2} \end{bmatrix} \text{mm/s}^2 \tag{4.208}$$

Rearranging (4.208) yields the next set of three equations required to solve the analysis:

$$\text{Equation 7} \quad 176\alpha_{4_y} + 58\alpha_{4_z} + A_{Px} = 6.755 \tag{4.209}$$

$$\text{Equation 8} \quad -2070 f_{\alpha 2} - 176\alpha_{4x} + 7\alpha_{4_z} + A_{Py} = -41\,375.361 \tag{4.210}$$

$$\text{Equation 9} \quad -63\,250 f_{\alpha 2} - 58\alpha_{4x} - 7\alpha_{4_y} = 1511.419 \tag{4.211}$$

As with the velocity analysis this leaves us with nine equations and 10 unknowns. The last equation is again obtained by constraining the rotation of the tie rod (Body 5) to prevent spin about its own axis:

$$\{\alpha_5\}_1 \bullet \{R_{HJ}\}_1 = 0 \tag{4.212}$$

$$[\alpha_{5x} \alpha_{5y} \alpha_{5z}] \begin{bmatrix} 0 \\ 228 \\ -8 \end{bmatrix} = 0 \text{ mm/s} \tag{4.213}$$

$$\text{Equation 10} \qquad 228\alpha_{5y} - 8\alpha_{5z} = 0 \tag{4.214}$$

The 10 equations can now be set up in matrix form ready for solution:

$$\begin{bmatrix} 0 & 3346 & 0 & 216 & 31 & 0 & 0 & 0 & 0 & 0 \\ 2070 & -1840 & -216 & 0 & -19 & 0 & 0 & 0 & 0 & 0 \\ 63\,250 & -54\,970 & -31 & 19 & 0 & 0 & 0 & 0 & 0 & 0 \\ 0 & 3346 & 0 & -51 & -44 & 0 & -8 & -228 & 0 & 0 \\ 0 & -1840 & 51 & 0 & 144 & 8 & 0 & 0 & 0 & 0 \\ 0 & -54\,970 & 44 & -144 & 0 & 228 & 0 & 0 & 0 & 0 \\ 0 & 0 & 0 & 176 & 58 & 0 & 0 & 0 & 1 & 0 \\ -2070 & 0 & -176 & 0 & 7 & 0 & 0 & 0 & 0 & 1 \\ -63\,250 & 0 & -58 & -7 & 0 & 0 & 0 & 0 & 0 & 0 \\ 0 & 0 & 0 & 0 & 0 & 0 & 228 & -8 & 0 & 0 \end{bmatrix} \begin{bmatrix} f_{\alpha 2} \\ f_{\alpha 3} \\ \alpha_{4x} \\ \alpha_{4y} \\ \alpha_{4z} \\ \alpha_{5x} \\ \alpha_{5y} \\ \alpha_{5z} \\ A_{Px} \\ A_{Py} \end{bmatrix} = \begin{bmatrix} -112.881 \\ -5906.732 \\ 415.833 \\ 32.229 \\ -1539.678 \\ -73.753 \\ 6.755 \\ -41\,375.361 \\ 1511.419 \\ 0 \end{bmatrix} \tag{4.215}$$

Solving equation (4.215) yields the following answers for the 10 unknowns:

$f_{\alpha 2} = -5.126 \times 10^{-2}$ rad/mm.s^2

$f_{\alpha 3} = -8.182 \times 10^{-2}$ rad/mm.s^2

$\alpha_{4x} = 29.386$ rad/s^2

$\alpha_{4y} = 3.737$ rad/s^2

$\alpha_{4z} = -20.847$ rad/s^2

$\alpha_{5x} = -23.361$ rad/s^2

$\alpha_{5y} = 6.466 \times 10^{-2}$ rad/s^2

$\alpha_{5z} = 1.843$ rad/s^2

$A_{Px} = 558.211$ mm/s^2

$A_{Py} = -36\,163.671$ mm/s^2

It is now possible to use the two scale factors, $f_{\alpha 2}$ and $f_{\alpha 3}$, to calculate the angular acceleration vectors $\{\alpha_2\}_1$ and $\{\alpha_3\}_1$:

$$\{\alpha_2\}_1 = f_{\alpha 2}\{R_{EF}\}_1 = -5.126 \times 10^{-2} \begin{bmatrix} 230 \\ 0 \\ 0 \end{bmatrix} = \begin{bmatrix} -11.790 \\ 0 \\ 0 \end{bmatrix} \text{rad/s}^2 \quad (4.216)$$

$$\{\alpha_3\}_1 = f_{\alpha 3}\{R_{AB}\}_1 = -8.182 \times 10^{-2} \begin{bmatrix} 230 \\ 0 \\ 14 \end{bmatrix} = \begin{bmatrix} -18.819 \\ 0 \\ -1.145 \end{bmatrix} \text{rad/s}^2 \quad (4.217)$$

In summary the angular acceleration vectors for the rigid bodies are as follows:

$\{\alpha_2\}_1^T = [-11.790 \quad 0 \quad 0]$ rad/s^2

$\{\alpha_3\}_1^T = [-18.819 \quad 0 \quad -1.145]$ rad/s^2

$\{\alpha_4\}_1^T = [29.386 \quad 3.737 \quad -20.847]$ rad/s^2

$\{\alpha_5\}_1^T = [-23.361 \quad 6.466 \times 10^{-2} \quad 1.843]$ rad/s^2

We can now proceed to calculate the translational accelerations at all the moving points, C, D, G, H and P, within this part of the model:

$$\{A_C\}_1 = \{A_{CA}\}_1 = \{\omega_3\}_1 \times \{V_C\}_1 + \{\alpha_3\}_1 \times \{R_{CA}\}_1 \quad (4.218)$$

$$\begin{bmatrix} A_{Cx} \\ A_{Cy} \\ A_{Cz} \end{bmatrix} = \begin{bmatrix} 0 & -0.855 & 0 \\ 0.855 & 0 & -14.039 \\ 0 & 14.039 & 0 \end{bmatrix} \begin{bmatrix} -120.555 \\ 435.157 \\ 1979.499 \end{bmatrix} + \begin{bmatrix} 0 & 1.146 & 0 \\ -1.146 & 0 & 18.819 \\ 0 & -18.819 & 0 \end{bmatrix} \begin{bmatrix} -115 \\ 141 \\ -38 \end{bmatrix} \text{mm/s}^2 \quad (4.219)$$

$$\begin{bmatrix} A_{Cx} \\ A_{Cy} \\ A_{Cz} \end{bmatrix} = \begin{bmatrix} -372.059 \\ -27\,893.260 \\ 6109.169 \end{bmatrix} + \begin{bmatrix} 161.445 \\ -583.447 \\ -2653.479 \end{bmatrix} = \begin{bmatrix} -210.614 \\ -28\,476.707 \\ 3455.690 \end{bmatrix} \text{mm/s}^2 \quad (4.220)$$

$$\{A_D\}_1 = \{A_{DA}\}_1 = \{\omega_3\}_1 \times \{V_D\}_1 + \{\alpha_3\}_1 \times \{R_{DA}\}_1 \quad (4.221)$$

$$\begin{bmatrix} A_{Dx} \\ A_{Dy} \\ A_{Dz} \end{bmatrix} = \begin{bmatrix} -96.030 \\ -47\,281.651 \\ 1576.804 \end{bmatrix} + \begin{bmatrix} 0 & 1.145 & 0 \\ -1.145 & 0 & 18.819 \\ 0 & -18.819 & 0 \end{bmatrix} \begin{bmatrix} -11 \\ 239 \\ -15 \end{bmatrix}$$

$$= \begin{bmatrix} 177.625 \\ -47\,432.261 \\ -2920.973 \end{bmatrix} \text{mm/s}^2 \quad (4.223)$$

$$\{A_G\}_1 = \{A_{GE}\}_1 = \{\omega_2\}_1 \times \{V_G\}_1 + \{\alpha_2\}_1 \times \{R_{GE}\}_1 \quad (4.224)$$

$$\begin{bmatrix} A_{Gx} \\ A_{Gy} \\ A_{Gz} \end{bmatrix} = \begin{bmatrix} 0 \\ -41\,375.058 \\ 1354.093 \end{bmatrix} + \begin{bmatrix} 0 & 0 & 0 \\ 0 & 0 & 11.791 \\ 0 & -11.791 & 0 \end{bmatrix} \begin{bmatrix} -115 \\ 275 \\ -9 \end{bmatrix} = \begin{bmatrix} 0 \\ -41\,481.177 \\ -1888.432 \end{bmatrix} \text{mm/s}^2 \quad (4.225)$$

$$\{A_H\}_1 = \{A_{HJ}\}_1 = \{\omega_5\}_1 \times \{V_H\}_1 + \{\alpha_5\}_1 \times \{R_{HJ}\}_1 \quad (4.226)$$

$$\begin{bmatrix} A_{Hx} \\ A_{Hy} \\ A_{Hz} \end{bmatrix} = \begin{bmatrix} 9.602 \times 10^{-3} \\ -45\,743.094 \\ 1605.022 \end{bmatrix} + \begin{bmatrix} 0 & -1.843 & 0.06466 \\ 1.843 & 0 & -23.361 \\ -0.06466 & 23.361 & 0 \end{bmatrix} \begin{bmatrix} 0 \\ 229 \\ -9 \end{bmatrix}$$

$$= \begin{bmatrix} -422.619 \\ -45\,953.343 \\ -3744.647 \end{bmatrix} \text{mm/s}^2 \quad (4.227)$$

The acceleration vector $\{A_P\}_1$ is already available from the initial bump analysis and the solution of equation (4.215). In summary the acceleration vectors for the moving points are as follows:

$\{A_C\}_1^T = [-210.614 \quad -28\,476.707 \quad 3455.690]$ mm/s^2
$\{A_D\}_1^T = [177.625 \quad -47\,432.261 \quad -2920.973]$ mm/s^2
$\{A_G\}_1^T = [0.0 \quad -41\,481.177 \quad -1888.432]$ mm/s^2
$\{A_H\}_1^T = [-422.619 \quad 45\,953.343 \quad -3744.647]$ mm/s^2
$\{A_P\}_1^T = [558.211 \quad -36\,163.671 \quad 0.0]$ mm/s^2

Having found the acceleration $\{A_C\}_1$ at the bottom of the damper unit we can now proceed to carry out a separate analysis of the unit to find the components of acceleration acting between Bodies 6 and 7.

As with the velocity analysis, this phase of the acceleration analysis can be facilitated by the modelling of three coincident points, C_3 on Body 3,

C_6 on Body 6 and C_7 on Body 7, all located at point C. Note that we already have

$$\{A_{C3}\}_1 = \{A_{C7}\}_1 = \{A_C\}_1 = \begin{bmatrix} -210.614 \\ -28\,476.707 \\ 3455.690 \end{bmatrix} \text{mm/s}^2 \tag{4.228}$$

We can also calculate the acceleration $\{A_{C6}\}_1$ from

$$\{A_{C6}\}_1 = \{A_{C6I}\}_1 = \{\omega_6\}_1 \times \{V_{C6I}\}_1 + \{\alpha_6\}_1 \times \{R_{CI}\}_1 \tag{4.229}$$

where

$$\{V_{C6I}\}_1 = \{V_{C6}\}_1 = \{V_{C6C7}\}_1 - \{V_{C7}\}_1 \tag{4.230}$$

$$\{V_{C6I}\} = \begin{bmatrix} 13.628 \\ -41.045 \\ -1988.378 \end{bmatrix} - \begin{bmatrix} -120.555 \\ 435.157 \\ 1979.499 \end{bmatrix} = \begin{bmatrix} 134.183 \\ -476.202 \\ -3967.877 \end{bmatrix} \text{mm/s} \tag{4.231}$$

therefore $\{A_{C6}\}_1$ is given by

$$\begin{bmatrix} A_{C6x} \\ A_{C6y} \\ A_{C6z} \end{bmatrix} = \begin{bmatrix} 0 & -1.159 & 0.245 \\ 1.159 & 0 & -0.904 \\ -0.245 & 0.904 & 0 \end{bmatrix} \begin{bmatrix} 134.183 \\ -476.202 \\ -3967.877 \end{bmatrix} + \begin{bmatrix} 0 & -\alpha_{6z} & \alpha_{6y} \\ \alpha_{6z} & 0 & -\alpha_{6x} \\ -\alpha_{6y} & \alpha_{6x} & 0 \end{bmatrix} \begin{bmatrix} 3 \\ -9 \\ -436 \end{bmatrix} \text{mm/s}^2 \tag{4.232}$$

$$\begin{bmatrix} A_{C6x} \\ A_{C6y} \\ A_{C6z} \end{bmatrix} = \begin{bmatrix} -420.212 \\ 3742.479 \\ -463.361 \end{bmatrix} + \begin{bmatrix} 9\alpha_{6z} - 436\alpha_{6y} \\ 3\alpha_{6z} + 436\alpha_{6x} \\ -3\alpha_{6y} - 9\alpha_{6x} \end{bmatrix} \text{mm/s}^2 \tag{4.233}$$

If we now consider the relative acceleration vector $\{A_{C6C7}\}_1$ we can see that this involves the relative acceleration between points on two bodies where relative rotation and sliding occurs. Referring back to Chapter 2 we can now identify the four components of acceleration associated with the combined rotation and sliding motion as the centripetal acceleration $\{A^p{}_{C6C7}\}_1$, the transverse acceleration $\{A^t{}_{C6C7}\}_1$, the Coriolis acceleration $\{A^c{}_{C6C7}\}_1$ and the sliding acceleration$\{A^s{}_{C6C7}\}_1$:

$$\{A^p{}_{C6C7}\}_1 = \{\omega_6\}_1 \times \{\{\omega_6\}_1 \times \{R_{C6C7}\}_1\} \tag{4.234}$$

$$\{A^t{}_{C6C7}\}_1 = \{\alpha_6\}_1 \times \{R_{C6C7}\}_1 \tag{4.235}$$

$$\{A^c{}_{C6C7}\}_1 = 2\{\omega_6\}_1 \times \{V_s\}_1 \tag{4.236}$$

$$\{A^s{}_{C6C7}\}_1 = |A^s{}_{C6C7}|\ \{l_{CI}\}_1 \tag{4.237}$$

Since the C_6 and C_7 are coincident points it follows that $\{A^p{}_{C6C7}\}_1$ and $\{A^t{}_{C6C7}\}_1$ are zero. It also follows that the sliding velocity $\{V_s\}_1$ is equal to

$\{V_{C6C7}\}_1$. We can also introduce a scale factor A_s to simplify the sliding acceleration calculation giving

$$\{A^c{}_{C6C7}\}_1 = 2\{\omega_6\}_1 \times \{V_{C6C7}\}_1 \tag{4.238}$$

$$\{A^s{}_{C6C7}\}_1 = A_s\{R_{CI}\}_1 \tag{4.239}$$

Combining these components of acceleration gives $\{A_{C6C7}\}_1$ as

$$\{A_{C6C7}\}_1 = 2\{\omega_6\}_1 \times \{V_{C6C7}\}_1 + A_s\{R_{CI}\}_1 \tag{4.240}$$

$$\begin{bmatrix} A_{C6C7x} \\ A_{C6C7y} \\ A_{C6C7z} \end{bmatrix} = 2\begin{bmatrix} 0 & -1.159 & 0.245 \\ 1.159 & 0 & -0.904 \\ -0.245 & 0.904 & 0 \end{bmatrix}\begin{bmatrix} 13.682 \\ -41.045 \\ -1988.378 \end{bmatrix} + A_s\begin{bmatrix} 3 \\ -9 \\ -436 \end{bmatrix} \text{mm/s}^2 \tag{4.241}$$

$$\begin{bmatrix} A_{C6C7x} \\ A_{C6C7y} \\ A_{C6C7z} \end{bmatrix} = \begin{bmatrix} -879.162 \\ 3626.702 \\ -80.457 \end{bmatrix} + A_s\begin{bmatrix} 3 \\ -9 \\ -436 \end{bmatrix} \text{mm/s}^2 \tag{4.242}$$

Applying the triangle law of vector addition yields

$$\{A_{C6C7}\}_1 = \{A_{C6}\}_1 - \{A_{C7}\}_1 \tag{4.243}$$

$$\begin{bmatrix} -879.162 \\ 3626.702 \\ -80.457 \end{bmatrix} + A_s\begin{bmatrix} 3 \\ -9 \\ -436 \end{bmatrix} = \begin{bmatrix} -420.212 \\ 3742.479 \\ -463.361 \end{bmatrix} + \begin{bmatrix} 9\alpha_{6z} - 436\alpha_{6y} \\ 3\alpha_{6z} + 436\alpha_{6x} \\ -3\alpha_{6y} - 9\alpha_{6x} \end{bmatrix} - \begin{bmatrix} -210.614 \\ -28\,476.707 \\ 3455.690 \end{bmatrix} \text{mm/s}^2 \tag{4.244}$$

Rearranging (4.244) yields three equations that can be used to solve this part of the analysis:

Equation 1 $$3A_s + 436\alpha_{6y} - 9\alpha_{6z} = 669.564 \tag{4.245}$$

Equation 2 $$-9A_s - 436\alpha_{6x} - 3\alpha_{6z} = 28\,592.484 \tag{4.246}$$

Equation 3 $$-436A_s + 9\alpha_{6x} + 3\alpha_{6y} = -3838.594 \tag{4.247}$$

This leaves us with four unknowns, α_{6x}, α_{6y}, α_{6z} and A_s, but only three equations. We can use the same approach here as used in the preceding velocity analysis. Since the spin degree of freedom of Body 6 about the axis C–I has no bearing on the overall solution we can again use the vector dot product to enforce perpendicularity of $\{\alpha_6\}_1$ to $\{R_{CI}\}_1$. This will yield the fourth equation as follows:

$$\{\alpha_6\}_1 \bullet \{R_{CI}\}_1 = 0 \tag{4.248}$$

$$[\alpha_{6x}\alpha_{6y}\alpha_{6z}]\begin{bmatrix} 3 \\ -9 \\ -436 \end{bmatrix} = 0 \text{ mm/s} \tag{4.249}$$

Equation 4 $$3\alpha_{6x} - 9\alpha_{6y} - 436\alpha_{6z} = 0 \tag{4.250}$$

The four equations can now be set up in matrix form ready for solution:

$$\begin{bmatrix} 3 & 0 & 436 & -9 \\ -9 & -436 & 0 & -3 \\ -436 & 9 & 3 & 0 \\ 0 & 3 & -9 & -436 \end{bmatrix} \begin{bmatrix} A_s \\ \alpha_{6x} \\ \alpha_{6y} \\ \alpha_{6z} \end{bmatrix} = \begin{bmatrix} 669.564 \\ 28\,592.484 \\ -3838.594 \\ 0 \end{bmatrix} \tag{4.251}$$

Solving equation (4.251) yields the following answers for the four unknowns:

$A_s = 7.457\,\text{s}^{-2}$

$\alpha_{6x} = -65.730\,\text{rad/s}^2$

$\alpha_{6y} = 1.147\,\text{rad/s}^2$

$\alpha_{6z} = -0.483\,\text{rad/s}^2$

This gives us the last two angular acceleration vectors for the upper and lower damper bodies:

$$\{\alpha_6\}_1^T = [-65.730 \;\; 1.147 \;\; -0.483]\;\text{rad/s}^2$$

$$\{\alpha_7\}_1^T = [-65.730 \;\; 1.147 \;\; -0.483]\;\text{rad/s}^2$$

From equation (4.240) we now have

$$\{A_{C6C7}\}_1 = 2\{\omega_6\}_1 \times \{V_{C6C7}\}_1 + A_s\{R_{CI}\}_1 \tag{4.252}$$

$$\{A_{C6C7}\}_1 = \begin{bmatrix} -879.162 \\ 3626.702 \\ -80.457 \end{bmatrix} + 7.457 \begin{bmatrix} 3 \\ -9 \\ -436 \end{bmatrix} = \begin{bmatrix} -856.791 \\ 3559.589 \\ -3331.709 \end{bmatrix} \text{mm/s}^2 \tag{4.253}$$

A comparison of the angular accelerations found from the preceding calculations and those found using an equivalent MSC.ADAMS model is shown in Table 4.12.

Table 4.12 Comparison of angular acceleration vectors computed by theory and MSC.ADAMS

Body	Angular acceleration vectors					
	Theory			MSC.ADAMS		
	α_x (rad/s^2)	α_y (rad/s^2)	α_z (rad/s^2)	α_x (rad/s^2)	α_y (rad/s^2)	α_z (rad/s^2)
2	−11.790	0.0	0.0	−11.791	0.0	0.0
3	−18.819	0.0	−1.145	−18.823	0.0	−1.146
4	29.386	3.737	−20.847	29.395	3.737	−20.840
5	−23.361	0.065	1.843	−23.384	0.157	2.053
6	−65.730	1.147	−0.483	−57.204	2.663	−0.449
7	−65.730	1.147	−0.483	−57.204	2.663	−0.449

Table 4.13 Comparison of translational acceleration vectors computed by theory and MSC.ADAMS

Point	Translational acceleration vectors					
	Theory			MSC.ADAMS		
	A_x (mm/s^2)	A_y (mm/s^2)	A_z (mm/s^2)	A_x (mm/s^2)	A_y (mm/s^2)	A_z (mm/s^2)
C	−210.614	−28 476.707	3455.690	−210.385	−28 478.60	3456.320
D	177.625	−47 432.261	−2920.973	177.846	−47 433.70	−2921.760
G	0.0	−41 481.177	−1888.432	0.0	−41 480.60	−1888.430
H	−422.619	−45 953.343	−3744.647	−420.215	−45 933.00	−3722.660
P	558.211	−36 163.671	0.0	557.780	−36 161.60	0.0
C_6C_7	−856.791	3559.589	−3331.709	−957.170	3 544.09	−2566.940

A comparison of the translational accelerations found at points within the suspension system from the preceding calculations and those found using an equivalent MSC.ADAMS model is shown in Table 4.13.

4.10.4 Static analysis

As discussed in this chapter a starting point for suspension component loading studies is to use equivalent static forces to represent the loads acting through the road wheel, associated with real world driving conditions. In this example the vector analysis method is used to carry out a static analysis where a vertical load of 10 000 N is applied at the tyre contact patch, this being representative in magnitude of the loads used for a 3G bump case on a typical vehicle of this size.

In this analysis we are ignoring gravity and the self-weight of the suspension components as this contribution tends to be minor compared with overall vehicle loads reacted at the tyre contact patch and diffused into the suspension system. For completeness the effects of self-weight will be included in a follow-on demonstration of a dynamic analysis.

Before attempting any vector analysis to determine the distribution of forces it is necessary to prepare a free-body diagram and label the bodies and forces in an appropriate manner as shown in Figure 4.73.

For the action–reaction forces shown acting between the bodies in Figure 4.73 Newton's third law would apply. The interaction, for example, at point D between Body 3 and Body 4 requires $\{F_{D43}\}_1$ and $\{F_{D34}\}_1$ to be equal and opposite equal. Thus instead of including the six unknowns F_{D43x}, F_{D43y}, F_{D43z}, F_{D34x}, F_{D34y} and F_{D34z} we can reduce this to three unknowns F_{D43x}, F_{D43y}, F_{D43z}. In a similar manner looking at the connections at points G and H we can see for all connections to Body 4 that the following applies:

$$\{F_{D43}\}_1 = -\{F_{D34}\}_1 \tag{4.254}$$

$$\{F_{G42}\}_1 = -\{F_{G24}\}_1 \tag{4.255}$$

$$\{F_{H45}\}_1 = -\{F_{H54}\}_1 \tag{4.256}$$

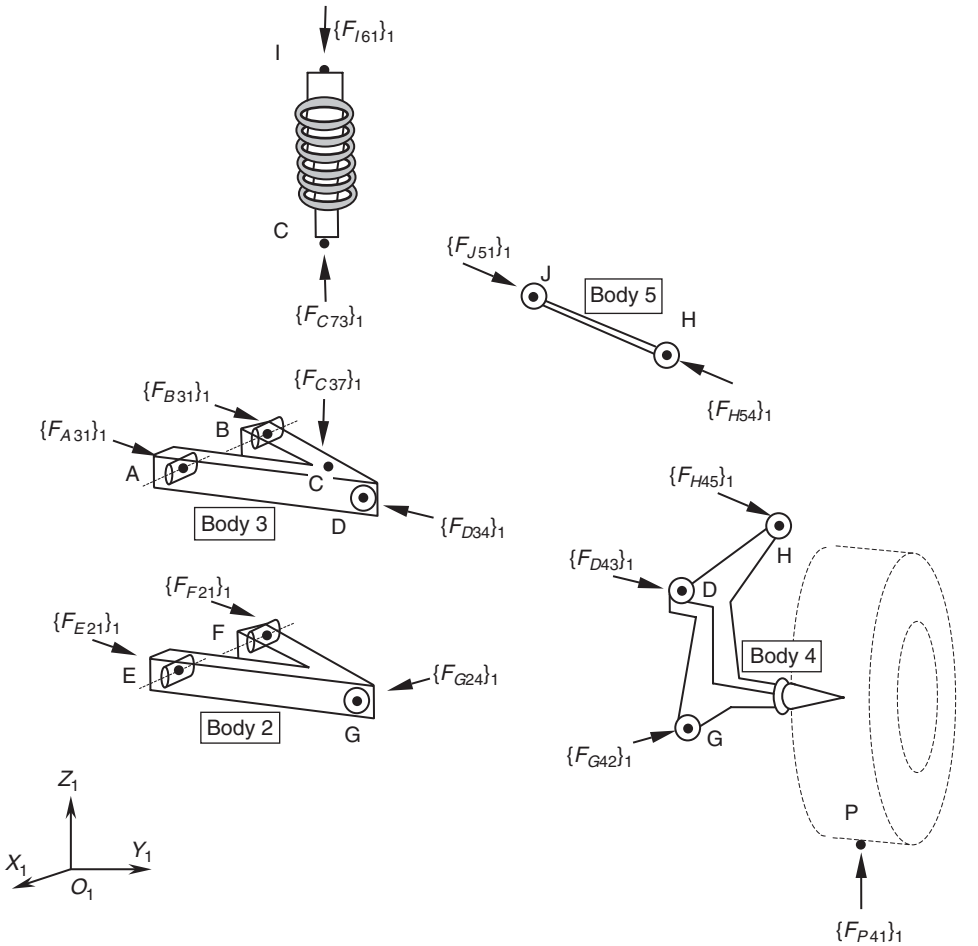

Fig. 4.73 Free-body diagram for double wishbone suspension system static force analysis

In this model we are treating the connections and mounts as pin-jointed, or as the equivalent spherical joints in an MBS model. For the track rod, Body 5, both ends of the linkage are pin-jointed and the force by definition must, if we allow ourselves the assumption to ignore gravity for this study, act along the axis H–J. In a similar manner the force acting on Body 7 at the base of the strut at point C must be equal and opposite to the force acting at the top on Body 6 at point I:

$$\{F_{J51}\}_1 = -\{F_{H54}\}_1 \tag{4.257}$$

$$\{F_{C37}\}_1 = -\{F_{C73}\}_1 = \{F_{I61}\}_1 \tag{4.258}$$

The number of unknowns can be reduced even further, by using scale factors to exploit the knowledge that the lines of action of the forces are known:

$$\{F_{H54}\}_1 = f_{S1}\{R_{JH}\}_1 \tag{4.259}$$

$$\{F_{C37}\}_1 = f_{S2}\{R_{CI}\}_1 \tag{4.260}$$

This results in the following set of 20 unknowns that must be found to solve for static equilibrium:

$F_{A31x}, F_{A31y}, F_{A31z}$
$F_{B31x}, F_{B31y}, F_{B31z}$
$F_{D43x}, F_{D43y}, F_{D43z}$
$F_{E21x}, F_{E21y}, F_{E21z}$
$F_{F21x}, F_{F21y}, F_{F21z}$
$F_{G24x}, F_{G24y}, F_{G24z}$
f_{S1}, f_{S2}

The problem can be solved by setting up the equations of equilibrium for Bodies 2, 3 and 4. The use of scale factors to model the forces acting along Body 5 and the strut, Bodies 6 and 7, means that these bodies cannot be used to generate any useful equations to solve the problem. Thus we could generate 18 equations as follows:

For Body 2 summing forces and taking moments about point G gives

$$\sum\{F_2\}_1 = \{0\}_1 \tag{4.261}$$

$$\sum\{M_{G2}\}_1 = \{0\}_1 \tag{4.262}$$

For Body 3 summing forces and taking moments about point D gives

$$\sum\{F_3\}_1 = \{0\}_1 \tag{4.263}$$

$$\sum\{M_{D3}\}_1 = \{0\}_1 \tag{4.264}$$

For Body 4 summing forces and taking moments about point G gives

$$\sum\{F_4\}_1 = \{0\}_1 \tag{4.265}$$

$$\sum\{M_{G4}\}_1 = \{0\}_1 \tag{4.266}$$

This leaves us with the requirement to generate another two equations for solution. The answer comes from a more considered study of the connections or mounts between the upper and lower wishbones and the ground part. Four possible MBS modelling solutions are shown in Figure 4.74.

In Figure 4.74(a) the wishbone is mounted using two bush force elements. Using this configuration the wishbone is mounted on an elastic foundation and the body has 6 rigid body degrees of freedom relative to the part on which it is mounted, which for this example is a non-moving ground part. If the actual wishbone is mounted on the vehicle in this way this would be the MBS modelling solution of choice if as discussed earlier the simulation aimed to produce accurate predictions of the mount reaction forces. The movement of the wishbone relative to the part on which it is mounted is controlled by the compliance in the bushes. This typically would allow relatively little resistance to rotation about an axis through the bushes, while strongly resisting motion in the other 5 degrees of freedom.

In Figure 4.74(b) the wishbone is constrained by a spherical joint at each bush location. Each spherical joint constrains 3 degrees of freedom. This is in fact equivalent to our vector-based model shown as a free-body diagram in Figure 4.73 where we currently have three constraint reaction forces at each of our mount locations A, B, E and F. The problem with this approach

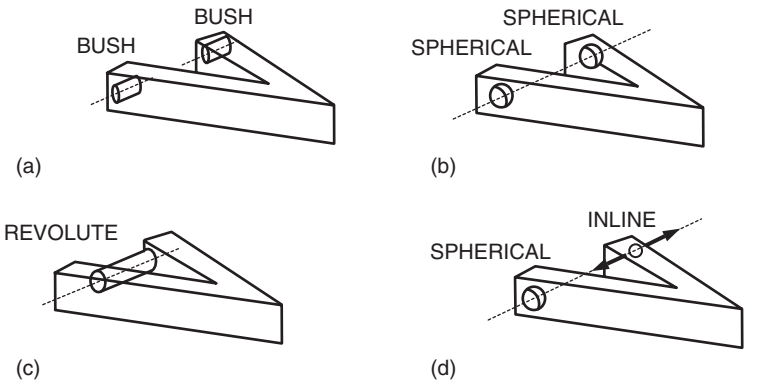

Fig. 4.74 Wishbone mount modelling strategies: (a) wishbone mounted by two bushes; (b) wishbone mounted by two spherical joints; (c) wishbone mounted by a single revolute joint; (d) wishbone mounted by a spherical joint and inline joint primitive.

is that the wishbone initially has 6 degrees of freedom and the two spherical joints remove three each leaving for the wishbone body a local balance of zero degrees of freedom. This is clearly not valid as in the absence of friction or other forces the wishbone is not physically constrained from rotating about an axis through the two spherical joints.

This is a classic MBS modelling problem where we have introduced a redundant constraint or overconstrained the model. It should also be noted that this is the root of our requirement for two more equations for the manual analysis, each equation being related to the local overconstraint of each wishbone. Early versions of MBS programs such as MSC.ADAMS were rather unforgiving in these circumstances and any attempt to solve such a model would cause the solver to fail with the appropriate error messages. More modern versions are able to identify and remove redundant constraints allowing a solution to proceed. While this undoubtedly adds to the convenience of model construction it does isolate less experienced users from the underlying theory and modelling issues we are currently discussing. In any event if the required outcome is to predict loads at the mount points the removal of the redundant constraints, although not affecting the kinematics, cannot be relied on to distribute correctly the forces to the mounts.

In Figure 4.74(c) the two wishbone mount connections are represented by a single revolute joint. This is the method suggested earlier as a suitable start for predicting the suspension kinematics but will again not be useful for prediction the mount reaction forces. In this model the single revolute joint will carry the combined translational reaction forces at both mounts with additional moment reactions that would not exist in the real system.

The final representation shown in Figure 4.74(d) allows a model that uses rigid constraint elements and can predict reaction forces at each mount without using the ‘as is’ approach of including the bush compliances or introducing redundant constraints. This is achieved by modelling one

mount with a spherical joint and modelling the other mount with an inline joint primitive, as described earlier in Chapter 3. The inline primitive constrains 2 degrees of freedom to maintain the mount position on the axis through the two mount locations. This constraint does not prevent translation along the axis through the mounts, this 'thrust' being reacted by the single spherical joint. Thus this selection of rigid constraints provides us with a solution that is not overconstrained. Although the MBS approach would best utilize the model with two bushes to predict the mount reaction forces the model in Figure 4.74(d) provides us with an understanding of the overconstraint problem and a methodology we can adapt to progress the vector-based analytical solution.

If we return now to the analytical solution and consider the lower wishbone Body 2, we can see in Figure 4.75 that a comparable approach to the use of the MBS inline joint primitive constraint is to ensure that the line of action of one of the mount reaction forces, say $\{F_{F21}\}_1$, is perpendicular to the axis E–F through the two wishbone mounts.

Thus we can derive the final two equations needed to progress the analytical solution using the familiar approach with the vector dot product to constrain the reaction force at the mount to be perpendicular to an axis through the mounts at, say, point B for the upper wishbone and point F for the lower wishbone:

$$\{F_{F21}\}_1 \bullet \{R_{EF}\}_1 = 0 \tag{4.267}$$

$$\{F_{B31}\}_1 \bullet \{R_{AB}\}_1 = 0 \tag{4.268}$$

Having established the 20 equations required for solution, it is possible to set up the equations starting with the force equilibrium of Body 2:

$$\Sigma\{F_2\}_1 = \{0\}_1 \tag{4.269}$$

$$\{F_{E21}\}_1 + \{F_{F21}\}_1 + \{F_{G24}\}_1 = \{0\}_1 \tag{4.270}$$

$$\begin{bmatrix} F_{E21x} \\ F_{E21y} \\ F_{E21z} \end{bmatrix} + \begin{bmatrix} F_{F21x} \\ F_{F21y} \\ F_{F21z} \end{bmatrix} + \begin{bmatrix} F_{G24x} \\ F_{G24y} \\ F_{G24z} \end{bmatrix} = \begin{bmatrix} 0 \\ 0 \\ 0 \end{bmatrix} \text{N} \tag{4.271}$$

The summation of forces in (4.271) leads to the first set of three equations:

$$\text{Equation 1} \qquad F_{E21x} + F_{F21x} + F_{G24x} = 0 \tag{4.272}$$

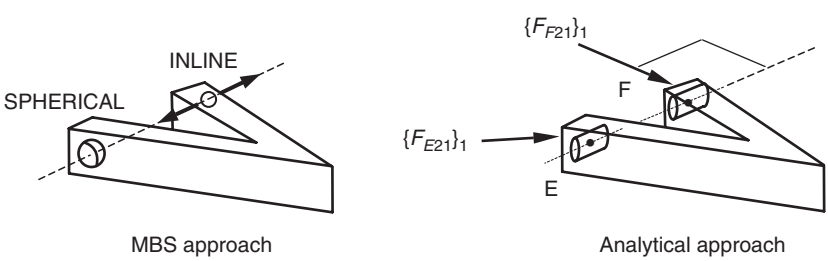

Fig. 4.75 Comparable MBS and analytical wishbone mounting models

Equation 2 $$F_{E21y} + F_{F21y} + F_{G24y} = 0 \tag{4.273}$$

Equation 3 $$F_{E21z} + F_{F21z} + F_{G24z} = 0 \tag{4.274}$$

Taking moments about point G for the forces acting on Body 2 gives

$$\sum\{M_{G2}\}_1 = \{0\}_1 \tag{4.275}$$

$$\{R_{EG}\}_1 \times \{F_{E21}\}_1 + \{R_{FG}\}_1 \times \{F_{F21}\}_1 = \{0\}_1 \tag{4.276}$$

$$\begin{bmatrix} 0 & -9 & -275 \\ 9 & 0 & -115 \\ 275 & 115 & 0 \end{bmatrix} \begin{bmatrix} F_{E21x} \\ F_{E21y} \\ F_{E21z} \end{bmatrix} + \begin{bmatrix} 0 & -9 & -275 \\ 9 & 0 & 115 \\ 275 & -115 & 0 \end{bmatrix} \begin{bmatrix} F_{F21x} \\ F_{F21y} \\ F_{F21z} \end{bmatrix} = \begin{bmatrix} 0 \\ 0 \\ 0 \end{bmatrix} \text{N mm} \tag{4.277}$$

Multiplying out the matrices in (4.277) yields the next set of three equations:

Equation 4 $$-9F_{E21y} - 275F_{E21z} - 9F_{F21y} - 275F_{F21z} = 0 \tag{4.278}$$

Equation 5 $$9F_{E21x} - 115F_{E21z} + 9F_{F21x} + 115F_{F21z} = 0 \tag{4.279}$$

Equation 6 $$275F_{E21x} + 115F_{E21y} + 275F_{F21x} - 115F_{F21y} = 0 \tag{4.280}$$

Consider next Body 3 and the equations required for force equilibrium:

$$\sum\{F_3\}_1 = \{0\}_1 \tag{4.281}$$

$$\{F_{A31}\}_1 + \{F_{B31}\}_1 + f_{S2}\{R_{CI}\}_1 + \{F_{D34}\}_1 = \{0\}_1 \tag{4.282}$$

$$\begin{bmatrix} F_{A31x} \\ F_{A31y} \\ F_{A31z} \end{bmatrix} + \begin{bmatrix} F_{B31x} \\ F_{B31y} \\ F_{B31z} \end{bmatrix} + f_{S2} \begin{bmatrix} 3 \\ -9 \\ -436 \end{bmatrix} + \begin{bmatrix} F_{D34x} \\ F_{D34y} \\ F_{D34z} \end{bmatrix} = \begin{bmatrix} 0 \\ 0 \\ 0 \end{bmatrix} \text{N} \tag{4.283}$$

The summation of forces in (4.283) leads to the next set of three equations:

Equation 7 $$F_{A31x} + F_{B31x} + 3f_{S2} + F_{D34x} = 0 \tag{4.284}$$

Equation 8 $$F_{A31y} + F_{B31y} - 9f_{S2} + F_{D34y} = 0 \tag{4.285}$$

Equation 9 $$F_{A31z} + F_{B31z} - 436f_{S2} + F_{D34z} = 0 \tag{4.286}$$

Taking moments about point D for the forces acting on Body 3 gives

$$\sum\{M_{D3}\}_1 = \{0\}_1 \tag{4.287}$$

$$\{R_{AD}\}_1 \times \{F_{A31}\}_1 + \{R_{BD}\}_1 \times \{F_{B31}\}_1 + \{R_{CD}\}_1 \times f_{S2}\{R_{CI}\}_1 = \{0\}_1 \tag{4.288}$$

$$\begin{bmatrix} 0 & -15 & -239 \\ 15 & 0 & -115 \\ 239 & 115 & 0 \end{bmatrix} \begin{bmatrix} F_{A31x} \\ F_{A31y} \\ F_{A31z} \end{bmatrix} + \begin{bmatrix} 0 & -1 & -239 \\ 1 & 0 & 115 \\ 239 & -115 & 0 \end{bmatrix} \begin{bmatrix} F_{B31x} \\ F_{B31y} \\ F_{B31z} \end{bmatrix} + f_{S2} \begin{bmatrix} 0 & 23 & -98 \\ -23 & 0 & 0 \\ 98 & 0 & 0 \end{bmatrix} \begin{bmatrix} 3 \\ -9 \\ -436 \end{bmatrix} = \begin{bmatrix} 0 \\ 0 \\ 0 \end{bmatrix} \text{N mm} \tag{4.289}$$

Multiplying out the matrices in (4.289) yields the next set of three equations:

Equation 10 $$-15F_{A31y} - 239F_{A31z} - 1F_{B31y} - 239F_{B31z} + 42\,521f_{S2} = 0 \tag{4.290}$$

Equation 11 $$15F_{A31x} - 115F_{A31z} + 1F_{B31x} + 115F_{B31z} - 69f_{S2} = 0 \tag{4.291}$$

Equation 12 $$239F_{A31x} + 115F_{A31y} + 239F_{B31x} - 115F_{B31y} + 294f_{S2} = 0 \tag{4.292}$$

Consider last Body 4 and the equations required for force equilibrium:

$$\sum\{F_4\}_1 = \{0\}_1 \tag{4.293}$$

$$\{F_{P41}\}_1 - \{F_{D34}\}_1 - \{F_{G24}\}_1 - f_{S1}\{R_{JH}\}_1 = \{0\}_1 \tag{4.294}$$

$$\begin{bmatrix} 0 \\ 0 \\ 10\,000 \end{bmatrix} - \begin{bmatrix} F_{D34x} \\ F_{D34y} \\ F_{D34z} \end{bmatrix} - \begin{bmatrix} F_{G24x} \\ F_{G24y} \\ F_{G24z} \end{bmatrix} - f_{S1}\begin{bmatrix} 0 \\ -228 \\ 8 \end{bmatrix} = \begin{bmatrix} 0 \\ 0 \\ 0 \end{bmatrix} \text{N} \tag{4.295}$$

The summation of forces in (4.295) leads to the next set of three equations:

Equation 13 $$-F_{D34x} - F_{G24x} = 0 \tag{4.296}$$

Equation 14 $$-F_{D34y} - F_{G24y} + 228f_{S1} = 0 \tag{4.297}$$

Equation 15 $$-F_{D34z} - F_{G24z} - 8f_{S1} = -10\,000 \tag{4.298}$$

Taking moments about point G for the forces acting on Body 4 gives

$$\sum\{M_{G4}\}_1 = \{0\}_1 \tag{4.299}$$

$$\{R_{PG}\}_1 \times \{F_{P41}\}_1 - \{R_{DG}\}_1 \times \{F_{D34}\}_1 - \{R_{HG}\}_1 \times f_{S1}\{R_{JH}\}_1 = \{0\}_1 \tag{4.300}$$

$$\begin{bmatrix} 0 & 176 & 58 \\ -176 & 0 & 7 \\ -58 & -7 & 0 \end{bmatrix}\begin{bmatrix} 0 \\ 0 \\ 10\,000 \end{bmatrix} - \begin{bmatrix} 0 & -216 & -31 \\ 216 & 0 & 19 \\ 31 & -19 & 0 \end{bmatrix}\begin{bmatrix} F_{D34x} \\ F_{D34y} \\ F_{D34z} \end{bmatrix} - f_{S1}\begin{bmatrix} 0 & -267 & -75 \\ 267 & 0 & 163 \\ 75 & -163 & 0 \end{bmatrix}\begin{bmatrix} 0 \\ -228 \\ 8 \end{bmatrix} = \begin{bmatrix} 0 \\ 0 \\ 0 \end{bmatrix} \text{Nmm} \tag{4.301}$$

Multiplying out the matrices in (4.301) yields the next set of three equations:

Equation 16 $$216F_{D34y} + 31F_{D34z} - 60\,276f_{S1} = -580\,000 \tag{4.302}$$

Equation 17 $$-216F_{D34x} - 19F_{D34z} - 1304f_{S1} = 0 = -70\,000 \tag{4.303}$$

Equation 18 $$-31F_{D34x} + 19F_{D34y} - 37\,164f_{S1} = 0 \tag{4.304}$$

Finally applying the vector dot product to ensure that no thrust for the force $\{F_{F21}\}_1$ acts along the axis E–F gives

$$\{F_{F21}\}_1 \bullet \{R_{EF}\}_1 = 0 \tag{4.305}$$

$$[F_{F21x}F_{F21y}F_{F21z}]\begin{bmatrix}230\\0\\0\end{bmatrix} = 0 \text{ N mm} \tag{4.306}$$

$$230F_{F21x} = 0 \tag{4.307}$$

For this particular suspension system the line E–F is parallel to the model x-axis yielding the trivial result F_{F21x} being equal to zero. In this case we can therefore ignore F_{F21x} in the following matrix solution of the system equations.

The axis A–B for the upper wishbone is not parallel to a model axis and therefore applying the vector dot product to ensure that $\{F_{B31}\}_1$ is perpendicular to the line A–B yields the final equation needed to solve the remaining 19 unknowns:

$$\{F_{B31}\}_1 \bullet \{R_{AB}\}_1 = 0 \tag{4.308}$$

$$[F_{B31x}F_{B31y}F_{B31z}]\begin{bmatrix}230\\0\\14\end{bmatrix} = 0 \text{ N mm} \tag{4.309}$$

$$\text{Equation 19} \quad 230F_{B31x} + 14F_{B31z} = 0 \tag{4.310}$$

The 19 equations can now be set up in matrix form ready for solution:

$$\begin{bmatrix}
0 & 0 & 0 & 0 & 0 & 0 & 0 & 0 & 0 & 1 & 0 & 0 & 0 & 0 & 1 & 0 & 0 & 0 & 0\\
0 & 0 & 0 & 0 & 0 & 0 & 0 & 0 & 0 & 0 & 1 & 0 & 1 & 0 & 0 & 1 & 0 & 0 & 0\\
0 & 0 & 0 & 0 & 0 & 0 & 0 & 0 & 0 & 0 & 0 & 1 & 0 & 1 & 0 & 0 & 1 & 0 & 0\\
0 & 0 & 0 & 0 & 0 & 0 & 0 & 0 & 0 & 0 & -9 & -275 & -9 & -275 & 0 & 0 & 0 & 0 & 0\\
0 & 0 & 0 & 0 & 0 & 0 & 0 & 0 & 0 & 9 & 0 & -115 & 0 & 115 & 0 & 0 & 0 & 0 & 0\\
0 & 0 & 0 & 0 & 0 & 0 & 0 & 0 & 0 & 275 & 115 & 0 & -115 & 0 & 0 & 0 & 0 & 0 & 0\\
1 & 0 & 0 & 1 & 0 & 0 & 1 & 0 & 0 & 0 & 0 & 0 & 0 & 0 & 0 & 0 & 0 & 0 & 3\\
0 & 1 & 0 & 0 & 1 & 0 & 0 & 1 & 0 & 0 & 0 & 0 & 0 & 0 & 0 & 0 & 0 & 0 & -9\\
0 & 0 & 1 & 0 & 0 & 1 & 0 & 0 & 1 & 0 & 0 & 0 & 0 & 0 & 0 & 0 & 0 & 0 & -436\\
0 & -15 & -239 & 0 & -1 & -239 & 0 & 0 & 0 & 0 & 0 & 0 & 0 & 0 & 0 & 0 & 0 & 0 & 42\,521\\
15 & 0 & -115 & 1 & 0 & 115 & 0 & 0 & 0 & 0 & 0 & 0 & 0 & 0 & 0 & 0 & 0 & 0 & -69\\
239 & 115 & 0 & 239 & -115 & 0 & 0 & 0 & 0 & 0 & 0 & 0 & 0 & 0 & 0 & 0 & 0 & 0 & 294\\
0 & 0 & 0 & 0 & 0 & 0 & -1 & 0 & 0 & 0 & 0 & 0 & 0 & 0 & -1 & 0 & 0 & 0 & 0\\
0 & 0 & 0 & 0 & 0 & 0 & 0 & -1 & 0 & 0 & 0 & 0 & 0 & 0 & 0 & -1 & 0 & 228 & 0\\
0 & 0 & 0 & 0 & 0 & 0 & 0 & 0 & -1 & 0 & 0 & 0 & 0 & 0 & 0 & 0 & -1 & -8 & 0\\
0 & 0 & 0 & 0 & 0 & 0 & 0 & 216 & 31 & 0 & 0 & 0 & 0 & 0 & 0 & 0 & 0 & -60\,276 & 0\\
0 & 0 & 0 & 0 & 0 & 0 & -216 & 0 & -19 & 0 & 0 & 0 & 0 & 0 & 0 & 0 & 0 & -1304 & 0\\
0 & 0 & 0 & 0 & 0 & 0 & -31 & 19 & 0 & 0 & 0 & 0 & 0 & 0 & 0 & 0 & 0 & -37\,164 & 0\\
0 & 0 & 0 & 230 & 0 & 14 & 0 & 0 & 0 & 0 & 0 & 0 & 0 & 0 & 0 & 0 & 0 & 0 & 0
\end{bmatrix}
\begin{bmatrix}
F_{A31x}\\F_{A31y}\\F_{A31z}\\F_{B31x}\\F_{B31y}\\F_{B31z}\\F_{D34x}\\F_{D34y}\\F_{D34z}\\F_{E21x}\\F_{E21y}\\F_{E21z}\\F_{F21y}\\F_{F21z}\\F_{G21x}\\F_{G24y}\\F_{G24z}\\f_{S1}\\f_{S2}
\end{bmatrix}
=
\begin{bmatrix}
0\\0\\0\\0\\0\\0\\0\\0\\0\\0\\0\\0\\0\\0\\-10\,000\\-580\,000\\-70\,000\\0\\0
\end{bmatrix} \tag{4.311}$$

Examination of the square matrix in (4.311) indicates a large number of zero terms, hence the matrix is referred to as sparse. As discussed in Chapter 3 this is a typical characteristic of the matrices generated in MBS and is one of the reasons why fast and efficient matrix inversion techniques can be deployed. The overall result is that MBS programs appear to solve quite complex engineering problems with a much lower requirement for computational effort than comparable other CAE methods such as non-linear

finite element analysis. Solving equation (4.311) yields the following answers for the 20 unknowns:

$F_{A31x} = 645.173$ N
$F_{A31y} = 2006.948$ N
$F_{A31z} = 3412.360$ N
$F_{B31x} = -204.112$ N
$F_{B31y} = 3022.800$ N
$F_{B31z} = 3353.266$ N
$F_{D34x} = -557.482$ N
$F_{D34y} = -4680.486$ N
$F_{D34z} = 10\,154.217$ N
$f_{S1} = -1.92786767$ N/mm
$F_{E21x} = -557.482$ N
$F_{E21y} = -1453.911$ N
$F_{E21z} = 47.583$ N
$F_{F21x} = 0$ N
$F_{F21y} = -2787.021$ N
$F_{F21z} = 91.212$ N
$F_{G24x} = 557.482$ N
$F_{G24y} = 4240.9322$ N
$F_{G24z} = -138.979$ N
$f_{S2} = 38.8069785$ N/mm

It is now possible to use the two scale factors found, f_{S1} and f_{S2}, to calculate the force vectors $\{F_{H54}\}_1$ and $\{F_{C37}\}_1$:

$$\{F_{H54}\}_1 = f_{S1}\{R_{JH}\}_1 = -1.92786767 \begin{bmatrix} 0 \\ -228 \\ 8 \end{bmatrix} = \begin{bmatrix} 0 \\ 439.554 \\ -15.942 \end{bmatrix} \text{N} \quad (4.312)$$

$$\{F_{C37}\}_1 = f_{S2}\{R_{CI}\}_1 = 38.8069785 \begin{bmatrix} 3 \\ -9 \\ -436 \end{bmatrix} = \begin{bmatrix} 116.421 \\ -349.263 \\ -16\,919.843 \end{bmatrix} \text{N} \quad (4.313)$$

In summary the force vectors are as follows:

$\{F_{A31}\}_1^T = [645.173 \;\; 2006.948 \;\; 3412.360]$ N

$\{F_{B31}\}_1^T = [-204.112 \;\; 3022.800 \;\; 3353.266]$ N

$\{F_{D34}\}_1^T = [-557.482 \;\; -4680.486 \;\; 10\,154.217]$ N

$\{F_{E21}\}_1^T = [-557.482 \;\; -1453.911 \;\; 47.583]$ N

$\{F_{F21}\}_1^T = [0 \;\; -2787.021 \;\; 91.212]$ N

$\{F_{G24}\}_1^T = [557.482 \;\; 4240.932 \;\; -138.979]$ N

$\{F_{H54}\}_1^T = [0 \;\; 439.554 \;\; -15.942]$ N

$\{F_{C37}\}_1^T = [116.421 \;\; -349.263 \;\; -16919.843]$ N

A comparison of the forces found, at points within the suspension system, from the preceding calculations and those found using an equivalent MSC.ADAMS model is shown in Table 4.14.

4.10.5 Dynamic analysis

Having carried out a static analysis it is possible to progress to a full dynamic analysis of the system. For the suspension system considered here a theoretical solution could be formulated on the basis of the same set of

Table 4.14 Comparison of force vectors computed by theory and MSC.ADAMS

Force	Force vectors					
	Theory			MSC.ADAMS		
	F_x (N)	F_y (N)	F_z (N)	F_x (N)	F_y (N)	F_z (N)
F_{A31}	645.173	2006.948	3412.360	645.173	2006.950	3412.360
F_{B31}	−204.112	3022.800	3353.266	−204.112	3022.800	3353.270
F_{C37}	116.421	−349.263	−16 919.843	116.421	−349.263	−16 919.800
F_{D34}	−557.482	−4680.486	10 154.217	−557.482	−4680.490	10 154.200
F_{E21}	−557.482	−1453.911	47.583	−557.482	−1453.910	47.582
F_{F21}	0.0	−2787.021	91.212	0.0	−2787.020	91.212
F_{G24}	557.482	4240.932	−138.979	557.482	4240.930	−138.794
F_{H54}	0.0	439.554	−15.942	0.0	439.554	−15.423

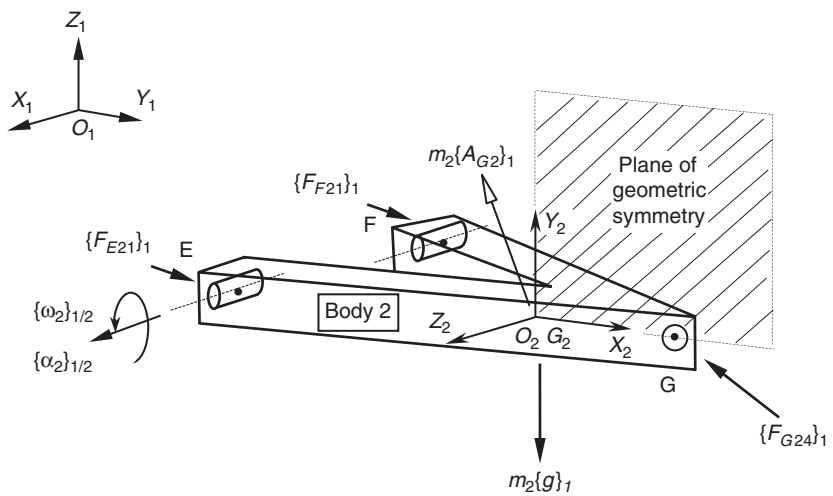

Fig. 4.76 Free-body diagram for suspension lower wishbone Body 2

20 unknown constraint forces as used in the previous static analysis. Referring back to Chapter 2, however, the reader will realize that the addition of inertial forces and the use of a local body centred co-ordinate system for the moment balance will add to the complexity of the solution. For brevity a full theoretical solution will not be performed here but rather the six equations of motion for Body 2 will be set up using, by way of example, the velocities and accelerations found earlier. The process of setting up the equations of motion for the other bodies would follow in a similar manner. Body 2 can be considered in isolation as illustrated with the free-body diagram shown in Figure 4.76.

For the dynamic analysis we can take it that the physical properties of the suspension component, mass, mass moments of inertia, centre of mass location and orientation of the body principal axis system, are all known.

The co-ordinate data provided with this example has only provided definitions so far for the locations of points such as those defining suspension

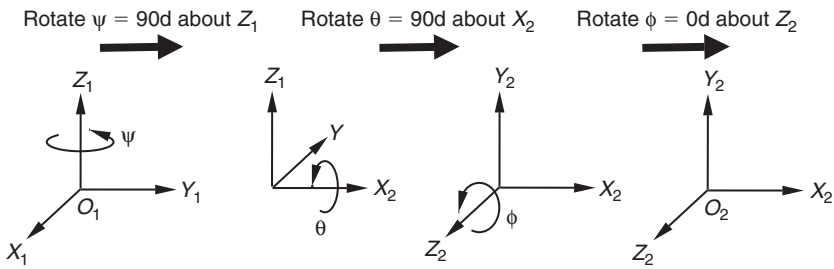

Fig. 4.77 Definition of body principal axis system using Euler angle rotations

mounts and joints connecting the linkages. Mass centre positions have not been provided. For a dynamic analysis the mass centre locations of all moving bodies are required in order to set up the equations of motion. For this example using Body 2 the position of the mass centre G_2 relative to the inertial reference frame O_1 is defined by the position vector $\{R_{G2O1}\}_1$ and assumed to be

$$\{R_{G2O1}\}_1^T = [7 \;\; 500 \;\; -85] \text{ mm}$$

The mass of Body 2, m_2, is taken to be 3.5 kg. It should also be noted from Figure 4.76 that the principal axes of Body 2 are located at the mass centre G_2 and are defined by the reference frame O_2. The transformation from reference frame O_1 to O_2 is obtained through a set of three Euler angle rotations as shown in Figure 4.77.

The mass moments of inertia for Body 2, measured about the principal axes of the body O_2, are taken to be for this example:

$$I_{21} = I_{2xx} = 1.5 \times 10^3 \text{ kg mm}^2$$
$$I_{22} = I_{2yy} = 38 \times 10^3 \text{ kg mm}^2$$
$$I_{23} = I_{2zz} = 38 \times 10^3 \text{ kg mm}^2$$

The X_2Y_2 plane of O_2 is taken to be a plane of geometric symmetry for the part so that all cross products of inertia are zero. The inertia matrix for Body 2 $[I_2]_{2/2}$ measured from and referred to reference frame O_2 is therefore

$$[I_2]_{2/2} = \begin{bmatrix} 1.5 \times 10^3 & 0 & 0 \\ 0 & 38 \times 10^3 & 0 \\ 0 & 0 & 38 \times 10^3 \end{bmatrix} \text{kg mm}^2 \tag{4.314}$$

From the previous velocity and acceleration analysis we also have

$$\{\omega_2\}_1^T = [12.266 \;\; 0 \;\; 0] \text{ rad/s}$$

$$\{\alpha_2\}_1^T = [-10.642 \;\; 0 \;\; 0] \text{ rad/s}^2$$

Before progressing to set up the equations of motion we need to do one more calculation to find the acceleration $\{A_{G2}\}_1$ of the mass centre for Body 2:

$$\{A_{G2}\}_1 = \{A_{G2E}\}_1 = \{\omega_2\}_1 \times \{V_{G2}\}_1 + \{\alpha_2\}_1 \times \{R_{G2E}\}_1 \tag{4.315}$$

where

$$\{V_{G2}\}_1 = \{V_{G2E}\}_1 = \{\omega_2\}_1 \times \{R_{G2E}\}_1 \tag{4.316}$$

$$\begin{bmatrix} V_{G2x} \\ V_{G2y} \\ V_{G2z} \end{bmatrix} = \begin{bmatrix} 0 & 0 & 0 \\ 0 & 0 & -12.266 \\ 0 & 12.266 & 0 \end{bmatrix} \begin{bmatrix} -115 \\ 155 \\ -5 \end{bmatrix} = \begin{bmatrix} 0 \\ 61.33 \\ 1901.23 \end{bmatrix} \text{mm/s} \tag{4.317}$$

therefore

$$\begin{bmatrix} A_{G2x} \\ A_{G2y} \\ A_{G2z} \end{bmatrix} = \begin{bmatrix} 0 & 0 & 0 \\ 0 & 0 & -12.266 \\ 0 & 12.266 & 0 \end{bmatrix} \begin{bmatrix} 0.0 \\ 61.33 \\ 1901.23 \end{bmatrix} + \begin{bmatrix} 0 & 0 & 0 \\ 0 & 0 & 10.642 \\ 0 & -10.642 & 0 \end{bmatrix} \begin{bmatrix} -115 \\ 155 \\ -5 \end{bmatrix} \text{mm/s}^2 \tag{4.318}$$

$$\begin{bmatrix} A_{G2x} \\ A_{G2y} \\ A_{G2z} \end{bmatrix} = \begin{bmatrix} 0 \\ -23\,372.797 \\ -869.336 \end{bmatrix} \text{mm/s}^2 \tag{4.319}$$

Before progressing further it is important to refer back to Chapter 3 and state that Newton's second law is only applicable for a consistent set of units. In effect this means either converting from millimetres to metres before carrying out the dynamic analysis or incorporating a units consistency factor *UCF* in the equations of motion:

$$\sum \{F_2\}_1 = \frac{m_2\{A_{G2}\}_1}{UCF} \tag{4.320}$$

Since our current dimensions for length are in mm and we need to work in SI our *UCF* value here is 1000. So converting $\{A_{G2}\}_1$ to m/s^2 gives

$$\begin{bmatrix} A_{G2x} \\ A_{G2y} \\ A_{G2z} \end{bmatrix} = \begin{bmatrix} 0 \\ -23.373 \\ -0.869 \end{bmatrix} \text{m/s}^2 \tag{4.321}$$

We also need to define a vector $\{g\}_1$ for gravitational acceleration which for the reference frame O_1 used here would be

$$\begin{bmatrix} g_x \\ g_y \\ g_z \end{bmatrix} = \begin{bmatrix} 0 \\ 0 \\ -9.81 \end{bmatrix} \text{m/s}^2 \tag{4.322}$$

For Body 2 summing forces and applying Newton's second law gives

$$\sum \{F_2\}_1 = m_2\{A_{G2}\}_1 \tag{4.323}$$

$$\{F_{E21}\}_1 + \{F_{F21}\}_1 + \{F_{G24}\}_1 + m_2\{g\}_1 = m_2\{A_{G2}\}_1 \tag{4.324}$$

$$\begin{bmatrix} F_{E21x} \\ F_{E21y} \\ F_{E21z} \end{bmatrix} + \begin{bmatrix} F_{F21x} \\ F_{F21y} \\ F_{F21z} \end{bmatrix} + \begin{bmatrix} F_{G24x} \\ F_{G24y} \\ F_{G24z} \end{bmatrix} + 3.5 \begin{bmatrix} 0 \\ 0 \\ -9.81 \end{bmatrix} = 3.5 \begin{bmatrix} 0 \\ -23.373 \\ -0.869 \end{bmatrix} \text{N} \tag{4.325}$$

The summation of forces in (4.325) leads to the first set of three equations:

$$\text{Equation 1} \qquad F_{E21x} + F_{F21x} + F_{G24x} = 0 \tag{4.326}$$

$$\text{Equation 2} \qquad F_{E21y} + F_{F21y} + F_{G24y} = -81.806 \tag{4.327}$$

$$\text{Equation 3} \qquad F_{E21z} + F_{F21z} + F_{G24z} = 31.294 \tag{4.328}$$

For the rotational equations it is convenient to refer the vectors to the reference frame O_2 fixed in and rotating with Body 2. The rotational equations of motion for Body 2 may be written as Euler's equations of motion in vector form as

$$\sum \{M_{G2}\}_{1/2} = [I_2]_{2/2}\{\alpha_2\}_{1/2} + [\omega_2]_{1/2}[I_2]_{2/2}\{\omega_2\}_{1/2} \tag{4.329}$$

Before progressing the angular velocity vector $\{\omega_2\}_1$ and angular acceleration vector $\{\alpha_2\}_1$ need to be transformed from reference frame O_1 to O_2 to give $\{\omega_2\}_{1/2}$ and $\{\alpha_2\}_{1/2}$. By inspection it can be seen from Figure 4.77 that the transformation is trivial and that due to the wishbone geometry and constraints ω_{2x} and α_{2x} in frame O_1 simply become ω_{2z} and α_{2z} when referenced to frame O_2. The process of vector transformation described in Chapter 2 will, however, be applied to illustrate the process for more general geometries. In this case we have only two rotations to account for, the first being 90 degrees ψ about the z-axis followed by a 90 degrees rotation θ about the x-axis. Thus for the angular velocity vector we have:

$$\{\omega_2\}_{1/2} = \begin{bmatrix} \omega_{2x2} \\ \omega_{2y2} \\ \omega_{2z2} \end{bmatrix} = \begin{bmatrix} 1 & 0 & 0 \\ 0 & \cos\theta & \sin\theta \\ 0 & -\sin\theta & \cos\theta \end{bmatrix} \begin{bmatrix} \cos\psi & \sin\psi & 0 \\ -\sin\psi & \cos\psi & 0 \\ 0 & 0 & 1 \end{bmatrix} \begin{bmatrix} \omega_{2x1} \\ \omega_{2y1} \\ \omega_{2z1} \end{bmatrix} \text{rad/s} \tag{4.330}$$

$$\{\omega_2\}_{1/2} = \begin{bmatrix} \omega_{2x2} \\ \omega_{2y2} \\ \omega_{2z2} \end{bmatrix} = \begin{bmatrix} 1 & 0 & 0 \\ 0 & 0 & 1 \\ 0 & -1 & 0 \end{bmatrix} \begin{bmatrix} 0 & 1 & 0 \\ -1 & 0 & 0 \\ 0 & 0 & 1 \end{bmatrix} \begin{bmatrix} 12.266 \\ 0 \\ 0 \end{bmatrix} = \begin{bmatrix} 0 \\ 0 \\ 12.266 \end{bmatrix} \text{rad/s} \tag{4.331}$$

The transformation of the angular acceleration vector takes place in a similar manner so that we have:

$$\{\omega_2\}_{1/2}^T = [0 \quad 0 \quad 12.266] \text{ rad/s}$$

$$\{\alpha_2\}_{1/2}^T = [0 \quad 0 \quad -10.642] \text{ rad/s}^2$$

Referring back to equation (4.329) and the free-body diagram in Figure 4.76 we can see that it is convenient to sum moments of forces acting on Body 2 about the mass centre G_2 to eliminate the inertial force $m_2\{A_2\}_1$ acting through the mass centre. In order to carry out the moment balance we will need to establish new relative position vectors $\{R_{EG2}\}_{1/2}$, $\{R_{FG2}\}_{1/2}$ and $\{R_{GG2}\}_{1/2}$. We will also need to define the vector components in metres for consistency. Working first in frame O_1 we have:

$$\{R_{EG2}\}_1^T = [0.115 \quad -0.155 \quad 0.005] \text{ m}$$
$$\{R_{FG2}\}_1^T = [-0.115 \quad -0.155 \quad 0.005] \text{ m}$$
$$\{R_{GG2}\}_1^T = [0.0 \quad 0.120 \quad -0.004] \text{ m}$$

Applying a vector transformation for the vector $\{R_{EG2}\}_1$ from frame O_1 to O_2 gives

$$\{R_{EG2}\}_{1/2} = \begin{bmatrix} 1 & 0 & 0 \\ 0 & 0 & 1 \\ 0 & -1 & 0 \end{bmatrix} \begin{bmatrix} 0 & 1 & 0 \\ -1 & 0 & 0 \\ 0 & 0 & 1 \end{bmatrix} \begin{bmatrix} 0.115 \\ -0.155 \\ 0.005 \end{bmatrix} = \begin{bmatrix} -0.155 \\ 0.005 \\ 0.115 \end{bmatrix} \text{m} \tag{4.332}$$

Applying the same vector transformation to $\{R_{FG2}\}_{1/2}$ and $\{R_{GG2}\}_{1/2}$ gives us the three relative position vectors, referenced to the correct frame O_2 and in consistent units, needed for the moment balance:

$$\{R_{EG2}\}_{1/2}^T = 10^{-3}[-155 \quad 5 \quad 115] \text{ m}$$

$$\{R_{FG2}\}_{1/2}^T = 10^{-3}[-155 \quad 5 \quad -115] \text{ m}$$

$$\{R_{GG2}\}_{1/2}^T = 10^{-3}[120 \quad 4 \quad 0] \text{ m}$$

Before writing the rotational equations of motion we can first determine the moment balance of the constraint forces acting at E, F and G:

$$\begin{aligned} \sum \{M_{G2}\}_{1/2} &= \{R_{EG2}\}_{1/2} \times \{F_{E21}\}_{1/2} + \{R_{FG2}\}_{1/2} \times \{F_{F21}\}_{1/2} + \{R_{GG2}\}_{1/2} \times \{F_{G24}\}_{1/2} \\ &= 10^{-3} \begin{bmatrix} 0 & -115 & 5 \\ 115 & 0 & 155 \\ -5 & -155 & 0 \end{bmatrix} \begin{bmatrix} F_{E21x2} \\ F_{E21y2} \\ F_{E21z2} \end{bmatrix} + 10^{-3} \begin{bmatrix} 0 & 115 & 5 \\ -115 & 0 & 155 \\ -5 & -155 & 0 \end{bmatrix} \begin{bmatrix} F_{F21x2} \\ F_{F21y2} \\ F_{F21z2} \end{bmatrix} \\ &\quad + 10^{-3} \begin{bmatrix} 0 & -4 & 0 \\ 4 & 0 & -120 \\ 0 & 120 & 0 \end{bmatrix} \begin{bmatrix} F_{G24x2} \\ F_{G24y2} \\ F_{G24z2} \end{bmatrix} \text{Nm} \end{aligned} \tag{4.333}$$

Considering next the rotational inertial terms we have:

$$\sum \{M_{G2}\}_{1/2} = [I_2]_{2/2}\{\alpha_2\}_{1/2} + [\omega_2]_{1/2}[I_2]_{2/2}\{\omega_2\}_{1/2} \tag{4.334}$$

$$\sum\{M_{G2}\}_{1/2} = \begin{bmatrix} I_{2xx} & 0 & 0 \\ 0 & I_{2yy} & 0 \\ 0 & 0 & I_{2zz} \end{bmatrix} \begin{bmatrix} \alpha_{2x2} \\ \alpha_{2y2} \\ \alpha_{2z2} \end{bmatrix} + \begin{bmatrix} 0 & -\omega_{2z2} & \omega_{2y2} \\ \omega_{2z2} & 0 & -\omega_{2x2} \\ -\omega_{2y2} & \omega_{2x2} & 0 \end{bmatrix} \begin{bmatrix} I_{2xx} & 0 & 0 \\ 0 & I_{2yy} & 0 \\ 0 & 0 & I_{2zz} \end{bmatrix} \begin{bmatrix} \omega_{2x2} \\ \omega_{2y2} \\ \omega_{2z2} \end{bmatrix} \text{Nm}$$

$$= \begin{bmatrix} 1.5 \times 10^{-3} & 0 & 0 \\ 0 & 38 \times 10^{-3} & 0 \\ 0 & 0 & 38 \times 10^{-3} \end{bmatrix} \begin{bmatrix} 0 \\ 0 \\ -10.642 \end{bmatrix} + \begin{bmatrix} 0 & -12.266 & 0 \\ 12.266 & 0 & 0 \\ 0 & 0 & 0 \end{bmatrix} \begin{bmatrix} 1.5 \times 10^{-3} & 0 & 0 \\ 0 & 38 \times 10^{-3} & 0 \\ 0 & 0 & 38 \times 10^{-3} \end{bmatrix} \begin{bmatrix} 0 \\ 0 \\ 12.266 \end{bmatrix} \text{Nm} \tag{4.335}$$

Equating (4.333) with (4.335) yields the rotational equations of motion for Body 2:

Equation 4

$$(-115F_{E21y2} + 5F_{E21z2} + 115F_{F21y2} + 5F_{F21z2} - 4F_{G24y2}) \times 10^{-3} = 0 \tag{4.336}$$

Equation 5

$$(115F_{E21x2} + 155F_{E21z2} - 115F_{F21x2} + 155F_{F21z2} + F_{G24x2} - 0.120F_{G24z2}) \times 10^{-3} = 0 \tag{4.337}$$

Equation 6

$$(-5F_{E21x2} - 155F_{E21y2} - 5F_{F21x2} - 155F_{F21y2} + 120F_{G24y2}) \times 10^{-3} = -404.396 \times 10^{-3} \tag{4.338}$$

At this stage the observant reader will note the inertial terms in (4.335) have only yielded a numerical value for the moment balance about the principal Z_2-axis. This makes sense as the Z_2-axis has been chosen to be parallel to the fixed axis of body rotation through points E and F. In the absence of components of angular velocity or acceleration about X_2 and Y_2 equations (4.336) and (4.337) above simplify to a static moment balance. It should also be noted that when rotation is constrained about a single principal axis the right-hand part of (4.334), $[\omega_2]_{1/2}[I_2]_{2/2}[\omega_2]_{1/2}$, is entirely zero to indicate a lack of gyroscopic terms in the absence of rotational coupling. Choosing a body centred axis system for the upper wishbone Body 3, with an axis parallel to an axis through points A and B, would yield a similar formulation. This would not, however, be the case, for example, if we continued to set up the equations for Body 4 where there is no single fixed axis of rotation.

Before leaving the area of formulating equations of motion for dynamic analysis we should also ensure that the impression is not given that the use

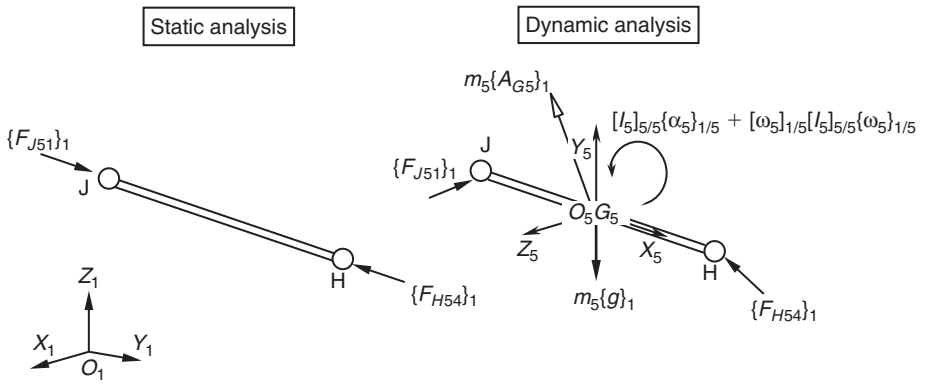

Fig. 4.78 Free-body diagrams for static and dynamic analysis of the tie rod

of a two-force body type scale factor, as used for the static analysis with the tie rod Body 5, can be employed here. Figure 4.78 shows free-body diagrams for both a static and dynamic analysis of the tie rod. For the static analysis it can be seen that with the assumption that gravity is ignored the reaction forces at J and H act along the axis of the tie rod allowing a scale factor to be used. For the dynamic analysis it can be seen that the inertial forces do not allow such an assumption and that a set of six equations of motion for Body 5 will be required for the solution.

If at this stage we ignore the mass effects of the damper assembly we can represent the force $\{F_{C37}\}_1$ acting on Body 3 at point C using as before a scalar. Since the line of action of $\{F_{C37}\}_1$ is known to act along the line C–I it is possible to define the force using the magnitude of the magnitude $|F_{C37}|$ factored with the unit vector $\{l_{CI}\}_1$, acting along the line from I to C, as follows:

$$\{F_{C37}\}_1 = F_s\{l_{CI}\}_1 \tag{4.339}$$

where F_s is the magnitude of the force $|F_{C37}|$ with a sign assigned that is positive if the force acts towards point C from I. In this analysis, and under normal driving conditions, F_s will be positive.

A consideration of the complete suspension system indicates that the following set of 25 unknowns must be found to solve for dynamic forces:

F_{A31x}, F_{A31y}, F_{A31z}
F_{B31x}, F_{B31y}, F_{B31z}
F_{D43x}, F_{D43y}, F_{D43z}
F_{E21x}, F_{E21y}, F_{E21z}
F_{F21x}, F_{F21y}, F_{F21z}
F_{G24x}, F_{G24y}, F_{G24z}
F_{H54x}, F_{H54y}, F_{H54z}
F_{J51x}, F_{J51y}, F_{J51z}
F_s

Each moving body, Bodies 2, 3, 4 and 5, yields six equations of motion that can be used to solve the dynamic analysis. Using the same approach as

demonstrated with Body 2 the following equations would be generated for all the bodies:

$$\sum \{F_2\}_1 = m_2\{A_{G2}\}_1 \tag{4.340}$$

$$\sum \{M_{G2}\}_{1/2} = [I_2]_{2/2}\{\alpha_2\}_{1/2} + [\omega_2]_{1/2}[I_2]_{2/2}\{\omega_2\}_{1/2} \tag{4.341}$$

$$\sum \{F_3\}_1 = m_3\{A_{G3}\}_1 \tag{4.342}$$

$$\sum \{M_{G3}\}_{1/3} = [I_3]_{3/3}\{\alpha_3\}_{1/3} + [\omega_3]_{1/3}[I_3]_{3/3}\{\omega_3\}_{1/3} \tag{4.343}$$

$$\sum \{F_4\}_1 = m_4\{A_{G4}\}_1 \tag{4.344}$$

$$\sum \{M_{G4}\}_{1/4} = [I_4]_{4/4}\{\alpha_4\}_{1/4} + [\omega_4]_{1/4}[I_4]_{4/4}\{\omega_4\}_{1/4} \tag{4.345}$$

$$\sum \{F_5\}_1 = m_5\{A_{G5}\}_1 \tag{4.346}$$

$$\sum \{M_{G5}\}_{1/5} = [I_5]_{5/5}\{\alpha_5\}_{1/5} + [\omega_5]_{1/5}[I_5]_{5/5}\{\omega_5\}_{1/5} \tag{4.347}$$

The equations of motion above yield 24 equations leaving one further equation to be derived to solve the 25 unknowns. The final equation allows us to formulate the scalar F_s with the appropriate magnitude and sign to represent the force acting along the strut. Referring back to the discussion of spring and damper forces in Chapter 3 we are reminded that for a linear formulation based on the spring stiffness k, free length L, and the damping coefficient c, of the damper we can formulate the force using

$$F_s = k(L - |R_{CI}|) - c \times VR_{CI} \tag{4.348}$$

The term $(L - |R_{CI}|)$ represents the deflection of the spring relative to the free length. The term VR_{CI} represents the radial line of sight velocity. This is effectively the magnitude of the velocity vector $\{V_{CI}\}_1$ given a sign so that VR_{CI} is negative when points C and I are approaching each other in bump and is positive when separating in rebound. The result of this is that the component of spring force is positive when the spring is compressed and the damper force component is positive during bump movement.

4.10.6 Geometry analysis

The preceding use of vectors to carry out three-dimensional velocity, acceleration, static force and dynamic force analyses of the double wishbone suspension system should have provided the reader with an insight into the computational work performed by an MBS program during the solution phase. An important aspect of this is that in all the preceding analyses the geometry has been assumed fixed throughout the solution. This is in fact not fully representative of the problem. For example, for the static analysis the damper acting between C and I is assumed to be locked so that although

the reaction force at C can be determined the suspension does not move despite a considerable vertical load being applied at the tyre contact patch.

In reality the damper has a sliding degree of freedom that allows the length C–I to shorten until the additional compression of the spring produces the force required for the suspension system to be in static equilibrium. This mechanism is the key behind the iterations described in Chapter 3 that take place during a solution step at a given point in time. In effect all the preceding vector analysis can be considered typical of the computations during one of many analysis iterations at a given point in time.

To demonstrate the final phase in this process a vector analysis will now be performed to determine the new position of the movable points throughout the suspension system due to a deflection in the suspension spring unit. In this case we will shorten the line C–I by 100 mm taking this to be representative of the movement for this suspension with typical spring and damper properties. We can consider that we are looking here at the suspension moving between the defined or model input position, to the full bump position. During a typical analysis iteration the movement would in fact be far less than this but the following calculations will illustrate the process and complete our treatment of vector analysis in this chapter.

Before proceeding with the analysis Figure 4.79 is provided to remind us of the suspension configuration, the point labelling system and to illustrate the shortening of the damper unit.

In order to establish the position of any point that has moved in the suspension system we must work from three points for which the co-ordinates

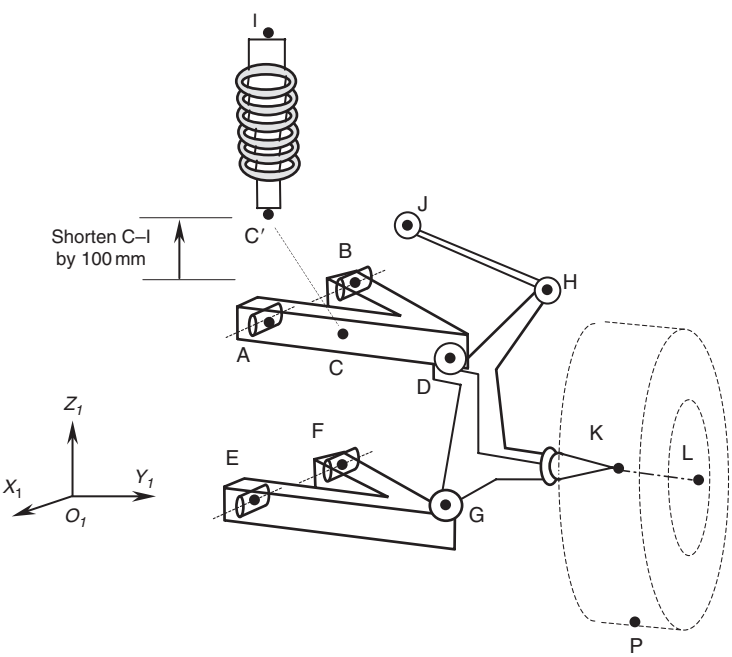

Fig. 4.79 Shortening of damper unit for double wishbone suspension geometry analysis

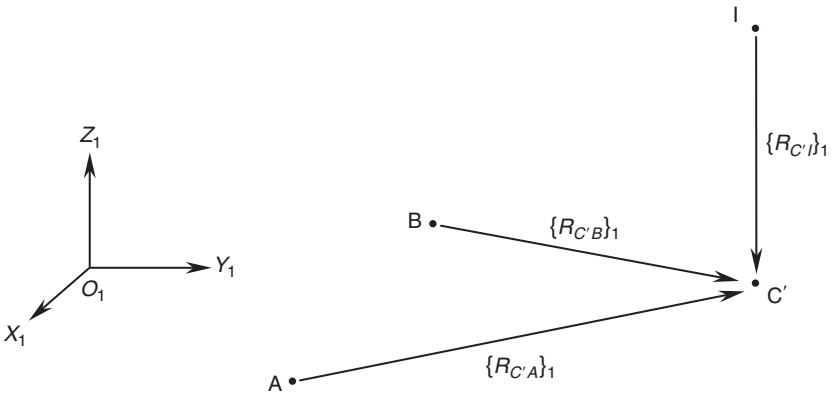

Fig. 4.80 Locating new point C′ by triangulation

are already established. To begin the analysis we can consider finding the new position of point C′ working from three points A, B and I that are fixed and cannot move as shown in Figure 4.80.

In this example the positions of A, B and I are known as are the lengths *AC*, *BC* and *IC′*. The length *IC′* takes into account the shortening of the strut by 100 mm but the lengths *AC* and *BC* are unchanged. The new position of *C′* is unknown and must be solved. In terms of vectors this can be expressed using the following known inputs:

$\{R_A\}_1^T = [Ax\ Ay\ Az]$
$\{R_B\}_1^T = [Bx\ By\ Bz]$
$\{R_I\}_1^T = [Ix\ Iy\ Iz]$
$|R_{CA}|$
$|R_{CB}|$
$|R_{C'I}|$

In order to solve the three unknowns $C'x$, $C'y$ and $C'z$, which are the components of the position vector $\{R_{C'}\}_1$, it is necessary to set up three equations as follows:

$$|R_{C'A}|^2 = (Cx - Ax)^2 + (C'y - Ay)^2 + (C'z - Az)^2 \tag{4.349}$$

$$|R_{C'B}|^2 = (C'x - Bx)^2 + (C'y - By)^2 + (C'z - Bz)^2 \tag{4.350}$$

$$|R_{C'I}|^2 = (C'x - Ix)^2 + (C'y - Iy)^2 + (C'z - Iz)^2 \tag{4.351}$$

In Chapter 2 it was demonstrated that the simultaneous solution of equations (4.349) to (4.251) results in a quadratic with two solutions, one of which will be correct, for $C'x$, $C'y$ and $C'z$. Having demonstrated in Chapter 2 the manipulations required to solve a set of three such equations we will content ourselves here to show the process followed to set up all the equations for this suspension system but use a computer program written in Basic to solve them.

Figure 4.81 illustrates the process that would be followed to solve the co-ordinates of all movable points where at each stage the positions of the three reference points must be either fixed or previously found if movable.

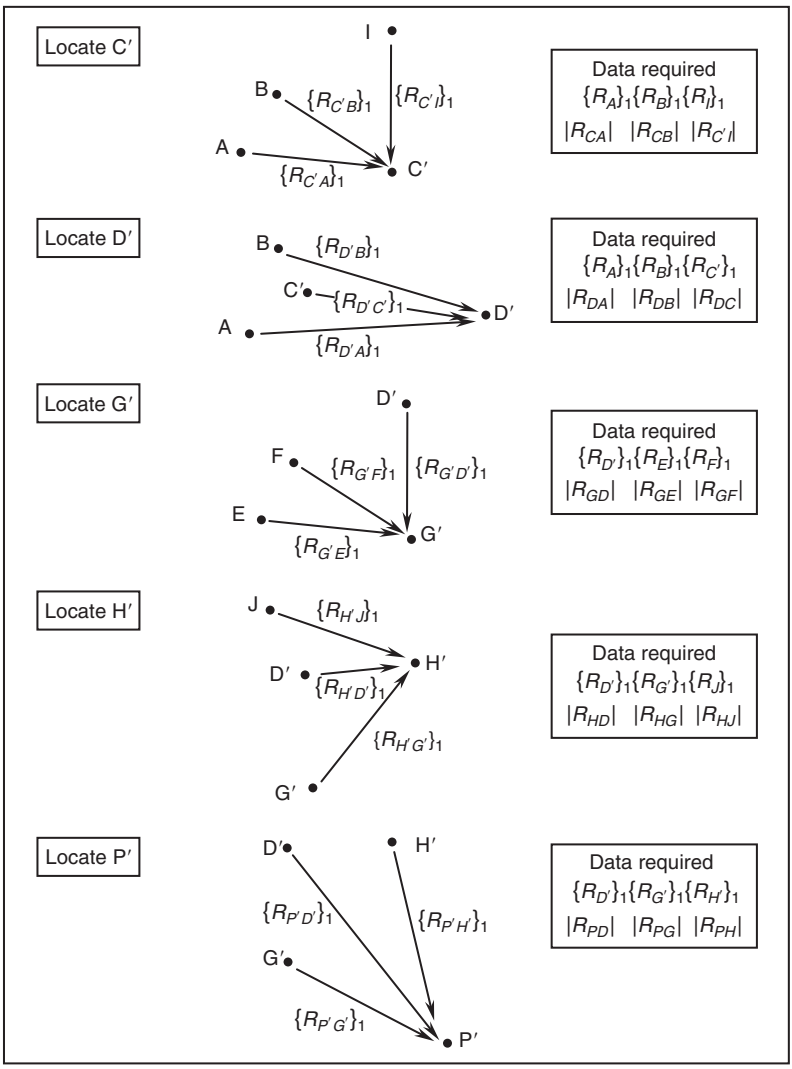

Fig. 4.81 Calculation sequence to solve double wishbone suspension geometry

The length between each of the three reference points and the movable point must also be fixed and known. This will only work if the movable point lies on the same rigid body as each of the reference points.

In addition to locating the movable points just described we will also need to determine the new positions K′ and L′ of the two points located on the wheel spin axis as shown in Figure 4.82. These two positions will be used with the starting locations K and L to determine the change in steer and camber angle between the two suspension configurations.

Having followed the process outlined here we obtain the new positions shown in Table 4.15. The results obtained using vector theory are compared

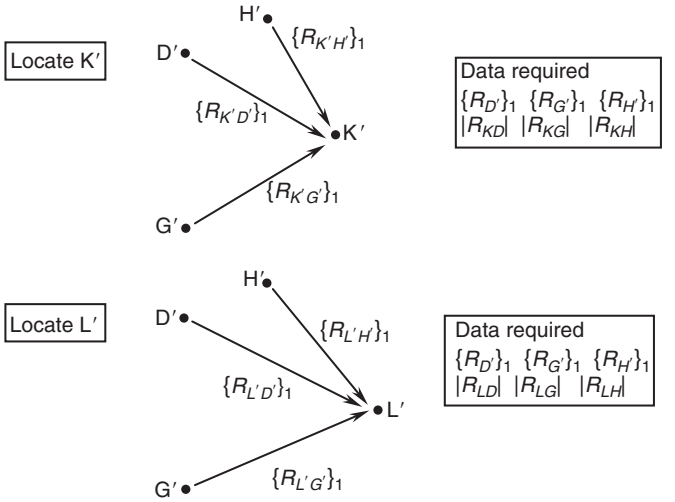

Figure 4.82 Location of points K′ and L′ on the wheel spin axis

Table 4.15 Comparison of movable point locations computed by theory and MSC.ADAMS

Point	Suspension position vectors					
	Theory			MSC.ADAMS		
	R_x (mm)	R_y (mm)	R_z (mm)	R_x (mm)	R_y (mm)	R_z (mm)
C′	−18.133	476.250	204.752	−18.133	476.250	204.753
D′	−21.719	534.601	286.699	−21.721	534.604	286.696
G′	7.0	573.627	73.087	7.0	573.629	73.084
H′	−168.982	493.368	330.131	−168.984	493.371	330.127
P′	8.978	638.864	−100.491	8.979	638.867	−100.494
K′	−4.232	550.301	160.835	−4.233	550.305	160.832
L′	−1.781	628.197	164.076	−1.783	628.199	164.073

with those from the equivalent MSC.ADAMS model where a motion input has been used to shorten the strut by 100 mm.

Having calculated the new positions of all the movable nodes the movement of the tyre contact patch, in this case taken to be point P, could be used to establish, for example, the lateral movement or half-track change. Referring back to Chapter 2 we can also use the methods described there to determine the bump steer as shown in Figure 4.83.

The change in steer angle or bump steer can be determined by finding the angle δ between the projection of KL and $K'L'$ onto the global X_1Y_1 plane. The projection is achieved after setting the z co-ordinates of all four position vectors to zero and then applying the vector dot product as shown in equation (4.352):

$$\cos\delta = \{R_{KL}\}_1 \bullet \{R_{K'L'}\}/|R_{KL}|\,|R_{K'L'}| \tag{4.352}$$

The change in camber angle γ is obtained in a similar manner where the projection this time takes place in the global Y_1Z_1 plane by setting all the x co-ordinates to zero.

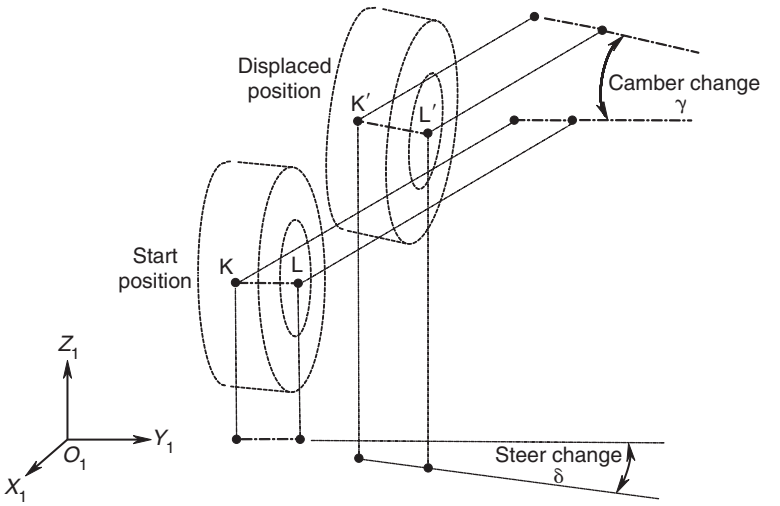

Fig. 4.83 Using vectors to determine camber and steer angle change

Table 4.16 Comparison of steer and camber angle change computed by theory and MSC.ADAMS

	Theory Change in angle (degrees)	**MSC.ADAMS Change in angle (degrees)**
Steer	1.802	1.802
Camber	−2.383	−2.382

$$\cos\gamma = \{R_{KL}\}_1 \bullet \{R_{K'L'}\}/|R_{KL}|\,|R_{K'L'}| \tag{4.353}$$

Note that in Figure 4.83 the changes in steer and camber angles are both shown as positive for this suspension located on the front left-hand side of the vehicle with the X_1-axis pointing forwards. A comparison of the answers found by theory with those from MSC.ADAMS is given in Table 4.16.

5 Tyre characteristics and modelling

5.1 Introduction

The handling performance and directional response of a vehicle are greatly influenced by the mechanical force and moment generating characteristics of the tyres. In road vehicle dynamics the manner in which a vehicle accelerates, brakes and corners is controlled by the forces generated over four relatively small tyre contact patches. If the tread pattern and the road texture are also considered it is clear that the area of frictional contact is reduced even more significantly. Figure 5.1 shows the deflection of a vehicle's tyres under hard cornering and helps to illustrate the significant requirements on the tyre to produce forces that control the relatively large mass of the vehicle.

It is not intended here to discuss the construction of the tyre carcass, materials or tread pattern. This is addressed by more general texts on vehicle dynamics (Gillespie, 1992) or more focused books on the subject of tyres (French, 1989; Moore, 1975). Rather this chapter will start by describing the mechanisms required to generate the vertical tyre forces that support the vehicle, the longitudinal forces required for driving and braking and the lateral forces needed for cornering. The distribution of pressure and stress will also generate local moments acting at the tyre contact patch. A good

Fig. 5.1 An example of tyre deflection under hard cornering (courtesy of *Auto Motor und Sport*)

understanding of these force and moment characteristics is essential before introducing the various mathematical tyre models available and describing the methods used to implement these with MBS vehicle models.

Before a computer simulation can be performed the tyre force and moment characteristics must be estimated or obtained from experimental tests. A traditional approach is to test the tyre using a tyre test machine and to measure the resulting force and moment components for various camber angles, slip angles and values of vertical force. The measured data is set up in tabular form, which is interpolated during the computer simulation in order to transfer the forces to the full vehicle model. Alternatively mathematical functions are used to fit equations to the measured test data. These equations provide a mathematical tyre model that can be incorporated into the full vehicle model. This method requires the generation of a number of parameters that must be derived from the measured data before the simulation can proceed. The quality of the model will be a compromise between the accuracy of the fit, relevance of the parameters, and the availability of methods to generate the parameters.

5.2 Tyre axis systems and geometry

5.2.1 The SAE and ISO tyre axis systems

To assist with the description of the forces and moments generated by a tyre, an axis system shown in simplified form in Figure 5.2 has been defined by the SAE (1976). In this system the *X*-axis is the intersection of the wheel plane and the road plane with the positive direction taken for the wheel moving forward. The *Z*-axis is perpendicular to the road plane with a positive direction assumed to be acting downwards. The *Y*-axis is in the road plane, its direction dictated by the use of a right-handed orthogonal axis system. The angles α and γ represent the slip angle and camber angle respectively. The SAE system will be used throughout this text unless stated.

It should be noted that not all practitioners adhere rigidly to this system in their publications and another system, the ISO tyre system, is gaining favour. This system, shown simplified in Figure 5.3, is likely to become the standard for future tyre models.

It will be seen later that distortions in the tyre carcass will cause the contact patch to move away from the rigid wheel plane shown in Figures 5.2 and 5.3. Although the components of force are still assumed to act through the contact point P the distortions will introduce offsets and additional components of moment also acting about the point P.

5.2.2 Definition of tyre radii

The definition of tyre radii is important for the formulation of slip in the contact patch. In general we consider a tyre to have an unloaded radius, a loaded radius and an effective rolling radius. The unloaded tyre radius, R_u, is straightforward to comprehend and is shown in Figure 5.4. For a rigid disc with radius R_u rolling forward with no sliding (fully geared to the road), during one revolution the disc will move forward a distance $2\pi R_u$.

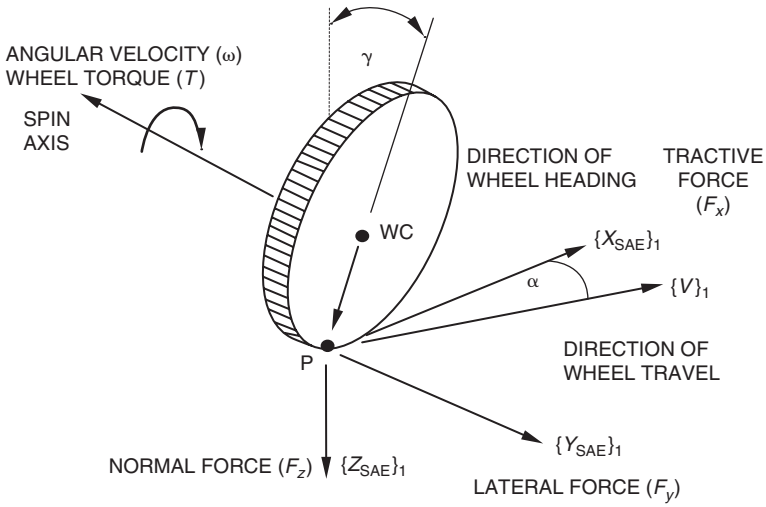

Fig. 5.2 SAE tyre axis system

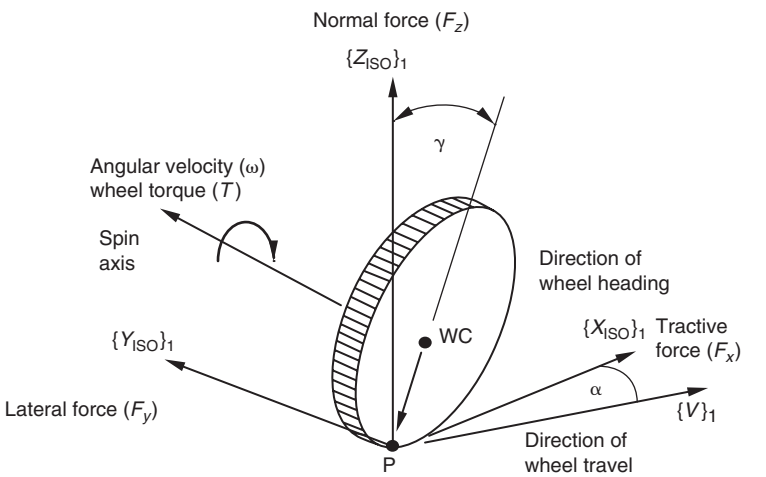

Fig. 5.3 ISO tyre axis system

As can be seen from Figure 5.4, due to tyre deflection the distance moved forward will be less than for the rigid disc and can be related to the effective rolling radius giving

$$R_u > R_e > R_l \tag{5.1}$$

Another definition of effective rolling radius is provided by Moore (1975), this being the distance from the wheel centre to a point C where the distance AC is taken to be one quarter of the total tyre contact patch length AB.

The following are other definitions related to tyre radius provided in SAE J670e (SAE Publication, 1976):

(i) The loaded radius, R_l, is the distance from the centre of the tyre contact patch to the wheel centre measured in the wheel plane.

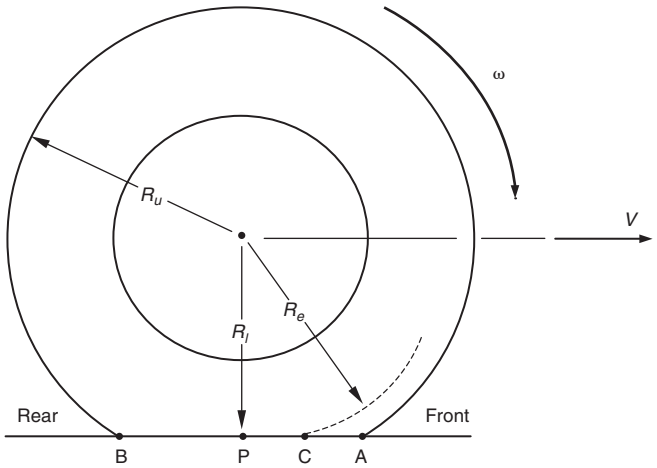

Fig. 5.4 Definition of tyre radii

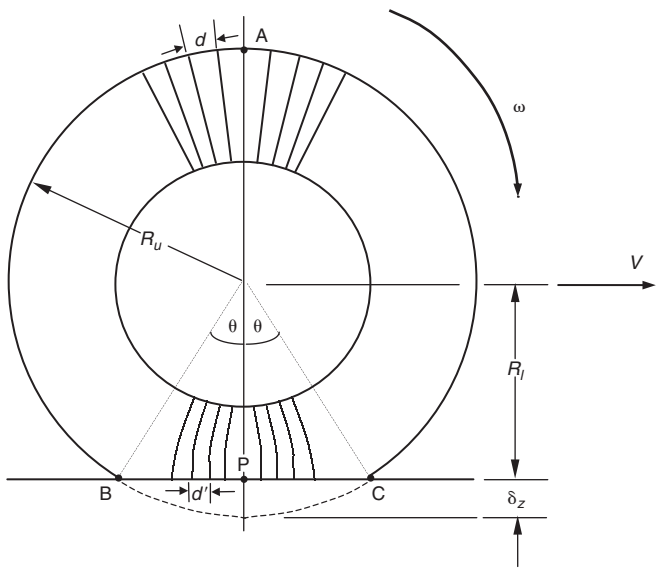

Fig. 5.5 Deformation of rolling tyre

(ii) The static loaded radius is the *loaded radius* of a stationary tyre inflated to the normal recommended pressure.

(iii) The effective rolling radius, R_e, is the ratio of the linear velocity of the wheel centre in the X_{SAE} direction to the angular velocity of the wheel.

A more detailed treatment of effective rolling radius is provided by Phillips (2000) based on the representation given in Figure 5.5 which allows the effective rolling radius to be related to the unloaded radius and tyre deflection. For the tyre shown in Figure 5.5, the wheel axle is considered fixed and the road moving such that the relative forward velocity of the wheel is V. If a

number of equidistant radial lines are drawn on the tyre the number passing point A in a given time must be the same as the number passing point P in the contact patch.

If we take

d = the distance between the radial lines at the tyre outer radius near A
d' = the distance between the radial lines at the contact patch near P

then

$$\frac{\omega R_u}{d} = \frac{V}{d'} \tag{5.2}$$

therefore

$$R_e = \frac{V}{\omega} = R_u \frac{d'}{d} \tag{5.3}$$

The tread band is subject to a longitudinal compressive strain within the contact patch ε where

$$\varepsilon = \frac{d - d'}{d} \tag{5.4}$$

$$d' = d\,(1 - \varepsilon) \tag{5.5}$$

therefore

$$R_e = R_u(1 - \varepsilon) \tag{5.6}$$

Assuming that the strain in the contact line is constant we have (assuming $\sin\theta = \theta - (\theta^3/3!) + (\theta^5/5!) \cdots$)

$$1 - \varepsilon = \frac{\text{cord } BC}{\text{arc } BC} = \frac{\sin\theta}{\theta} \approx 1 - \frac{\theta^2}{6} \tag{5.7}$$

From Figure 5.5 we also have (assuming $\cos\theta = 1 - (\theta^2/2!) + (\theta^4/4!) \ldots$)

$$\delta_z = R_u(1 - \cos\theta) \approx R_u \frac{\theta^2}{2} \tag{5.8}$$

From equations (5.7) and (5.8) we have

$$1 - \varepsilon = 1 - \frac{\delta_z}{3R_u} \tag{5.9}$$

From equations (5.6) and (5.9) we have

$$R_e = R_u - \frac{\delta_z}{3} \tag{5.10}$$

If we substitute the loaded radius as $R_1 = R_u - \delta_z$ into (5.10) we get

$$R_e = R_1 + \frac{2\delta_z}{3} \tag{5.11}$$

5.2.3 Tyre asymmetry

Although it is not intended to address the construction of a tyre in this textbook a brief mention is needed of two types of tyre asymmetry that can occur, these being conicity and plysteer. Both types of asymmetry can occur during tyre fabrication and have the effect of introducing small amounts of lateral force and aligning moment when a tyre is running at zero slip angle. It will be seen later in this chapter that these offsets in lateral force or aligning moment are visible when plotted against slip angle and that representation in a simulation will depend on the sophistication of the tyre model used.

In a modern vehicle these effects become more important when considering refinement and the 'on-centre' feel of the vehicle, particularly when driving for long periods at high motorway speeds.

Conicity is an effect that arises due to assuming the tyre to have the shape of a truncated cone as shown in Figure 5.6.

When considering the effect of conicity it must be realized that incorporation in a tyre model must take careful account of the tyre axis sytem used. In Figure 5.6, for example, the tyres shown with exaggerated conicity produce a force towards the apex of the cone as the vehicle travels on a straight heading. For the tyre on the left side this is a force that is positive when referred to the Y_{SAE}-axis. If the same tyre is now switched to the right side of the vehicle, reversing the direction of rotation, the force is still towards the apex but is now negative when referred to the Y_{SAE}-axis.

Ply steer is an effect that arises due to a small bias in the positioning of the cords within the tyre belt layers. This is shown in Figure 5.7 where it is

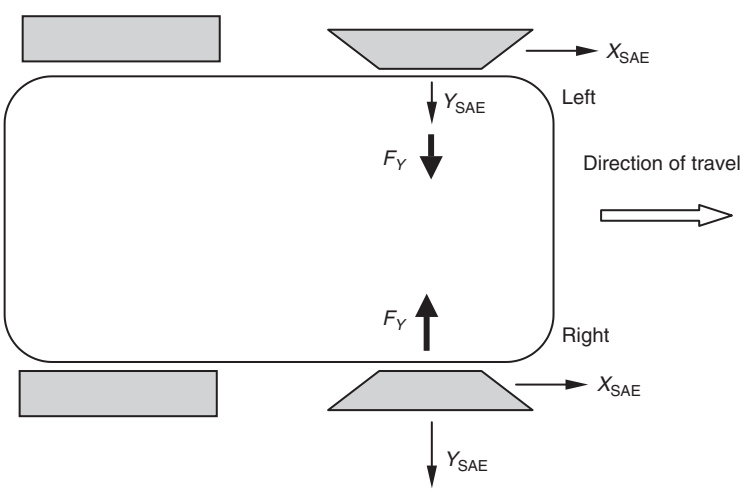

Fig. 5.6 Generation of tyre lateral forces due to conicity

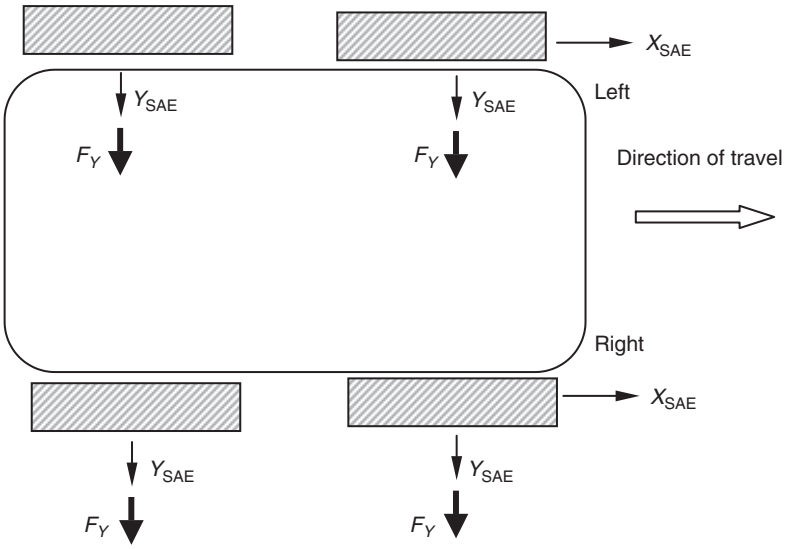

Fig. 5.7 Generation of tyre lateral forces due to plysteer

evident that the opposite occurs to conicity in that switching a tyre from the left to the right of the vehicle does not reverse the lateral force direction. Thus for a vehicle fitted with tyres all exhibiting the same plysteer there will be a tendency for the vehicle to drift off a straight course without some steering correction. A correction will modify the course of the vehicle but will cause the rear wheels to 'track' to the side of the front wheels so that the vehicle progresses with a crab like motion, albeit imperceptible to the driver.

5.3 The tyre contact patch

5.3.1 Friction

The classical laws of friction as often taught to undergraduates can be summarized as:

1. Friction is a property of two contacting surfaces. It does not make sense to discuss friction as if it were a material property.
2. Frictional force is linearly proportional to normal force and can be defined using a coefficient of friction (frictional force/normal force).
3. The coefficient of friction is independent of contact area between the two surfaces.
4. The static coefficient of friction (stiction) is greater than the kinetic (sliding) coefficent of friction.
5. The coefficient of friction is independent of sliding speed.

A detailed treatment of this subject with regard to tyres is given by Moore (1975), where it is shown that the above laws are flawed, or limited in certain

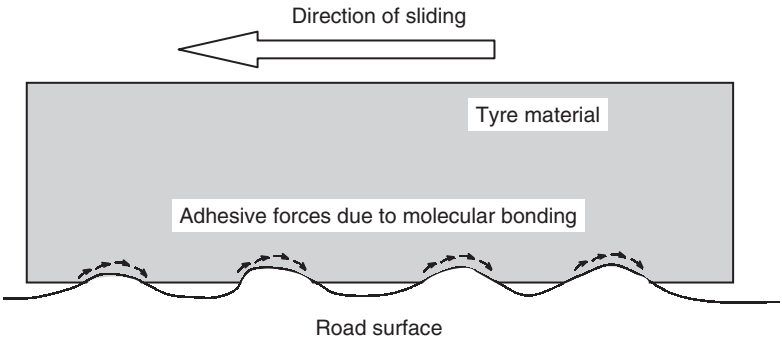

Fig. 5.8 Frictional force component due to adhesion

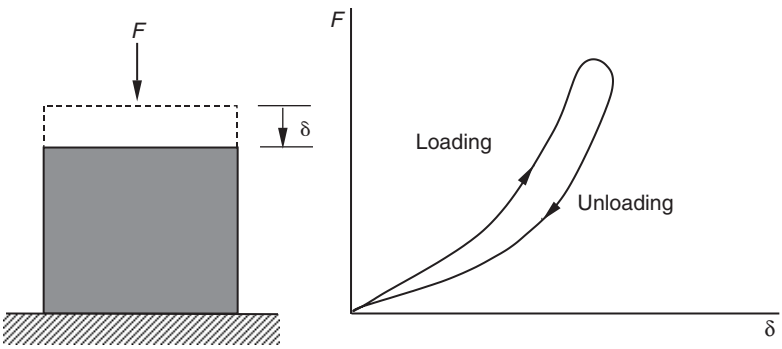

Fig. 5.9 Hysteresis in rubber

conditions such as high tyre pressures. The concept of a coefficient of friction associated with static and sliding conditions will, however, prove useful for describing the tyre models used later in this chapter.

For tyres the friction generated between the tread rubber and the road surface is generated through two mechanisms these being adhesion and hysteresis. The adhesive component, shown in Figure 5.8, results from molecular bonds generated between the exposed surface atoms of rubber and road material in the contact area. This is the larger component of friction on dry roads but is greatly reduced when the road surface is contaminated with water or ice. Hence the use of 'slick' tyres, with no tread and increased surface contact area, for racing on dry roads.

In order to understand the hysteresis mechanism consider a block of rubber subjected to an increasing and then a decreasing load as shown in Figure 5.9. As the rubber is loaded and unloaded it can be seen that for a given displacement δ the force F is greater during the loading phase than the unloading phase.

If we continue to consider the situation where a non-rotating tyre is sliding over a non-smooth surface with a coefficient of friction μ assumed to

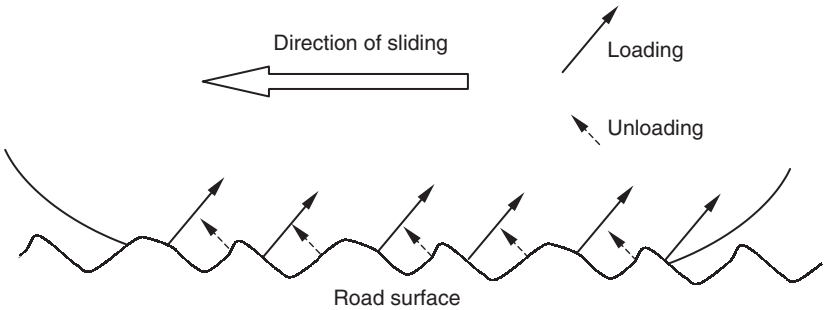

Fig. 5.10 Loading and unloading of tyre rubber in the contact patch

be zero it can be seen from Figure 5.10 that an element of rubber in the contact patch will be subject to continuous compressive loading and unloading.

In the idealized situation of no friction as the tyre slides over the irregular road surface compressive forces normal to the surface are generated as the rubber is loaded and unloaded. Due to the hysteresis in the rubber the sum of the loaded forces is greater than the sum of the unloaded forces resulting in, for example here, a resultant braking force opposing the direction of sliding.

5.3.2 Pressure distribution in the tyre contact patch

In order to understand the manner by which forces and moments are generated in the contact patch of a rolling tyre an initial appreciation of the stresses acting on an element of tread rubber in the contact patch is required. Each element will be subject to a normal pressure p and a shear stress τ acting in the road surface. In theory the element will not slip on the road if $\tau < \mu p$ where μ is the coefficient of friction between the tread rubber and the road surface.

The pressure distribution depends on tyre load and whether the tyre is stationary, rolling, driven or braked. The pressure distribution is not uniform and will vary both along and across the contact patch. In order to understand the mechanics involved with the generation of forces and moments in the contact patch some simplification of the pressure distribution will be adopted here starting with Figure 5.11 where typical pressure distributions in the tyre contact patch for a stationary tyre and the effects of inflation pressure are considered.

Generally the pressure rises steeply at the front and rear of the contact patch to a value that is approximately equal to the tyre inflation pressure. Overinflation causes an area of higher pressure in the centre of the contact patch while underinflation leads to an area of reduced pressure in the centre of the patch.

When the tyre is rolling it will be shown later that pressure distribution in the contact patch is not symmetric and is greater towards the front of the contact patch.

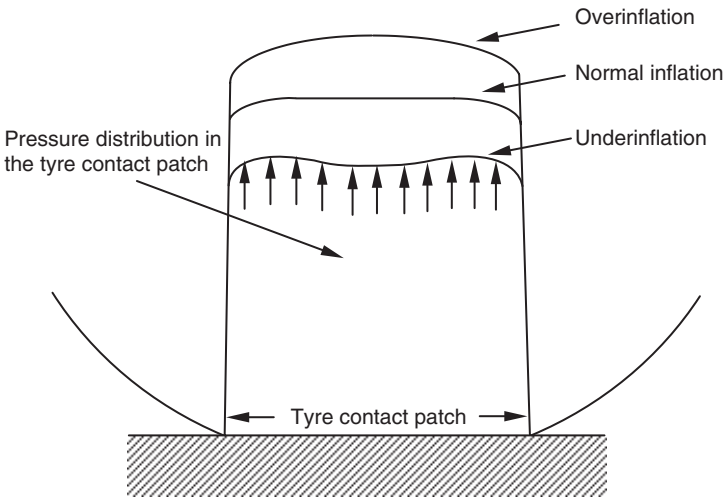

Fig. 5.11 Pressure distribution in a stationary tyre contact patch

5.4 Tyre force and moment characteristics

5.4.1 Components of tyre force and stiffness

The local pressures and stresses distributed over the tyre contact patch can be integrated to produce forces and moments referenced to a local co-ordinate system within the contact patch. Using the SAE tyre axis system the full set of forces and moments is as shown in Figure 5.12.

The following section will explain the mechanical characteristics of each force and moment component. The order in which these components are described will be that which most facilitates an understanding of the mechanisms and dependencies rather than following the local order of the SAE tyre axis system. The tractive force F_x and lateral force F_y depend on the magnitude of the normal force component F_z. Hence the normal force is described first.

It should also be noted that more than one mechanism will be involved in the generation of each component. The tractive force has formulations involving driving, braking and rolling resistance. The lateral force is dependent on both slip and camber angle. It is also not possible to treat components of force and moment in isolation. It is, for example, necessary to provide a single explanation as to how the self-aligning moment and lateral force resulting from slip angle arise due to stress distributions within the tyre contact patch.

Finally the reader should also be reminded that vehicle dynamics is traditionally a subject where various terms are used to describe the same thing. For example, vertical force, normal force and tyre load may be used to mean the same thing by various authors. Other examples where confusion may arise include the use of aligning torque, aligning moment or self-aligning moment, longitudinal or tractive force and lateral or cornering force.

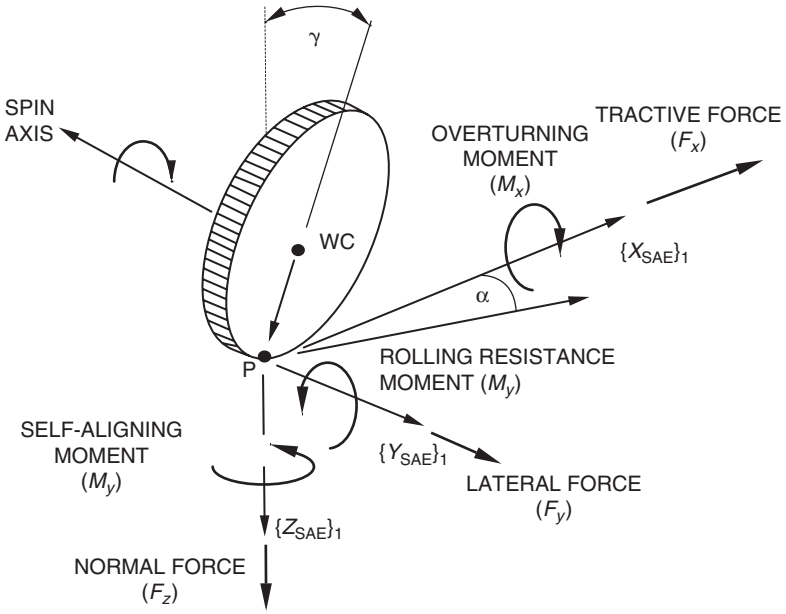

Fig. 5.12 Tyre forces and moments shown acting in the SAE tyre axis system

The use of the term stiffness can also add confusion to newcomers to the subject area. A traditional static force/displacement approach is used by Moore (1975) to define longitudinal, lateral and torsional stiffness of a tyre. In each case a non-rolling tyre is mounted on a plate and incrementally loaded as indicated in Figure 5.13 until complete sliding occurs. Plotting graphs of force or moment against displacement or rotation allows the stiffness parameters to be obtained from the slopes at the origin.

We will see later that terms such as cornering stiffness and aligning moment stiffness are associated with a rolling tyre and should not be confused with the lateral and torsional stiffness defined here. The term longitudinal stiffness can be particularly misleading as another definition is commonly used when longitudinal tractive forces due to driving and braking are discussed.

The explanations that follow will initially deal with each force mechanism in isolation, for example lateral forces arising due to slip angle and camber angle are considered separately with no simultaneous longitudinal tractive force. Following this, a more complex treatment involving combinations of the various force components will be addressed.

5.4.2 Normal (vertical) force calculations

The calculation of normal force in the tyre is relatively straightforward compared with the calculation of longitudinal or lateral forces. The normal force will, however, always be negative when computed using the SAE tyre axis system. This is not particularly elegant when presenting the dependencies of other force components on the normal force. To overcome this a positive value of this force component is often referred to as vertical force or tyre load. In SAE J670e (SAE Publication, 1976) vertical load is taken as the negative of normal force.

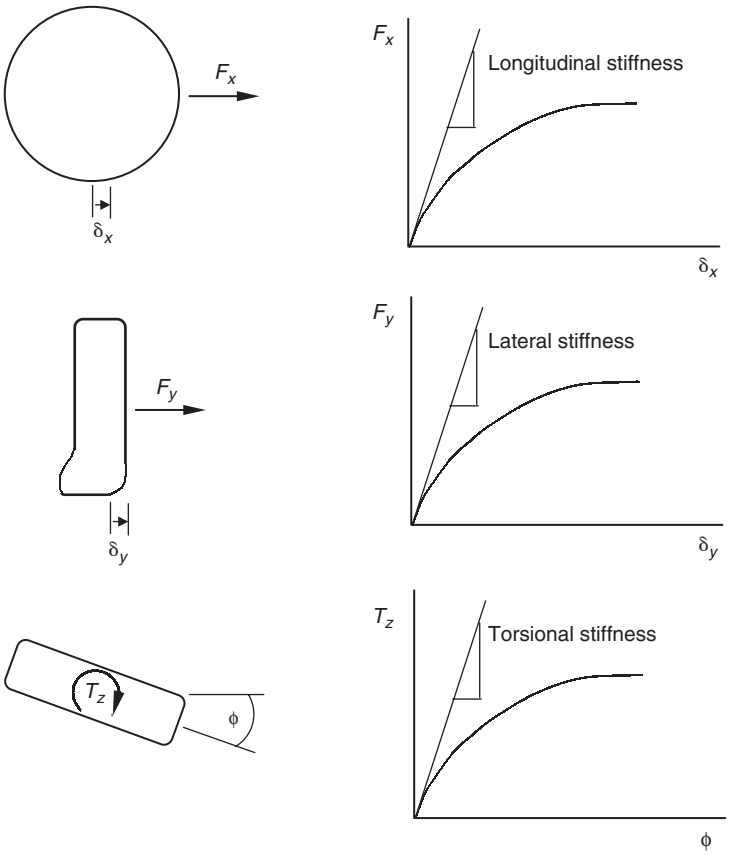

Fig. 5.13 Measurement of stiffness in a non-rolling tyre

It is generally sufficient to treat the tyre as a linear spring and damper when computing the vertical force component. The calculation of the vertical force F_z acting at point P in the tyre contact patch has a contribution due to stiffness F_{zk} and a contribution due to damping F_{zc}. These forces act in the direction of the $\{Z_{\mathrm{SAE}}\}_1$ vector shown in Figure 5.14:

$$F_z = F_{zk} + F_{zc} \tag{5.12}$$

$$F_{zk} = -k_z \delta_z \tag{5.13}$$

$$F_{zc} = -c_z V_z \tag{5.14}$$

where

$$c_z = 2.0\,\zeta\sqrt{m_t k_z}$$

and
m_t = mass of tyre
k_z = radial tyre stiffness
ζ = radial damping ratio
δ_z = tyre penetration
V_z = rate of change of tyre penetration

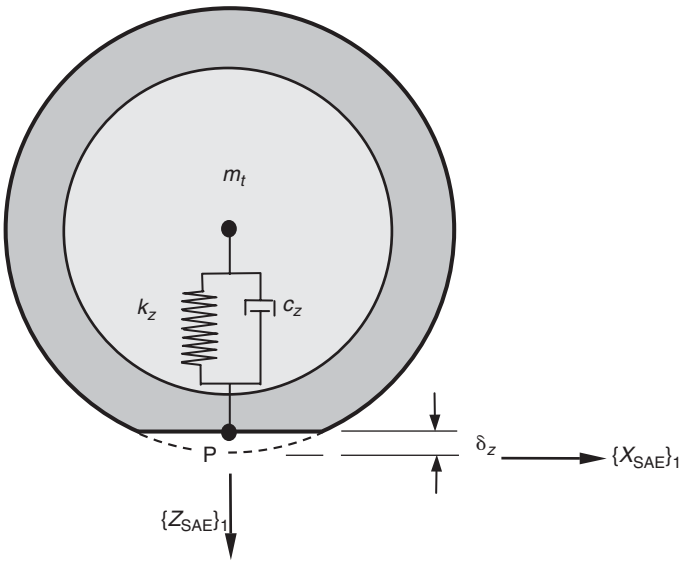

Fig. 5.14 Vertical tyre force model based on a linear spring damper

A linear model of tyre vertical force may need to be extended to a non-linear model for applications involving very heavy vehicles or studies where the tyre encounters obstacles in the road or terrain of a similar size to the contact patch or smaller. This could also be applicable for parallel work in the aircraft industry where established tyre models have been formulated to simulate the behaviour of the aircraft on the runway, particularly on landing, and potential problems with wheel shimmy (Smiley, 1957; Smiley and Horne, 1960). Where a non-linear model of vertical tyre force is required the most straightforward approach would be to represent the stiffness-based component of the force by a cubic spline interpolation of measured static force–displacement data.

5.4.3 Longitudinal force in a free rolling tyre (rolling resistance)

Under normal driving conditions a tyre is continually subject to a wide range of tractive driving and braking forces. This section discusses the formulation of driving and braking forces under pure slip conditions, i.e. straight-line motion only. The more complex situation of combined slip, for example simultaneous braking and cornering, is addressed later in this chapter.

As a starting point it can be shown that slip will always be present in the tyre contact patch even in the absence of tractive driving and braking forces. Consider first the free rolling tyre shown in Figure 5.15 and the mechanism that leads to the generation of longitudinal slip. The model used in Figure 5.15 has simplifications but will help to develop an initial understanding. As the tyre rolls forward the radius reduces as tread material approaches point A at the front of the tyre contact patch. At this point we can say that the forward velocity V of the wheel relative to the road surface is given by

$$V = \omega R_e \tag{5.15}$$

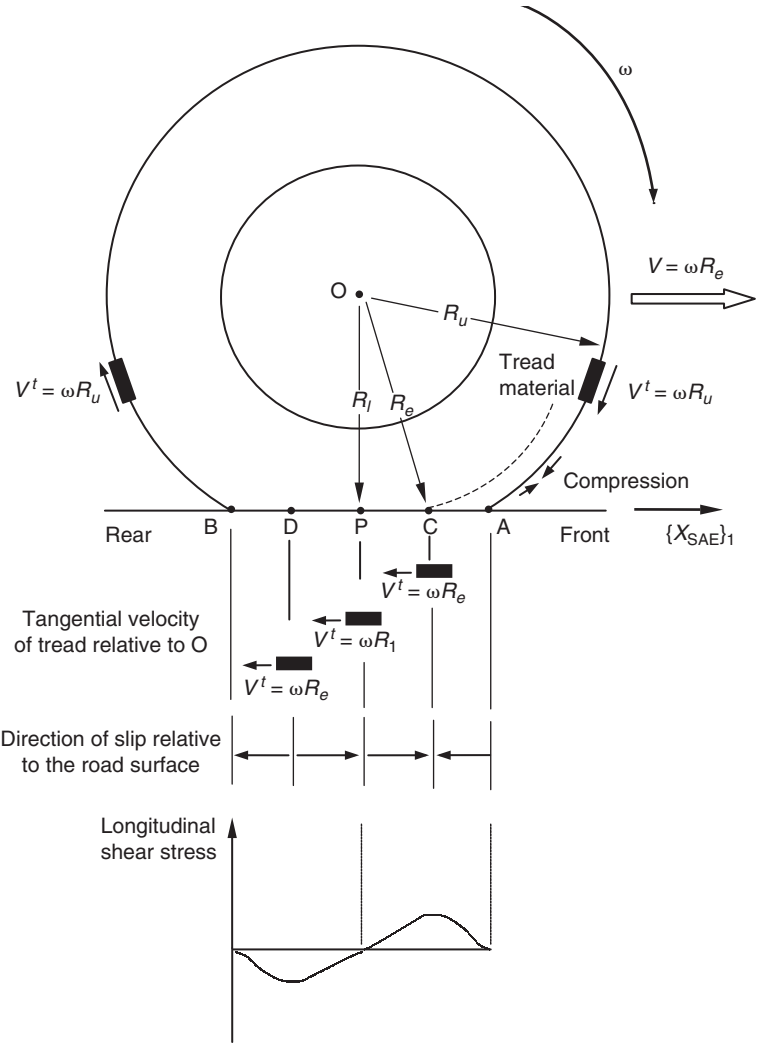

Fig. 5.15 Generation of slip in a free rolling tyre

The tread material approaching the front of the contact patch will have a tangential velocity V^t relative to the wheel centre O given by

$$V^t = \omega R_u \tag{5.16}$$

As the tread material gets close to the start of the contact patch the tyre radius decreases causing the tangential velocity of the tread material to decrease causing circumferential compression of tread material just before it enters the contact patch.

As the tread material enters the contact patch at point A the rearward tangential velocity relative to the wheel centre is just slightly greater than the forward velocity of the vehicle. This results in initial rearward slip of tread material relative to the road surface between point A and C. At point C it is assumed

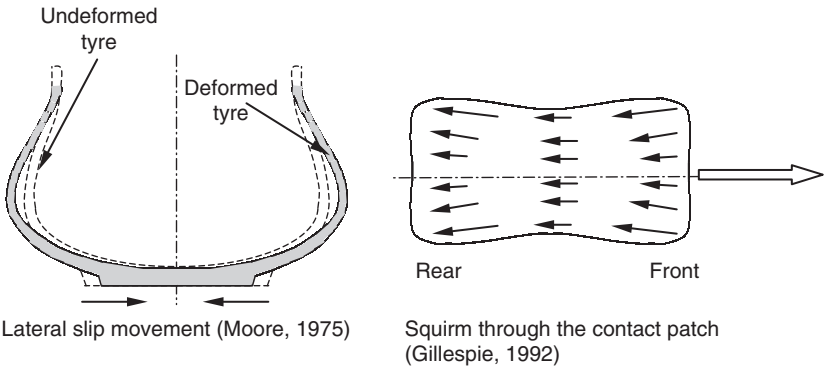

Fig. 5.16 Lateral distortion of the contact patch for a free rolling tyre

that the radius has reduced to a value equivalent to the effective rolling radius R_e resulting in the rearward tangential velocity matching the forward vehicle velocity and theoretically producing a point of zero slip in the tyre. Over the central region of the contact patch between C and D the radius reduces to a value below the effective rolling radius reversing the slip in the tyre to the forward direction. At the centre of the patch P the radius reduces to the loaded radius R_l. In theory this point would produce the lowest tangential velocity and the highest forward slip although experimental observations (Moore, 1975) indicate that the tangential speed does not reduce to this level. Between point D and B the radius recovers to a value greater than the effective rolling radius causing the direction of slip to reverse again to a rearward direction.

It is clear that the direction of slip changes several times as tread moves through the contact patch resulting in the distribution of longitudinal shear stress of the type shown at the bottom of Figure 5.15. The shear stress is plotted to be consistent with the SAE reference frame and is not symmetric with the net effect being to produce an overall force, the rolling resistance, acting in the negative X_{SAE} direction.

It should be noted that the two-dimensional model presented is not fully representative as components of lateral slip are also introduced in a free rolling tyre due to deformation of the side walls as shown in Figure 5.16.

As the tyre carcass deforms in the vicinity of the contact patch the deformation of the side walls creates additional inwards movement of the tread material (Moore, 1975). This causes the contact patch to assume an hourglass shape creating an effect referred to as ‘squirm’ (Gillespie, 1992) as the tread material moves through the contact patch.

Before moving on to consider the driven or braked tyre we will now consider the rolling resistance forces generated in a free rolling tyre. Rolling resistance results from energy losses in the tread rubber and side walls. Energy loss in the tread rubber is produced by hysteresis. If we refer again to Figure 5.9 it is clear for a block of rubber, or tread material, that there is more force required at any given displacement during the loading phase than the unloading phase. As tread material moves through the contact

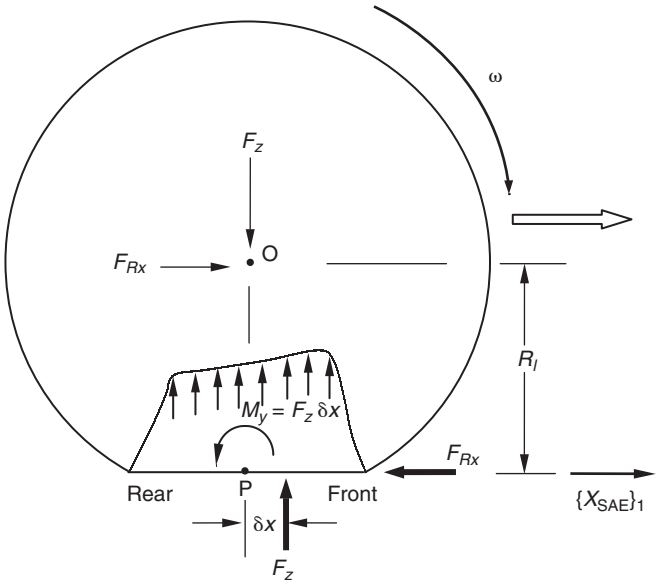

Fig. 5.17 Generation of rolling resistance in a free rolling tyre

patch it will be loaded until it reaches the midpoint of the contact patch and unloaded as it moves to the rear of the contact patch. This and the additional losses due to hysteresis in the side walls lead to a pressure distribution that is not symmetrical as shown for the stationary tyre in Figure 5.11 and has a greater pressure distribution in the front half of the contact patch as shown in Figure 5.17.

The pressure distribution implies that the resultant tyre load F_z acts through the centre of pressure a distance δx forward of the wheel centre. For equilibrium a couple exists that must oppose the tyre load and its reaction acting down through the wheel centre. The couple that reacts the wheel load couple results from the rolling resistance force F_{Rx} acting longitudinally in the negative X_{SAE} axis and reacted at the wheel centre where

$$F_{Rx} = \frac{F_z \delta x}{R_l} \tag{5.17}$$

The rolling resistance may also be referenced by a rolling resistance coefficient, this being the rolling resistance force F_{Rx} divided by the tyre load F_z. By definition therefore the rolling resistance moment, M_y, is $F_z \delta x$ and the rolling resistance moment coefficient is δx. Rigorous adherence to the sign convention associated with the tyre reference frame is essential when implementing these formulations in a tyre model. In Figure 5.17, to assist understanding, F_z is represented as the vertical force acting on the tyre rather than the negative normal force computed in the Z_{SAE} direction.

The rolling resistance force is very small in comparison with other forces acting at the contact patch, a rolling resistance coefficient of the order 0.01 being typical for a car tyre. This and the fact that the rolling resistance force

may vary by up to 30% of the average value during one revolution (Phillips, 2000) make accurate measurement difficult.

5.4.4 Braking force

During braking the activation of the brake mechanism will apply forces to the rotating wheel that at this stage may be treated as a brake torque T_B acting about the wheel centre and opposing the rolling motion of the wheel. During this process the tread material in the tyre will begin to slide relative to the road, giving rise to slip. As the angular velocity of the wheel reduces a braking force is generated that tends to move the contact patch rearwards relative to the wheel centre. This effect will introduce circumferential tension in the tread just before entering the contact patch as opposed to the compression noted earlier in this area for a free rolling tyre. As the contact patch distorts rearward during braking compression will instead be generated in the tread just leaving the patch as shown in Figure 5.18.

During braking, as for free rolling, as tread material approaches the contact patch the radius will reduce with a consequent reduction in the tangential speed of the tread material relative to the wheel centre. For moderate braking, the tread initially entering the contact patch will initially bend rearward under the action of shear stresses for a short distance before the tangential velocity of the tread material slows to the forward velocity of the tyre ωR_e and slip begins to progressively develop as the tread material moves back through the contact patch.

As the tread approaches the rear of the tread the pressure begins to unload releasing the deformation in the tread. The tangential velocity of the tread material begins to increase and the frictional braking force reduces rapidly to zero at the rear of the patch. These actions produce distributions of pressure, slip and longitudinal shear stress of the type shown at the bottom of Figure 5.18 where the shear stress is plotted as negative in accordance with the resultant braking force resolved in the SAE tyre co-ordinate system. It should also be noted that when braking, the pressure distribution tends to differ from that in a free rolling tyre as the peak, and hence resultant tyre load, move further forward in the tyre contact patch.

If the resulting braking force is maintained the angular velocity of the tyre will reduce from its free rolling value and will eventually become zero when the wheel is fully locked. A measure of the slip generated can be defined by a slip ratio or percentage slip. In this text the term slip ratio S will be used:

$$S = \frac{\omega_0 - \omega_B}{\omega_0} \tag{5.18}$$

where

ω_0 is the angular velocity of the free rolling wheel
ω_B is the angular velocity of the braked wheel

If we consider the case of a braked wheel it can be seen from equation (5.18) that for the free rolling state the slip ratio will be zero and that for the fully locked and skidding wheel the slip ratio will be 1.0. Multiplying slip ratio by 100 gives the term percentage slip.

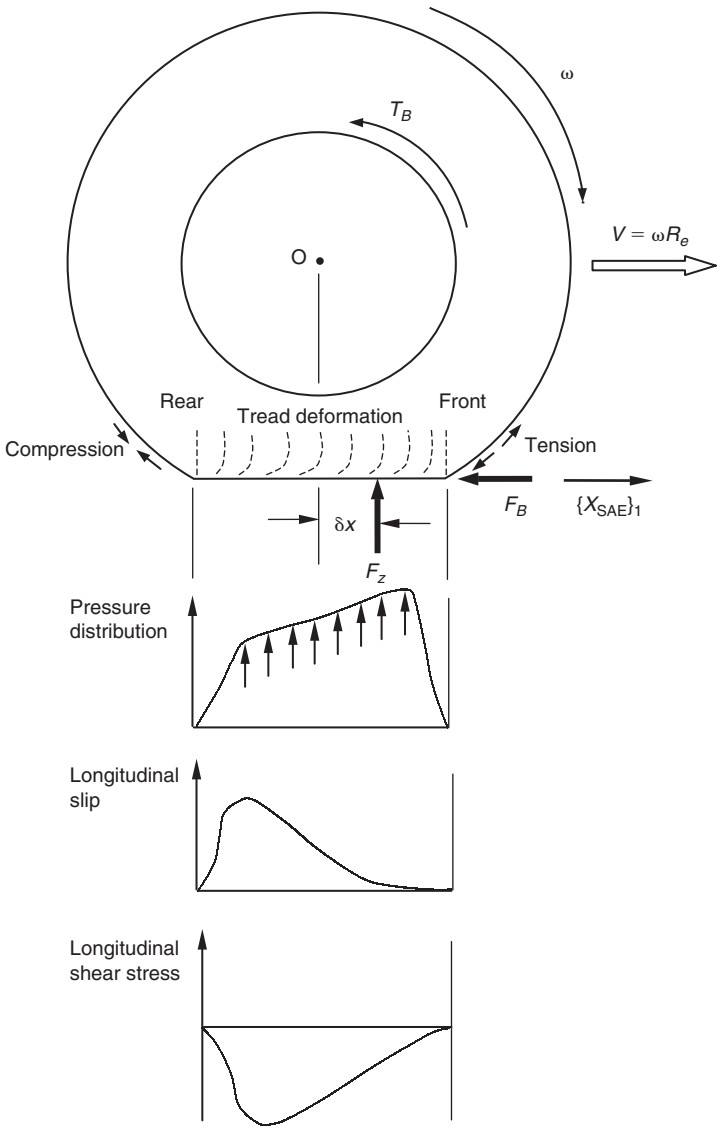

Fig. 5.18 Generation of force in a braked tyre

In SAE J670e (SAE Publication, 1976) the sign is reversed to produce a slip ratio of -1.0 for the fully locked wheel, convenient when plotting braking force that is negative in the SAE system against slip ratio:

$$S = \frac{\omega_B - \omega_0}{\omega_0} \tag{5.19}$$

A further definition that is popular is to substitute $V = \omega_0 R_e$ into equation (5.18) giving

$$S = \frac{V - \omega_B R_e}{V} \tag{5.20}$$

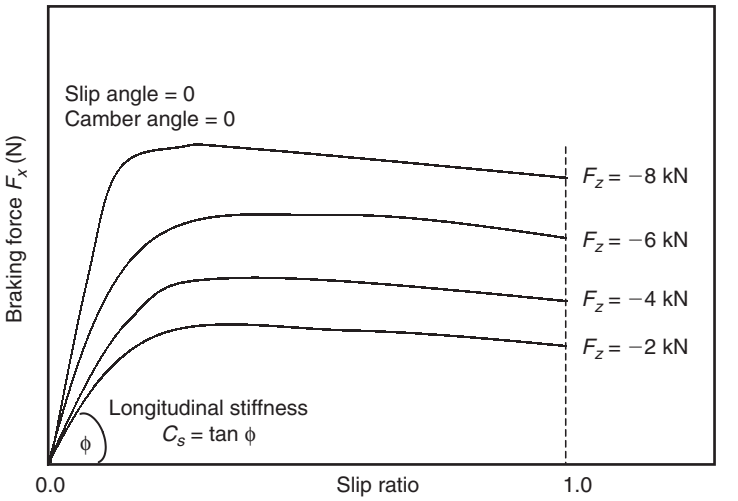

Fig. 5.19 Braking force versus slip ratio

It should be noted that slip ratio has been subject to various definitions by researchers and research groups in tyre companies, several are listed in Milliken and Milliken (1995). Some tyre models use R_l instead of R_e when formulating slip ratio which may require careful consideration when using a general-purpose MBS program to model ABS (Ozdalyan and Blundell, 1998).

Plotting curves of braking force, for convenience shown positive here, against slip ratio for a range of tyre loads will generally produce curves of the type shown in Figure 5.19.

Examination of the curves in Figure 5.19 reveals that at each vertical load the braking force increases rapidly in a linear manner to reach a peak value that, depending on tyre design and road conditions, would typically occur at a slip ratio anywhere between 0.15 and 0.3. After this point the braking force will level out or reduce as the wheel approaches the fully locked situation. Examination of curves such as these, sometimes called 'mu-slip' curves, facilitates an understanding of ABS operation where cycling the brake pressure maintains a slip ratio near the peak braking force position for each wheel on the vehicle. This is desirable not only to maximize braking effort but also to maintain a rolling wheel for cornering and directional stability.

An important property of each curve is the slope at the origin, referred to as the longitudinal stiffness, C_s. It can be seen that this is not a constant but increases with load which is significant when considering the capability of any tyre model to be used in braking simulations. In Figure 5.19 the curves are shown to pass through the origin. In practice a small vertical offset in longitudinal force will be apparent for a free rolling tyre, this being the rolling resistance discussed earlier.

It is important to reiterate that frictional forces are not the property of the tyre alone. The effects of road material and texture, or contamination with water and ice, are also significant. Figure 5.20 demonstrates typical curves of braking force against slip ratio, at a given tyre load for various road conditions (Phillips, 2000). These curves demonstrate that on wet roads peak

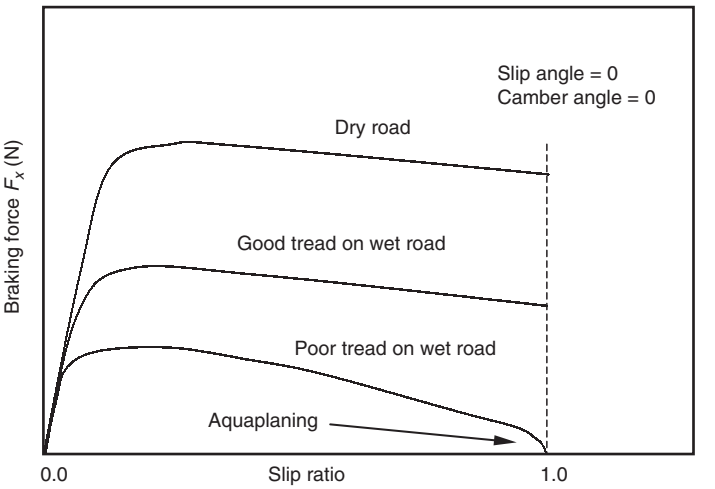

Fig. 5.20 The effect of road contamination on braking

values of braking force as expected reduce and that for a locked wheel with poor tread a dangerous situation known as hydroplaning or aquaplaning can arise where the tyre runs on a film of water and traction is effectively lost. The curves of braking force can also be categorized by two coefficients of friction associated with the peak braking force and that associated with total sliding at a slip ratio of 1.0. On dry roads it is possible to obtain a coefficient of friction for good tyres in excess of 1.0, on wet roads this would typically reduce to about 0.5 or lower for tyres with poor tread while a road contaminated with ice may only achieve a peak value of 0.1.

It can be seen when examining the curves in Figure 5.20 that the longitudinal stiffness is relatively unaffected by surface contamination. This is particularly dangerous for a road with ice or the poor tyre on a wet road. In these conditions the peak braking force occurs rapidly at low slip ratio causing the vehicle to skid before any possible corrective action from the average driver.

In addition to the above it is also known that an increase in vehicle speed will reduce peak values of braking force and that other parameters such as tyre inflation pressure will have an effect, a more detailed treatment of which is given by Gillespie (1992).

5.4.5 Driving force

During driving the transmission will impart a driving torque T_D to the rotating wheel as shown in Figure 5.21. As the angular velocity of the wheel increases a driving force is generated that tends to move the contact patch forward relative to the wheel centre. This effect will introduce circumferential compression in the tread just before entering the contact patch and tension on leaving as opposed to braking.

As the wheel is driven the tread entering the contact patch will initially bend forward under the action of shear stresses for a short distance. As the tread approaches the rear of the tread the pressure begins to unload releasing

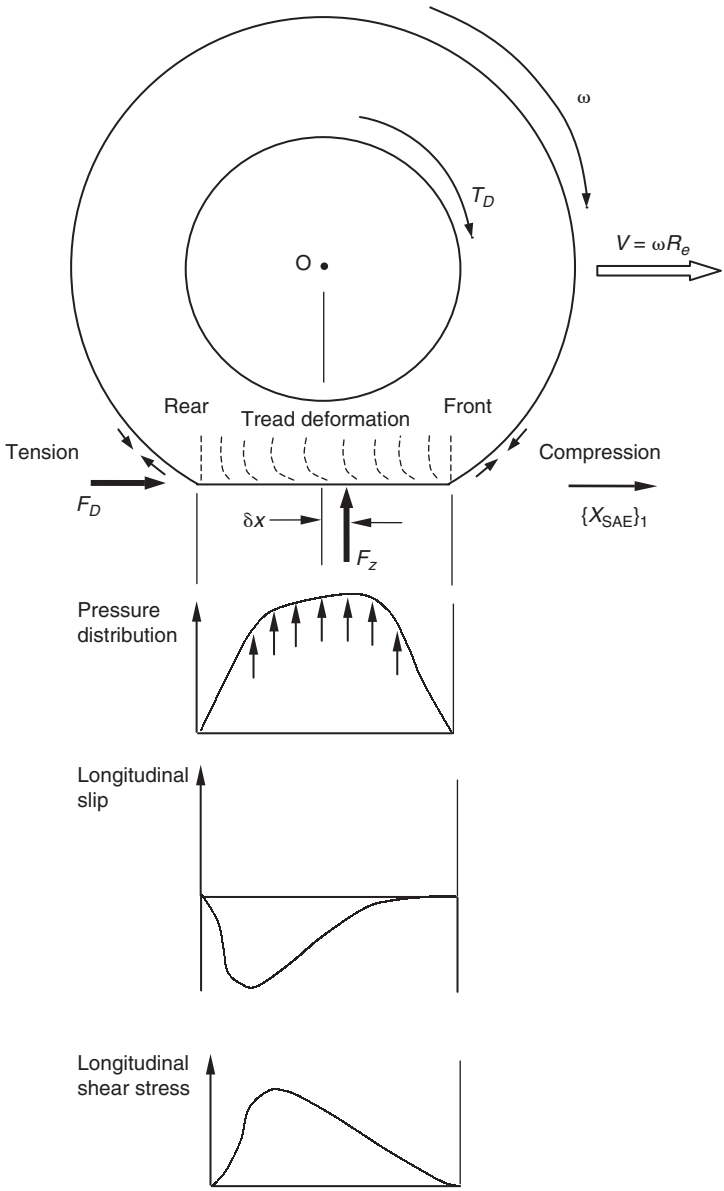

Fig. 5.21 Generation of force in a driven tyre

the deformation in the tread and progressive sliding develops. These actions produce distributions of pressure, slip and longitudinal shear stress of the type shown at the bottom of Figure 5.21. It can also be seen that when driving, the pressure distribution tends to differ from that in a braked tyre as the peak, and hence resultant tyre load, move further to the rear in the tyre contact patch reducing the offset δx.

If the resulting driving force is maintained the angular velocity of the tyre will increase from its free rolling value and will eventually begin to spin.

A measure of the slip generated for the driven tyre can be defined by a further modification to the slip ratio S:

$$S = \frac{\omega_D - \omega_0}{\omega_0} \tag{5.21}$$

where

ω_0 is the angular velocity of the free rolling wheel

ω_D is the angular velocity of the driven wheel

For driving a slip ratio of 1.0 is sometimes taken to define the onset of wheel spin. From equation (5.21) this will occur when the angular velocity of the driven wheel reaches a value of twice that for free rolling. Unlike braking, the slip ratio in driving can exceed 1.0 as the wheel angular velocity continues to increase. This definition of 'spin' is somewhat arbitrary. For both tractive and braking cases the relationship between longitudinal force and slip ratio is such that the wheel behaviour converges for slip ratios smaller than those at which peak force is produced. However, for larger slip ratios the wheel behaviour diverges rapidly. For spin in particular, angular velocity increases very quickly until torque is reduced.

5.4.6 Generation of lateral force and aligning moment

The generation of lateral force and aligning moment in the tyre results from combinations of the same mechanisms and are thus treated together here. As a starting point it is helpful to consider Figure 5.22, which is adapted from the sketches for forces and torques provided by Olley (1945). Figure 5.22 is particularly useful for relating the sign convention for the lateral forces and aligning moments plotted and discussed throughout this chapter.

From Figure 5.22 it can be seen that for a tyre rolling with a slip angle α at zero camber angle the lateral force generated due to the distribution of shear stress in the contact patch acts to the rear of the contact patch centre creating a lever arm known as the pneumatic trail. This mechanism introduces the aligning moment and has a stabilizing or 'centring' effect on the road wheel. This is an important aspect of the steering 'feel' that is fed back to the driver through the steering system.

Similarly it can be seen from Figure 5.22 that for a tyre rolling with a camber angle γ at zero slip angle the lateral force generated is called camber thrust. Due to the conditions in the contact patch the camber thrust acts in front of the contact patch centre creating a mechanism that creates a moment. Although this is referred to here as an aligning moment it has the opposite effect of the aligning moment resulting from slip angle and is sometimes called the camber torque as there is no resultant aligning action on the road wheel.

5.4.7 The effect of slip angle

In order to understand the mechanisms that lead to the generation of lateral force and aligning moment resulting due to slip angle it is useful to start with Figure 5.23 showing the distribution of pressure p, and the lateral stress in the contact patch. The upper part of the figure provides a side view

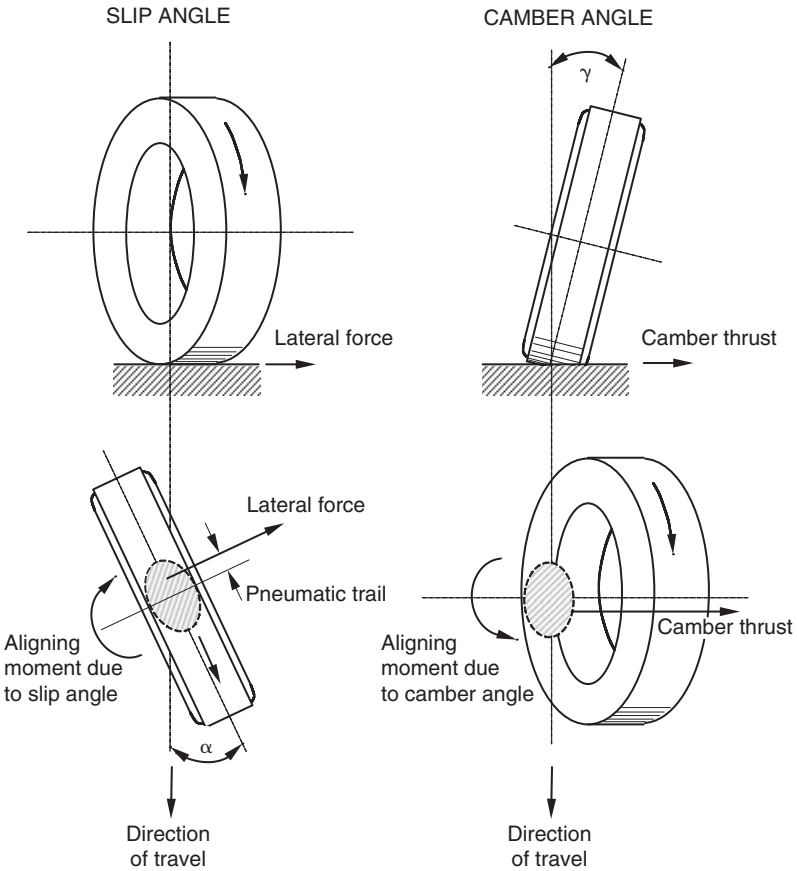

Fig. 5.22 Forces and moments due to slip and camber angle

and the lower part is a top view looking down on to the contact patch. The lateral stress boundary μp represents the limit available between the tread rubber and the road surface. If the lateral stress is below this limit no sliding will occur but once the lateral stress reaches this limit the tread rubber will commence sliding.

When the tyre rolls at a slip angle α, tread rubber that is put down on the road surface at the front of the contact patch moves back through the patch at the same slip angle, deforming the sidewalls of the tyre, so that the lateral stress in the tread rubber steadily increases as shown. At a certain point in the contact patch the lateral stress reaches the limit boundary after which sliding takes place until the tread rubber leaves the rear of the contact patch and the lateral stress returns to zero.

As the slip angle increases the rate at which lateral stress is generated as the tread rubber moves back through the contact patch increases so that the point at which slippage commences moves forward in the contact patch. It can also be seen that as the slip angle increases the area under the lateral stress curve increases. This area is a measure of the resulting lateral force F_y generated by integrating the stress over the contact patch. At low slip

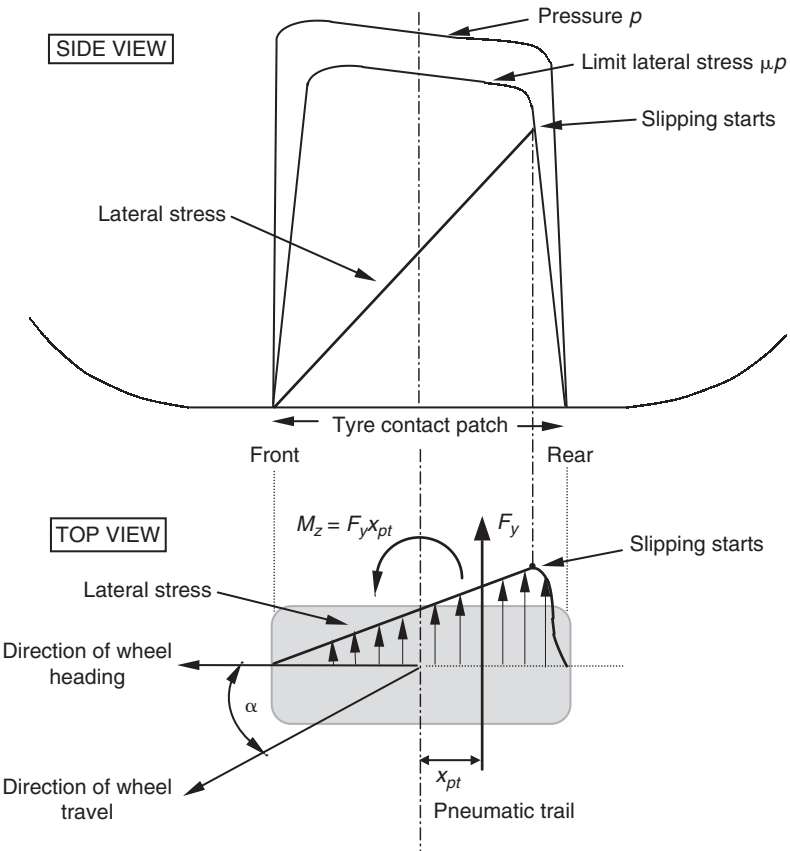

Fig. 5.23 Generation of lateral force and aligning moment due to slip angle

angles, when the lateral stress shape is substantially triangular, there is a nearly linear relationship between lateral force and slip angle. In general this linearity only extends to 1 or 2 degrees of slip angle. As the slip angle increases, the amount of rubber involved in sliding gradually extends from the rear of the tyre contact patch until all the rubber is sliding and the lateral stress follows the boundary limit μp distribution.

Since the form of the pressure distribution is a measure of the tyre load $(-F_z)$, it follows that the maximum lateral force $F_{y\,\max}$ is found from

$$F_{y\,\max} = -\mu F_z \tag{5.22}$$

In practice this maximum is achieved at slip angles above 20 degrees for most tyres. Figure 5.24 shows a typical plot of lateral force F_y with slip angle α for increasing tyre load with the camber angle set at zero. For the convenience of plotting results in the positive quadrant negative slip angle is used in this plot. From the plot it can be seen that the cornering stiffness C_α is the gradient of the curve measured at zero slip angle at a given tyre load. As the tyre load increases so does the cornering stiffness although it will be seen later that at higher tyre loads the magnitude of the cornering stiffness begins to level off. In Figure 5.24 the curves are shown to pass through the

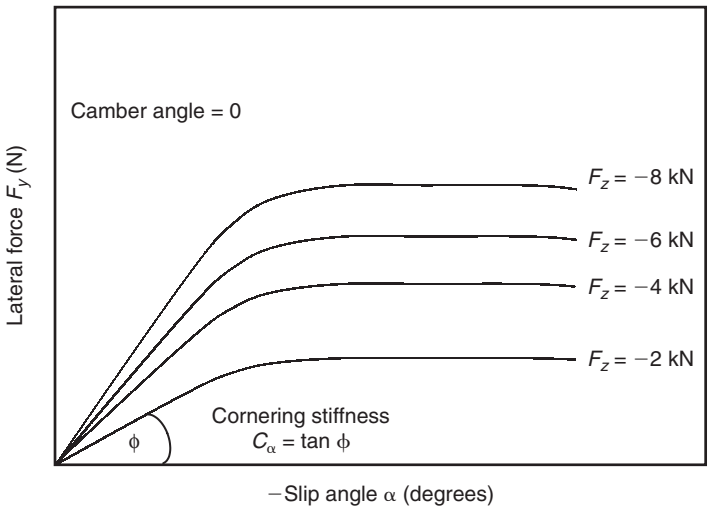

Fig. 5.24 Plotting lateral force versus slip angle

origin. In practice a small offset in lateral force will be apparent at zero slip angle due to the effects of conicity and plysteer discussed earlier.

Looking back to Figure 5.23 it can be seen that as the shape of the lateral stress distribution is approximately triangular the lateral force F_y acts through the centroid of this area that is to the rear of the wheel centre line by a distance referred to as the pneumatic trail. Inspection of Figure 5.23 should indicate that as the slip angle increases the line of action of F_y moves forward reducing the pneumatic trail eventually to zero. The aligning moment M_z is the product of the lateral force and the pneumatic trail and will reduce accordingly eventually becoming negative usually for lightly loaded tyres at high slip angles. In these situations the extent of sliding occurs to such an extent throughout the contact patch that the lateral stress distribution approaches the shape of the μp curve moving the centroid through which F_y acts forward of the centre. A typical plot of aligning moment with slip angle, for a given tyre load and zero camber angle, is shown in Figure 5.25. From the plot it can be seen that the aligning moment stiffness is the gradient of the curve measured at zero slip angle at a given tyre load.

The aligning moment curve is nearly linear at low slip angles and reaches a maximum value for most tyres at a slip angle of 4 to 6 degrees. The gradient of the curve measured at a zero slip angle is the aligning moment stiffness. In Figure 5.25 the curves are shown to pass through the origin. In practice a small offset in aligning moment will be apparent at zero slip angle due to the effects of conicity and plysteer discussed earlier.

5.4.8 The effect of camber angle

The lateral force that arises due to an inclination of the tyre from the vertical is referred to as camber thrust. The SAE definition of positive camber angle is taken for the top of the tyre leaning outwards relative to the vehicle. The fact that this differs from side to side does not lead to consistency when developing a tyre model. For understanding it is useful to remember that

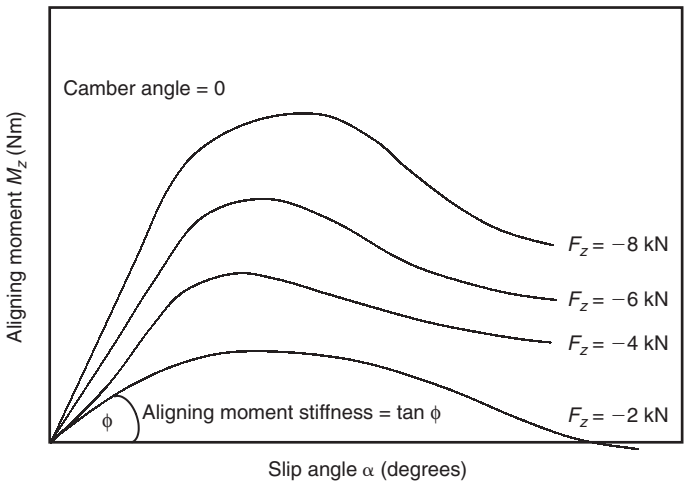

Fig. 5.25 Plotting aligning moment versus slip angle

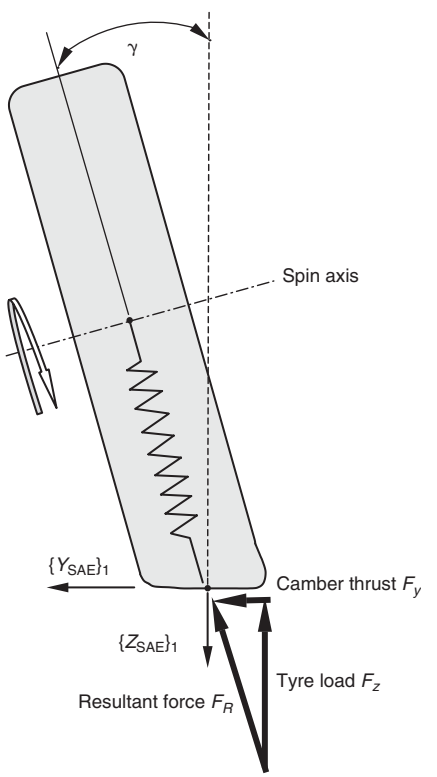

Fig. 5.26 Generation of lateral force due to camber angle

the camber thrust will always act in the direction that the tyre is inclined as shown in Figure 5.26. For the SAE system shown here a positive camber angle γ will produce a positive camber thrust for all tyres on the vehicle modelled in that system.

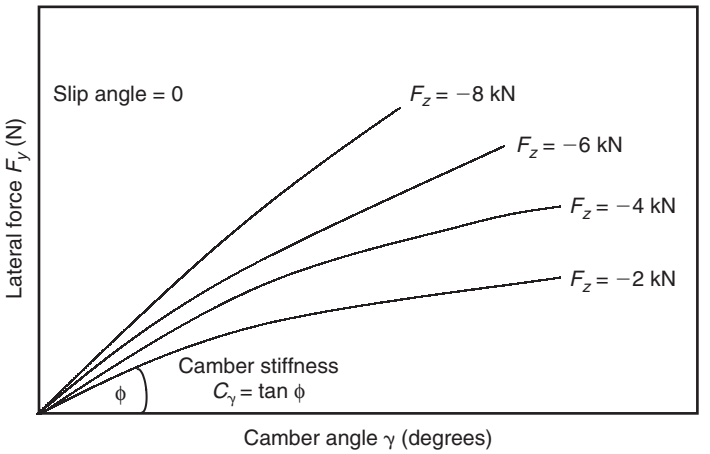

Fig. 5.27 Plotting lateral force versus camber angle

If the tyre is inclined at a camber angle γ, then deflection of the tyre and the associated radial stiffness will produce a resultant force, F_R, acting towards the wheel centre. Resolving this into components will produce the tyre load and the camber thrust.

An alternative explanation provided in Milliken and Milliken (1995) compares a stationary and rolling tyre. For the stationary tyre experimental observations of tread in the contact patch indicate a curved shape. As the tyre rolls the tread moving through the contact patch is constrained by the road to move along a straight line, the net reaction of these forces being the camber thrust.

Figure 5.27 shows a typical plot of lateral force F_y with camber angle γ for increasing tyre load with the slip angle set to zero. From the plot it can be seen that the camber stiffness C_γ is the gradient of the curve measured at zero camber angle at a given tyre load.

In order to understand why a cambered tyre rolling at zero slip angle produces an aligning moment, it is useful to consider the effect of the shape of the contact patch. Consider the situation shown in Figure 5.28 where the wheel and tyre are rolling at a camber angle γ with the slip angle equal to zero. The lower part of Figure 5.28 is a plan view on the tyre contact patch. The three points A, B and C, shown in Figure 5.28, are initially in line across the centre of the contact patch. If the tyre rolls so that point B moves to B′ at the rear of the contact patch then the rubber in the centre line is not subjected to any longitudinal stress.

Due to the camber the tyre will corner and point A on the inside of the tyre will roll at a smaller radius of bend to point C on the outside of the tyre. If the tyre rubber was not subject to any longitudinal stress these points would move to A″ and C″ respectively. If it is assumed that the stiffness of the tyre restricts this and the points remain in line across the rear of the contact patch (A′, B′ and C′) then a longitudinal tensile stress acts on the inner A side and a compressive stress acts on the outer C side.

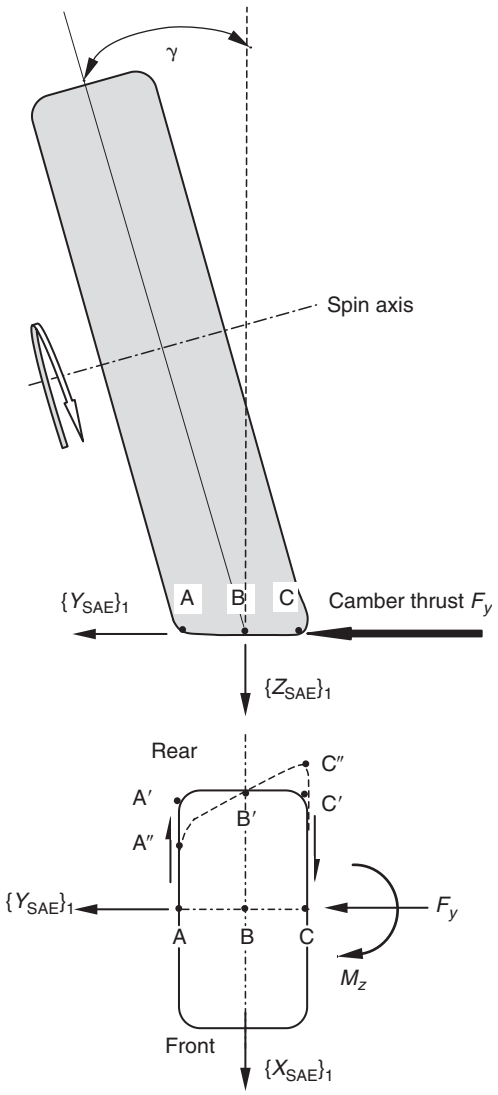

Fig. 5.28 Generation of self-aligning moment due to camber angle

The longitudinal stresses produce an effective force couple M_z shown in Figure 5.28 acting along the inner and outer side of the patch. A typical plot of aligning moment with camber angle, for a given tyre load and zero slip angle, is shown in Figure 5.29. From the plot it can be seen that the aligning moment camber stiffness is the gradient of the curve measured at zero camber angle at a given tyre load.

The lateral forces due to camber angle tend to be small when compared with those resulting from slip angle for a typical car tyre. In the linear range it would not be untypical to generate as much as 20 times the amount of lateral force per degree of slip angle compared with that generated per degree of camber angle. For motorcycle tyres, with a more rounded profile, it is

possible for riders to incline the motorcycle to produce camber angles between the tyre and road in excess of 45°, resulting in camber thrust being the most significant component of lateral force.

5.4.9 Combinations of camber and slip angle

The treatment so far has considered the generation of lateral force due to slip angle and camber angle in isolation. For a road car, while slip angle dominates the generation of lateral force, some amount of camber will occur at the same time. The effect of adding camber to slip angle is shown in Figure 5.30 where for a given tyre load the lateral force against slip angle curve is plotted at 0°, 5° and 10° of camber angle. It should be noted that

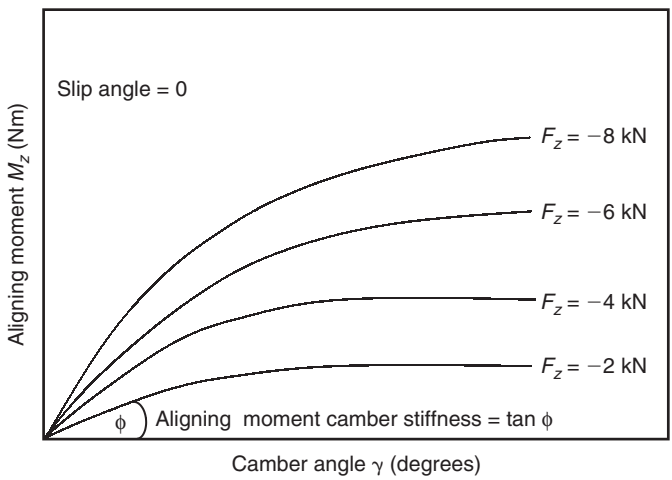

Fig. 5.29 Plotting aligning moment versus camber angle

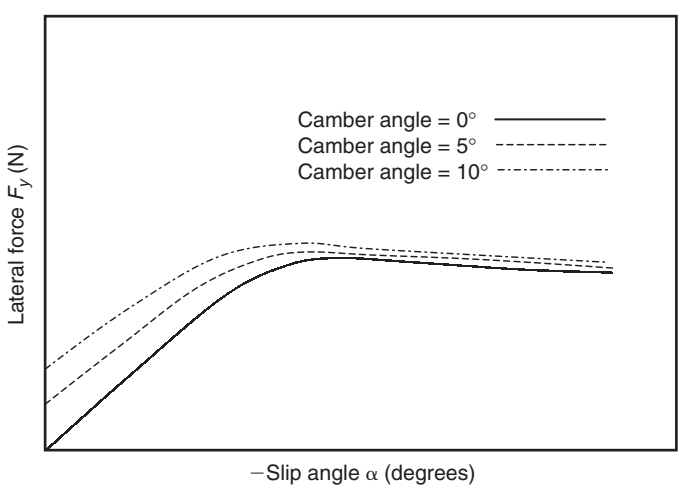

Fig. 5.30 The effect of combined camber and slip angle on lateral force

the curves here are plotted with assisting camber angle where the wheels are leaning into the turn. A similar reduction in lateral force will occur where the camber angle is reversed and the wheels lean out of the turn.

At zero degrees of slip angle the introduction of camber angle introduces an offset from the origin, this being the camber thrust discussed earlier occurring at a zero slip angle. The small offsets in lateral force due to conicity and plysteer, discussed in section 5.2.3, are ignored in Figure 5.30. In the linear range the contributions in lateral force due to slip and camber may be added together but during the transition towards sliding it can be seen that the additive effect of camber will reduce although the peak value of lateral force is still increased. The maximum increase in peak lateral force will occur at different camber angles for different wheel loads. Thus for a given tyre on a given vehicle it is possible (Milliken and Milliken, 1995) to optimize camber angle for a given combination of slip angle and tyre load.

5.4.10 Overturning moment

Two of the components of moment acting in the tyre contact patch have been discussed. The generation of rolling resistance moment was described while discussing the free rolling tyre in section 5.4.3. The self-aligning moment arising due to slip or camber angle was discussed in sections 5.4.7 and 5.4.8. For completeness the final component of moment acting at the tyre contact patch that requires description is the overturning moment that would arise due to deformation in the tyre as shown in Figure 5.31. The forces and moments as computed in the SAE reference frame are formulated to act at P, this being the point where the wheel plane intersects the ground plane at a point longitudinally aligned with the wheel centre.

In Figure 5.31 it can be seen that distortion of the side walls results in a lateral shift of the contact patch, which may result from either slip angle or

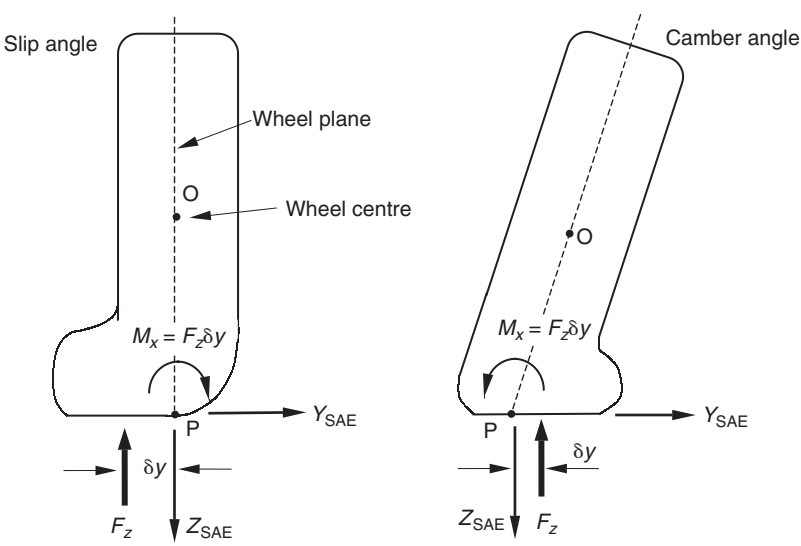

Fig. 5.31 Generation of overturning moment in the tyre contact patch

camber angle or a combination of the two. The resulting offset tyre load introduces an additional component of moment M_x. Attention to the sign convention associated with the tyre reference frame is again needed if the moment is to be included in a tyre model. In Figure 5.31, to assist understanding, F_z is represented as the tyre load acting on the tyre rather than the negative normal force computed in the Z_{SAE} direction.

A consideration of the overturning moment is generally more important where relatively large displacements in the tyre occur, as with aircraft tyres (Smiley, 1957; Smiley and Horne, 1960). Overturning effects are also of major importance for motorcycle tyres, particularly in terms of matching the behaviour of front and rear tyres. The lateral offset, δy, also applies to the longitudinal forces and is responsible for the 'stand up under light braking' that all motorcycles display.

5.4.11 Combined traction and cornering (comprehensive slip)

The treatment of longitudinal braking or driving forces and lateral cornering forces has so far dealt with the two components of force in isolation. The simulation of vehicle behaviour involving tyre forces acting in this manner leads to what is termed pure cornering or pure tractive (i.e. driving or braking) behaviour. In reality longitudinal and lateral forces often occur simultaneously during vehicle manoeuvres. A typical situation would be to initiate braking before entering a bend and continue braking into the corner. It is also typical, once the driver feels sufficient confidence, to begin applying throttle, and driving forces, during cornering before exiting the bend. For such situations a tyre model must be able to deal with combined tractive and cornering forces, a situation referred to as comprehensive slip.

The basic law of friction relating frictional force to normal force can be of assistance when considering combinations of longitudinal driving or braking forces with lateral cornering forces. The treatment here concentrates on lateral forces due to slip angle with camber angle set to zero. Figure 5.32 initially shows a tyre subject to pure braking or cornering force where in each case the slip in the ground plane is such that the tyre force produced is a peak value this being μF_z, the peak coefficient of friction multiplied by tyre load.

For pure cornering the peak force will occur at a relatively large slip angle where in Figure 5.32 some lateral distortion of the contact patch is indicated together with a small amount of pneumatic trail.

For a tyre running at a large slip angle with additional braking force the resultant ground plane force is still equal to μF_z but the resultant force direction opposes the direction of sliding. The longitudinal and lateral forces F_x and F_y are now components of the resultant force. Thus it can be seen that the simultaneous action of longitudinal and lateral slip reduces the amount of cornering or braking/driving force that may be obtained independently.

Figure 5.33 shows a plot of lateral force against longitudinal force for a range of slip angles at a given tyre load and with the camber angle set to zero. The x-axis represents the tyre at zero slip angle running from a maximum braking force value equal to μF_z at point A to a maximum driving force value equal to μF_z at point B, these points being consistent with the slip ratios that would produce peak force for a straight running tyre.

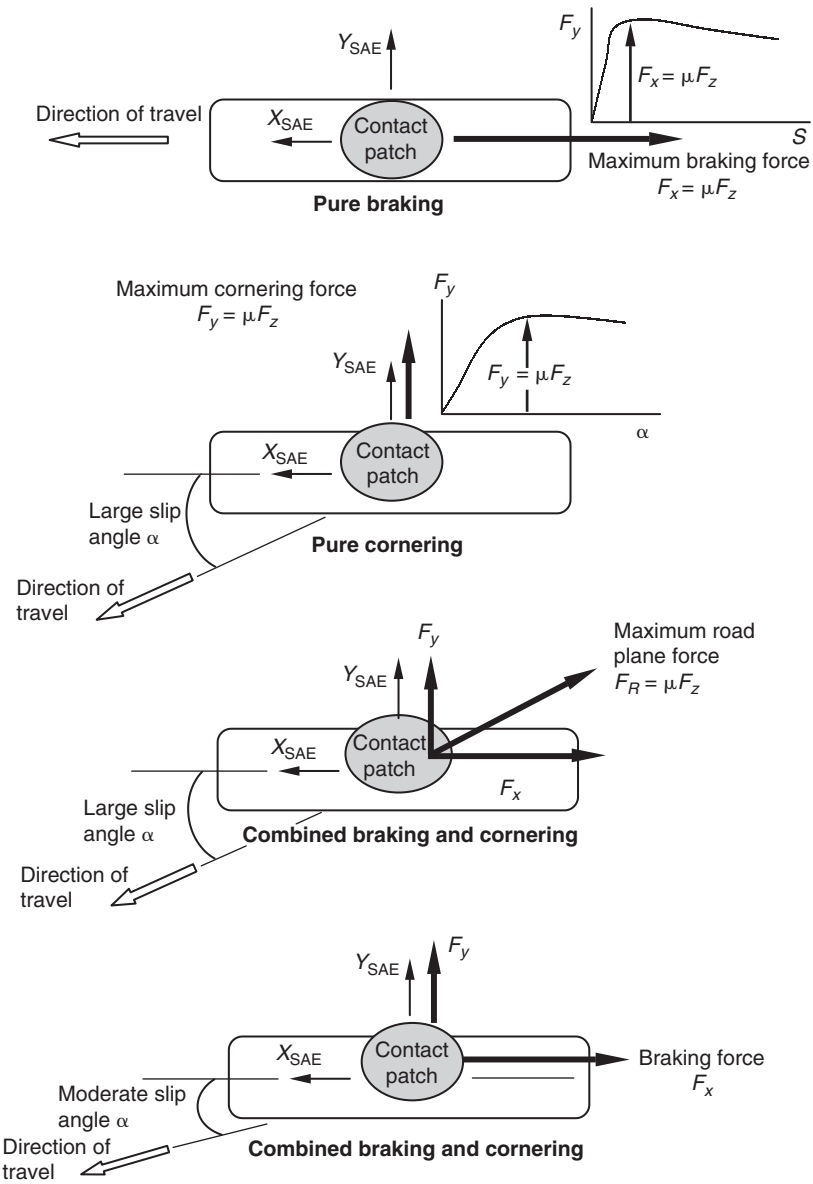

Fig. 5.32 Pure and combined braking and cornering forces

In the absence of braking or driving force the maximum lateral force equal to μF_z that can be achieved occurs at point C. Measurements of F_y at points along the *y*-axis intersected by curves at the set slip angles shown would provide a plot of lateral force against slip angle at the given tyre load. As driving or braking force is added the maximum resultant force that can be achieved is defined by points lying on a curve of radius μF_z referred to as the 'friction circle' or sometimes the 'friction ellipse' as some tyres will have more capability in traction or cornering leading to an elliptical boundary shape.

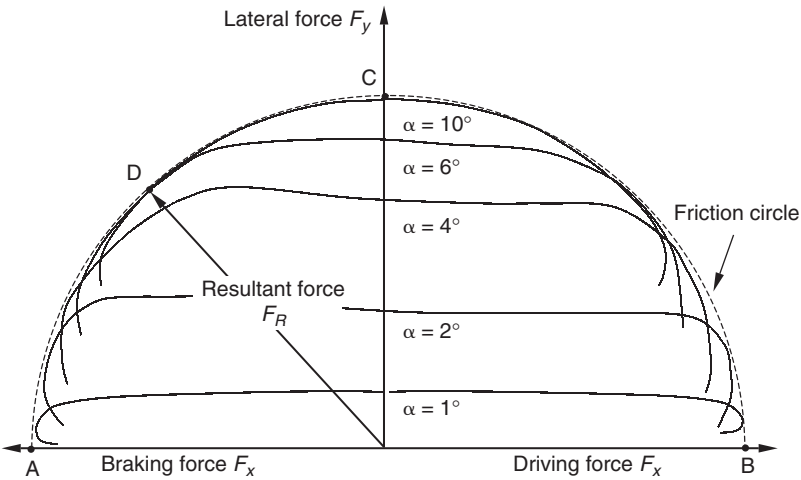

Fig. 5.33 Plotting lateral force against longitudinal force (friction circle)

Figure 5.33 shows, for a typical tyre, the general form of the friction circle diagram for the full range of driving and braking forces. Note that only lateral forces due to positive slip angle are presented and a similar diagram would exist for measurements taken at negative slip angles. Point D represents an example of a position where the tyre is operating at the friction limit for combined braking and cornering, as shown in Figure 5.32 where it is clear that the amount of braking or cornering force that could be produced independently is reduced and that the magnitude of F_R is simply

$$F_R = \sqrt{F_x^2 + F_x^2} \tag{5.23}$$

It can also be noted that the curves are not symmetric in that lateral forces initially increase slightly as braking force is applied. As discussed earlier the braking force adds circumferential tension to the tyre material entering the contact patch. This stress stiffening effect can be seen to raise the lateral force slightly while the reversal of longitudinal force to driving leads to a reduction. As the curves approach the friction limit it can be observed that they turn inwards. For a fixed slip angle the longitudinal slip is increased moving along the curves, for either braking or driving, until the point where both lateral force and longitudinal force reduce, hence causing the curves to bend back.

Plotting curves of aligning moment on the y-axis against longitudinal force on the x-axis it is possible to show that the opposite can occur (Phillips, 2000) and that adding braking force reduces aligning moment and adding driving force adds to it. Referring back to Figure 5.32, the bottom diagram shows a tyre running at moderate slip angle producing a lateral force F_y along a line of action set back from the centre by the pneumatic trail. The contact patch is shown displaced laterally due to the cornering force so that for simultaneous braking the braking force produces a moment that would subtract from the existing aligning moment due to the product of lateral force and pneumatic trail. From the diagram at the bottom of Figure 5.32 it is also clear that the simultaneous application of a driving force would produce

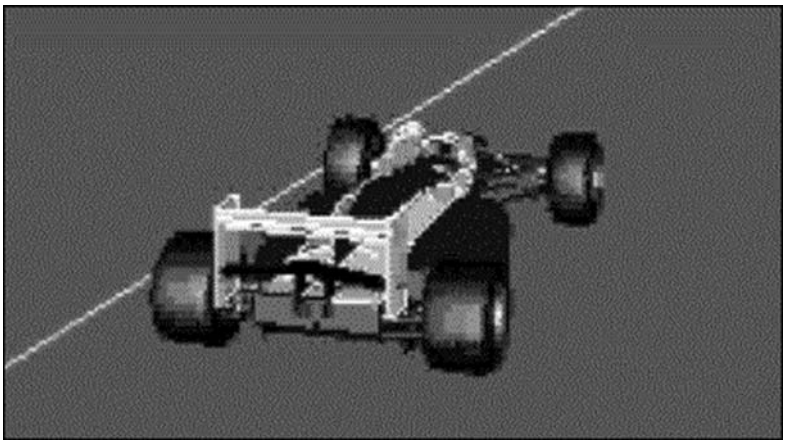

Fig. 5.34 Race car simulation model (provided courtesy of MSC.Software)

a moment that would add to the aligning moment due to the product of lateral force and pneumatic trail. At higher braking forces the effect may cause the aligning moment to go negative.

The friction circle or ellipse is also a way to monitor the performance of a race car driver using instrumented measurements of lateral and longitudinal accelerations, sometimes called the 'g–g' diagram. Comparing this diagram with known tyre data it is possible to see how well the driver performs keeping the vehicle close to the friction limits of the tyres.

A similar exercise is possible using an MBS model of a vehicle with a road model to represent the circuit. With the MBS model, extraction of longitudinal and lateral tyre force time histories is possible for a simulated lap of the circuit. This in theory allows investigation into the influence of tyre or vehicle model parameter changes and steering inputs on tyre limit behaviour.

5.4.12 Relaxation length

For cornering it has been shown that the generation of lateral force due to slip angle is of prime importance. In practice the generation of lateral force is not instantaneous but is subject to a delay generally referred to as 'tyre lag'. Without modelling some form of time lag a tyre model will compute the force and pass this to the MBS vehicle model so that the lateral force is applied instantly at that integration time step. It has been shown (Loeb et al., 1990) that the tyre must roll a certain distance, 'relaxation length', for the tyre to deflect sufficiently to generate the lateral force.

A possible method to measure relaxation length is to set the tyre up at a given slip angle in a test rig with the drum or belt not yet moving. On starting the machine the distance rolled before the forces and moments reach steady state can be recorded, hence giving a measure of relaxation length. An improved method for vehicle dynamics (Loeb et al., 1990) is to start the test with the tyre running at low speed in the straight ahead configuration and apply a rapid step input of steer angle to the tyre producing a time

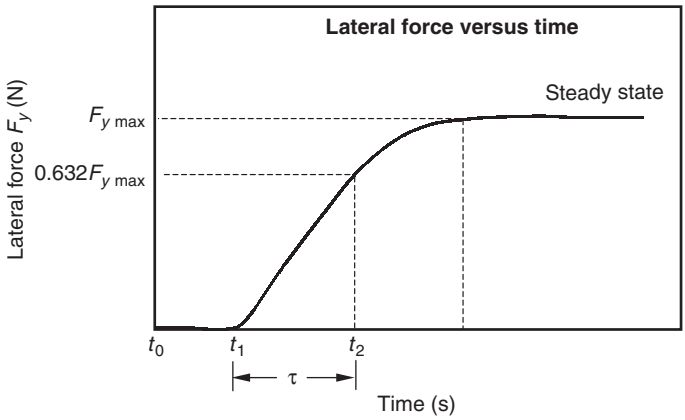

Fig. 5.35 Development of lateral force following step steering input

history plot, similar to that shown in Figure 5.35, indicating the build-up in lateral force.

The results obtained (Loeb et al., 1990) for the lateral force response appear exponential indicating a first order dynamic system where the time constant τ, equal to $t_2 - t_1$ in Figure 5.35, is the time required to achieve 63.2% of the final steady state response.

Incorporation of a lag effect for tyre lateral force within an MBS program requires an understanding of the mathematical integration process used to solve the equations of motion as discussed in Chapter 3 of this text. For the MSC.ADAMS program the approach taken is to compute a theoretical value of slip angle, α_l, that includes a lag effect and to input this to the appropriate tyre model algorithm for lateral force due to slip angle. As a starting point the tyre relaxation length L_R is taken as an input parameter from which, for a forward speed V_x, the time constant τ can be found using

$$\tau = L_R/V_x \tag{5.24}$$

Thus by this definition the relaxation length L_R is the distance through which the tyre must roll in order to develop 63.2% of the required lateral force. This leads to an initial expression:

$$\frac{d\alpha_l}{dt} = \frac{\alpha_c - \alpha_l}{\tau} \tag{5.25}$$

where

α_c is the computed value of slip angle (instantaneous) at the current time
α_l is the value of slip angle corrected to account for lag

An estimate of the term $d\alpha_l/dt$ in equation (5.25) can be obtained from equation (5.26). Additional understanding of the terms can be obtained by reference to Figure 5.36 where for clarity the integration time step, $t - t_{\text{last}}$, is shown with exaggerated magnitude:

$$\frac{d\alpha_l}{dt} \approx \frac{\alpha_l - \alpha_{\text{last}}}{t - t_{\text{last}}} \tag{5.26}$$

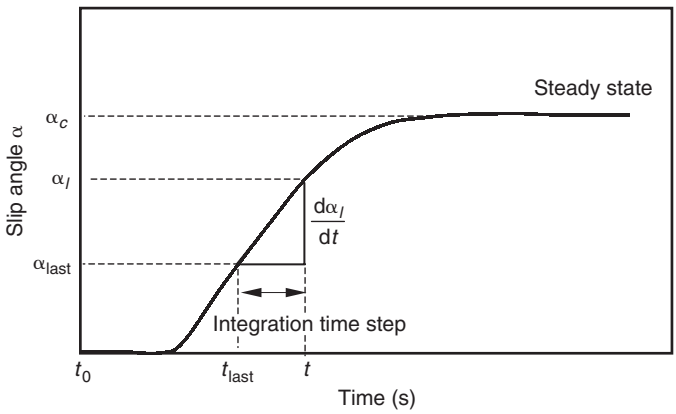

Fig. 5.36 Build-up of slip angle in an MBS model to represent tyre lag

where

α_{last} is the value of α_l computed at the last successful integration time step
t is the current simulation time
t_{last} is the time for the last successful integration time step

An estimate of the term $(\alpha_c - \alpha_l)/\tau$ in equation (5.25) can be obtained from

$$\frac{\alpha_c - \alpha_l}{\tau} = \frac{\alpha_c - \alpha_{last}}{\tau} \tag{5.27}$$

Combining equations (5.26) and (5.27) allows the value of α_l required to compute lateral force at the current time step to be obtained from

$$\alpha_l = \left(\frac{\alpha_c - \alpha_l}{\tau}\right)\left(t - t_{last}\right) + \alpha_{last} \tag{5.28}$$

Using data for the baseline vehicle used throughout this text it is possible to carry out a calculation to estimate a time delay, tyre lag, for a vehicle travelling at 100 kph. The load on the tyre F_z is taken as 4500 N and the radial stiffness of the tyre k_z is taken as 160 N/mm. From this it is possible to calculate the static tyre deflection δ_z:

$$\delta_z = \frac{F_z}{k_z} = 28.1\,\text{mm} \tag{5.29}$$

Referring back to equation (5.10) the effective rolling radius, R_e, can be calculated using the tyre deflection δ_z from equation (5.29) and an unloaded tyre radius, R_u, of 318.5 mm from

$$R_e = R_u - \frac{\delta_z}{3} = 309.1\,\text{mm} \tag{5.30}$$

Typically a tyre would roll through between 0.5 and 1 revolution (Gillespie, 1992) in order to develop the lateral force following a change in slip angle. If we assume that the tyre must complete 0.5 revolutions then for a speed of 100 kph the tyre lag on this vehicle is 0.035 s.

5.5 Experimental testing

In order to obtain the data needed for the tyre modelling required for simulation a series of tests may be carried out using tyre test facilities, typical examples being the machines that are illustrated in Figures 5.37 and 5.38. The following is typical of tests performed (Blundell, 2000) used to obtain the tyre data that supports the baseline vehicle used throughout this text.

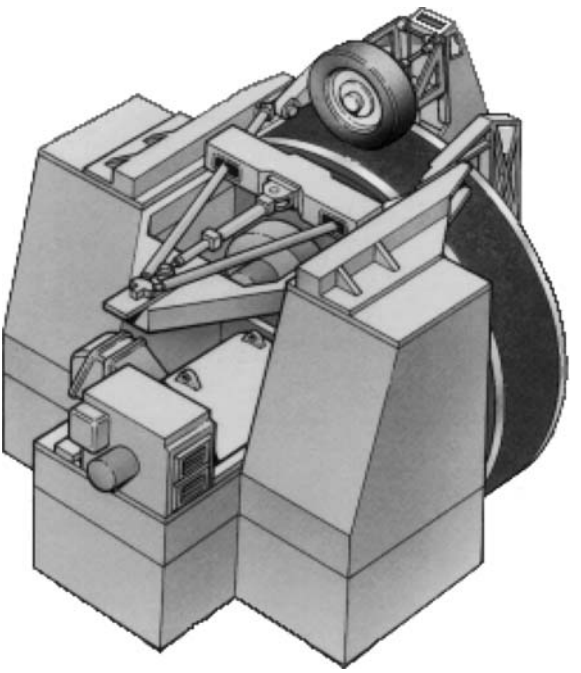

Fig. 5.37 High Speed Dynamics machine for tyre testing formerly at Dunlop Tyres Ltd (courtesy of Dunlop Tyres Ltd)

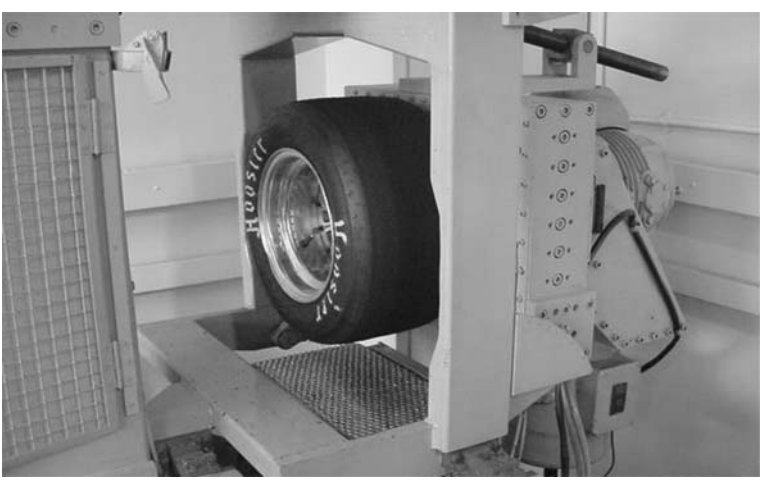

Fig. 5.38 Flat Bed Tyre Test machine at Coventry University

The measurements of forces and moments were taken using the SAE co-ordinate system for the following configurations:

(i) Varying the vertical load in the tyre 200, 400, 600, 800 kg.

(ii) For each increment of vertical load the camber angle is varied from −10 to 10 degrees with measurements taken at 2 degree intervals. During this test the slip angle is fixed at 0 degrees.

(iii) For each increment of vertical load the slip angle is varied from −10 to 10 degrees with measurements taken at 2 degree intervals. During this test the camber angle is fixed at 0 degrees.

(iv) For each increment of vertical load the slip and camber angle are fixed at zero degrees and the tyre is gradually braked from the free rolling state to a fully locked skidding tyre. Measurements were taken at increments in slip ratio of 0.1.

The test programme outlined here can be considered a starting point in the process of obtaining tyre data to support a simulation exercise. In practice obtaining all the data required to describe the full range of tyre behaviour discussed in the preceding sections will be extremely time consuming and expensive. The test programme described here does not, for example, consider effects such as varying the speed of the test machine, changes in tyre pressure or wear, changes in road texture and surface contamination by water or ice. The testing is also steady state and does not consider the transient state during transition from one orientation to another.

Most importantly the tests do not consider the complete range of combinations that can occur in the tyre. The longitudinal force testing described is limited by only considering the generation of braking force. To obtain a complete map of tyre behaviour it would also, for example, be necessary to test not only for variations in slip angle at zero degrees of camber angle but to repeat the slip angle variations at selected camber angles. For comprehensive slip behaviour it would be necessary at each slip angle to brake or drive the tyre from a free rolling state to one that approaches the friction limit, hence deriving the 'friction circle' for the tyre.

Extending a tyre test programme in this way may be necessary to generate a full set of parameters for a sophisticated tyre model but will significantly add to the cost of testing. Obtaining data requires the tyre to be set up at each load, angle or slip ratio and running in steady state conditions before the required forces and moments can be measured. By way of example the basic test programme described here required measurements to be taken for the tyre in 132 configurations. Extending this, using the same pattern of increments and adding driving force to consider combinations of slip angle with camber or slip ratio would extend the testing to 1452 configurations. In practice this could be reduced by judicious selection of test configurations but it should be noted the tests would still be for a tyre at constant pressure and constant speed on a given test surface. Examples of test results for a wider range of tyres and settings can be obtained by general reference to the tyre specific publications quoted in this chapter and in particular to the textbook by Pacejka (2002).

For the tyre tests described here the following is typical of the series of plots that would be produced in order to assess the force and moment

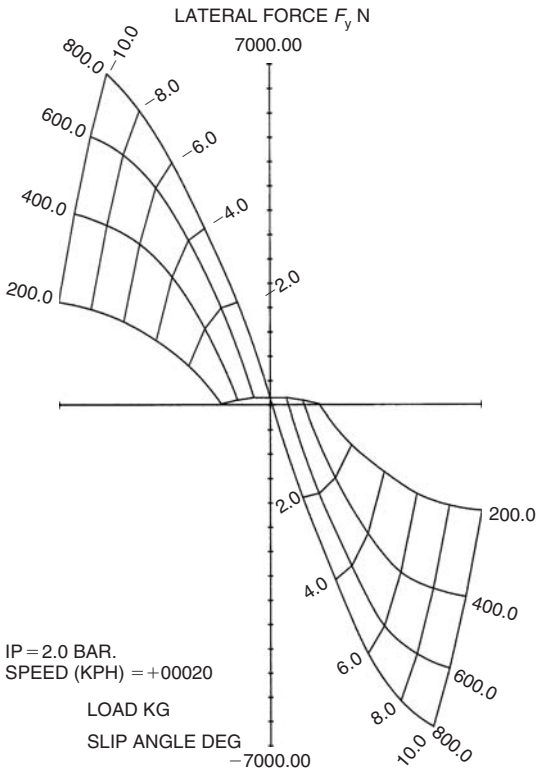

Fig. 5.39 Lateral force F_y with slip angle α (courtesy of Dunlop Tyres Ltd)

characteristics. The results are presented in Figures 5.39 to 5.48 where a carpet plot format is used for the lateral force and aligning moment results:

(i) Lateral force F_y with slip angle α

(ii) Aligning moment M_z with slip angle α

(iii) Lateral force F_y with aligning moment M_z (Gough plot)

(iv) Cornering stiffness with load

(v) Aligning stiffness with load

(vi) Lateral force F_y with camber angle γ

(vii) Aligning moment M_z with camber angle γ

(viii) Camber stiffness with load

(ix) Aligning camber stiffness with load

(x) Braking force with slip ratio

Before continuing with the treatment of tyre modelling readers should note the findings (van Oosten et al., 1999) of the TYDEX Workgroup. In this study a comparison of tyre cornering stiffness for a tyre tested on a range

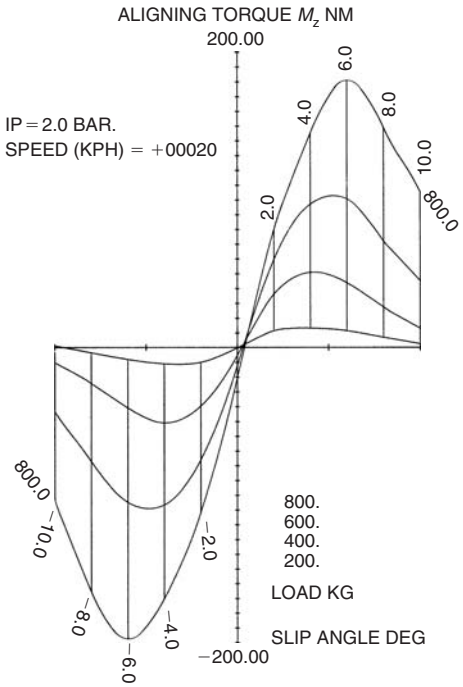

Fig. 5.40 Aligning moment M_z with slip angle α (courtesy of Dunlop Tyres Ltd)

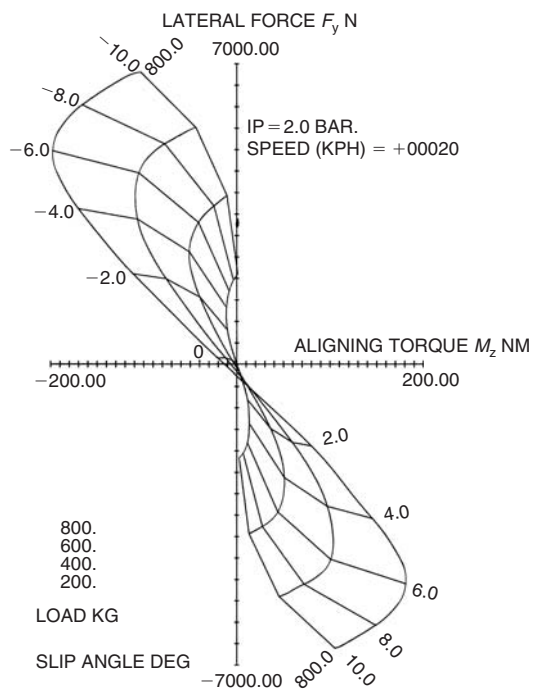

Fig. 5.41 Lateral force F_y with aligning moment M_z (Gough plot) (courtesy of Dunlop Tyres Ltd)

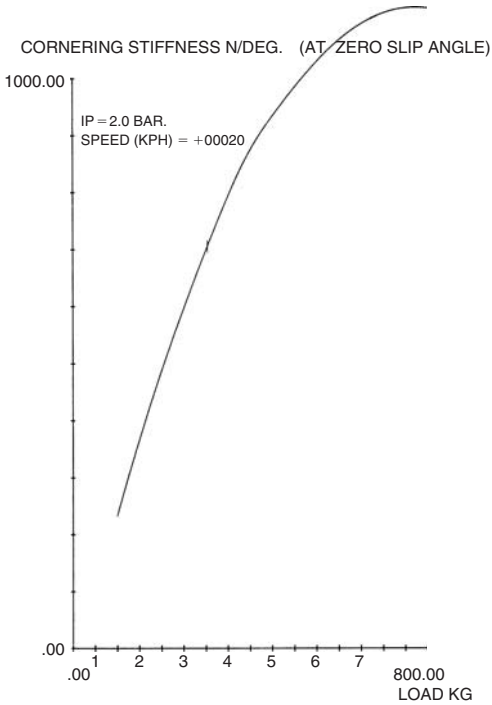

Fig. 5.42 Cornering stiffness with load (courtesy of Dunlop Tyres Ltd)

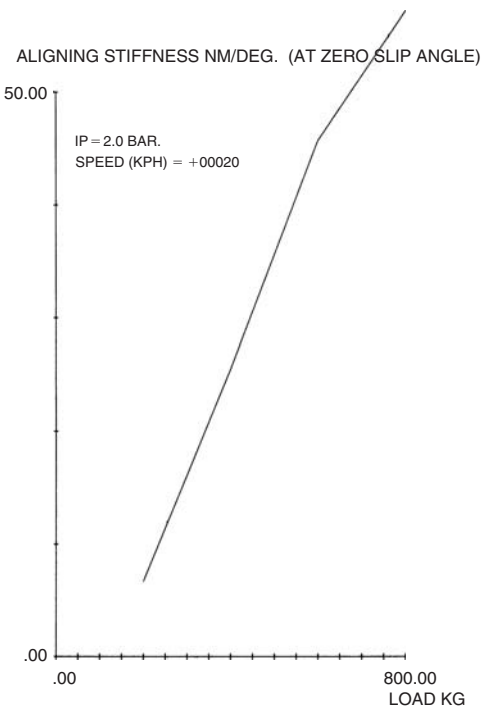

Fig. 5.43 Aligning stiffness with load (courtesy of Dunlop Tyres Ltd)

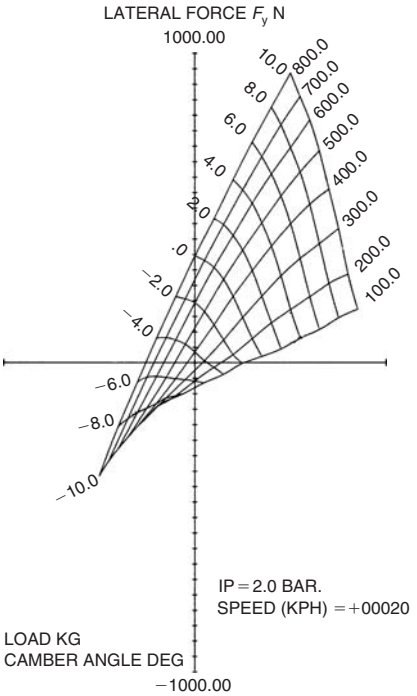

Fig. 5.44 Lateral force F_y with camber angle γ (courtesy of Dunlop Tyres Ltd)

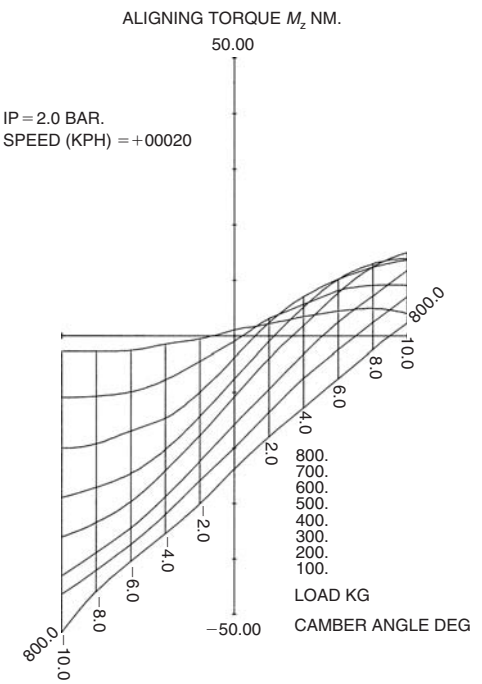

Fig. 5.45 Aligning moment M_Z with camber angle γ (courtesy of Dunlop Tyres Ltd)

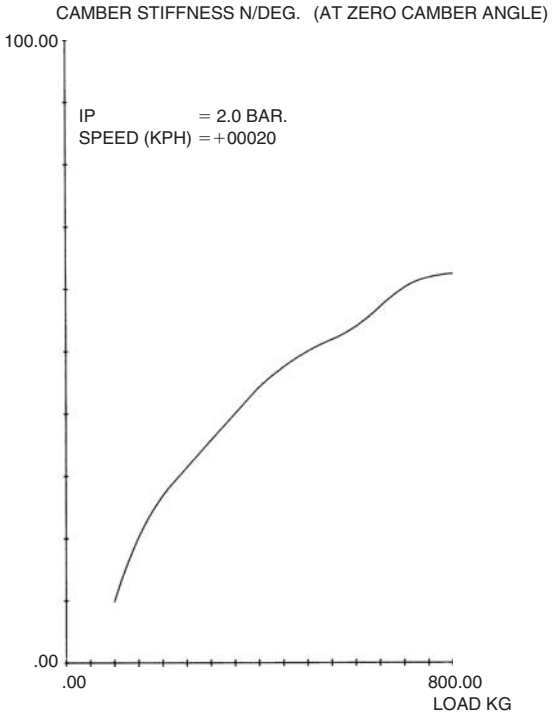

Fig. 5.46 Camber stiffness with load (courtesy of Dunlop Tyres Ltd)

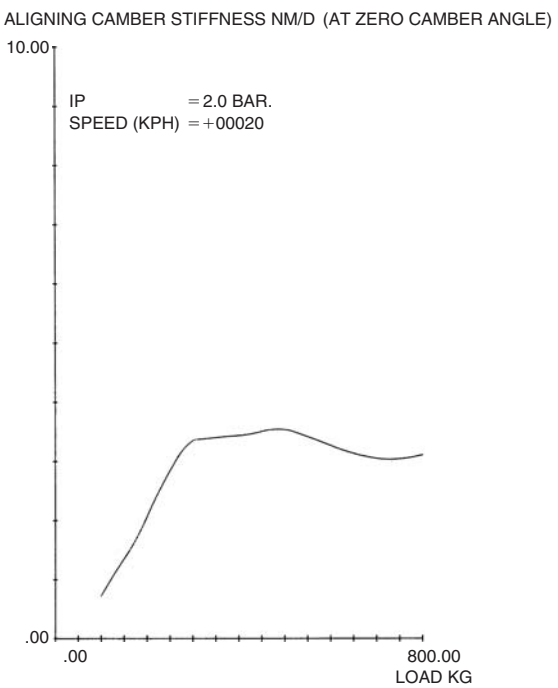

Fig. 5.47 Aligning camber stiffness with load (courtesy of Dunlop Tyres Ltd)

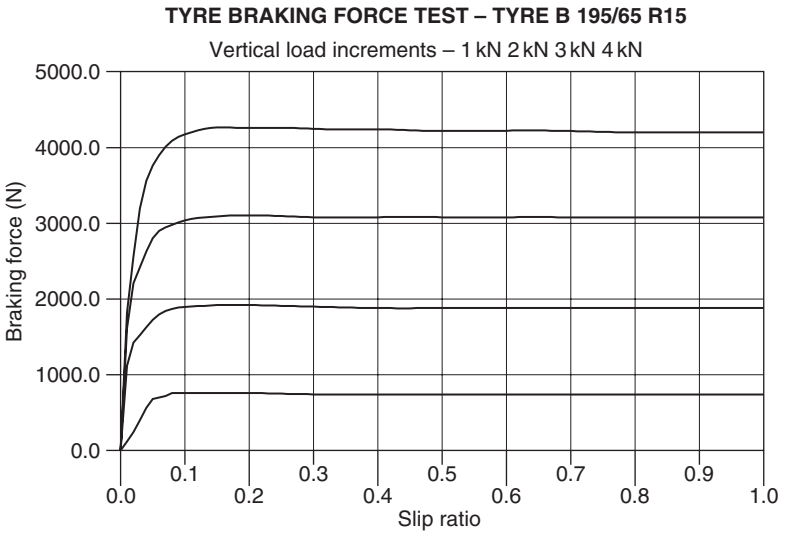

Fig. 5.48 Braking force with slip ratio

of comparable tyre test machines gave differences between minimum and maximum measured values of up to 46%. Given the complexities of the tyre models that are described in the following section the starting point should be a set of measured data that can be used with confidence to form the basis of a tyre model.

5.6 Tyre modelling

5.6.1 Overview

The modelling of the forces and moments at the tyre contact patch has been the subject of extensive research in recent years. A review of some of the most common tyre models was provided by Pacejka and Sharp (1991), where the authors state that it is necessary to compromise between the accuracy and complexity of the model. The authors also state that the need for accuracy must be considered with reference to various factors including the manufacturing tolerances in tyre production and the effect of wear on the properties of the tyre. This would appear to be a valid point not only from the consideration of computer modelling and simulation but also in terms of track testing where new tyres are used to establish levels of vehicle performance. A more realistic measurement of how a vehicle is going to perform in service may be to consider testing with different levels of wear or incorrect pressure settings.

One of the methods discussed by Pacejka and Sharp (1991) focuses on a multi-spoke model developed by Sharp where the tyre is considered to be a series of radial spokes fixed in a single plane and attached to the wheel hub. The spokes can deflect in the radial direction and bend both circumferentially and laterally. Sharp provides more details on the radial spoke model approach in Sharp and El-Nashar (1986) and Sharp (1990, 1993). The other

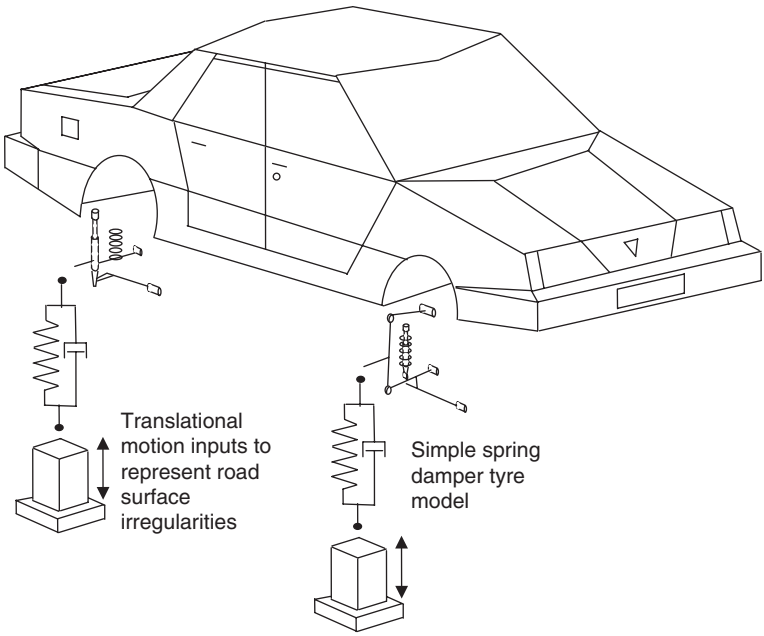

Fig. 5.49 A simple tyre model for ride and vibration studies. (This material has been reproduced from the Proceedings of the Institution of Mechanical Engineers, K1 Vol. 214 'The modelling and simulation of vehicle handling. Part 3: tyre modelling', M.V. Blundell, page 4, by permission of the Council of the Institution of Mechanical Engineers)

method of tyre modelling reviewed is based on the 'Magic Formula' that will be discussed in more detail later in this section. Another review of tyre models is given by Pacejka (1995), where the influence of the tyre is discussed with regard to 'active' control of vehicle motion. The radial-spoke and 'Magic Formula' models are again discussed.

Before considering tyre models in more detail it should be stated that tyre models are generally developed according to the type of application the vehicle simulation will address. For ride and vibration studies the tyre model is often required to transmit the effects from a road surface where the inputs are small but of high frequency. In the simplest form the tyre may be represented as a simple compression-only spring and damper acting between the wheel centre and the surface of the road. The simulation may in fact recreate the physical testing using a four-poster test rig with varying vertical inputs at each wheel. A concept of the tyre model for this type of simulation is provided in Figure 5.49 where for clarity only the right side of the vehicle is shown.

In suspension loading or durability studies the tyre model must accurately represent the contact forces generated when the tyre strikes obstacles such as potholes and road bumps. In these applications the deformation of the tyre as it contacts the obstacle is of importance and is a factor in developing the model. These sort of tyre models are often developed for agricultural or construction type vehicles used in an off-road environment and dependent on the tyre to a larger extent in isolating the driver from the

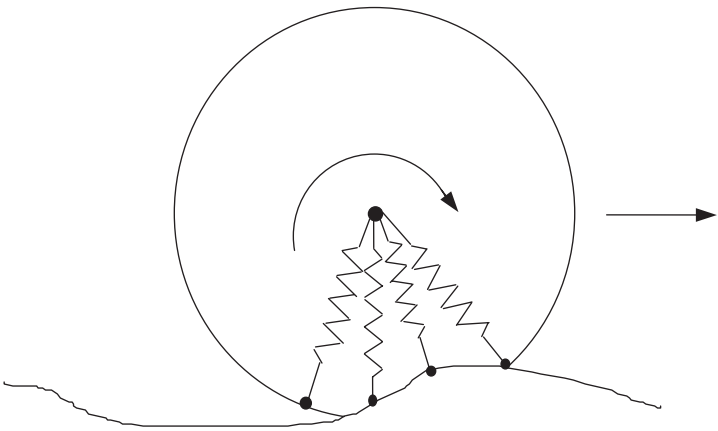

Fig. 5.50 A radial spring terrain enveloping tyre model. (This material has been reproduced from the Proceedings of the Institution of Mechanical Engineers, K1 Vol. 214 'The modelling and simulation of vehicle handling. Part 3: tyre modelling', M.V. Blundell, page 4, by permission of the Council of the Institution of Mechanical Engineers)

ground surface inputs. An example of this sort of tyre model is described by Davis (1974) where a radial spring model was developed to envelop irregular features of a rigid terrain. The tyre is considered to be a set of equally spaced radial springs that when in contact with the ground will provide a deformed profile of the tyre as it envelops the obstacle. The deformed shape is used to redefine the rigid terrain with an 'equivalent ground plane'. The concept of an equivalent ground plane model was used in the early ADAMS/Tire™ model for the durability application but has the main limitation that the model is not suitable for very small obstacles that the tyre might completely envelop. This is clarified by Davis (1974) where it is stated that the wavelength of surface variations in the path of the tyre should be at least three times the length of the tyre to ground contact patch. The other and most basic limitation of this type of model is that the simulation is restricted to straight-line motion and would only consider the vertical and longitudinal forces being generated by the terrain profile. An example of a radial spring tyre model is shown in Figure 5.50.

The work carried out by Kisielewicz and Ando (1992) describes how two different programs have been interfaced to carry out a vehicle simulation where the interaction between the tyre and the road surface has been calculated using an advanced non-linear finite element analysis program.

For vehicle handling studies we are generally concerned with the manoeuvring of the vehicle on a flat road surface. The function of the tyre model is to establish the forces and moments occurring at the tyre to road contact patch and resolve these to the wheel centre and hence into the vehicle as indicated in Figure 5.51.

For each tyre the tyre model will calculate the three orthogonal forces and the three orthogonal moments that result from the conditions arising at the tyre to road surface contact patch. These forces and moments are applied at each wheel centre and control the motion of the vehicle. In terms of

modelling the vehicle is actually 'floating' along under the action of these forces at each corner. For a handling model the forces and moment at the tyre to road contact patch which are usually calculated by the tyre model are:

(a) F_x – longitudinal tractive or braking force

(b) F_y – lateral cornering force

(c) F_z – vertical normal force

(d) M_z – aligning moment

The other two moments which occur at the patch, M_x the overturning moment and M_y the rolling resistance moment, are generally not significant for a handling tyre model for passenger cars. The calculation of these forces and moments at the contact patch is the essence of a tyre model and will be discussed in more detail later.

As a simulation progresses and the equations for the vehicle and tyre are solved at each solution point in time there is a flow of information between the vehicle model and the tyre model. The tyre model must continually receive information about the position, orientation and velocity at each wheel centre and also the topography of the road surface in order to calculate the forces and moment at the contact patch. The road surface is usually flat but may well have changing frictional characteristics to represent varying surface textures or changes between dry, wet or ice conditions. Inclined or cambered road surfaces can also be modelled if needed. The information

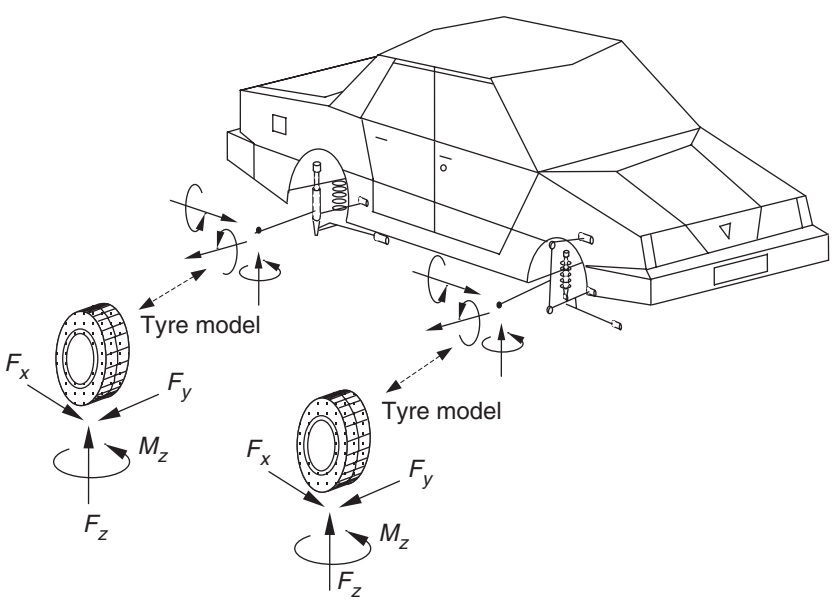

Fig. 5.51 Interaction between vehicle model and tyre model. (This material has been reproduced from the Proceedings of the Institution of Mechanical Engineers, K1 Vol. 214 'The modelling and simulation of vehicle handling. Part 3: tyre modelling', M.V. Blundell, page 5, by permission of the Council of the Institution of Mechanical Engineers)

from the wheel centre such as the height, camber angle, slip angle, spin velocity and so on are the inputs to the tyre model at each point in time and will dictate the calculation of the new set of forces at the contact patch.

These newly computed tyre conditions are then fed back to the vehicle model at each wheel centre. This will produce a change in the vehicle position at the next solution point in time. The conditions at each wheel centre will change and will be relayed back to the tyre model again. A new set of tyre forces and moments will then be calculated and so the process will continue.

The treatment of tyre models that follows in this section is based on methods that have been developed for vehicle handling simulations. A later section will deal with tyre models for durability analysis. As stated earlier the computation of vertical force is straightforward based on the equations in section 5.4.2. For the handling models described here the 'model' focuses on the calculation of longitudinal driving or braking forces and lateral forces. The formulation of rolling resistance and aligning moments is also covered. Before discussing individual tyre models it is necessary to describe the calculations carried out in the main MBS program to provide the tyre model with the necessary position, orientation and velocities of the road wheel.

5.6.2 Calculation of tyre geometry and velocities

A tyre model, for handling or durability analysis, requires input regarding the position and orientation of the wheel relative to the road together with velocities used to determine the slip characteristics. The implementation of these computations as a tyre model with an MBS program is best described using the full three-dimensional vector approach outlined in Chapter 2. The following description is based on the methods used in MSC.ADAMS but is applicable to any vehicle simulation model requiring tyre force and moment input. As a starting point the tyre can be modelled using the input radii R_1 and R_2 as shown in Figure 5.52.

Using the tyre model geometry based on a torus it is possible to determine the geometric outputs that are used in the subsequent force and moment

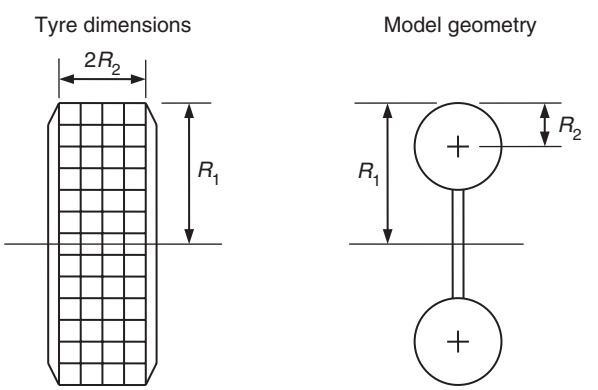

Fig. 5.52 Tyre model geometry. (This material has been reproduced from the Proceedings of the Institution of Mechanical Engineers, K1 Vol. 214 'The modelling and simulation of vehicle handling. Part 3: tyre modelling', M.V. Blundell, page 6, by permission of the Council of the Institution of Mechanical Engineers)

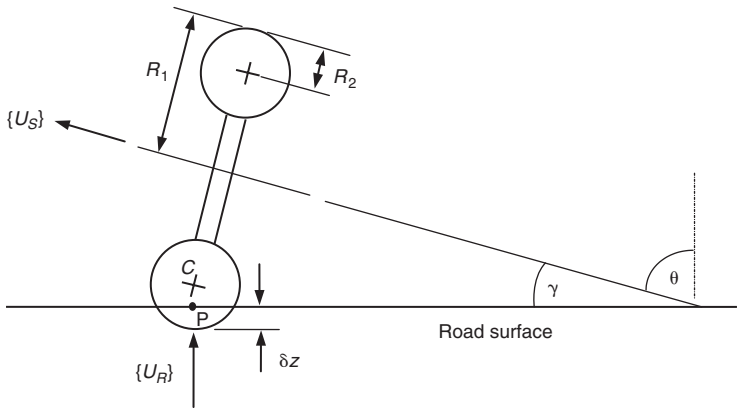

Fig. 5.53 Inclined tyre geometry

calculations. Consider first the view in Figure 5.53 looking along the wheel plane at the tyre inclined on a flat road surface.

The vector $\{U_s\}$ is a unit vector acting along the spin axis of the tyre. The vector $\{U_r\}$ is a unit vector that is normal to the road surface and passes through the centre of the tyre carcass at C. The contact point P between the tyre and the surface of the road is determined as the point at which the vector $\{U_r\}$ intersects the road surface. For the purposes of this document it is assumed the road is flat and only one point of contact occurs.

The camber angle γ between the wheel plane and the surface of the road is calculated using:

$$\gamma = \pi/2 - \theta \tag{5.31}$$

where

$$\theta = \arccos(\{U_r\} \bullet \{U_s\}) \tag{5.32}$$

The vertical penetration of the tyre δ_z at point P is given by:

$$\delta z = R_2 - |\mathrm{CP}| \tag{5.33}$$

In order to calculate the tyre forces and moment it is also necessary to determine the velocities occurring in the tyre. In Figure 5.54 the SAE co-ordinate system is located at the contact point P. This is established by the three unit vectors $\{X_{\mathrm{SAE}}\}_1$, $\{Y_{\mathrm{SAE}}\}_1$ and $\{Z_{\mathrm{SAE}}\}_1$. Note that referring back to Chapter 2 the subscript 1 indicates that the components of a vector are resolved parallel to reference frame 1, which in this case is the Ground Reference Frame (GRF).

Using the triangle law of vector addition it is possible to locate the contact point P relative to the fixed Ground Reference Frame O_1:

$$\{R_P\}_1 = \{R_W\}_1 + \{R_{PW}\}_1 \tag{5.34}$$

At this stage it should be said that the vector $\{R_{PW}\}_1$ represents the loaded radius and not the effective rolling radius of the tyre. Should this be significant for the work in hand, such as the modelling and simulation of ABS (Ozdalyan and Blundell, 1998), then further modification of the tyre model may be necessary.

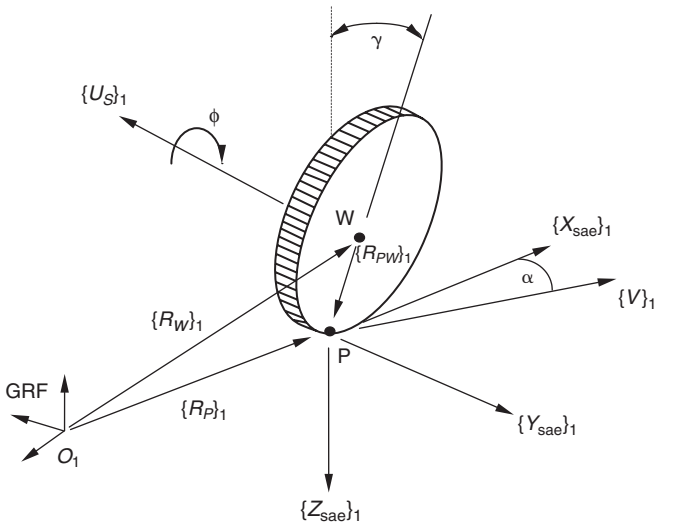

Fig. 5.54 Tyre geometry and kinematics. (This material has been reproduced from the Proceedings of the Institution of Mechanical Engineers, K1 Vol. 214 'The modelling and simulation of vehicle handling. Part 3: tyre modelling', M.V. Blundell, page 7, by permission of the Council of the Institution of Mechanical Engineers)

If the angular velocity vector of the wheel is denoted by $\{\omega\}_1$ then the velocity $\{V_P\}_1$ of point P is given by:

$$\{V_P\}_1 = \{V_W\}_1 + \{V_{PW}\}_1 \tag{5.35}$$

where

$$\{V_{PW}\}_1 = \{\omega\}_1 \times \{R_{PW}\}_1 \tag{5.36}$$

It is now possible to determine the components of $\{V_P\}_1$ which act parallel to the SAE co-ordinate system superimposed at P. The longitudinal slip velocity V_{XC} of point P is given by:

$$V_{XC} = \{V_P\}_1 \bullet \{X_{\text{SAE}}\}_1 \tag{5.37}$$

The lateral slip velocity V_Y of point P is given by:

$$V_Y = \{V_P\}_1 \bullet \{Y_{\text{SAE}}\}_1 \tag{5.38}$$

The vertical velocity V_Z at point P, which will be used to calculate the damping force in the tyre, is given by:

$$V_Z = \{V_P\}_1 \bullet \{Z_{\text{SAE}}\}_1 \tag{5.39}$$

Considering the angular velocity vector of the wheel $\{\omega\}_1$ in more detail we can represent the vector as follows. The wheel develops a slip angle α which is measured about $\{Z_{\text{SAE}}\}_1$, a camber angle γ which is measured about $\{X_{\text{SAE}}\}_1$ and a spin angle ϕ which is measured about $\{U_S\}_1$. The total angular velocity vector of the wheel is the summation of all three motions and is given by:

$$\{\omega\}_1 = \dot{\alpha}\{Z_{\text{SAE}}\}_1 + \dot{\gamma}\{X_{\text{SAE}}\}_1 + \dot{\varphi}\{U_s\}_1 \tag{5.40}$$

It is possible to consider an angular velocity vector $\{\omega_S\}_1$ that only considers the spinning motion of the wheel and does not contain the contributions due to α and γ. This vector for angular velocity that only considers spin is given by:

$$\{\omega_S\}_1 = \dot{\varphi}\{U_S\} \tag{5.41}$$

Using this it is possible to determine V_C the 'circumferential velocity' component of point P relative to the centre of the wheel W and measured parallel to $\{X_{\mathrm{SAE}}\}_1$:

$$V_C = (\{\omega_S\}_1 \times \{R_{PW}\}_1) \bullet \{X_{\mathrm{SAE}}\}_1 \tag{5.42}$$

At this stage it may be worth considering the usual two-dimensional representation of longitudinal slip for straight-line braking. Referring back to section 5.4.4 a definition of slip ratio, S, during braking was given by

$$S = \frac{V - \omega_B R_e}{V} \tag{5.43}$$

Based on the velocities which have been determined for the three-dimensional case it is now possible to calculate a longitudinal slip ratio, S, during braking which is given by:

$$S = \frac{V_{XC}}{|V_X|} \tag{5.44}$$

For this formulation of slip ratio V_{XC} can be considered to be the contact patch velocity relative to the road surface. This is equivalent to $V - \omega_B R_e$ in the two-dimensional model, albeit using the loaded radius in the vector-based formulation. The circumferential velocity V_C of P measured relative to the wheel centre can be subtracted from V_{XC} to give V_X the actual longitudinal velocity of P ignoring the rotation effect. This can be thought of as the velocity of an imaginary point in the ground that follows the contact patch and is also equivalent to V in the two-dimensional model. During traction, the longitudinal slip ratio is formulated using:

$$S = \frac{V_{XC}}{|V_c|} \tag{5.45}$$

The lateral slip of the contact patch relative to the road is defined by the slip angle α where

$$\alpha = \arctan\{V_Y/V_X\} \tag{5.46}$$

During braking a lateral slip ratio S_α is computed as:

$$S_\alpha = |\tan\alpha| = |V_Y/V_X| \tag{5.47}$$

During braking S_α will have a value of zero when V_Y is zero and can have a maximum value of 1.0, which equates to a slip angle α of 45 degrees. Slip angles in excess of this are not usual for vehicle handling but may occur in other applications where a tyre model is used, for example, to simulate aircraft taxiing on a runway.

During traction the formulation becomes:

$$S_\alpha = (1 - S)|\tan\alpha| = |V_Y/V_C| \tag{5.48}$$

5.6.3 Road surface/terrain definition

It is easy to forget when discussing tyres that the resultant forces and moments are a product, as with any friction-based model, of the interaction between the tyre and the road and not a property of the tyre in isolation. Early tyre models treated the road or terrain as simply an infinite flat surface requiring only a vertical datum for definition. This was extended to two-dimensional models that allowed a terrain to be defined as a series of sections. This allowed for durability type analysis, with forward motion only, to encounter potholes, bumps and other road obstacles. A typical current approach is to represent the geometry and frictional characteristics of the road surface or terrain using a finite element approach as shown in Figure 5.55.

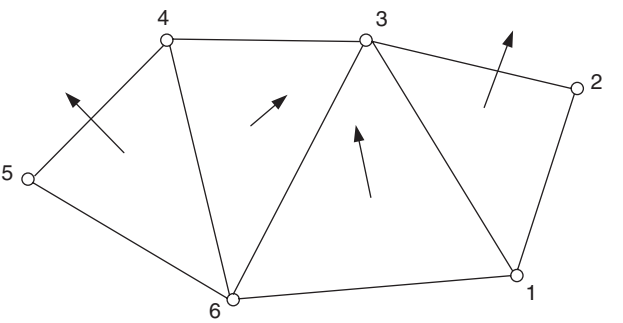

Fig. 5.55 Definition of road surface using finite element approach. (This material has been reproduced from the Proceedings of the Institution of Mechanical Engineers, K1 Vol. 214 'The modelling and simulation of vehicle handling. Part 3: tyre modelling', M.V. Blundell, page 9, by permission of the Council of the Institution of Mechanical Engineers)

The road surface is defined as a system of triangular patches. As with finite elements the outward normal of the element is defined by numbering the nodes for each element using a sequence that is positive when considering a rotation about the outward normal. For each element it is possible to define frictional constants that are factored with the friction parameters associated with a tyre property file. This would allow simulations when the vehicle encounters changing road conditions as with driving from dry to wet conditions or simulation of 'mu-split' conditions where one side of the vehicle is braking in the dry and the other on ice.

The ability to model a road surface as a continuous three-dimensional surface is required not only for durability work but is also needed for handling simulations on non-flat road surfaces. As with any finite element model the accuracy of the road surface definition will be a function of the mesh refinement. Current practice among some users in industry is to model the road using the more sophisticated mesh generation tools provided with finite element software and then run a small translation program to reformat the data file as, for example, an MSC.ADAMS road file.

5.6.4 Interpolation methods

Early tyre models for handling such as the initial ADAMS/Tire model used the results of laboratory rig testing directly to generate 'look-up' tables of

data that were used directly by the tyre model to interpolate the lateral force and aligning moment at the contact patch. Figure 5.56 illustrates a sample of some results which might typically be obtained from a tyre rig test where for variations in vertical load F_z the lateral forces F_y are plotted as a function of slip angle at zero camber angle.

For this set of data the independent variables that are set during the test are the camber angle, the vertical force, and the slip angle. The measured dependent variable is the lateral force. Using this measured data the tyre model, really a method rather than a model, uses a curve fit to obtain a value for the lateral force for the value of F_z and slip angle determined by the wheel centre position and orientation. If the instantaneous camber angle lies between two sets of measured data at different camber angles set during the test then the tyre model can use linear interpolation between the two camber angles. If the instantaneous camber angle is, for example, 2.4 degrees and measured data is available at 2 and 3 degrees, then the curve fitting as a function of F_z and slip angle is carried out at the two bounding camber angles and the linear interpolation is carried out between these two points. The approach described here for lateral force is applied in exactly the same manner when determining by interpolation a value for the aligning moment. There are some disadvantages in using an interpolation tyre model:

(i) The process of interpolating large quantities of data at every integration step in time may not be an efficient simulation approach and is often considered to result in increases in computer solution times for the analysis of any given manoeuvre.

(ii) This sort of model does not lend itself to any design modification or optimization involving the tyre. The tyre must already exist and have been tested. In order to investigate the influence of tyre design changes on vehicle handling and stability then the tyre model must be reduced to parameters that can be related to the tyre force and moment characteristics. This has led to the development of tyre models represented by formulae that will now be discussed.

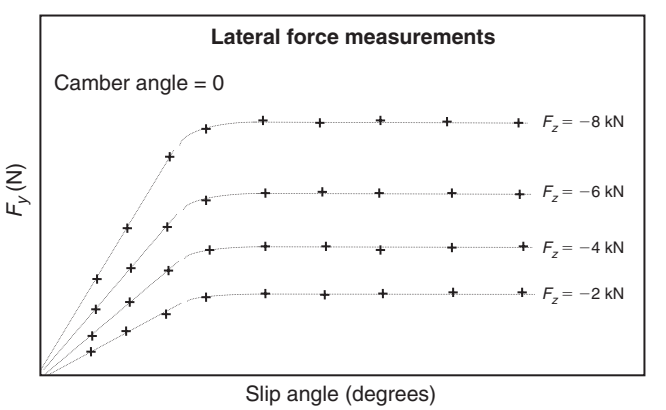

Fig. 5.56 Interpolation of measured tyre test data. (This material has been reproduced from the Proceedings of the Institution of Mechanical Engineers, K1 Vol. 214 'The modelling and simulation of vehicle handling. Part 3: tyre modelling', M.V. Blundell, page 14, by permission of the Council of the Institution of Mechanical Engineers)

5.6.5 The 'Magic Formula' tyre model

The tyre model which is now most well established and has generally gained favour is based on the work by Pacejka and as mentioned earlier is referred to as the 'Magic Formula'. The 'Magic Formula' is not a predictive tyre model but is used to represent the tyre force and moment curves and is undergoing continual development. The early version (Bakker et al., 1986, 1989) is sometimes referred to as the 'Monte Carlo version' due to the conference location at which this model was presented in the 1989 paper. The tyre models discussed here are based on the formulations described in Bakker et al. (1989) and a later version (Pacejka and Bakker, 1993) referred to as version 3 of the 'Magic Formula'. Other authors have developed systems based around the 'Magic Formula'. The BNPS model (Schuring et al., 1993) is a particular version of the 'Magic Formula' that automates the development of the coefficients working from measured test data. The model name BNPS is in honour of Messrs Bakker, Nyborg and Pacejka who originated the 'Magic Formula' and the S indicates the particular implementation developed by Smithers Scientific Services Inc.

In the original 'Magic Formula' paper Bakker et al. (1986) discuss the use of formulae to represent the force and moment curves using established techniques based on polynomials or a Fourier series. The main disadvantage with this approach is that the coefficients used have no engineering significance in terms of the tyre properties and as with interpolation methods the model would not lend itself to design activities. This is also reflected in Sitchen (1983) where the author describes a representation based on polynomials where the curves are divided into five regions but this still has the problem of using coefficients which do not typify the tyre force and moment characteristics.

The general acceptance of the 'Magic Formula' is reinforced by the work carried out at Michelin and described in Bayle et al. (1993). In this paper the authors describe how the 'Magic Formula' has been tested at Michelin and 'industrialized' as a self-contained package for the pure lateral force model. The authors also considered modifications to the 'Magic Formula' to deal with the complicated situation of combined slip.

The 'Magic Formula' model is undergoing continual development, which is reflected in a further publication (Pacejka and Besselink, 1997) where the model is not restricted to small values of slip and the wheel may also run backwards. The authors also discuss a relatively simple model for longitudinal and lateral transient responses restricted to relatively low time and path frequencies. The tyre model in this paper also acquired a new name and is referred to as the 'Delft Tyre 97' version.

The 'Magic Formula' has been developed using mathematical functions that relate:

(i) The lateral force F_y as a function of slip angle α

(ii) The aligning moment M_z as a function of slip angle α

(iii) The longitudinal force F_x as a function of longitudinal slip κ

When these curves are obtained from steady state tyre testing and plotted the general shape of the curves is similar to that indicated in Figure 5.57.

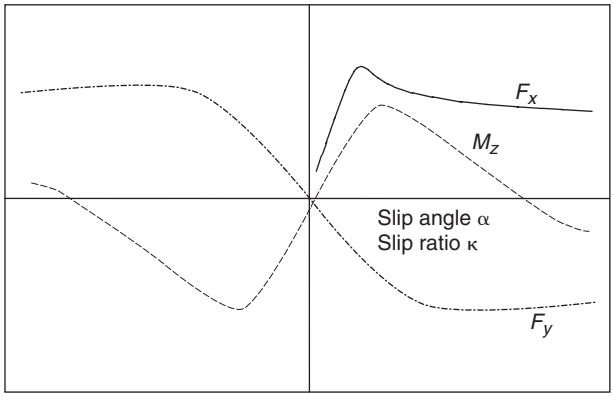

Fig. 5.57 Typical form of tyre force and moment curves from steady state testing

It is important to note that the data used to generate the tyre model is obtained from steady state testing. The lateral force F_y and the aligning moment M_z are measured during pure cornering, i.e. cornering without braking, and the longitudinal braking force during pure braking, i.e. braking without cornering.

The basis of this model is that tyre force and moment curves obtained under pure slip conditions and shown in Figure 5.57 look like sine functions that have been modified by introducing an arctangent function to 'stretch' the slip values on the x-axis.

The general form of the model as presented in Bakker et al. (1986) is:

$$y(x) = D \sin[C \arctan\{Bx - E(Bx - \arctan(Bx))\}] \tag{5.49}$$

where

$$Y(X) = y(x) + S_v \tag{5.50}$$

$$x = X + S_h \tag{5.51}$$

S_h = horizontal shift

S_v = vertical shift

In this case Y is either the side force F_y, the aligning moment M_z or the longitudinal force F_x and X is either the slip angle α or the longitudinal slip, for which Pacejka uses κ. The physical significance of the coefficients in the formula become more meaningful when considering Figure 5.58.

For lateral force or aligning moment the offsets S_v and S_h arise due to adding camber or physical features in the tyre such as conicity and ply steer. For the longitudinal braking force this is due to rolling resistance.

Working from the offset XY-axis system the main coefficients are:

D – is the peak value.

C – is a shape factor that controls the 'stretching' in the x direction. The value is determined by whether the curve represents lateral force, aligning moment, or longitudinal braking force. These values can be modified to

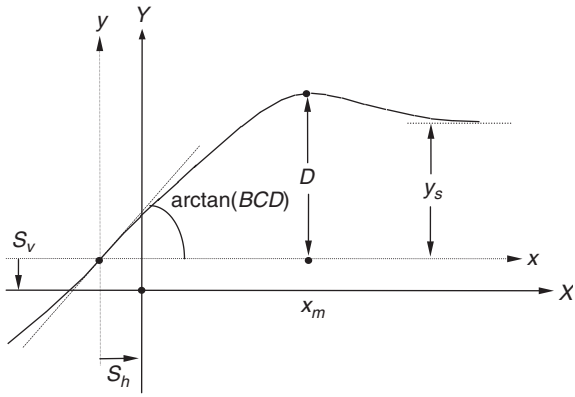

Fig. 5.58 Coefficients used in the 'Magic Formula' tyre

fit a particular tyre or if suitable taken as the constants given in Bakker et al. (1986):

1.30 – lateral force curve

1.65 – longitudinal braking force curve

2.40 – aligning moment curve

B – is referred to as a 'stiffness' factor. From Figure 5.58 it can be seen that BCD is the slope at the origin, i.e. the cornering stiffness when plotting lateral force. Obtaining values for D and C leads to a value for B.

E – is a 'curvature' factor that effects the transition in the curve and the position x_m at which the peak value if present occurs. E is calculated using:

$$E = \frac{Bx_m - \tan(\pi/2C)}{Bx_m - \arctan(Bx_m)} \tag{5.52}$$

y_s – is the asymptotic value at large slip values and is found using:

$$y_s = D \sin(\pi C/2) \tag{5.53}$$

The curvature factor E can be made dependent on the sign of the slip value plotted on the x-axis:

$$E = E_0 + \Delta E \operatorname{sgn}(x) \tag{5.54}$$

This will allow for the lack of symmetry between the right and left side of the diagram when comparing driving and braking forces or to introduce the effects of camber angle γ. This effect is illustrated in Pacejka and Bakker (1993) by the generation of an asymmetric curve using coefficients $C = 1.6$, $E_O = 0.5$ and $\Delta E = 0.5$. This is recreated here using the curve shape illustrated in Figure 5.59. Note that the plots have been made non-dimensional by plotting y/D on the y-axis and BCx on the x-axis.

The 'Magic Formula' utilizes a set of coefficients a_0, a_1, a_2, … as shown in Tables 5.1 and 5.2. In Figure 5.60 it can be seen that at zero camber the cornering stiffness BCD_y reaches a maximum value defined by the coefficient a_3 at a given value of vertical load F_z that equates to the coefficient a_4.

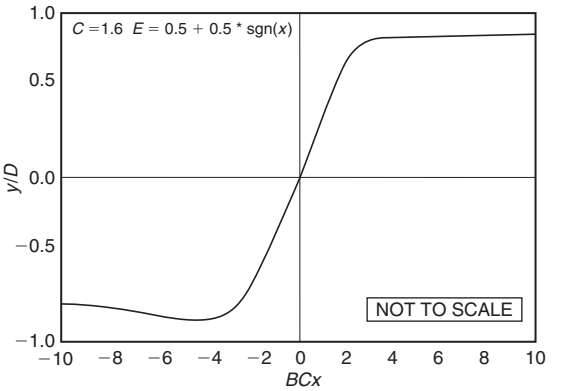

Fig. 5.59 Generation of an asymmetric curve

Table 5.1 Pure slip equations for the 'Magic Formula' tyre model (Monte Carlo version)

General formula

$y(x) = D \sin[C \arctan\{Bx - E(Bx - \arctan(Bx))\}]$
$Y(X) = y(x) + S_v$
$x = X + S_h$
B = stiffness factor
C = shape factor
D = peak factor
S_h = horizontal shift
S_v = vertical shift
$B = (dy/dx_{(x=0)})/CD$
$C = (2/\pi) \arcsin(y_s/D)$
$D = y$ max
$E = (Bx_m - \tan(\pi/2C))/(Bx_m - \arctan(Bx_m))$

Lateral force

$X_y = \alpha$
$Y_y = F_y$
$D_y = \mu_y F_z$
$\mu_y = a_1 F_z + a_2$
$BCD_y = a_3 \sin(2 \arctan(F_z/a_4))(1 - a_5|\gamma|)$
$C_y = a_0$
$E_y = a_6 F_z + a_7$
$B_y = BCD_y/C_y D_y$
$S_{hy} = a_8\gamma + a_9 F_z + a_{10}$
$S_{vy} = a_{11} F_z \gamma + a_{12} F_z + a_{13}$

Longitudinal force

$X_x = \kappa$
$Y_x = F_x$
$D_x = \mu_x F_z$
$\mu_x = b_1 F_z + b_2$
$BCD_x = (b_3 F_z^2 + b_4 F_z) \exp(-b_5 F_z)$
$C_x = b_0$
$E_x = b_6 F_z^2 + b_7 F_z + b_8$
$B_x = BCD_x/C_x D_x$
$S_{hx} = b_9 F_z + b_{10}$
$S_{vy} = 0$

Aligning moment

$X_z = \alpha$
$Y_z = M_z$
$D_z = c_1 F_z^2 + c_2 F_z$
$BCD_z = (c_3 F_z^2 + c_4 F_z)(1 - c_6|\gamma|) \exp(-c_5 F_z)$
$C_z = c_0$
$E_z = (c_7 F_z^2 + c_8 F_z + c_9)(1 - c_{10}|\gamma|)$
$B_z = BCD_z/C_z D_z$
$S_{hz} = c_{11}\gamma + c_{12} F_z + c_{13}$
$S_{vz} = (c_{14} F_z^2 + c_{15} F_z)\gamma + c_{16} F_z + c_{17}$

This relationship is illustrated in Figure 5.60 where the slope at zero vertical load is taken as $2a_3/a_4$.

This model has been extended to deal with the combined slip situation where braking and cornering occur simultaneously. A detailed account of the combined slip model is given in Pacejka and Bakker (1993). The equations for pure slip only and as developed for the Monte Carlo model (Bakker et al., 1989) are summarized in Table 5.1 and similarly for version 3 (Pacejka and Bakker, 1993) in Table 5.2. As can be seen a large number of parameters are involved and great care is needed to avoid confusion between each version.

Table 5.2 Pure slip equations for the 'Magic Formula' tyre model (version 3)

General formula

$y(x) = D \sin[C \arctan\{Bx - E(Bx - \arctan(Bx))\}]$
$Y(X) = y(x) + S_v$
$x = X + S_h$
B = stiffness factor
C = shape factor
D = peak factor
S_h = horizontal shift
S_v = vertical shift
$B = (dy/dx_{(x=0)})/CD$
$C = (2/\pi) \arcsin(y_s/D)$
$D = y$ max
$E = (Bx_m - \tan(\pi/2C))/(Bx_m - \arctan(Bx_m))$

Longitudinal force

$X_x = \kappa$
$Y_x = F_x$
$D_x = \mu_x F_z$
$\mu_x = b_1 F_z + b_2$
$BCD_x = (b_3 F_z^2 + b_4 F_z) \exp(-b_5 F_z)$
$C_x = b_0$
$E_x = (b_6 F_z^2 + b_7 F_z + b_8) \times (1 - b_{13} \operatorname{sgn}(\kappa + S_{hx}))$
$B_x = BCD_x/C_x D_x$
$S_{hx} = b_9 F_z + b_{10}$
$S_{vy} = b_{11} F_z + b_{12}$
Brake force only ($b_{11} = b_{12} = b_{13} = 0$)

Lateral force

$X_y = \alpha$
$Y_y = F_y$
$D_y = \mu_y F_z$
$\mu_y = (a_1 F_z + a_2)(1 - a_{15}\gamma^2)$
$BCD_y = a_3 \sin(2 \arctan(F_z/a_4))(1 - a_5|\gamma|)$
$C_y = a_0$
$E_y = (a_6 F_z + a_7)(1 - (a_{16}\gamma + a_{17}) \operatorname{sgn}(\alpha + S_{hy}))$
$B_y = BCD_y/C_y D_y$
$S_{hy} = a_8 F_z + a_9 + a_{10}\gamma$
$S_{vy} = a_{11} F_z + a_{12} + (a_{13} F_z^2 + a_{14} F_z)\gamma$

Aligning moment

$X_z = \alpha$
$Y_z = M_z$
$D_z = (c_1 F_z^2 + c_2 F_z)(1 - c_{18}\gamma^2)$
$BCD_z = (c_3 F_z^2 + c_4 F_z)(1 - c_6|\gamma|) \exp(-c_5 F_z)$
$C_z = c_0$
$E_z = (c_7 F_z^2 + c_8 F_z + c_9)(1 - (c_{19}\gamma + c_{20}) \operatorname{sgn}(\alpha + S_{hz}))/(1 - c_{10}|\gamma|)$
$B_z = BCD_z/C_z D_z$
$S_{hz} = c_{11} F_z + c_{12} + c_{13}\gamma$
$S_{vz} = c_{14} F_z + c_{15} + (c_{16} F_z^2 + c_{17} F_z)\gamma$

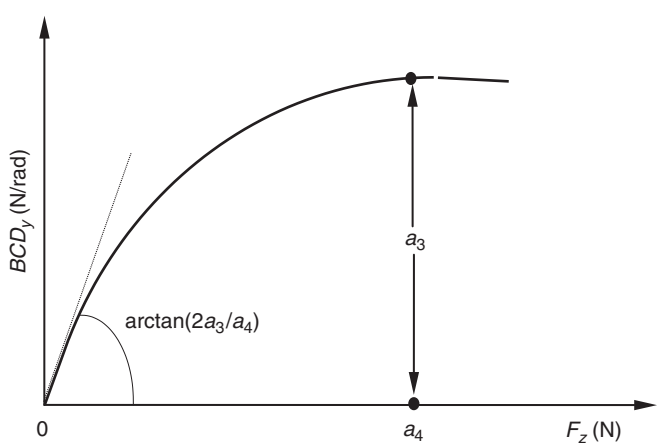

Fig. 5.60 Cornering stiffness as a function of vertical load at zero camber angle

Apart from implementing the model into a multibody systems analysis program for vehicle simulation some method is needed to obtain the coefficients from raw test data. In Sharp (1992) a suggested approach is to use an appreciation of the properties of the 'Magic Formula' to fix C based on the values suggested in Pacejka and Bakker (1993) for lateral force, longitudinal force and aligning moment. For each set of load data it is then possible to obtain the peak value D and the position at which this occurs x_m. Using the slope at the origin and the values for C and D it is now possible to determine

the stiffness factor B and hence obtain a value for E. Having obtained these terms at each load the various coefficients are determined using curve fitting techniques to express B, C, D and E as functions of load. An issue that occurs when deriving the coefficients for this model is whether those that have physical significance should be fixed to match the tyre or set to values that give the best curve fit.

van Oosten and Bakker (1993) describe their work using measured data and software developed at the TNO Road-Vehicles Research Institute to apply a regression method and obtain the coefficients. Schuring et al. (1993) have also automated the process for the BNPS version of the model. Comparisons of output from the 'Magic Formula' with measured test data (Bakker et al., 1986, 1989) indicate good correlation. A study in Makita and Torii (1992) comparing the results of this model with those obtained from vehicle testing under pure slip conditions also indicates the high degree of accuracy which can be obtained using this tyre model.

5.6.6 The Fiala tyre model

The Fiala tyre model (Fiala, 1954) is probably most well known to MSC.ADAMS users as it is provided as a standard feature of the program. Although limited in capability this model has the advantage that it only requires 10 input parameters and that these are directly related to the physical properties of the tyre. The input parameters are shown in Table 5.3.

The parameters R_1, R_2, k_z, ζ, are all used to formulate the vertical load in the tyre and are required for all tyre models that are used here, including the Pacejka and Interpolation models. As the Fiala model ignores the influence of camber angle the coefficient which defines lateral stiffness due to camber angle, C_γ, is not used. This means that the generation of longitudinal forces, lateral forces and aligning moments with the Fiala model is controlled using just five parameters (C_s, C_α, C_r, μ_0 and μ_1).

Table 5.3 Fiala tyre model input parameters

R_1	The unloaded tyre radius (units – length)
R_2	The tyre carcass radius (units – length)
k_z	The tyre radial stiffness (units – force/length)
C_s	The longitudinal tyre stiffness. This is the slope at the origin of the braking force F_x when plotted against slip ratio (units – force)
C_α	Lateral tyre stiffness due to slip angle. This is the cornering stiffness or the slope at the origin of the lateral force F_y when plotted against slip angle α (units – force/radians)
C_γ	Lateral tyre stiffness due to camber angle. This is the cornering stiffness or the slope at the origin of the lateral force F_y when plotted against camber angle γ (units – force/radians)
C_r	The rolling resistant moment coefficient which when multiplied by the vertical force F_z produces the rolling resistance moment M_y (units – length)
ζ	The radial damping ratio. The ratio of the tyre damping to critical damping. A value of zero indicates no damping and a value of one indicates critical damping (dimensionless)
μ_0	The tyre to road coefficient of 'static' friction. This is the y intercept on the friction coefficient versus slip graph, effectively the peak coefficient of friction
μ_1	The tyre to road coefficient of 'sliding' friction occurring at 100% slip with pure sliding

Despite the advantage of a simple parameter set the main limitations of the model include:

(i) The model cannot represent combined cornering and braking or cornering and driving.

(ii) Lateral force and aligning moment resulting from camber angle are not modelled.

(iii) The variation in cornering stiffness at zero slip angle with tyre load is not considered.

(iv) The offsets in lateral force or aligning moment at zero slip angle due to conicity and ply steer are not represented.

In order to calculate the longitudinal and lateral forces it is first necessary to understand how the Fiala tyre model determines a resultant friction coefficient μ as a function of the comprehensive slip ratio $S_{L\alpha}$ as shown in Figure 5.61. The comprehensive slip ratio $S_{L\alpha}$ is taken to be the resultant of the longitudinal slip coefficient S and the lateral slip coefficient S_α:

$$S_{L\alpha} = \sqrt{S^2 + S_\alpha^2} \tag{5.55}$$

The instantaneous value of the tyre to road friction coefficient μ can then be obtained by linear interpolation:

$$\mu = \mu_0 - S_{L\alpha}(\mu_0 - \mu_1) \tag{5.56}$$

The value of μ obtained can now be used to obtain a critical value of longitudinal slip ratio S^*, beyond which the tyre is sliding:

$$S^* = \left| \frac{\mu F_z}{2C_s} \right| \tag{5.57}$$

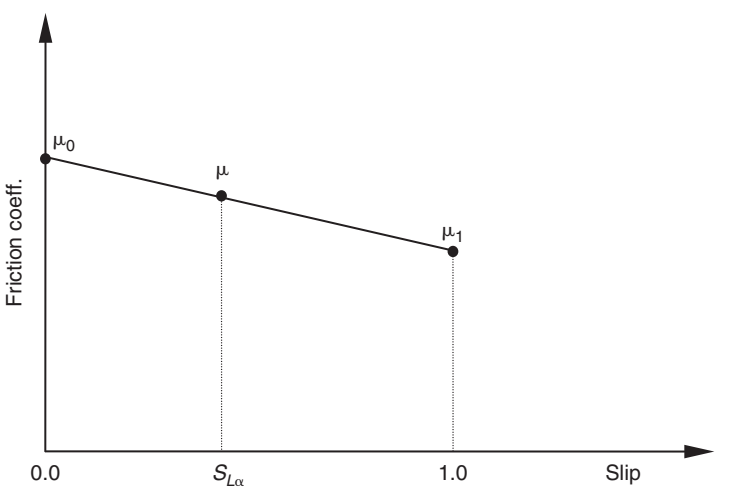

Fig. 5.61 Linear tyre to road friction model. (This material has been reproduced from the Proceedings of the Institution of Mechanical Engineers, K1 Vol. 214 'The modelling and simulation of vehicle handling. Part 3: tyre modelling', M.V. Blundell, page 13, by permission of the Council of the Institution of Mechanical Engineers)

If $|S|$ is less than S^* the tyre is considered to be in an elastic deformation state and

$$F_x = -C_s S \tag{5.58}$$

If $|S|$ is greater than S^* the tyre is considered to be in a complete sliding state and

$$F_x = -\text{sgn}(S)\{\mu F_z - [(\mu F_z)^2/4|S|C_s]\} \tag{5.59}$$

For the lateral force a critical slip angle α^* is calculated using:

$$\alpha^* = \arctan |3\mu F_z/C_\alpha| \tag{5.60}$$

If $|\alpha|$ is less than α^* then the tyre is considered to be in a state of elastic deformation and

$$H = 1 - C_\alpha|\tan \alpha|/3\mu|F_z| \tag{5.61}$$

$$F_y = -\mu|F_z|(1 - H^3)\ \text{sgn}(\alpha) \tag{5.62}$$

If $|\alpha|$ is greater than α^* then the tyre is considered to be sliding and

$$F_y = -\mu|F_z|\ \text{sgn}(\alpha) \tag{5.63}$$

The rolling resistance moment M_y is given by:

$$M_y = -C_r F_z \quad \text{(forward motion)} \tag{5.64}$$

$$M_y = C_r F_z \quad \text{(backward motion)} \tag{5.65}$$

For the aligning moment M_z if $|\alpha|$ is less than α^* (elastic deformation state) then:

$$H = 1 - C_\alpha|\tan \alpha|/3\mu|F_z| \tag{5.66}$$

$$M_z = 2\mu|F_z|R_2(1 - H)H^3\ \text{sgn}(\alpha) \tag{5.67}$$

If $|\alpha|$ is greater than α^* (complete sliding state) then:

$$M_z = 0.0 \tag{5.68}$$

Note that the Fiala tyre model formulation does not allow for the possibility of negative aligning moments occurring at high slip angles.

5.6.7 Tyre models for durability analysis

The modelling of suspension systems for durability analysis where component loads are needed for follow-on stress and fatigue analysis was discussed in Chapter 4. As discussed the models are developed to simulate tests carried out on the proving ground to represent impacts with road obstacles of the type shown in Figure 5.62. If an actual vehicle has been taken on the proving ground and instrumented to take readings at the wheel centre, then the recorded data can be used as input to a suspension or vehicle model and the need for a durability tyre model is negated.

As vehicle design processes move towards more use of virtual prototypes the need to carry out full dynamic simulations of proving ground procedures requires more sophisticated tyre models to interact with the terrain. In the extreme simulations recreating the testing of off-road vehicles involving conditions of the type shown in Figure 5.63 requires a tyre model that

Fig. 5.62 Proving ground measurements at the wheel centre for durability analysis (provided courtesy of MSC.Software)

Fig. 5.63 Off-road testing conditions involving a wide range of terrain

can deal with a wide range of terrain. The tyre models developed for such work are based on a physical representation of the tyre carcass geometry and material rather than a mathematical model of the measured force and moment behaviour used for vehicle handling tyre models.

A tyre model that has been developed at TNO on the foundation of the 'Magic Formula' and subsequent Delft-Tyre models has been shown to handle a wide range of road inputs allowing handling simulations to be combined with highly non-linear road inputs. The SWIFT (Short Wavelength Intermediate Frequency Tyre) model is described by van Oosten and Jansen (1999) as a model intended for the development of

active chassis control systems and optimizing vehicle ride properties with capabilities including:

(i) The use of the 'Magic Formula' for slip force calculations

(ii) A sophisticated contact for short wavelength slip variations

(iii) An effective method to model road obstacles (durability)

(iv) A rigid ring model to accommodate tyre belt vibrations to 80 Hz

(v) Tyre characteristics that can vary with speed and load

The model has been validated through the extensive tyre test capabilities at TNO and has been shown (van Oosten and Jansen, 1999) to be accurate for durability applications, such as rolling over cleats and enveloping steps in the road surface, when comparing simulations with experimental measurements.

A comprehensive description of this complex tyre model is not possible here. Rather the reader is referred to the companion text in this series (Pacejka, 2002) where a complete chapter is dedicated to describing the formulations within the SWIFT tyre model.

The MSC.ADAMS durability tyre model (Vesimaki, 1997) was originally developed to deal with off-road applications. An example of this would be the simulation of very large vehicles used by the timber industry in the forests of the author's home country, Finland. The tyre model developed for such an application would be required to deal with a vehicle cornering on a steep uneven slope where the tyres are going to encounter obstacles such as tree stumps. The requirements for such a tyre model are summarized by the author as:

(i) to enable handling simulation on an uneven 3D road surface

(ii) to allow a road/terrain definition based on geometry

(iii) to accommodate varying friction over the terrain

(iv) to account for the cross-sectional tyre dimension and geometry

Such a model requires a physical representation of the tyre profile in order to model the boundaries of the tyre carcass as they envelop obstacles. The tyre model input consists of points that model one half of the tyre profile, as shown on the left side of Figure 5.64. The tyre model uses the input geometry to compute interpolated internal points, each of which defines the radius and lateral position of a disc representing a slice of the tyre cross-section.

As with any model based on a physical discretization, the model refinement or number of cross-sectional elements must be such that the width of the 'slices' is sufficiently small to deal with obstacles that are narrow compared with the overall width of the tyre. The road model is based on the finite element representation described in section 5.6.3.

The algorithm developed carries out initial iterations to identify road elements that are subject to potential contact, at the current integration time step, before evaluating the position of each tyre element slice with each of the candidate road elements. An example of this is shown schematically in Figure 5.65 where one tyre cross-sectional element is seen to intersect a step defined by a number of triangular road elements.

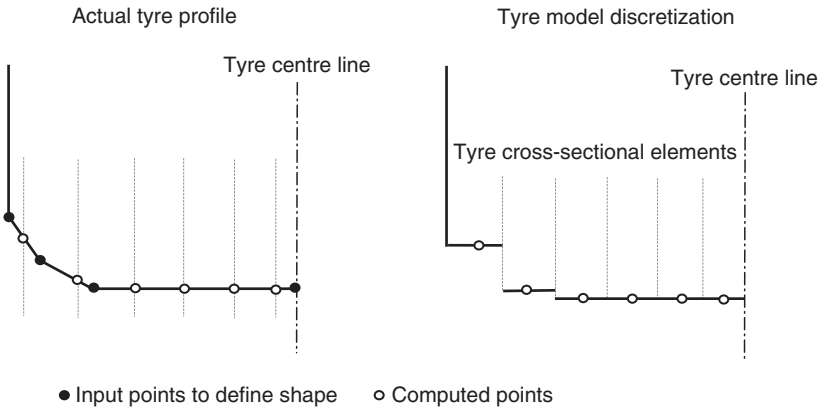

Fig. 5.64 Discretization of tyre profile for durability analysis

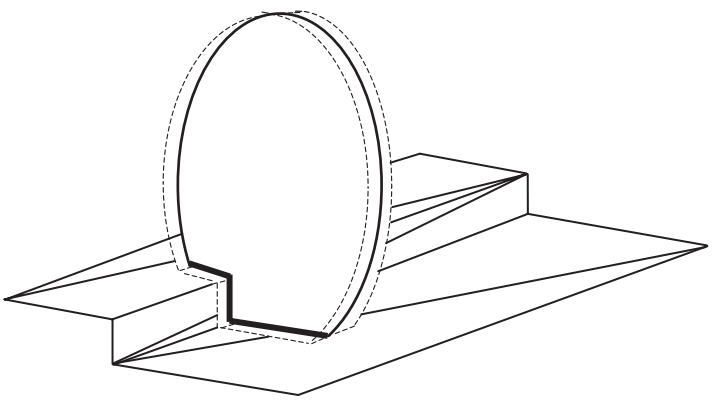

Fig. 5.65 Intersection of durability tyre model element with road surface element

For each of the discrete elements used to model the tyre cross-section the interaction with the road surface elements produces a line projection of the intersection on the tyre element.

From this it is possible to compute the area and hence volume related to the penetration of tyre cross-sectional element by the road, for example by summing the three components shown in Figure 5.66. For a tyre with n cross-sectional elements, where each element has m components of penetrated area, the effective penetrated volume, V_{eff}, for the complete tyre is given by

$$V_{\text{eff}} = \sum_{i=1}^{n} \sum_{j=1}^{m} A_m w_n \tag{5.69}$$

where

A_m is the penetrated area of the mth component of area within the cross-sectional tyre element
w_n is the width of the nth cross-sectional element of the tyre

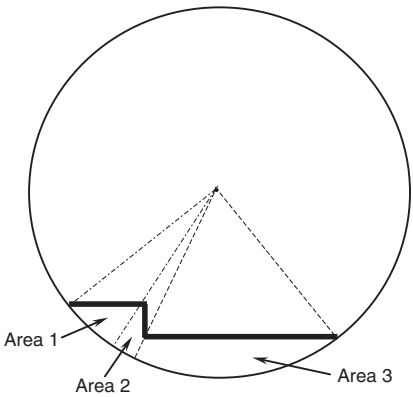

Fig. 5.66 Penetration of tyre elemental slice by road surface elements

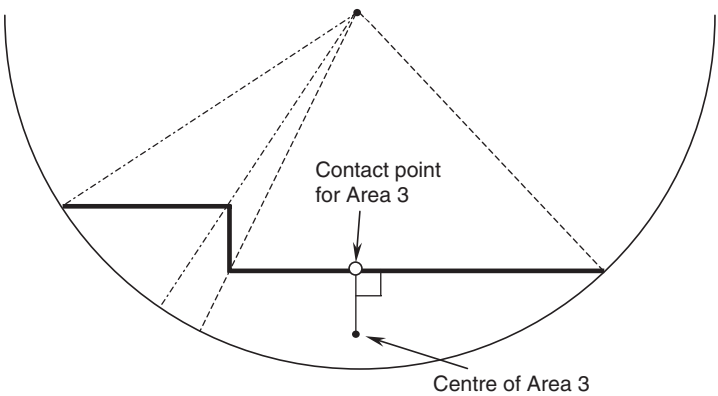

Fig. 5.67 Determination of effective contact point

The location of the effective contact point, within the deformed volume of tyre, is found by taking a weighted average of the contact point locations associated with each component of area within each cross-sectional element of the tyre. In Figure 5.67 it can be seen that for the component of area shown, the associated contact point is located where the road surface is intersected by a line normal to the road surface and passing through the centre of area. On this basis the x co-ordinate, X_{ecp}, for the effective contact point of the tyre would be found from

$$X_{\text{ecp}} = \sum_{i=1}^{n} \sum_{j=1}^{m} \frac{A_m w_n}{V_{\text{eff}}} X_m \tag{5.70}$$

where

X_m is the x co-ordinate of the contact point for the mth component of area within the cross-sectional tyre element.

The y and z co-ordinates of the effective contact point are found using the same approach used to determine X_{ecp} in equation (5.71). Having located

an overall effective contact point for the tyre at the given moment of interaction with the terrain it is necessary to determine an effective normal vector to the road surface acting through the contact point. Once again Vesimaki (1997) uses a weighted average approach. The road normal can therefore be defined by using again the x component X_{ern} as an example:

$$X_{\text{ern}} = \sum_{i=1}^{n} \sum_{j=1}^{m} \frac{A_m w_n}{V_{\text{eff}}} Xn_m \tag{5.71}$$

where

Xn_m is the x component of the road normal for the mth component of area within the cross-sectional tyre element.

Having found a volume, contact point and road normal vector for the deformed tyre at the given integration point in time it is necessary to compute a normal force acting on the tyre from the road. This involves an intermediate step where the effective volume of penetration, V_{eff}, is related to effective radial penetration of the tyre. This involves interpolation of a look-up table held within the tyre model that relates, for the defined tyre profile, the tyre penetration to penetrated volume when the tyre is compressed onto a flat surface.

The final computation required by the tyre model is to determine the effective coefficient of friction, μ_{eff}, due to contact with the terrain:

$$\mu_{\text{eff}} = \sum_{i=1}^{n} \sum_{j=1}^{m} \frac{A_m w_n}{V_{\text{eff}}} \mu_m \tag{5.72}$$

where

μ_m is the coefficient of friction associated with the mth component of area within the cross-sectional tyre element.

For off-road simulation a useful aspect of this approach is that the coefficient of friction can be factored to vary for each road element as described in section 5.6.3.

Another tyre model, FTire, specifically developed for ride and durability simulations has been developed by COSIN Software in Germany (Gipser, 1999) and made available through an interface in MSC.ADAMS.

The model comprises a rigid rim surrounded by elements with elastic interconnections that form a surrounding flexible belt or ring and has been developed to deal with frequencies up to 120 Hz and to encompass obstacles in the longitudinal direction of rolling with wavelengths half the length of the tyre contact patch. In the transverse direction the model can handle inclination of the road surface but not obstacles that vary across the tyre lateral direction, hence the model is referred to as a '2½-dimensional' nonlinear vibration model. The model can also accommodate the effects of stiffening and radial growth associated with high angular spin velocities. The model input parameters comprise tyre geometry and measured physical characteristics, with the optional input of natural frequencies and damping factors associated with the lower vibration modes of an unloaded tyre on a rigid rim. The belt or flexible ring is modelled as 50 to 100 lumped mass elements elastically interconnected and mounted to the rigid rim.

The elements have interconnecting stiffness to account for relative bending, extension, radial and tangential motion in the circumferential and lateral directions. The radial connection between elements on the belt and the rigid rim is a combined spring damper that allows the model to account for centrifugal dynamic stiffening at high angular spin velocities.

Each of the interconnected belt elements has 5 to 10 massless tread blocks each having non-linear stiffness and damping in the radial, tangential and lateral directions, hence allowing the tread blocks to transmit normal forces from the road directly to the belt. Frictional forces in both the circumferential and lateral directions can be transmitted through the shear forces acting on the massless tread elements. The resultant forces and moments acting on the rigid rim are found by integrating the forces acting throughout the elastic foundation of the belt.

5.7 Implementation with MBS

MBS software intended for use in vehicle dynamics will often have specialized modules intended for tyre modelling. As stated the Fiala tyre model is the default in MSC.ADAMS and at this time can be implemented directly without any special programs. Implementation of the 'Magic Formula' tyre model and the Interpolation method can be achieved using a specialized module ADAMS/Tire or by writing FORTRAN subroutines and linking these to provide a customized user executable of MSC.ADAMS. Current versions of programs such as ADAMS/Car make the incorporation of a tyre model appear seamless. Example tyre model subroutines developed by the authors are provided in Appendix B, some of which form the basis of a tyre modelling, checking and plotting facility (Blundell, 2000).

One interface between MSC.ADAMS and a tyre model is through a user-written TIRSUB subroutine. The subroutine defines a set of three forces and three torques acting at the tyre to road surface contact patch and formulated in the SAE co-ordinate system. The equations used to formulate these forces and moments have been programmed into the subroutines to represent the various tyre models. The transformation of the forces and moments from the tyre contact patch to the wheel centre is performed internally by the program. The TIRSUB subroutine is called from within the model data set by a TIRE statement for each tyre on the vehicle. Tyre data can be passed from the TIRE statement, from SPLINE and ARRAY statements within the data set, or programmed into the subroutine. In addition MSC.ADAMS passes a number of variables, which describe the current set of contact properties and may be used in any model formulation. These variables, which are computed in the SAE co-ordinate system, are listed below:

(i) Longitudinal slip ratio

(ii) Lateral slip angle (radians)

(iii) Camber angle (radians)

(iv) Normal deflection of tyre into road surface

(v) Normal velocity of penetration of tyre into road surface

(vi) Longitudinal sliding velocity of contact patch

(vii) Distance from wheel centre to contact point (loaded radius)

(viii) Angular velocity about the spin axis of the tyre

(ix) Longitudinal velocity of tyre tread base

(x) Lateral velocity of tyre tread base

In addition to the TIRSUB that uses the SAE tyre co-ordinate system later versions of the software include a TYRSUB that uses the ISO tyre co-ordinate system.

5.7.1 Virtual tyre rig model

A functional model of the Flat Bed Tyre Test machine at Coventry University has been developed in MSC.ADAMS and forms part of the system described here. The rig model has been developed in order to address the situation where a tyre data file has been supplied for a particular model but the test data is not available either in tabular format or graphically as plotted curves. It is clearly desirable to use the tyre data parameters or coefficients to generate the sort of plots produced from a tyre test programme and to inspect these plots before using the data files with an actual full vehicle model.

The tyre rig model is also useful where test data has been used to extract mathematical model parameters. The plots obtained from the mathematical model can be compared with test data to ensure the mathematical parameters are accurate and represent the actual tyre. The tyre test rig model performs a useful function for vehicle simulation system activities developed around MSC.ADAMS. The process that this involves is shown conceptually in Figure 5.68.

The orientation of the global axis system and the local axis system for the tyre has been set up using the same methodology as that required when generating a full vehicle model in MSC.ADAMS as shown in Figure 5.69.

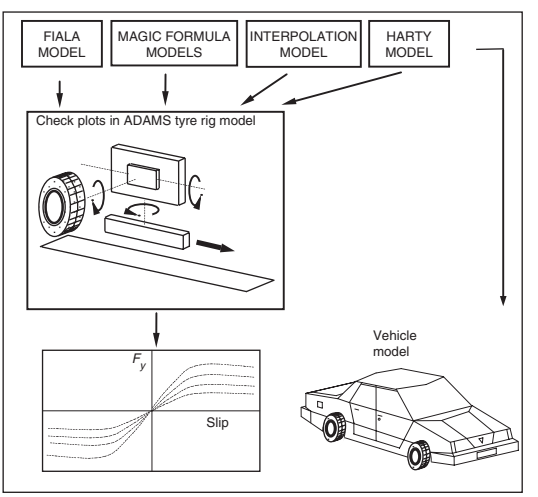

Fig. 5.68 Overview of the tyre modelling system

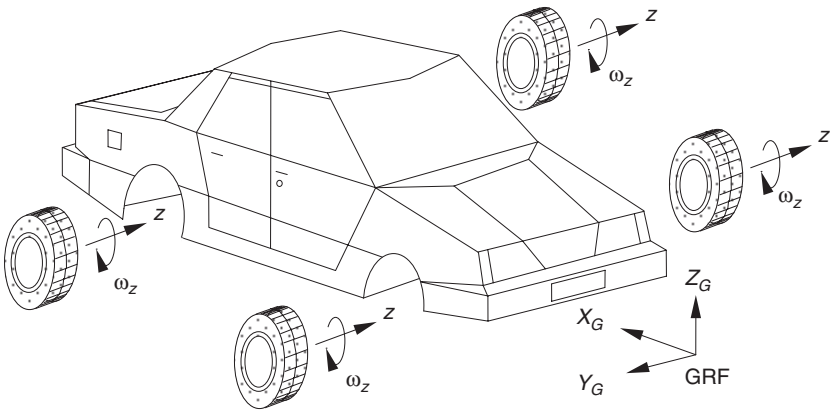

Fig. 5.69 Orientation of tyre co-ordinate systems on the full vehicle model. (This material has been reproduced from the Proceedings of the Institution of Mechanical Engineers, K1 Vol. 214 'The modelling and simulation of vehicle handling. Part 3: tyre modelling', M.V. Blundell, page 16, by permission of the Council of the Institution of Mechanical Engineers)

The usual approach with full vehicle modelling is to set up a global co-ordinate system or Ground Reference Frame (GRF) where the x-axis points back along the vehicle, the y-axis points to the right of the vehicle and the z-axis is up. The local z-axis of each tyre part is orientated to point towards the left side of the vehicle so that the wheel spin vector is positive when the vehicle moves forward during normal motion. Note that this is the co-ordinate system as set up at the wheel centre and should not be confused with the SAE co-ordinate system, which is used at the tyre contact patch in order to describe the forces and moments occurring there.

The model of the tyre test machine presented here contains a tyre part, which rolls forward on a flat uniform road surface in the same way that the tyre interacts with a moving belt in the actual machine. In this model the road is considered fixed as opposed to the machine where the belt represents a moving road surface and the tyre is stationary. Considering the system schematic of the model shown in Figure 5.70 the tyre part 02 is connected to a carrier part 03 by a revolute joint aligned with the spin axis of the wheel. The carrier part 03 is connected to another carrier part 04 by a revolute joint that is aligned with the direction of travel of the vehicle. A motion input applied at this joint is used to set the required camber angle during the simulation of the test process. The carrier part 04 is connected to a sliding carrier part 05 by a cylindrical joint, which is aligned in a vertical direction. A rotational motion is applied at this joint, which will set the slip angle of the tyre during the tyre test simulation. The cylindrical joint allows the carrier part 04 to slide up or down relative to 05 which is important as a vertical force is applied downwards on the carrier part 04 at this joint and effectively forces the tyre down on to the surface of the road. The model has been set up to ignore gravitational forces so that this load can be varied and set equal to the required wheel vertical load which would be set during the tyre test process. The sliding carrier part 05 is connected to the ground part 01 by a translational joint aligned with the direction of travel of the wheel. A motion input applied at this joint will control the forward velocity of the tyre during the test.

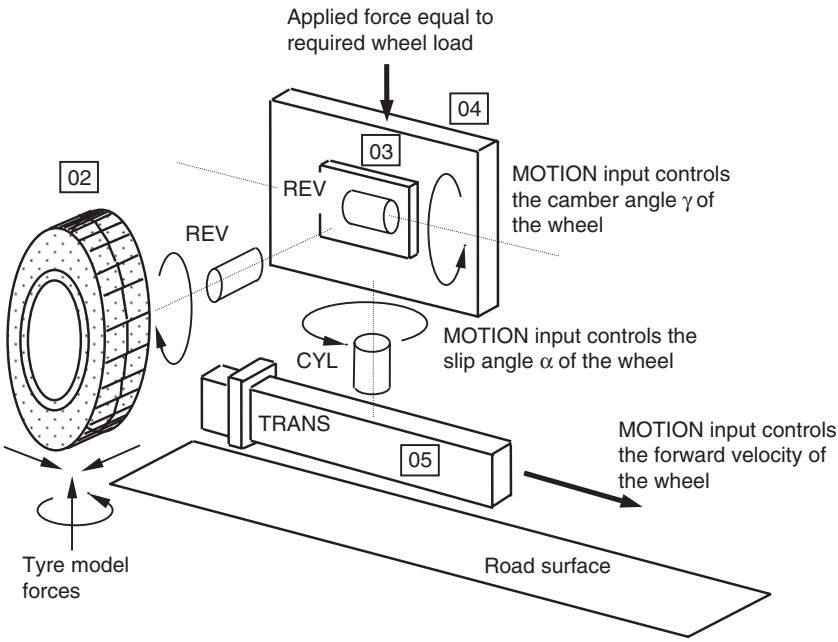

Fig. 5.70 MSC.ADAMS model of a flat bed tyre test machine. (This material has been reproduced from the Proceedings of the Institution of Mechanical Engineers, K1 Vol. 214 'The modelling and simulation of vehicle handling. Part 3: tyre modelling', M.V. Blundell, page 17, by permission of the Council of the Institution of Mechanical Engineers)

Table 5.4 Degree-of-freedom balance equation for the tyre rig model

Model component	DOF	Number	Total DOF
Parts	6	4	24
Revolutes	−5	2	−10
Translational	−5	1	−5
Cylindrical	−4	1	−4
Motions	−1	3	−3
			$\sum_{DOF} = 2$

The joint controlling camber angle can be located at the tyre contact patch rather than at the wheel centre. This will avoid introducing lateral velocity and hence slip angle for the change in camber angle during a dynamic simulation.

The model of the tyre test machine has 2 rigid body degrees of freedom as demonstrated by the calculation of the degree of freedom balance in Table 5.4. One degree of freedom is associated with the spin motion of the tyre, which is dependent on the longitudinal forces generated and the slip ratio. The other degree of freedom is the height of the wheel centre above the road, which is controlled by the applied force representing the wheel load.

The tyre test rig model has been used to read the tyre model data files used in a study (Blundell, 2000a) to plot tyre force and moment graphs. The graphics of the tyre rig model are shown in Figure 5.71.

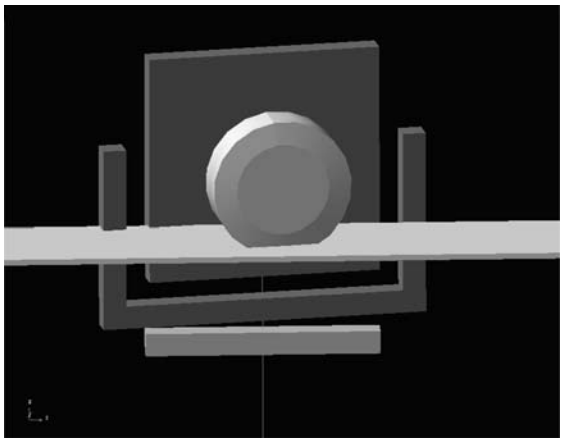

Fig. 5.71 Computer graphics for the tyre rig model

5.8 Examples of tyre model data

The results obtained from a series of tyre tests (Blundell, 2000a) have been used to set up the data needed for the various modelling approaches described here. In summary the following procedure was followed:

(i) For the Interpolation method the measured numerical values were reformatted directly into the SPLINE statements within an MSC.ADAMS data file as shown in Table 5.5. For each spline shown in Table 5.5 the *X* values correspond to either the slip or camber angle and are measured in degrees. The first value in each *Y* array corresponds to the vertical load measured in kg. The following values in the *Y* arrays are the measured lateral forces (N) or the aligning moments (Nm) which correspond with the matching slip or camber angles in the *X* arrays. All the required conversions to the vehicle model units are carried out in the FORTRAN subroutine for the Interpolation tyre model listed in Appendix B.

(ii) The coefficients for the 'Magic Formula' model were provided by Dunlop Tyres using in-house software to fit the values. The 'Magic Formula' tyre model (version 3) parameters are shown in Table 5.9. It should be noted that the parameters due to camber effects were not available from this set of tests.

(iii) The parameters for the Fiala model were obtained by simple measurements from the plots produced during tyre testing. The Fiala model requires a single value of cornering stiffness to be defined although in reality cornering stiffness varies with tyre load. For the purposes of comparing the tyre models the parameters for the Fiala tyre model shown in Table 5.6 have been derived from the test data at the average of the front and rear wheel loads of the vehicle considered in this study. Fiala parameters obtained at front and rear wheel loads are given in Tables 5.7 and 5.8. Using the data for each of these models the tyre rig model described in the previous section was run for vertical loads of 200, 400, 600 and 800 kg. In each case the slip angle was varied between plus and minus 10 degrees.

Table 5.5 Spline data for Interpolation model

```
LATERAL FORCE (N) WITH SLIP ANGLE (DEG) AND LOAD (KG)
SPLINE/100
,X = -10,-8,-6,-4,-2,0,2,4,6,8,10
,Y = 200,2148,2050,1806,1427,867,16,-912,-1508,-1881,-2067,-2151
,Y = 400,3967,3760,3409,2727,1620,75,-1587,-2776,-3482,-3759,-3918
,Y = 600,5447,5099,4436,3385,1962,94,-1893,-3397,-4557,-5049,-5269
,Y = 800,6738,5969,4859,3533,2030,66,-1971,-3662,-5122,-6041,-6500
ALIGNING MOMENT (NM) WITH SLIP ANGLE (DEG) AND LOAD (KG)
SPLINE/200
,X = -10,-8,-6,-4,-2,0,2,4,6,8,10
,Y = 200,4.6,-0.1,-6,-11.1,-10.9,-1.3,10.6,11.2,7.9,3.2,-0.3
,Y = 400,-4.8,-19.6,-39,-52.1,-41.9,-6.7,35.8,49.1,38.6,23.4,10.1
,Y = 600,-36.5,-73.1,-102.6,-107.9,-78.7,-14.2,60.6,96.2,93.4,65.8,40.7
,Y = 800,-105.1,-181.1,-206.1,-172.4,-116.0,-3.6,79.9,143.3,172.2,141.5,98.5
LATERAL FORCE (N) WITH CAMBER ANGLE (DEG) AND LOAD (KG)
SPLINE/300
,X = -10,-8,-6,-4,-2,0,2,4,6,8,10
,Y = 100,-123.3,-96.3,-64.6,-39.3,-3,19,46,80.6,108.3,146,173.3
,Y = 200,-142.6,-106.6,-57.3,-14.6,28,78,127,169.6,212.3,255,285.6
,Y = 300,-173.6,-106.6,-44,20.6,87.6,159,223.6,291.3,344.3,393.3,443.6
,Y = 400,-194,-115.6,-31.3,53,141.6,237,319.6,396.3,468.6,526.3,579
,Y = 500,-219.6,-121.6,-17.3,91,199,304,403.3,487,572.6,651.3,717
,Y = 600,-247.6,-128.3,-9.3,109.3,234,351,453.3,557.3,651.6,734.6,829.6
,Y = 700,-278,-138.6,-3.6,126.3,254,381,499.3,616,723,827,922.6
,Y = 800,-318.6,-165,-21,128,261.3,404.0,524.3,656,780,895,1012
ALIGNING MOMENT (NM) WITH CAMBER ANGLE (DEG) AND LOAD (KG)
SPLINE/400
,X = -10,-8,-6,-4,-2,0,2,4,6,8,10
,Y = 100,-5,-5,-4.3,-2.2,-0.9,1.2,2.6,4.2,5.8,7,6.4
,Y = 200,-14.6,-13.7,-12,-9.2,-4.9,-0.9,3.6,6.7,9.6,11,11.7
,Y = 300,-24.1,-22.6,-19.6,-16.7,-11.1,-4.2,2.8,8.1,11.9,15.2,17
,Y = 400,-34.2,-31.8,-28.5,-22.9,-15.8,-8.2,-0.3,6.5,12.2,15.6,17.7
,Y = 500,-41.5,-38,-32.7,-26.5,-18.8,-10.8,-2.5,3.9,10.7,16.5,19.6
,Y = 600,-48.7,-43.6,-38,-31.6,-23.9,-15.9,-8.1,-0.4,6.4,12.1,16.8
,Y = 700,-52.5,-47.5,-40.9,-34.4,-26.6,-19.5,-11.9,-4.7,1.3,7.2,12.6
,Y = 800,-56.9,-51.3,-44.2,-37.9,-30.7,-23.9,-16.7,-10.1,-4,2.4,8.3
```

Table 5.6 Fiala tyre model parameters (average wheel load)

R_1 = 318.5 mm	R_2 = 97.5 mm
k_z = 150 N/mm	C_s = 110 000 N
C_α = 51 560 N/rad	C_γ = 2580 N/rad
C_r = 0.0 mm	ξ = 0.05
μ_0 = 1.05	μ_1 = 1.05

Table 5.7 Fiala tyre model parameters (front wheel load)

R_1 = 318.5 mm	R_2 = 97.5 mm
k_z = 150 N/mm	C_s = 110 000 N
C_α = 54 430 N/rad	C_γ = 2750 N/rad
C_r = 0.0 mm	ξ = 0.05
μ_0 = 1.05	μ_1 = 1.05

Table 5.8 Fiala tyre model parameters (rear wheel load)

R_1 = 318.5 mm	R_2 = 97.5 mm
k_z = 150 N/mm	C_s = 110 000 N
C_α = 46 980 N/rad	C_γ = 2350 N/rad
C_r = 0.0 mm	ξ = 0.05
μ_0 = 1.05	μ_1 = 1.05

Table 5.9 'Magic Formula' tyre model (version 3) parameters

Lateral force	Aligning moment
A0 = .103370E+01	C0 = .235000E+01
A1 = −.224482E−05	C1 = .266333E−05
A2 = .132185E+01	C2 = .249270E−02
A3 = .604035E+05	C3 = −.159794E−03
A4 = .877727E+04	C4 = −.254777E−01
A5 = 0.0	C5 = .142145E−03
A6 = .458114E−04	C6 = 0.00
A7 = .468222	C7 = .197277E−07
A8 = .381896E−06	C8 = −.359537E−03
A9 = .516209E−02	C9 = .630223
A10 = 0.00	C10 = 0.00
A11 = −.366375E−01	C11 = .120220E−06
A12 = −.568859E+02	C12 = .275062E−02
A13 = 0.00	C13 = 0.00
A14 = 0.00	C14 = −.172742E−02
A15 = 0.00	C15 = .544249E+01
A16 = 0.00	C16 = 0.00
A17 = .379913	C17 = 0.00
	C18 = 0.00
	C19 = 0.00
	C20 = 0.00

5.9 Case study 6 – Comparison of vehicle handling tyre models

Using the data derived from the tyre tests and the MSC.ADAMS tyre test rig the following plots have been produced here by way of example:

(i) Lateral force for a range of plus and minus 10 degrees of slip angle

(ii) Lateral force for a range of plus and minus 2 degrees of slip angle (near zero)

For each plot a set of three curves is presented showing the variation in force or moment for each of the three tyre models. The comparisons are made separately at vertical loads of 200, 400, 600 and 800 kg. Using the Interpolation model as a benchmark the results plotted for the 'Magic Formula' and Fiala models are compared in Figures 5.72 to 5.79.

The plots show that the more detailed 'Magic Formula' will produce a better match than the simpler Fiala model when examining the variation in lateral force with slip angle. Comparing the 'Magic Formula' with the

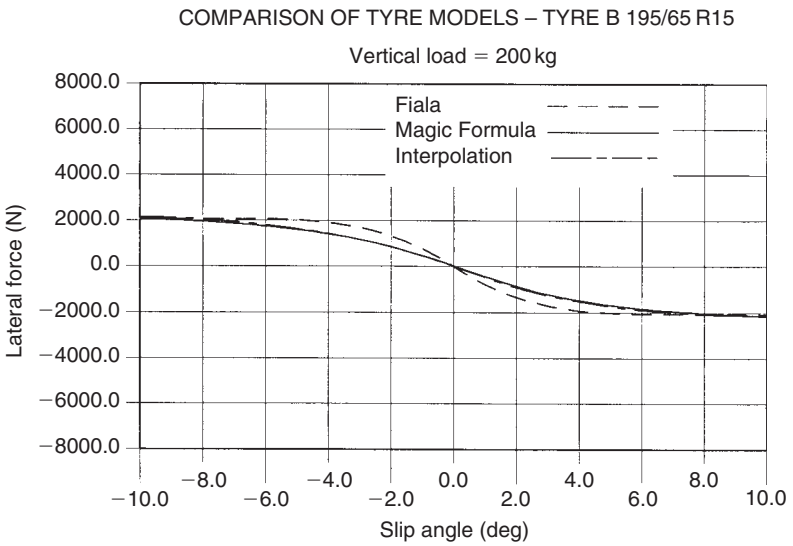

Fig. 5.72 Comparison of tyre models – lateral force with slip angle. (200 kg load). (This material has been reproduced from the Proceedings of the Institution of Mechanical Engineers, K1 Vol. 214 'The modelling and simulation of vehicle handling. Part 3: tyre modelling', M.V. Blundell, page 19, by permission of the Council of the Institution of Mechanical Engineers)

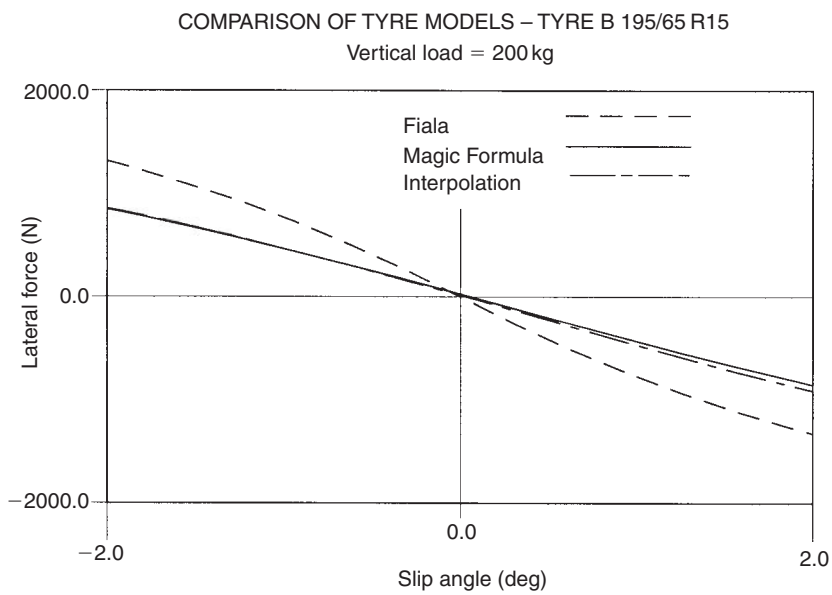

Fig. 5.73 Comparison of tyre models – lateral force at near zero slip angle (200 kg load). (This material has been reproduced from the Proceedings of the Institution of Mechanical Engineers, K1 Vol. 214 'The modelling and simulation of vehicle handling. Part 3: tyre modelling', M.V. Blundell, page 19, by permission of the Council of the Institution of Mechanical Engineers)

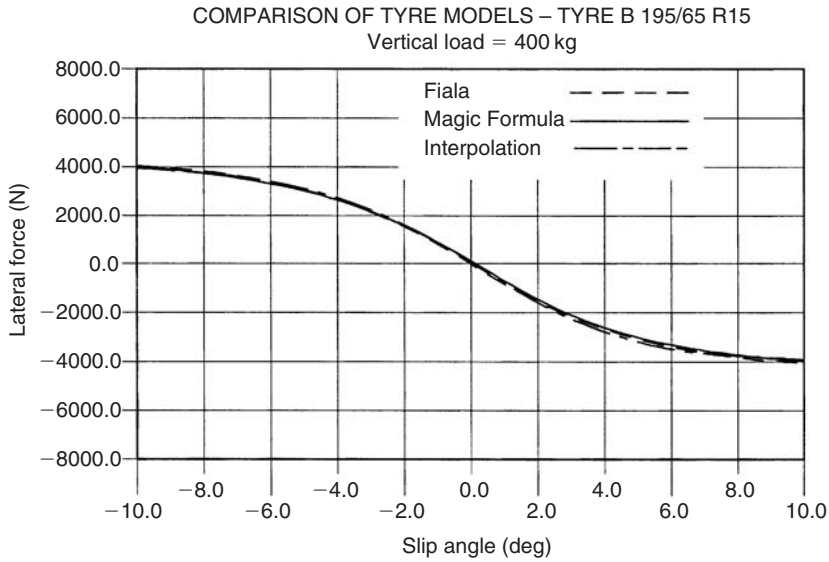

Fig. 5.74 Comparison of tyre models – lateral force with slip angle. (400 kg load). (This material has been reproduced from the Proceedings of the Institution of Mechanical Engineers, K1 Vol. 214 'The modelling and simulation of vehicle handling. Part 3: tyre modelling', M.V. Blundell, page 20, by permission of the Council of the Institution of Mechanical Engineers)

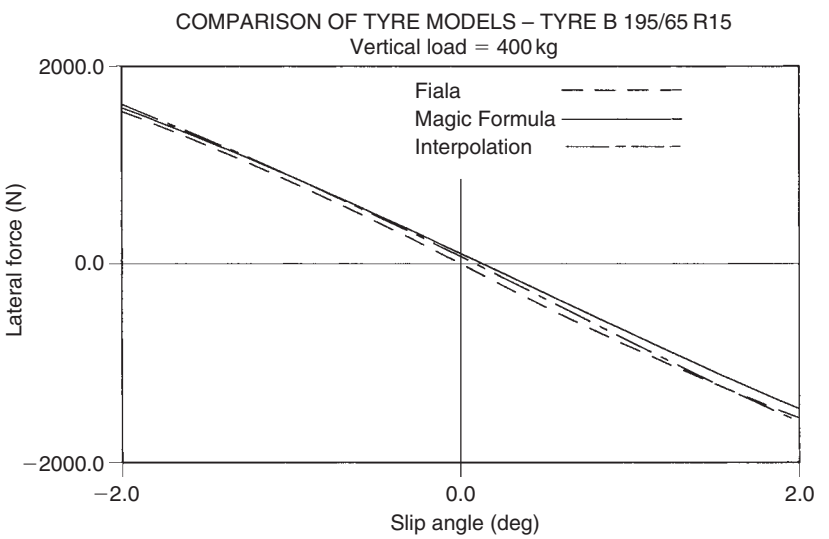

Fig. 5.75 Comparison of tyre models – lateral force at near zero slip angle (400 kg load). (This material has been reproduced from the Proceedings of the Institution of Mechanical Engineers, K1 Vol. 214 'The modelling and simulation of vehicle handling. Part 3: tyre modelling', M.V. Blundell, page 20, by permission of the Council of the Institution of Mechanical Engineers)

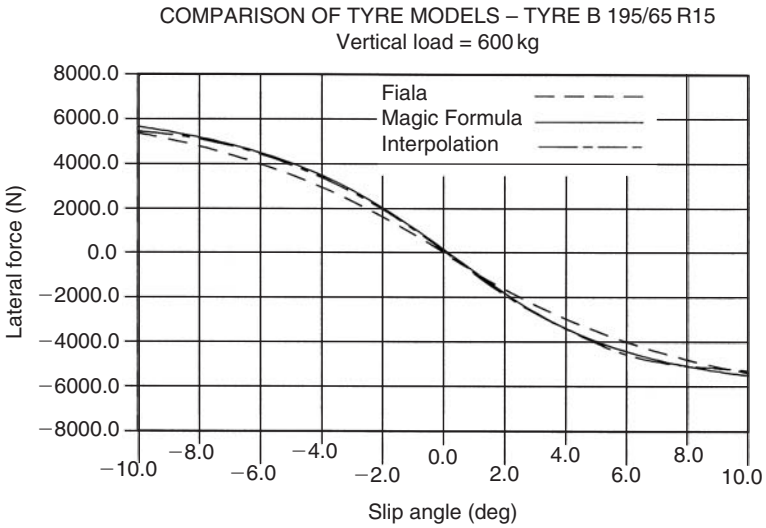

Fig. 5.76 Comparison of tyre models – lateral force with slip angle. (600 kg load). (This material has been reproduced from the Proceedings of the Institution of Mechanical Engineers, K1 Vol. 214 'The modelling and simulation of vehicle handling. Part 3: tyre modelling', M.V. Blundell, page 21, by permission of the Council of the Institution of Mechanical Engineers)

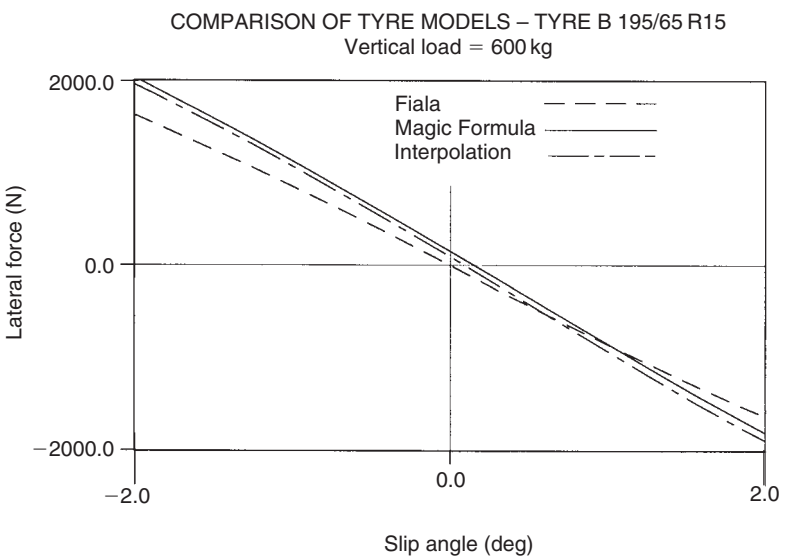

Fig. 5.77 Comparison of tyre models – lateral force at near zero slip angle (600 kg load). (This material has been reproduced from the Proceedings of the Institution of Mechanical Engineers, K1 Vol. 214 'The modelling and simulation of vehicle handling. Part 3: tyre modelling', M.V. Blundell, page 19, by permission of the Council of the Institution of Mechanical Engineers)

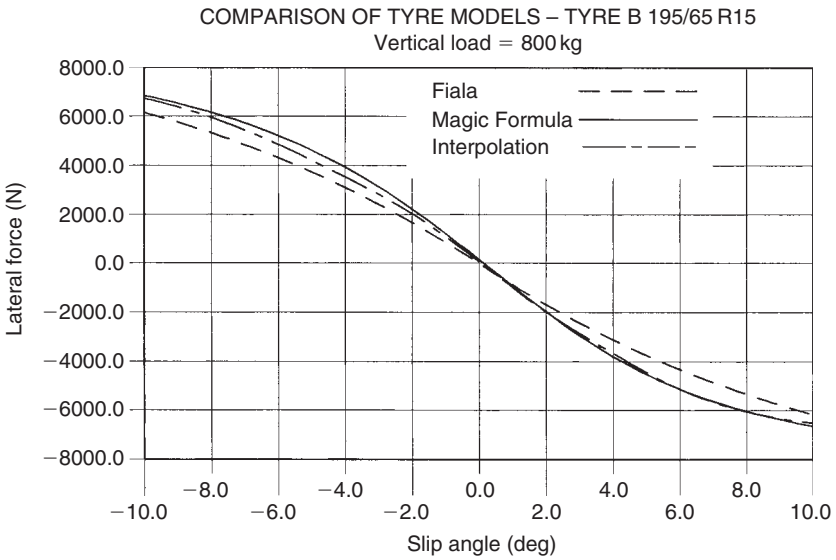

Fig. 5.78 Comparison of tyre models – lateral force with slip angle. (800 kg load). (This material has been reproduced from the Proceedings of the Institution of Mechanical Engineers, K1 Vol. 214 'The modelling and simulation of vehicle handling. Part 3: tyre modelling', M.V. Blundell, page 22, by permission of the Council of the Institution of Mechanical Engineers)

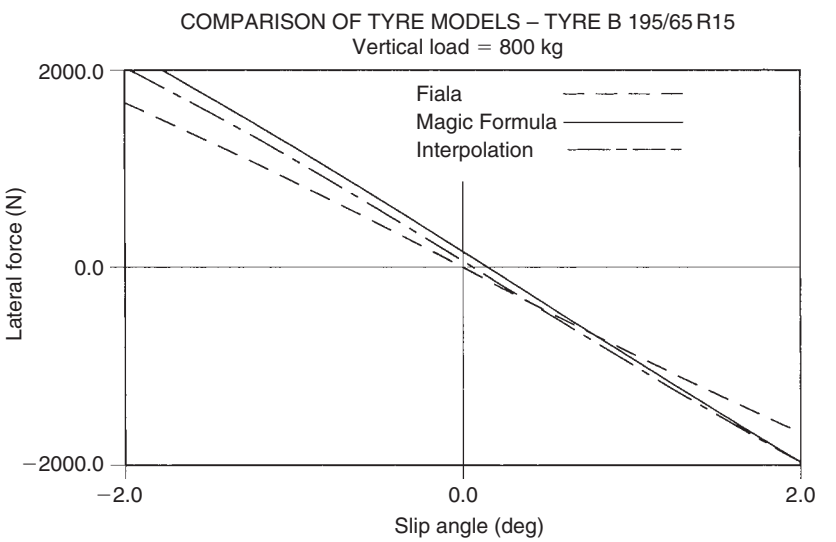

Fig. 5.79 Comparison of tyre models – lateral force at near zero slip angle (800 kg load). (This material has been reproduced from the Proceedings of the Institution of Mechanical Engineers, K1 Vol. 214 'The modelling and simulation of vehicle handling. Part 3: tyre modelling', M.V. Blundell, page 22, by permission of the Council of the Institution of Mechanical Engineers)

Interpolation data there is little to distinguish between the two sets of curves. The plots also indicate that the 'Magic Formula' can accurately represent offsets in lateral force at zero slip angle due to ply steer and conicity. Looking at the plots for the Fiala model it can be seen that the model underestimates lateral force where higher slip angles coincide with higher wheel loads. These plots also confirm that the Fiala model is ignoring lateral force offsets at zero slip angle.

The case study here is presented as an example of good practice to interrogate a tyre model and parameters before incorporation in a vehicle simulation exercise. The comparison of lateral force variation with slip angle and load shown here can be extended using the virtual rig to consider the effects of camber angle, braking, traction and combinations thereof on the significant forces and moments predicted by the model.

6 Modelling and assembly of the full vehicle

6.1 Introduction

In this chapter we will address the main systems that must be modelled and assembled to create and simulate the dynamics of the full vehicle system. The term 'full vehicle system' needs to be understood within the context of this textbook. The use of powerful modern multibody systems software allows the modelling and simulation of a range of vehicle subsystems representing the chassis, engine, driveline and body areas of the vehicle. This is illustrated in Figure 6.1 where it can be seen that multibody systems models

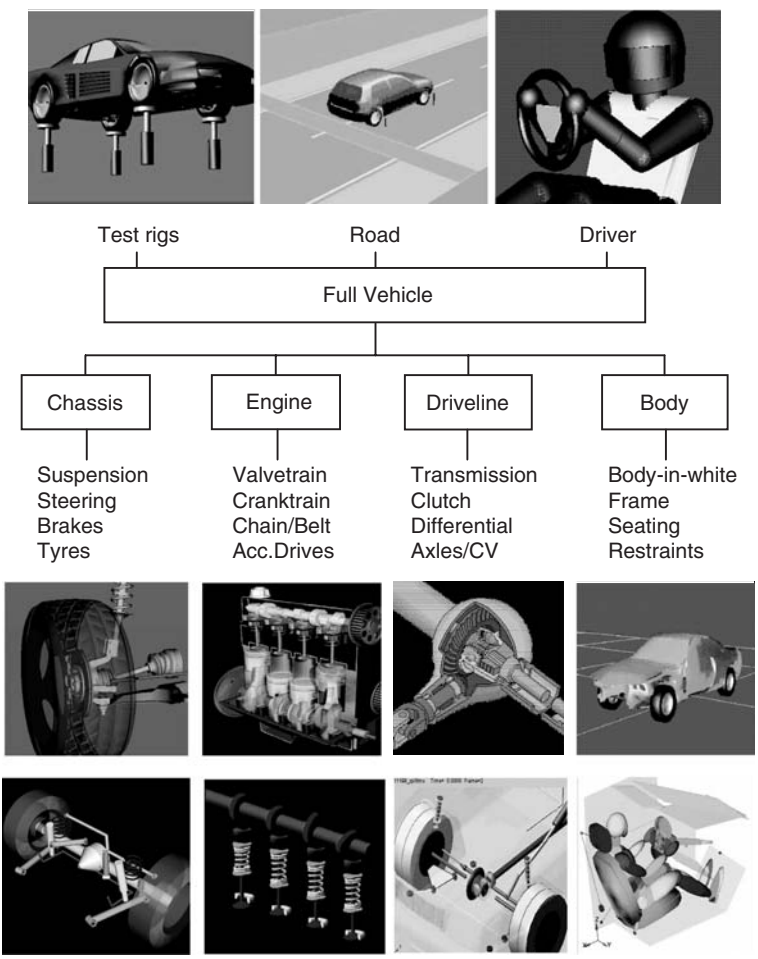

Fig. 6.1 Integration of subsystems in a full vehicle model (provided courtesy of MSC.Software)

for each of these areas are integrated to provide a detailed 'literal' representation of the full vehicle. Note that Figure 6.1 includes the modelling of the driver and road as elements of what is considered to constitute a full vehicle system model.

In this chapter we restrict our discussion of 'full vehicle system' modelling to a level appropriate for the simulation of the vehicle dynamics. As such the modelling of the suspension systems, anti-roll bars, steering system, steering inputs, brake system and drive inputs to the road wheels will all be covered. With regard to steering the modelling of the driver inputs will also be described with a range of driver models.

Note at this stage we do not consider the active elements of vehicle control other than to introduce the modelling of ABS for vehicle braking. Chapter 8 is dedicated to the modelling of active systems.

For the vehicle dynamics task a starting point involving models of less elaborate construction than that suggested in Figure 6.1 will provide useful insights much earlier in the design process. Provided such models correctly distribute load to each tyre and involve a usefully accurate tyre model, such as the 'Magic Formula' described in Chapter 5, good predictions of the vehicle response for typical proving ground manoeuvres can be obtained.

The modelling of the suspension system was considered in detail in Chapter 4. The treatment that follows in this chapter will discuss a range of options that addresses the representation of the suspension in the full vehicle as either an assembly of linkages or using simpler 'conceptual' models. It is necessary here to start with the discussion of suspension representation in the full vehicle to set the scene for following sections dealing with the modelling of springs in simple suspension models or the derivation of roll stiffness. A case study provided at the end of this chapter will compare the simulated outputs for a simulated vehicle manoeuvre using a range of suspension modelling strategies that are described in Section 6.4.

6.2 The vehicle body

For the vehicle dynamics task the mass, centre of mass position and mass moments of inertia of the vehicle body require definition within the multibody data set describing the full vehicle. It is important to note that the body mass data may include not only the structural mass of the body-in-white but also the mass of the engine, exhaust system, fuel tank, vehicle interior, driver, passengers and any other payload. A modern CAD system, or the pre-processing capability, for example, in ADAMS/View, can combine all these components to provide the analyst with a single lumped mass.

Figure 6.2 shows a detailed representation of a full vehicle model. In a model such as this there are a number of methods that might be used to represent the individual components. Using a model that most closely resembles the actual vehicle, components such as the engine might, for example, be elastically mounted on the vehicle body using bush elements to represent the engine mounts.

Fig. 6.2 A detailed multibody systems vehicle model (provided courtesy of MSC.Software)

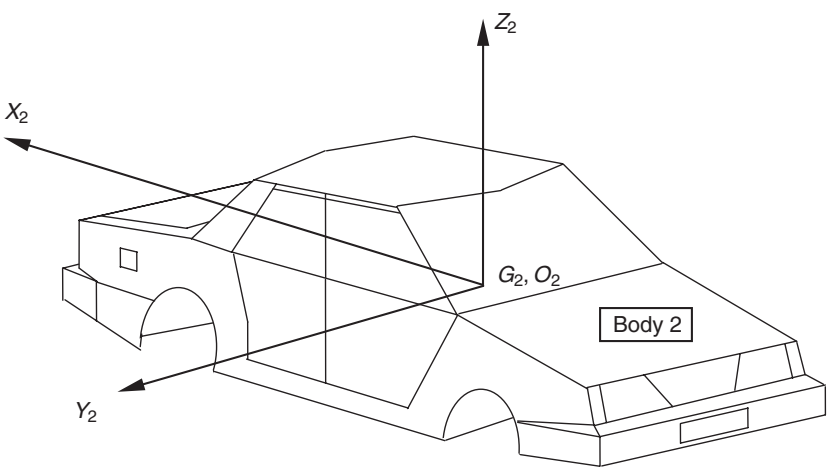

Fig. 6.3 Vehicle body reference frame

The penalty for this approach will be the addition of 6 degrees of freedom for each mass treated in this way. Alternatively a fix joint may be used to rigidly attach the mass to the vehicle body. Although this would not add degrees of freedom, the model would be less efficient through the introduction of additional equations representing the extra body and the fix joint constraint. The use of fix joint constraints may also introduce high reaction moments that would not exist in the model when using elastic mounts distributed about the mass.

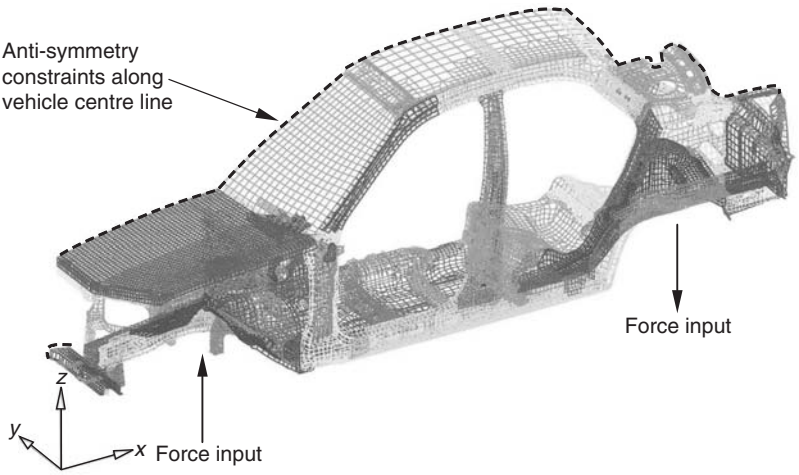

Fig. 6.4 Finite element model of body-in-white

An example of a vehicle body referenced frame O_2 located at the mass centre G_2 for Body 2 is shown in Figure 6.3. For this model the XZ plane is located on the centre line of the vehicle with gravity acting parallel to the negative Z_2 direction. Using an approach where the body is a single lumped mass representing the summation of the major components the mass centre position can be found by taking first moments of mass and the mass moments of inertia can be obtained using the methods described in Chapter 2. From inspection of Figure 6.3 it can be seen that a value would exist for the I_{xz} cross product of inertia but that I_{xy} and I_{yz} should approximate to zero given the symmetry of the vehicle. In reality there may be some asymmetry that results in a CAD system outputting small values for the I_{xy} and I_{yz} cross products of inertia.

The dynamics of the actual vehicle are greatly influenced by the yaw moment of inertia I_{zz} of the complete vehicle, to which the body and associated masses will make the dominant contribution. A parameter often discussed is the ratio k^2/ab, sometimes referred to as the 'Dynamic Index', where k is the radius of gyration associated with I_{zz} and a and b locate the vehicle mass centre longitudinally relative to the front and rear axles respectively, as shown earlier in Figure 4.47. The significance of this is discussed later in Chapter 7.

The assumption so far has been that the vehicle body is represented as a single rigid body but it is possible to model the torsional stiffness of the vehicle structure if it is felt that this could influence the full vehicle simulations. A simplistic representation of the torsional stiffness of the body may be used (Blundell, 1990) where the vehicle body is modelled as two rigid masses, front and rear half body parts, connected by a revolute joint aligned along the longitudinal axis of the vehicle and located at the mass centre. The relative rotation of the two body masses about the axis of the revolute joint is resisted by a torsional spring with a stiffness corresponding to the torsional stiffness of the vehicle body. Typically, the value of torsional stiffness may be obtained using a finite element model of the type shown in Figure 6.4. For efficiency symmetry has been exploited here to model with

finite elements only one half of the vehicle body. This requires the use of anti-symmetry constraints along the centre line of the finite element model, for all nodes on the plane of geometric symmetry, to carry out the asymmetric torsion case.

It is also possible to incorporate a finite element representation of the vehicle body within the multibody system full vehicle model. An example of this was shown in Figure 4.3 where the flexibility of a racing cart frame was included in the model. Despite the capability of modern engineering software to include this level of detail it will be seen from Case study 7 at the end of this chapter that a single lumped mass is an efficient and accurate representation of a relatively stiff modern vehicle body for the simulation of a vehicle handling manoeuvre.

6.3 Measured outputs

Before continuing in this chapter to describe the subsystems that describe the full vehicle we need to consider the typical outputs measured on the proving ground and predicted by simulation. This will be dealt with more extensively at the start of Chapter 7 but an initial treatment is given here to support the following discussion and the case study presented at the end of this chapter. For a full vehicle system simulation the predicted outputs are generally plotted as time history graphs where the outputs are the computed in a reference frame fixed in the vehicle body as indicated in Figure 6.5. Typical outputs can include:

(i) Forward velocity

(ii) Lateral acceleration

(iii) Roll angle

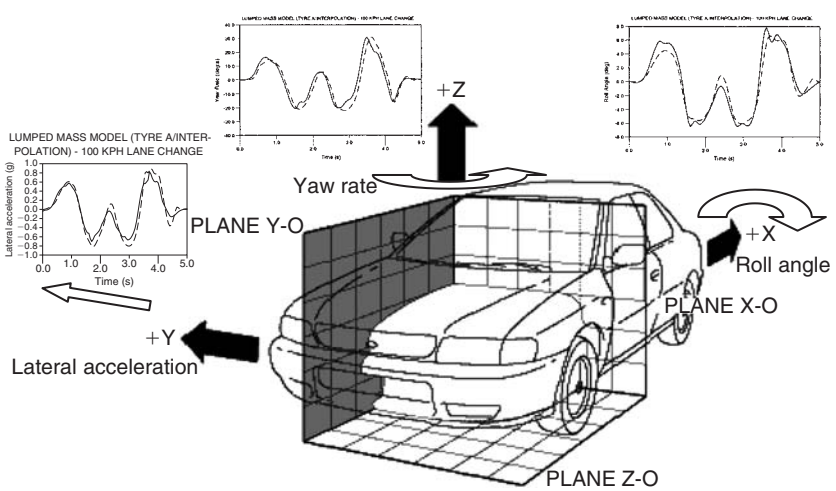

Fig. 6.5 Typical lateral responses measured in vehicle co-ordinate frame

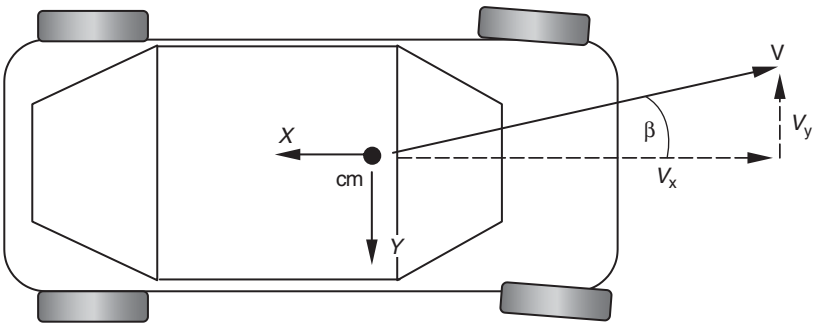

Fig. 6.6 Body slip angle

(iv) Pitch angle

(v) Yaw rate

(vi) Roll rate

Another measure often determined during test or simulation is the body slip angle, β. This is the angle of the vehicle velocity vector measured from a longitudinal axis through the vehicle as shown in Figure 6.6. The components of velocity of the vehicle mass centre V_x and V_y, measured in vehicle body reference frame, can be used to readily determine this.

6.4 Suspension system representation

6.4.1 Overview

In Chapter 4 the modelling and analysis of the suspension system was considered in isolation. In this section the representation of the suspension as a component of the full vehicle system model will be considered. As stated the use of powerful multibody systems analysis programs often results in modelling the suspension systems as installed on the actual vehicle. In the following discussion a vehicle modelled with the suspension represented in this manner is referred to as a 'Linkage model'.

Before the advent of computer simulation classical vehicle dynamicists needed to simplify the modelling of the vehicle to a level where the formulation of the equations of motion was manageable and the solution was amenable with the computational tools available at the time. Such an approach encouraged efficiency with the analyst identifying the modelling issues that were important in representing the problem in hand. The use of modern software need not discourage such an approach. The following sections summarize four vehicle models, one of which is based on modelling the suspension linkages with three other models that use alternative simplified implementations. All four models have been used to simulate a double lane change manoeuvre (Blundell, 2000) and are compared in Case study 7 at the end of this chapter. The four models described here

involve levels of evolving detail and elaboration and can be summarized as follows:

(i) A *lumped mass model*, where the suspensions are simplified to act as single lumped masses which can only translate in the vertical direction with respect to the vehicle body.

(ii) An *equivalent roll stiffness model*, where the body rotates about a single roll axis that is fixed and aligned through the front and rear roll centres.

(iii) A *swing arm model*, where the suspensions are treated as single swing arms that rotate about a pivot point located at the instant centres for each suspension.

(iv) A *linkage model*, where the suspension linkages and compliant bush connections are modelled in detail in order to recreate as closely as possible the actual assemblies on the vehicle.

6.4.2 Lumped mass model

For the lumped mass model the suspension components are considered lumped together to form a single mass. The mass is connected to the vehicle body at the wheel centre by a translational joint that only allows vertical sliding motion with no change in the relative camber angle between the road wheels and the body. The camber angle between the road wheels and the

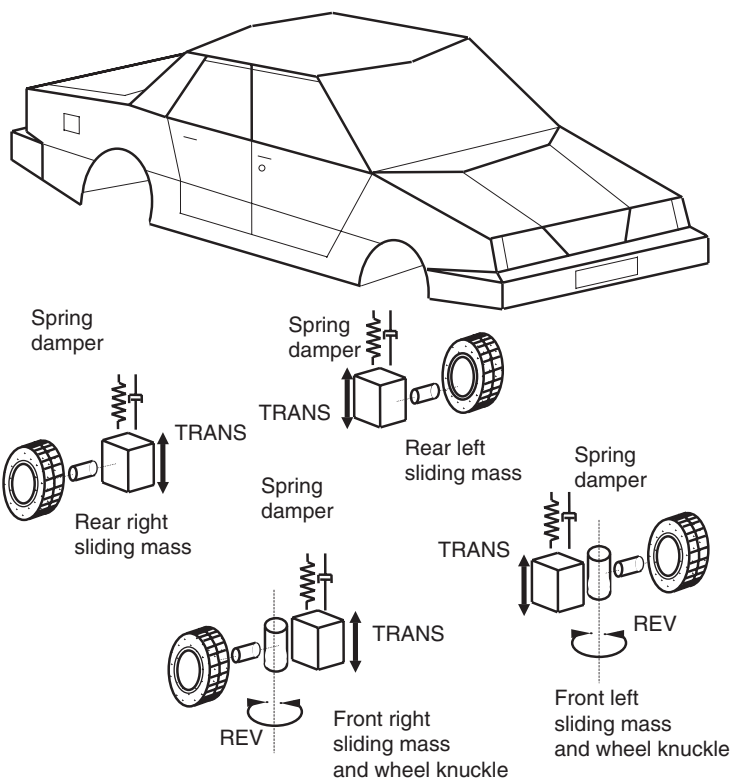

Fig. 6.7 Lumped mass model approach

road will therefore be directly related to the roll angle of the vehicle. Spring and damper forces act between the suspensions and the body. Such suspensions have been used on early road vehicles, notably the Lancia Lambda (1908–1927), where it was termed 'sliding pillar'.

The front wheel knuckles are modelled as separate parts connected to the lumped suspension parts by revolute joints. The steering motion required for each manoeuvre is achieved by applying time dependent rotational motion inputs about these joints. Each road wheel is modelled as a part connected to the suspension by a revolute joint. The lumped mass model is shown schematically in Figure 6.7.

6.4.3 Equivalent roll stiffness model

This model is developed from the lumped mass model by treating the front and rear suspensions as rigid axles connected to the body by revolute joints. The locations of the joints for the two axles are their respective 'roll centres' as described in Chapter 4. A torsional spring is located at the front and rear roll centres to represent the roll stiffness of the vehicle. The determination of the roll stiffness of the front and rear suspensions required an investigation as described in the following section. The equivalent roll stiffness model is shown schematically in Figure 6.8.

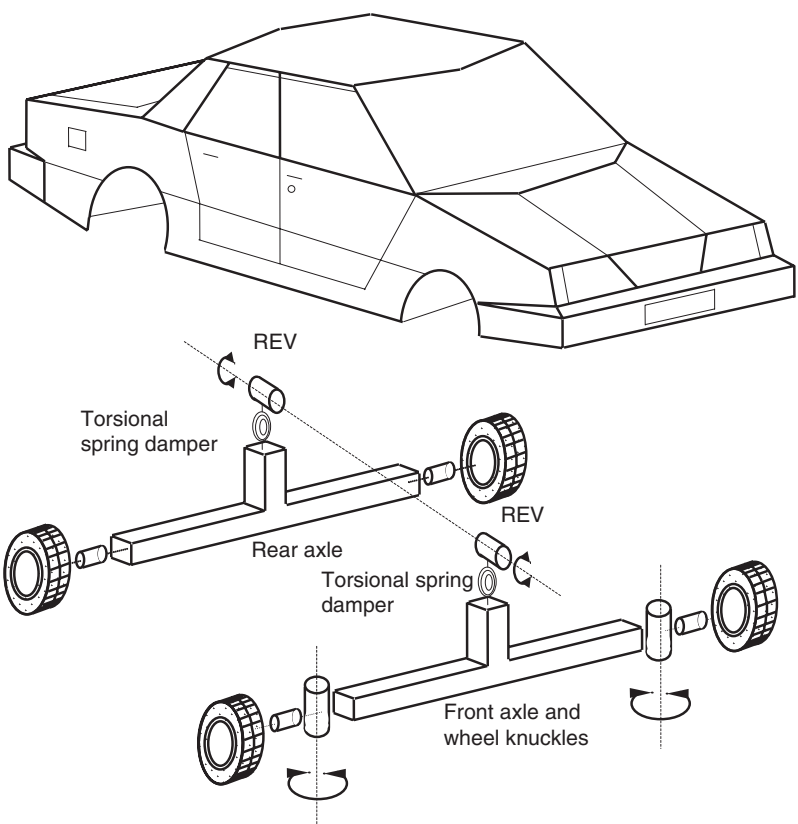

Fig. 6.8 Equivalent roll stiffness model approach

Note that this model shows the historical background to much of the current unclear thinking about roll centres and their influence on vehicle behaviour. With beam axles, as were prevalent in the 1920s, this model is a good equivalent for looking at handling behaviour on flat surfaces and ignoring ride inputs. For independent suspensions where the anti-roll geometry remains relatively consistent with respect to the vehicle and where the roll centres are relatively low (i.e. less than around 100 mm for a typical passenger car) – a fairly typical double wishbone setup, for example – then this approximation can be useful despite its systematic inaccuracy. However, drawing general conclusions from such specific circumstances can be dangerous; vehicles which combine a strut suspension at one end (with very mobile anti-roll geometry) and double wishbone at the other (with relatively constant anti-roll geometry) may not be amenable to such simplifications. With this and all other simplified models, the analyst must consider whether or not the conclusions that are drawn reflect upon the simplification adopted or actually reveal some useful insight. The case study presented at the end of the chapter shows a vehicle that behaves acceptably when modelled in this way.

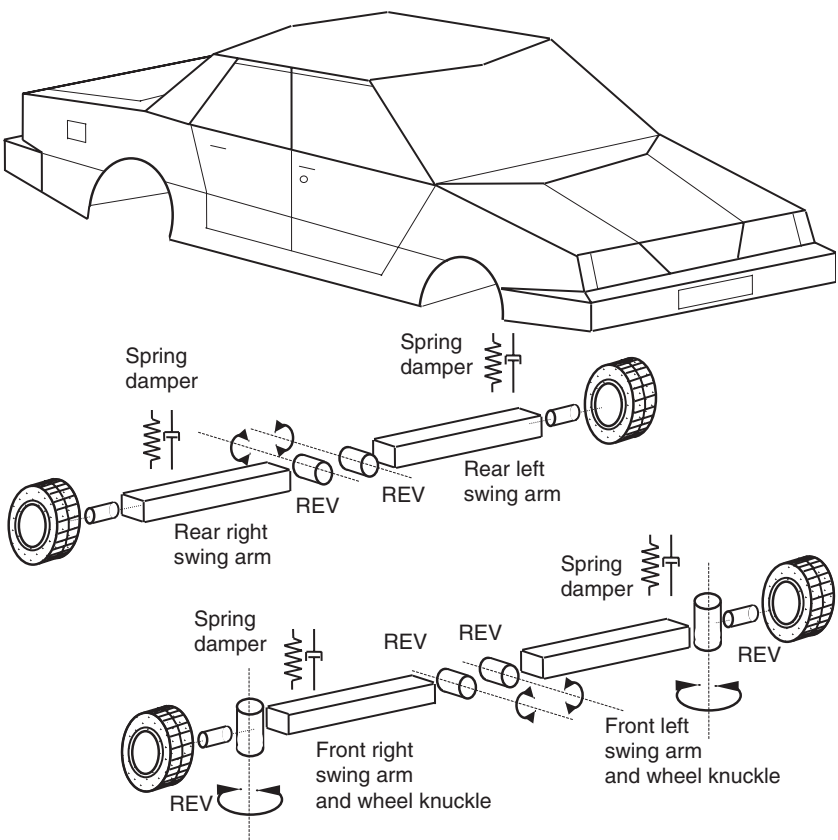

Fig. 6.9 Swing arm model approach

6.4.4 Swing arm model

This model is developed from the equivalent roll stiffness mass model by using revolute joints to allow the suspensions for all four wheels to 'swing' relative to the vehicle body rather than using the suspensions linked on an axle. The revolute joints are located at the instant centres of the actual suspension linkage assembly. These positions are found by modelling the suspensions separately as described in Chapter 4. The swing arm model has an advantage over the roll centre model in that it allows the wheels to change camber angle independently of each other and relative to the vehicle body. The swing arm model is shown schematically in Figure 6.9. Although in the sketch the swing arms are shown with an axis parallel to the vehicle axis this need not be so in general. Also, although in the sketch the swing arms are shown as a 'plausible' mechanical arrangement (i.e. not overlapping) this also need not be so; in general contact between elements is not modelled for vehicle dynamics studies and in general the instant centres are widely spaced and not necessarily within the physical confines of the vehicle body. The swing arm model has the advantage over the equivalent roll stiffness model in that the heave and pitch ride behaviour can be included.

6.4.5 Linkage model

The model based on linkages as shown in Figure 6.10 is the model that most closely represents the actual vehicle. This sort of vehicle model is the

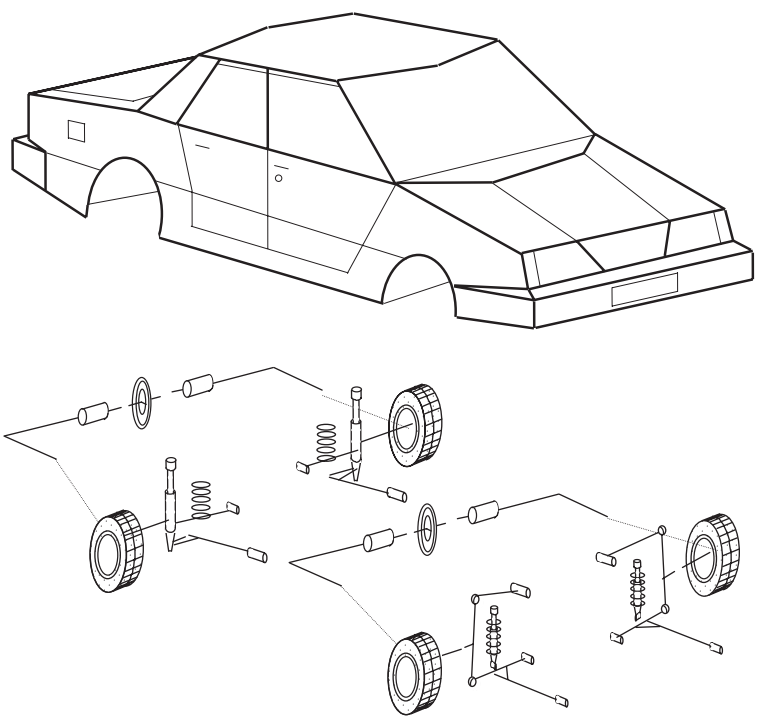

Fig. 6.10 Linkage model 'as is' approach

most common approach adopted by MSC.ADAMS users in the automotive industry often extending the model definition to include full non-linear bush characteristics.

A simplification of a model based on linkages is to treat the joints as rigid and generate a kinematic representation of the suspension system. As described in Chapter 4 a double wishbone arrangement is typical of a suspension system that can be modelled in this way and used for handling simulations (Pilling, 1995).

6.4.6 The concept suspension approach

In addition to the four suspension modelling approaches just described another form of suspension model simplification (Scapaticci and Minen, 1992) considers an approach where the model contains no elements representing a physical connection between the road wheel and the chassis. Instead the movement of the road wheel with respect to the chassis is described by a functional representation, which describes the wheel centre

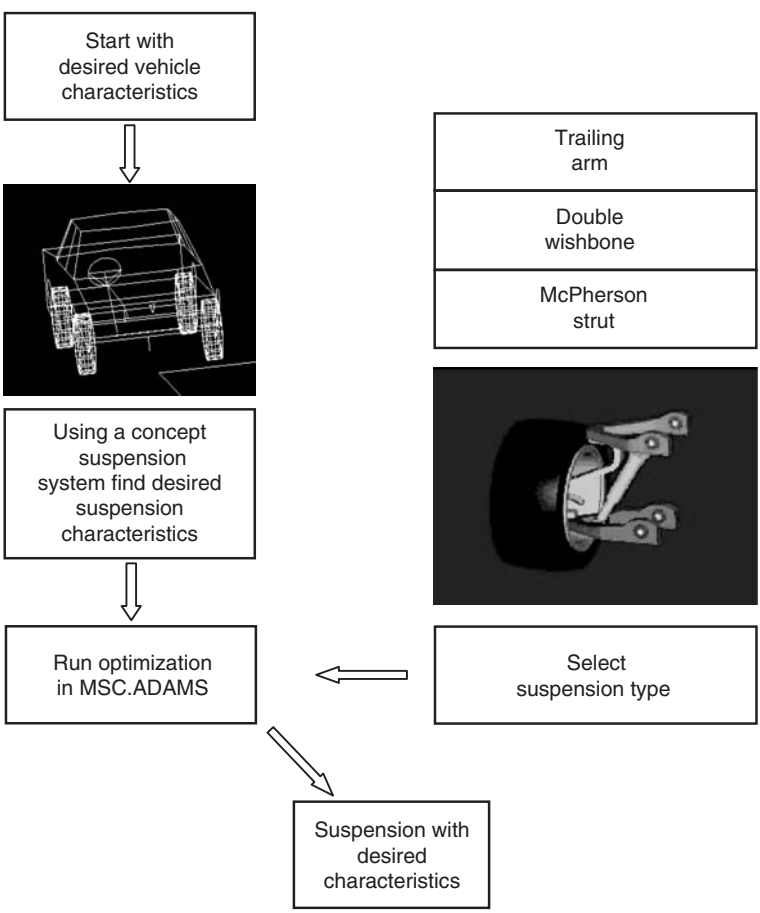

Fig. 6.11 Application of a Concept Suspension model (provided courtesy of MSC.Software)

trajectory and orientation as it moves vertically between full bump and rebound positions. Scapaticci and Minen (1992) describe this approach as the implementation of synthetic wheel trajectories. Such a method has been adopted within MSC.ADAMS where the model is referred to as a 'Concept Suspension' and is the basis of many dedicated vehicle dynamics modelling software tools such as Milliken Research Associate's VDMS, MSC's CarSim, University of Michigan's ArcSim, and Leeds University's VDAS. The way in which such a model is applied is summarized in Figure 6.11. In essence the vehicle model containing the concept suspension can be used to investigate the suspension design parameters that can contribute to the delivery of the desired vehicle handling characteristics without modelling of the suspension linkages. In this way, the analyst can gain a clear understanding of the dominant issues affecting some aspect of vehicle dynamics performance. A case study is given in section 6.14 describing the use of a reduced (3 degree of freedom) linear model to assess the influence of suspension characteristics on straight-line stability. These models belong very firmly in the 'analysis' segment of the overall process diagram described in Chapter 1, Figure 1.6.

The functional representation of the model is based on components that describe effects due to kinematics dependent on suspension geometry and also elastic effects due to compliance within the suspension system. A schematic to support an explanation of the function of this model is provided in Figure 6.12.

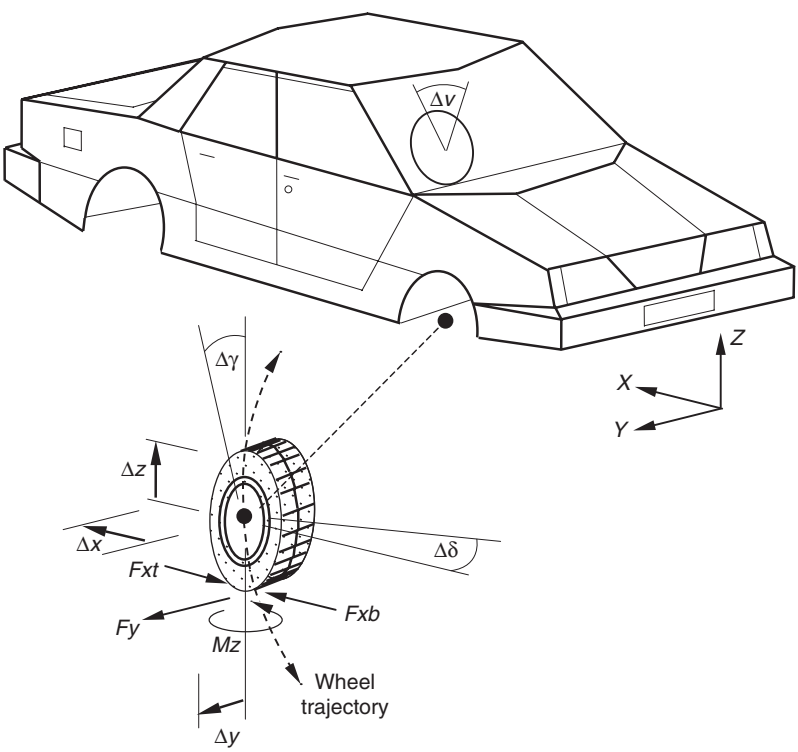

Fig. 6.12 Concept Suspension system model schematic

If we consider first the kinematic effects due to suspension geometry we can see that there are two variables that provide input to the model:

Δz is the change in wheel centre vertical position (wheel travel)
Δv is the change in steering wheel angle

The magnitude of the wheel travel Δz will depend on the deformation of the surface, the load acting vertically through the tyre resulting from weight transfer during a simulated manoeuvre and a representation of the suspension stiffness and damping acting through the wheel centre. The magnitude of the change in steering wheel angle Δv will depend on either an open loop fixed time dependent rotational motion input or a closed loop torque input using a controller to feed back vehicle position variables so as to steer the vehicle to follow a predefined path. The modelling of steering inputs is discussed in more detail later in this chapter. The dependent variables that dictate the position and orientation of the road wheel are:

Δx is the change in longitudinal position of the wheel
Δy is the change in lateral position (half-track) of the wheel
$\Delta\delta$ is the change in steer angle (toe in/out) of the wheel
$\Delta\gamma$ is the change in camber angle of the wheel

The functional dependencies that dictate how the suspension moves with respect to the input variables can be obtained through experimental rig measurements, if the vehicle exists and is to be used as a basis for the model, or by performing simulation with suspension models as described in Chapter 4. For example, the dependence of camber angle $\Delta\gamma$ on wheel travel can be derived from the curves plotted for Case study 1 in Chapter 4.

The movement of the suspension due to elastic effects is dependent on the forces acting on the wheel. In their paper Scapaticci and Minen (1992) describe the relationship using the equation shown in (6.1) where the functional dependencies due to suspension compliance are defined using the matrix F_E:

$$\begin{bmatrix} \Delta x \\ \Delta y \\ \Delta\delta \\ \Delta\gamma \end{bmatrix} = \begin{bmatrix} \\ F_E \\ \\ \end{bmatrix} \begin{bmatrix} Fxt \\ Fxb \\ Fy \\ Mz \end{bmatrix} \tag{6.1}$$

and the inputs are the forces acting on the tyre:

Fxt is the longitudinal tractive force
Fxb is the longitudinal braking force
Fy is the lateral force
Mz is the self-aligning moment

Note that the dimensions of the matrix F_E are such that cross-coupling terms, such as toe change under braking force, can exist. The availability of such data early in the design phase can be difficult but the adoption of such a generalized form allows the user to speculate on such values and thus use the model to set targets for acceptable behaviour.

6.5 Modelling of springs and dampers

6.5.1 Treatment in simple models

The treatment of road springs and dampers in a vehicle where the suspensions have been modelled using linkages is generally straightforward. A road spring is often modelled as linear but the damper will usually require a non-linear representation as discussed in Chapter 3. It is also common for the bump travel limiter to be engaged early and to have both stiffness and damping elements to its behaviour; both those aspects may be modelled using the methods discussed here. The choice of whether to combine them with the road spring and damper forces is entirely one of modelling convenience; the authors generally find the ease of debugging and auditing the model is worth the carriage of two not strictly necessary additional force generating terms.

For the simplified modelling approach used in the lumped mass and swing arm models the road springs cannot be directly installed in the vehicle model as with the linkage model. Consider the lumped mass model when compared with the linkage model as shown in Figure 6.13.

Clearly there is a mechanical advantage effect in the linkage model that is not present in the lumped mass vehicle model. At a given roll angle for the lumped mass model the displacement and hence the force in the spring will be too large when compared with the corresponding situation in the linkage model.

For the swing arm model the instant centre about which the suspension pivots is often on the other side of the vehicle. In this case the displacement in the spring is approximately the same as at the wheel and a similar problem occurs as with the lumped mass model. For all three simplified models this

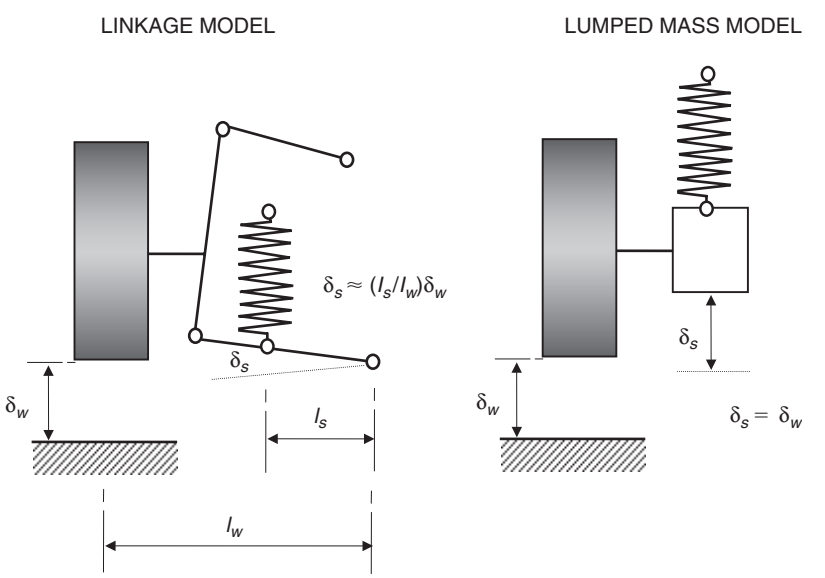

Fig. 6.13 Road spring in linkage and lumped mass models

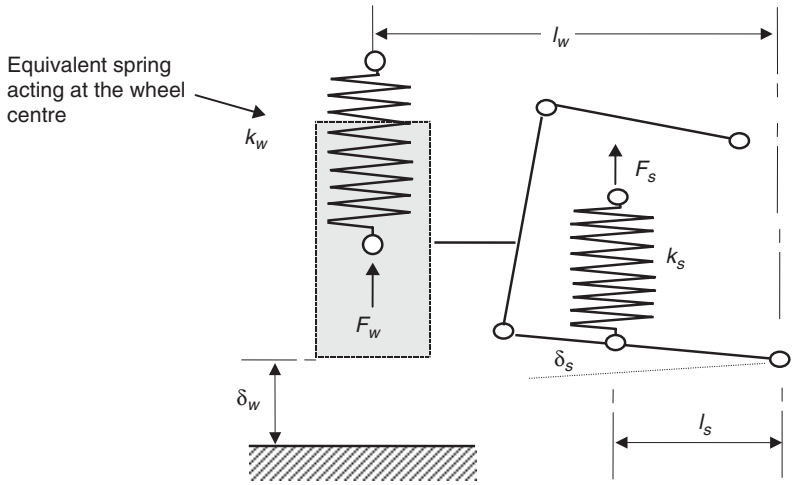

Fig. 6.14 Equivalent spring acting at the wheel centre

problem can be overcome as shown in Figure 6.14 by using an 'equivalent' spring which acts at the wheel centre.

As an approximation, ignoring exact suspension geometry, the expression (6.2) can be used to represent the stiffness k_w of the equivalent spring at the wheel:

$$k_w = F_w/\delta_w = (l_s/l_w)F_s/(l_w/l_s)\delta_s = (l_s/l_w)^2 k_s \tag{6.2}$$

The presence of a square function in the ratio can be considered a combination of both the extra mechanical advantage in moving the definition of spring stiffness to the wheel centre and the extra spring deflection at the wheel centre.

6.5.2 Modelling leaf springs

Although the modelling of leaf springs is now rare on passenger cars they are still fitted extensively on light trucks and goods vehicles where they offer the advantage of providing relatively constant rates of stiffness for large variations in load at the axle. The modelling of leaf springs has always been more of a challenge in an MBS environment when compared with the relative simplicity of modelling a coil spring. Several approaches may be adopted the most common of which are shown in Figure 6.15.

Early attempts at modelling leaf springs utilized the simple approach based on equivalent springs to represent the vertical and longitudinal force–displacement characteristic of the leaf spring. On the actual vehicle the leaf springs also contribute to the lateral positioning of the axle, with possible additional support from a panhard rod. Although not shown in Figure 6.15 lateral springs could also be incorporated to represent this.

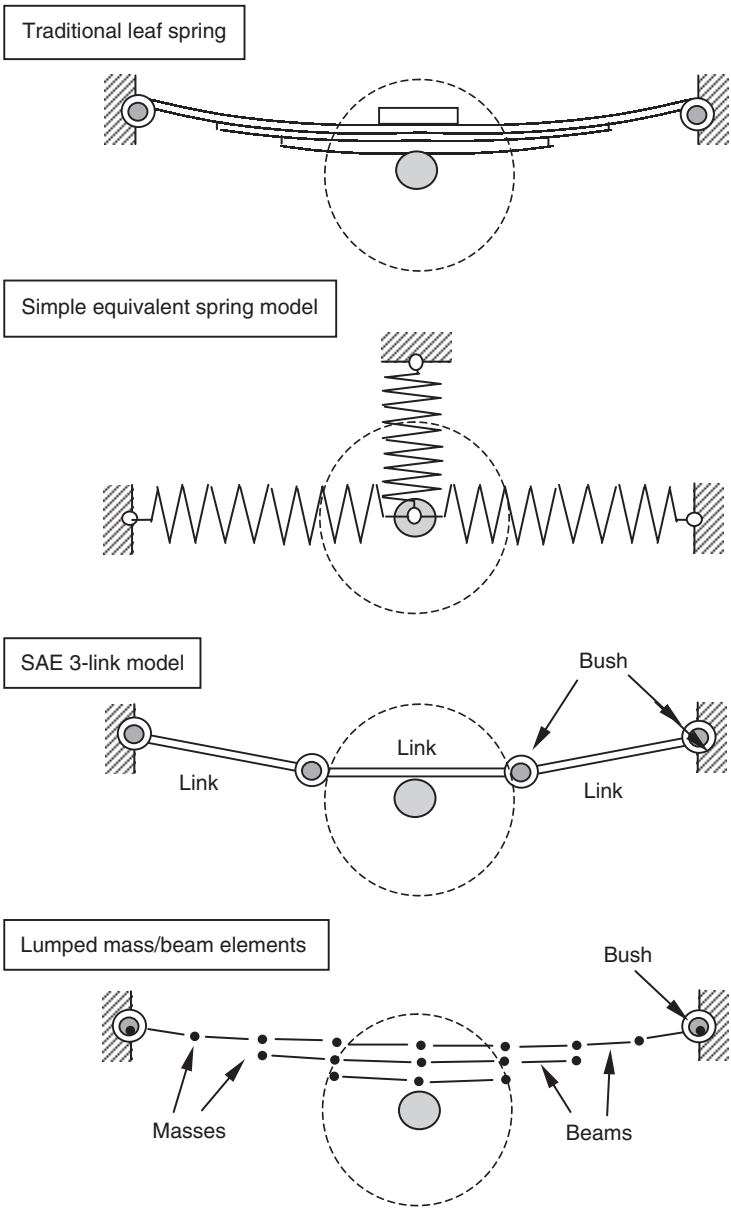

Fig. 6.15 Leaf spring modelling strategies

The next approach is based on modelling the leaf spring as three bodies (SAE 3-link model) interconnected by bushes or revolute joints with an associated torsional stiffness that provides equivalent force–displacement characteristics as found in the actual leaf spring. The last approach shown in Figure 6.15 uses a detailed 'as is' approach representing each of the leaves as a series of distributed lumped masses interconnected by beam elements with the correct sectional properties for the leaf. This type of model is also

complicated by the need to model the interleaf contact forces between the lumped masses with any associated components of sliding friction.

6.6 Anti-roll bars

As shown in Figure 6.16 anti-roll bars may be modelled using two parts connected to the vehicle body by revolute joints and connected to each other by a torsional spring located on the centre line of the vehicle. In a more detailed model the analyst could include rubber bush elements rather than the revolute joints shown to connect each side of the anti-roll bar to the vehicle. In this case for a cylindrical bush the torsional stiffness of the bush would be zero to allow rotation about the axis, or could have a value associated with the friction in the joint. In this model the connection of the anti-roll bars to the suspension system is not modelled in detail, rather each anti-roll bar part is connected to the suspension using an inplane joint primitive that allows the vertical motion of the suspension to be transferred to the anti-roll bars and hence produce a relative twisting motion between the two sides.

A more detailed approach, shown in Figure 6.17, involves including the drop links to connect each side of the anti-roll bar to the suspension systems. The drop link is connected to the anti-roll bar by a universal joint and is connected to the suspension arm by a spherical joint. This is similar to the modelling of a tie rod as discussed in Chapter 4 where the universal joint is used to constrain the spin of the link about an axis running along its length, this degree of freedom having no influence on the overall behaviour of the model.

The stiffness K_T of the torsional spring can be found directly from fundamental torsion theory for the twisting of bars with a hollow or solid circular cross-section. Assuming here a solid circular bar and units that are consistent with the examples that support this text we have

$$K_T = \frac{GJ}{L} \tag{6.3}$$

where

G is the shear modulus of the anti-roll bar material (N/mm^2)

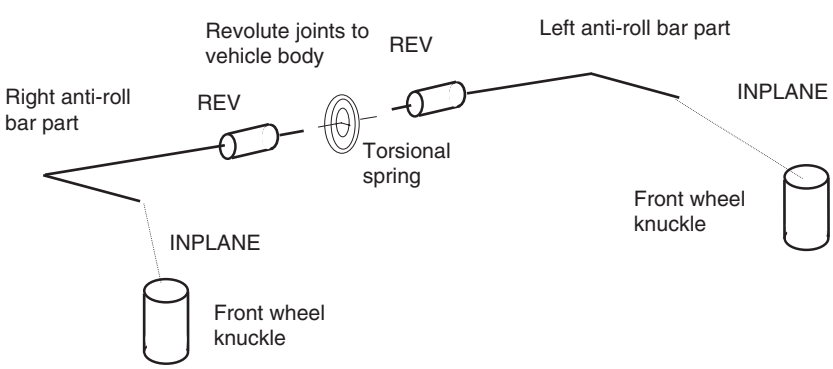

Fig. 6.16 Modelling the anti-roll bars using joint primitives

J is the second moment of area (mm^4)
L is the length of the anti-roll bar (mm)

Note that the length L used in equation (6.3) is the length of the bar subject to twisting. For the configuration shown in Figure 6.17 this is the transverse length of the anti-roll bar across the vehicle and does not include the fore–aft lengths of the system that connect to the drop links. These lengths of the bar provide the lever arms to twist the transverse section of bar and are subject to bending rather than torsion. An externally solved FE model could be used to give an equivalent torsional stiffness for a simplified representation such as this.

Given that bending or flexing of the roll bar may have an influence the next modelling refinement of the anti-roll bar system uses finite element beams, of the type described in Chapter 3, to interconnect a series of rigid bodies with lumped masses distributed along the length of the bar. Such sophistication becomes necessary to investigate anti-roll bar interactions with steer torque, or anti-roll bar lateral 'walking' problems in the vehicle; in general though, such detail is not required for vehicle behaviour modelling.

Again these joints could be modelled with bushes if needed. Such a model is shown in Figure 6.18 would be to model the drop links with lumped masses and beams if the flexibility of these components needed to be modelled.

The modelling described so far has been for the modelling of the conventional type of anti-roll bar found on road vehicles. Vehicles with active components in the anti-roll bar system might include actuators in place of the drop links or a coupling device connecting the two halves of the system providing variable torsional stiffness at the connection. Space does not permit a description of the modelling of such systems here, but with ever more students becoming involved in motorsport this section will conclude with a description of the type of anti-roll bar model that might be included

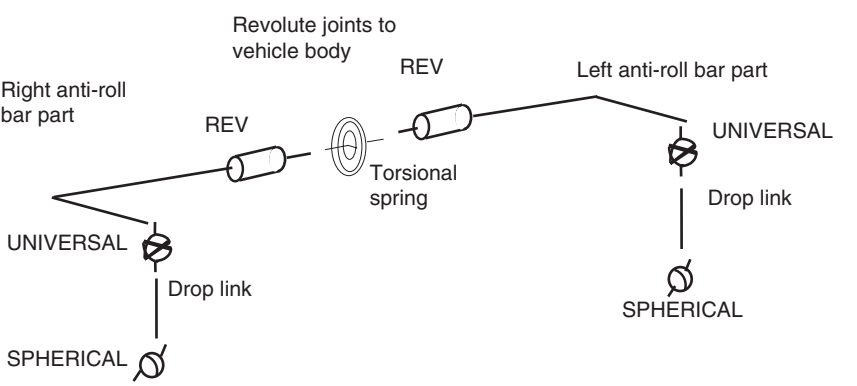

Fig. 6.17 Modelling the anti-roll bars using drop links. (This material has been reproduced from the Proceedings of the Institution of Mechanical Engineers, K2 Vol. 213 'The modelling and simulation of vehicle handling. Part 2: vehicle modelling', M.V. Blundell, page 131, by permission of the Council of the Institution of Mechanical Engineers)

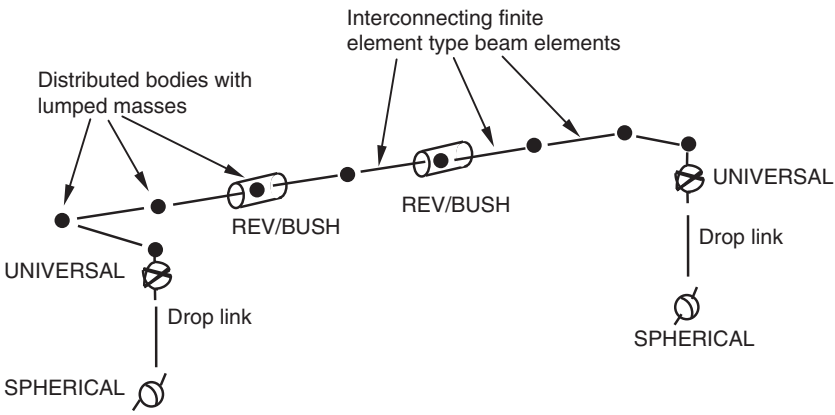

Fig. 6.18 Modelling the anti-roll bars using interconnected finite element beams

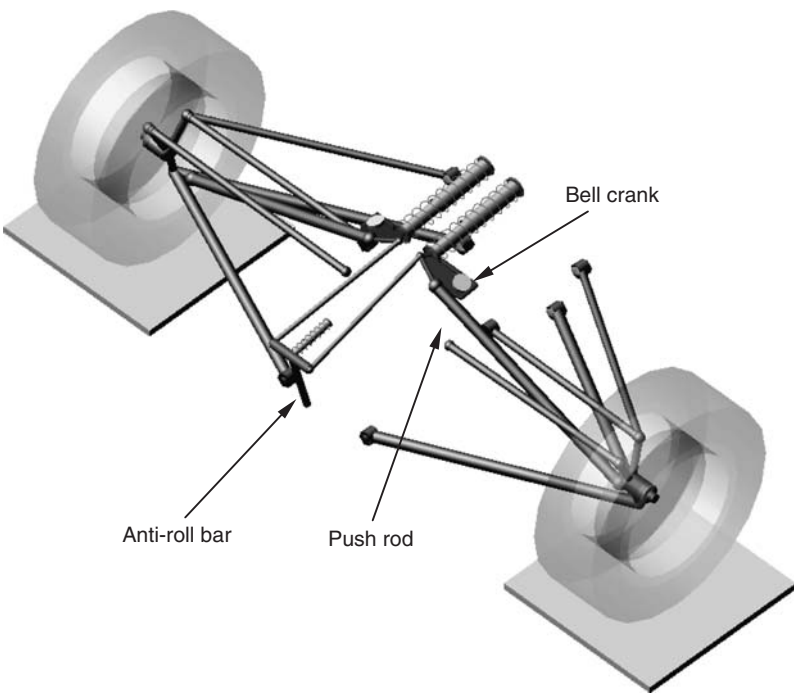

Fig. 6.19 Graphic of anti-roll bar in typical student race vehicle (provided courtesy of MSC.Software)

in a typical student race vehicle. A graphic for the system is shown in Figure 6.19.

The modelling of this system is illustrated in the schematic in Figure 6.20 where it can be seen that the anti-roll bar is installed vertically and is connected to the chassis by a revolute joint. The revolute joint allows the

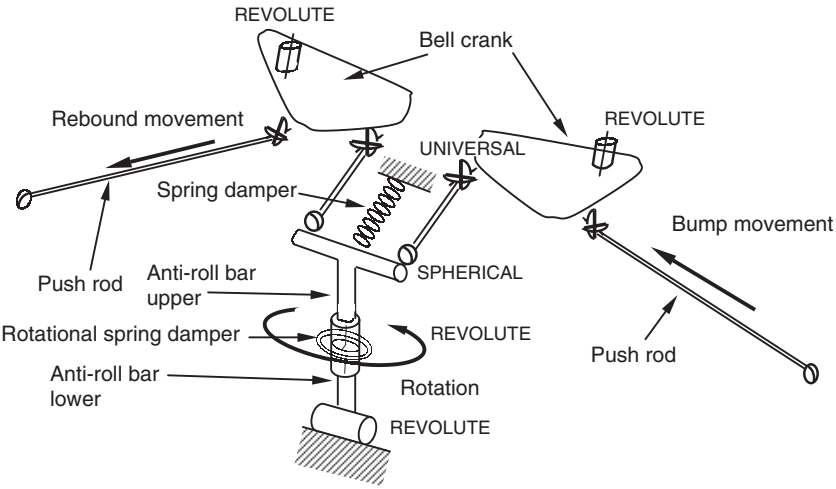

Fig. 6.20 Modelling of anti-roll bar mechanism in student race car

anti-roll bar to rock back and forward as the bell cranks rotate during parallel wheel travel but prevents rotation during opposite wheel travel when the body rolls. As the body rolls the torsional stiffness of the anti-roll bar, modelled with the rotational spring damper, resists the pushing motion of one push rod as the suspension moves in bump on one side and the pulling motion as the suspension moves in rebound on the other side. The small spring damper helps to locate the anti-roll bar with respect to the vehicle chassis and adds to the heave stiffness and damping. Alternative linkage designs are possible that allow the use of a translational spring element and hence allow independent control of damping in roll compared to damping in heave. Such 'three spring' systems are common in higher formula motorsports events when allowed by the rules.

6.7 Determination of roll stiffness for the equivalent roll stiffness model

In order to develop a full vehicle model based on roll stiffness it is necessary to determine the roll stiffness and damping of the front and rear suspension elements separately. The estimation of roll damping is obtained by assuming an equivalent linear damping and using the positions of the dampers relative to the roll centres to calculate the required coefficients. If a detailed vehicle model is available the procedure used to find the roll stiffness for the front suspension elements involves the development of a model as shown in Figure 6.21. This model includes the vehicle body, this being constrained to rotate about an axis aligned through the front and rear roll centres. The roll centre positions can be found using the methods described in Chapter 4. The vehicle body is attached to the ground part by a cylindrical joint located at the front roll centre and aligned with the rear roll centre. The rear roll centre is attached to the ground by a spherical joint in order to prevent the vehicle sliding along the roll axis. A motion input is applied at the cylindrical

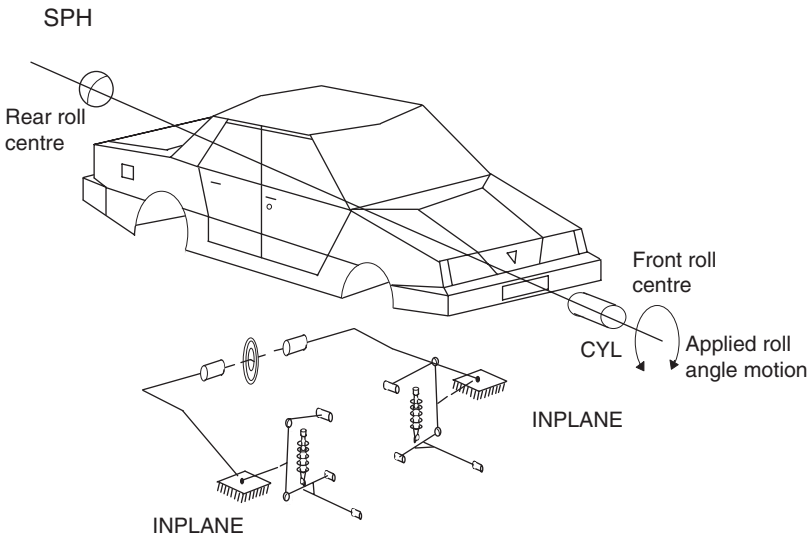

Fig. 6.21 Determination of front end roll stiffness. (This material has been reproduced from the Proceedings of the Institution of Mechanical Engineers, K2 Vol. 213 'The modelling and simulation of vehicle handling. Part 2: vehicle modelling', M.V. Blundell, page 127, by permission of the Council of the Institution of Mechanical Engineers)

joint to rotate the body through a given angle. By requesting the resulting torque acting about the axis of the joint it is possible to calculate the roll stiffness associated with the front end of the vehicle. The road wheel parts are not included nor are the tyre properties. The tyre compliance is represented separately by a tyre model and should not be included in the determination of roll stiffness. The wheel centres on either side are constrained to remain in a horizontal plane using inplane joint primitives. Although the damper force elements can be retained in the suspension models they have no contribution to this calculation as the roll stiffness is determined using static analysis. The steering system, although not shown in Figure 6.21, may also be included in the model. If present a motion input is needed to lock the steering in the straight-ahead position during the roll simulation.

For the rear end of the vehicle the approach is essentially the same as for the front end, with in this case a cylindrical joint located at the rear roll centre and a spherical joint located at the front roll centre.

For both the front and rear models the vehicle body can be rotated through an appropriate angle either side of the vertical. For the example vehicle used in this text the body was rotated 10 degrees each way. The results for the front end model are plotted in Figure 6.22. The gradient at the origin can be used to obtain the value for roll stiffness used in the equivalent roll stiffness model described earlier.

In the absence of an existing vehicle model that can be used for the analysis described in the preceding section, calculations can be performed to estimate the roll stiffness. In reality this will have contributions from the road springs, anti-roll bars and possibly the suspension bushes. Figure 6.23

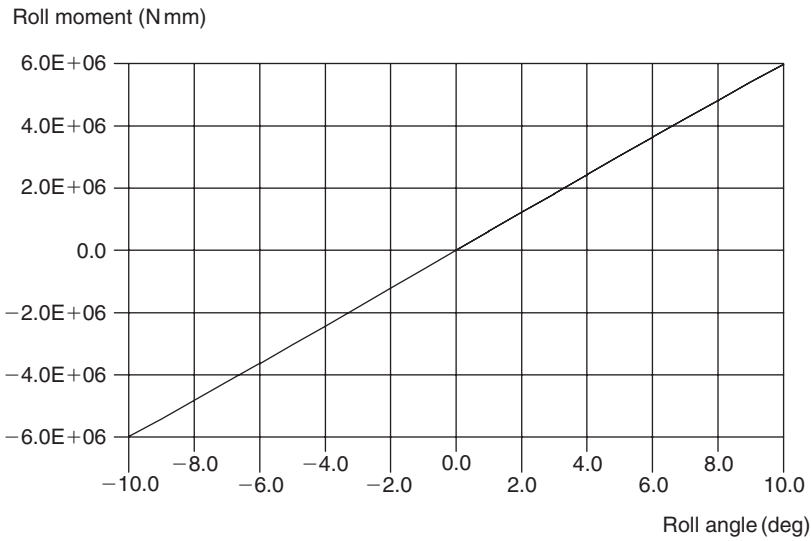

Fig. 6.22 Front end roll simulation

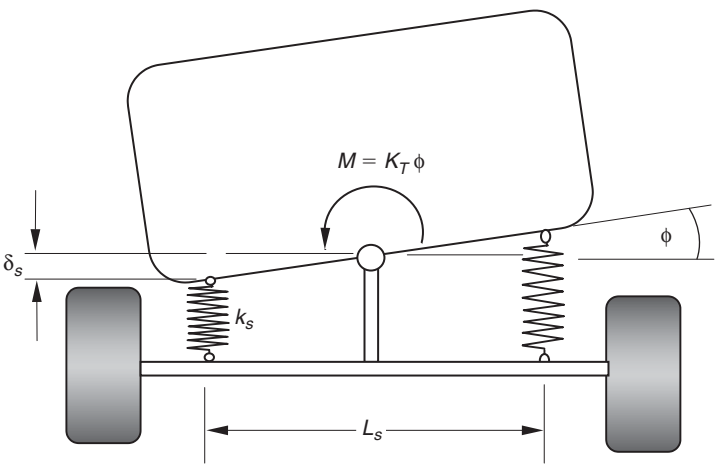

Fig. 6.23 Calculation of roll stiffness due to road springs

provides the basis for a calculation of the road spring contribution for the simplified arrangement shown. In this case the inclination of the road springs is ignored and have a separation across the vehicle given by L_s.

As the vehicle rolls through an angle ϕ the springs on each side are deformed with a displacement δ_s given by

$$\delta_s = \phi L_s/2 \tag{6.4}$$

The forces generated in the springs F_s produce an equivalent roll moment M_s given by

$$M_s = F_s L_s = k_s \delta_s L_s = k_s \phi L_s^2/2 \tag{6.5}$$

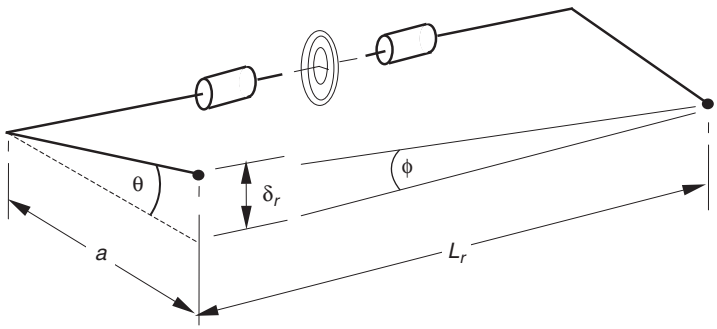

Fig. 6.24 Calculation of roll stiffness due to the anti-roll bar

The roll stiffness contribution due to the road springs K_{Ts} at the end of the vehicle under consideration is given by

$$K_{Ts} = M_s/\phi = k_s L_s^2/2 \tag{6.6}$$

In a similar manner the contribution to the roll stiffness at one end of the vehicle due to an anti-roll bar can be determined as shown in Figure 6.24.

In this case if the ends of the anti-roll bar are separated by a distance L_r and the vehicle rolls through an angle ϕ, the relative deflection of one end of the anti-roll bar to the other δ_r is given by

$$\delta_r = a\theta = \phi L_r \tag{6.7}$$

The angle of twist in the roll bar is given by

$$\theta = \frac{TL_r}{GJ} \tag{6.8}$$

where as discussed earlier G is the shear modulus of the anti-roll bar material, J is the polar second moment of area and T is the torque acting about the transverse section of the anti-roll bar. Note that in this analysis we are ignoring the contribution due to bending. The forces acting at the ends of the anti-roll bar F_r produce an equivalent roll moment M_r given by

$$M_r = F_r L_r = TL_r/a = \theta GJ/a = \phi L_r GJ/a^2 \tag{6.9}$$

The roll stiffness contribution due to the anti-roll bar K_{Tr} at the end of the vehicle under consideration is given by

$$K_{Tr} = M_r/\phi = L_r GJ/a^2 \tag{6.10}$$

The contribution of both the road springs and the anti-roll bar can then be added, ignoring suspension bushes here, to give the roll stiffness K_T:

$$K_T = K_{Ts} + K_{Tr} \tag{6.11}$$

Note that current practice in vehicles is to have relatively soft springs and fit stiffer anti-roll bars than was the norm some years ago. If vehicles achieve a large proportion of their roll stiffness from anti-roll bars, the subjective phenomenon of 'roll rock' (also known as 'lateral head toss') becomes problematic. A rule of thumb is that such phenomena begin to emerge when the

anti-roll bars form more than about one third of the overall roll stiffness – in other words if K_{Tr} is greater than $0.5\,K_{Ts}$.

6.8 Aerodynamic effects

Some treatment of aerodynamics is generally given in existing text books (Milliken and Milliken, 1995; Gillespie, 1992) dealing with vehicle dynamics. Other textbooks are dedicated to the subject (Hucho and Ahmed, 1998). The flow of air over the body of a vehicle produces forces and moments acting on the body resulting from the pressure distribution (form) and friction between the air and surface of the body. The forces and moments are considered using a body centred reference frame where longitudinal forces (drag), lateral forces, and vertical forces (lift or down thrust) will arise. The aerodynamic moments will be associated with roll, pitch and yaw rotations about the corresponding axes.

Current practice is generally to ignore aerodynamic forces for the simulation of most proving ground manoeuvres but for some applications and classes of vehicle this is clearly not representative of the vehicle dynamics in the real world, for example winged vehicles. It is often said that for some vehicles of this type the down thrust is so great that this could overcome the weight of a vehicle, allowing it, for example, to drive upside-down through a tunnel, although this has never been demonstrated.

The lack of speed limits on certain autobahns in Germany also means that a vehicle manufacturer selling a high performance vehicle to that market will need to test the vehicle at speeds well over twice the legal UK limit. The possibility of aerodynamic forces at these high speeds destabilizing the vehicle needs to be investigated and where physical testing is to be done, equivalent computer simulation is also desirable. Other effects such as side gusting are also tested for and have been simulated by vehicle dynamicists in the past.

An approach that has been commonly used is to apply forces and moments to the vehicle body using measured results, look-up tables, from wind tunnel testing. As the vehicle speed and the attitude of the body change during the simulation the forces and moments are interpolated from the measured data and applied to the vehicle body. A difficulty with such an approach is that the measured results are for steady state in each condition and that transient effects are not included in the simulation. Consideration has been given to the use of a computational fluid dynamics (CFD) program to calculate aerodynamic forces and moments in parallel with (co-simulation) an MBS program solving the vehicle equations of motion. The problem at the current time with this approach is the mismatch in the computation time for both methods. MBS models of a complete vehicle can simulate vehicle handling manoeuvres in seconds, or even real time, whereas complex CFD models can involve simulation times running into days. Current CFD methods also have difficulty with aerodynamic transient effects (e.g. vortex shedding) although an emerging group of 'multi-physics' codes look set to address these problems. Thus there is no realistic prospect of the practical use of transient aerodynamics effects being modelled in the near future. However, genuine transient aerodynamic effects, such as those involved in so-called 'aeroelastic

flutter' – an unsteady aerodynamic flow working in sympathy with a structural resonance – are extremely rare in ground vehicles.

In order to introduce readers to the fundamentals consider a starting point where it is intended only to formulate an aerodynamic drag force acting on the vehicle body.

The drag force F_D can be considered to act at a frontal centre of pressure for the vehicle centre of pressure (*CP*) and have the following formulation:

$$F_D = \frac{1}{2}\frac{\rho V^2 C_D A}{GC} \tag{6.12}$$

where

C_D = the aerodynamic drag coefficient
ρ = the density of air
A = the frontal area of the vehicle (projected onto a yz plane)
V = the velocity of the vehicle in the direction of travel
GC = a gravitational constant

The gravitational constant is included in equation (6.12) to remind readers that this is a dynamic force. If the model units are SI then *GC* is equal to 1. If as commonly used the model units for length are mm then *GC* is equal to 1000. When formulating the aerodynamic drag force it should be considered that the force acts at the *CP* and that this point generally moves as the vehicle changes attitude. Similarly the drag coefficient C_D and projected frontal area *A* also change as the body moves. For the position shown in Figure 6.25 it is clear that for anything other than straight-line motion it is going to be necessary to model the forces as components in the body centred axis system. If we consider the vehicle moving only in the *xy* plane then this is going to require at least the formulation of a longitudinal force *Fx*, a lateral force *Fy* and a yawing moment *Mz* all resolved from the centre of pressure to the body centred axis system, usually located at the mass centre. Wind tunnel testing or computational fluid dynamic analysis is able to yield coefficients for all six possible forces and moments acting on the body, referred back to the mass centre. Note that for passenger vehicles it is typical that the aerodynamic yaw moment is as shown in the figure, i.e. is such to make the vehicle turn away from the wind. For other vehicles this may not be true and individual research on the vehicle in question is needed.

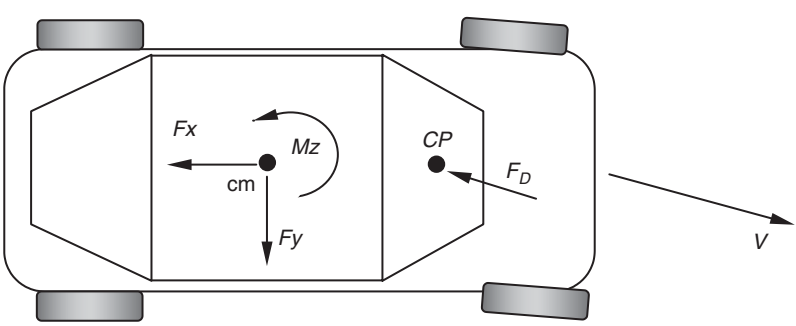

Fig. 6.25 Application of aerodynamic drag force

6.9 Modelling of vehicle braking

In Chapter 5 the force and moment generating characteristics of the tyre were discussed and it was shown how the braking force generated at the tyre contact patch depends on the slip ratio as the wheel is braked from a free rolling wheel with a slip ratio of zero to a fully locked wheel where the slip ratio is unity. In this section we are not so much concerned with the tyre, given that we would be using a tyre model interfaced with our full vehicle model to represent this behaviour. Rather we now address the modelling of the mechanisms used to apply a braking torque acting about the spin axis of the road wheel that produces the change in slip ratio and subsequent braking force.

Clearly as the vehicle brakes, as shown in Figure 6.26, there is weight transfer from the rear to the front of the vehicle. Given what we know about the tyre behaviour the change in the vertical loads acting through the tyres will influence the braking forces generated. As such the braking model may need to account for real effects such as proportioning the braking pressures to the front and rear wheels or the implementation of anti-lock braking systems (ABS). Before any consideration of this we need to address the mechanism to model a braking torque acting on a single road wheel.

If we consider a basic arrangement the mechanical formulation of a braking torque, based on a known brake pressure, acting on the piston can be derived from Figure 6.27.

The braking torque B_T is given by

$$B_T = n\mu pAR_d \tag{6.13}$$

where

n = the number of friction surfaces (pads)
μ = the coefficient of friction between the pads and the disc
p = the brake pressure
A = the brake piston area
R_d = the radius to the centre of the pad

Note that depending on the sophistication of the model the coefficient of friction μ may be constant or defined as a run-time variable as a function of brake rotor temperature. Obtaining such data is usually relatively easy, but the calculation of rotor temperature can be a little more involved.

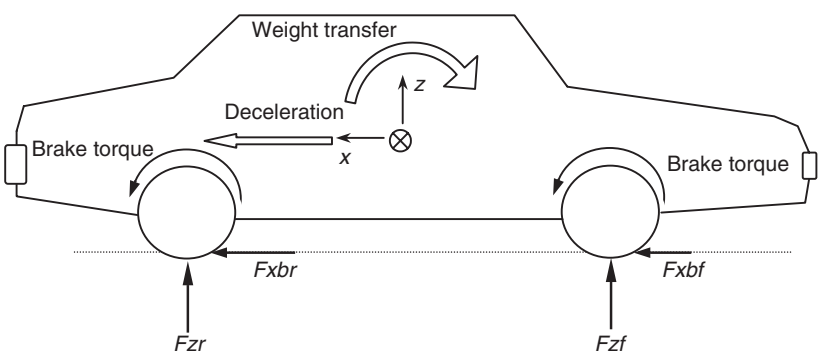

Fig. 6.26 Braking of a full vehicle

Figure 6.28 shows typical specific heat capacity versus temperature characteristics for different brake rotor materials. Brake rotor temperature, T, can be calculated using the expression:

$$T = T_0 + \frac{B_T \omega t - hA_c(T - T_{\text{env}})}{mc} \tag{6.14}$$

where

T_0 = initial brake rotor temperature (K)
ω = brake rotor spin velocity (rads second^{-1})
t = time (seconds)
h = brake rotor convection coefficient (Wm^{-2}K^{-1})
A_c = convective area of brake disc (m^2)
T_{env} = environmental temperature (K)
m = mass of brake rotor (kg)
c = specific heat capacity of brake rotor (J kg^{-1} K^{-1})

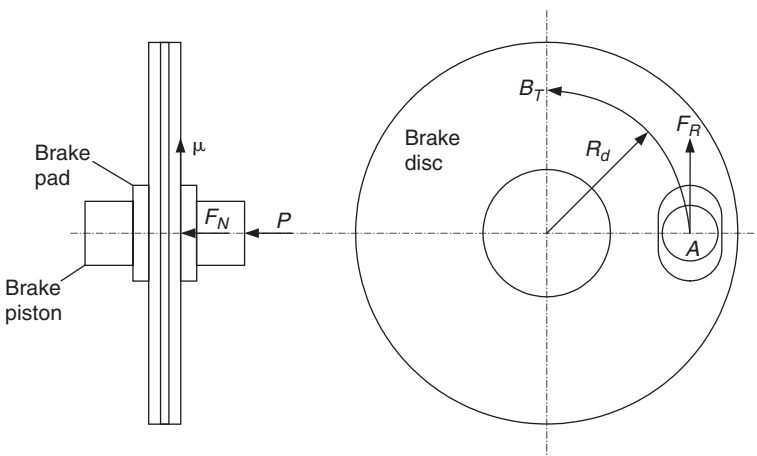

Fig. 6.27 Braking mechanism

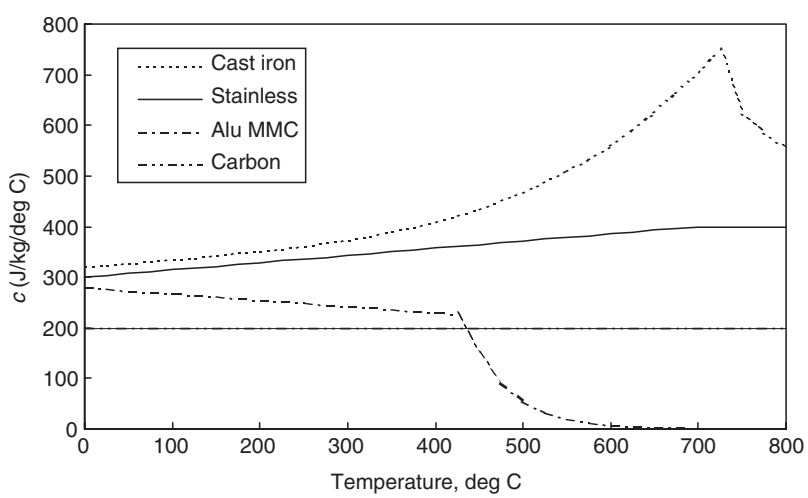

Fig. 6.28 Specific heat capacity, c, versus temperature, T (Farr, 1999)

For the most common brake rotor material, cast iron, the specific heat versus temperature characteristic can be approximated in the working range (0–730°C) by the expression:

$$c = 320 + 0.15T + 1.164 \times 10^{-9}T^4 \tag{6.15}$$

Note that in the above expression, temperature T is in centigrade (Celsius) and not Kelvin. The brake torque and temperature models may be used easily within a multibody system model using a combination of design variables (declared in MSC.ADAMS using the 'variable create' command) and run-time variables (declared in MSC.ADAMS using 'data_element create' variable) as shown in Table 6.1 where we are using for the first time here an input format that corresponds to a command language used in MSC.ADAMS. Note the need for an explicit iteration since the temperature depends on the heat capacity and the heat capacity depends on the temperature. When modelling such behaviour in a spreadsheet, it is sufficient to refer to the temperature of the preceding time step. Although this is possible within many multibody system packages, it can be awkward to implement and can also lead to models with some degree of numerical delicacy.

Note also that it is common practice within brake manufacturers to separate the brake energizing event from the brake cooling event for initial design calculations, leading to a systematic overestimation of the temperature during fade/recovery testing. This conservative approach is unsurprising given the consequences of brake system underdesign. The example given is a relatively simple one, with convection characteristics that are independent of vehicle velocity and no variation of brake friction with brake temperature. Although in practice these simplifications render the results slightly inaccurate, they are useful when used for comparative purposes – for example, if the brake temperature model is used with an ESP algorithm it can rank control strategies in terms of the energy added to individual brake rotors. Similar modelling is of course possible for other frictional systems within

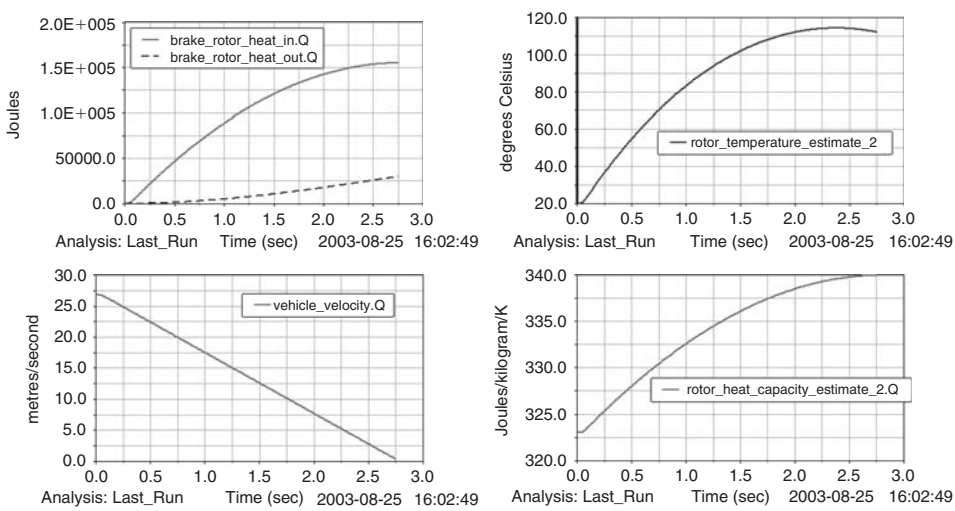

Fig. 6.29 Output from the brake temperature model shown in Table 6.1 during a 60 mph–0 stop

Table 6.1 A brake rotor temperature model based on brake torque

```
!--------------------- Function definitions --------------------!
!
part create equation differential_equation &
   differential_equation_name = .model_1.brake_heating_integral &
   adams_id = 2 &
   comments = "Brake Heat Input Integral" &
   initial_condition = 0.0 &
   function = "VARVAL(Brake_Torque)*VARVAL(vehicle_velocity)/0.3" &
   implicit = off &
   static_hold = off


data_element create variable &
   adams_id = 102 &
   variable_name = brake_rotor_heat_in &
   function = "DIF(2)"
!
data_element create variable &
   variable_name = "rotor_temperature_kelvin_estimate_1" &
   function = "T_env + VARVAL(brake_rotor_heat_in)/(rotor_mass*350)"
!
data_element create variable &
   variable_name = "rotor_temperature_estimate_1" &
   function = "VARVAL(rotor_temperature_kelvin_estimate_1)-273"
!
data_element create variable &
   variable_name = "rotor_heat_capacity_estimate_2" &
   function = "320 + 0.15*VARVAL(rotor_temperature_estimate_1)", &
              " + 1.164E-9*VARVAL(rotor_temperature_estimate_1)**4"
!
part create equation differential_equation &
   differential_equation_name = .model_1.brake_cooling_integral &
   adams_id = 3 &
   comments = "Brake Heat Rejection Integral" &
   initial_condition = 0.0 &
   function = "hAc*(VARVAL(rotor_temperature_kelvin_estimate_1)-T_env)" &
   implicit = off &
   static_hold = off


data_element create variable &
   adams_id = 103 &
   variable_name = brake_rotor_heat_out &
   function = "DIF(3)"
!
data_element create variable &
   variable_name = "rotor_temperature_kelvin_estimate_2" &
   function = "T_env + ", &
              "(VARVAL(brake_rotor_heat_in) - VARVAL(brake_rotor_heat_out))/", &
              "(rotor_mass*VARVAL(rotor_heat_capacity_estimate_2) + 0.001)"
!
data_element create variable &
   variable_name = "rotor_temperature_estimate_2" &
   function = "VARVAL(rotor_temperature_kelvin_estimate_2)-273"
```

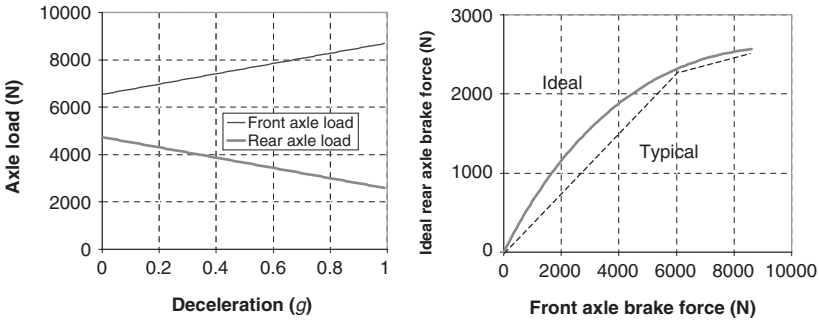

Fig. 6.30 Force distribution for ideal and typical braking events

the vehicle, such as drive or transmission clutches. Typical values of the convection constant hAc are around $150\,\mathrm{W\,K^{-1}}$ for a front disc brake installation, around $80\,\mathrm{W\,K^{-1}}$ for a rear brake installation and as low as $20\,\mathrm{W\,K^{-1}}$ for a rear drum brake.

A further key factor in modelling brake performance is the distribution of brake torques around the vehicle. While decelerating, the vertical loads on the axles change as described in section 4.8.1 due to the fact that the mass centre of the vehicle is above the ground.

It may be presumed that for ideal braking, the longitudinal forces should be distributed according to the vertical forces. Using the above expressions, the graphs in Figure 6.30 can be calculated for vertical axle load versus deceleration. Knowing the total force necessary to decelerate the vehicle it is possible to calculate the horizontal forces for 'ideal' (i.e. matched to vertical load distribution) deceleration. Plotting rear force against front force leads to the characteristic curve shown in Figure 6.30. However, in general it is not possible to arrange for such a distribution of force and so the typical installed force distribution is something like that shown by the dashed line in the figure. Note that the ideal distribution of braking force varies with loading condition and so many vehicles have a brake force distribution that varies with vehicle loading condition. For more detailed information on brake system performance and design, Limpert (1999) gives a detailed breakdown of performance characteristics and behaviour, all of which may be incorporated within a multibody system model of the vehicle using an approach similar to that shown in Table 6.1 if desired.

Described in some detail in Limpert's work is the function of a vehicle ABS system. The key ingredient of such a system is the ability to control brake pressure in one of three modes, often described as 'hold, dump and pump'. Hold is fairly self-explanatory, the wheel cylinder pressure is maintained regardless of further demanded increases in pressure from the driver's pedal. 'Dump' is a controlled reduction in pressure, usually at a predetermined rate and 'pump' is a controlled increase in pressure, again usually at a predetermined rate.

The main variable is the brake pressure p. In the work by Ozdalyan (1998) a slip control model was initially developed as a precursor to the implementation of an ABS model. This is illustrated in Figure 6.31 where it can be seen that on initial application of the brakes the brake force rises approximately

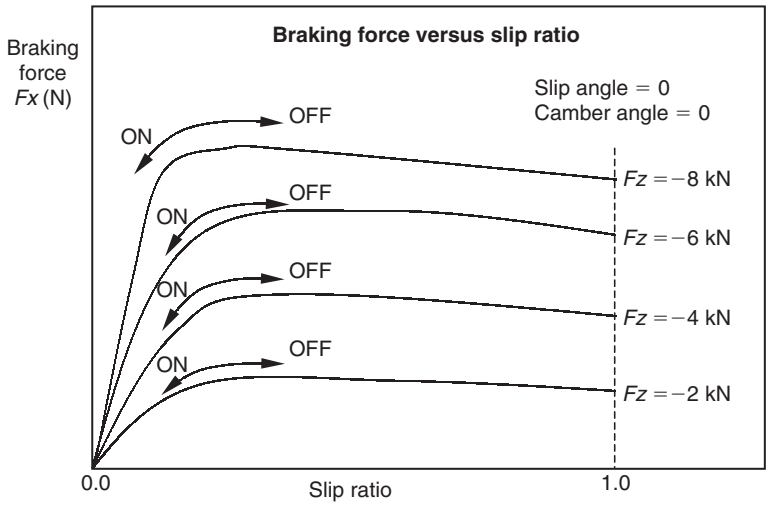

Fig. 6.31 Principle of a brake slip control model

linearly with slip ratio depending on the wheel load. If the braking is severe the slip ratio increases past the point where the optimum brake force is generated. To prevent the slip ratio increasing further to the point where the wheel is locked an ABS system will then cycle the brake pressure on and off maintaining peak braking performance and a rolling wheel to assist manoeuvres during the braking event.

In this model the brake pressure is found by integrating the rate of change of brake pressure, this having set values for any initial brake application or subsequent application during the ABS cycle phase. Implementation of these changing dump, pump and hold states requires care to ensure no discontinuities in the brake pressure formulation.

The modelling in MBS of more realistic ABS algorithms (van der Jagt et al., 1989) is more challenging as the forward velocity and hence slip ratio is not directly available for implementation in the model. The implementation of such a model allows the angular velocity of the wheel to be factored with the rolling radius to produce an output commonly referred to as wheel speed by practitioners in this area. A plot of wheel speed is compared with vehicle speed in Figure 6.32 where the typical oscillatory nature of the predicted wheel speed reflects the cycling of the brake pressure during the activation of the ABS model in this vehicle simulation.

6.10 Modelling traction

For some simulations it is necessary to maintain the vehicle at a constant velocity. Without some form of driving torque the vehicle will ‘drift’ through the manoeuvre using the momentum available from the velocity defined with the initial conditions for the analysis. Ignoring rolling resistance and aerodynamic drag will reduce losses but the vehicle will still lose momentum during the manoeuvre due to the ‘drag’ components of tyre cornering forces generated during the manoeuvre. An example is provided

Fig. 6.32 Plot of vehicle speed and wheel speed during ABS braking simulation

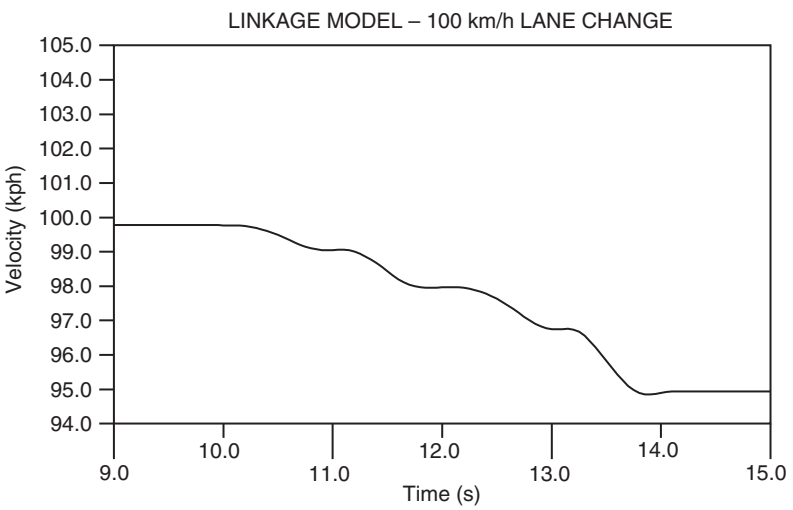

Fig. 6.33 Loss in velocity as vehicle 'drifts' through the lane change manoeuvre

in Figure 6.33 where for a vehicle lane change manoeuvre it can be seen that during the 5 seconds taken to complete the manoeuvre the vehicle loses about 5 km/h in the absence of any tractive forces at the tyres.

The emphasis with programs such as ADAMS/Car and ADAMS/Chassis is to include a driveline model as part of the full vehicle as a means to impart torques to the road wheels and hence generate tractive driving forces at the tyres. Space does not permit a detailed consideration of driveline modelling here but as a start a simple method of imparting torque to the driven wheels is shown in Figure 6.34.

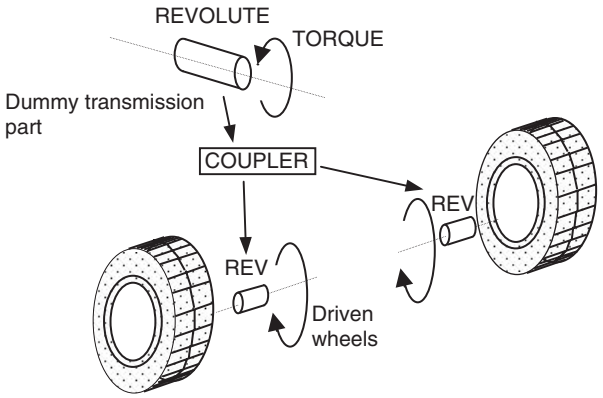

Fig. 6.34 Simple drive torque model

The rotation of the front wheels is coupled to the rotation of the dummy transmission part shown in Figure 6.34. The coupler introduces the following constraint equation:

$$s_1 \cdot r_1 + s_2 \cdot r_2 + s_3 \cdot r_3 = 0 \tag{6.16}$$

where s_1, s_2 and s_3 are the scale factors for the three revolute joints and r_1, r_2 and r_3 are the rotations. In this example suffix 1 is for the driven joint and suffixes 2 and 3 are for the front wheel joints. The scale factors used are $s_1 = 1$, $s_2 = 0.5$ and $s_3 = 0.5$ on the basis that 50% of the torque from the driven joint is distributed to each of the wheel joints. This gives a constraint equation linking the rotation of the three joints:

$$r_1 = 0.5r_2 + 0.5r_3 \tag{6.17}$$

Note that this equation is not determinant. For a given input rotation r_1, there are two unknowns r_2 and r_3 but only the single equation. In order to solve r_2 and r_3 this equation must be solved simultaneously with all the other equations representing the motion of the vehicle. This is important particularly during cornering where the inner and outer wheels must be able to rotate at different speeds.

6.11 Other driveline components

The control of vehicle speed is significantly easier than the control of vehicle path inside a vehicle dynamics model. In the real vehicle, speed is influenced by the engine torque, brakes and aerodynamic drag. As discussed earlier these are relatively simple devices to represent in a multibody systems model, with the exception of turbochargers and torque converters. Even these latter components can be represented using differential equations of the form:

$$T_{\mathrm{BOOST}} = T_2 \cdot \hat{T}_{\mathrm{BOOST}} \tag{6.18}$$

$$\frac{\mathrm{d}}{\mathrm{d}t}(T_2) = \frac{T_1}{k_2} \cdot (t_{\mathrm{boost}} - T_2) \tag{6.19}$$

Table 6.2 Example MSC.ADAMS command statements for an empricial mean-state turbocharger

```
! -- First First Order Differential Equation --
part create equation differential_equation &
   differential_equation_name = turbo_lag_equation_1 &
   adams_id = 12 &
   comments = "Lag Equation 1 - Explicit" &
   initial_condition = 0.0 &
   function = "varval(K1_now) * ( varval(boost_throttle)*100-DIF(12) )" &
   implicit = off &
data_element create variable &
   variable_name=K2 &
   function="STEP(varval(throttle_derivative),", &
            "-10, 100.0,", &
            " -1, (DIF(12))/varval(K2_divisor_now)", &
            "   )"

! -- Second First Order Differential Equation --
part create equation differential_equation &
   differential_equation_name = turbo_lag_equation_2 &
   adams_id = 13 &
   comments = "Lag Equation 2 - Explicit" &
   function = "varval(K2) * ( varval(boost_throttle)*100-DIF(13) )" &
   implicit = off &
data_element create variable &
   variable_name = boost_torque_scaling &
   function = "DIF(13)/100"

! -- Sum both normally aspirated and turbocharged (delayed) component
data_element create variable &
   variable_name = prop_torque &
   function = "(", &
              " VARVAL(na_engine_torque)*VARVAL(throttle)*1000", &

" +VARVAL(boosted_engine_torque)*VARVAL(boost_torque_scaling)*1000", &
        ")"
```

$$\frac{\mathrm{d}}{\mathrm{d}t}(T_1) = k_1 \cdot (t_{\text{boost}} - T_1) \tag{6.20}$$

where $\hat{T}_{\text{BOOST}}$ is the maximum possible torque available, t_{boost} is the throttle setting to be applied to the boost torque (which may be different to the throttle setting applied to the normally aspirated torque to model the rapid collapse of boost off-throttle) and $k_{1,2}$ are mapped, state dependent values to calibrate the behaviour of the engine (i.e. large delays at low engine speed, reducing delays with rising engine speed). An example of the statements required to model the resulting torque is shown in Table 6.2.

In this example the variable throttle runs from $-$ 0.3 to 1.0 to simulate overrun torque. The variable boost_throttle is a clipped version from 0 to 1.0 since no turbocharger boost is available on overrun. Throttle_derivative is the first time derivative of throttle. All the other variables (varvals) are retrieved from the relevant curves (splines) plotted in Figure 6.35.

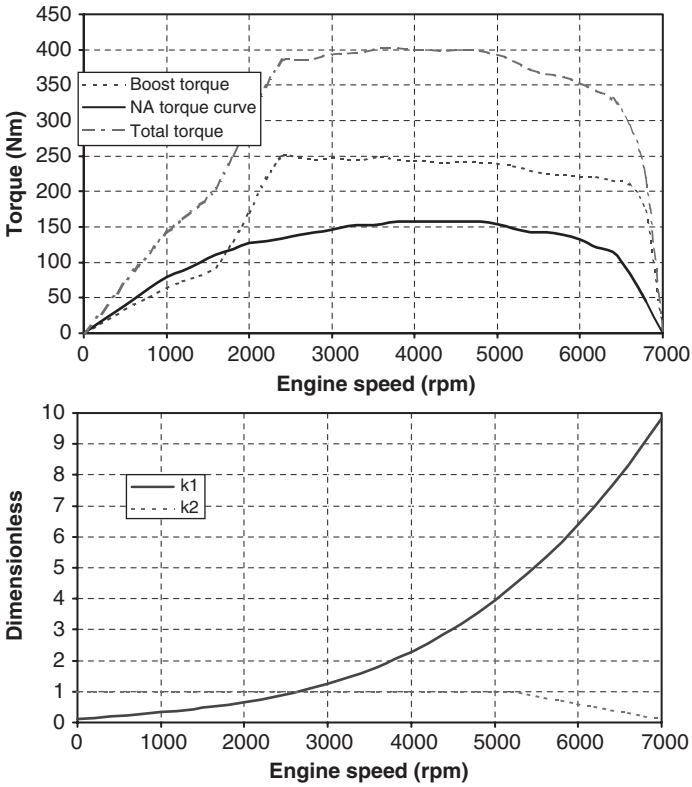

Fig. 6.35 Empricial mean-state turbocharger model

The delays inherent in a torque converter are amenable to such modelling techniques using typical torque converter characteristic data in a similar empirical manner.

Once the physical elements of the system are modelled, the task of modelling the driver behaviour is largely similar to that for path following described later. In order to represent, for example, the effect of a driver using the throttle to maintain a steady velocity through a manoeuvre a controller can be developed to generate the torque shown in Figure 6.34.

A simple but workable solution is to model the driving torque T, with the following formulation:

$$T = K * (Vs - Va) * \text{STEP (Time, 0, 0, 1, 1)} \tag{6.21}$$

where

K = a constant which is tuned to stabilize the torque
Vs = the desired velocity for the simulation
Va = the forward velocity of the vehicle, which can be obtained using a system variable

The purpose of the STEP FUNCTION is to define a change of state in the expression that is continuous.

The step function can be used to factor a force function by ramping it on over a set time period. In this case the driving torque is being switched on between time = 0 and time = 1 second. This is important because it is necessary to perform an initial static analysis of the vehicle at time = 0 when $Va = 0$ and the torque must not act.

As can be seen a 'reference' (desired) state is needed, an error term is defined by the difference between the current state and the reference state and finally, responses to that in terms of throttle or brake application to adjust the speed back towards the reference value. There are two possible approaches; the simplest provides a speed 'map' for the track, similar to the curvature map description of it. More elaborately, it is possible to examine the path curvature map locally and decide (through a knowledge of the ultimate capabilities of the vehicle, perhaps) whether or not the current speed is excessive, appropriate or insufficient for the local curvature and use brakes or engine appropriately. For the development of vehicles, open loop throttle or brake inputs may be preferable and are sometimes mandated in defined test manoeuvres, rendering the whole issue of speed control moot.

In many ways the skill of the competition driver lies entirely in this ability to judge speed and adjust it appropriately. It is also a key skill to cultivate for limit handling development and arguably for road driving too, so as not to arrive at hazards too rapidly to maintain control of the vehicle. For this functionality, some form of preview is essential. It is both plausible and reasonable to run a 'here and now at the front axle' model for the path follower and a 'previewing' speed controller within the same model, described in subsequent sections.

6.12 The steering system

6.12.1 Modelling the steering mechanism

There are a number of steering system configurations available for cars and trucks based on linkages and steering gearboxes. The treatment in the following sections is limited to a traditional rack and pinion system. Space does not permit discussion of the modelling of power steering or steer-by-wire here.

For the simple full vehicle models discussed earlier, such as that modelled with lumped mass suspensions, there are problems when trying to incorporate the steering system. Consider first the arrangement of the steering system on the actual vehicle and the way this can be modelled on the detailed linkage model as shown in Figure 6.36. In this case only the suspension on the right-hand side is shown for clarity.

The steering column is represented as a part connected to the vehicle body by a revolute joint with its axis aligned along the line of the column. The steering inputs required to manoeuvre the vehicle are applied as motion or torque inputs at this joint. The steering rack part is connected to the vehicle body by a translational joint and connected to the tie rod by a universal

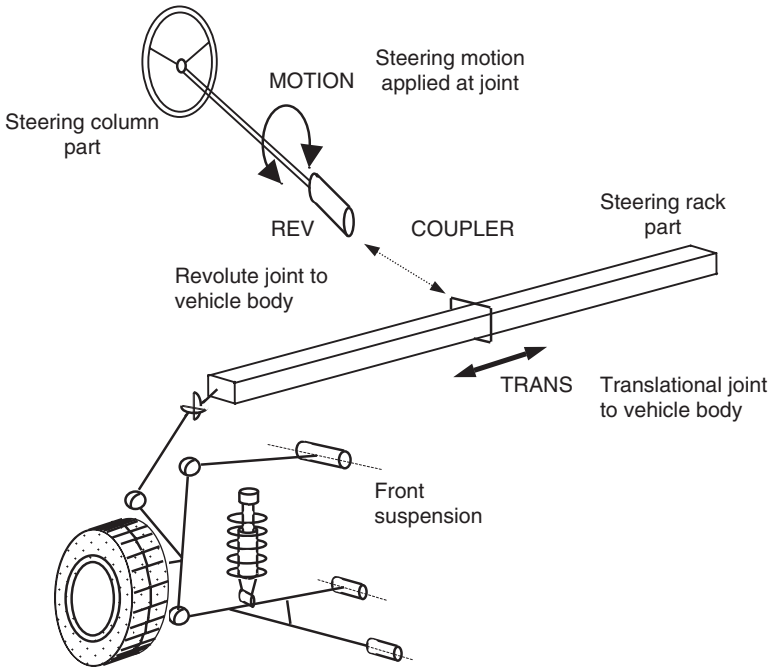

Fig. 6.36 Modelling the steering system. (This material has been reproduced from the Proceedings of the Institution of Mechanical Engineers, K2 Vol. 213 'The modelling and simulation of vehicle handling. Part 2: vehicle modelling', M.V. Blundell, page 129, by permission of the Council of the Institution of Mechanical Engineers)

joint. The translation of the rack is related to the rotation of the steering column by a coupler statement that defines the ratio. An example of a statement that would define the ratio is

```
COUPLER/510502,JOINTS = 501,502,TYPE = T:R
,SCALES = 8.45D,1.0
```

In this case joint 501 is the translational joint and 502 is the revolute joint. The coupler statement ensures that for every 8.45 degrees of column rotation there will be 1 mm of steering rack travel.

Attempts to incorporate the steering system into the simple models using lumped masses, swing arms and roll stiffness will be met with a problem when connecting the steering rack to the actual suspension part. This is best explained by considering the situation shown in Figure 6.37.

The geometry of the tie rod, essentially the locations of the two ends, is designed with the suspension linkage layout and will work if implemented in an 'as-is' model of the vehicle including all the suspension linkages. Physically connecting the tie rod to the simple suspensions does not work. During an initial static analysis of the full vehicle, to settle at kerb height, the rack moves down with the vehicle body relative to the suspension system.

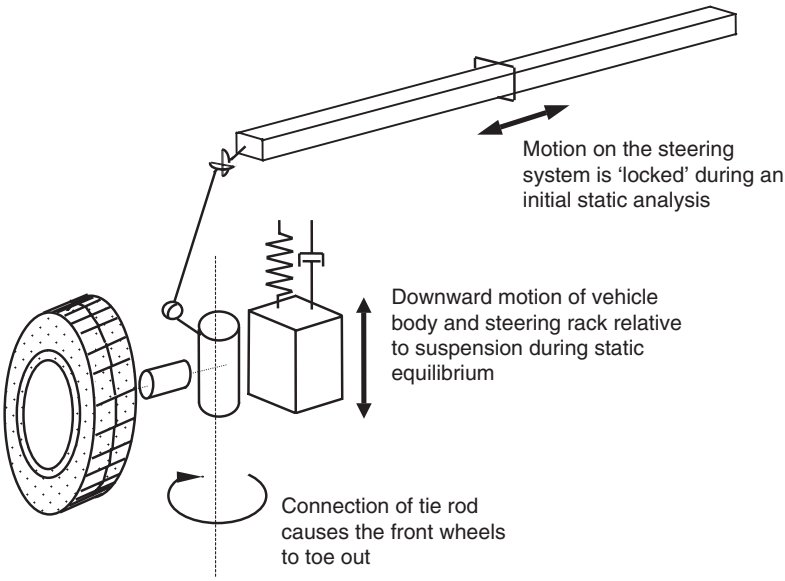

Fig. 6.37 Toe change in front wheels at static equilibrium for simple models. (This material has been reproduced from the Proceedings of the Institution of Mechanical Engineers, K2 Vol. 213 'The modelling and simulation of vehicle handling. Part 2: vehicle modelling', M.V. Blundell, page 129, by permission of the Council of the Institution of Mechanical Engineers)

This has a pulling effect, or pushing according to the rack position, on the tie rod that causes the front wheels to steer during the initial static analysis. The solution to this is to establish the relationship between the steering column rotation and the steer change in the front wheels and to model this as a direct ratio using two coupler statements to link the rotation between the steering column and each of the front wheel joints as shown in Figure 6.38.

6.12.2 Steering ratio

In order to implement the ratios used in the couplers shown in Figure 6.38 linking the rotation of the steering column with the steer change at the road wheels it is necessary to know the steering ratio. At the start of a vehicle dynamics study the steering ratio can be a model design parameter. In the examples here a ratio of 20 degrees of handwheel rotation to 1 degree of road wheel steer is used. On some vehicles this may be lower and on trucks or commercial vehicles it may be higher. To treat steering ratio as linear is a simplification of the situation on a modern vehicle. For example, the steering ratio may vary between a higher value on centre to a lower value towards the limits of rack travel or vice versa. This would promote a feeling of stability for smaller handwheel movements at higher motorway speeds and assist lower speed car park manoeuvres.

Using the multibody systems approach the steering ratio can be investigated through a separate study carried out using the front suspension system connected to the ground part instead of the vehicle body. The

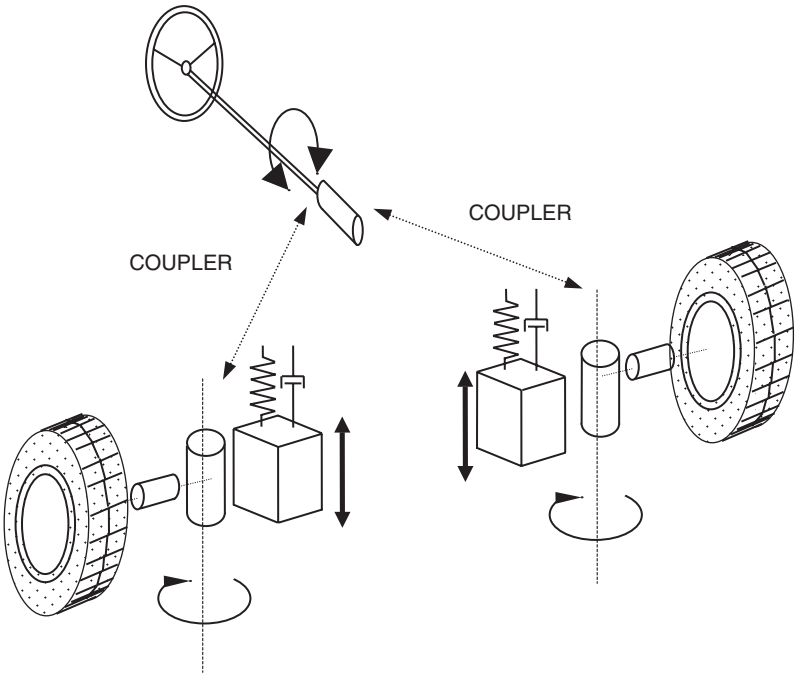

Fig. 6.38 Coupled steering system model. (This material has been reproduced from the Proceedings of the Institution of Mechanical Engineers, K2 Vol. 213 'The modelling and simulation of vehicle handling. Part 2: vehicle modelling', M.V. Blundell, page 130, by permission of the Council of the Institution of Mechanical Engineers)

modelling of these two subsystems, with only the suspension on the right side shown, is illustrated in Figure 6.39.

The approach of using a direct ratio to couple the rotation between the steering column and the steer angle of the road wheels is common practice in simpler models but may have other limitations in addition to the treatment of the ratio as linear:

(i) In the real vehicle and the linkage model the ratio between the column rotation and the steer angle at the road wheels would vary as the vehicle rolls and the road wheels move in bump and rebound.

(ii) For either wheel the ratio of toe out or toe in as a ratio of left or right handwheel rotation would not be exactly symmetric.

Modelling the suspension with linkages will capture these effects. Although this may influence the modelling of low speed turning they have little effect for handling manoeuvres with comparatively small steer motions.

With simpler vehicle models, not including suspension linkages, the ratio would need to be functionally dependent on the vertical movement of the suspension and direction of handwheel rotation if the behaviour is to be modelled. It should also be noted that compliance in the steering rack or rotational compliance in the steering column could be incorporated if the analysis dictates this.

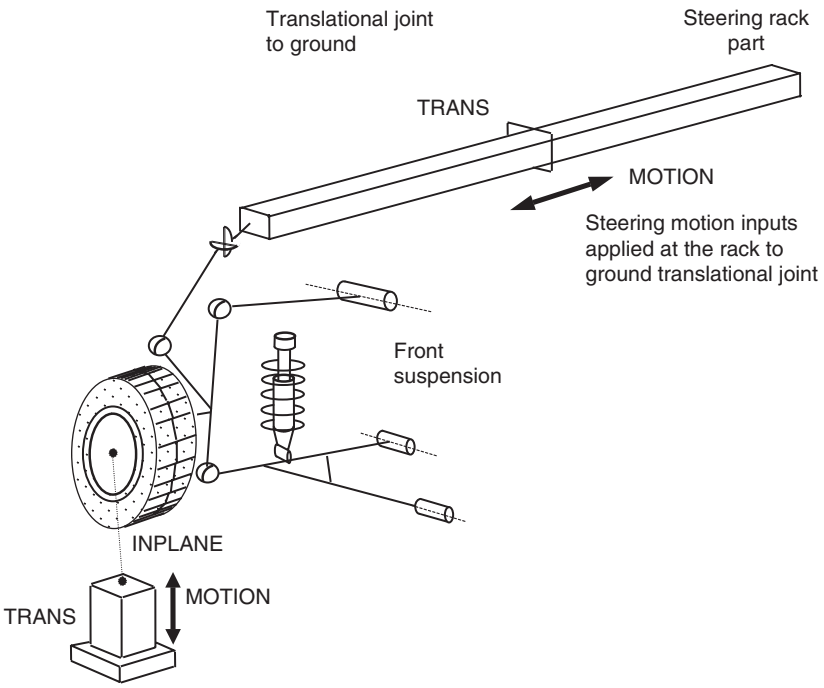

Fig. 6.39 Front suspension steering ratio test model

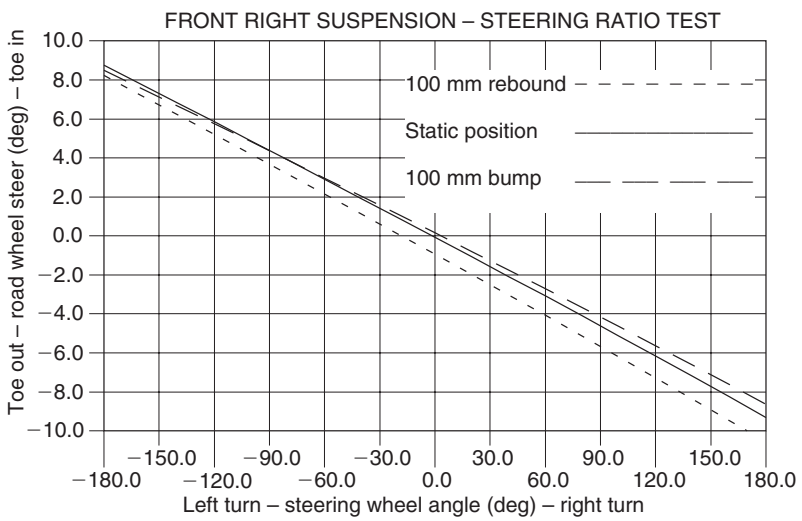

Fig. 6.40 Results of steering ratio test for MSC.ADAMS front right suspension model

In the following example the geometric ratio between the rotation of the steering column and the travel of the rack is already known, so it is possible to apply a motion input at the rack to ground joint that is equivalent to handwheel rotations either side of the straight ahead position. The jack part shown in Figure 6.39 can be used to set the suspension height during

a steering test simulation. Typical output is shown in Figure 6.40 where the steering wheel angle is plotted on the *x*-axis and the road wheel angle is plotted on the *y*-axis. The three lines plotted represent the steering ratio test for the suspension in the static (initial model set up here), bump and rebound positions.

Having decided on the suspension modelling strategy and how to manage the relationship between the handwheel rotation and steer change at the road wheels the steering inputs from the driver and the manoeuvre to be performed need to be considered.

6.12.3 Steering inputs for vehicle handling manoeuvres

The modelling of steering inputs suggests for the first time some representation of the driver as part of the full vehicle system model. Any system can be considered to consist of three elements – the 'plant' (the item to be controlled), the input to the plant and the output from the plant (Figure 6.41). Inputs to the system (i.e. handwheel inputs) are referred to as 'open loop' or 'closed loop'. An open loop steering input requires a time dependent rotation to be applied to the part representing a steering column or handwheel in the simulation model. In the absence of these bodies an equivalent translational input can be applied to the joint connecting a rack part to the vehicle body or chassis, assuming a suspension linkage modelling approach has been used. Examples will be given here where the time dependent motion is based on a predetermined function or equation to alter the steering inputs or a series of measured inputs from a vehicle on the proving ground.

Any system can be considered to consist of three elements – the 'plant' (the item to be controlled), the input to the plant and the output from the plant (Figure 6.41).

When a closed-loop controller is added to the system, its goal is to allow the input to the plant to be adjusted so as to produce the desired output. The desired output is referred to as the 'reference' state; a difference between the actual output and the reference is referred to as an 'error' state. The goal of the control system is to drive the error to zero.

We can consider an example of a closed loop steering input that requires a torque to be applied to the handwheel or steering column such that the vehicle will follow a predetermined path during the simulation. A mechanism must be modelled to measure the deviation of the vehicle from the path and process this in a manner that feeds back to the applied steering torque.

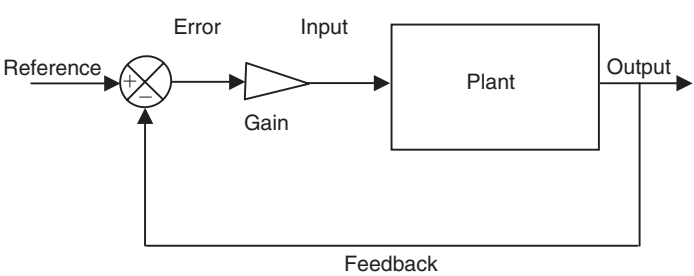

Fig. 6.41 An open-loop system, in black, is a subset of a closed-loop system, in grey

As the simulation progresses the torque is constantly modi-fied based on the observed path of the vehicle and the desired trajectory. Such an input is referred to as closed loop since the response is observed and fed back to the input, thus closing the control loop.

To return to the open-loop case, we can consider an example of an open loop manoeuvre for a steering input where we want to ramp a steering input of 90 degrees between 1 and 1.5 seconds of simulation time. Using an MSC.ADAMS solver statement the function applied to the steering motion would be:

FUNCTION = STEP(TIME, 1, 0, 1.5, 90D)

In a similar manner if we wanted to apply a sinusoidal steering input with an amplitude of 30 degrees and a frequency of 0.5 Hz we could use:

FUNCTION = 30D * SIN(TIME*180D)

For the lane change manoeuvre described earlier the measured steering wheel angles from a test vehicle can be extracted and input as a set of *XY* pairs, which can be interpolated using a cubic spline fit. A time history plot for the steering inputs is shown in Figure 6.42 for lane change manoeuvres at 70 and 100 km/h.

By way of example the MSC.ADAMS statements which apply the steering motion to the steering column to body revolute joint and the spline data are shown in Table 6.3 for a 100 km/h lane change. The *x* values are points in time and the *y* values are the steering inputs in degrees. In the absence of measured data it is possible to construct an open loop single or double lane change manoeuvre using a combination of nested arithmetic IF functions with embedded step functions with some planning and care over syntax. Note that for a fixed steering input a change in vehicle configuration will produce a change in response so that the vehicle fails to follow a path.

For a closed loop steering manoeuvre a torque is applied to the steering column, or a force to the steering rack if the column is not modelled, that will vary during the simulation so as to maintain the vehicle on a predefined

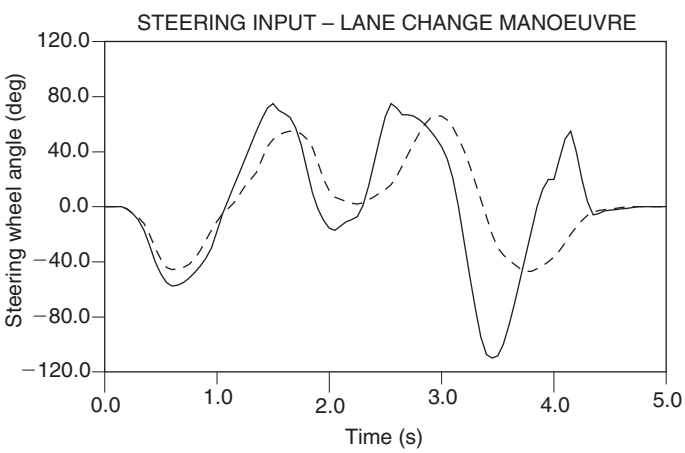

Fig. 6.42 Steering input for the lane change manoeuvre at 70 km/h (dashed line) and 100 km/h (solid line)

Table 6.3 MSC.ADAMS statements for lane change steering inputs

```
MOTION/502,JOINT=502,ROT
,FUNC=(PI/180)*CUBSPL(TIME,0,1000)

SPLINE/1000
,X=0,1,2,3,4,5,6,7,8,9
,9.1,9.2,9.3,9.4,9.5,9.6,9.7
,9.8,9.9,10,10.1,10.2,10.3,10.4,10.5,10.6,10.7,10.8,10.9,11
,11.1,11.2,11.25,11.3,11.4,11.5,11.6,11.7,11.8,11.9,12,12.1
,12.2,12.3,12.4,12.5,12.6,12.7,12.8,12.9,13,13.1,13.2,13.3
,13.4,13.5,13.6,13.7,13.75,13.8,13.9,14,14.1,14.2,14.3,14.4,14.5
,14.6,14.7,14.8,14.9,15
,Y = 0,0,0,0,0,0,0,0,0,0
,0,0,0,0,0,0,0
,0,0,-5,-17,-40,-55,-57,-52,-43,-30,-5,15,35,55,72,75,70,65,45,10
,-10,-17,-11,-7,15,50,75,67,66,60,50,35,0,-50,-95,-110,-100,-70,-35,0
,20,20,35,55,20,-6,-3,-2,-1,0,0,0,0,0,0
```

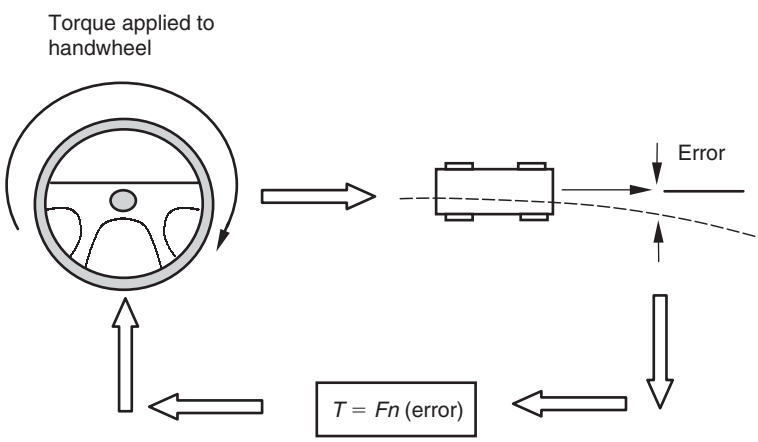

Fig. 6.43 Principle of a closed loop steering controller

path. This requires a steering controller to process feedback of the observed deviation from the path (error) and to modify the torque accordingly as illustrated in Figure 6.43.

6.13 Driver behaviour

It becomes inevitable with any form of vehicle dynamics modelling that the interaction of the operator with the vehicle is a source of both input and disturbance. In flight dynamics, the phenomenon of 'PIO' – pilot induced oscillation – is widely known. This occurs when inexperienced pilots, working purely visibly and suffering from some anxiety, find their inputs are somewhat excessive and cause the aircraft to, for example, pitch rhythmically instead of holding a constant altitude (Figure 6.44).

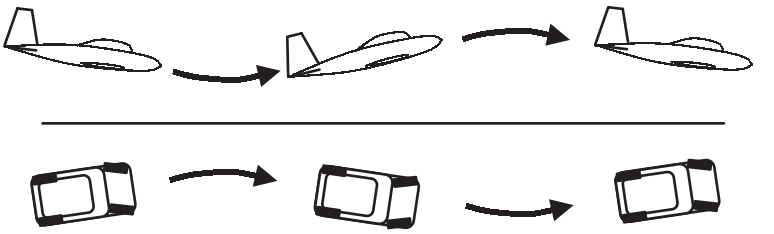

Fig. 6.44 Pilot Induced Oscillation (PIO) – not exclusively an aeronautical phenomenon

PIO is caused when the operator is unable to recognize the effects of small control inputs and therefore increases those inputs, before realizing they were excessive and reversing them through a similar process. It is analogous to the 'excess proportional control gain oscillation' discussed in classical control theory (Leva et al., 2002). For road vehicles, drivers most likely to induce PIO in steering tend to be inexperienced or anxious drivers travelling at a speed with which they are uncomfortable. This type of PIO is not to be confused with the typical experience of drivers of skidding vehicles when the initial skid is corrected but the vehicle subsequently 'fishtails' or simply departs in the opposite direction – this is a 'phasing at resonance' control error. The driver fails to apply a 'feed forward' (open loop, knowledge-based) correction in advance of the vehicle's response to compensate for the delay in vehicle response.

PIO also occurs in tractive (i.e. throttle) control inputs and is the reason even experienced drivers are incapable of travelling at a constant speed on highways; perception of changes in following distance is universally poor. If too little attention is spent on the driving task or if insufficient following distance is left, these PIOs become successively amplified by following drivers until the speed variation results in a 'shunt' accident. Radar-based cruise control systems will alleviate this risk but are no substitute for attentive driving while anything less than the whole vehicle fleet is fitted with it.

6.13.1 Steering controllers

There are a variety of controller models suitable for modelling driver behaviour in existence. Some, such as ADAMS/Driver™ developed as part of the MSC.ADAMS modelling package, are very complete – others, such as the two-loop feedback control model used by the authors, are simpler. The analyst must consider the needs of the simulation (and the financial constraints of the company) and choose the most appropriate level of modelling to achieve the task at hand. Driver models in general fall into two categories:

(1) Optimum control models. Optimum control models use some form of 'penalty function' – a measure used to assess the quality of control achieved. For example, for a vehicle steering model the appropriate variable might be lateral deviation from the intended path. Optimum control models use repeated simulations of the event and numerical optimization methods to 'tune' the parameters for a control system to minimize the value(s) of the penalty function(s) over the duration of the event of interest. For learned

events, such as circuit driving, these methods are excellent in producing a prediction of likely driver behaviour. However, some care must be exercised with their use. For road vehicles, drivers are generally unskilled and so the application of modelling techniques in which repeated solutions are used to discover the 'best' way of achieving a manoeuvre may not be appropriate when simulating a manoeuvre that the driver has only one attempt at completing, for example emergency evasive manoeuvres. For race vehicle simulation, some care must also be exercised lest extended calculations result in the proof that the driver can adapt to a remarkable variety of vehicle changes – without any real insight into which will improve performance in a competition environment.

(2) Moment-by-moment feedback models[1]. Such models are really a subset of the optimum control models described above – the optimum control method repeatedly uses feedback models in order to discern the best state of tune for the controller. When the feedback controllers are used alone, the analyst must set their tuning. Although the absence of 'automated' correlation makes them less appropriate for circuit racing, it also adds clarity in the sense that the parameters, once set, remain constant and so changes in the vehicle behaviour and/or driver inputs can be readily understood.

In general, the driver behaves as the most generic form of loop-closing controller. There are several attractive control technologies represented in the literature and some of their proponents believe they represent a 'one size fits all' solution for the task of applying control to any system. The competing technologies are outlined for comparison:

(i) Logic controller. A logic controller produces output that has only certain possible values. For example, if a driver model were implemented using logic, the logic might be 'if the vehicle is to the left of the intended path, steer right and vice versa'. With a logic controller, the amount of steer is fixed and so any control of the vehicle would be achieved as a series of jerks, oscillating about the intended path. While probably functional it would be unlikely to represent any normal sort of driver.

(ii) PID controller. As stated PID stands for 'Proportional, Integral and Derivative'. The error is used in three ways; used directly, a control effort is applied in proportion to (and opposition to) the error – this is the 'P', proportional, element of the control. The fact that the control effort is in opposition to the error is important, since otherwise the control effort would increase the error instead of reducing it. For this reason, such systems are

[1]Feedback models ought to be known as 'instantaneous feedback' models but the word instantaneous has become slightly muddled in recent times. It should be used unambiguously to mean 'existing for a moment in time' but has become sadly confused with 'instant', meaning immediate. Instant feedback would imply the inability to represent transport delays and the like in the controller model, which is incorrect. The use of moment-by-moment is therefore preferred although it introduces confusion with moment in the sense of torque.

often referred to as 'negative feedback' systems. The error can also be integrated and differentiated, with control forces applied proportional to the integral and the differential – these are the 'I' and the 'D' terms in the controller. One or more of the terms may not be used at all in any particular controller. An analogy for PID controllers can be found in vehicle suspensions. If the ride height is thought of as the desired output, then individual components of the suspension behave as parts of a control system. The springs produce a force proportional to the change in ride height and the dampers produce a force proportional to the derivative of ride height. Real dampers are often non-linear in performance, and there is nothing to stop non-linear gains being used for any of the control terms. The D term has the effect of introducing damping into the control system. An analogy for the I term is a little harder to come by. The best analogy is that of a self-levelling unit fitted to the suspension, which applies a restoring force related to the length of time the vehicle has been at the wrong ride height and how wrong the ride height is. (This is an imperfect analogy for many reasons but allows the notion to be understood at least.) In real systems, when the output is *nearly* the same as the reference state it is frequently the case that the control forces become too small to influence the system, either because of mechanical hysteresis or sensor resolution or some similar issue. One important measure of the quality of any control system is the accuracy with which it achieves its goals. Such an offset characterizes an inaccurate system; an integral term 'winds up' from a small error until powerful enough to restore the system to the reference state. Thus for classical control, integral terms are important for accuracy. However, since they take some time to act they can introduce delays into the system. In general PID controllers have the advantage that they produce 'continuous' output – that is to say all the derivatives are finite, the output has no steps – which is quite like the behaviour of real people.

(iii) Fuzzy logic. Fuzzy logic was first described in the 1960s but found favour in the 1980s as a fashionable 'new' technology. Notions of 'true' and 'false' govern 'logic' in computer algorithms. Simple control systems assess a set of conditions and make a decision based on whether or not such variables are true or false. Fuzzy logic simply defines 'degrees of truth' by using numbers between 0 and 1 such that the actions taken are some blend of actions that would be taken were something completely true and other actions that would be taken were something completely false. Fuzzy logic is most applicable to control systems where actions taken are dependent on circumstance and where a simple PID controller is unable to produce the correct output in every circumstance. For example, throttle demand in a rear-wheel drive vehicle model might be controlled with a PID controller to balance understeer; however, too much throttle would cause oversteer and some more sophisticated blend of steer and throttle input would be required to retain control under these circumstances.

(iv) Neural networks. Where the system of interest is highly non-linear and a lot of data exists that describes desired outputs of the system for many different combinations of inputs, it is possible to use a neural network to 'learn' the patterns inherently present in the data. A neural network is quite simply a network of devices that is 'neuron-like'. Neurons are the brain's building blocks and are switches with multiple inputs and some

threshold to decide when they switch. In general, neural networks are run on transistor devices or in computer simulations. They require a period of 'training' when they learn what settings need to be made for individual neurons in order to produce the required outputs. Once trained, they are extremely rapid in operation since there is very little 'processing' as such, simply a cascade of voltage switching through the transistor network. If the network is implemented as semiconductor transistors then it works at a speed governed only by the latency of the semiconductor medium – extremely fast indeed. Neural networks are extremely useful for controlling highly non-linear systems for which it is too difficult to code a traditional algorithm. However, the requirement for a large amount of data can make the learning exercise a difficult one. Recent advances in the field reduce the need for precise data sets of input and corresponding outputs; input data and 'desirable outcome' definitions allow neural networks to learn how to produce a desirable outcome by identifying patterns in the incoming data. Such networks are extremely slow in comparison to the more traditional types of network during the learning phase. In general, for driver modelling there is little applicability for neural networks at present due to the lack of fully populated data sets with which to teach them. It is also worth commenting that for any input range that was not encountered during the learning phase, the outputs are unknown and may not prove desirable. This latter feature is not dissimilar to real people; drivers who have never experienced a skid are very unlikely to control it at the first attempt.

(v) System identification. System identification is a useful technique, not dissimilar in concept to neural networking. A large amount of data is passed through one of several algorithms that produce an empirical mathematical formulation that will produce outputs like the real thing when given the same set of inputs. The formulation is more mathematical than neural networking and so the resulting equations are amenable to inspection – although the terms and parameters may lack any immediately obvious significance if the system is highly non-linear. System identification methods select the level of mathematical complexity required to represent the system of interest (the 'order' of the model) and generate parameters to tune a generic representation to the specific system of interest. As with neural networks, the representation of the system for inputs that are beyond the bounds of the original inputs (used to identify the model) is undefined. System identification is useful as a generic modelling technique and so has been successfully applied to components such as dampers as well as control system and plant modelling. System identification is generally faster to apply than neural network learning but the finished model cannot work as quickly. The same data set availability problems for neural networking also mean system identification is not currently applicable to driver modelling.

(vi) Adaptive controllers. Adaptive control is a generic term to describe the ability of a control system to react to changes in circumstances. In general, people are adaptive in their behaviour and so it would seem at first glance that adaptive control is an appropriate tool for modelling driver behaviour. Optimum control models, described above, generally use some form of adaptive control to optimize the performance of a given controller architecture to the system being controlled and the task at hand. Adaptation is a problem in real world testing since it obscures real differences in performance;

equally it can obscure performance changes and so adaptive modelling of driver behaviour is not preferred except for circuit driving. Several techniques come under the headline of adaptive control; the simplest is to change the control parameters in a predetermined fashion according to the operating regime, an operation referred to as 'gain scheduling'. Gain is the term used for any treatment given to an error state before it is fed to an input – thus the PID controller described above has a P-gain, an I-gain and a D-gain. It might be, for example, that under conditions of opposite lock the P-gain is increased since the driver needs to work quickly to retain control, or under conditions of increasing speed the P-gain is reduced since slower inputs are good for stability at higher speeds. A more complex method is to carry a model of the plant on board in the controller and to use it to better inform some form of gain scheduling, perhaps using information that cannot readily be discerned from on-board instrumentation – such as body slip angle. This is referred to as a Model Reference Adaptive Scheme (MRAS). A further variation on the theme is to use the controller to calculate model parameters using system or parameter identification methods (described above). The control system parameters can be modified based on this information – in effect there is an ongoing redesign of the control system using a classical deterministic method, based on the reference state and the plant characteristics according to the latest estimate. This is referred to as a 'self-tuning-regulator' and is useful for unpredictably varying systems. Finally, a method known as 'dual control' intentionally disturbs the system in order to learn its characteristics, while simultaneously controlling it towards a reference state. In many ways this is similar to a top level rally driver stabbing the brakes in order to assess friction levels while disturbing the overall speed of the vehicle as little as possible; the knowledge gained allows the driver to tune their braking behaviour according to recently learned characteristics. Such behaviour is in marked contrast to circuit drivers, who concentrate on learned braking points and sometimes have difficulty adapting to changing weather conditions. With the exception of the simplest gain scheduling methods, in general adaptive control techniques are unsuitable for the modelling of driver behaviour as part of any practicable process. Once again the variation in simulation output cannot readily be traced to any particular aspect of the system and hence the success or otherwise of an intended modification is difficult to interpret.

In the light of the preceding description, the authors believe a PID controller, with some form of simple gain scheduling, is most appropriate for the modelling of driver behaviour in a multibody system context. The art of implementing a successful model is in selecting the state variables within the model to use with the controller.

6.13.2 A path following controller model

The first hurdle to be crossed is the availability of suitable state variables and the use of gain terms to apply to them. Typically in a multibody system model, many more variables are available than in a real vehicle. Within the model, these variables can be the subject of differential equations in order to have available integral and differential terms. Table 6.4 shows a portion

Table 6.4 A portion of an MSC.ADAMS command file showing the implementation of differential equations to retrieve and use integral and derivative terms for a state variable

```
! -- Derivative Term - not generally used --
part create equation differential_equation &
   differential_equation_name = .test.yaw_rate_error_equation_1 &
   adams_id = 3 &
   comments = "Yaw Rate Error Equation - Implicit" &
   initial_condition = 0.0 &
   function = "DIF(3)-varval(yaw_rate_error)" &
   implicit = on &
   static_hold = off
data_element create variable &
   variable_name = yaw_rate_error_derivative &
   function = "DIF1(3)"

! -- Integral Term --
part create equation differential_equation &
   differential_equation_name = .test.yaw_rate_error_equation_2 &
   adams_id = 4 &
   comments = "Yaw Rate Error Equation - Explicit" &
   initial_condition = 0.0 &
   function = "varval(yaw_rate_error)" &
   implicit = off &
   static_hold = off
data_element create variable &
   variable_name = yaw_rate_error_integral &
   function = "(DIF(4))"

! Steer input torque in response to path error.
force create direct single_component_force &
     single_component_force_name = yaw_rate_handwheel_torque &
     type_of_freedom = rotational &
     action_only = on &
     i_marker_name = .hand_wheel_column.m_wheel_column &
     j_marker_name = .hand_wheel_column.m_wheel_column &
     function = "(", &
        "   VARVAL(yaw_rate_error)           * VARVAL(yp_gain) ", &
        " + VARVAL(yaw_rate_error_integral)  * VARVAL(yi_gain) ", &
        " + VARVAL(yaw_rate_error_derivative)* VARVAL(yd_gain) ", &
       ")", &
       "* STEP(TIME,0.0,0.0,1.0,1.0)"
```

of a command file from MSC.ADAMS implementing those terms for yaw rate. While it is a working example, no claim is made that is in any sense optimum.

Such variables can usually be manipulated within the model using the programming syntax provided with the code being used. For simulation codes such as MSC.ADAMS, the format of such calculations can appear a little clumsy but this soon disappears with familiarity. The most recent versions of MSC.ADAMS include a 'control toolbox' to facilitate the implementation of PID controllers. For codes such as MATLAB/Simulink the implementation of control systems is arguably easier since they are written with the prime objective of control system modelling. However, the modelling of the vehicle as a plant is more difficult within these systems and so there

is an element of swings and roundabouts if choosing between the codes. In general, codes like MSC.ADAMS have a history in very accurate simulation of mechanical systems and can be coerced into representing control systems. Codes like MATLAB and MATLAB/Simulink are the reverse; they have a history in very detailed control system simulation and can be coerced into representing mechanical systems. For this reason, a recent development suggests using each code to perform the tasks at which it is best; this is often referred to as 'co-simulation'. The authors' experiences to date have been universally disappointing for entirely prosaic reasons – the speed of execution is extremely poor and the robustness of the software suppliers in dealing with different releases of each other's product has been somewhat inconsistent. The effort required to persuade the relevant software to work in an area where it is weak is usually made only once and in any case the additional understanding gained is almost always worthwhile for the analyst involved. Until the performance and robustness of the software improve, the authors do not favour co-simulation except for the most detailed software verification exercises.

The next hurdle to be crossed is the representation of the intended behaviour of the vehicle – the 'reference' states. Competition-developed lap simulation tools use a 'track map' based on distance travelled and path curvature. This representation allows the reference path to be of any form at all and allows for circular or crossing paths (e.g. figures of eight) to be represented without the one-to-many mapping difficulties that would be encountered with any sort of y-versus-x mapping. Integrating the longitudinal velocity for the vehicle gives a distance-travelled measure that shows itself to be tolerably robust against drifting within simulation models. Using this measure, the path curvature can be surveyed in the vicinity of the model.

Some authors favour the use of a preview distance for controlling the path of the vehicle, with an error based on lateral deviation from the intended path. However, there is usually a difficulty associated with this since the lateral direction must be defined with respect to the vehicle. (Failure to anchor the reference frame to the vehicle means that portions of the path approaching 90 degrees to the original direction of travel rapidly diverge to large errors.) Projecting a preview line forward of the mass centre based on vehicle centre line is unsatisfactory due to the body slip angle variations mentioned previously. Either the proportional gain must be reduced to avoid 'PIO' type behaviour, which leads to unsatisfactory behaviour through aggressive avoidance manoeuvres, or else some form of gain scheduling must be applied. Alternatively, the preview vector can be adjusted for body slip angle before it is used if oscilliatory behaviour is to be avoided. The length of the preview vector must be adjusted with speed if reasonably consistent behaviour is to be produced. For 'normal' driving this type of model can produce acceptably plausible results but for manoeuvres such as the ISO 3888 Lane Change the behaviour becomes unacceptably oscilliatory particularly after the manoeuvre.

An alternative method, used by the authors with some success for a variety of extreme manoeuvres, is to focus on the behaviour of the front axle. This model fits with one of the author's (Harty) experience of driving at or near the handling limit, particularly on surfaces such as snow where large body

slip angles highlight the mechanisms used in the driver's mind. High performance driving coaches (Palmer, 1999) rightly concentrate on the use of a 'model' the driver needs in order to retain control in what would otherwise become stressful circumstances of non-linear vehicle behaviour and multiple requirements for control – typically vehicle orientation (body slip angle) and velocity (path control). Useful learning occurs on low grip environments that can be readily transferred across to high grip. In low grip environments, the extreme non-linearity of response of the vehicle can be explored at low speeds and with low stress levels, allowing the driver to piece together a model to be used within their own heads; it is then a matter of practise to transfer the lessons to a high grip environment. The same concepts can be used to explore the behaviour of a driver model within a multibody system environment such as MSC.ADAMS.

The formulation used is described below. All subscripts x and y are in the vehicle reference frame. The ground plane velocity V_g is given from the components V_x and V_y using

$$V_g = \sqrt{V_x^2 + V_y^2} \tag{6.22}$$

The demanded yaw rate ω_d is found from the forward velocity V_x and path curvature k using

$$\omega_d = V_g k \tag{6.23}$$

The body slip angle β is found from the velocities V_y and V_g using

$$\beta = \arcsin\left(\frac{V_y}{V_g}\right) \tag{6.24}$$

The centripetal acceleration A^p is given from the components of acceleration A_x and A_y using

$$A^p = A_y \cos(\beta) + A_x \sin(\beta) \tag{6.25}$$

The front axle no-slip yaw rate ω_{fNS} is found from the centripetal acceleration A^p, the yaw acceleration α_z, the distance, a, from the mass centre to the front axle and the ground plane velocity V_g using

$$\omega_{fNS} = \frac{A^P - \alpha_z a}{V_g} \tag{6.26}$$

The yaw error ω_{err} is then found from the demanded yaw rate ω_d and the front axle no-slip yaw rate ω_{fNS} using

$$\omega_{\text{err}} = \omega_d - \omega_{fNS} \tag{6.27}$$

The implementation of equations (6.22) to (6.27) is illustrated, using again an example of the MSC.ADAMS command file format, in Table 6.5.

Table 6.5 MSC.ADAMS command file sample for 'front axle control' driver model

```
data_element create variable &
   variable_name = ground_plane_velocity &
   function = "(              (", &
      "VX(m_body_CG,base)**2 +", &
      "VY(m_body_CG,base)**2", &
         ")**0.5 ) / 1000"

data_element create variable &
   variable_name = demanded_yaw_rate &
   function = "varval(ground_plane_velocity) *", &
              "AKISPL(varval(path_length),0,path_curvature_spline)"

data_element create variable &
   variable_name = beta &
   function="ASIN(VY(m_body_CG,base,m_body_CG)/", &
            "(varval(ground_plane_velocity) + 0.00001))"

data_element create variable &
   variable_name = centacc &
   function = "(VARVAL(latacc)*COS(VARVAL(beta))) +", &
               "(VARVAL(longacc)*SIN(VARVAL(beta)))"

data_element create variable &
   variable_name = front_axle_no_slip_yaw &
   function = "-(", &
            "VARVAL(centacc) ", &
            "- WDTZ(m_body_CG,base,m_body_CG)", &
            "* DX(m_body_CG,mfr_upright_wheel_centre,m_body_CG)", &
         " )", &
         " /", &
         " ( varval(ground_plane_velocity) + 0.00001 )"

data_element create variable &
   variable_name = yaw_rate_error &
   function = " varval(demanded_yaw_rate) - varval(front_axle_no_slip_yaw)"
```

For a variety of events, this formulation produces good driver/vehicle behaviour, representative of real vehicle and driver behaviour (Figure 6.45). The simulated driver and vehicle behaviour for a post-limit turn-in event is compared here to a real vehicle. Note the freewheeling analytical model (of a significantly different vehicle) displays greater body slip angle, while the real vehicle displays greater oversteer.

6.13.3 Body slip angle control

Skilled drivers, particularly rally drivers, frequently operate at large body slip angles. Colloquially, there is much talk of body slip angles being in excess of 45 degrees but recorded data suggests this is not the case despite appearances. Large body slip angles generally slow progress; although some of the yaw transients are rapid, in general the actual body slip angles are comparatively small (Figure 6.46). In general, drivers greatly overestimate body slip angle subjectively.

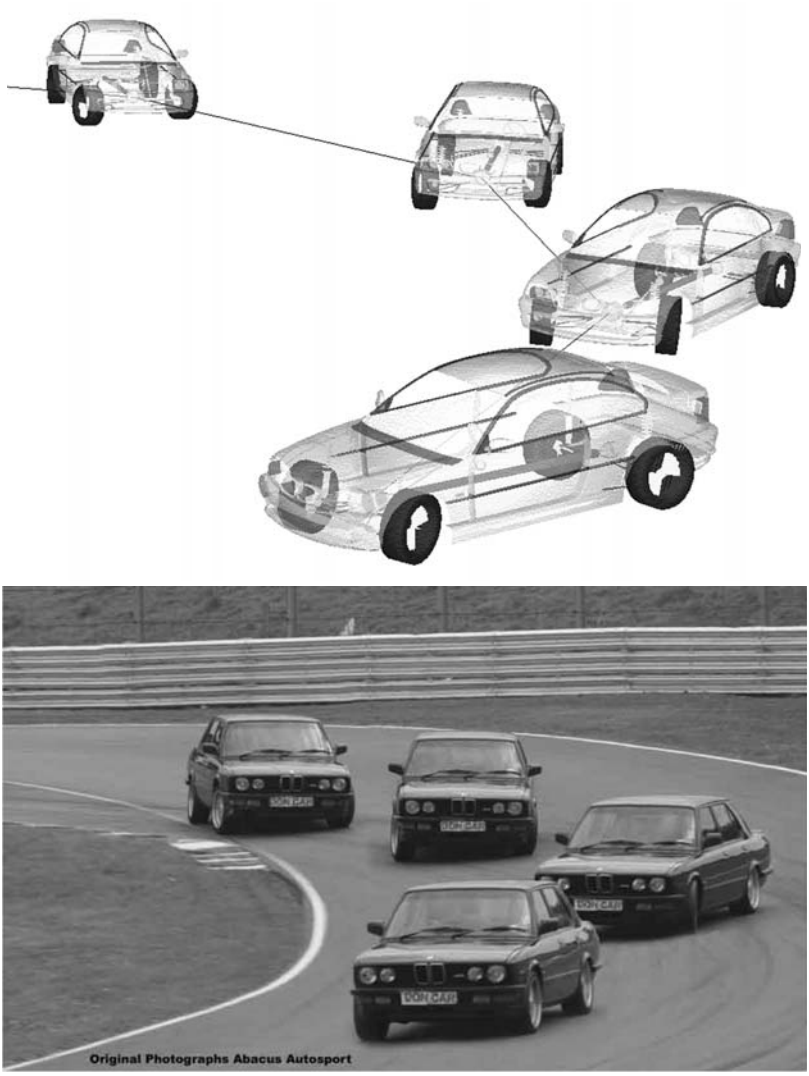

Fig. 6.45 Driver and vehicle behaviour for a post-limit turn-in event (photograph courtesy of Don Palmer, www.donpalmer.co.uk)

The steering system on a vehicle has only 20–25 degrees (less on the rally car) of lock and so realistically, control beyond these body slip angles is unlikely without very large amounts of space indeed.

Most drivers are acutely sensitive to the rate of change of body slip angle, albeit they do not always respond correctly to it. Instead a 'threshold' behaviour appears common, with drivers neglecting body slip angle until either the angle becomes large or its rate of change becomes large. For road cars, our goals are to have a road car manage its own body slip angle so as not to put pressure on drivers in an area where in general skill is lacking. For driver modelling purposes, a separate body slip angle control loop is desirable to catch spins but need not be terribly sophisticated since if it is

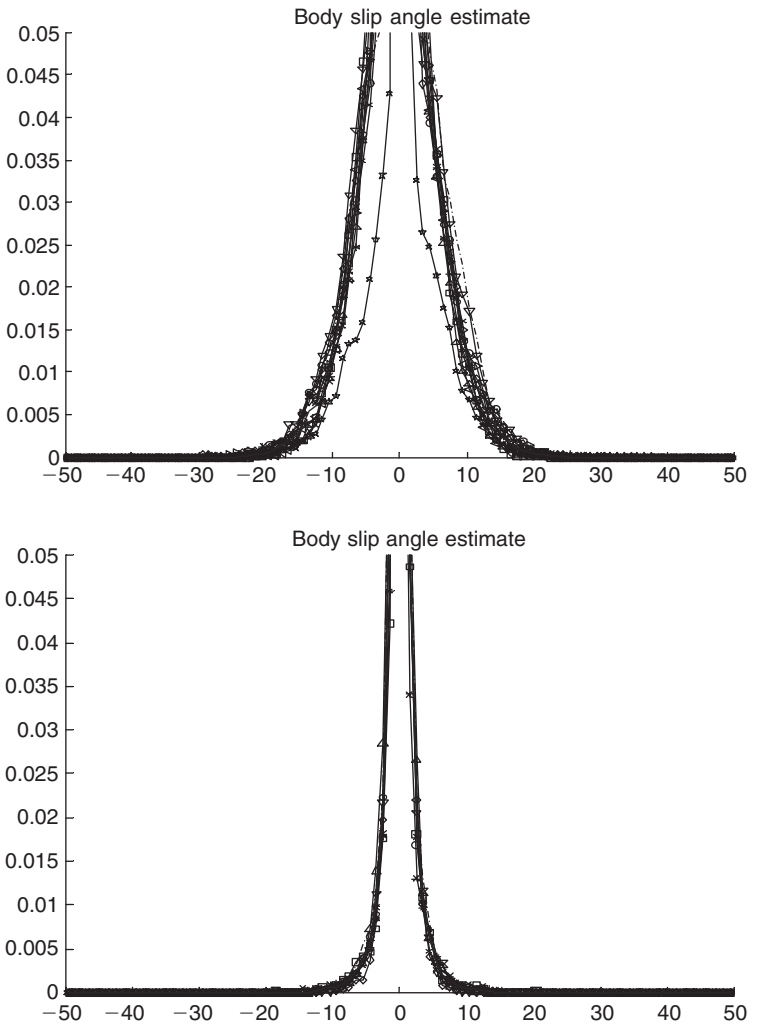

Fig. 6.46 Probability density for body slip angle estimates – Greece 2002 (top) and Germany 2002 (bottom) for Petter Solberg, Subaru World Rally Team

invoked then we have to some extent failed. Such behaviour is desirable in the real vehicle too and is the goal of active intervention systems such as brake-based stability control systems; however, the robust sensing of body slip angle still proves elusive in a cost-effective manner despite its apparent simplicity.

6.13.4 Two-loop driver model

For general use, the authors favour a simple and robust two-loop driver model comprising a path follower and spin catcher, with a separate speed control as appropriate to the task at hand. Figure 6.48 shows such a model.

Fig. 6.47 Large body slip angles are unavailable to normal drivers except as part of an accident. Subaru WRC, Greece 2002 (courtesy of Prodrive)

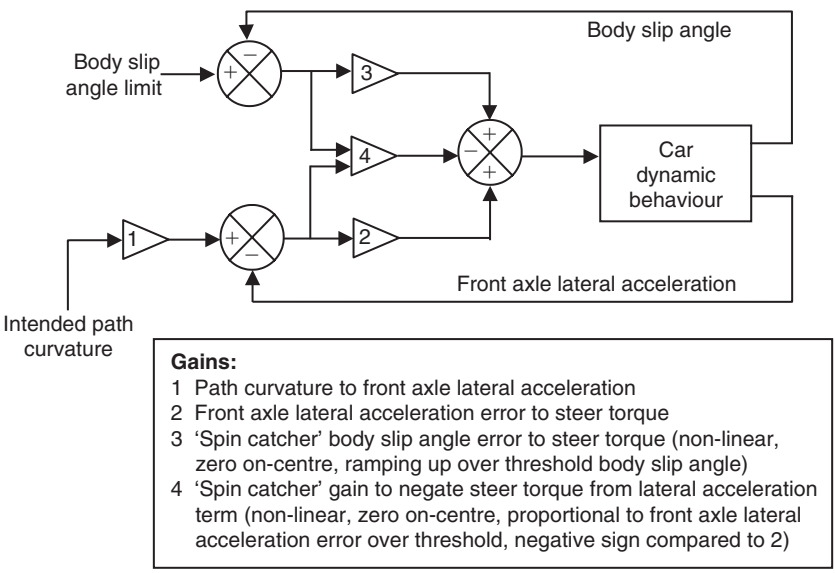

Fig. 6.48 A typical two-loop driver model

6.14 Case study 7 – Comparison of full vehicle handling models

As mentioned at the start of this chapter the use of modern multibody systems software provides users with the capability to develop a model of a full vehicle that incorporates all the major vehicle subsystems. Clearly the development of such a model is dependent on the stage of vehicle design and the availability of the data needed to model all the subsystems. For the

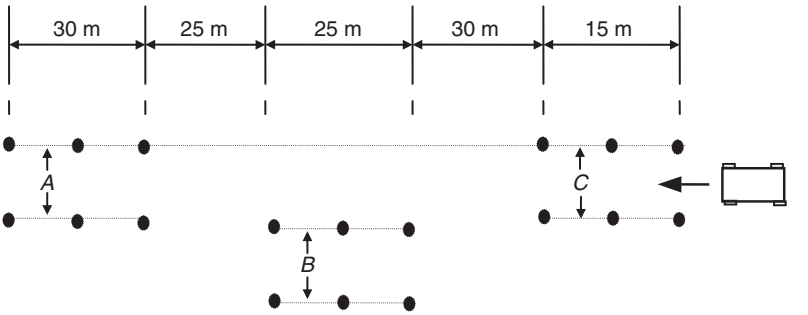

A – 1.3 times vehicle width + 0.25 m

B – 1.2 times vehicle width + 0.25 m

C – 1.1 times vehicle width + 0.25 m

Fig. 6.49 Lane change test procedure. (This material has been reproduced from the Proceedings of the Institution of Mechanical Engineers, K2 Vol. 214 'The modelling and simulation of vehicle handling. Part 4: handling simulation', M.V. Blundell, page 74, by permission of the Council of the Institution of Mechanical Engineers)

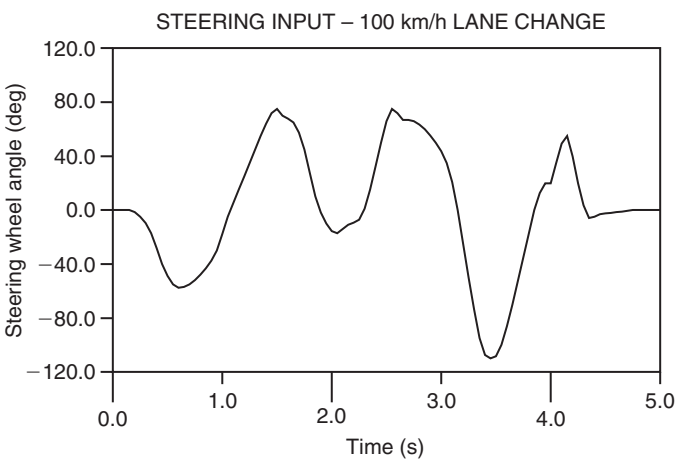

Fig. 6.50 Steering input for the lane change manoeuvre

vehicle dynamics task, however, the automotive engineer will want to carry out simulations before the design has progressed to such an advanced state.

In this case study the level of vehicle modelling detail required to simulate a 'full vehicle' handling manoeuvre will be explored. The types of manoeuvres performed on the proving ground are discussed in the next chapter but as a start we will consider a 100 km/h double lane change manoeuvre. The test procedure for the double lane change manoeuvre is shown schematically in Figure 6.49.

For the simulations performed in the case study the measured steering wheel inputs from a test vehicle have been extracted and applied as a time dependent handwheel rotation (Figure 6.50) as described in section 6.12.3.

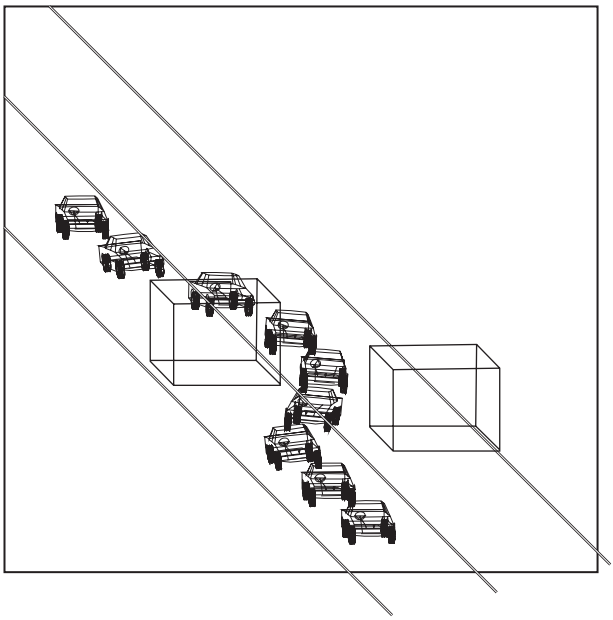

Fig. 6.51 Superimposed graphical animation of a double lane change manoeuvre

To appreciate the use of computer simulations to represent this manoeuvre an example of the superimposed animated wireframe graphical outputs for this simulation is given in Figure 6.51.

In this study the influence of suspension modelling on the accuracy of the simulation outputs is initially discussed based on results obtained using the four vehicle models described in section 6.4 and summarized schematically again here in Figure 6.52. The models shown can be thought of as a set of models with evolving levels of elaboration leading to the final linkage model that involves the modelling of the suspension linkages and the bushes.

For each of the vehicle models described here it is possible to estimate the model size in terms of the degrees of freedom in the model and the number of equations that MSC.ADAMS uses to formulate a solution. The calculation of the number of degrees of freedom (DOF) in a system is based on the Greubler equation given in Chapter 3. It is therefore possible for any of the vehicle models to calculate the degrees of freedom in the model. An example is provided here for the equivalent roll stiffness model where the degrees of freedom can be calculated as follows:

$$\begin{aligned} \text{Parts} \quad & 9 \times 6 \;\; = 54 \\ \text{Rev} \quad & 8 \times -5 = -40 \\ \text{Motion} \quad & 2 \times -1 = -2 \\ \hline & \Sigma_{DOF} = 12 \end{aligned}$$

In physical terms it is more meaningful to describe these degrees of freedom in relative terms as follows. The vehicle body part has 6 degrees of freedom. The two axle parts each have 1 rotational degree of freedom relative to the

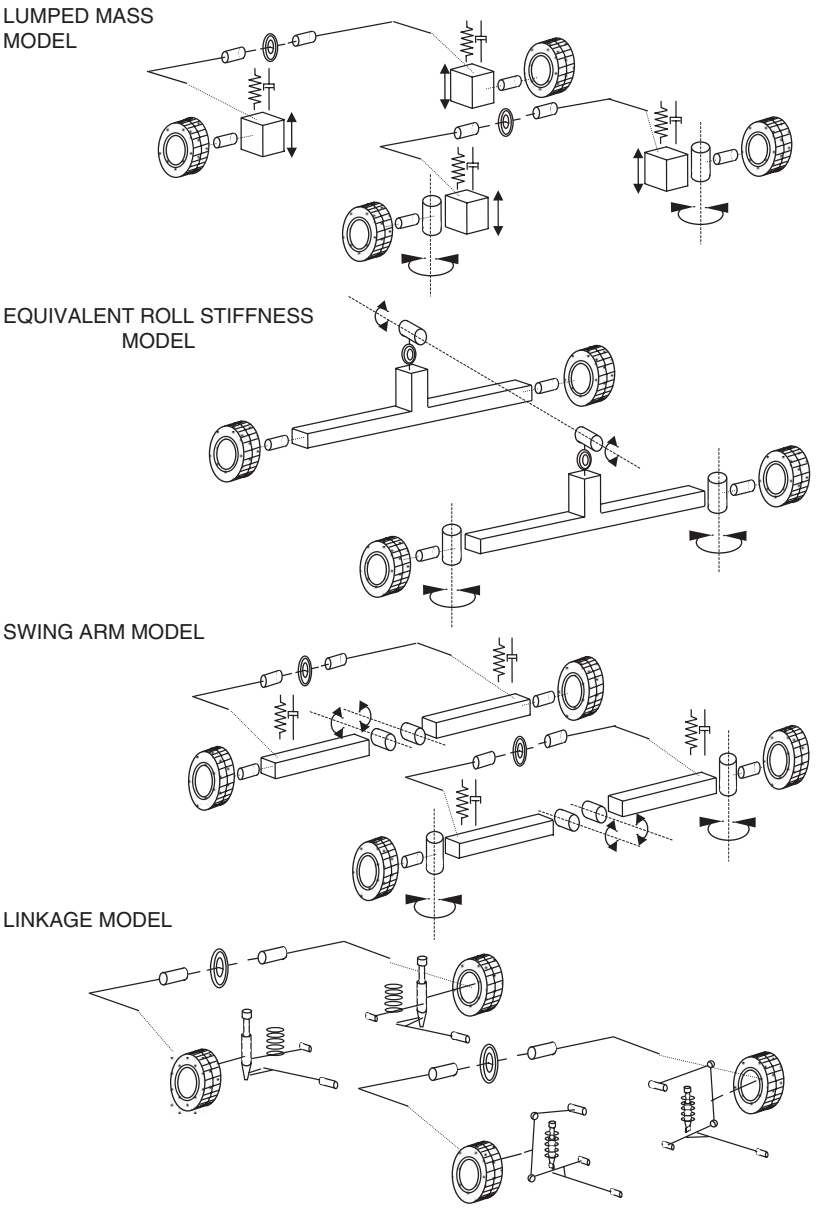

Fig. 6.52 Modelling of suspension systems

body. Each of the four road wheel parts has 1 spin degree of freedom relative to the axles making a total of 12 degrees of freedom for the model.

When a simulation is run in MSC.ADAMS the program will also report the number of equations in the model. As discussed in Chapter 3 the software will formulate 15 equations for each part in the model and additional equations representing the constraints and forces in the model. On this basis the size of all the models is summarized in Table 6.6.

Table 6.6 Vehicle model sizes

Model	Degrees of freedom	Number of equations
Linkage	78	961
Lumped mass	14	429
Swing arm	14	429
Roll stiffness	12	265

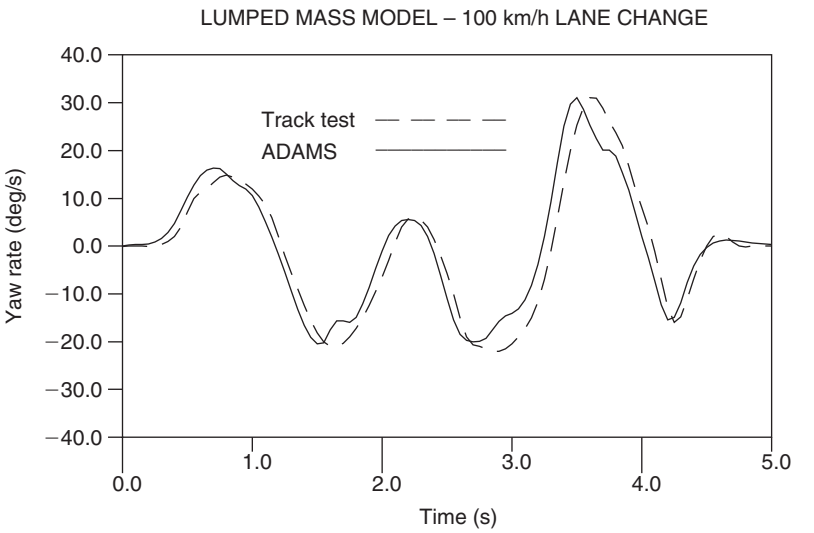

Fig. 6.53 Yaw rate comparison – lumped mass model and test. (This material has been reproduced from the Proceedings of the Institution of Mechanical Engineers, K2 Vol. 214 'The modelling and simulation of vehicle handling. Part 4: handling simulation', M.V. Blundell, page 80, by permission of the Council of the Institution of Mechanical Engineers)

The size of the model and the number of equations is not the only issue when considering efficiency in vehicle modelling. Of perhaps more importance is the engineering significance of the model parameters. The roll stiffness model, for example, may be preferable to the lumped mass model. It is not only a simpler model but is also based on parameters such as roll stiffness that will have relevance to the practising vehicle dynamicist. The roll stiffness can be measured on an actual vehicle or estimated during vehicle design. This model does, however, incorporate rigid axles eliminating the independent suspension characteristics. Note that in this case study an interpolation tyre model of the type described in Chapter 5 has been used with each vehicle model.

Measured outputs including lateral acceleration, roll angle and yaw rate can be compared with measurements taken from the vehicle during the same manoeuvre on the proving ground to assess the accuracy of the models. By way of example the yaw rate predicted by simulation with all four models is compared with measured track test data in Figures 6.53 to 6.56.

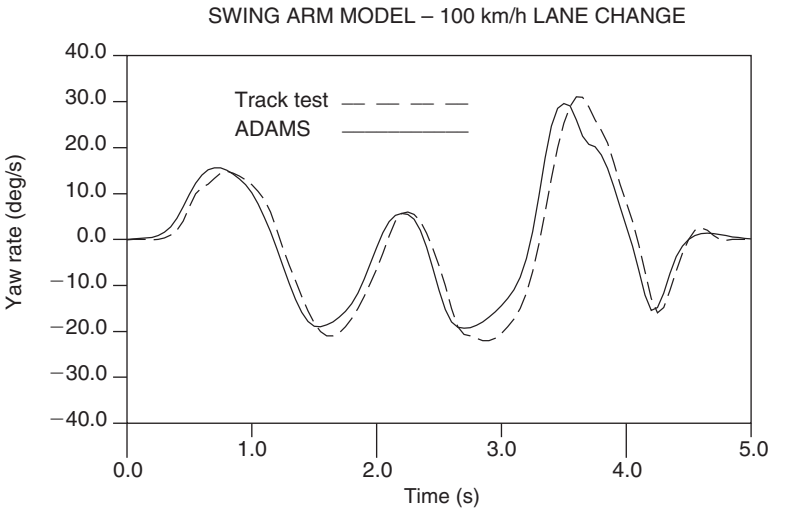

Fig. 6.54 Yaw rate comparison – swing arm model and test. (This material has been reproduced from the Proceedings of the Institution of Mechanical Engineers, K2 Vol. 214 'The modelling and simulation of vehicle handling. Part 4: handling simulation', M.V. Blundell, page 80, by permission of the Council of the Institution of Mechanical Engineers)

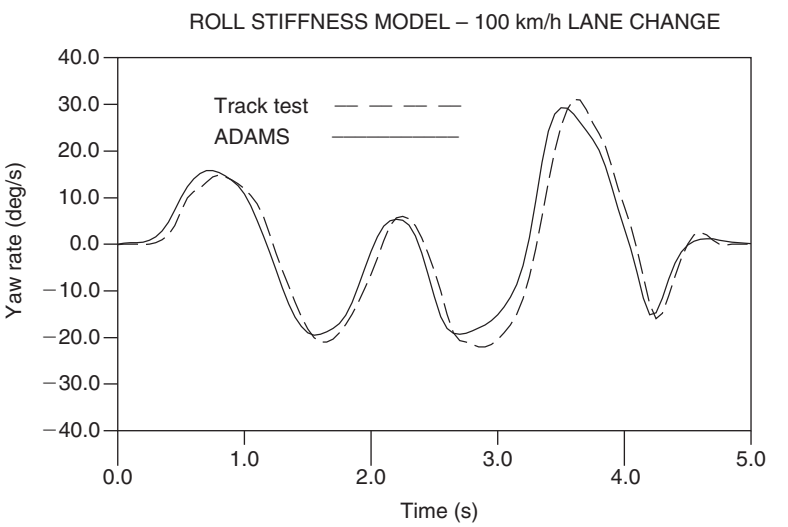

Fig. 6.55 Yaw rate comparison – roll stiffness model and test. (This material has been reproduced from the Proceedings of the Institution of Mechanical Engineers, K2 Vol. 214 'The modelling and simulation of vehicle handling. Part 4: handling simulation', M.V. Blundell, page 81, by permission of the Council of the Institution of Mechanical Engineers)

Examination of the traces in Figures 6.53 to 6.56 raises the question as to how an objective assessment of the accuracy of the simulations may be made. Accuracy is not a 'yes/no' quantity, but instead a varying absence of difference exists between predicted (calculated) behaviour and measured

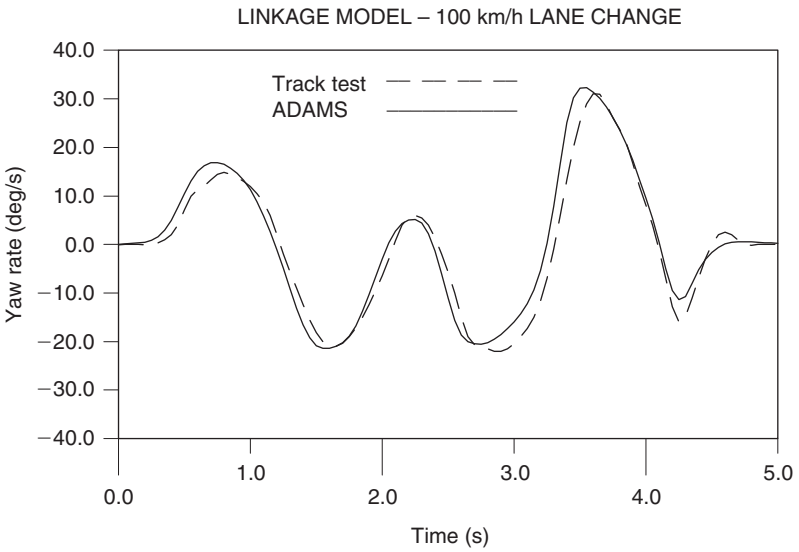

Fig. 6.56 Yaw rate comparison – linkage model and test. (This material has been reproduced from the Proceedings of the Institution of Mechanical Engineers, K2 Vol. 214 'The modelling and simulation of vehicle handling. Part 4: handling simulation', M.V. Blundell, page 81, by permission of the Council of the Institution of Mechanical Engineers)

behaviour. Such a 'difference' is commonly referred to as 'error'. This definition neatly sidesteps two other difficulties:

- Is the measured data what actually happens in the absence of measurement?
- Is the measured data what actually happens during service?

For example, the mass-loading effect of accelerometers may introduce inaccuracies at high frequencies and could mean that the system of interest behaves differently when being measured to when not. The accuracy of controlled measurements in discerning the behaviour of the system when in normal uncontrolled use is another matter entirely. Both topics are far from trivial.

In this case other questions arise such as:

- Does the model data accurately represent the vehicle conditions on the day of the test?
- Does the tyre test data obtained on a tyre test machine accurately represent the condition of the test surface and tyres used on the day of the test?
- How repeatable are the experimental test results used to make an assessment of model accuracy?
- Is there a model data input error common to all the models?

Comparing the performance of the equivalent roll stiffness model with that of the linkage model in Figures 6.55 and 6.56 it is possible to look, for

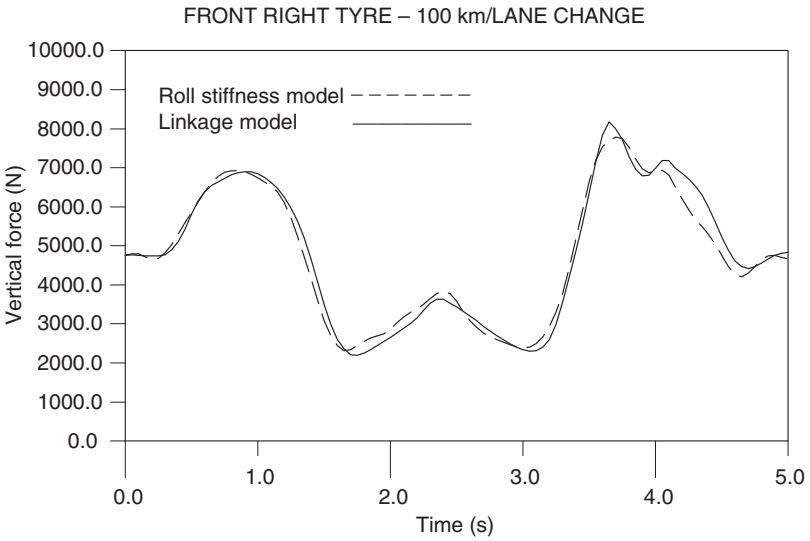

Fig. 6.57 Vertical tyre force comparison – linkage and roll stiffness models

example, at the error measured between the experimental and simulated results for the peaks in the response or to sum the overall error from start to finish. On that basis it may seem desirable to somehow 'score' the models giving, say, the linkage model 8/10 and the roll stiffness model 7/10. In light of the above questions the validity of such an objective measure is debatable and it is probably more appropriate to simply state:

> *For this vehicle, this manoeuvre, the model data, and the available benchmark test data the equivalent roll stiffness model provides reliable predictions when compared with the linkage model for considerably less investment in model elaboration.*

Clearly it is also possible to use an understanding of the physics of the problem to aid the interpretation of model performance. An important aspect of the predictive models is whether the simplified suspension models correctly distribute load to each tyre and model the tyre position and orientation in a way that will allow a good tyre model to determine forces in the tyre contact patch that impart motion to the vehicle and produce the desired response. Taking this a step further we can see that if we use the equivalent roll stiffness and linkage models as the basis for further comparison it is possible in Figures 6.57 and 6.58 to compare the vertical force in, for example, the front right and left tyres. The plots indicate the performance of the simple equivalent roll stiffness model in distributing the load during the manoeuvre. The weight transfer across the vehicle is also evident as is the fact that tyre contact with the ground is maintained throughout. It should also be noticed that in determining the load transfer to each wheel the equivalent roll stiffness model does not include the degrees of freedom that would allow the body to heave or pitch relative to the suspension systems.

In Figures 6.59 and 6.60 a similar comparison between the two models is made, this time considering, for example, the slip and camber angles predicted in the front right tyre.

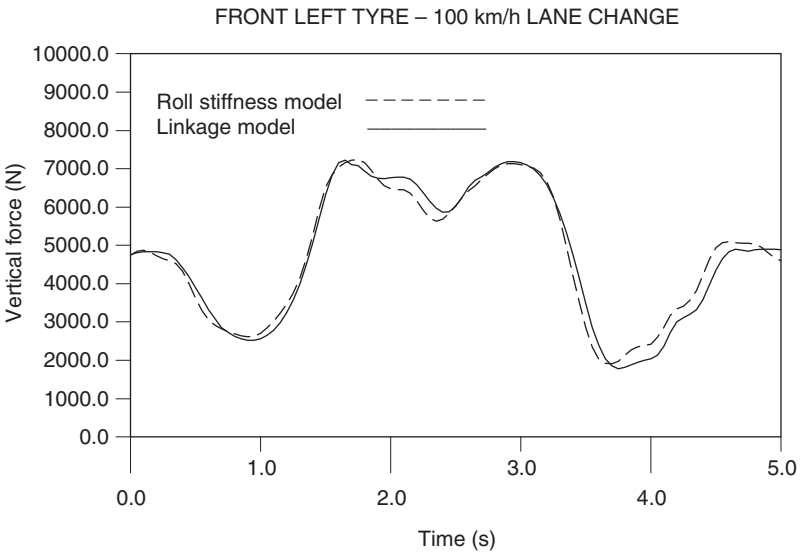

Fig. 6.58 Vertical tyre force comparison – linkage and roll stiffness models

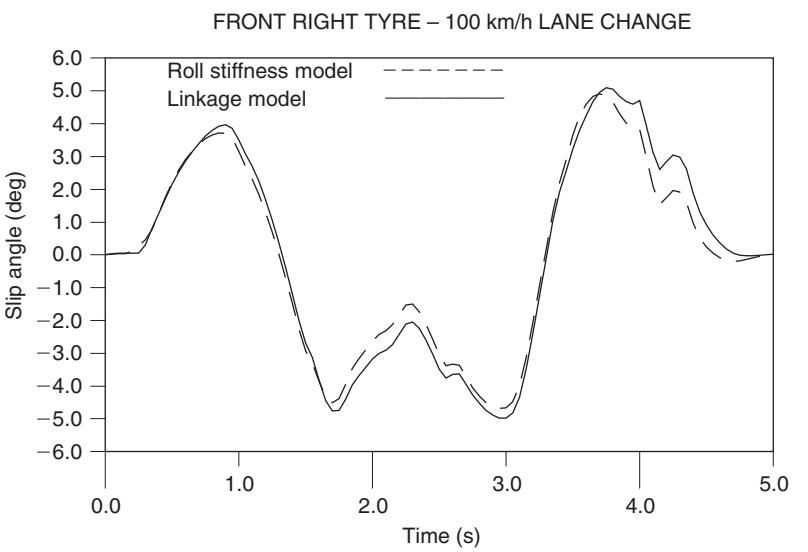

Fig. 6.59 Slip angle comparison – linkage and roll stiffness models

Although the prediction of slip angle agrees well it can be seen in Figure 6.60 that the equivalent roll stiffness model with a maximum value of about 1.5 degrees underestimates the amount of camber angle produced during the simulation when compared with the linkage model where the camber angle approaches 5 degrees. Clearly the wheels in the effective roll stiffness model do not have a camber degree of freedom relative to the rigid axle parts and the camber angle produced here is purely due to tyre deflection.

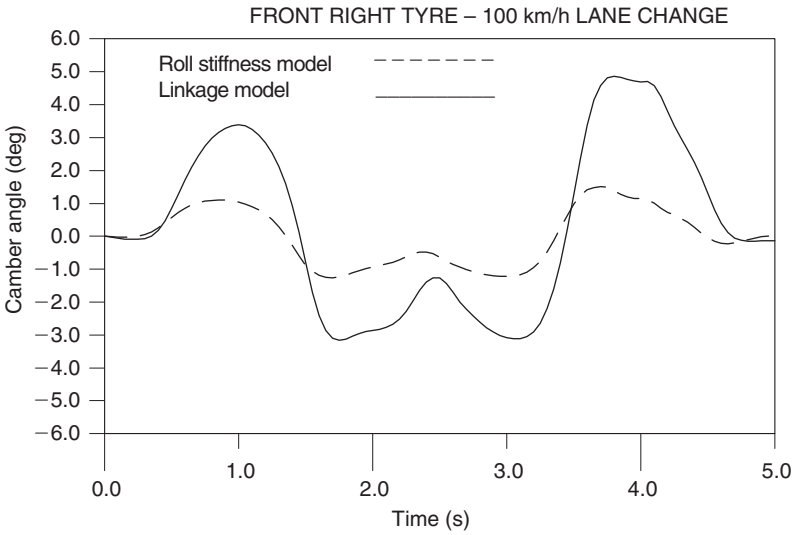

Fig. 6.60 Camber angle comparison – linkage and roll stiffness models

As discussed in Chapter 5 it is perhaps fortuitous in this case that for a passenger car of the type used here the lateral tyre force produced due to slip angle is considerably more significant than that arising due to camber between the tyre and road surface. Further investigations can be carried out to establish the significance of a poor camber angle prediction input to the tyre model. In Figure 6.61 the linkage model has been run using an interpolation tyre model where it has been possible to deactivate the generation of lateral force arising from camber angle. In this plot it can be seen that the prediction of yaw rate, for example, is not sensitive for this vehicle and this manoeuvre to the modelling of camber thrust.

To conclude this case study it is possible to consider an alternative modelling and simulation environment for the prediction of the full vehicle dynamics. As discussed earlier the incorporation of microprocessor control systems in a vehicle may involve the use of a simulation method that involves:

(i) the use of multibody systems software where the user must invest in the modelling of the control systems

(ii) the use of software such as MATLAB/Simulink where the user must invest in the implementation of a vehicle model or

(iii) a co-simulation involving parallel operation of the multibody systems and control simulation software

In this example the author (Wenzel et al., 2003)[2] has chosen the second of the above options and a vehicle model (Figure 6.62) is developed from first

[2]Wenzel et al. (2003) describe preliminary work undertaken in a collaborative research project with Jaguar Cars Ltd, Coventry, UK and funded by the Control Theory and Applications Centre, Coventry University, Coventry, UK. It forms the PhD programme for Thomas A. Wenzel.

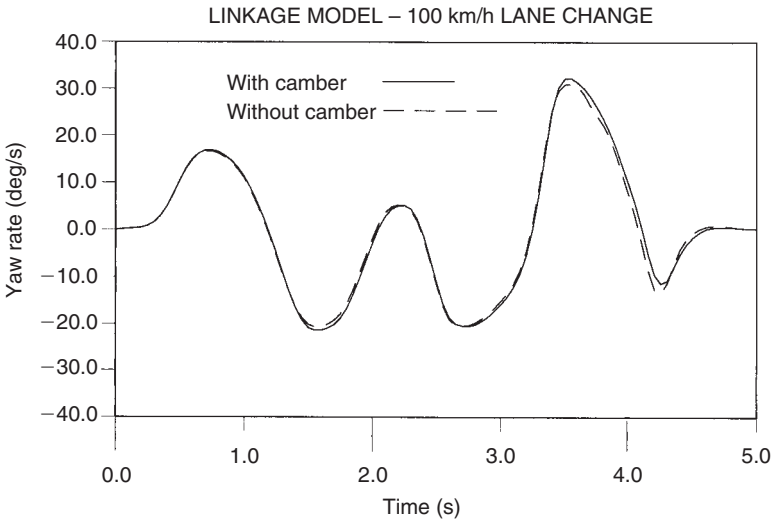

Fig. 6.61 Yaw rate comparison – Interpolation tyre model. (This material has been reproduced from the Proceedings of the Institution of Mechanical Engineers, K2 Vol. 214 'The modelling and simulation of vehicle handling. Part 4: handling simulation', M.V. Blundell, page 83, by permission of the Council of the Institution of Mechanical Engineers)

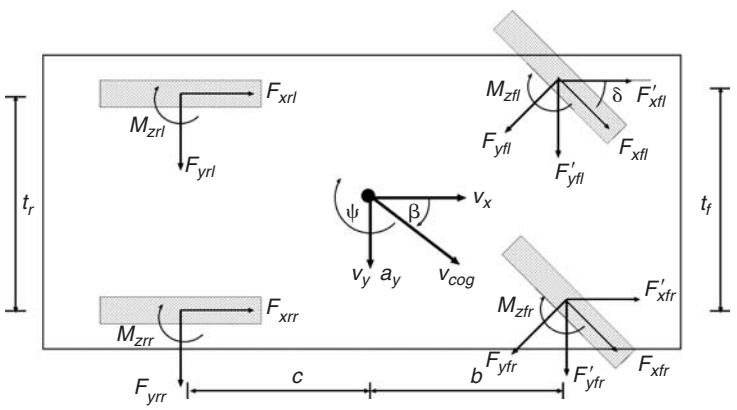

Fig. 6.62 Three-degree-of-freedom vehicle model (Wenzel et al., 2003)

principles and implemented in Simulink. The model developed here is based on the same data used for this case study with 3 degrees of freedom: the longitudinal direction x, the lateral direction y and the yaw around the vertical axis z.

The vehicle parameters used in the following model include:

v_x = longitudinal velocity (m/s)
v_y = lateral velocity (m/s)
v_{cog} = centre of gravity velocity (m/s)
a_x = longitudinal acceleration (m/s^2)

a_y = lateral acceleration (m/s^2)
Γ = torque around z-axis (Nm)
δ = steer angle (rad)
β = side slip angle (rad)
α_{ij} = wheel slip angles (rad)
$\dot{\psi}$ = yaw rate (rad/s)
F_{zij} = vertical forces on each wheel (N)
ij = position: i = front(f)/rear(r), j = left(l)/right(r)

Note that steer angle δ and the velocity of the vehicle's centre of gravity v_{cog} are specified as model inputs.

The relationship between the dynamic vehicle parameters can be formulated as differential equations. Most of these can be found in the standard literature. Using formulas by Wong (2001) and Will and Żak (1997) the following differential equations for acceleration, torque and yaw rate can be derived:

$$\dot{v}_x = \frac{1}{m}\left(F_{xfl}\cos\delta - F_{yfl}\sin\delta + F_{xfr}\cos\delta - F_{yfr}\sin\delta + F_{xrl} + F_{xrr}\right) + v_y\dot{\psi} \tag{6.28}$$

$$\dot{v}_y = \frac{1}{m}\left(F_{yfl}\cos\delta + F_{xfl}\sin\delta + F_{yfr}\cos\delta + F_{xfr}\sin\delta + F_{yrl} + F_{yrr}\right) - v_x\dot{\psi} \tag{6.29}$$

$$\begin{aligned}\Gamma = {} & \frac{t_f}{2}F'_{xfl} - \frac{t_f}{2}F'_{xfr} + \frac{t_r}{2}F_{xrl} - \frac{t_r}{2}F_{xrr} + bF'_{yfl} + bF'_{yfr} - cF_{yrl} - cF_{yrr} \\ & + M_{zfl} + M_{zfr} + M_{zrl} + M_{zrr}\end{aligned} \tag{6.30}$$

$$\ddot{\psi} = \frac{\Gamma}{J_z} \tag{6.31}$$

where the additional parameters are defined as:

F_{xij} = longitudinal forces on tyre ij (N)
F_{yij} = lateral forces on tyre ij (N)
F'_{xij} = longitudinal forces on tyre ij in the vehicle's co-ordinate system (N)
F'_{yij} = lateral forces on tyre ij in the vehicle's co-ordinate system (N)
M_{zij} = self-aligning moment on tyre ij (Nm)
m = mass of vehicle (kg)
J_z = moment of inertia around vertical axis (Nm^2)
t_f, t_r = front and rear track width (m)
b, c = position of centre of gravity between wheels (m)

Other important states are the wheel slip angles α_{ij} and the body slip angle β, defined as follows:

$$\alpha_{fl/r} = \delta - \arctan\left(\frac{v_y + b\dot{\psi}}{v_x \pm \frac{1}{2}t_f\dot{\psi}}\right) \tag{6.32}$$

$$\alpha_{rl/r} = \arctan\left(\frac{-v_y + c\dot{\psi}}{v_x \pm \frac{1}{2}t_r\dot{\psi}}\right) \tag{6.33}$$

$$\beta = \arctan\left(\frac{v_y}{v_x}\right) \tag{6.34}$$

In this model roll and pitch of the vehicle are neglected but weight transfer is included to determine the vertical load at each wheel as defined by Milliken and Milliken (1995):

$$F_{zfl/r} = \left(\frac{1}{2}mg \pm m\frac{a_y h}{t}\right)\frac{c}{\ell} - ma_x\,\frac{h}{\ell} \tag{6.35}$$

$$F_{zrl/r} = \left(\frac{1}{2}mg \pm m\frac{a_y h}{t}\right)\frac{b}{\ell} + ma_x\,\frac{h}{\ell} \tag{6.36}$$

The additional parameters are the height h of the vehicle's centre of gravity, the wheelbase ℓ and the gravitational acceleration g.

In equations (6.37) and (6.38) it has to be considered that $a_x \neq \dot{v}_x$ and $a_y \neq \dot{v}_y$. The yaw motion of the vehicle has to be taken in account (Wong, 2001) giving:

$$a_x = \dot{v}_x - v_y\dot{\psi} \tag{6.37}$$

$$a_y = \dot{v}_y + v_x\dot{\psi} \tag{6.38}$$

In this work the author (Wenzel et al., 2003) has simulated a range of vehicle manoeuvres using both the 'Magic Formula' and Fiala tyre models described in Chapter 5. The example shown here is for the lane change manoeuvre used in this case study with a reduced steer input applied at the wheels as shown in the bottom of Figure 6.63.

Also shown in Figure 6.63 are the results from the Simulink model and a simulation run with the MSC.ADAMS linkage model. For this manoeuvre and vehicle data set the Simulink and MSC.ADAMS models can be seen to produce similar results.

In completing this case study there are some conclusions that can be drawn. For vehicle handling simulations it has been shown here that simple models such as the equivalent roll stiffness model can provide good levels of accuracy. It is known, however, that roll centres will 'migrate' as the vehicle rolls, particularly as the vehicle approaches limit conditions. The plots for Case Study 1 in Chapter 4 show the vertical movement of the roll centre along the centre line of the vehicle as the suspension moves between bump and rebound. On the complete vehicle the roll centre will also move laterally off the centre line as the vehicle rolls.

Using a multibody systems approach to develop a simple model may also throw up some surprises for the unsuspecting analyst. The equivalent roll

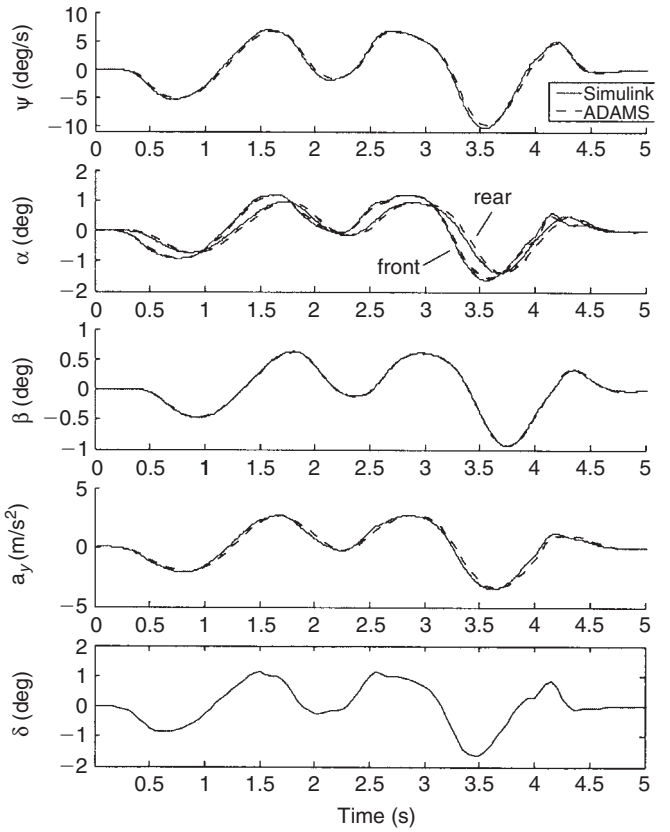

Fig. 6.63 Comparison of Simulink and MSC.ADAMS predictions of vehicle response

stiffness model, for example, does not include heave and pitch degrees of freedom relative to the front and rear axles. During the simulation, however, the degrees of freedom exist for the body to heave and pitch relative to the ground inertial frame. These degrees of freedom must still be solved and in this case are damped only by the inclusion of the tyre model. In the 3 degrees of freedom model these motions are ignored and solution is only performed on the degrees of freedom that have been modelled. While the main theme in this book is to demonstrate the use of multibody systems analysis the Matlab/Simulink model is useful here in providing the basis for additional modelling and simulation of the modern control systems involved in enhancing the stability and dynamics of the vehicle. The effort invested in this modelling approach also provides educational benefits reinforcing fundamental vehicle dynamics theory.

6.15 Summary

Many different possibilities exist for modelling the behaviour of the vehicle driver. That none has reached prominence suggests that none is correct for

every occasion. In general, the road car vehicle dynamics task is about delivering faithful behaviour during accident evasion manoeuvres – where most drivers rarely venture. Positioning the vehicle in the linear region is relatively trivial and need not exercise most organizations unduly, but delivering a good response, maintaining yaw damping and keeping the demands on the driver low are of prime importance in the non-linear accident evasion regime. For this reason, controllers that take time to 'learn' the behaviour of the vehicle are inappropriate – road drivers do not get second attempts. For road vehicles, the closed loop controller based on front axle lateral acceleration gives good results and helps the analyst understand whether or not the vehicle is actually 'better' in the sense of giving an average driver the ability to complete a manoeuvre.

In motorsport applications, however, drivers are skilled and practised and so controllers with some feed-forward capability (to reflect 'learned' responses), plus closed loop control of body slip angle are appropriate to reflect the high skill level of the driver. Whether or not advanced gain scheduling models, such as the Model Reference Adaptive Scheme or Self-Tuning Regulator, are in use depends very much on whether or not data exists to support the verification of such a model. The authors preference is that 'it is better to be simple and wrong than complicated and wrong' – in other words, all other things being equal, the simplest model is the most useful since its shortcomings are more easily understood and judgements based on the results may be tempered accordingly. With elaborate schemes, particularly self-tuning ones, there is a strong desire to believe the complexity is in and of itself a guarantee of success.

In truth if a relatively simple and robust model cannot be made to give useful results it is more likely to show a lack of clarity in forming the question than a justification for further complexity.

7 Simulation output and interpretation

7.1 Introduction

Vehicle handling simulations are intended to recreate the manoeuvres and tests that vehicle engineers carry out using prototype vehicles on the test track or proving ground. Some are defined by the International Standards Organization, which outlines recommended tests in order to substantiate the handling performance of a new vehicle:

ISO 3888-1:1999	Passenger cars – Test track for a severe lane-change manoeuvre – Part 1: Double lane-change
ISO 3888-2:2002	Passenger cars – Test track for a severe lane-change manoeuvre – Part 2: Obstacle avoidance
ISO 4138:1996	Passenger cars – Steady-state circular driving behaviour – Open-loop test procedure
ISO 7401:2003	Road vehicles – Lateral transient response test methods – Open-loop test methods
ISO 7975:1996	Passenger cars – Braking in a turn – Open-loop test procedure
ISO/TR 8725:1988	Road vehicles – Transient open-loop response test method with one period of sinusoidal input
ISO/TR 8726:1988	Road vehicles – Transient open-loop response test method with pseudo-random steering input
ISO 9815:2003	Road vehicles – Passenger-car and trailer combinations – Lateral stability test
ISO 9816:1993	Passenger cars – Power-off reactions of a vehicle in a turn – Open-loop test method
ISO 12021-1:1996	Road vehicles – Sensitivity to lateral wind – Part 1: Open-loop test method using wind generator input
ISO 13674-1:2003	Road vehicles – Test method for the quantification of on-centre handling – Part 1: Weave test
ISO 14512:1999	Passenger cars – Straight-ahead braking on surfaces with split coefficient of friction – Open-loop test procedure
ISO 15037-1:1998	Road vehicles – Vehicle dynamics test methods – Part 1: General conditions for passenger cars
ISO 15037-2:2002	Road vehicles – Vehicle dynamics test methods – Part 2: General conditions for heavy vehicles and buses

ISO 17288-1:2002	Passenger cars – Free-steer behaviour – Part 1: Steering-release open-loop test method
ISO/TS 20119:2002	Road vehicles – Test method for the quantification of on-centre handling – Determination of dispersion metrics for straight-line driving

Standards also exist for categories of vehicles other than passenger cars and manufacturers in those markets will use them as appropriate. Manufacturers will probably go beyond these minimum procedures in most market segments. The goal of excellence in handling performance is driven not by the need to meet fixed legislation but rather the increasing demands of a competitive marketplace.

The attractions of simulation are summarized in Chapter 1 as:

- improved comprehension and ranking of design variables
- rapid experimentation with design configurations and
- genuine optimization of numerical response variables

Also apparent is the ability to consider the behaviour of a vehicle before that vehicle exists physically. The cost for prototype vehicles can easily be £250 000 at the time of writing. Prudent use of simulation can ensure that only worthwhile prototype designs are turned into hardware. In many ways, well-considered simulation gives an equivalent to the use of a comprehensively instrumented vehicle in order to understand the sensitivity of the behaviour to the design variables available.

The use of instrumented vehicles to investigate handling performance can be traced back to the work of Segal in the early 1950s, which as mentioned in Chapter 1 was the subject of one of the seminal 'IME Papers' (Segel, 1956). Testing was carried out using a 1953 Buick Super four-door sedan (saloon), to investigate steady state behaviour with a fixed steering input at various speeds and also transient response to sudden pulse inputs at the steering wheel. The instrumentation used at that time allowed the measurement of the following:

(i) Left front wheel steer
(ii) Right front wheel steer
(iii) Steering wheel rotation
(iv) Lateral acceleration
(v) Roll angle
(vi) Pitch angle
(vii) Yaw rate
(viii) Roll rate
(ix) Forward velocity

Some of these responses are shown in Figure 7.1. The trajectory (path) of the vehicle can also be recorded. With simulation this is straightforward but in the past has been difficult to measure on the test track, testers resorting to measuring a trail of dye left by the vehicle on the test track surface.

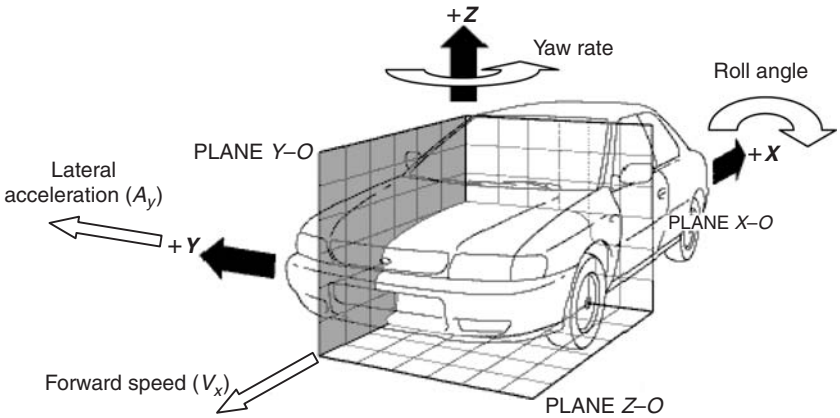

Fig. 7.1 Typical lateral responses measured in one of several possible vehicle co-ordinate frames

Modern satellite-based instrumentation has improved on this somewhat. For each handling manoeuvre, or simulation, it is necessary for vehicle engineers to decide which responses are to be measured during the testing process.

All test and analytical activities are directed at understanding and improving the overall dynamic behaviour of the vehicle. As discussed in Chapter 1, the difficulty with the vehicle dynamics field is not the complexity of the effects in play but the level of interaction between them. A further difficulty is the level of change in behaviour required for a vehicle to be usefully 'improved'. Typically, strong impressions of change are made with only modest variations of physical measures. When the difficulty of repeatable testing and the variation of impression with individual testers are both thrown in, the vehicle dynamics process lacks 'capability' – in the sense of quality control – compared to the task it is set. To explain this further, consider the following example.

7.2 Case study 8 – Variation in measured data

Several attempts have been made to define single number measures for vehicle dynamic performance. A popular measure in the USA is limiting lateral acceleration – frequently referred to as 'grip'. Table 7.1 shows data that might be recorded during a steady state test, using a stopwatch to time a lap of a marked 200 m diameter circle.

If an honest error estimation is made in the recorded data then the results with the stopwatch are probably accurate to ± 0.1 second. Thus the raw data would appear as shown in Figure 7.2, with error bars on the figure as shown. This is a typical set of data for such a test; prolonging the test further might well degrade the tyres on the vehicle and lead to a 'skewed' result favouring the first test configuration with fresher tyres. It could be argued that tests should be repeated on fresh tyres for each different configuration to be examined but while academically sound, this argument neglects the commercial and temporal pressures placed on vehicle testing,

Table 7.1 Time to complete lap of a marked 200 m diameter circle (seconds)

	Test 1	Test 2	Test 3	Test 4	Test 5
Configuration A	21.38	21.71	21.57	21.61	21.50
Configuration B	21.60	21.49	21.29	21.39	21.53

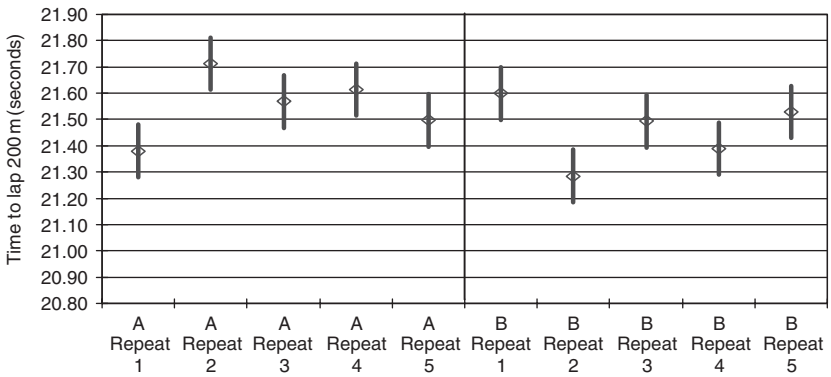

Fig. 7.2 Raw data from steady state test with error bars

Table 7.2 Statistical summary of test data

	Mean	Population standard deviation
Configuration A	0.866*g*	0.010*g*
Configuration B	0.874*g*	0.010*g*
Difference A − B	0.008*g*	

particularly in intermediate configurations before matters are finalized and particularly if the tyres themselves are prototype items.

If these measurements are manipulated into lateral acceleration figures using the simple relationship

$$A_y = \frac{(200\pi/t)^2}{100} \tag{7.1}$$

then treated as the results that might be obtained from a production process and manipulated accordingly, the results in Table 7.2 emerge.

It is clear that the extrapolation to a population from only five samples is somewhat poor practice. However, it is equally clear that the difference between the two configurations is significantly less than the spread of the distribution of the tests. In statistical process control, a process is regarded as 'capable' if six times the standard deviation (so-called '6σ') is less than 75% of the tolerance on the measured attribute. For the measurement processes above, the 'capability' is no less than $6 \times 0.01 \times 4/3 = 0.08g$ – 10 times

the difference actually observed in the test. In other words, differences of less than $0.08g$ cannot be controlled reliably using such a measurement process. However, such a difference is a significant one between otherwise similar vehicles, representing something around 10% of the total lateral acceleration available.

While the dataset shown in the example is fictitious, the statistical character of the measurements is entirely typical, even under well-controlled conditions. When a vehicle is nearly optimized, this problem is typical. The resolution of the process in use – the test facilities and so on – is comparable to or greater than the control required to optimize the vehicle further. For this reason, in both motorsport and production vehicle engineering, a great deal of the final optimization is based on subjective judgements of a few well-chosen individuals.

7.3 A vehicle dynamics overview

7.3.1 Travel on a curved path

At this point, it is appropriate to develop some basic notions about vehicle dynamics. These definitions will be used later to suggest an interpretation of the subjective/objective relationship; however, it should be clear that by its very nature the absolute quantification of subjective qualities is impossible.

The driver has two primary concerns in controlling the vehicle. These are speed and path. Speed is controlled with engine power and braking systems. The use of separate controls for acceleration and deceleration is logical when the systems are separate but may become less so if vehicle architecture changes significantly; for example, some system with a 'motor in each wheel' that both accelerates and brakes might have a single pedal for control, of the type prototyped by Nomix AB in Sweden (http://www.nomix.se/nomixl.html) and under investigation by the Swedish National Road Administration at the time of writing. Variation of speed is governed by vehicle mass and tractive/brake power availability at all but the lowest speed, and is easily understood.

The adjustment of path curvature at a given speed is altogether more interesting. In a passenger car the driver has a handwheel, viewed by the authors as a 'yaw rate' demand – a demand for rotational velocity of the vehicle when viewed from above. The combination of a yaw rate and a forward velocity vector, which rotates with the vehicle, gives rise to a curved path. The curved path of the vehicle requires some lateral acceleration. The tyres on a car exert a force towards the centre of a turn and the body mass is accelerated by those forces centripetally – in a curved path. Thus the sum of the lateral forces that the tyres exert on the car is the centripetal force that produces the centripetal acceleration (Figure 7.3). Note that the authors do not favour the use of the equivalent inertial ('D'Alembert') force since it can be misleading; it gives the impression that the analysis of the cornering vehicle is a static equilibrium problem, which it most certainly is not. The idea of an analogous static equilibrium condition is not in itself problematic but inappropriate 'static' thinking quickly becomes torturous and unwieldy. For example, a common obsession is to attempt to

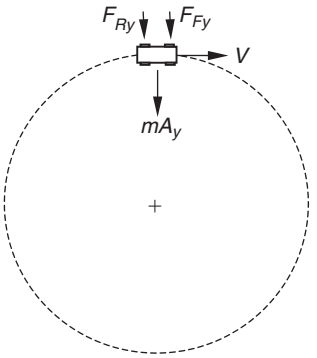

$$\Sigma F_y = mA_y \tag{7.2}$$

where A_y is the centripetal acceleration acting towards the centre of the corner

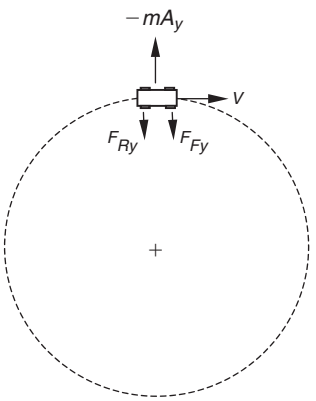

$$\Sigma F_y - mA_y = 0 \tag{7.3}$$

where $-mA_y$ is the d'Alembert force

Fig. 7.3 Representation of inertial force during cornering

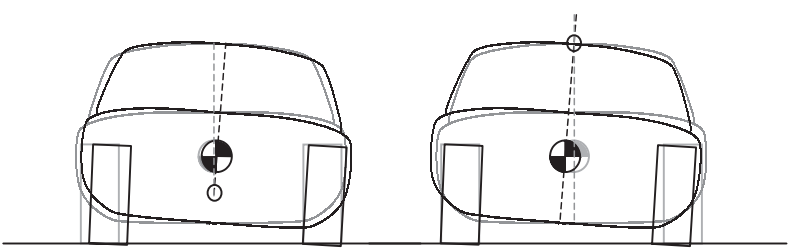

Fig. 7.4 The difficulty with arbitrary reference frames applied to 'pseudo-static' cornering as suggested by the use of D'Alembert forces

find a 'centre of rotation in roll'. This is usually performed with some sort of 'point of zero lateral velocity' logic but the reality is that this 'zero velocity' point is with respect to some arbitrary and ill-defined reference frame. Figure 7.4 shows the same vehicle represented in two equally arbitrary reference frames; the first is anchored at the outboard wheel contact patch and the second at the inboard wheel contact patch. Given that most independent suspensions are not symmetric, the 'lateral displacement' for a given roll angle is entirely dependent on the choice of reference frame. Thus the idea of some 'centre of instantaneous motion' is difficult to pin

down and even more difficult to ascribe any meaning to. If the reference frame is anchored somewhere on the vehicle body then that point becomes a point of zero translation, and the concept is again seen to be of no value. Nevertheless, within the authors' experience there has been a great deal of effort to track down 'centres of motion' using elaborate static equilibrium analogies.

7.3.2 The classical treatment based on steady state cornering

The classical assessment of the behaviour of a vehicle was developed by the early work of vehicle dynamicists such as Olley, Milliken and Segel and has been documented in several textbooks dealing with the subject. In the following sections the classical treatment will be summarized followed by a consideration based on the transient dynamics of the driven vehicle.

The classical assessment of the behaviour of a vehicle is based on either testing or simulating steady state cornering. 'Steady state' means the vehicle states are unchanging with time – the car is 'settled' in a corner at constant speed, on a constant radius and so on. Note that steady state is not the same as 'static'. Two traditional evaluation methods exist. The first involves driving the vehicle around a constant radius circle at a range of constant speeds that correspond to a range of increments in lateral acceleration. The second method involves driving the vehicle at a constant speed but with a progressive increase in handwheel angle that reduces the radius of turn with time and consequently increases the lateral acceleration. Which method is in use in a particular organization is likely to be governed by the test facilities available and previous practice rather than on the merits or otherwise of one or other test method. In particular, the first method is very practicable to perform and so it will be used for the basis of the following discussion.

The starting point for the consideration of steady state cornering behaviour is an assessment of the vehicle cornering at low speed (Figure 7.5).

The minimum radius available in normal driving is the turning circle. At higher speeds the limit to path curvature is not the amount the wheels can be turned but rather the maximum centripetal force that can be generated. This is governed by the limiting coefficient of friction (μ) between tyres and road, typically around 0.9. Simplistically, if friction is independent of area (the Newtonian model), the theoretical maximum centripetal acceleration in units of g is identical to the friction coefficient, μ:

$$\frac{A_y}{g} = \frac{F_y}{mg} = \frac{mg\mu}{mg} = \mu \tag{7.4}$$

This is for vehicles without additional force pressing them into the road – i.e. not 'winged' racing cars. Therefore, the maximum yaw rate possible (in degrees/second) is shown in Figure 7.6 for a typical vehicle.

The yaw rate from 'geometry', ω_{geom}, as shown in Figure 7.6 is the maximum possible steering and varies with speed according to the simple relationship

$$\omega_{geom} = \frac{V(\delta_i + \delta_o)/2}{L}\left(\frac{180}{\pi}\right) \tag{7.5}$$

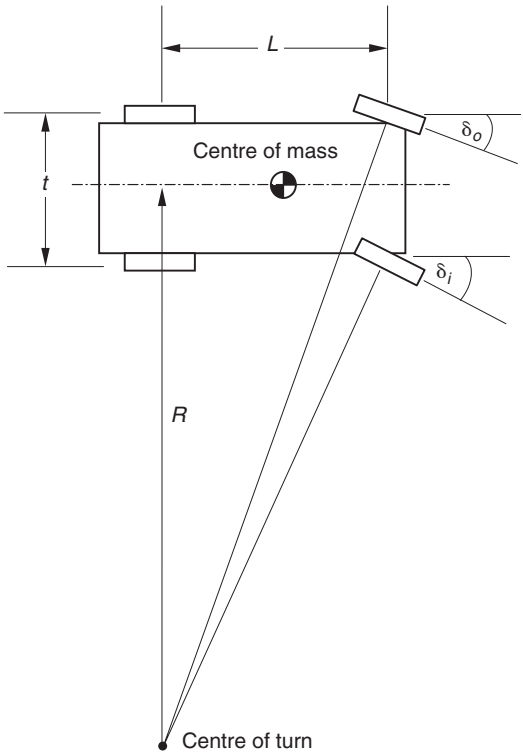

Fig. 7.5 Cornering at low speed

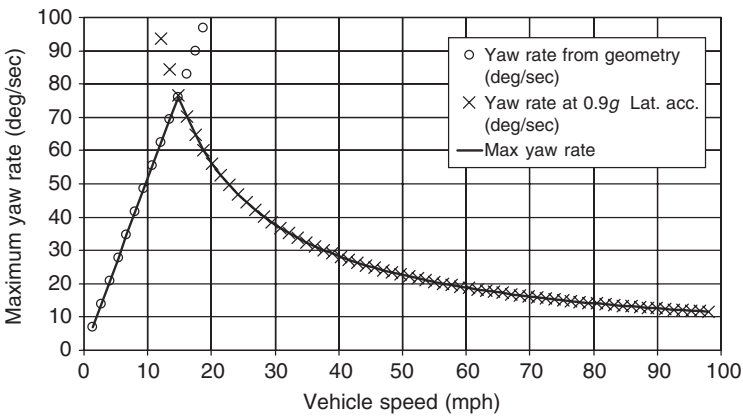

Fig. 7.6 Maximum possible yaw rate for a typical vehicle

where V is the forward velocity in m/s, δ_i, δ_o are the steer angles in radians as shown in Figure 7.5 and L is the wheelbase in m.

Yaw rate from limiting friction, ω_{friction}, is equally simple:

$$\omega_{\text{friction}} = \left(\frac{180}{\pi}\right)\frac{\mu g}{V} \tag{7.6}$$

So it can be seen that above a limiting speed, given by

$$V_{\text{lowlimit}} = \sqrt{\frac{\mu g L}{((\delta_i + \delta_o)/2)(\pi/180)}} \tag{7.7}$$

it is the surface grip that determines the limiting yaw rate and hence path curvature. For typical passenger cars, the region in which geometry dominates steering behaviour is small – up to about 15 mph. This is the speed that may be counted as 'low' and in which Figure 7.5 is a reasonable description of the behaviour of the vehicle. For vehicles such taxis and heavy goods vehicles, the low speed region is of more importance simply because these vehicles make more low speed, minimum radius manoeuvres. However, they rarely perform these manoeuvres at speeds exceeding walking pace and so the yaw rates remain low.

The steer angles required to avoid scrubbing at the inner and outer road wheels, δ_o and δ_i are:

$$\delta_o = \frac{L}{(R + 0.5t)}\left(\frac{180}{\pi}\right) \tag{7.8}$$

$$\delta_i = \frac{L}{(R - 0.5t)}\left(\frac{180}{\pi}\right) \tag{7.9}$$

The angle of a notional 'average' wheel on the vehicle centre line, δ, is the 'Ackermann' angle – the approximate form is in common usage:

$$\delta = \frac{LR}{(R - 0.25t^2)}\left(\frac{180}{\pi}\right) \approx \frac{L}{R}\left(\frac{180}{\pi}\right) \tag{7.10}$$

In 1817, Rudolph Ackermann patented geometry similar to this as an improvement over a steered axle as was common on horse-drawn vehicles. That the geometry we today call 'Ackermann' was in fact a modification proposed by the Frenchman Charles Jeantaud in 1878 has been lost in the mists of time. Some measure of how accurately the steering geometry corresponds to the Ackermann/Jeantaud description is often quoted although rarely defined. The authors use a description as given in Figure 7.7, which in turn uses the simplified form of equation (7.10).

The Ackermann/Jeantaud angles are calculated as given in equations (7.8) and (7.9). These are compared with the angles actually achieved by the front wheels. A fraction of the compensation is expressed for the outer wheel using δ_{mean} for the mean of the actual angles:

$$\textit{Ackermann fraction} = \frac{\delta_{o\_\text{actual}} - \delta_{\text{mean}}}{\left[L/\left[(180/\pi)(L/\delta_{\text{mean}}) + 0.5t\right]\right](180/\pi) - \delta_{\text{mean}}} \tag{7.11}$$

This is the quantity graphed in Figure 7.7 as '% Ackermann'. The values shown (around 40%) are typical for road cars. There exists some confusion over the significance of Ackermann geometry. For ride and handling work,

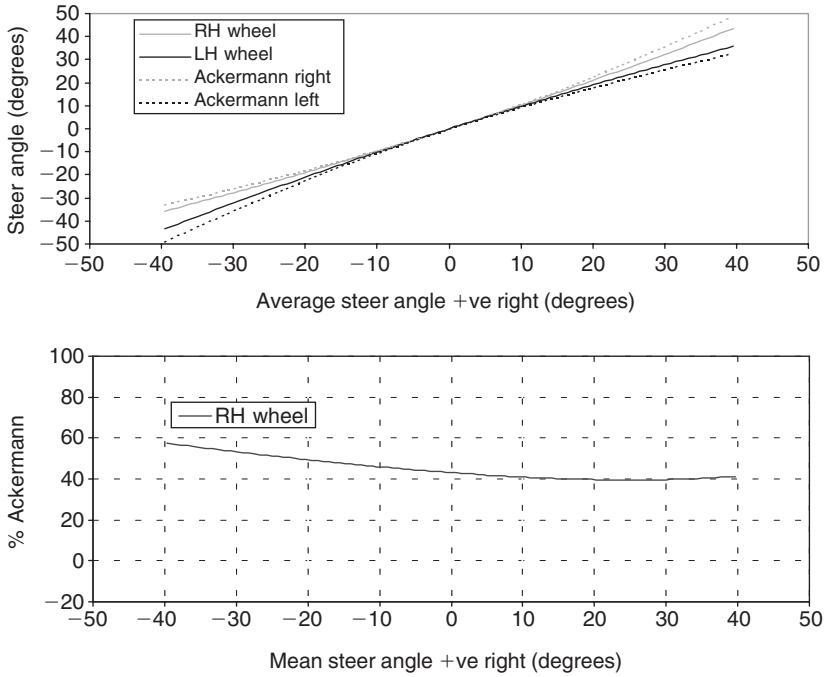

Fig. 7.7 Steering geometry in comparison with Ackermann/Jeantaud geometry

the significance is sometimes overstated. Considering Figure 7.5, a turn at 50 mph (22 ms^{-1}) road speed at 0.4g lateral acceleration may be calculated as producing a yaw rate of 10.2 degrees/second. For a 2.7 m wheelbase vehicle, this requires a mean steer angle of 1.26 degrees. The radius of turn is 123 m and so the Jeantaud modification gives 1.25018 degrees on the inner wheel and 1.26552 degrees on the outer wheel – an included angle of 0.015 degrees. For a typical cornering stiffness of 1500 N/degree, this gives a lateral force variation of 23 N between 0% Ackermann and 100% Ackermann. The lateral forces to achieve 0.4g at 50 mph are over 5900 N for a typical 1500 kg vehicle, so the Ackermann effect amounts for lateral forces of some 0.4% of the total – a small modifier on the vehicle as a whole.

The level of Ackermann effect does come into play at parking speeds, however. Typically, there is some inclination of the vehicle's steering axis when viewed from the front and side of the vehicle. These inclinations are known as castor and steer axis inclination (SAI), or kingpin inclination (KPI) respectively and are shown in Figure 7.8. Together with the offsets at ground level between the geometric centre of the wheel, these inclinations have the effect of moving the inboard wheel down and the outboard wheel up. Figure 7.9 shows the inboard wheel being moved down as it goes onto back lock. Given the constraint of the ground, this has the effect of imposing a roll moment on the vehicle that is reacted by the front and rear suspensions in series (Figure 7.10). The loading of the vehicle wheels becomes asymmetric.

This asymmetry is of the order of 10 N in a typical family saloon and is of little consequence. However, in a more stiffly sprung vehicle if the steering

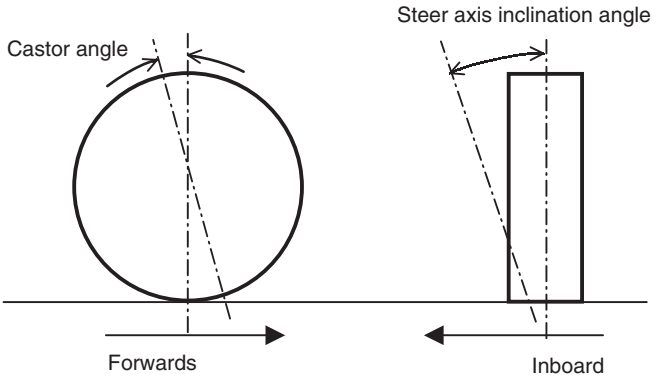

Fig. 7.8 Steer angle geometry definitions

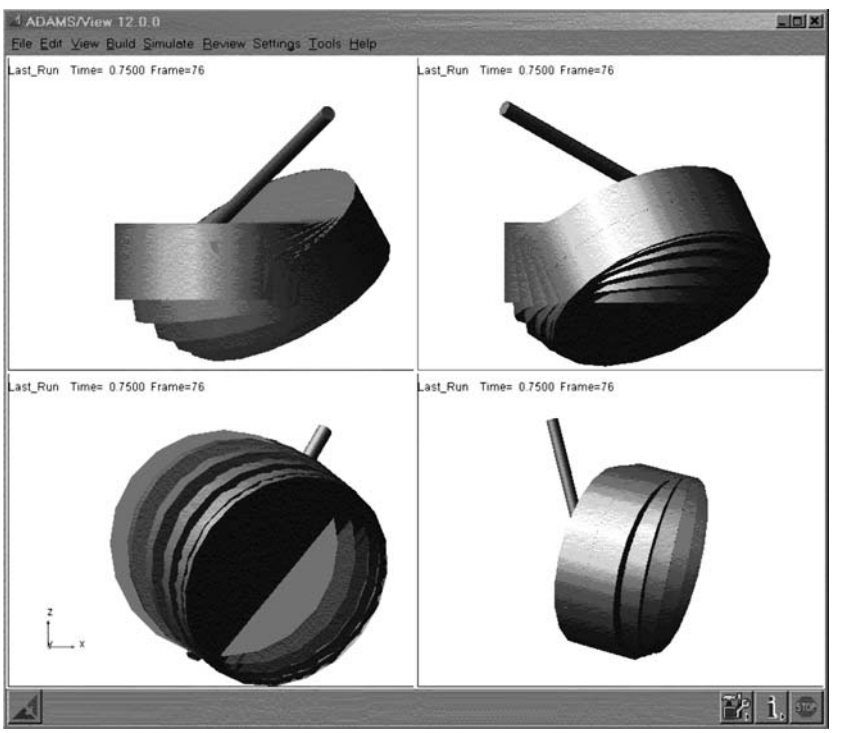

Fig. 7.9 Steering geometry effects on wheel vertical position: fully constrained body and suspension, model runs from straight ahead to full back lock. Plan view (top left) rear view (top right), left view (bottom left) and three-quarter view (bottom right) of front left wheel with steering axis indicated by cylindrical graphic. Note the steering geometry used is atypical for emphasis

geometry is not constructed with care, the asymmetry can be more than 100 N. If this loading is applied in conjunction with significantly low Ackermann fractions, the result is that the inner wheel is emphasized over the outer wheel.

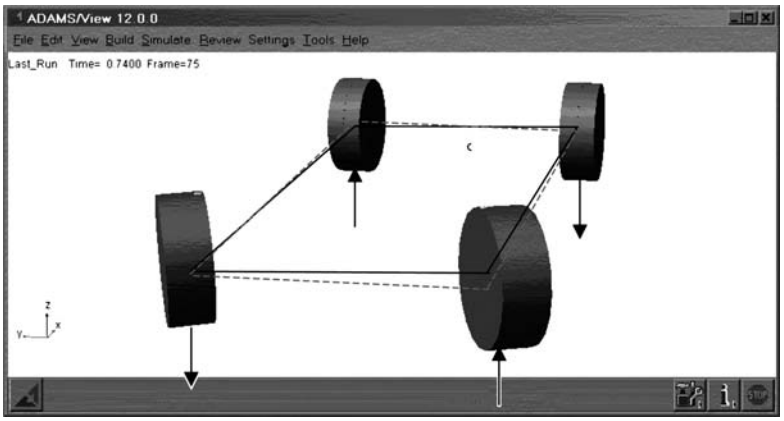

Fig. 7.10 Platform motion during steering at low speed (black) in comparison with the static platform position (grey dashed). Changes in wheel weight are indicated; front left wheel has an increased reaction force

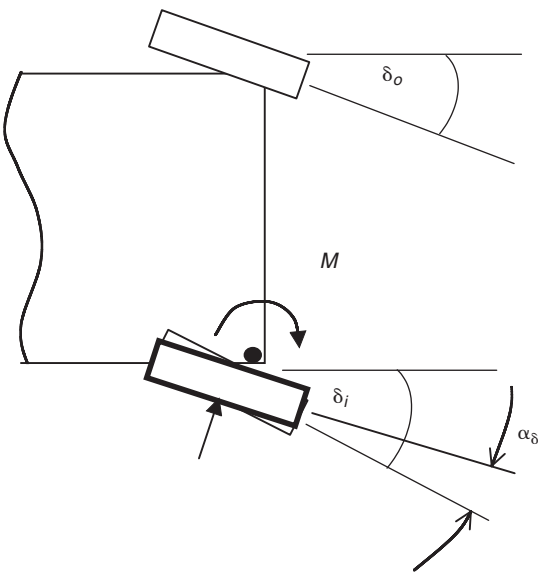

Fig. 7.11 Effect of inside wheel loading in producing an excess side force due to slip angle α_δ when the vehicle is in motion

This emphasis has the consequence of producing an effective side force from the tyre because it is operating at a comparatively large slip angle. Normally, side forces from both tyres work in opposition if the wheels are effectively toed in when the Ackermann fraction is less than unity. However, if the forces are not in balance (because of the weight imbalance between inboard and outboard tyres) the additional side force on the inboard tyre has the effect of reducing the steer aligning torque when the vehicle is in motion. If the Ackermann fraction is particularly low, the vehicle will have a 'wind on to lock' behaviour at car park speeds beyond certain steer angles.

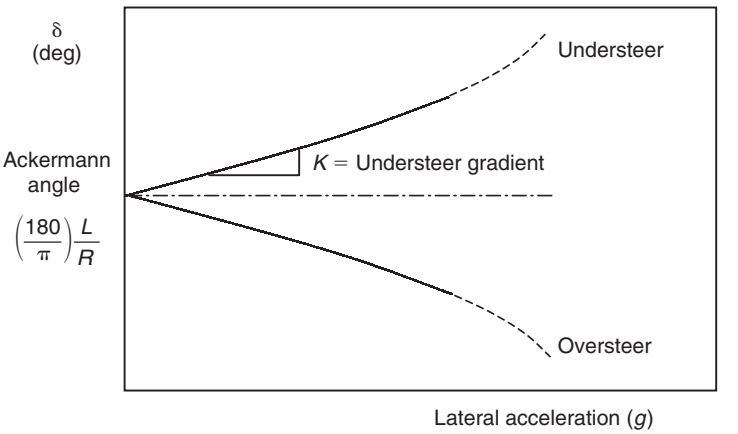

Fig. 7.12 Determination of understeer gradient (Gillespie, 1992)

Vehicles with stiff suspension, high steer axis angles and wide tyres are more prone to this effect.

Returning to the more general steady state cornering behaviour, the constant radius turn test procedure (ISO 4138), the procedure may be summarized as:

- Start at slow speed, find Ackermann angle.
- Increment speed in steps to produce increments in lateral acceleration of typically $0.1g$.
- Corner in steady state at each speed and measure steering inputs.
- Produce a graph similar to that shown in Figure 7.12.

Considering the diagram, two regions are apparent. In the 'understeer' region, more steer angle is necessary compared to the Ackermann angle to hold the chosen radius. This may not seem intuitive unless the view is taken that the vehicle steers less than is expected ('under' the Ackermann response) and more steer angle is needed to compensate for it. Similarly, the 'oversteer' region needs less steer angle compared to the Ackermann angle. If the oversteer is large, the steer might need to become negative to trim the vehicle in the steady state. For many, oversteer is marked by the use of steer in the opposite direction to the corner – so-called 'opposite lock'. However, the strict definition only requires that less steer than the Ackermann angle is applied – the transition to opposite lock merely marks a further degree of oversteer but there is nothing especially significant about the sign change. If the steer angle does not vary with lateral acceleration the vehicle is said to be 'neutral steering'.

At low lateral acceleration the road wheel angle δ can be expressed using (7.12):

$$\delta = \left(\frac{180}{\pi}\right)\frac{L}{R} + KA_y \tag{7.12}$$

where

δ = road wheel angle (deg)
K = understeer gradient (deg/g)
A_y = lateral acceleration (g)
L = wheelbase (m)
R = radius (m)

Note that the use of understeer gradient in degrees/g can be expressed at either the axle or the handwheel if appropriate regard is taken of the steering reduction ratio. For vehicle dynamicists it is easy to declare that the only measure of consequence is the axle steer; however, this is to ignore the subjective importance of handwheel angle to the operator of the vehicle. Note also that this parameter K is not to be confused with the more common 'stability factor' K as developed by Milliken and Segel and used later in this chapter.

Olley makes an important distinction between what he calls the primary effects on the car affecting the tyre slip angles and secondary effects affecting handwheel angles and body attitudes, which are acutely sensed by the operator (Milliken and Milliken, 2001). Perhaps the biggest source of difficulty between practical and theoretical vehicle dynamicists is that the large modifiers of the primary vehicle dynamics are generally fixed by the time the practical camp get their hands on a vehicle and so are not considered by them; the secondary modifiers used to great effect to deliver the required subjective behaviour of the vehicle for its marketplace are frequently overlooked by the theoretical camp as being 'small modifiers' despite being important to the emotional reaction of the driver to the vehicle. For this entirely prosaic reason it is common that members of each fraternity understand little of what goes on in the other.

7.3.3 Some further discussion of vehicles in curved path

Below the limiting yaw rate it is tempting to think that for a real vehicle the behaviour is largely geometric in nature (Figure 7.13). This is essentially a repeat of the Ackermann diagram in Figure 7.5 and equation (7.5).

The geometric yaw rate is achieved by some notional vehicle that may be thought of as running on 'blade' wheels on indestructible ice – no sideslip

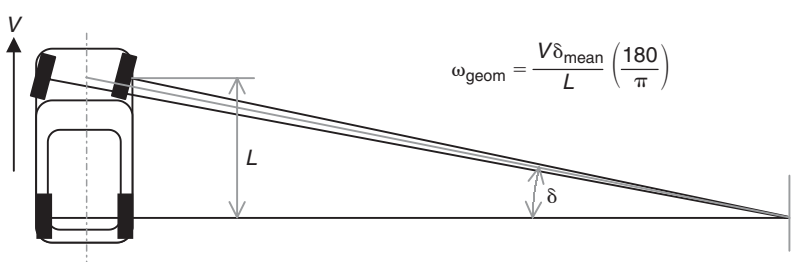

Fig. 7.13 Geometric yaw rate expectations

of the wheels is possible. It is important for vehicle dynamicists to remember that the overwhelming majority of the driving population genuinely believe this is the way in which their vehicles function. For many typical drivers, the belief exists that the tyres are little miniature 'rails' that the vehicle carries around with itself to 'lay tracks' as it goes along.

In order to express something useful from the infinite number of combinations of speed and steering angle that exist, the notion of a 'gain' becomes helpful – an output divided by an input. Thus for a purely geometric vehicle, the Yaw Rate Gain (*YRG*) could be expressed as

$$YRG_{\text{geom}} = \frac{\omega}{\delta_{\text{mean}}} = \frac{V}{L} \tag{7.13}$$

This may be recognized as describing the low speed region of Figure 7.6. The higher speed region, even with a simplistic Newtonian friction model, can be seen to have a non-linear *YRG* characteristic (Figure 7.14) since it is possible to turn the front wheels to an angle that corresponds to a yaw rate greater than that which the vehicle can achieve. The similarity between Figures 7.6 and 7.14 should be apparent to the reader.

As previously noted, when a vehicle yaws less than expected, the term 'understeer' is used – the response of the vehicle is less than ('under') what might have been expected. When a vehicle yaws more than expected, the term 'oversteer' is used – the response of the vehicle exceeds (is 'over') what might have been expected. So far only mechanisms for generating understeer have been discussed. Remaining with the Newtonian friction to describe the behaviour of the tyres, one further fundamental point is worth establishing. For a vehicle travelling in a circular path, forward speed, V, yaw rate, ω, and lateral (centripetal) acceleration, A_y, are related with

$$A_y = \omega V \tag{7.14}$$

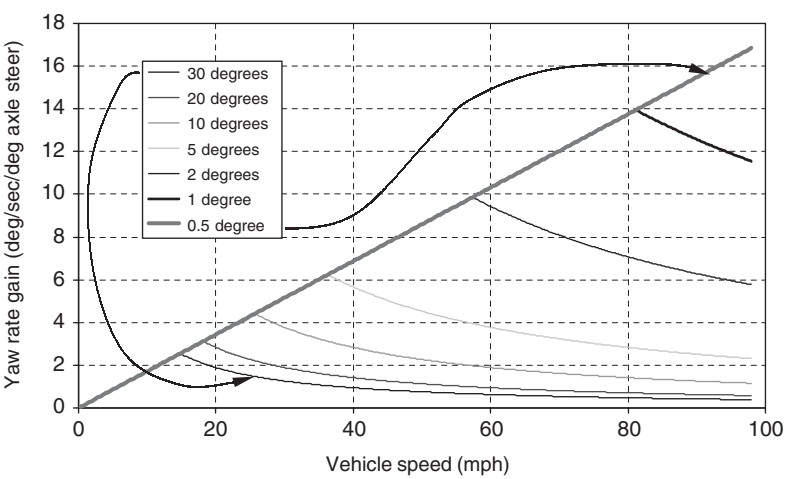

Fig. 7.14 Yaw rate gains for an idealized vehicle with Newtonian friction

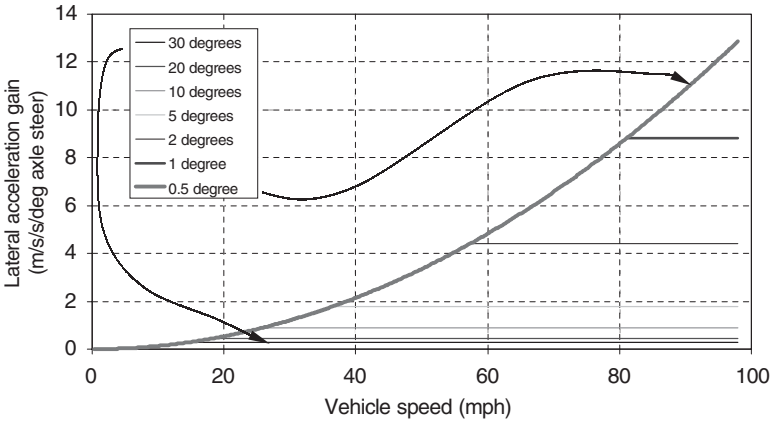

Fig. 7.15 Lateral acceleration gains for an idealized vehicle with Newtonian friction

Using the preceding relationship for geometric yaw rate gain, a geometric lateral acceleration gain (AyG_{geom}) can be deduced for the geometric vehicle in the region where

$$AyG_{\text{geom}} = \frac{A_y}{\delta_{\text{mean}}} = \frac{\omega_{\text{geom}} V}{\delta_{\text{mean}}} = V^2 L \tag{7.15}$$

At high speeds it can be seen that axle steer inputs of much in excess of half a degree cause the available friction to saturate and that to retain proportional control, the driver must keep inputs below this level. For this reason, quite high reduction ratios are generally used in steering gears to give a reasonable level of input sensitivity at the handwheel. For a European passenger car, a reduction ratio of around 16–18:1 is typical (16 degrees of handwheel giving 1 degree of axle steer), meaning that at the highest speeds shown in Figures 7.14 and 7.15 handwheel inputs of 10–20 degrees are enough to saturate the vehicle with respect to the available friction in a high grip environment. For vehicles travelling faster – for example, on unrestricted autobahns or competition vehicles – it can be seen that the overall steering ratio is of importance in order not to have the vehicle overly sensitive to driver inputs. There is, however, a trend among vehicle manufacturers to fit numerically lower steering ratios over time – compare a 1966 Ford Cortina at 23.5:1 with its current cousin the Focus at 17.5:1 – to promote a perception of agility. This fashion will require the adoption of more adventurous variable steering ratios (for example, as promoted by Bishop Technologies or as implemented by BMW and ZF in the 2003 5 series 'Active Front Steer' system) in order to retain sensitivity at high speeds. In low-grip environments, the handwheel inputs needed to saturate the vehicle at speed are tiny, scaling down with coefficient of friction, μ.

The range of lateral acceleration gains, from $0.6\,\text{ms}^{-2}$/degree at 20 mph to $12.9\,\text{ms}^{-2}$/degree at 100 mph, is quite a wide range to ask the driver to accommodate. When high speed road systems lack curves of any kind there is no feedback information to allow the driver to adapt and so extremely straight designs of roads are unhelpful in this respect. Thus it is often true that normal drivers get into difficulty when faced with an emergency evasive

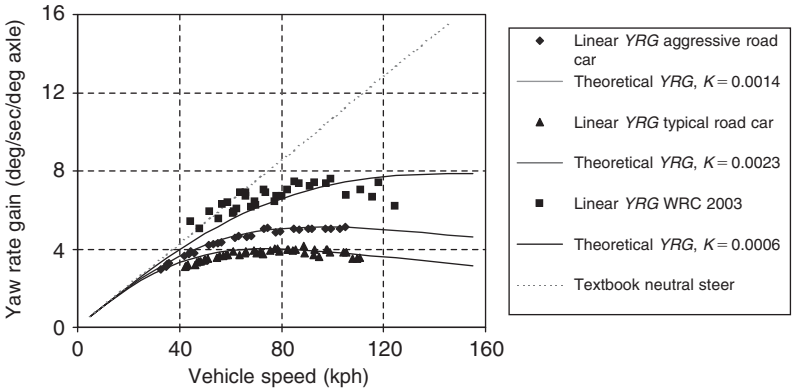

Fig. 7.16 Yaw rate gain characteristics for three different vehicles. The stability factor, *K*, is defined later in the text

manoeuvre at high speed. Some component of this is simply because the saturation (in terms of grip) at a comparatively low yaw rate of the car surprises the driver. Typically, road infrastructures are constructed so as not to need high lateral accelerations at high speeds. For normal drivers the difficulty is largely masked in day-to-day driving, which contributes to some complacency. In general, vehicles are tuned to have reduced *YRG* (and hence *AyG*) at higher speeds to compensate for this problem. The level of this tuning differs widely between different markets.

7.3.4 The subjective/objective problem

As suggested in the opening chapter, there are two strongly divided camps in the vehicle dynamics field – practitioners and theoreticians. One of the reasons for the difficulties between the two camps is the use of common vocabulary with different meanings. On the theoretical side, for example, there are clear definitions of such basic terms as 'understeer' and 'oversteer'. Subjectively, these terms are used to describe quite different behaviours.

Understeer and oversteer have been defined in section 7.3.3 as yaw rates under and over what might be expected, respectively. The subjective/objective problem has a great deal to do with *the nature of the expectation*.

Objectively, what is expected is the 'idealized' or 'geometric' yaw rate (Figure 7.14). At the lowest vehicle speeds this corresponds very closely with the performance of the actual vehicle, as noted earlier. As vehicle speeds rise then the frictional limitations on yaw rate mean the vehicle is unable to achieve the geometric yaw rate for large steering angles. For typical road vehicles, further modifications to the characteristics of the vehicle are performed to further reduce the yaw rate gain even when the tyres are not saturated. Figures 7.16 and 7.17 compare two road cars with a non-winged competition car.

Objectively, understeer (*US*) is when the actual yaw rate is less than the idealized yaw rate and is often expressed as the ratio of the two:

$$US = \frac{\omega_{\text{geom}}}{\omega} \tag{7.16}$$

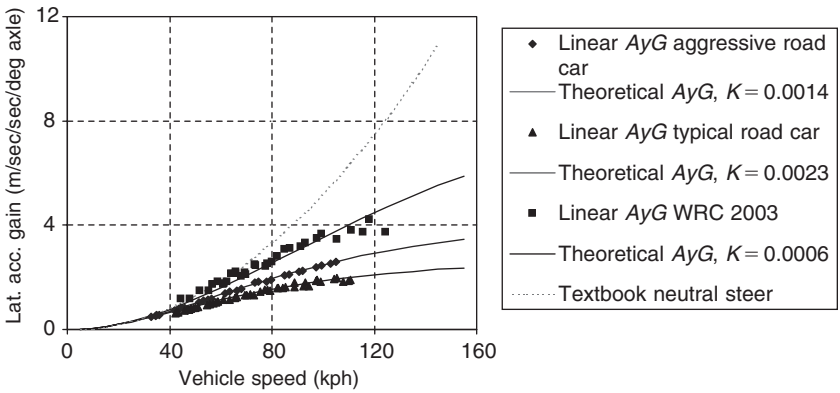

Fig. 7.17 Lateral acceleration gain characteristics for three different vehicles

If *US* is greater than unity, the vehicle is understeering and if *US* is less than unity the vehicle is oversteering. A vehicle that produces the geometric yaw rate is described as 'neutral steering' and is often regarded as something of a holy grail. However, for all the reasons described in section 7.3.3 it is rarely engineered in vehicles. In Figure 7.16, all three cars understeer in their linear regions. The range of lateral acceleration gains is greatly reduced for the understeering road car in Figure 7.17, requiring less skilful adaptation to vehicle behaviour as speed varies compared with a textbook neutral steer vehicle. For the competition car the lateral acceleration gain can be seen to be substantially linear with speed.

Subjectively, drivers instinctively learn these base characteristics of vehicles very quickly. Only the most inexperienced novice drivers have difficulty with the steering ratios being higher or lower than expected. Within a few hours of driving experience, errors in steering (as distinct from positional errors caused by the size of the vehicle) are almost entirely absent. When the vehicle is driven at low lateral accelerations (i.e. when there is significant grip in reserve) the vehicle behaves in a substantially linear fashion – i.e. more steering gives more yaw rate in a proportional manner. Under these conditions, vehicles are rarely evaluated as 'understeering' although the vast majority of road cars do in fact understeer at highway speeds. These gains (both yaw and lateral) become the 'datum' condition, which is often rendered as 'neutral' when described subjectively. Differences between vehicles, in particular with yaw rate gain, are likely to be ascribed to differences in steering ratio and not differences in fundamental vehicle behaviour.

As lateral accelerations rise towards some significant fraction of the available coefficient of friction (typically above 50–60% of μ), the vehicle behaviour becomes non-linear due to the behaviour of the tyres. Depending on suspension geometry, tyre characteristics, elasto-kinematic behaviour of the suspension and suspension calibration, the yaw rate characteristics in the non-linear region can vary in either direction – either up or down – from the linear characteristics. Of particular interest is the relationship between lateral acceleration and yaw rate gains in the non-linear region. Figure 7.18 graphically suggests three possibilities for the departure from linearity for a vehicle. The situation imagined is that a vehicle has been driven steadily

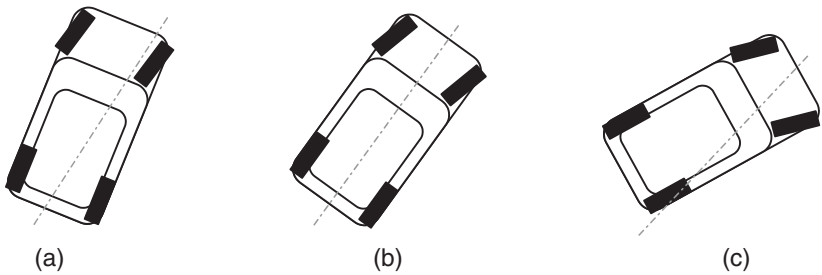

Fig. 7.18 Possibilities for departure from linearity

close to the subjective linearity limit and then the vehicle speed is increased in order to increase the lateral acceleration. The increase in vehicle speed is gradual and so details such as driveline layout are not relevant because the drive torque is low. This situation might occur, for example, on a long, constant radius, downhill motorway interchange 'cloverleaf'.

The three scenarios illustrated in Figure 7.18 can be summarized as:

(a) reduced *AyG* and further reduced *YRG*

(b) reduced *AyG* and *YRG* in proportion to each other

(c) reduced *YRG* and further reduced *AyG*

In scenario (a), yaw rate gain is reduced further than lateral acceleration gain. In order to accommodate the changes in both lateral acceleration and yaw rate, the radius of the path must increase and so the vehicle has a period of adjustment to a new, wider line in the curve. Most drivers notice this and instinctively reduce vehicle speed to restore the desired path over the ground. It is described subjectively as an 'understeer departure' or 'pushing' or perhaps in the USA as 'plowing' (ploughing). If uncompensated, it leads to a vehicle departing the course (road, track, etc.) in an attitude that is basically forwards. This is by far the most common behaviour for road vehicles. It is desirable since, if the vehicle does leave the road, it is least likely to roll over and will correctly present the engineered crash structure between the occupants and any obstacles encountered. For sporty drivers the sensation of the vehicle 'turning out' of the corner as it departs from linearity can become tiresome.

In scenario (b), lateral acceleration and yaw rate gain change in some connected manner and the vehicle will maintain course although it might need some modification to steering input. Subjectively this vehicle will be described as 'neutral' although objectively it might well be understeering. Excess speed for a curve will lead to the vehicle running wide but with no sense of 'turning out of the curve'. Such a vehicle generally feels benign although the progressive departure can mean it is unnoticed by inattentive drivers. Enthusiastic drivers will not be so frustrated by this behaviour.

In scenario (c), lateral acceleration gain reduces more than yaw rate gain. This leads to an 'over-rotation' of the vehicle when viewed in plan. Depending on the severity of the mismatch, the change may lead to a spin out of the curve. From inside the vehicle there is a pronounced sense of the rear end

of the vehicle departing first but objectively the vehicle may not actually oversteer in the classical sense – it may simply move 'towards neutrality'. This is the nature of rear-wheel-drive vehicles when driven to departure using the throttle. Subjectively, there is a pronounced sense of 'oversteer' – sometimes described as 'loose' in the USA. Vehicles that preserve yaw rate gain as they lose linearity are widely regarded as fun to drive and sporty.

A further difficulty between theoretical and practical dynamicists is that the former group often consider the vehicle on the basis of 'fixed control' and 'free control' where the latter almost always use 'driver input to complete a set task'. With fixed and free control, the inputs are consistent and the response of the vehicle is used to evaluate it. With driver input, the vehicle response is substantially constant and the vehicle is evaluated on the basis of the required changes in driver input to complete a task. More and more, so-called 'black lakes' – large flat areas of high grip surface – are being added to vehicle testing facilities to allow the evaluation of fixed and free control manoeuvres for experimental correlation purposes. Also gaining in popularity are theoretical 'driver models'. These range from simple path-followers to sophisticated multi-loop, multi-pass adaptive controllers. At present there are many such models and none has gained precedence, suggesting perhaps that none is ideal for the task at hand – understanding and improving vehicle behaviour. Methods for modelling driver behaviour are discussed in Chapter 6. A very real problem with such models is that there is a fine line between evaluating the quality of the driver model and evaluating the change on the vehicle. Did the vehicle performance improve because the modification suited the driver model? Does that behaviour reflect a typical driver in an emergency situation? These criticisms are not unique to modelling and can also be levelled at highly skilled development drivers. Indeed, within motorsport circles this particular difficulty is widely recognized. There are drivers who can drive a given setup in the fastest way that it can be driven but who cannot articulate how the vehicle could be faster. Such drivers are an asset on race days but less so during development testing. For this reason, 'test' or 'development' drivers are frequently employed who have a different set of skills to event drivers.

In summary then, the subjective evaluation of a vehicle depends largely on the nature of its departure from linearity while objective evaluation is an absolute positioning against a neutral datum. From inside the vehicle it is generally difficult to distinguish between a vehicle that is operating at a large body slip angle and one that is truly oversteering. In any case, to control a large body slip angle it is frequently necessary to reduce or reverse steering input ('opposite lock'), changing the measured yaw rate gains substantially towards oversteer.

7.3.5 Mechanisms for generating under- and oversteer

To understand the vehicle parameters that have an influence on oversteer, understeer and departure behaviour, we can use the roll stiffness model described earlier to consider a series of free bodies and the force moment balance on each during steady state cornering. Figure 7.19 shows a version of the roll stiffness model while travelling in a curved path, with a lateral acceleration A_y.

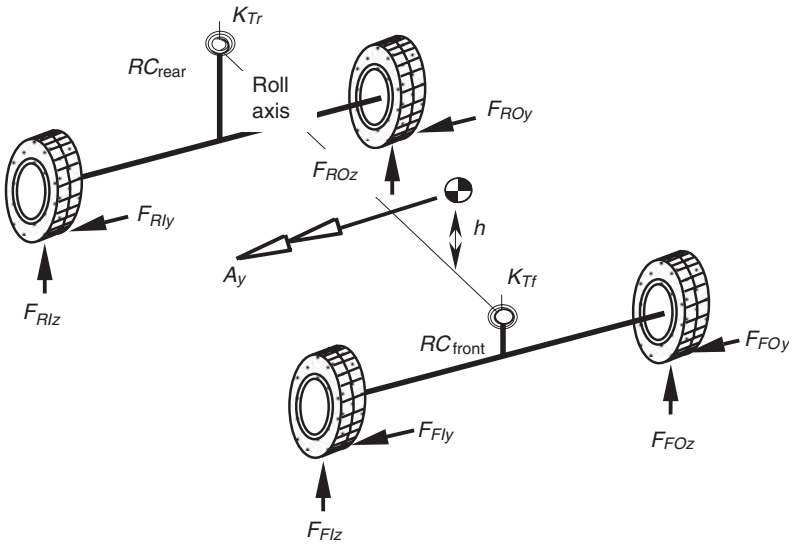

Fig. 7.19 Free-body diagram roll stiffness model during cornering

Consider next the components of force and moment acting on the vehicle body in isolation.

Using the roll stiffness model as the basis for the analysis we are treating the body as a single rigid axis with forces and moments transmitted from the front and rear suspensions (axles) at points representing the front and rear roll centres as shown in Figure 7.20. Consider the forces and moments acting on the vehicle body rigid roll axis. Note that we are ignoring the inclination of the roll axis. A roll moment ($mA_y \cdot h$) acts about the axis and is resisted in the model by the moments M_{FRC} and M_{RRC} resulting from the front and rear roll stiffnesses K_{Tf} and K_{Tr}:

$$F_{FRCy} + F_{RRCy} - mA_y = 0 \tag{7.17}$$

$$M_{FRC} + M_{RRC} - mA_y \cdot h = 0 \tag{7.18}$$

The roll moment causes weight transfer between inner and outer wheels (Figure 7.21). Taking moments for each of the front and rear axles shown gives:

$$\Delta F_{FzM} = \frac{M_{FRC}}{t_f} = ma_y \cdot h\left(\frac{K_{Tf}}{K_{Tf} + K_{Tr}}\right)\frac{1}{t_f} \tag{7.19}$$

$$\Delta F_{RzM} = \frac{M_{RRC}}{t_r} = ma_y \cdot h\left(\frac{K_{Tr}}{K_{Tf} + K_{Tr}}\right)\frac{1}{t_r} \tag{7.20}$$

It can be seen from equations (7.19) and (7.20) that if the front roll stiffness K_{Tf} is greater than the rear roll stiffness K_{Tr} there will be more weight transfer at the front (and vice versa). It can also be seen that an increase in track

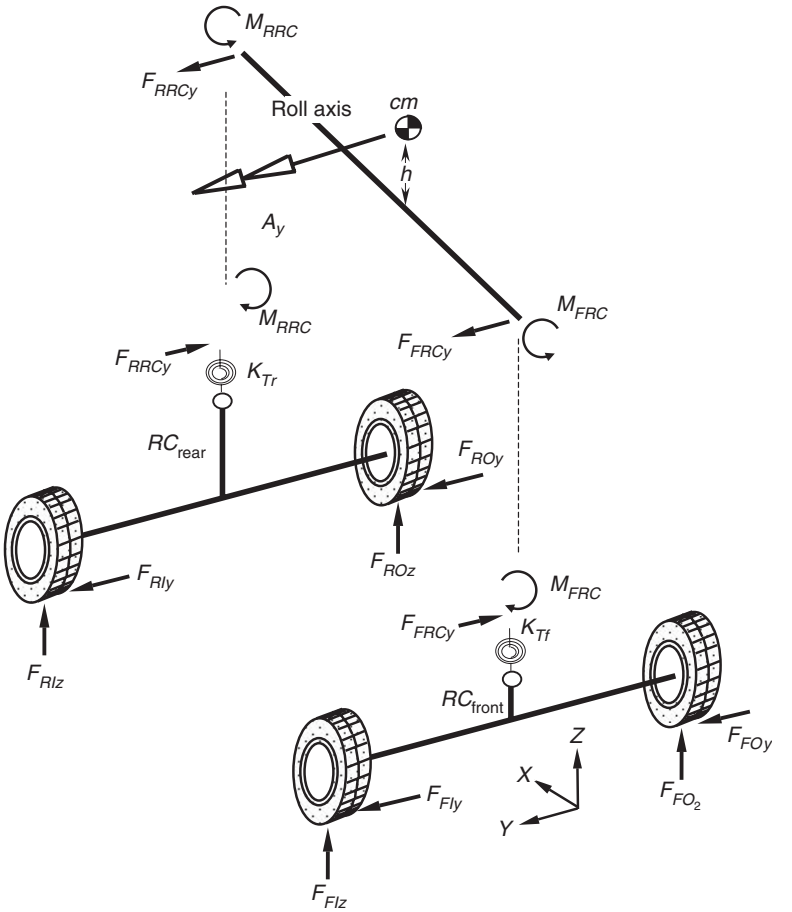

Fig. 7.20 Forces and moments acting at the roll axis

will reduce weight transfer. Consider again a free-body diagram of the body roll axis and the components of force acting at the front and rear roll centres.

This gives:

$$F_{FRCy} = ma_y \left(\frac{b}{a+b} \right) \tag{7.21}$$

$$F_{RRCy} = ma_y \left(\frac{a}{a+b} \right) \tag{7.22}$$

From equations (7.21) and (7.22) we can see that moving the body centre of mass forward would increase the force, and hence weight transfer, reacted through the front roll centre (and vice versa). We can now proceed to find the additional components, ΔF_{FzL} and ΔF_{RzL}, of weight transfer due to the lateral forces transmitted through the roll centres.

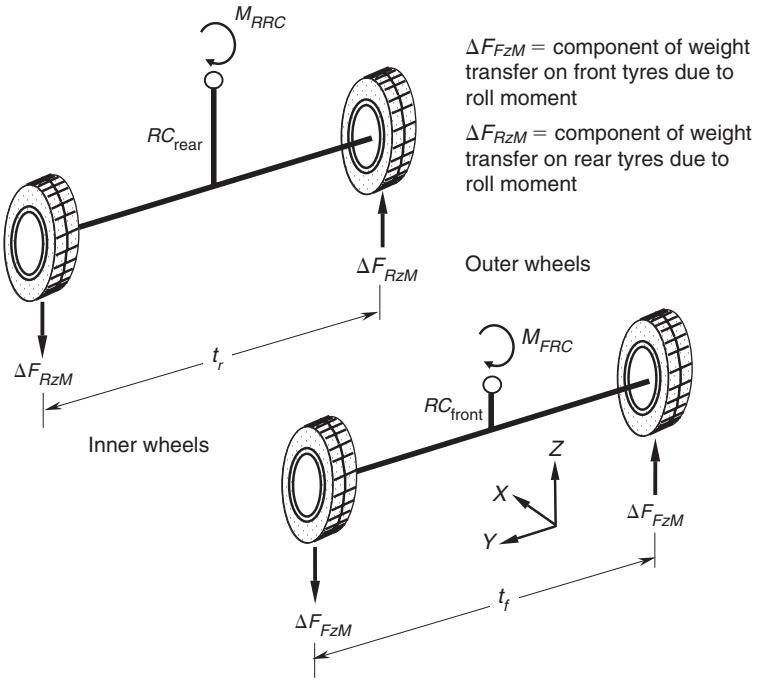

Fig. 7.21 Components of weight transfer due to roll moment

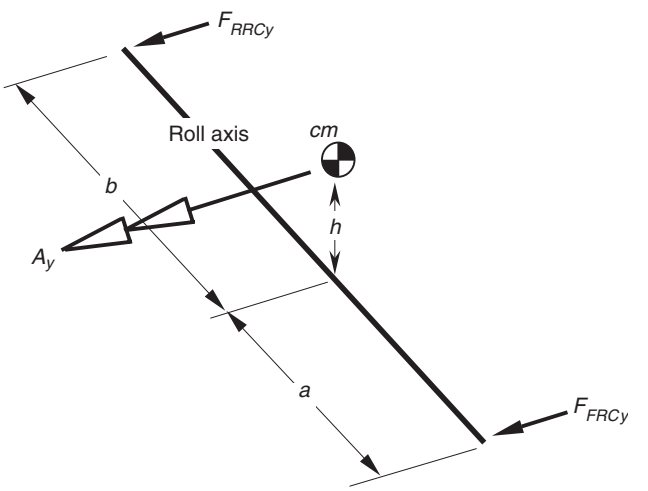

Fig. 7.22 Forces acting on the body roll axis

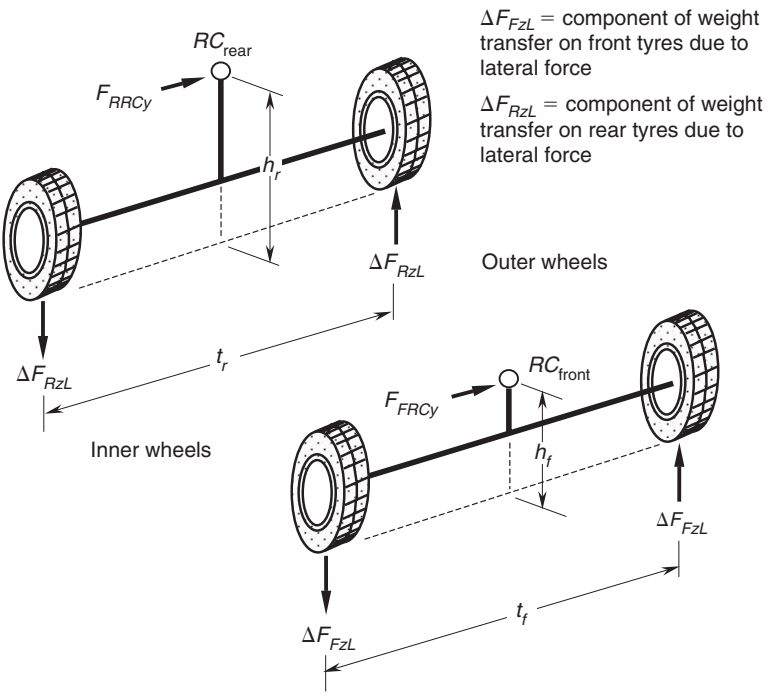

Fig. 7.23 Components of weight transfer due to lateral force

Taking moments again for each of the front and rear axles shown in Figure 7.23 gives:

$$\Delta F_{FzL} = F_{FRCy}\left(\frac{h_f}{t_f}\right) = ma_y \cdot h\left(\frac{b}{a+b}\right)\left(\frac{h_f}{t_f}\right) \tag{7.23}$$

$$\Delta F_{RzL} = F_{RRCy}\left(\frac{h_r}{t_r}\right) = ma_y \cdot h\left(\frac{a}{a+b}\right)\left(\frac{h_r}{t_r}\right) \tag{7.24}$$

It can be seen from equations (7.23) and (7.24) that if the front roll centre height h_f is increased there will be more weight transfer at the front (and vice versa).

We can now find the resulting load shown in Figure 7.24 acting on each tyre by adding or subtracting the components of weight transfer to the front and rear static tyre loads (F_{FSz} and F_{RSz}).

This gives:

$$F_{FIz} = F_{FSz} - \Delta F_{FzM} - \Delta F_{FzL} \tag{7.25}$$

$$F_{FOz} = F_{FSz} + \Delta F_{FzM} + \Delta F_{FzL} \tag{7.26}$$

$$F_{RIz} = F_{RSz} - \Delta F_{RzM} - \Delta F_{RzL} \tag{7.27}$$

$$F_{ROz} = F_{RSz} + \Delta F_{RzM} + \Delta F_{RzL} \tag{7.28}$$

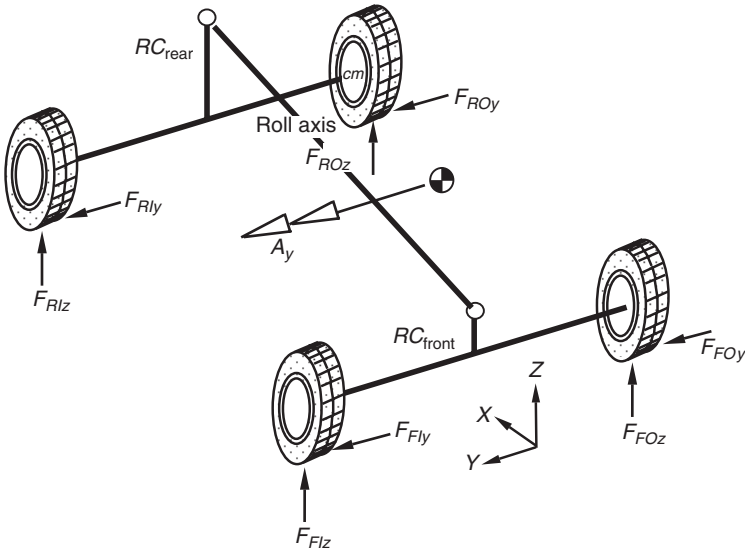

Fig. 7.24 Resulting forces acting at the inner and outer tyres

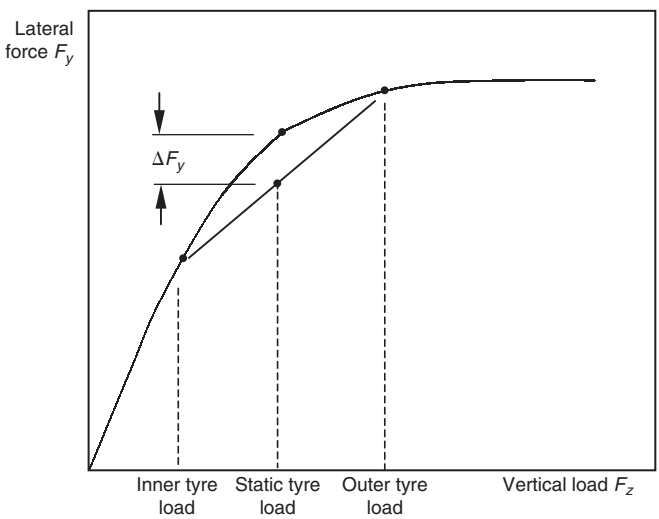

Fig. 7.25 Loss of cornering force due to non-linear tyre behaviour

At this stage we must consider the tyre characteristics. The tyre cornering force F_y varies with the tyre load F_z but the relationship is not linear (as shown in Chapter 5).

Figure 7.25 shows a typical plot of tyre lateral force with tyre load at a given slip angle. The total lateral force produced at either end of the vehicle is the average of the inner and outer lateral tyre forces. From the figure it can be seen that ΔF_y represents a theoretical loss in tyre force

resulting from the averaging and the non-linearity of the tyre. Tyres with a high load will not produce as much lateral force (in proportion to tyre load) compared with other tyres on the vehicle.

More weight transfer at either end therefore reduces the total lateral force produced by the tyres and causes that end to drift out of the turn. It should be noted that this behaviour is true for all slip angles of interest; at low slip angles, the cornering stiffness of the tyre is reduced non-linearly with increasing load, promoting a larger slip angle at an axle with a greater roll moment. At saturated slip angles, the peak lateral force is reduced as a proportion of the vertical load, producing a lower coefficient of friction for an axle with a greater roll moment. Thus mechanisms that adjust sub-limit under- and oversteer also adjust departure plough and spin behaviour.

Although substantially simplified, the preceding analysis helps with understanding the essential mechanisms in play when a vehicle is cornering.

7.4 Transient effects

Vehicle dynamics would be a very simple field if the preceding text described it entirely. However, the pneumatic tyres in use have some features that add complication. The most significant of these is the need for the tyres to have a slip angle in order to generate a lateral force. This can be seen intuitively to lead to the need for a slip angle of the body as a whole (Figure 7.26).

The need for a body slip angle gives rise to an additional yaw rate, rotating the body to the correct slip angle, for a brief period near the start of any manoeuvre. There is also a corresponding yaw rate reduction at the end of a manoeuvre required to bring the vehicle back to its trimmed, straight-ahead state. *These variations in yaw rate are acutely remarked by even the least skilled driver and greatly influence the emotional reaction of the driver to the car – although the driver might not consciously recognize it.*

A vehicle that rotates slowly to give the required body slip angle feels sluggish and unresponsive; a vehicle that overshoots and oscillates feels lively and poorly controlled. Subjectively, these two states might be described as

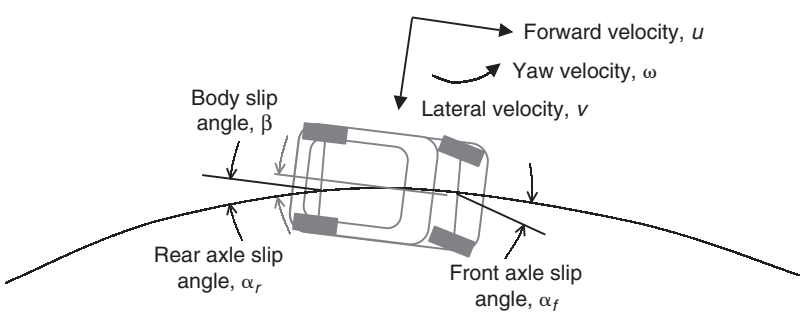

Fig. 7.26 Pneumatic tyres give rise to the need for a body slip angle

'transient understeer' and 'transient oversteer' respectively – although the latter might not objectively be oversteer, it is certainly a greater yaw rate than might be expected. Objectively, the quantity of interest is the rate of change of body slip angle, known as β or 'beta-dot'. The bulk yaw rate of the vehicle is made up of two components: the first is the yaw rate associated with a curved path – it might be thought of as the yaw rate that would be experienced by a stone on a string being swung around. Milliken and others refer to this as the 'no-slip yaw rate' – the yaw rate predicted without any body slip angle. The second is the beta-dot component. By inspection, it can be seen that:

$$\dot{\beta} = \frac{A_y}{V} - \omega \tag{7.29}$$

Thus in general, beta-dot is available as a simple combination of vehicle states, particularly during multibody simulation work. For real vehicles, noise on accelerometer data and the difficulty of knowing the genuine forward speed of the vehicle under conditions of longitudinal tyre slip mean that beta-dot is difficult to discern in real time, although it is amenable to offline processing.

With changes in suspension configuration, elasto-kinematic calibration and damper behaviour, beta-dot can be modified significantly. The overall behaviour of the vehicle may well only be slightly modified and so to concentrate merely on bulk yaw rate would be to underestimate the significance of the change from the driver's perspective.

In the steady state, the body slip angle is constant and so it is of little consequence except when something changes. In practice, real vehicles spend very little time in the steady state and so the short-lived events – described as 'transients' – are very important to the driver's reaction to the vehicle because of the acute perception of beta-dot. This perception is not only in terms of absolute levels but also in terms of delays between driver requests and vehicle response. When the handwheel is in motion, the driver is implicitly requesting a change in body slip angle, since body slip angle is linked to lateral acceleration. If the change in body slip angle occurs in a way that is substantially connected to the change in steering, the driver feels reassured. If, however, the change in body slip angle occurs with perhaps a significant delay or perhaps with a characteristic shape different to the steer rate, the driver forms an impression that the vehicle has 'a mind of its own'. This leads to poor subjective ratings for handling confidence whatever the objective measures might say. Thus the correlation between steer rate and beta-dot is a useful one in measuring improvements in vehicle behaviour using theoretical models and real vehicles alike.

Transients are also important to the objective behaviour of the whole vehicle. Under circumstances of a steering reversal, particularly at or near the grip limit, there is a substantial increase in yaw rate transiently. To understand this, imagine the vehicle travelling in a steady curve with a body slip angle of, say, 5 degrees. Now imagine the steering is reversed to produce a lateral acceleration in the other direction with a corresponding slip angle of -5 degrees. If the adjustment of the body slip angle took place over a 1 second period, this would make a transient yaw rate of 10 degrees/second.

Considering Figure 7.6, it can be seen this is a substantial proportion of the total available yaw rate at speeds over about 50 mph. If the steady state lateral acceleration produced a yaw rate of, say, 15 degrees/second (below the friction limit) then the addition of 10 degrees/second transient yaw rate would be more than the vehicle is capable of sustaining. For this reason alone, vehicles that converge (i.e. settle to a steady state solution) under normal conditions may well become unstable (spin) under conditions of steer reversal. Therefore any studies of transient vehicle dynamics must at some stage consider responses to steer reversals.

Vehicle mass and particularly inertia properties are a modifier to vehicle behaviour. There is a popular belief that the minimum mass moment of inertia in yaw is the best. However, this is not necessarily so. To understand this, consider a vehicle manoeuvring in the ground plane, which may be described by the classical 2-degree-of-freedom formulation:

$$C_{\alpha f}\alpha_f a - C_{\alpha r}\alpha_r b = \dot{\omega} I_{zz} \tag{7.30}$$

$$C_{\alpha f}\alpha_f + C_{\alpha r}\alpha_r = mu\omega + m\dot{v} \tag{7.31}$$

At the moment of turn-in, yaw rate ω and rear slip angle α_r are both zero. Assuming a constant acceleration solution for the differential equations (a reasonable assumption for the first few moments of a turn-in event or following a disturbance at the front axle), the response of the builds in the manner given in equations (7.32) and (7.33):

$$\omega = \frac{C_{\alpha f}\alpha_f at}{I_{zz}} \tag{7.32}$$

$$v = \frac{C_{\alpha f}\alpha_f t}{m} \tag{7.33}$$

Combining these quantities gives an instant centre at a distance c behind the mass centre:

$$c = \frac{v}{\omega} = \frac{(C_{\alpha f}\alpha_f t)/m}{(C_{\alpha f}\alpha_f at)/I_{zz}} = \frac{I_{zz}}{ma} = \frac{mk^2}{ma} = \frac{k^2}{a} \tag{7.34}$$

Expressing the distance c as a fraction of the distance to the rear axle b leads to

$$\frac{c}{b} = \frac{k^2}{ab} \tag{7.35}$$

This quantity may be recognized as the 'Dynamic Index' (*DI*) defined by the SAE and used to good effect by Olley, albeit in pitch rather than yaw. Its importance for vehicle behaviour is that a *DI* less than unity results in an increase in lateral velocity at the rear axle, and hence an increase in slip angle at the rear tyres (Figure 7.26). If *DI* is greater than unity then lateral velocity – and hence slip angles – are reduced. In a situation where the

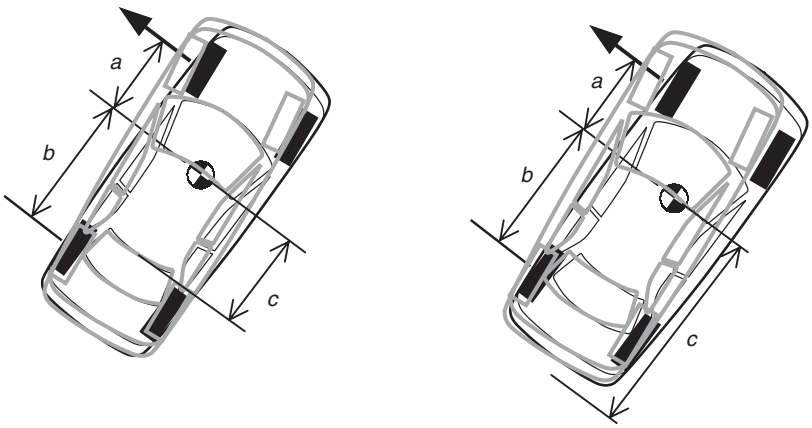

Fig. 7.27 Dynamic Index influences the centre of rotation of the vehicle in yaw

vehicle is cornering at the critical slip angle, it can be seen that a *DI* less than unity will increase the rear slip angle and therefore reduce the cornering force available at the rear axle – promoting the tendency to spin. Low yaw inertia does indeed promote agility and speed of response, but excessively low inertia – as quantified by *DI* – makes the car difficult even for skilled drivers to manage in yaw. There is thus a trade-off between response and ease of control; for a broad spectrum of vehicles from the Mk 1 Lotus Elan to the BMW M5, this trade-off is a *DI* of just over 0.9. Motorsport vehicles differ significantly from road cars and the exact figures are jealously guarded. It can be seen with some reflection that a low-mass mid-engined car errs towards a *DI* that is 'too low' since the wheels have to be a certain distance from each other to accommodate engine and passengers. The interested reader is invited to compare the mass and wheelbase of a Fiat X/1-9 and an MG-F.

In general, an important goal for vehicle dynamicists is to have the vehicle 'look after itself' from a body slip angle point of view. Most drivers have no conscious knowledge of body slip angle and beta-dot until they become large. The authors estimate that a body slip rate of less than around 5 degrees/second is probably the threshold between subconscious and conscious awareness of body slip rate, but this is necessarily extremely sensitive to context. This means that a body slip angle of 5 degrees or more can develop more or less unnoticed by a typical driver. In general, body slip angles of greater than 10 degrees are difficult for the majority of the driving population to recover control from, and so 5 degrees represents something 'halfway to irrecoverable'. When the body slip rate and/or angle exceeds some threshold, drivers suddenly become aware that something is amiss and so they report that vehicles 'abruptly' skid because the event was well developed before they recognized it. For this reason, an unexpected skid during otherwise normal driving can be surprisingly traumatic and leave people with a large amount of anxiety since they felt 'ambushed' by the vehicle. Drivers become sensitized and acclimatized to variations in body slip rate and angle through familiarity and for this reason, skid pan training for normal drivers is an excellent idea.

7.5 Steering feel as a subjective modifier

A further difficulty for theoretical dynamicists is the question of steering 'feel'. Subjectively, impressions of vehicle behaviour are gathered to a significant extent through the handwheel, whether consciously or subconsciously. A great deal of effort is concentrated in modern road cars on the manner in which torque is transmitted back to the driver up the steering column. Those skilled in the art have no difficulty distinguishing between steering issues and vehicle issues. However, a lack of clarity can lead to confusion if steer effects are not separated from vehicle effects. For example, two otherwise identical vehicles with different steering ratios will be judged quite differently by most drivers. Presuming the underlying behaviour of the vehicle is satisfactory, most drivers will rate a numerical reduction in steering ratio ('quicker' steering) as giving 'better' handling due to the increased yaw rate gain of the vehicle as seen by the driver from the handwheel. Yet the vehicles are identical and it would be possible to reproduce the behaviour of one vehicle by steering at a different rate in the other, to different final positions.

Steering feel is correctly given a great deal of importance in road car design since it is the primary means by which the customer comprehends the dynamics of the vehicle. Accurate modelling of steering feel is difficult and requires a great deal of data about friction in individual joints, plus also a good characterization of the hydraulic or electrical power assistance used in the steering system. Nevertheless, work to understand the relative importance of individual contributions is possible with comparatively inaccurate models so long as good judgement is used and conclusions are correlated with work on real systems.

Changes in steering torque are a primary input for skilled drivers to detect vehicle behaviour. When driving normally, the tyres generate forces by distortions in the contact patch (see Chapter 5) that result in a moment attempting to return the tyre to a zero slip angle condition. This is referred to as 'aligning torque' and, if the steering system is well designed, is delivered with very little corruption from vehicle weight and frictional effects directly to the hands of the driver. As the front tyre gets close to its frictional limit, the deformed shape of the contact patch changes such that the aligning torque falls substantially and may even reverse slightly. Attentive drivers note this and are thus pre-emptively aware they are approaching the friction limit. In addition, if a vehicle starts to spin then the steering system informs the driver within around 0.1 second using the 'castoring' torque generated by operating the entire vehicle at a large slip angle. This mechanism ensures minimum handwheel torque when the wheels are placed so as recover the skid; in this way the steering system fairly directly signals the current body slip angle to the driver. Skilled drivers are extremely sensitive to these messages, which arrive ahead of the brain's processing of the results of its data from the inner ear and significantly ahead of messages decoded purely from the visual environment.

7.6 Roll as an objective and subjective modifier

So far, no mention has been made of body roll. There are two important effects of roll, one objective and one subjective. In Chapter 4, some discussion of

the so-called 'roll centre' was put forward as well as the notion of suspension movement leading to adjustments of the wheel camber and toe angle as the body rolls.

Both these effects lead to a modification of the way the tyre is presented to the road. These in turn lead to variations in the yaw moment on the car and therefore some real (objective) influence on the behaviour of the vehicle. These are mostly quite straightforward. For example, toe out on bump on the front suspension will lead to a reduction in the toe angle of the wheel as the vehicle rolls out of the turn, reducing the yaw moment on the vehicle and hence reducing the steady state yaw rate if no adjustment is made by the driver. A slightly more subtle effect is associated with the typical inclination of the so-called roll axis. If the vehicle is imagined to rotate purely about its longitudinal axis (to roll in a pure sense) then the lower front anti-roll geometry will lead to a greater lateral velocity of the front wheels in comparison with the rear. This modification of the lateral velocity will modify the tyre slip angles, with a correspondingly greater increase in front slip angle than rear. As a result, the tyres will produce a yaw moment out of the turn – against the yaw rate but phased with roll rate. Although the motion of the vehicle is not purely roll when entering a turn or reacting to a disturbance, this mechanism may be seen to be one that couples roll and yaw.

Modern road vehicles are comparatively taut in roll, with compliances of 6 degrees/lateral *g* and less being commonplace on quite ordinary vehicles. This is in comparison with 20 years ago, when roll compliances of 12 degrees/lateral *g* were quite normal. Circuit competition cars are typically at something under 2 degrees/lateral *g*. Low levels of roll compliance mean that body roll is no longer the modifier to vehicle dynamics that it once was – its effect is now quite small in the overall scheme of things.

Subjectively, roll has an important effect. Upon entering a turn, the vehicle may be thought of as 'relaxing out' to a final body roll angle. This means the lateral response of the driver's head, high in the vehicle, is reduced during the transient roll-out section of turn-in. Consideration of the expression for beta-dot, above, shows that subjectively this leads to a momentary overestimation of body slip rate by the driver and hence roll transients often degrade driver confidence by introducing a delay in perceived lateral acceleration. Note that for vehicles typically instrumented, delay is not captured by an accelerometer mounted on the floor of the passenger compartment and some processing of roll rate is necessary to compute the lateral response of the vehicle at driver's head height. This is also true of multibody system models. Although the driver subconsciously compensates for motion of their head on the flexibility of their neck, they do not generally compensate for motion of the platform of the vehicle in the same manner.

The nature of the roll-out event is also important, with many in the vehicle dynamics community believing that roll acceleration profiles and roll jerk (the time derivative of roll acceleration) are important modifiers in the perception of roll as a modifier to platform dynamics. Makers of motion simulators understand and use this effect to 'simulate' angular events, applying an angular jerk and then providing a visual environment to suggest the roll rate is persisting. Although quite reproducible, these small events are difficult to capture with instrumentation on vehicles and so there exists a belief that these phenomena are not amenable to objective quantification. That

this is currently true is a consequence of pragmatism rather than any underlying principle – it is very quick to have someone experienced and skilled in the art develop damper tuning for these subjective qualities, compared to instrumenting a vehicle and going through a research programme to define numerical goals at which to aim. In general, a fluid development of initial roll rate and a progressive deceleration to the final roll angle are recognized as necessary to reduce the perception of roll angle. Directional changes towards this end are certainly amenable to predictive analysis with multibody system models, and simulation work using the final, released damper calibrations would go a long way towards improving the quality of work on the next vehicle programme. However, institutionally there is little time in modern engineering organizations for such work since it does not immediately contribute to the task at hand. Historically it has been difficult to get good data to define vehicle dampers (primary modifiers for roll transients) although modern system identification techniques mean this is more possible than it once was.

There is some work that suggests that roll-pitch interaction is important for subjective evaluation of roll (Kawagoe et al., 1997) and this certainly seems plausible. Again, such behaviour is amenable to analysis with multibody system modelling and allows directional selection of design alternatives if not final tuning on the real vehicle. Essentially, a pitch nose-upward that accompanies roll is often subjectively described as 'the rear of the vehicle rolling more than the front' – a statement that is quite mystifying to objective vehicle dynamicists but common currency among skilled development drivers. It is recognized as undesirable and a small but not excessive amount of nose-down pitch is preferred for road vehicles. The exact amount varies with market segment and changes over time as market tastes change. This is something of a challenge for vehicle dynamicists since often there is a desire to have the vehicle roll onto front bump stops before rear in order to guarantee limit understeer, and hence stability – unfortunately this promotes subjectively undesirable pitch nose-up with large roll transients. Development work with multibody system models and real vehicles allows combinations of damper tuning and anti-roll geometry to overcome this difficulty. Once again, a fluid development of initial pitch rate and progressive deceleration to the final pitch angle are recognized as necessary to reduce the perception of pitch angle.

7.7 Frequency response

As mentioned in section 7.4, a transient demand for yaw rate change (a non-zero steering rate) is also a transient demand for a change in body slip angle. That is to say there is a strong link between expectations of beta-dot and rate of handwheel motion. Delays between the two are also acutely remarked.

The seminal IME papers in 1957 showed the existence of a yaw/sideslip mode of vibration for the vehicle, which can be illustrated with only a 2-degree-of-freedom model. The mode of vibration may be thought of as analogous to a pendulum but in the ground plane. It is this mode of vibration that rally drivers use when they 'flick' the car from one side to the other before a turn. Like any other vibrating system, the gains of the

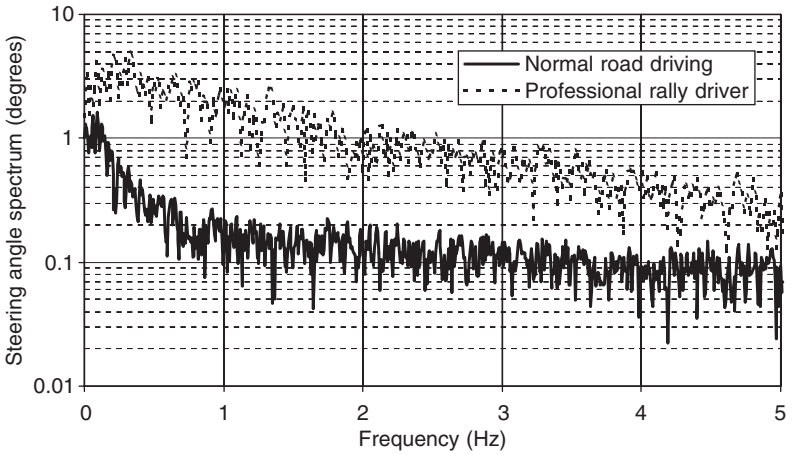

Fig. 7.28 A frequency-domain comparison between road and competition driving

vehicle vary with frequency. Substantially below the resonant frequency, the behaviour of the vehicle is as already described. Around the resonant frequency, the gain is controlled by the level of damping present and above the resonant frequency the gain is controlled by the mass and inertia of the vehicle.

Also like any other vibrating system, a phase shift builds up between input and output as input frequencies approach resonance. At resonance, response is 90 degrees behind input and beyond resonance, response is 180 degrees behind input. For normal drivers this is particularly problematic. When driving normally, the significant frequency content of steer input is very low, typically below the primary ride frequencies at around 1 Hz. A professional rally driver, in contrast, makes rapid and high frequency steering inputs. Figure 7.28 shows a pair of spectral estimates made from handwheel angle recorded over time. The spectral density measure of degrees/Hz is multiplied by the spectral resolution of the two estimates to allow meaningful overplotting of signals sampled at different rates. A single 4096 point buffer, tapered using the 'Hanning' (cosine) window function has been used for both signals. At the lowest frequency, the professional driver (Petter Solberg during the third special stage of the 2002 Argentina round of the World Rally Championship) is using around three times as much steering input as the road driver, the author (Harty) on a Saturday in Warwickshire. By 0.5 Hz, the normal road driver's steer input is nearing the noise floor and is around one eighth of its peak. In contrast, the professional driver's input is more or less flat to 1 Hz and tails off slowly, extending all the way to 5 Hz before reaching the same levels as the normal road driver's input at 0.5 Hz. At 0.5 Hz, the professional driver is using between eight and nine times the normal road driver's steer input – and this on a rack ratio that is some 50% faster than the road car on which the data was gathered.

Thus the Milliken assertion (Milliken and Milliken, 1995) that for road use the vehicle can be treated as a series of connected quasi-static events is mostly true – this is the basis of the automotive statics analysis embodied in the MRA Moment Method software (Milliken and Milliken, 1995). However,

during emergency manoeuvres, the amplitude and frequency content of driver's steer inputs rise tremendously. Published data suggests that the highest steer rate sustained for 200 ms or more is likely to be around 1100 degrees/second by the population as a whole (Bartlett, 2000). Data from the World Rally Championship series confirms this is the highest rate used by those drivers also; the authors' logged data also achieves – but has never exceeded – these levels on occasion.

When such large and high frequency inputs are used, the response of the vehicle is no longer controlled only by the steady state yaw characteristics but may also be amplified compared to the base level as well having a phase delay imposed as described previously. The dynamic amplification is a result of the yaw/sideslip resonance of the vehicle being excited to produce responses that may be substantially greater as well as delayed by some 150 milliseconds compared to the linear result that the driver might be expecting.

7.8 The problems imposed by ...

7.8.1 Circuit racing

Here the authors draw unashamedly on the material (Milliken and Milliken, 1995) presented in Chapter 1 of the Milliken and Milliken book *Race Car Vehicle Dynamics*. Circuit racing is about using the acceleration vector of the vehicle to maximum effect at all times, be it in braking, accelerating, turning, or some combination thereof. Circuit racing is a highly rehearsed behaviour with 'braking points' and 'turn-in points' all being prescribed for a given type of vehicle. The driver's task is to apply control in a largely open loop manner and to add minor trim inputs in a closed loop manner. The 'Milliken Moment Method' uses, as one of several tools, a diagram that describes the manoeuvring envelope for the vehicle by plotting yaw moment against lateral force (or some variants thereof). Some examples are given of the diagrams for various possible configurations. Notionally, the 'ideal' circuit car is one which is neutral steering and retains its yaw rate gain characteristic right to the limit of adhesion since this maximizes the lateral acceleration possible. In truth, most circuit cars exhibit a small amount of 'push' or 'plough' right at the limit but to a first approximation, the yaw moment versus lateral force diagram looks a little like that shown in Figure 7.29. The right-hand vertex aligns with the A_Y-axis, indicating a departure that is neither 'push' nor 'loose'.

7.8.2 Rallying

In contrast, rallying is largely unrehearsed, with line-of-sight driving plus prompts from co-drivers. These prompts take the form of memory-joggers: 'left 5, 150 over crest; caution, do not cut'. This is interpreted by the driver as 'left [turn, of severity] 5 [where 1 is gentle and 5 is aggressive based on likely speed before braking commences], 150 [metres] over crest; caution, do not cut [the inside of the corner because there is some hazard not obvious on entry]'. A great deal of skill and rapport is required; both driver and co-driver need to mould each other's expectations on the style of the co-driver's prompts. This information, though, is very incomplete compared to the

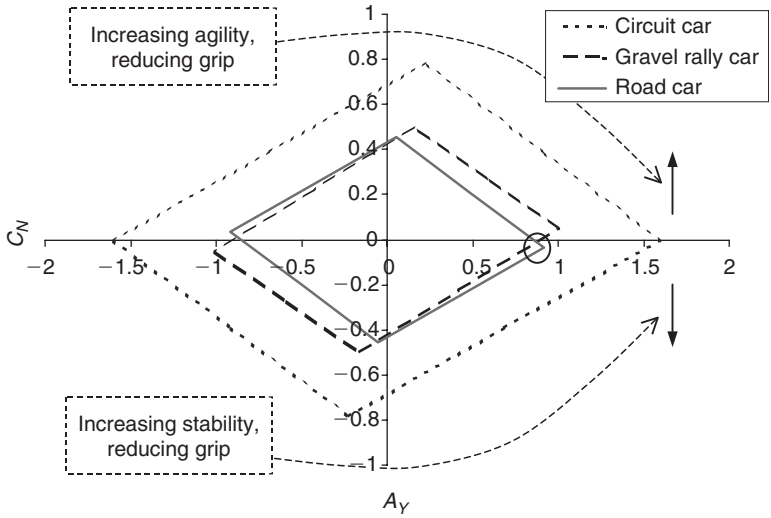

Fig. 7.29 F–M diagrams for circuit racing, rally and road car performance – based on static weight distribution

circuit-racer's knowledge. Rally driving is all about control and adaptation. The driver's inputs have a very small open loop content and very large and active closed loop (trim) content. During a typical drift event lasting 2 seconds, there are five changes of steering angle direction (i.e. from left to right) and handwheel rates as defined in Bartlett (2000) exceed 1000 degrees/second regularly despite the use of ultra-low ('fast') steering ratios. The yaw moment versus lateral force diagram is typically skewed much more towards control, which often produces stability concerns at the very highest speeds (Figure 7.29). The right-hand vertex is above the A_Y-axis, indicating a departure that is 'loose' – that is to say the vehicle will spin unless actively trimmed by the driver.

7.8.3 Accident avoidance

Accident avoidance in road cars is quite different to both the previous scenarios. In terms of the percentage of miles driven it is statistically insignificant; if it weren't for the fact that collisions have such serious consequences we would ignore it altogether. This is important because it means the driver is (in general) unpractised and unprepared. The driving task may be thought of as possessing two components – the *command* component, concerned with the speed and path of the vehicle, and the *control* component, concerned with maintaining the heading of the vehicle in line with its path. That this split mimics the way the authors model the driver behaviour (Chapter 6) is no coincidence. Under normal circumstances the control part of the driving task is minimal. However, during aggressive manoeuvres it emerges to become an important component of the overall task because of the transient and frequency domain issues outlined earlier. Typically, the importance of command decisions is also high at these times, leading to either a loss of control or poor command decisions under circumstances where the vehicle could have been physically able to evade the emergent hazards, had the

driver been 'more able'. For normal driving tuition, only command driving is taught and control is presumed linear. Progression into the non-linear region is regarded as a failure and so is inadequately addressed. In the UK, for example, a single 'emergency stop' manoeuvre is the only non-linear event in DSA test. While notionally it is true that perfect command decisions could maintain the vehicle always in the linear region, most individuals are imperfect and will misjudge matters from time to time – either misjudging their own speed and position or that of others, requiring some emergency avoidance driving of one form or another.

There are two requirements for the vehicle under these circumstances. The first is that it must have sufficient cornering ability to be able to curve the vehicle path in such a manner as to avoid the hazards. The second is that it be stable – that is to say that the control demands on the user are minimized. A strongly desirable attribute is that the vehicle displays behaviour that does not distract the attention of the driver by thinking he 'might' need some control in the near future. In general this is linked with stability but not necessarily in a direct manner. Considering the force–moment diagram in Figure 7.29, the right-hand vertex (circled) is below the the A_Y-axis, indicating a departure that is 'push' – that is to say the vehicle loses yaw rate gain with increasing lateral acceleration, gaining stability. If stability were the only criterion, then it would be easy to simply ensure an early 'push' departure with the vehicle design. However, increasing expectations for cornering ability to avoid hazards means that excessive sacrifice of grip for stability (a traditional recipe for the North American market) is becoming less and less acceptable.

7.9 The use of analytical models with a signal-to-noise ratio approach

The attraction of using predictive methods is mentioned in Chapter 1 and reiterated in section 7.1. One key benefit of analytical methods is that they are very repeatable – the same simulation run twice will generally yield the same results. There are specific exceptions to this, where 'random' numbers are included in analyses but in general it holds as a premise. This removes an important obstacle in vehicle dynamics – the lack of repeatability of measured data as mentioned at the start of the chapter. This is certainly one form of 'noise' but not the form referred to in the title of the section. In general, drivers expect linearity from their vehicles. A departure from linearity may be regarded as 'noise' compared to the 'signal' that represents the driver's inputs.

Most readers will be familiar with the idea of variation in output being some measure of repeatability. For example, if a machine is required to produce a piece of a certain nominal size then a better 'quality' machine will produce pieces closer to that nominal size than a worse 'quality' machine. To quantify the level of match between machine and desired results, we use the notion, introduced in section 7.1, of 'Process Capability', C_p:

$$C_p = \frac{0.75\Delta_d}{6\sigma_d} \tag{7.36}$$

where Δ_d is the allowable range for the attribute d and σ_d is the standard deviation of the attribute d as produced by the process. If C_p is greater than unity, the process is 'capable' and if not, it isn't. This notion is used to assess production methods for intended tolerances and to focus attention on the least capable processes where resources are limited. As previously noted, the capability for the vehicle dynamics measurement process is questionable at best – though analytical methods improve the capabability of the process at the risk of introducing systematic inaccuracies through modelling errors and the like.

As part of a design process, the idea of a signal-to-noise ratio (SN ratio) becomes much more useful. If we imagine that same manufacturing process, SN ratio is the ability of the process to produce any desired value of d. Thus, for some form of CNC machine tool, some dimension d might be anywhere from 10 mm to 500 mm. A snapshot of the device's ability to produce, say, 276 mm is less useful than an overall knowledge of the relationship between input (desired dimension) and output (dimension produced). There are three types of 'lack of quality' that concern us:

- *Linearity*: the proportionality of output to input. For example, if on small dimensions the stiffness of the workpiece reduced, the machine might systematically make smaller things than required but as the dimension increases this effect might become less significant.
- *Variability*: the consistency of output to input. If the machine is insufficiently stiff then random vibrations induced by the cutting action might lead to random variations in the size of the workpiece.
- *Sensitivity*: the scale of output to input. If some calibration error were present between sensors and tool positioning shafts, it could be that so-called 'millimetres' in one axis were different to 'millimetres' on another axis.

A fourth effect is the ability of our measuring technique to discern the output to the required resolution. If we ask for a 0.1 mm change in size of the product but can only measure to the nearest millimetre, we are unable to discern whether or not we have been successful. This, however, is a matter of good experimental or analytical technique rather than something innate in the process itself and so it is laid aside as a difficulty for the moment.

To capture all three types of 'lack of quality', a single measure is used – the SN ratio. This is simply defined as

$$SN = \eta = 10 \log_{10}\left(\frac{\kappa^2}{\sigma^2}\right) \tag{7.37}$$

where κ is the sensitivity of the process (i.e. the amount the output changes for a unit input change) and σ is the standard deviation of the results from the nominal.

To successfully use the idea of SN ratio in vehicle dynamics design, a process is required that looks something like that shown in Figure 7.30. Notice the similarity between this and Figure 1.6 in Chapter 1. This type of process is variously and vaguely known as robust design, parameter design or the Taguchi method.

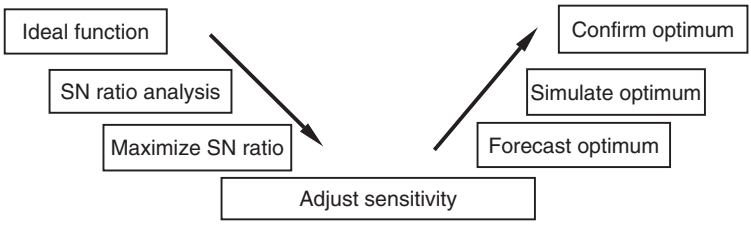

Fig. 7.30 The robust design process

The first and crucial step is to define the so-called 'ideal function'. In vehicle dynamics it is very easy to become mired in talk of detailed effects of springs, dampers, bump rubbers, anti-roll bar bushings and so on and to dive into an intensive programme of investigation that quickly spirals out of control. It is only the experience of the empirical vehicle dynamicists that delivers vehicles that perform under these circumstances. Those same empirical vehicle dynamicists have become rightly suspicious of analytical methods since they can take a long time and run the risk of delivering little if not well directed. This need not be so. The authors suggest that the ideal functions should be generic enough to be applicable to any vehicle, without exception; only the tuning of sensitivities should need matching to the application.

If we consider the brake system as an example, it is simple to state an ideal function:

> *to proportionally transfer the driver's inputs from the pedal to the deceleration of the vehicle up to the available friction level.*

Brake systems have several unintended functions as implemented. Squeal, judder and so on are of prime concern to road vehicle manufacturers and the ability to use all the available friction is of prime concern in motorsport applications. The conditions under which this 'ideal function' holds are simple – all conditions under which the vehicle operates. This includes in reverse (when drum brake systems can be startlingly ineffective), in car parks, when cold, when hot, when wet, when new, when worn, without the engine running and so on. Individually, these circumstances lead to a great deal of elaborate testing. However, when using SN ratio methods they can be robustly combined into a relatively small number of tests that will deliver the best performance available from the existing combination of ingredients and design variables.

'Signal' is that part of the input to the system, via the design variables ('control factors') under the engineer's control, that is intended to produce a response. 'Noise' is the collection of all other factors that influence the response. For the brake system, these are ambient temperature, brake temperature, vehicle loading condition, direction of travel, fluid condition and so on. Design variables available to the engineer will be such things as disc mass, friction material, calliper stiffness, seal material, master cylinder mounting stiffness, pipe stiffness and so on. Some knowledge of the most likely dominant variables is preferred since the number of variables can become unmanageable. Wherever possible, variables should be compounded together for initial studies. If identified as important, further work can be performed to isolate the effects of individual variables. For example, calliper

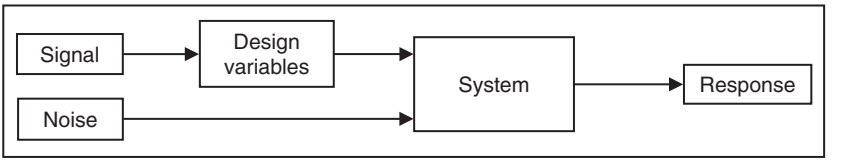

Fig. 7.31 A generic system from the robust design perspective

stiffness, master cylinder mounting stiffness and pipe stiffness come together under 'system stiffness'. As long as our tests incorporate some contribution from each of the compounded 'sub-variables' then the conclusions will be valid. Similarly, noise inputs can be compounded together to give a 'noise reducing performance the most' and 'noise increasing performance the most'. For example, the former condition might be very cold brakes, fully loaded, worn brake pads. The latter condition might be optimally warm brakes, driver only, new bedded-in brake pads.

Each variable could be varied individually while maintaining the others constant. While this is a valid method, it rapidly leads to a large number of experiments with only a small number of variables. For example, with eight variables the number of experiments required to test two levels of each variable is $2 \times 2 \times 2 \times 2 \times 2 \times 2 \times 2 \times 2 = 256$ experiments. The use of orthogonal arrays allows meaningful results to be produced from a reduced set of experiments. With only eight variables, results can be obtained from only 72 runs. Adhering to so-called 'Taguchi' principles and using dynamic signal-to-noise ratios as described allows interactions between inputs to be ruled out, allowing eight variables to be handled in just 16 experimental runs. Modern multibody system codes usually come with some form of experimental design built into them, although not necessarily the dynamic signal-to-noise ratio calculations described.

To perform the experiment, several levels of 'signal' are set and the design configuration is set. Results are collected at each signal level, in each design configuration for both noise conditions. The nature of those results should be such that the comparison with the ideal function is a meaningful one. For the brake system, mean deceleration between two speeds is suggested as a suitable response variable. Any modern data logging or multibody system analysis software can easily capture and process such data. Signal factors should be chosen to give a reasonable spread of results over the operating envelope. In the case of a brake system, three levels of deceleration might be suggested as $0.2g$, $0.5g$ and $0.8g$, with the pedal inputs selected to give results around these levels. Note that the signal factors (i.e. pedal inputs) should remain as consistent as possible. The actual array to be used is best selected from an existing library of such arrays; there is no particular need to derive one's own. Figure 7.32 shows a typical such array.

Once the results have been generated – either by an experiment or by simulation – they are processed to calculate signal-to-noise ratio and sensitivity for each of the conditions in the orthogonal array. For vehicle dynamic behaviour, the most useful form for the signal-to-noise ratio calculation is the so-called 'linear' form, which presumes that output is

	A	B	A×B	C	A×C	B×C	D×E	D	A×D	B×D	C×E	C×D	B×E	A×E	E
1	−	−	+	−	+	+	−	−	+	+	−	+	−	−	+
2	+	−	−	−	−	+	+	−	−	+	+	+	+	−	−
3	−	+	−	−	+	−	+	−	+	−	+	+	−	+	−
4	+	+	+	−	−	−	−	−	−	−	−	+	+	+	+
5	−	−	+	+	−	−	+	−	+	+	−	−	+	+	−
6	+	−	−	+	+	−	−	−	−	+	+	−	−	+	+
7	−	+	−	+	−	+	−	−	+	−	+	−	+	−	+
8	+	+	+	+	+	+	+	−	−	−	−	−	−	−	−
9	−	−	+	−	+	+	−	+	−	−	+	−	+	+	−
10	+	−	−	−	−	+	+	+	+	−	−	−	−	+	+
11	−	+	−	−	+	−	+	+	−	+	−	−	+	−	+
12	+	+	+	−	−	−	−	+	+	+	+	−	−	−	−
13	−	−	+	+	−	−	+	+	−	−	+	+	−	−	+
14	+	−	−	+	+	−	−	+	+	−	−	+	+	−	−
15	−	+	−	+	−	+	−	+	−	+	−	+	−	+	−
16	+	+	+	+	+	+	+	+	+	+	+	+	+	+	+

Fig. 7.32 An $L_{16}^{(5\text{-}1)}$ two-level orthogonal array used for processing five variables in 16 runs. Columns A × B handle interactions between A and B, and so on.

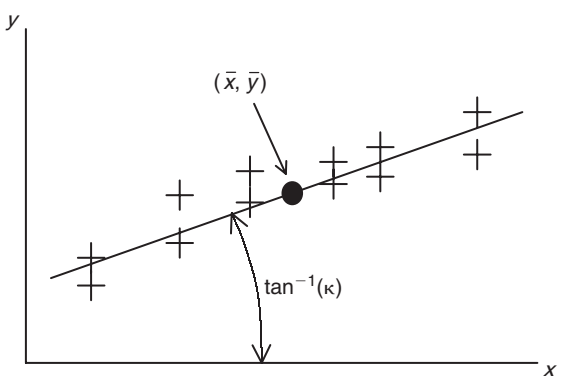

Fig. 7.33 Linear form of presumed response

related to input in the following manner:

$$y = \kappa(x - \bar{x}) + \bar{y} + e \tag{7.38}$$

where y is the response, x is the signal, and e is the error. $\bar{y}$ and $\bar{x}$ are the averages over the whole experimental data set.

If the system is non-linear (as is typical), the ideal function is defined such that the linear form of this equation can still be applied. As a further example, if acceleration performance is being considered then the ideal function is 'constant power acceleration' such that

$$Pt = \frac{1}{2}mv^2 \tag{7.39}$$

that is to say all of the power of the engine goes into kinetic energy in the vehicle. The ideal function may be expressed as:

$$x = V_0 + \sqrt{2P(t - t_0)/m},\ y = V \tag{7.40}$$

If various speed intervals are used for testing then the constant power formulation allows the expected results, or signal values, to be set according to this formulation. Actual test values can be compared with them using the linear formulation to calculate signal-to-noise ratios and sensitivity. Changes that improve the sensitivity will be reduced losses in the system (i.e. better efficiency) and changes that improve the signal-to-noise ratio will be improved robustness. For example, lower levels of driveline vibration reducing random losses, reduced aerodynamic drag maintaining constant power acceleration to a higher speed and improved area under the torque curve giving reduced sensitivity to gear ratios will all improve signal-to-noise ratio.

So how then should this be applied to simulation models to improve the lateral dynamics of vehicles? The key to success lies totally in the definition of ideal functions. We have already discussed the brake system and powertrain. The handwheel remains the only driver input left. Its function is as a yaw rate demand. Previously, the behaviour of typical vehicles and drivers has been discussed. On the basis of this, a suggested ideal function for the handwheel is:

> *to deliver a yaw rate proportional to handwheel angle, related to speed by the stability factor for the vehicle in question, up to the limit of available friction.*

Figure 7.16 shows the linear yaw rate gain in relation to speed for some different vehicles. Thus, the ideal function for the handwheel could be expressed:

$$x = \frac{V\delta}{L(1 + KV^2)},\ y = \omega \tag{7.41}$$

With n pieces of logged or predicted information, signal-to-noise ratio, η, is calculated according to the following method:

$$\eta = 10 \cdot \log_{10}\left[\frac{S_\kappa - V_e}{\left[\sum_{n=1}^{n}(x_i - \bar{x})^2\right] \cdot V_e}\right] \tag{7.42}$$

where the following intermediate calculations are defined:

Error variance
$$V_e = \frac{S_e}{n - 2} \tag{7.43}$$

Error variation
$$S_e = S_T - S_\kappa \tag{7.44}$$

Total variation
$$S_T = \sum_{i=1}^{n} y_i^2 - \frac{\left(\sum_{i=1}^{n} y_i\right)^2}{n} \tag{7.45}$$

Variation due to linear effect $$S_\kappa = \frac{\left(\sum_{i=1}^{n} y_i(x_i - \bar{x})\right)^2}{\sum_{i=1}^{n}(x_i - \bar{x})^2} \tag{7.46}$$

In addition, the sensitivity of the data set (the ratio of input to output) is calculated thus:

$$\kappa = \frac{\sum_{i=1}^{n} y_i(x_i - \bar{x})}{\sum_{i=1}^{n}(x_i - \bar{x})^2} \tag{7.47}$$

The similarity to the standard least squares method is apparent. The interested reader is urged to consult Wu and Wu (2000) for further, more detailed description and background to the method. In that text, the symbols used differ slightly. The symbols used here have been chosen to avoid a clash with the familiar vehicle dynamics symbols in use. To use the method, a typical set of predicted or logged values is taken, consisting of yaw rate $\omega(t)$, handwheel angle $\delta(t)$ and forward speed $V(t)$. Values for stability factor, K, and wheelbase, L, are presumed known for the vehicle. Using the ideal function, 'expected' values for ω are calculated and taken as the input data series, x. The 'real' – either logged or predicted – values of ω are taken as the output y and the calculations for η and κ performed as described above.

Once signal-to-noise ratios have been calculated for each 'state' in the orthogonal array, they are processed to produce an effects plot of the type shown in Figure 7.34. In this case, the array was an $L_{16}^{(5\text{-}1)}$ two-level array for processing five design variables and their possible interactions. Variable A is shown to be dominant, with variables B and E important also. The signs of the effects are not all the same; variable A is 'less A gives *more* response' while B and E are 'less B/E gives *less* response'. There are no significant interactions between the variables. Effects plots are produced for κ and η separately. To calculate effects with the array shown in Figure 7.32, results from runs 1, 3, 5, 7, 9, 11, 13 and 15 are averaged to give the '−' result for variable A. The remaining columns give the '+' result for variable A. For variable B, runs 1, 2, 5, 6, 9, 10, 13 and 14 give the '−' result, and so

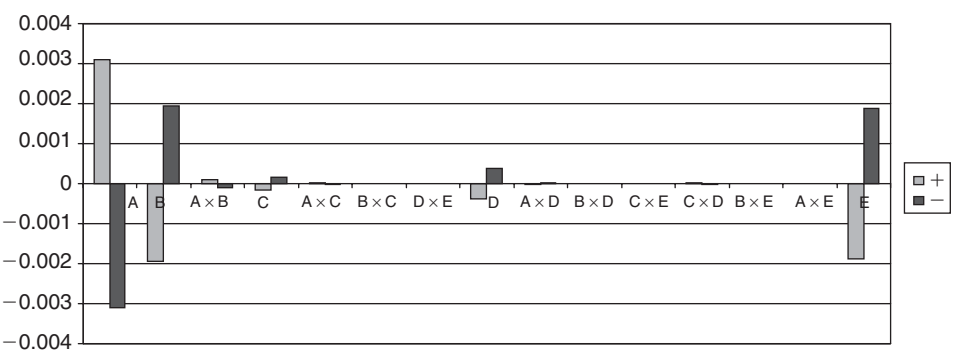

Fig. 7.34 A typical effects plot produced by processing the results from an orthogonal array

on. The combination of design variables is selected to maximize signal-to-noise ratio to maximize robustness of the system. The following steps in the process are the adjustments to the sensitivity, κ, being made through those variables showing themselves as affecting κ but of less influence on η.

Such an approach to the ideal function for the steering and handling behaviour covers a great many different situations although for motorsport applications, in particular rallying, it may lack one important aspect.

Rally drivers use the non-linearity of the car to their advantage. Recall the force–moment diagram in Figure 7.29. This is derived on the basis of quasi-static calculations. However, professional rally drivers use the dynamic amplification of the yaw–sideslip resonance along with features such as ruts and road surface edges (Figure 7.35) to achieve yaw accelerations significantly greater than that suggested by the Milliken moment method, as shown by the comparison in Figure 7.36.

The lightest data in the centre represents the highest speeds achieved during the stage and fits well within the estimated boundaries of the F–M diagram. However, the two other shades show extremely large levels of yaw acceleration at high lateral acceleration in strong contrast to the general form of the Milliken diagram. This is a symptom of the use of the dynamic amplification in the yaw–sideslip mode as used by the rally drivers. The use of an ideal function that relates steer angle to yaw rate will promote an increase in yaw damping, which is good for road cars but precludes the 'flick' style of driving preferred by rally drivers.

Figure 7.37, by contrast, shows the behaviour of the rally car on tarmac and suggests that the vehicle stays well within the quasi-static boundary predicted by the Milliken moment method.

Fig. 7.35 Tommi Makinen hooks the front left wheel of his 2003 Subaru WRC off the tarmac and ensures a large yaw moment will be available shortly (courtesy of Prodrive)

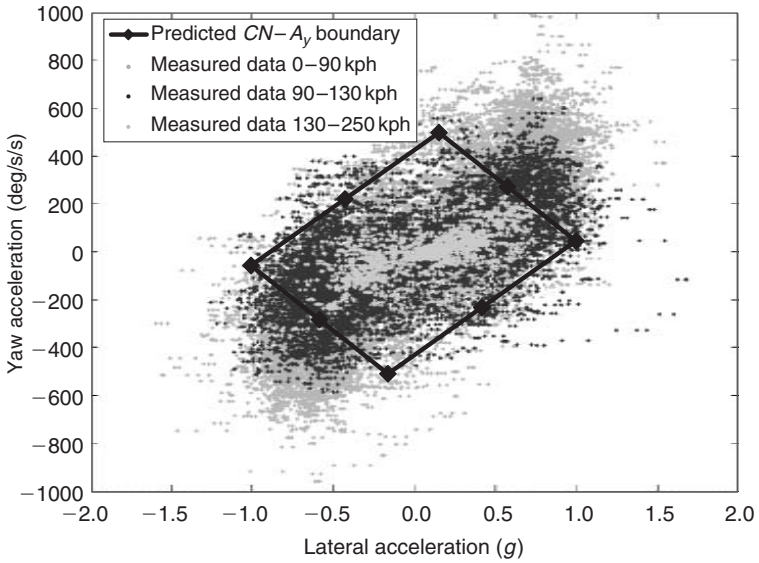

Fig. 7.36 Yaw acceleration versus lateral acceleration for the Subaru WRC 2002, Petter Solberg, Argentina

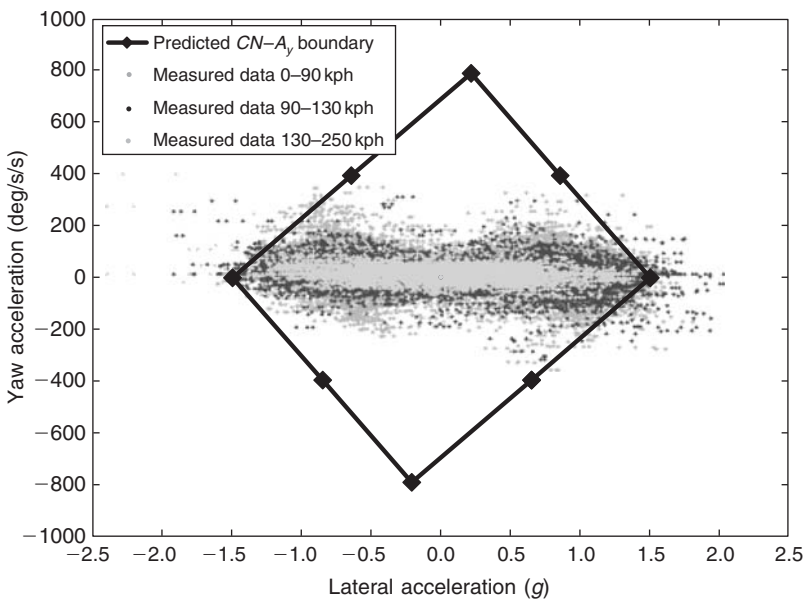

Fig. 7.37 Yaw acceleration versus lateral acceleration for Subaru WRC 2002, Petter Solberg, Germany

Examination of the recorded data shows there is little 'steady state' about the rally stage on loose surfaces and the character of the handwheel angle versus yaw rate trace for the entire stage has a distinctly 'circular' quality about it (Figure 7.38). This indicates that output (yaw) has a phase shift of around 90 degrees – an indication that the system is indeed at resonance. In

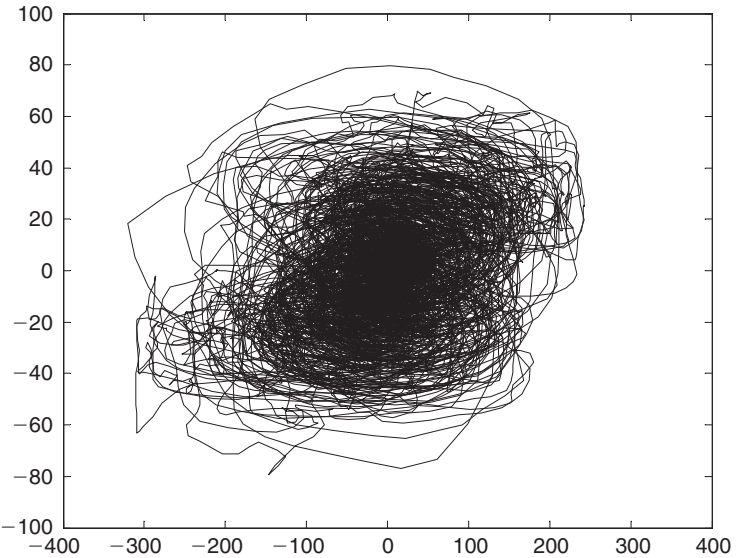

Fig. 7.38 Yaw versus steer angle – note the circular quality of the data traces, indicating a 90 degree phase difference between the two quantities

this instance the proposed ideal function is inadequate. Commercial proprieties prevent the discussion of this particular topic in any further detail but readers are assured there is indeed an appropriate ideal function.

7.10 Some consequences of using signal-to-noise ratio

Previously, vehicle dynamicists have sought to address a wide range of phenomena – unintended yaw rate change following lift-off in a turn, delays following turn-in, non-linearity with increasing lateral acceleration and so on. It is eminently possible to attack each of these issues in turn, although it is also likely that solutions to some may become problematic for others.

The use of a single measure – signal-to-noise ratio – and an ideal function allows experimentation to optimize the performance of the vehicle in its entirety. Questions of balancing one attribute against another no longer become subjective but can be expressed objectively, since an increase in yaw damping will increase signal-to-noise ratio where it controls yaw overshoots in response to disturbances but reduce signal-to-noise ratio where it blunts turn-in. This is not to say that the endeavour of optimizing vehicle dynamics will become trivial; defining the correct 'handling sign-off' usage over which to record signal-to-noise ratio remains difficult, instrumentation challenges remain, and the difficulties of accurately simulating vehicle and driver behaviour over a lengthy handling sign-off test are far from trivial. Also non-trivial is the engineering of areas of vehicle behaviour where the departure from the ideal function might be regarded as 'character' rather than a non-optimum. An example of such behaviour is

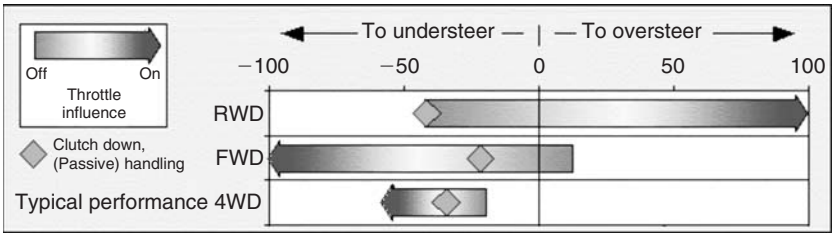

Fig. 7.39 Vehicle behaviour on-throttle – flaws or brand attributes? The illustration is informal, the quantities of understeer and oversteer being some undefined '%'

the oversteer departure – i.e. the loose behaviour at the limit – of rear-wheel-drive vehicles (Figure 7.39). If smart systems on board disallow such a departure, keeping the vehicle stubbornly linear until the end of the available friction, will it surprise the driver when the friction is exceeded? Will it bore the driver and tempt him or her to buy a different, less perfect brand next time? Or will the retention of *YRG* as *AyG* falls off give a uniformly better driving experience, less tainted by some of today's compromises?

Certainly the use of signal-to-noise ratio can potentially address many issues simultaneously:

- linearity of yaw rate gain with lateral acceleration
- delays in response degrading driver confidence
- roll/yaw interaction
- disturbance rejection
- throttle/steer interaction
  - FWD – minimizing 'push' under power
  - RWD – reducing oversteer departure tendency under power
  - 4WD – minimizing 'push' under power
- brake/steer interaction

Of some importance for the successful application of the method is the balancing of the proportion of different events in the overall signal-to-noise calculation. For instance, when comparing the influence of crosswind disturbance rejection with the influence of roll–yaw interaction, due account must be taken of how many 'crosswind' events there are for every 'aggressive turn-in' event and so on, lest one become unduly weighted in comparison with others. It is likely that the selection of the sign-off cycle will be what ultimately determines the dynamic brand attributes of the vehicle. This is not so different to the current situation where vehicles are tuned to match the preferences of key individuals at their preferred test facilities. These differences are a source of richness and diversity in vehicle design and are part of the larger commercial process of 'differentiation' to retain or increase market share.

8 Active systems

8.1 Introduction

Modern passenger vehicles are developed to a very high level in terms of their dynamic behaviour. Indeed, there are many who believe that little more can be done to improve the performance of the road car with passive means. While it may be a little premature to make such a statement, there have been many steps forward that have been made since the start of the vehicle engineering industry:

- addition of suspension damping
- adoption of independent suspension
- adoption of hydraulic suspension damping
- adoption of hydraulic brakes
- progressive stiffening of body structure
- addition of isolating elastomers in suspension
- adoption of radial tyre construction
- decoupling of lateral and longitudinal loadpaths
- optimization of suspension geometry
- optimization of elasto-kinematic behaviour
- adoption of low profile radial tyre construction

It is probably true that there is less to do than has been done. However, some fundamental difficulties remain with pneumatically tyred vehicles. In particular, the fall-off in yaw damping with speed is problematic. Since the fundamental nature of the tyres is to generate side forces with respect to slip angle, this leads to increased lateral velocities at increased vehicle speeds in order to respond to a given level of disturbance (Figure 8.1). This

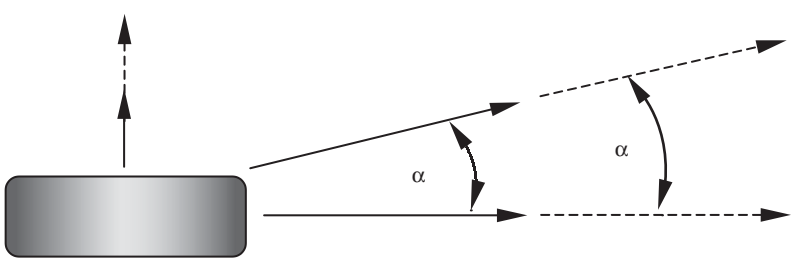

Fig. 8.1 An increase in forward speed requires an increase in lateral speed to respond to the same disturbance

behaviour leads directly to Fonda's 'tyre-as-damper' analogy (Fonda, 1956). Since lane width in general does not increase with speed, this means the vehicle's ability to reject a given disturbance within the lane is reduced with increasing speed and hence driver workload increases. As well as the straightforward increase in lateral velocity, consideration of the stability derivatives for the classical vehicle dynamics equations given in Milliken and Milliken (1995) shows that four important derivatives have vehicle speed as a denominator:

$$Y_r = \left(\frac{a \cdot C_F - b \cdot C_r}{V_x} \right) \tag{8.1}$$

$$N_r = \left(\frac{a^2 \cdot C_F - b^2 \cdot C_r}{V_x} \right) \tag{8.2}$$

$$Y_{VY} = \frac{C_F + C_R}{V_x} \tag{8.3}$$

$$N_{VY} = \frac{a \cdot C_F - b \cdot C_r}{V_x} \tag{8.4}$$

The dimensions a and b are the longitudinal distances of the vehicle mass centre from the front and rear axles as shown previously in Figure 7.22. The first two derivatives are the side force and yaw moment with respect to yaw velocity. The remaining two are side force and yaw moment with respect to body slip angle, which may be expressed as a function of lateral and forward velocities and hence implicitly contains forward velocity in the denominator. It is thus a fundamental consequence of the tyre behaviour that the vehicle loses restoring force with speed. This is in marked contrast to aircraft (in the subsonic region, at least) where restoring forces increase with speed since aerodynamic forces rise with the square of speed.

Note the contrast between these statements and those at the start of Chapter 7, where the control gains for ground vehicles can be seen to increase significantly with speed. This presents vehicle engineers with some particular problems since control authority is increasing while system stability is reducing – a 'closing gap' scenario in which the safe behaviour of vehicles at autobahn speeds remains difficult to engineer.

8.2 Active systems

For this reason, the industry as a whole is considering the use of active systems to complement the passive behaviour of the vehicle. Traditionally, 'active' has meant a system in which energy is added in some form. In modern usage, this distinction is becoming lost and so the term is being used for any system that performs something other than a passive mechanical reaction. Previously, systems that modified their behaviour without adding energy were referred to as 'adaptive'. In general, systems that combine

mechanical actuation with electronic control are referred to as 'mechatronic', although this term appears infrequently in industry literature.

To model any type of mechatronic system requires the introduction of 'sensors' into the vehicle model and the implementation of the control law. This is most conveniently performed as state variables in a manner similar to that described for driver modelling. One important difference, however, is that the driver model is 'continuous' – that is to say the resulting outputs may be differentiated without discontinuity. An aspect of many active systems is that they use 'logic controller' principles (see Chapter 6) and thus may branch between conditions in a very short space of time. If carelessly modelled, this may give convergence problems inside the vehicle model and so the use of some smoothing method is required. Note that these difficulties are present when implementing real life systems and not confined to simulation. In MSC.ADAMS, the STEP function described in Chapter 3 allows the transition between one level and another using a half sinusoidal form that is continuously differentiable.

8.2.1 Active suspension and variable damping

Lotus performed a great deal of work in the 1980s looking at 'active suspension', a fast acting system that varied the vertical load on each corner in accordance with control laws attempting to preserve ride height, minimize wheel load variation and minimize body acceleration. This system was undoubtedly very effective, particularly on the attitude-sensitive Formula 1 car. However, expensive components and significant power consumption mean that, to the authors' knowledge, only the Mercedes CL and S-Class's 'Active Body Control' system is on the road 20 years later (Figure 8.2). Even this is a down-specified version, working only with primary ride motions (up to around 5 Hz) rather than the higher frequency wheel-hop control achieved by the Lotus SID research vehicle. In April 1990, Inifinity, the luxury division of Nissan, introduced a similar hydraulic 5 Hz system for the 1991 model year Q45, badged as Q45a when carrying the 'Full Active Suspension' (FAS). This remained on the market only until the

Fig. 8.2 Mercedes Active Body Control (ABC) in action at high lateral accelerations – around 1 degree of body roll (a combination of tyre compliance and some programmed roll compliance for 'feel') with the ABC car compared to 4.5 degrees of body roll for the passively suspended car (courtesy of *Auto Motor und Sport*)

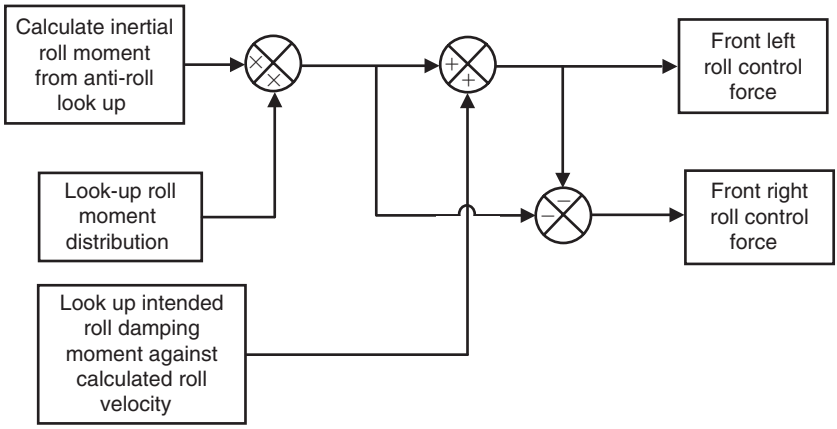

Fig. 8.3 Simplified active suspension model

1996 model year, when it was withdrawn the year before the facelifted model was introduced. Nissan cited low take-up of the FAS option as the reason for its deletion, with only 15% of US customers subscribing to it.[1]

Partial active systems, working only against body roll, have included Citroën's 'Activa' system fitted to the Xantia (not to be confused with the two concept cars of the same name) from 1995 until 2000, when it was replaced by the C5 model which reverted to the adaptive roll stiffness/damping system known as 'Hydractive II'. Land Rover's 'Active Cornering Enhancement' is a hydraulically actuated fast roll levelling system, working around 5 Hz and fitted to Land Rover Discoveries from the 1999 model year to date.

Active suspension systems and their cousins, continuously variable damper systems, are easy in concept to implement in multibody system models. Action–reaction force pairs are introduced into each vehicle suspension unit in addition to the normal spring, damper and anti-roll bar forces. The magnitude of these forces is controlled by control laws in a similar fashion to that in the real vehicle. For example, a system (Figure 8.3) might use an open loop roll moment method by applying forces proportional to the output from a lateral accelerometer. A further modification might be the addition of a roll damping term based on relative velocities of left and right suspension units, with a look-up table (spline) for use at different vehicle speeds.

Table 8.1 shows a sample of an MSC.ADAMS command file implementing such a system on the front suspension of a vehicle.

Active suspension in principle allows the control of individual tyre reaction forces in a manner decoupled from platform orientation. As well as allowing a level platform during braking and cornering events (preserving suspension travel for disturbance events and improving the angle at which the tyre is presented to the road), it allows the redistribution of roll moment reaction on a moment-by-moment basis. The mechanisms discussed in Chapter 7 for inducing over- and understeer can thus be harnessed and used to improve turn-in behaviour, yaw damping and so on.

[1]Source: Steve Parker, 'Car Nut TV', Palm Springs, California.

Table 8.1 MSC.ADAMS command file sample for simplified active suspension

```
data_element create variable &
   variable_name = inertial_sprung_roll_moment &
   function = "( VARVAL(latacc) * (mass) *", &
      "( DZ(m_body_CG,base) - ", &
      " ( AKISPL(varval(fl_suspension_position),0,front_anti_roll_ spline) ", &
      " * (front_track)/2 ) * varval(fl_suspension_load)/varval(total_load)", &
      " + AKISPL(varval(fr_suspension_position),0,front_anti_roll_ spline) ", &
      " * (front_track)/2 ) * varval(fr_suspension_load)/varval(total_load)", &
      " + AKISPL(varval(rl_suspension_position),0,rear_anti_roll_ spline) ", &
      " * (rear_track)/2 ) * varval(rl_suspension_load)/varval (total_load)", &
      " + AKISPL(varval(rr_suspension_position),0,rear_anti_roll_ spline) ", &
      " * (rear_track)/2 ) * varval(rr_suspension_load)/varval (total_load)", &
      ") ) )

data_element create variable &
   variable_name = roll_moment_load_front &
   function = "varval(inertial_sprung_roll_moment) *", &
              "AKISPL(varval(latacc),0,roll_moment_distribution_spline)", &
              " / (front_track)"

data_element create variable &
   variable_name = roll_damping_load &
   function = "( ", &
              " ( VZ(fl_damper_top,fl_damper_bottom) + ", &
              " VZ(rl_damper_top,rl_damper_bottom) ) -", &
              " ( VZ(fr_damper_top,fr_damper_bottom) + ", &
              " VZ(rr_damper_top,rr_damper_bottom) ) ", &
              ") * ( (front_track)+(rear_track) )/2 * ", &
              "* AKISPL(varval(velocity),0,roll_damping_velocity_spline)

force create direct single_component_force &
   single_component_force_name = front_left_active_force &
   i_marker_name = .fl_damper_top &
   j_marker_name = .fl_damper_bottom &
   function = "( + varval(roll_moment_load_front) + varval(roll_damping_load)", &
              "* STEP(TIME,0.0,0.0,1.0,1.0)"

force create direct single_component_force &
   single_component_force_name = front_right_active_force &
   i_marker_name = .fr_damper_top &
   j_marker_name = .fr_damper_bottom &
   function = "( - varval(roll_moment_load_front) - varval(roll_damping_load)", &
              "* STEP(TIME,0.0,0.0,1.0,1.0)"
```

Note that in the example no attempt has been made to filter the output down to any particular bandwidth. Filtering is a lengthy topic in its own right and is best not approached glibly. Many software environments allow the use of filtering techniques within their post-processing tools. However, for simulating active systems, some kind of filtering is almost always necessary at run time. Whether to simulate the limited bandwidth of an actuation device or to smooth noisy data, some form of filter must be implemented while the model is running.

Some MBS codes have access to a sophisticated run-time filtering library, such as those set up in the Matlab product environment. Others, like MSC.ADAMS, lack such run-time tools but do have the ability to enter a generic transfer function command. The filter transfer function itself must be

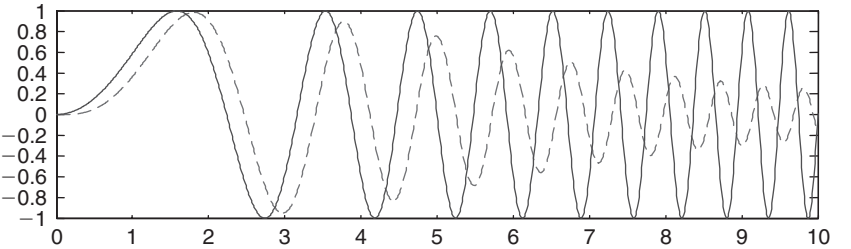

Fig. 8.4 Two-pole Butterworth filter described in equation (8.5) applied to signal in equation (8.6) (solid) – resulting signal in dashed line

arrived at using some external filter design tool. Particular caution is needed since some software environments use descending order for the terms in the transfer function while some use ascending order, as illustrated in equation (8.5), which represents a 1 Hz second order Butterworth filter in the Laplace domain as used in Matlab and MSC.ADAMS:

$$g(s) = \underbrace{\frac{39.884}{s^2 + 8.8869s + 39.884}}_{\text{Matlab description}} = \underbrace{\frac{39.884}{39.884 + 8.8869s + s^2}}_{\text{MSC.ADAMS Description}} \tag{8.5}$$

More sophisticated filtering is possible using higher order transfer functions and using the more general state–space modelling methods, which are available in most multibody system environments. The interested reader is referred to Blinchikoff and Zverev (2001) for detailed discussion of filtering methods and their repercussions. The most important thing to recognize is that almost any form of real-time/run-time filtering introduces some form of phase delay. Using the example transfer function in equation (8.5), an input chirp signal in Matlab defined as:

$$x = \sin\left(2\pi \cdot \frac{time^2}{10}\right) \tag{8.6}$$

produces an output as shown in Figure 8.4. Note that the amplitude attenuation is very gentle but that a phase delay has been introduced even at frequencies well below the notional cut-off frequency.

The 2-pole Butterworth filter represents a linear second order mechanical system and so its intelligent use can be very helpful in avoiding modelling complexity. The interested reader is encouraged to study its formulation and implementation in different forms – pole/zero and Laplace polynomial – as a launchpad to a deeper understanding of real-time filtering issues and complexities.

Adaptive damping logic can be implemented in a similar fashion to active suspension inside an MBS model, scaling a damper spline or adding a scaled 'damper variation' spline to a 'minimum damping' spline according to a controller demand. The 1988 Lancia Thema 8.32 is believed by the authors to be the first production implementation of an adaptive damping system, with

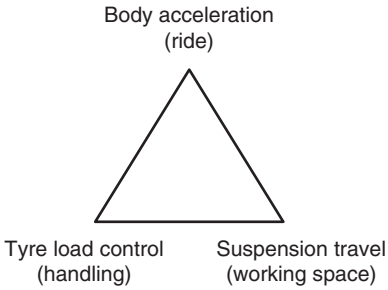

Fig. 8.5 Suspension trade-offs

two-state dampers switching rapidly between 'soft' and 'hard' settings according to an algorithm that examined ride accelerations and driver inputs.

Active suspensions and continuously variable dampers seek to address the traditional three-way trade-off in suspension calibration (Figure 8.5). Given enough working space it is possible to improve both ride and handling simultaneously, as evidenced by desert race vehicles.

However, in road cars with suspension travel limited by prosaic packaging constraints, generally ride is achieved at the expense of handling or vice versa. Crolla comments (Crolla, 1995) that good control of the suspension dampers delivers many of the benefits of active control without the power consumption. Thus it seems to the authors to be the 'thinking man's' solution to improved suspension calibration. It also offers the prospect of software control for calibration of suspension dampers, making inroads into development times and potentially delivering economies of scale by making the same damper hardware fit a wider range of vehicles than it does today.

8.2.2 Brake-based systems

Other systems are less comprehensive but can have large benefits. In 1978, Mercedes introduced the Bosch 'Anti-Blockier System' as an option on the Mercedes S-Class. This system, universally abbreviated to ABS (albeit with some contortions to translate the German expression for 'anti-lock' into English), releases, holds and reapplies brake pressure in individual wheel brakes in order to retain directional stability and steering control with no practicable sacrifice in braking capability. Although technically it is possible for a skilled driver to outbrake ABS, in truth the level of rehearsal this requires means it is unlikely in a road car in any realistic situation. Highly rehearsed circuit driving is an area where skilled drivers may improve over ABS performance and so circuit cars rarely use ABS.

In 1995 Mercedes introduced the Bosch 'Electronic Stability Program' (ESP) on the Mercedes S-Class. This system applies the brakes asymmetrically and without the driver's foot applied to the brake pedal, in order to exert restoring yaw moments on the vehicle. While previous ABS strategies had an element of open loop control to minimize the build-up of yaw moment for asymmetric braking situations, ESP proceeds to the next logical step of closed loop control of yaw rate. Desired yaw rate is mapped through extensive testing on the vehicle and compared with actual yaw rate. Conceptually

this is similar to the driver control model described in Chapter 7. However, a fundamental difference is that the brake actuators are not always controlled as proportional devices. To suppress understeer, brake torque is typically applied at the inside rear wheel in a manner substantially proportional to the magnitude of the understeer. For oversteer, a different strategy is employed. First, a threshold is set below which no intervention occurs and second, the system introduces a defined amount of brake torque for variable lengths of time to trim oversteer. It is also typical that engine torque will be reduced under these conditions. This gives rise to the typical 'lumpy' sensation of the operation of ESP and the belief for many drivers that it is a relatively crude system. In truth, it is extremely elaborate, but the requirement not to burn out the brakes during spirited driving means this 'threshold' control is necessary.

Both ABS and ESP control can be difficult to model for reasons of the discontinuities described in section 8.2. In the real world, finite hydraulic bandwidth imposes its own smoothing on the system but the operation of ABS systems remains subject to a repeated series of 'impact' noises during sharp hydraulic transients. Only the very latest electro-hydraulic braking technology succeeds in avoiding this. Co-simulation between multiple modelling codes is the answer suggested by the software industry for all these problems although this is not preferred for a variety of reasons, described in Chapter 6. Another alternative is so-called 'hardware-in-the-loop' simulation that uses a real physical brake system with pressure sensors to feed the behaviour of the brake system back into the model. The model computes the effects on the vehicle and feeds vehicle state information out to 'virtual sensors' that replace the real sensors on the vehicle, making its decisions and affecting the real brake system to complete the loop. Although potentially accurate, this type of modelling is more suited to confirmation work as shown on the right-hand side of Figure 7.29.

The biggest difficulty in real-world systems is the accurate discernment of the vehicle speed under conditions when the wheel speeds are only loosely connected to it and each other. This is usually referred to as the 'reference speed' problem. Another significant difficulty is the need to control the vehicle by varying longitudinal slip ratio when the actuator is a torque-control device. On ice, for example, 10 Nm may be enough to lock the wheel whereas on dry pavement, 10 Nm will produce barely any change in slip ratio. For both these reasons, ABS and ESP strategies are more complex than might first be imagined; differences in effectiveness and implementations largely come down to the sophistication of the reference speed calculation and friction estimation.

8.2.3 Active steering systems

In 1986, Nissan launched their High Capacity Active Steering (HICAS) system on the rear axle of the R31 Skyline Coupé. Honda followed with a mechanical system on the Prelude and Mitsubishi were close behind in the Lancer, using an electronically controlled system like the Nissan. Nissan used the notion of a compliant subframe with its location controlled by a hydraulic actuator, while Honda and Mitsubishi essentially duplicated the front steering system at the rear of the vehicle, using a central rack. The objectives of the systems were clear and there is a great deal of literature published on the subject (Ro and Kim, 1996). Four-wheel steer seeks to control the body slip angle and rate, and hence has a profound effect on driver

impressions of the vehicle. It also has the comparatively trivial effect of tightening the turning circle at low speeds. Honda has subsequently dropped four-wheel steer, declaring that 'advances in tyre technology have rendered it unnecessary'. Mitsubishi kept it until 1999 on their 3000 GTO model, while Nissan continue with a development now called Super-HICAS system on the Skyline.

A difficulty with four-wheel-steer is that, while it makes the vehicle feel excellent in the linear region (through enhanced body slip angle control), as the handling limit approaches the flat nature of the tyre side force versus slip angle curve means that its ability to improve vehicle control disappears. In this sense, it is possibly the worst type of system – enhancing driver confidence without actually improving limit capability. Four-wheel steer is easily simulated in multibody systems modelling, with an additional part to represent the rear steering rack and forces applied to it according to a control law as with other systems.

BMW has recently announced 'Active Front Steer' in conjunction with ZF for the 2004 model year 5-Series. Consideration of the behaviour of competition drivers, particularly rally drivers, suggests the potential for this system is high and that it offers a much more continuous control than brake-based systems. Although onerous, the potential failure modes have clearly been overcome. It also offers the chance to overcome the problem of increased control sensitivity at high speeds by reducing the yaw rate gain progressively with speed. It does not suffer any of the problems of rear-wheel steering in terms of limit control.

Prodrive has recently announced an 'Active Toe Control' system for application to all four wheels. This is primarily an on-centre modifier for the vehicle and is intended to complement the torque distribution systems they are also known for. Such a system is postulated in Lee et al. (1999) and has been prototyped on a research vehicle. The interaction between such a system and a torque-distribution system is explored in He et al. (2003).

8.2.4 Active camber systems

Milliken Research Associates produced an active camber Corvette in the mid-1980s with closed loop control of yaw rate following the success of the 'camber racer', which was recently run again at Goodwood on modern motorcycle tyres. Mercedes have also produced the F400 Carving, which runs an active camber system. Although attractive in function, the increased package requirements in the wheelhouse make active camber something that will probably not be applied to road cars.

8.2.5 Active torque distribution

Nissan's Skyline R32 Coupé had the somewhat bewilderingly named ATTESA-ETS (Advanced Total Traction Engineering System for All – Electronic Torque Split) system in 1989. The Porsche 959 had similar technology in the same year, although without the lengthy acronym. Since then, systems of torque redistribution according to handling (as against traction) priorities have remained elite in production cars. Prodrive has recently

revived interest with several low-cost ATD systems suitable for a wide variety of vehicles but none of these have achieved production status as yet. In essence, traditional driveline technology systems seek to minimize wheel spin whereas these systems seek to connect drive torque distribution to vehicle handling via closed loop feedback. From a modelling point of view, they are simple to implement in that some state variables are declared (typically a target yaw rate and current state, similar to ESP systems) and the actuation forces are implemented accordingly.

8.3 Which active system?

The North American market is currently resisting complexity in its best-selling light truck segment (pickups and SUVs), since the appeal from the vehicle manufacturer's perspective is the low cost of production, giving margins that are allowing the vehicle manufacturers to remain in business during lean times. Nevertheless, competition from offshore is causing consumer expectations in the USA for vehicle performance and quality to increase steadily. In Europe, an already sophisticated consumer is expecting steadily improving dynamic performance from their vehicle, while in Asia the predilection for 'gadgets' on vehicles has seen this market lead the way in terms of satellite navigation and so on. All three major world vehicle markets have their own reason for needing to improve vehicle dynamic performance over and above the level that can be achieved using conventional, passive technology. However, no one wants to be first to market with a system that initially gives them a cost penalty and runs the risk of delivering benefits that the customer does not notice – and is therefore not prepared to pay for.

Table 8.2 Which active system – and why?

Name	Lateral acceleration	Steering rate	Guiding principles	Applicable active system
Normal	0–0.3*g*	0–400°/second	• To steer the car, steer the wheels. • Ride matters.	Active rear toe, active front steer, adaptive dampers.
Spirited	0.3–0.6*g*	400–700°/second	• Intelligently combine drive and steer forces to deliver control without retardation. • Control body motion.	Active torque distributrion, *active rear toe, active front steer*, *adaptive dampers.*
Emergency	0.6*g* +	700+°/second	• Use brakes to reduce kinetic energy of the vehicle. • Minimize wheel load variation for maximum grip and control.	Brake-based system, *adaptive dampers*, active anti-roll bars.

Italics denote duplication – i.e. reuse

For this reason, detailed predictive work will be needed to sort the useful from the gimmick in terms of vehicle dynamics controls. The author's expectations for the use of active systems on vehicles are given in Table 8.2. Three driving regimes are identified, which may be described as 'normal', 'spirited' and 'accident avoidance'. These may be loosely classified as being 0–0.3*g* lateral acceleration, 0.3–0.6*g* lateral acceleration and 0.6*g* + lateral acceleration respectively. They are also characterized by driver inputs, particularly in terms of handwheel rates – 0–400 degrees/second, 400–700 degrees/second and 700–1100 degrees/second, respectively.

The results in Table 8.2 are not in any sense definitive but the authors considered views in the light of the available evidence. It is hoped that the readers of this text will be part of the group of engineers discovering just how good these judgements are.

Appendix A: Vehicle model system schematics and data sets

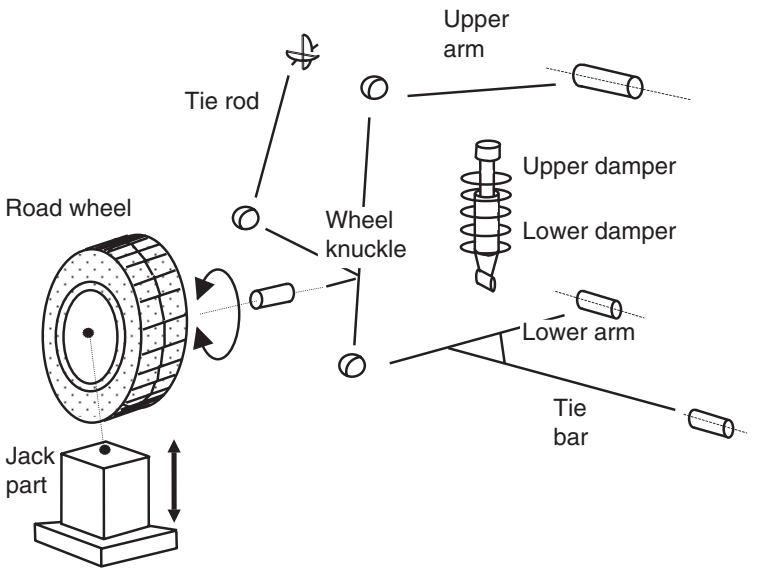

Fig. A.1 Front suspension components

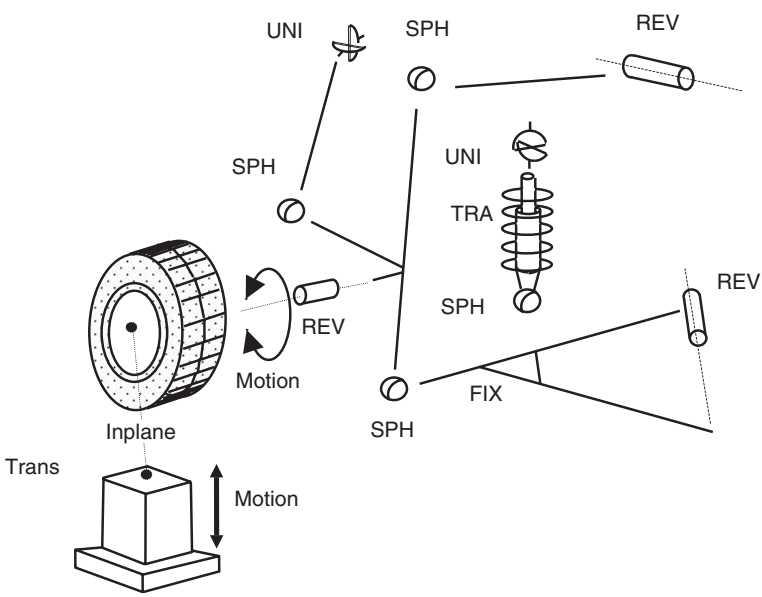

Fig. A.2 Front suspension with joints

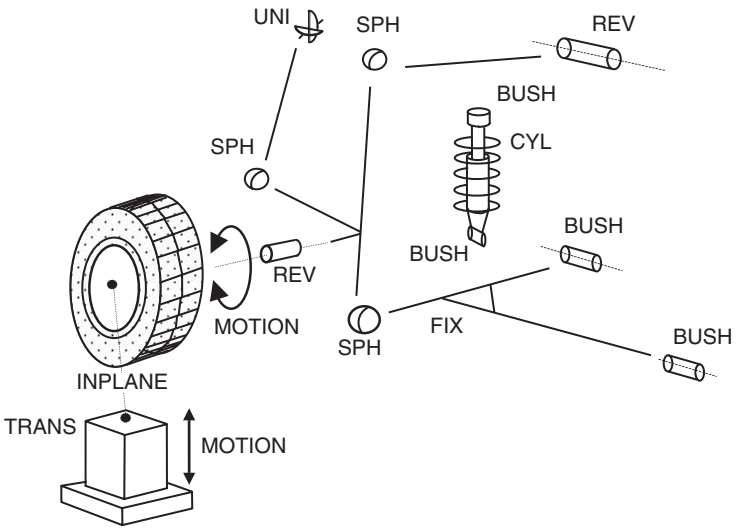

Fig. A.3 Front suspension with bushes

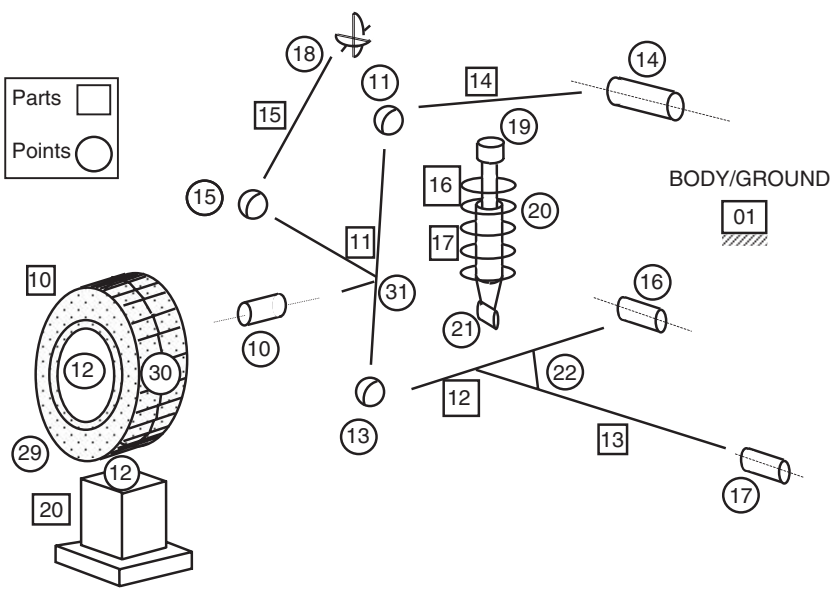

Fig. A.4 Front suspension numbering convention

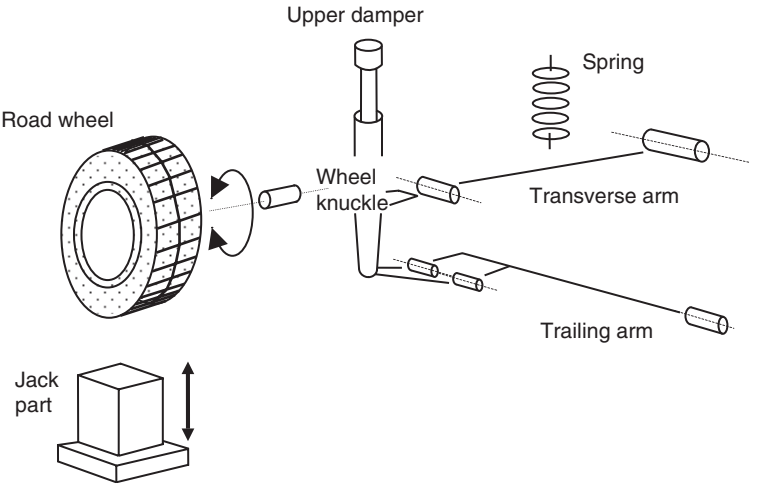

Fig. A.5 Rear suspension components

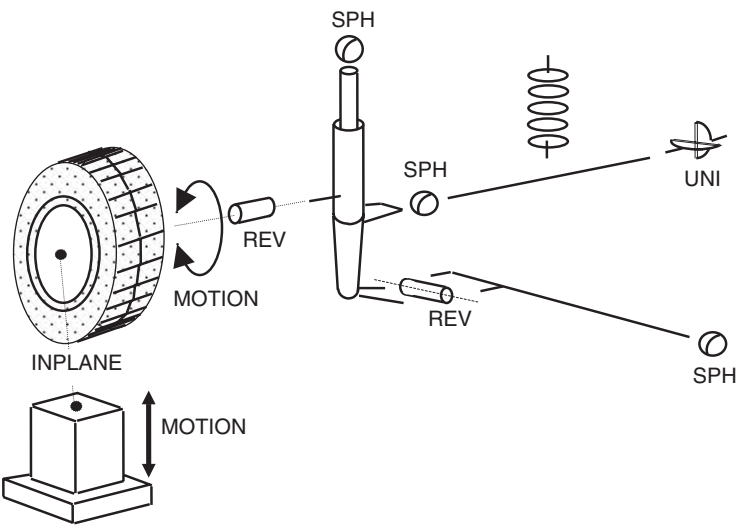

Fig. A.6 Rear suspension with joints

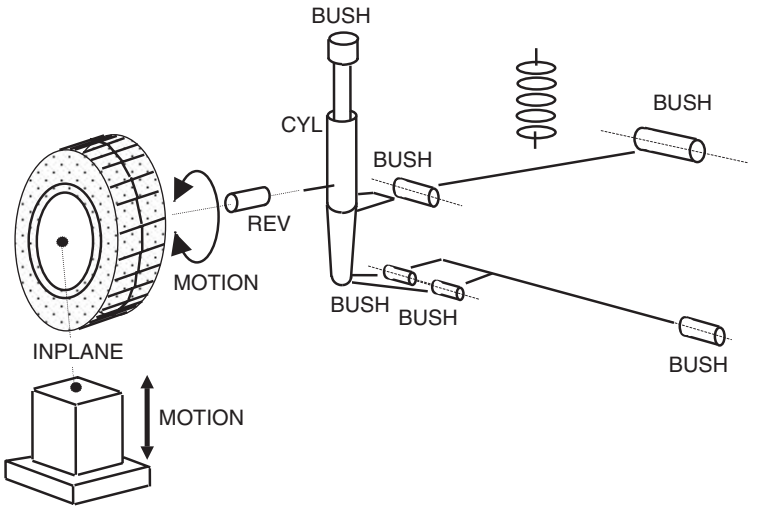

Fig. A.7 Rear suspension with bushes

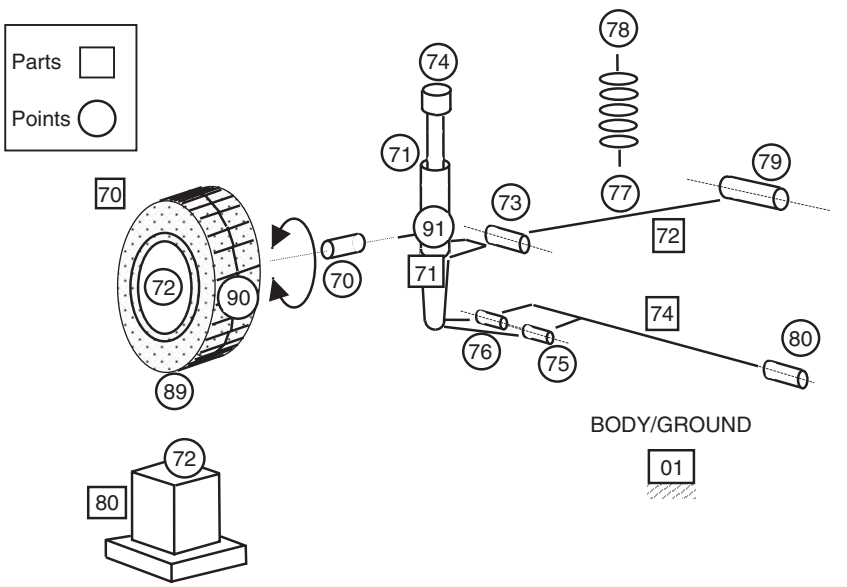

Fig. A.8 Rear suspension numbering convention

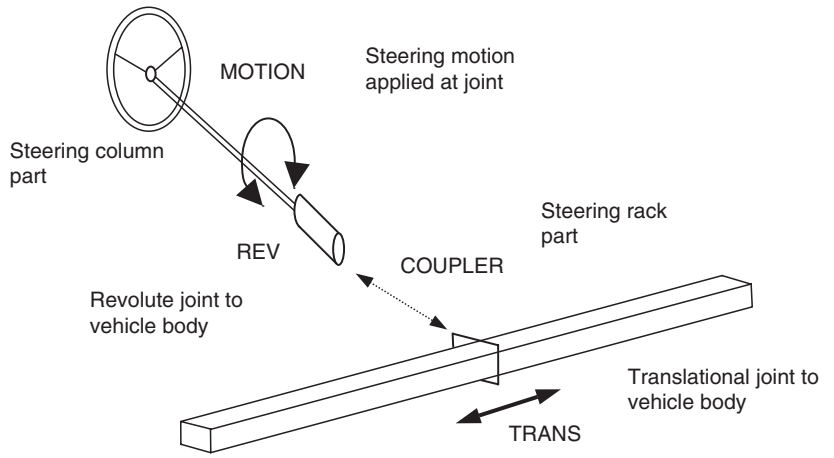

Fig. A.9 Steering system components and joints

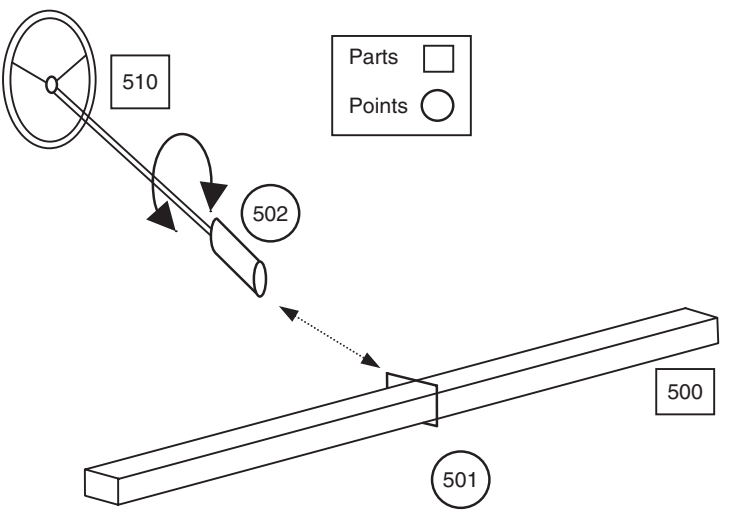

Fig. A.10 Steering system numbering convention

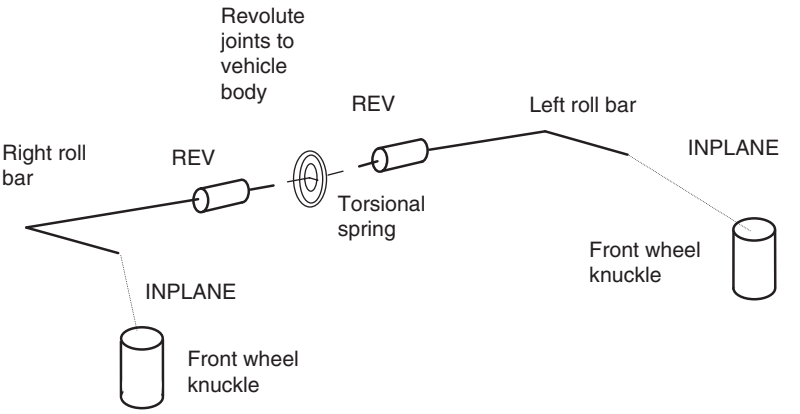

Fig. A.11 Front roll bar system components and joints

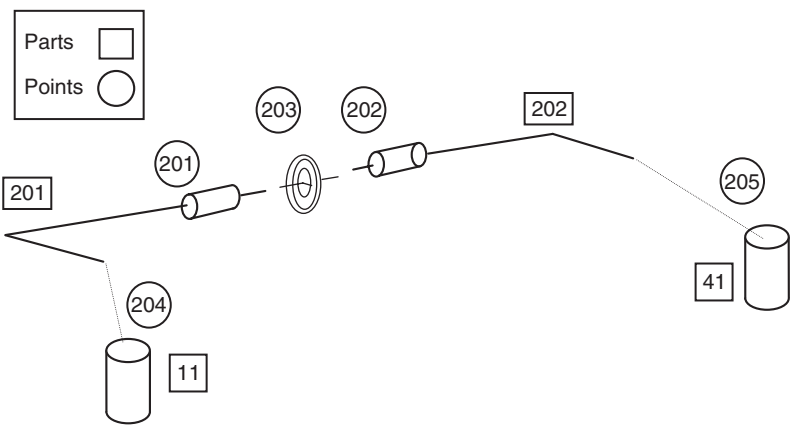

Fig. A.12 Front roll bar system numbering convention

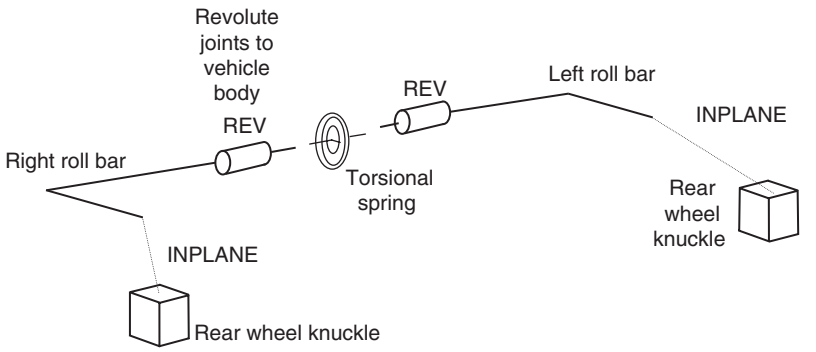

Fig. A.13 Rear roll bar system components and joints

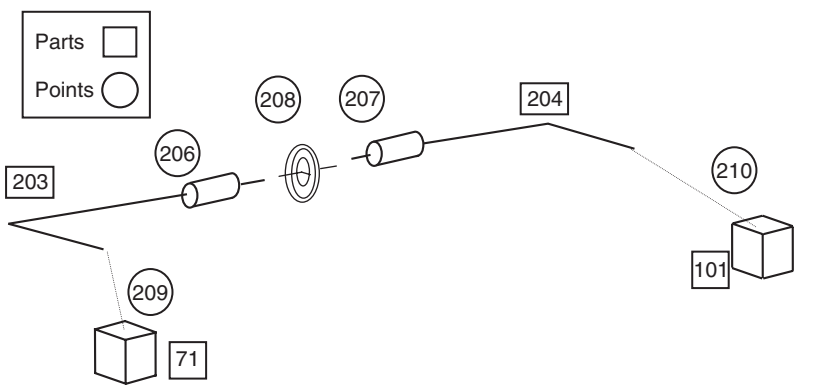

Fig. A.14 Rear roll bar system numbering convention

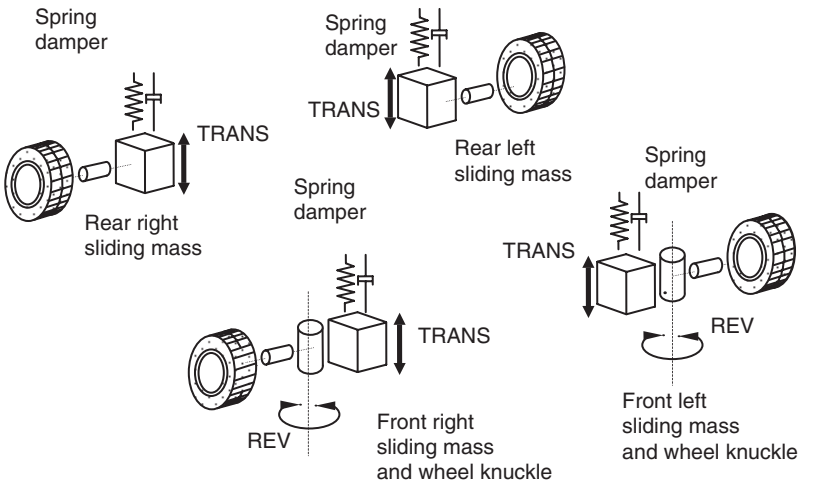

Fig. A.15 Lumped mass model suspension components and joints

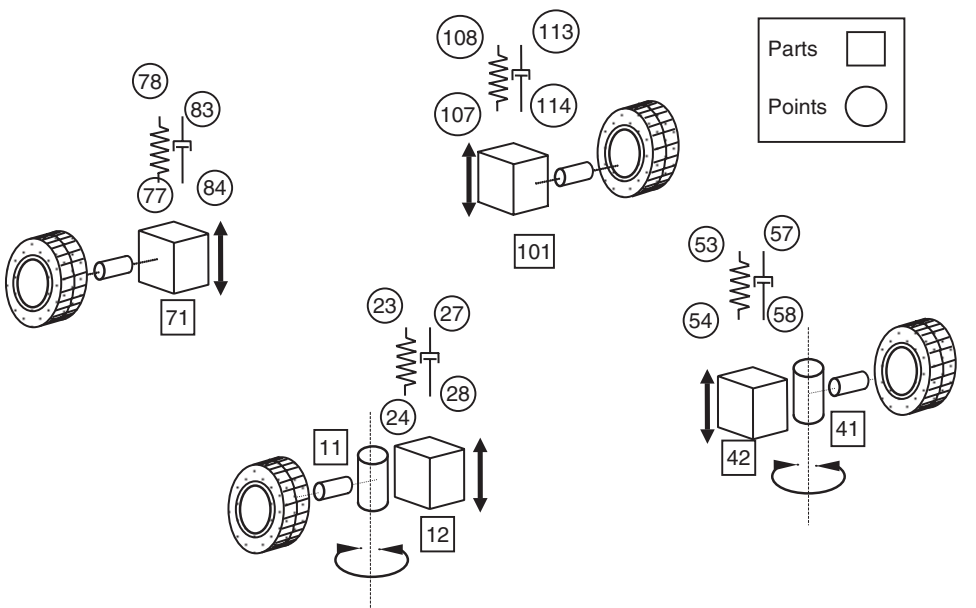

Fig. A.16 Lumped mass model suspension numbering convention

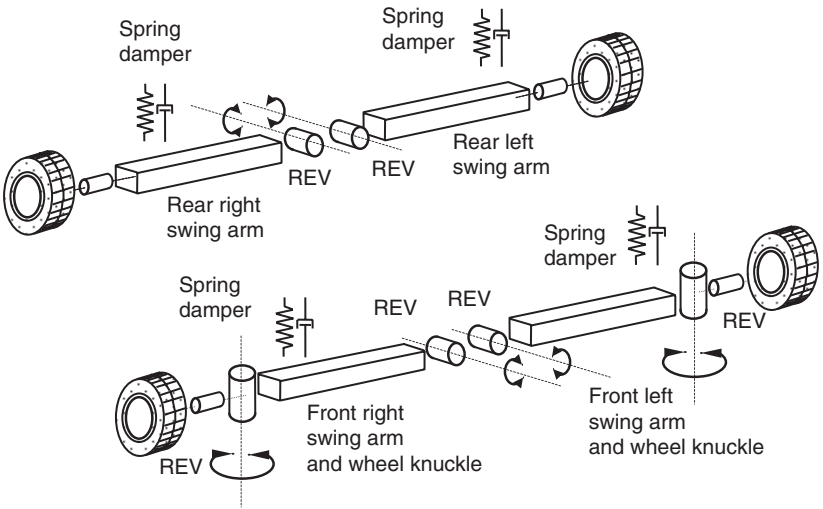

Fig. A.17 Swing arm model suspension components and joints

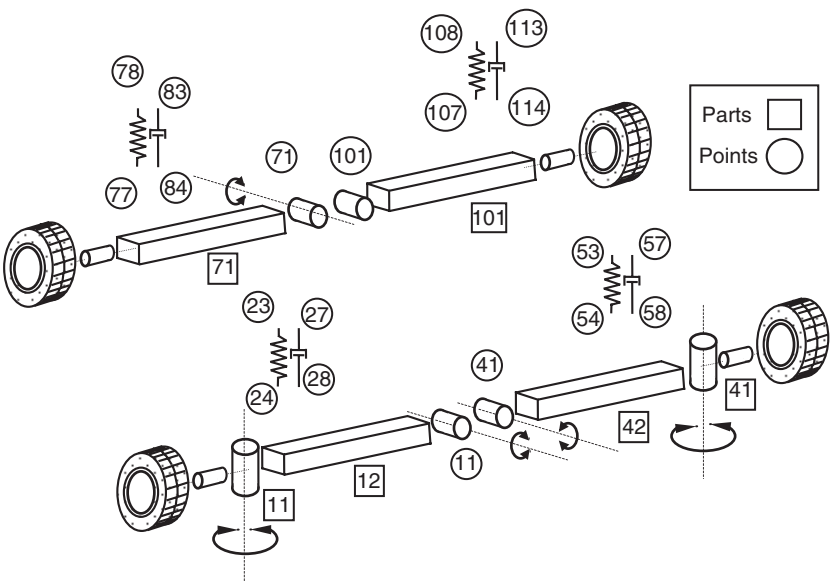

Fig. A.18 Swing arm model suspension numbering convention

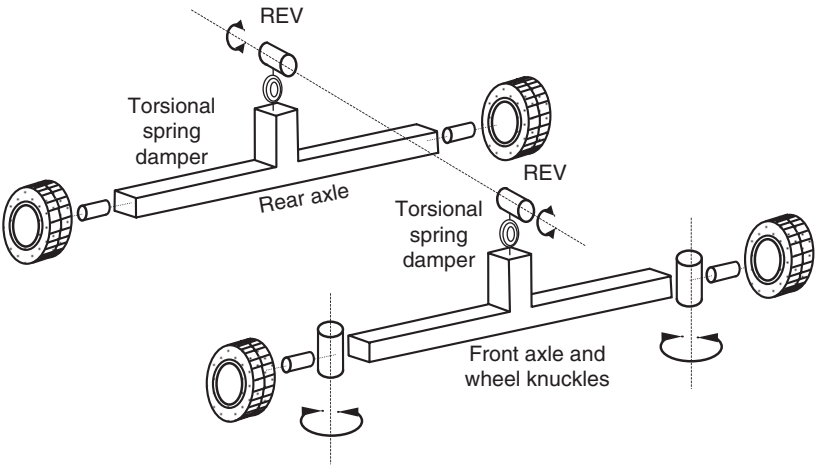

Fig. A.19 Roll stiffness model suspension components and joints

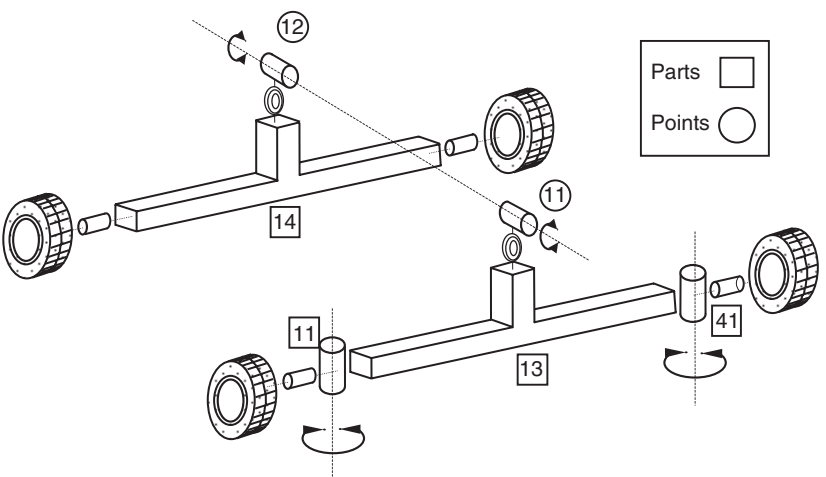

Fig. A.20 Roll stiffness model suspension numbering convention

Table A.1 Road wheel mass and moment of inertia data

Description	Part ID	CM marker	Mass (kg)	Mass moments of inertia (kg mm^2)		
				Ix	*Iy*	*Iz*
Front right wheel	10	*10	21.204	577.59E3	577.59E3 93	1.077E3
Front left wheel	40	*40	21.204	577.59E3	577.59E3 93	1.077E3
Rear right wheel	170	*70	21.204	577.59E3	577.59E3 93	1.077E3
Rear left wheel	100	*100	21.204	577.59E3	577.59E3 93	1.077E3

* The wheel parts are generated automatically by the TIRE statement. The centre of mass is taken to be at the location of the J marker for each tyre, i.e. locations 10, 40, 70, 100.

Table A.2 Front right suspension mass and moment of inertia data

Description	Part ID	CM marker	Mass (kg)	Mass moments of inertia (kg mm^2)		
				Ix	*Iy*	*Iz*
Wheel knuckle	11	1100	11.678	65.647E3	120.541E3	77.691E3
Lower arm	12	1200	3.4405	37.856E3	0.348E3	37.933E3
Tie bar	13	1300	2.64	0.023E3	3.876E3	3.876E3
Upper arm	14	1400	2.187	11.520E3	4.071E3	15.218E3
Tie rod	15	1500	0.575	3.876E3	0.023E3	3.876E3
Upper damper	16	1600	0.389	63.948E3	63.948E3	0.822E3
Lower damper	17	1700	6.215	107.364E3	107.364E3	4.972E3

Table A.3 Front left suspension mass and moment of inertia data

Description	Part ID	CM marker	Mass (kg)	Mass moments of inertia (kg mm^2)		
				Ix	*Iy*	*Iz*
Wheel knuckle	41	4100	11.678	65.647E3	120.541E3	77.691E3
Lower arm	42	1200	3.4405	37.856E3	1.348E3	37.933E3
Tie bar	43	1300	2.64	0.023E3	3.876E3	3.876E3
Upper arm	44	1400	2.187	11.520E3	4.071E3	15.218E3
Tie rod	45	1500	0.575	3.876E3	0.023E3	3.876E3
Upper damper	46	1600	0.389	63.948E3	63.948E3	0.822E3
Lower damper	47	1700	6.215	107.364E3	107.364E3	4.972E3

Table A.4 Rear right suspension mass and moment of inertia data

Description	Part ID	CM marker	Mass (kg)	Mass moments of inertia (kg mm^2)		
				Ix	*Iy*	*Iz*
Wheel knuckle	71	7100	12.036	165.994E3	196.457E3	34.224E3
Transverse arm	72	7200	6.424	101.389E3	15.215E3	113.237E3
Trailing arm	74	7400	4.322	12.826E3	190.372E3	199.393E3
Upper damper	73	7300	0.982	1.003E3	1.003E3	0.1E3

Table A.5 Rear left suspension mass and moment of inertia data

Description	Part ID	CM marker	Mass (kg)	Mass moments of inertia (kg mm^2)		
				Ix	*Iy*	*Iz*
Wheel knuckle	101	10100	12.036	165.994E3	196.457E3	34.224E3
Transverse arm	102	10200	6.424	101.389E3	15.215E3	113.237E3
Trailing arm	104	10400	4.322	12.826E3	190.372E3	199.393E3
Upper damper	103	10300	0.982	1.003E3	1.003E3	0.1E3

Table A.6 Body, rollbars and steering mass and moment of inertia data

Description	Part ID	CM marker	Mass (kg)	Mass moments of inertia (kg mm^2)		
				Ix	*Iy*	*Iz*
Body	200	20000	1427.3	379.0E6	2235.0E6	2269.0E6
Front right roll bar	201	20100	1.4	10.0	10.0	20.0
Front left roll bar	202	20200	1.4	10.0	10.0	20.0
Rear right roll bar	203	20300	1.4	10.0	10.0	20.0
Rear left roll bar	204	20400	1.4	10.0	10.0	20.0
Steering rack	500	50000	0.48	13357.0	48.0	13357.0
Steering column	510	51000	2.2	24.0E3	24.0E3	40762.0

Table A.7 Lumped mass model mass and moment of inertia data

Description	Part ID	CM marker	Mass (kg)	Mass moments of inertia (kg mm^2)		
				Ix	*Iy*	*Iz*
Right wheel knuckle	11	1100	11.678	65.647E3	120.541E3	77.691E3
Left wheel knuckle	41	4100	11.678	65.647E3	120.541E3	77.691E3
Front right mass	12	1200	15.447	86.818E3	159.445E3	102.765E3
Front left mass	42	4200	15.447	86.818E3	159.445E3	102.765E3
Rear right mass	71	7100	23.764	280.209E3	402.062E3	346.854E3
Rear left mass	101	10100	23.764	280.209E3	402.062E3	346.854E3

Table A.8 Swing arm model mass and moment of inertia data

Description	Part ID	CM marker	Mass (kg)	Mass moments of inertia (kg mm^2)		
				Ix	*Iy*	*Iz*
Right wheel knuckle	11	1100	11.678	65.647E3	120.541E3	77.691E3
Left wheel knuckle	41	4100	11.678	65.647E3	120.541E3	77.691E3
Front right arm	12	1200	15.447	86.818E3	159.445E3	102.765E3
Front left arm	42	4200	15.447	86.818E3	159.445E3	102.765E3
Rear right arm	71	7100	23.764	280.209E3	402.062E3	346.854E3
Rear left arm	101	10100	23.764	280.209E3	402.062E3	346.854E3

Table A.9 Roll stiffness model mass and moment of inertia data

Description	Part ID	CM marker	Mass (kg)	Mass moments of inertia (kg mm^2)		
				Ix	*Iy*	*Iz*
Right wheel knuckle	11	1100	11.678	65.647E3	120.541E3	77.691E3
Left wheel knuckle	41	4100	11.678	65.647E3	120.541E3	77.691E3
Front axle	13	1300	30.894	173.636E3	318.89E3	205.53E3
Rear axle	14	1400	47.528	560.418E3	804.124E3	693.708E3

Table A.10 Front right suspension geometry

Point ID	Co-ordinates (mm)			Euler angles (deg)			*ZP* (mm)		
	X	*Y*	*Z*	ψ	θ	ϕ	*X*	*Y*	*Z*
1100	966.1	743.9	165.9						
1200	1006.0	525.0	113.0	12D	−13.5D	0.0D			
1300	722.0	444.0	115.0						
1400	1064.0	500.0	566.0	28.5D	9D	0.0D			
1500	1129.0	534.0	189.0						
1600	954.4	509.6	497.3	163.66D	164.61D	0.0D			
1700	954.4	509.6	497.3	163.66D	164.61D	0.0D			
10	966.1	743.9	165.9	0D	90D	0.0D			
11	986.6	639.3	572.1						
13	962.2	703.1	90.7						
14	973.0	417.8	548.4	119.05D	91.03D	0.0D			
15	1106.2	673.9	171.7						
16	1050.0	348.3	137.0	−75.95D	90.87D	−172.78D			
17	474.0	332.0	115.0	−66.15D	90D	0.0D			
18	1145.0	392.0	196.0				1245.0	392.0	196.0*
19	945.9	480.4	607.7	163.66D	164.61D	0.0D			
20	954.4	509.6	497.3	163.66D	164.61D	0.0D			
21	987.0	620.0	76.5	−89.72D	98.11D	0.0D			
22	984.2	562.3	113.9						
23	945.9	480.4	607.7						
24	965.5	547.4	354.1						
25	945.9	480.4	607.7						
26	954.4	509.6	497.3						
27	945.9	480.4	607.7						
28	987.0	620.7	76.5						
31	966.1	693.1	165.9						
32	965.3	547.4	354.1						
33	945.9	480.4	607.7	163.66D	164.61D	0.0D			

* The *ZP* orientation is only applied to the marker which belongs to the rack part and is used for the universal joint connecting the rack to the tie rod.

Table A.11 Front left suspension geometry

Point ID	Co-ordinates (mm)			Euler angles (deg)			*ZP* (mm)		
	X	*Y*	*Z*	ψ	θ	ϕ	*X*	*Y*	*Z*
4100	966.1	−743.9	165.9						
4200	1006.0	−525.0	113.0	12D	−13.5D	0.0D			
4300	722.0	−444.0	115.0						
4400	1064.0	−500.0	566.0	28.5D	9D	0.0D			
4500	1129.0	−534.0	189.0						
4600	954.4	−509.6	497.3	−343.66D	164.61D	−180D			
4700	954.4	−509.6	497.3	−343.66D	164.61D	−180D			
40	966.1	−743.9	165.9	0D	90D	0D			
41	986.6	−639.3	572.1						
43	962.2	−703.1	90.7						
44	973.0	−417.8	548.4	−299.05D	91.03D	−180.0D			
45	1106.2	−673.9	171.7						
46	1050.0	−348.3	137.0	−104.05D	90.87D	−7.22D			
47	474.0	−332.0	115.0	−113.85D	90D	−180D			
48	1145.0	−392.0	196.0				1245.0	−392.0	196.0*
49	945.9	−480.4	607.7	−343.66D	164.61D	−180.0D			
50	954.4	−509.6	497.3	−343.66D	164.61D	−180D			
51	987.0	−620.0	76.5	89.72D	81.89D	0.0D			
52	984.2	−562.3	113.9						
53	945.9	−480.4	607.7						
54	965.5	−547.4	354.1						
55	945.9	−480.4	607.7						
56	954.4	−509.6	497.3						
57	945.9	−480.4	607.7						
58	987.0	−620.7	76.5						
61	966.1	−693.1	165.9						
62	965.3	−547.4	354.1						
63	945.9	−480.4	607.7	−343.66D	164.61D	180D			

* The *ZP* orientation is only applied to the marker which belongs to the rack part and is used for the universal joint connecting the rack to the tie rod.

Table A.12 Rear right suspension geometry

Point ID	Co-ordinates (mm)			Euler angles (deg)			*ZP* (mm)		
	X	*Y*	*Z*	ψ	θ	ϕ	*X*	*Y*	*Z*
7100	3732	725	167						
7200	3743	493	112	0D	4.55D	0.0D			
7300	3701.02	525.66	606.36	163.46D	166.09D	0.0D			
7400	3630	587	70						
70	3732	725	167	0D	90D	0.0D			
71	703.6	534.4	569.6	163.46D	166.09D	0.0D			
72	3732	725	167						
73	3747	706	109.5	88.809D	90D	−4.3376D			
74	3701	525.7	606.4	163.46D	166.09D	−195D			
75	3695.4	684.6	48.1	56.715D	97.334D	0.0D			
76	3803.4	613.7	34.2	56.716D	97.334D	0.0D			
77	3743	496	84.0						
78	3743	475	265.8						
79	3737	225	146	88.809D	90D	−4.3376D			
80	3203	600	144.5	75.0491D	98.3D	0.0D			
81	3703.5	533	573						
82	3693	499	714						
83	3693.3	499.7	715.9						
84	3729.7	622.2	200						
85	3701	525.7	606.4	163.46D	166.09D	0.0D			
86	3703.6	534.4	569.6						
91	3732	684.6	167						

Table A.13 Rear left suspension geometry

Point ID	Co-ordinates (mm)			Euler angles (deg)			*ZP* (mm)		
	X	*Y*	*Z*	ψ	θ	ϕ	*X*	*Y*	*Z*
10100	3732	−725	167						
10200	3743	−493	112	−180D	4.55D	−180D			
10300	3701.02	−525.66	606.36	−343.46D	166.09D	−180D			
10400	3630	−587	70						
100	3732	−725	167	0D	90D	0.0D			
101	3703.6	−534.4	569.6	163.46D	166.09D	0.0D			
102	3732	−725	167						
103	3747	−706	109.5	91.191D	90D	−175.6624D			
104	3701	−525.7	606.4	−343.46D	166.09D	15D			
105	3695.4	−684.6	48.1	123.284D	97.334D	180D			
106	3803.4	−613.7	34.2	123.284D	97.334D	180D			
107	3743	−496	84.0						
108	3743	−475	265.8						
109	3737	−225	146	91.191D	90D	−175.634D			
110	3203	−600	144.5	−255.049D	98.3D	180D			
111	3703.5	−533	573						
112	3693	−499	714						
113	3693.3	−499.7	715.9						
114	3729.7	−622.2	200						
115	3701	−525.7	606.4	−343.46D	166.09D	180D			
116	3703.6	−534.4	569.6						
121	3732	−684.6	167						

Table A.14 Body, roll bars and steering geometry

Point ID	Co-ordinates (mm)			Euler angles (deg)			*ZP* (mm)		
	X	*Y*	*Z*	ψ	θ	ϕ	*X*	*Y*	*Z*
20000	2150.4	0.0	452.0						
20100	1264	263	87	0.0D	90D	0.0D			
201	1264	263	87	0.0D	90D	0.0D			
203	1264	0.0	87	0.0D	90D	0.0D			
204	966.1	743.9	165.9						
20200	1264	−263	87	0.0D	90D	0.0D			
202	1264	−263	87	0.0D	90D	0.0D			
203	1264	0.0	87	0.0D	90D	0.0D			
205	966.1	−743.9	165.9						
20300	4142	508	268	0.0D	90D	0.0D			
206	4142	508	268	0.0D	90D	0.0D			
208	4142	0	268	0.0D	90D	0.0D			
209	3732	725	167						
20400	4142	−508	268	0.0D	90D	0.0D			
207	4142	−508	268	0.0D	90D	0.0D			
208	4142	0	268	0.0D	90D	0.0D			
210	3732	−725	167						
50000	1145	0	196						
501	1145	0	196	180D	90D	0.0D			
51000	1964	353	787.6				1698.6	348.6	604.4
502	1964	353	787.6				1698.6	348.6	604.4
5101	2072	353	631						
5102	1961	543	788						
5103	1967	163	788						
5104	1145	338	222						

Table A.15 Lumped mass model geometry

Point ID	Co-ordinates (mm)			Euler angles (deg)			*ZP* (mm)		
	X	*Y*	*Z*	ψ	θ	ϕ	*X*	*Y*	*Z*
1100	966.1	743.9	165.9						
1200	966.1	500	165.9						
4100	966.1	−743.9	165.9						
4200	966.1	−500	165.9						
7100	3732	500	167						
10100	3732	−500	167						
11	966.1	500	165.9						
41	966.1	−500	165.9						
39	966.1	743.9	165.9						
69	966.1	−743.9	165.9						
99	3732	500	167						
129	3732	−500	167						

Table A.16 Swing arm model geometry

Point ID	Co-ordinates (mm)			Euler angles (deg)			*ZP* (mm)		
	X	*Y*	*Z*	ψ	θ	ϕ	*X*	*Y*	*Z*
1100	966.1	743.9	165.9						
1200	966.1	500	165.9						
4100	966.1	−743.9	165.9						
4200	966.1	−500	165.9						
7100	3732	500	167.0						
10100	3732	−500	167.0						
39	966.1	743.9	165.9						
69	966.1	−743.9	165.9						
11	966.1	−1361	358.6						
41	966.1	1361	358.6						
71	3732	−576.5	206.2						
101	3732	576.5	206.2						

Table A.17 Roll stiffness model geometry

Point ID	Co-ordinates (mm)			Euler angles (deg)			*ZP* (mm)		
	X	*Y*	*Z*	ψ	θ	ϕ	*X*	*Y*	*Z*
1100	966.1	743.9	165.9						
4100	966.1	−743.9	165.9						
1300	966.1	0.0	165.9						
1400	3732.0	0.0	167.0						
39	966.1	743.9	165.9						
69	966.1	−743.9	165.9						
11	966.1	0.0	27.4						
12	3732.0	0.0	47.4						

Table A.18 Spring data

The springs are defined using the SPRINGDAMPER statement.	
Front spring:	
Stiffness	$k = 31.96$ N/mm
Free length	$L = 426$ mm
Rear spring:	
Stiffness	$k = 60.8$ N/mm
Free length	$L = 253$ mm

Table A.19 Front damper data

The dampers are defined using the SFORCE statement. The dampers are non-linear. The data provided shows the variation of force in the damper with velocity.	
Velocity (mm/s)	−5000, −3150, −2870, −2450, −2205, −1925, −1610, −1260, −910, −630, −470, − 400, −350, −300, −250, −230, −200, −190, −160, −120, −80, −55, −40, −20, −10, −1, −0.1, 0, 0.3, 3, 30, 40, 60, 80, 100, 200, 250, 400, 490, 770, 1050, 1330, 1820, 2060, 2485, 2590, 2730, 2835, 2940, 3080, 5000
Force (N)	10425, 5800, 5200, 4400, 4000, 3600, 3200, 2800, 2400, 2000, 1800, 1700, 1600, 1500, 1400, 1350, 1310, 1290, 1200, 1000, 700, 400, 210, 80, 40, 4, 0.4, 0, −1, −10, −100, −123, −150, −182, −200, −260, −300, −400, −500, −800, −1200, −1600, −2400, −2800, −3400, −3500, −3600, −3700, −3800, −4000, −7840

Table A.20 Rear damper data

The dampers are defined using the SFORCE statement. The dampers are non-linear. The data provided shows the variation of force in the damper with velocity.	
Velocity (mm/s)	−5000, −3150, −2800, −2450, −2100, −1750, −1400, −1050, −700, −560, −500, −450, −400, −350, −300, −250, −200, −150, −100, −50, −25, −5, −1, −0.1, 0, 0.1, 1, 5, 25, 50, 100, 200, 300, 400, 500, 700, 1050, 1400, 1750, 2100, 2450, 2800, 3150, 5000
Force (N)	7352, 3652, 3120, 2635, 2193, 1855, 1518, 1180, 927, 843, 800, 773, 722, 686, 658, 596, 560, 488, 329, 154, 77, 15.4, 3.08, 0.308, 0, −0.126, −1.26, −6.3, −31.5, −63, −126, −153.25, −180.5, −208, −235, −253, −380, −675, −970, −1349, −1788, −2277, −2867, −6567

Table A.21 Roll bar data

Front roll bar: Torsional stiffness	Kt = 490E3 N mm/rad
Rear roll bar: Torsional stiffness	Kt = 565E3 N mm/rad

Table A.22 Front suspension bush data

The following linear values are used to define the stiffness and damping in the bushes. For each bush data is listed as:

$K = kx, ky, kz$	Stiffness (N/mm)
$KT = ktx, kty, ktz$	Torsional stiffness (Nmm/rad)
$C = cx, cy, cz$	Damping (N s/mm)
$CT = ctx, cty, ctz$	Torsional damping (N mm s/rad)

LOWER ARM MOUNT BUSH (Location 12 and 42)
K = 7825, 7825, 944
KT = 2.5E6, 2.5E6, 500
C = 35, 35, 480
CT = 61 000, 61 000, 40

TIE BAR BUSH MOUNT
K = 5723, 5723, 6686
KT = 543 000, 543 000, 500
C = 400, 400, 300
CT = 18 400, 18 400, 4

UPPER DAMPER MOUNT
K = 14 353, 14 353, 10 000
KT = 120 000, 120 000, 400
C = 400, 400, 300
CT = 1200, 1200, 40

LOWER DAMPER MOUNT
K = 6385, 6385, 550
KT = 355 000, 355 000, 400
C = 640, 640, 50
CT = 35 000, 35 000, 40

Table A.23 Rear suspension bush data

The following linear values are used to define the stiffness and damping in the bushes. For each bush data is listed as:

K = *kx*, *ky*, *kz*	Stiffness (N/mm)
KT = *ktx*, *kty*, *ktz*	Torsional stiffness (N mm/rad)
C = *cx*, *cy*, *cz*	Damping (N s/mm)
CT = *ctx*, *cty*, *ctz*	Torsional damping (N mm s/rad)

REAR TRAILING LINK TO HUB BUSHES
K = 10 500, 10 500, 870
KT = 2.8E5, 2.8E5, 67 500
C = 1000, 1000, 100
CT = 25 000, 25 000, 40

REAR TRAILING LINK TO BODY BUSH
K = 660, 660, 175
KT = 260 300, 260 300, 40 000
C = 100, 100, 50
CT = 25 000, 25 000, 40

REAR UPPER DAMPER MOUNT
K = 540, 1300, 532
KT = 58 915, 180 750, 670
C = 200, 200, 70
CT = 5800, 5800, 67

The following linear values are used to define the stiffness and damping in the bushes. For each bush data is listed as:

K = *kx*, *ky*, *kz*	Stiffness (N/mm)
KT = *ktx*, *kty*, *ktz*	Torsional stiffness (N mm/rad)
C = *cx*, *cy*, *cz*	Damping (N s/mm)
CT = *ctx*, *cty*, *ctz*	Torsional damping (N mm s/rad)

REAR LOWER ARM TO BODY MOUNT
K = 10 800, 3420, 840
KT = 790 000, 380 000, 400
C = 1000, 400, 100
CT = 88 000, 40 000, 40

REAR LOWER ARM TO HUB BUSH
K = 5540, 5540, 515
KT = 210 540, 210 540, 400
C = 800, 800, 50
CT = 25 000, 25 000, 40

Appendix B: Fortran tyre model subroutines

B.1 Interpolation tyre model subroutine

```
      SUBROUTINE TIRSUB (ID, TIME, T0, CPROP, TPROP, MPROP,
     &                   PAR, NPAR, STR, NSTR, DFLAG,
     &                   IFLAG, FSAE, TSAE, FPROP)
C
C     This program is part of the CUTyre system - M Blundell, Feb 1997
C     This version is based on an interpolation approach using measured
C     tyre test data which is include in SPLINE statements. The model is
      referred to as the
C     Limited version based on the limited testing where camber and slip are
      varied
C     independently.
C
C
C     The coefficients in the model assume the following units:
C     slip angle: degrees
C     camber angle: degrees
C     Fz (load): kg
C     Fy and Fx: N
C     Tz: Nm
C
C     Note this subroutine is developed to not account for offsets
C     twice. The offsets are include for slip interpolation
C     but for camber the offset at zero camber is subtracted.
C
C Inputs:
C
      INTEGER           ID, NPAR, NSTR
      DOUBLE PRECISION TIME, T0
      DOUBLE PRECISION CPROP(*), TPROP(*), MPROP(*), PAR(*)
      CHARACTER*80 STR(*)
      LOGICAL           DFLAG, IFLAG, ERRFLG
C
C Outputs:
C
      DOUBLE PRECISION FSAE(*), TSAE(*), FPROP(*), ARRAY(3)
C
C Local Variables:
C
      DOUBLE PRECISION SLIP, ALPHA, DEFL, DEFLD
      DOUBLE PRECISION R2, CZ, CS, CA, CR, DZ, AMASS, WSPIN
C
      DOUBLE PRECISION GAMMA,CG,RALPHA,RGAMMA,FZL,
      TZL,TZLA,TZLG
      DOUBLE PRECISION CFY,DFY,EFY,SHFY,SVFY,PHIFY,TZLG0,
      TZLG1
```

```
      DOUBLE PRECISION CTZ,DTZ,ETZ,BTZ,SHTZ,SVTZ,PHITZ
      DOUBLE PRECISION CFX,DFX,EFX,BFX,SHFX,SVFX,PHIFX
C
      INTEGER          IORD
      DOUBLE PRECISION ZERO, ONE, SCFACT, DELMAX,FYA,
     FYG,FYG0,FYG1
      DOUBLE PRECISION FX, FY, FZ, FX1, FX2, TY, TZ, H, ASTAR,
     SSTAR
      DOUBLE PRECISION U, FZDAMP, FZDEFL, WSPNMX, DTOR,
     RTOD
      LOGICAL          ERFLG
C
      PARAMETER        (ZERO=0.0)
      PARAMETER        (ONE=1.0)
      PARAMETER        (IORD=0)
      PARAMETER        (WSPNMX=5.0D-1)
      PARAMETER        (DTOR=0.017453292)
      PARAMETER        (RTOD=57.29577951)
C
C
C     EXECUTABLE CODE
C
C
C     Extract data from input arrays
C
      SLIP    = CPROP(1)
      DEFL    = CPROP(4)
      DEFLD = CPROP(5)
      WSPIN = CPROP(8)
C
      AMASS = MPROP(1)
C
      R2  = TPROP(2)
      CZ  = TPROP(3)
      CS  = TPROP(4)
      CA  = TPROP(5)
      CR  = TPROP(7)
      DZ  = TPROP(8)
      U   = TPROP(11)
C
      RALPHA   = CPROP(2)
      RGAMMA = CPROP (3)
      CG           = TPROP (6)
      ALPHA      = RALPHA*RTOD
      GAMMA    = RGAMMA*RTOD
C
C     Initialize force values
C
      FX = 0.D0
      FY = 0.D0
      FZ = 0.D0
      TY = 0.D0
```

```
      TZ=0.D0
C
      IF(DEFL .LE. 0.D0) THEN
      GOTO 1000
      ENDIF
C
C     Calculate normal loads due to stiffness (always .LE. zero)
C
      FZDEFL = -DEFL*CZ
C
C     Calculate normal loads due to damping
C
      FZDAMP = -2.D0*SQRT(AMASS*CZ)*DZ*(DEFLD)
C
C     Calculate total normal force (fz)
C
      FZ = MIN (0.0D0, (FZDEFL + FZDAMP))
C
C     Convert to kg and change sign
C
      FZL = -FZ/9.81
C
C     Calculate critical longitudinal slip value
C
      SSTAR = ABS(U*FZ/(2.D0*CS))
C
C     Compute longitudinal force
C
      IF(ABS(SLIP) .LE. ABS(SSTAR)) THEN
        FX = -CS*SLIP
      ELSE
        FX1 = U*ABS(FZ)
        FX2 = (U*FZ)**2/(4.D0*ABS(SLIP)*CS)
        FX = -(FX1-FX2)*SIGN(1.0D0,SLIP)
      ENDIF
C
C     Compute lateral force
C
      CALL CUBSPL (ALPHA,FZL,100,0,ARRAY,ERRFLG)
      FYA=ARRAY(1)
      CALL CUBSPL (0,FZL,300,0,ARRAY,ERRFLG)
      FYG0=ARRAY(1)
      CALL CUBSPL (GAMMA,FZL,300,0,ARRAY,ERRFLG)
      FYG1=ARRAY(1)
      FYG=FYG1−FYG0
      FY=FYA+FYG
C
C     Compute self aligning moment
C
      CALL CUBSPL (ALPHA,FZL,200,0,ARRAY,ERRFLG)
      TZLA=ARRAY(1)
      CALL CUBSPL (0,FZL,400,0,ARRAY,ERRFLG)
```

```
      TZLG0=ARRAY(1)
      CALL CUBSPL (GAMMA,FZL,400,0,ARRAY,ERRFLG)
      TZLG1=ARRAY(1)
      TZLG=TZLG1-TZLG0
      TZL=TZLA+TZLG
C
C     Convert to Nmm
C
      TZ=TZL*1000.0
C
C     Copy the calculated values for FX, FY, FZ, TY & TZ to FSAE
C     and TSAE arrays
C
1000 FSAE(1) = FX
       FSAE(2) = FY
       FSAE(3) = FZ
C
      TSAE(1) = 0.0
      TSAE(2) = 0.0
      TSAE(3) = TZ
C
      FPROP(1) = 0.0
      FPROP(2) = 0.0
C
      RETURN
      END
```

B.2 'Magic Formula' tyre model (version 3) subroutine

```
      SUBROUTINE TIRSUB (ID, TIME, T0, CPROP, TPROP, MPROP,
     &                   PAR, NPAR, STR, NSTR, DFLAG,
     &                   IFLAG, FSAE, TSAE, FPROP)
C
C     This program is part of the CUTyre system - M Blundell, Feb 1997
C     This version is based on the Magic Formula tyre model (Version 3).
C     Coefficients are for TYRE B
C
C     The coefficients in the model assume the following units:
C     slip angle: radians
C     camber angle: radians
C     slip ratio %
C     Fz (load): N
C     Fy and Fx: N
C     Tz: Nm
C     Note sign changes between Paceka formulation and SAE convention
C     If camber is not included set A5,A10,A13,A14,A15,A16
C     and C6,C10,C13,C16,C17,C18,C19,C20 to zero
C
C Inputs:
C
```

```
      INTEGER          ID, NPAR, NSTR
      DOUBLE PRECISION TIME, T0
      DOUBLE PRECISION CPROP(*), TPROP(*), MPROP(*), PAR(*)
      CHARACTER * 80 STR(*)
      LOGICAL          DFLAG, IFLAG
C
C Outputs:
C
      DOUBLE PRECISION FSAE(*), TSAE(*), FPROP(*)
C
C Local Variables:
C
      DOUBLE PRECISION SLIP, ALPHA, DEFL, DEFLD
      DOUBLE PRECISION R2, CZ, CS, CA, CR, DZ, AMASS, WSPIN
C
C
C
      DOUBLE PRECISION GAMMA,CG,RALPHA,RGAMMA,FXP,
     FZP,FYP,TZP
      DOUBLE PRECISION A0,A1,A2,A3,A4,A5,A6,A7,A8,A9,A10,
     A11,A12,A13
      DOUBLE PRECISION A14,A15,A16,A17,SLIPCENT
      DOUBLE PRECISION C0,C1,C2,C3,C4,C5,C6,C7,C8,C9,C10,C11,
     C12,C13
      DOUBLE PRECISION C14,C15,C16,C17,C18,C19,C20
      DOUBLE PRECISION CFY,DFY,EFY,SHFY,SVFY,PHIFY
      DOUBLE PRECISION CTZ,DTZ,ETZ,BTZ,SHTZ,SVTZ,PHITZ
      DOUBLE PRECISION CFX,DFX,EFX,BFX,SHFX,SVFX,PHIFX,
     DUMTZ,DUMFY
C
      INTEGER          IORD
      DOUBLE PRECISION ZERO, ONE, SCFACT, DELMAX
      DOUBLE PRECISION FX, FY, FZ, FX1, FX2, TY, TZ, H, ASTAR,
     SSTAR
      DOUBLE PRECISION U, FZDAMP, FZDEFL, WSPNMX, DTOR,
     RTOD
      LOGICAL          ERFLG
C
      PARAMETER        (ZERO=0.0)
      PARAMETER        (ONE=1.0)
      PARAMETER        (IORD=0)
      PARAMETER        (WSPNMX=5.0D-1)
      PARAMETER        (DTOR=0.017453292)
      PARAMETER        (RTOD=57.29577951)
C
C     Define Pacejka Coefficients
C
      A0 = .103370E+01
      A1 = -.224482E-05
      A2 = .132185E+01
      A3 = .604035E+05
      A4 = .877727E+04
```

```
      A5   = 0.0
      A6   = .458114E-04
      A7   = .468222
      A8   = .381896E-06
      A9   = .516209E-02
      A10  = 0.00
      A11  = -.366375E-01
      A12  = -.568859E+02
      A13  = 0.00
      A14  = 0.00
      A15  = 0.00
      A16  = 0.00
      A17  = .379913
C
C
      C0   = .235000E+01
      C1   = .266333E-05
      C2   = .249270E-02
      C3   = -.159794E-03
      C4   = -.254777E-01
      C5   = .142145E-03
      C6   = 0.00
      C7   = .197277E-07
      C8   = -.359537E-03
      C9   = .630223
      C10  = 0.00
      C11  = .120220E-06
      C12  = .275062E-02
      C13  = 0.00
      C14  = -.172742E-02
      C15  = .544249E+01
      C16  = 0.00
      C17  = 0.00
      C18  = 0.00
      C19  = 0.00
      C20  = 0.00
C
C
C     EXECUTABLE CODE
C
C
C     Extract data from input arrays
C
      SLIP     = CPROP(1)
      DEFL     = CPROP(4)
      DEFLD    = CPROP(5)
      WSPIN    = CPROP(8)
C
      AMASS    = MPROP(1)
C
       R2 = TPROP(2)
       CZ = TPROP(3)
```

```
      CS  = TPROP(4)
      CA  = TPROP(5)
      CR  = TPROP(7)
      DZ  = TPROP(8)
      U   = TPROP(11)
C
C     Convert sign on alpha
C
      RALPHA   = CPROP(2)
      RGAMMA = CPROP (3)
      CG         = TPROP (6)
      ALPHA    = -RALPHA
      GAMMA   = RGAMMA
C
C     Initialize force values
C
      FX = 0.D0
      FY = 0.D0
      FZ = 0.D0
      TY = 0.D0
      TZ = 0.D0
C
      IF(DEFL .LE. 0.D0) THEN
        GOTO 1000
      ENDIF
C
C     Calculate normal loads due to stiffness (always .LE. zero)
C
      FZDEFL = -DEFL*CZ
C
C     Calculate normal loads due to damping
C
      FZDAMP = -2.D0*SQRT(AMASS*CZ)*DZ*(DEFLD)
C
C     Calculate total normal force (fz)
C
      FZ = MIN (0.0D0, (FZDEFL+FZDAMP) )
C
C     Convert to kN and change sign
C
      FZP = -FZ
C
C     Compute longitudinal force
C
      IF(ABS(SLIP) .LE. ABS(SSTAR)) THEN
        FX = -CS*SLIP
      ELSE
        FX1 = U*ABS(FZ)
        FX2 = (U*FZ)**2/(4.D0*ABS(SLIP)*CS)
        FX = -(FX1-FX2)*SIGN(1.0D0,SLIP)
      ENDIF
C
```

```
C    Compute lateral force
C
      CFY=A0
      SHFY=A8*FZP+A9+A10*GAMMA
      DFY=(A1*FZP+A2)*(1-A15*GAMMA**2)*FZP
      IF(ALPHA+SHFY.LT.0.0)THEN
        DUMFY=-1.0
      ELSE
        DUMFY=1.0
      ENDIF
      EFY=(A6*FZP+A7)*(1-(A16*GAMMA+A17)*DUMFY)
      BFY=((A3*SIN(2*ATAN(FZP/A4)))*(1-A5*ABS(GAMMA)))/
      (CFY+DFY)
      SVFY=A11*FZP+A12+(A13*FZP**2+A14*FZP)*GAMMA
      PHIFY=(1-EFY)*(ALPHA+SHFY)+(EFY/BFY)*
      ATAN (BFY*(ALPHA+SHFY))
      FYP=DFY*SIN(CFY*ATAN(BFY*PHIFY))+SVFY
C
C    Change sign
C
      FY=FYP
C
C    Compute self aligning moment
C
      CTZ=C0
      SHTZ=C11*FZP+C12+C13*GAMMA
      DTZ=(C1*FZP**2+C2*FZP)*(1-C18*GAMMA**2)
      IF(ALPHA+SHTZ.LT.0.0)THEN
        DUMTZ=-1.0
      ELSE
        DUMTZ=1.0
      ENDIF
      ETZ=(C7*FZP**2+C8*FZP+C9)*(1-(C19*GAMMA+C20)*
      DUMTZ)
      ETZ=ETZ/(1-C10*ABS(GAMMA))
      BTZ=((C3*FZP**2+C4*FZP)*(1-C6*ABS(GAMMA))*
      EXP(-C5*FZP))/(CTZ+DTZ)
      SVTZ=C14*FZP+C15+(C16*FZP**2+C17*FZP)*
      GAMMA
      PHITZ=(1-ETZ)*(ALPHA+SHTZ)+(ETZ/BTZ)*ATAN(BTZ*
      (ALPHA+SHTZ))
      TZP=DTZ*SIN(CTZ*ATAN(BTZ*PHITZ))+SVTZ
C
C    Convert to Nmm and change sign
C
      TZ=TZP*1000.0
C
C    Copy the calculated values for FX, FY, FZ, TY & TZ to FSAE
C    and TSAE arrays
C
1000 FSAE(1)=FX
       FSAE(2)=FY
```

```
      FSAE(3)=FZ
      TSAE(1)=0.0
      TSAE(2)=0.0
      TSAE(3)=TZ
     FPROP(1)=0.0
     FPROP(2)=0.0
C
      RETURN
      END
```

B.3 The Harty tyre model subroutine

```
C
C   MDI TIRSUB : Prodrive Concept Tyre Model
C
C   A Quick & Simplified Tyre Model which plugs in as the FIALA
C   model does, with a "TIRE" statement.
C
C   Unlike FIALA, critical slip angle is broadly independent
C   of load and initial cornering stiffness is strongly
C   load dependent.
C
C   The model does handle comprehensive slip. Lateral force
C   generation is zero at peak longitudinal force slip ratio
C   (typically about 20%) but returns to a value around one
C   tenth of the peak lateral force as the wheel progresses
C   beyond that limit. This may result in poor post-spin
C   performance. The force generated with locked wheels is
C   currently aligned with the wheel plane; this is incorrect.
C
C   Longitudinal force generation is assumed to be symmetric
C   for tractive and braking slip. This is not generally
C   true beyond the critical slip ratio for real tyres but
C   is reasonable up to that point. This tyre will over
C   estimate longitudinal forces for tractive slip and
C   slightly underestimate them for braking slip in the
C   post-critical regions.
C
C   Camber thrust is included as for the motorcycle tire
C   model using "taut string" logic. Lateral migration of
C   the contact patch is not included, unlike a motorcycle
C   tyre model.
C
C   Aligning Torque calculation includes the lateral force
C   due to camber. This is not quite right as the camber
C   force mechanism has no pneumatic trail associated with
C   it. Pay attention if using this for motorcycle work;
C   consider reworking it so that TZ does not include the
C   camber force. The form of the aligning torque is a
C   bit poor and would benefit from some more thought;
C   pneumatic trail collapses linearly with lateral force.
```

```
C
C   Relaxation Length is externally imposed as with the
C   Fiala tyre.
C
C   Tyre Data is taken from the tyre parameter file (.tpf)
C   but note that not all the data is used. The other
C   parameters are passed in via the UPARAMETERS argument
C   on the TIRE statement inside an MSC.ADAMS deck.
C
C   The model is quite empirical and has no basis in any sort
C   of established fact or theory. It may or may not bear a
C   passing resemblance to "Maltyre", a Malcolm Burgess model
C   implemented at Lotus, although this is unintended.
C
C   (c) DAH 24 Oct 1999
C
C   A quick note on the comment style. Before the
C   '$$$ EXECUTABLE CODE $$$' line, the comments are all
C   as standard in a TIRSUB
C   After that, process chunks are separated with some blank
C   lines and an 'open' comment. Comments which refer
C   specifically to the following lines of code start and
C   end with a double dash (--).
C
      SUBROUTINE TIRSUB (ID, TIME, T0, CPROP, TPROP, MPROP,
     &                   PAR, NPAR, STR, NSTR, DFLAG,
     &                   IFLAG, FSAE, TSAE, FPROP)
C
C Inputs:
C
      INTEGER           ID, NPAR, NSTR
      DOUBLE PRECISION TIME, T0
      DOUBLE PRECISION CPROP(*), TPROP(*), MPROP(*), PAR(*)
      CHARACTER*80          STR(*)
      LOGICAL           DFLAG, IFLAG
C
C Outputs:
C
      DOUBLE PRECISION FSAE(*), TSAE(*), FPROP(*)
C
C Local Variables:
C
      DOUBLE PRECISION SLIP, ALPHA, DEFL, DEFLD, CAMBER, CG
      DOUBLE PRECISION R1, R2, CZ, CS, CA, CR, DZ, AMASS,
      WSPIN
C
      DOUBLE PRECISION ALPHA_C, Ay, By, R_LOAD, dB_dFz,
      ALPHA_M
      DOUBLE PRECISION SLIP_C, Ax, SLIP_M, FR_ELLIP, CP_LEN
C
      INTEGER           IORD
      DOUBLE PRECISION ZERO, ONE, SCFACT, DELMAX
```

```
C    DOUBLE PRECISION FX, FY, FZ, FX1, FX2, TX, TY, TZ, H, ASTAR
     DOUBLE PRECISION FX, FY, FZ, TX, TY, TZ
C    DOUBLE PRECISION SSTAR, U, FZDAMP, FZDEFL, WSPNMX
     DOUBLE PRECISION FZDAMP, FZDEFL, WSPNMX
     DOUBLE PRECISION B, USLIP, SCMIN, LSLIP, TSCALE
     LOGICAL      ERFLG
C
     PARAMETER   (ZERO=0.0)
     PARAMETER   (ONE=1.0)
     PARAMETER   (IORD=0)
     PARAMETER   (WSPNMX=5.0D-1)
C
C
C$$$$$$$$$$$$$$$$ EXECUTABLE CODE $$$$$$$$$$$$$$$$$$$$$$
C
C
C    Extract data from input arrays
C
C -- Tyre States at Run-time: --
     SLIP       = CPROP(1)
     ALPHA    = CPROP(2)
     CAMBER = CPROP(3)
     DEFL       = CPROP(4)
     DEFLD    = CPROP(5)
     WSPIN    = CPROP(8)
C -- Wheel & Tyre Mass, scaled (see manual) --
       AMASS = MPROP(1)
C -- Tyre Properties, from .tpf file --
C            Unladen Radius
     R1       = TPROP(1)
C               Carcase width
     R2       = TPROP(2)
C               Vertical Stiffness
     CZ       = TPROP(3)
C               Longitudinal Stiffness - not used
     CS       = TPROP(4)
C               Cornering Stiffness - not used
     CA       = TPROP(5)
C               Camber Stiffness - not used
     CG       = TPROP(6)
C               Rolling Resistance Coeffiecient
     CR       = TPROP(7)
C               Damping Ratio in Z (viscous damping)
     DZ       = TPROP(8)
C               Static Friction Coefficient
C    MU     = TPROP(9)
C               Sliding Friction Coefficient
C    MU_S = TPROP(10)
C               Friction Coefficient at the current slip value
          U = TPROP(11)
C -- Tyre Properties from UPAR Array inside MSC.ADAMS Deck--
```

```
C                    Critical Slip Angle (Max Lateral Force) - degrees in
                     User Array
      ALPHA_C  =  PAR(1)
C                    Curvature Factor (exponential function to peak slip
                     angle)
      Ay       =  PAR(2)
C                    Scale Factor for Lateral Force at Rated Load
      By       =  PAR(3)
C                    Rated Load (N)
      R_LOAD   =  PAR(4)
C                    Diminution of Scale Factor with load
      dB_dFz   =  PAR(5)
C                    Max Slip angle
      ALPHA_M  =  PAR(6)
C                    Critical Slip Ratio (Max Longitudinal Force) %
      SLIP_C   =  PAR(7)
C                    Curvature Factor (exponential function to peak slip ratio)
      Ax       =  PAR(8)
C                    Max Slip Ratio
      SLIP_M   =  PAR(9)
C     -- Debug only - check we're getting what we think --
C     IF ( IFLAG .eq. .TRUE. ) THEN
C       WRITE(*,*) 'ALPHA_C ', ALPHA_C, ', Ay ', Ay, ', By ', By
C       WRITE(*,*) 'R_LOAD', R_LOAD, ', dB_dFz ', dB_dFz
C       WRITE(*,*) 'ALPHA_M ', ALPHA_M, ', SLIP_C ', SLIP_C,
        ', Ax ', Ax
C     WRITE(*,*) 'SLIP_M ', SLIP_M
C     ENDIF
C     Tyre Modelling Proper Begins
C     Initialize force values
C
      FX=0.D0
      FY=0.D0
      FZ=0.D0
      TX=0.D0
      TY=0.D0
      TZ=0.D0
C -- Wheel off the ground? Easy – everything zero --
      IF(DEFL .LE. 0.D0) THEN
        GOTO 1000
      ENDIF
C     Normal Loads; simple calculations as with sample tirsub.f;
C     Penetrations to hub are not accounted for.
C -- Calculate normal loads due to stiffness (always .LE. zero) --
      FZDEFL=-DEFL*CZ
C -- Calculate normal loads due to damping --
      FZDAMP=-2.D0*SQRT(AMASS*CZ)*DZ*(DEFLD)
C -- Ease up on the damping force scale factor at small deflections --
      DELMAX=0.01*R2
      IF (DEFL .LE. DELMAX) THEN
        CALL STEP(DEFL, ZERO, ZERO, DELMAX, ONE, IORD,
        SCFACT, ERFLG)
```

```
        FZDAMP=SCFACT*FZDAMP
       ENDIF
C -- Sum for total normal force --
       FZ=MIN (0.0D0, (FZDEFL+FZDAMP) )
C    Longitudinal Loads
C C   ************* FIALA CALCULATIONS *************
C C
C C   Calculate critical longitudinal slip value
C C
C    SSTAR=ABS(U*FZ/(2.D0*CS))
C C
C C   Compute longitudinal force (fx)
C C
C    IF(ABS(SLIP) .LE. ABS(SSTAR)) THEN
C      FX=-CS*SLIP
C    ELSE
C      FX1=U*ABS(FZ)
C      FX2=(U*FZ)**2/(4.D0*ABS(SLIP)*CS)
C      FX=-(FX1-FX2)*SIGN(1.0D0,SLIP)
C    ENDIF
C C
C C   ****************************************
C -- We're working in percent --
       SLIP=SLIP*100
       IF(ABS(SLIP) .LE. ABS(SLIP_C)) THEN
C -- Exponential Rise (1-e^-x) below critical slip ratio --
       FX=(1-EXP(-Ax*ABS(SLIP)/SLIP_C))*U*FZ*SIGN(1.0D0,SLIP)
       ELSE
C -- Linear Decay to Sliding Friction above critical slip ratio --
C -- MU_S Apparently not passed through? --
C    FX=-FZ*(1-EXP(-Ax))*(MU-(ABS(SLIP)-SLIP_C)/SLIP_M*
       (MU-MU_S))
C    FX=FX*SIGN(1.0D0,SLIP)
C -- Try U instead? --
       FX=FZ*(1-EXP(-Ax))*U*SIGN(1.0D0,SLIP)
       ENDIF
C    Lateral force and aligning torque (FY & TZ)
C    -- Scale Factor Diminished with Load FZ --
       B=By+(ABS(FZ)-R_LOAD)*dB_dFz
C -- We're working in degrees --
       ALPHA=ALPHA*45/ATAN(1.0)
       IF(ABS(ALPHA) .LE. 1.D-10) THEN
         FY=0.D0
         TZ=0.D0
       ELSE IF(ABS(ALPHA) .LE. ALPHA_C) THEN
C -- As for longitudinal forces, Exponential Rise (1-e^-x) below
C    critical slip angle --
C -- This line contains an even number of minus-sign errors --
       FY=(1-EXP(-Ay*ABS(ALPHA)/ALPHA_C))*U*B*FZ*SIGN
       (1.0D0,ALPHA)
       ELSE
```

```
C -- As for longitudinal forces, Linear Decay to Sliding Friction
C    above critical slip ratio --
C -- MU_S apparently not passed through? --
C    FY=FZ*(1-EXP(-Ay))*(MU-(ABS(ALPHA)−ALPHA_C)/
     ALPHA_M*(MU−MU_S))
C    FY=FY*B*SIGN(1.0D0,ALPHA)
C -- Try U instead? --
     FY=FZ*(1-EXP(-Ay))*U*B*SIGN(1.0D0,ALPHA)
     ENDIF
C C ********** FIALA CALCULATIONS **********
C C
C C Calculate critical value of slip angle
C C
C    ASTAR=ATAN(ABS(3.D0*U*FZ/CA))
C C
C C Compute Fiala lateral force and aligning torque (FY & TZ)
C C
C    IF(ABS(ALPHA) .LE. 1.D-10) THEN
C      FY=0.D0
C      TZ=0.D0
C    ELSE IF(ABS(ALPHA) .LE. ASTAR) THEN
C      H=1.D0 - CA*ABS(TAN(ALPHA))/(3.D0*U*ABS(FZ))
C      FY=-U*ABS(FZ)*(1.D0-H**3)*SIGN(1.0D0,ALPHA)
C      TZ=U*ABS(FZ)*2.D0*R2*(1.D0-H)*(H**3)*SIGN
       (1.0D0,ALPHA)
C    ELSE
C    FY=-U*ABS(FZ)*SIGN(1.0D0,ALPHA)
C    TZ=0.D0
C    ENDIF
C C
C C ******************************************
C -- Add camber force to FY - "Taut String" --
     FY=FY+FZ*TAN(CAMBER)
C    Mitigate FY depending on "Friction Ellipse"
     FR_ELLIP=(FX/(FZ*U))**2+(FY/(FZ*U*B))**2.0
     IF (FR_ELLIP .GT. 1.0) THEN
     LSLIP=SLIP_C-5.0
     IF(SLIP .LT. LSLIP) THEN
C -- Friction Ellipse treatment for comprehensive slip below
C    critical slip ratio --
     FY=-((1-(FX/(FZ*U))**2)*(FZ*U*B)**2)**0.5*SIGN
     (1.0D0,ALPHA)
     ELSE
C -- Just kill the lateral force if slip ratio is above
C    critical slip ratio --
     USLIP=SLIP_C+15.0
     SCMIN=0.03
     CALL STEP(SLIP, LSLIP, ONE, USLIP, SCMIN, IORD,
    *                SCFACT, ERFLG)
     FY=-((1-(FX/(FZ*U))**2)*(FZ*U*B)**2)**0.5*SIGN
     (1.0D0,ALPHA)
```

```
      FY=SCFACT*FY
      ENDIF
      ENDIF
C     Aligning Torque based on final FY including camber force
C     Not quite right as Camber force has no pneumatic trail.
C     Pay attention if using this for motorcycle work;
C     consider reworking so that TZ does not include camber force.
C     Aligning torque form is a bit poor anyway.
C -- Contact Patch Length −
      CP_LEN=(R1**2 - (R1+FZ/CZ)**2)**0.5*2.0
      IF(ABS(ALPHA) .GT. 1.D-10) THEN
       IF(ABS(ALPHA) .LE. ALPHA_C) THEN
        TZ=-FY*CP_LEN*(1-ABS(ALPHA)/ALPHA_C)/4
       ELSE
        TZ=0.0
       ENDIF
      ENDIF
C     Other Calculations as FIALA Tyre:
C     Rolling resistance moment (TY)
      CALL STEP(ABS(WSPIN), .25D0*WSPNMX, ZERO, WSPNMX,
     *                ONE, IORD, SCFACT, ERFLG)
      IF (WSPIN .GE. 0.0) THEN
       TY=-SCFACT*CR*FZ
      ELSE
       TY=SCFACT*CR*FZ
      ENDIF
C     Compute righting moment due to lateral Contact Patch Shift (TX)
C     Use CG as "shape factor" to add to or subtract righting moment
C     from MSC.ADAMS' Toroidal assumption. CG > 1 = fatter than toroid
C     CG < 1 = more like blade
C
C     TX=FZ*0.5*SIN(2*CAMBER)*R2/2*(CG - 1)
C     Copy the calculated values for FX, FY, FZ, TY & TZ to FSAE
C     and TSAE arrays and return. Scale them to start with to
C     let the simulation wake up gently. But not FZ, otherwise
C     we fall through the floor.
1000 CALL STEP(TIME, ZERO, ZERO, ONE, ONE, IORD, TSCALE,
ERFLG)
      FSAE(1)   = FX*TSCALE
      FSAE(2)   = FY*TSCALE
      FSAE(3)   = FZ
      TSAE(1)   = TX*TSCALE
      TSAE(2)   = TY*TSCALE
      TSAE(3)   = TZ*TSCALE
      FPROP(1) = 0.0
      FPROP(2) = 0.0
C
      RETURN
      END
```

Appendix C: Glossary of terms

Agility Ground vehicles are free roaming devices (with the exception of railed vehicles) in which the driver/rider seeks to influence path curvature and speed in order to follow an arbitrary course. The ease, speed and accuracy with which the operator can alter path curvature is agility. For motorcycles, the primary dictator of path curvature is roll angle, and therefore motorcycle agility discussions focus on roll behaviour; the handlebar is a roll acceleration demand. For finite track vehicles, path curvature arises from yaw rate; the handwheel is a yaw rate demand. Measures such as maximum speed through a given slalom crudely discern agility but not in a way which provides information on how to improve the design if more agility is desired.

Anti-aliasing Anti-aliasing is analogue filtering applied to a signal before it is digitally sampled. Digital data should not be collected without an appropriate anti-aliasing filter. Aliasing is when something happens between subsequent samples that is simply 'missed' by the sampling process.

Consider Figure C.1; a 5 Hz process has been sampled at 4.762 Hz. Nyquist's theory predicts that spectral content is wrapped around according to multiples of half the sampling frequency. For the above example, the wrapping occurs at $5 - (2*4.762/2) = 0.238$ Hz. Once data has been allowed to alias, it cannot be 'unaliased'.

Anti-lift Anti-lift is a geometric property of the suspension which means the reaction of traction-induced pitch moment is reacted entirely by tension in the mechanical suspension members (100% anti-lift), entirely by the roadspring(s) (0% anti-lift) or some combination of the two.

Anti-lift of less than 0% is described as 'pro-lift'. The concept is applicable only to a driven front wheel/axle and is thus generally inapplicable to

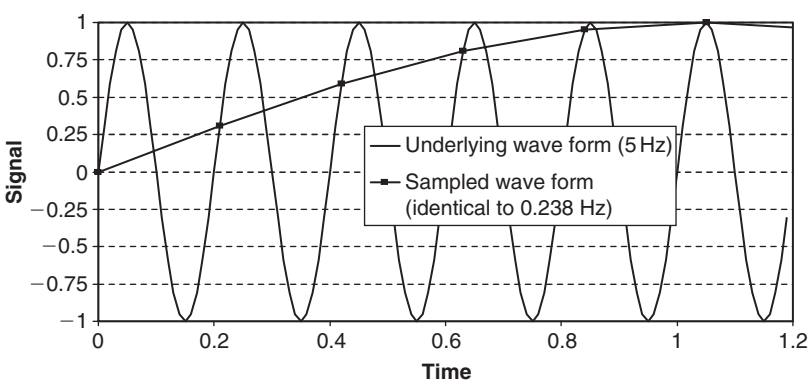

Fig. C.1 Anti-aliasing

motorcycles. Anti-lift is only applicable to a driven front wheel/axle. For a rear wheel/axle, the appropriate measure is anti-squat (q.v.).

Anti-lift is not a preferred term for the behaviour of rear suspension geometry under braking; the preferred term for this behaviour is 'anti-pitch' (q.v.).

Anti-pitch Anti-pitch is a geometric property of the suspension which means the reaction of brake-induced pitch moment is reacted entirely by compression in the mechanical suspension members (100% anti-pitch), entirely by the roadspring(s) (0% anti-pitch) or some combination of the two. Anti-pitch of less than 0% is described as 'pro-pitch'.

Road motorcycles have a typical inclination of the front suspension fork legs that provide pro-pitch behaviour. The rear swing arm is inclined at around 8 degrees to provide some anti-pitch, but little brake effort is apportioned to the rear of motorcycles braking hard and so it is generally ineffective at preventing pitch.

The term 'anti-dive' is not preferred since it has been used as a proprietary description for systems which modify front suspension damper calibration in order to resist brake-induced pitch in motorcycles.

For finite track vehicles, excessive anti-pitch geometry degrades refinement by forcing the wheel into any obstacles it encounters instead of allowing it to retreat from them. Brake-induced pitch behaviour is substantially modified by the use of inboard brakes.

Anti-roll Anti-roll is a geometric property of the suspension that means the reaction of roll moment is reacted entirely by compression in the mechanical suspension members (100% anti-roll), entirely by the suspension calibration (0% anti-roll) or some combination of the two. Less than 0% anti-roll is described as 'pro-roll'. This concept is meaningless for motorcycles.

One effect of anti-roll geometry is to speed the transfer of load into the tyre for a given roll moment. By modifying this load transfer differentially from front to rear strong changes in character can be wrought, though they rarely result in fundamental changes in vehicle behaviour. (This is not to say they are of no import; race performance hinges on 'character' since it leads towards or away from a confident driver.)

Different anti-roll geometry from front to rear also acts to provide a yaw/roll coupling mechanism. For typical saloons coupling is such that roll out of a turn produces a yaw moment out of the turn. This is given by more anti-roll at the rear than at the front axle. Vehicles with less anti-roll at the rear have a distinctive impression of sitting 'down and out' at the rear when driven aggressively; it rarely results in confidence.

Anti-squat Anti-squat is a geometric property of the suspension where the traction-induced pitch moment is reacted entirely by compression in the mechanical suspension members (100% anti-squat), entirely by the roadspring(s) (0% anti-squat) or some combination of the two. Less than 0% anti-squat is described as 'pro-squat'.

Road motorcycles have a typical inclination of the rear swing arm of around 8 degrees providing around 5% anti-squat. The calculation of anti-squat on

a chain-driven motorcycle is non-trivial and must include chain tension reaction components in the free-body diagram for the swing arm. Anti-squat is only applicable to a driven rear wheel/axle. For a front wheel/axle, the appropriate measure is anti-lift (q.v.).

Anti-squat is not a preferred term for the behaviour of front suspension geometry under braking; the preferred term for this behaviour is 'anti-pitch'. The term 'anti-dive' is not preferred since it has been used as a proprietary description for systems that modify front suspension damper calibration in order to resist brake-induced pitch.

Articulated An articulated vehicle is one in which two significant bodies are present and must pivot with respect to one another in order for the vehicle to follow a curved path. Motorcycles and tractor–trailer combinations are articulated.

Beta-dot See Body slip rate.

Body slip angle Body slip angle is the angle measured in the ground plane between the heading angle and the path of the vehicle. Heading may be thought of as what would be read by an on-board compass calibrated to the frame of reference in use. Path is the vector extending in the direction of travel at the current instant. Note that for all vehicles using pneumatic tyres, some body slip angle is inevitable to allow the rear tyres to generate a slip angle (q.v.) when travelling in a curved path.

Body slip rate Body slip rate is the first time derivative of body slip angle (q.v.). Body slip rate is an angular velocity associated solely with creating or removing body slip angle. The total vehicle yaw rate (q.v.) is made up of the no-slip yaw rate (q.v.) – that part necessary for travelling in a curved path – plus the body slip rate. Body slip rate is zero in the steady state; the relationship between body slip rate and handwheel rate is crucial in modifying driver confidence. Unfortunately, for vehicles other than road cars on high friction surfaces it is difficult to discern experimentally since it relies on 'the small difference of two large numbers' and is thus prone to sensor noise.

Bump Bump is a term used specifically to describe a motion of the suspension arrangement in which the wheel travels closer to the body. Its opposite is rebound (q.v.). Bump is also known as jounce.

Camber Camber is the angle between a vertical line passing through the wheel centre and the lateral projection of that line onto the wheel plane (the projection being in the lateral direction). Strictly, it is absolute relative to the ground. A totally upright wheel has zero camber. A wheel lying flat on the ground has 90 degree camber.

Confusion can occur with finite track vehicles as to whether camber is measured with reference to the body co-ordinate system or a co-ordinate system on the ground. To ease this, the angle relative to ground can be referred to as the 'presentation angle' and that relative to the body as camber angle. A clear and unambiguous statement of the reference frame as often as is necessary is recommended to preclude ambiguity.

Castor Castor is usually referred to as rake (q.v.) for motorcycles. For finite track vehicles, it is the angle that the steering axis makes with the vertical when projected onto the plane of symmetry of the vehicle.

Among the car community, there is frequent surprise at the notion that the steering axis need not pass through the wheel centre but may be offset from it when viewed the side; thus it is possible to have trail (q.v.) but no castor, or vice versa.

Centre of percussion See Inertial conjugate.

Centripetal force Centripetal forces are the unbalanced forces that result in acceleration of a body toward the centre of its path curvature. Without them there is no curvature of path. A body travelling in a curved path is not in equilibrium.

Cepstrum Cepstrum is a contrived word. It is an anagram of spectrum and is used to describe the Fourier transform of something already expressed in the frequency domain. The technique is used widely in sonar to identify patterns of frequency content such as that generated by rotating machinery. It is slowly creeping into industrial usage and may yet become a tool in the ground vehicle industry.

Coherence Coherence is an unambiguously defined calculated quantity that describes the consistency of phase relationship between two spectral estimates. Whenever a cross spectrum or transfer function is calculated, coherence should be calculated and used to assess the credibility of the results. Cross spectra with a coherence of less than 0.9 should be regarded cautiously and those below about 0.8 should be rejected. Note that these judgements are made on a spectral-line-by-spectral-line basis and it is acceptable for data at 5 Hz to be believable while that at 7 Hz is discarded.

Complex numbers Complex numbers are numbers containing real and imaginary components. The imaginary component of a complex number is a real number multiplied by the square root of -1. 'Complex' thus has a specific meaning and should be avoided to represent 'complicated' or 'elaborate' in general discussion.

Eigenvalues (q.v.) calculated using complex numbers are 'complex eigenvalues'; those calculated without are simply 'real eigenvalues'.

Computational fluid dynamics Computational fluid dynamics is a tool for addressing fluid dynamic problems. Closed form (classical) fluid dynamics solutions quickly become extremely cumbersome for any but the simplest problems and boundary layer complexity renders closed form fluid dynamics forms inapplicable for any object of interest except perhaps for artillery shells and the like.

In a manner similar to finite element analysis (q.v.), computational fluid dynamics uses a large number of finite volumes, known as cells, for which closed form solutions are known. The equations are coupled by imposing conditions of compatibility between adjacent cells and solving the resulting problem numerically. The solution is a time domain integration across

the whole problem region, which is extremely time consuming for even quite simple bodies.

Contact patch (tyre) The contact patch for a pneumatic tyre is that part of the tyre in contact with the ground.

Couple A couple is one or more forces acting at a distance from some point of interest such that a moment is exerted at that point.

In rigorous usage it is distinct from a torque, which is sometimes referred to as a 'pure moment' to differentiate it from a couple. Pure moments are unusual; couples are much more common.

This distinction is of little importance in day-to-day use, and unless the distinction between couples and torques is germane to the discussion it is best left unmade; it usually adds more confusion than it avoids. 'Torque' is commonly used for both, and 'pure torque' as a distinction is acceptable.

Damper A damper is a device that produces a force opposing a motion applied to it. Gyroscopic torques are not dampers although they are velocity dependent, since they do not act to oppose a motion applied but instead act at 90 degrees to that motion.

The term damper is frequently applied to mean a hydraulic device to the exclusion of other devices, but this is merely habit rather than preference. Dampers are not shock absorbers – they transmit shocks, not absorb them. The spring and damper assembly together could be described as a shock absorber. The term shock absorber, or 'shock' for short, is not preferred.

A dampener is something that adds moisture and has nothing to do with dynamics.

Dynamic absorber A dynamic absorber is an additional spring–mass–damper system added to a mechanical system to take a single resonance and modify it by forming two resonances, each of which is more damped than the single resonance in the unmodified system. One of the two resonances is at a lower frequency than the original and the other is at a higher frequency.

Mass–damper systems can also be added to dissipate energy uniformly across a wide frequency range, and these devices are also sometimes referred to as 'dynamic absorbers'. Finally, discrete lumped masses can be firmly attached to change resonant frequencies in order to decouple an excitation from a structural resonance. Such a device is frequently and confusingly referred to as a 'mass damper' although it would be less ambiguous to call it an inertial attenuator.

Dynamics The Greek word 'dynamos' (pronounced dunn-a-moss) means energy and is where we get our word dynamic from. In the sense frequently used today by mechanical engineers it is used to signify a time-varying exchange of energy between kinetic (motion), strain (stretching) and/or potential (height) states. Similar phenomena exist with electrical circuits and are crucial to the operation of radios and other elaborate equipment.

When this exchange occurs easily the system is said to be at resonance. It happens at characteristic frequencies (speeds of a repeated motion) for any

structure. If an event happens at a speed substantially similar to or greater than the speed (frequency) of the slowest resonance, it will be dynamic, or fast. If an event happens at less than that speed, it will be static, or slow. For a full system, such as a motorcycle, the same is true. Unlike a four wheeler, motorcycles have no static equilibrium (balanced) state. They do, however, have a dynamic equilibrium, which is why they are useful despite falling over when at a standstill. The correct understanding of the dynamic behaviour of vehicle systems at the design stage is vital to avoid costly mistakes being carried forward to the prototype stage or, worse, to production.

Eigensolution, eigenvalues, eigenvectors There is a clear mathematical description of characteristic solutions ('eigen' is German for 'characteristic') of matrix problems, but it is unhelpful for this glossary.

Eigensolutions, which consist of eigenvalues and eigenvectors, are quite simply free vibration solutions – that is to say resonances, or 'natural solutions' for the system described by the matrix problem. If the system is heavily damped (more than around 5% damping ratio) then complex numbers are necessary for useful eigensolutions of the system. If it is lightly damped then only real numbers are necessary.

Eigensolutions are also sometimes referred to as 'modal solutions', 'normal modes' and a variety of other titles. Thus a 'real normal modes' solution is one that solves the eigenvalue problem for a lightly damped system, using only real numbers. Note that it is a property of modes of vibration calculated in this manner, that they are normal (orthogonal) to one another; they produce a dot product of zero if the vectors are multiplied together. The concept of orthogonality requires at least two items for it to be meaningful.

Expected and unexpected response Expected response is not the subjective vagary it might be supposed. Expected response is defined clearly for dynamics usage as the product of the system inputs and the idealized characteristics of the system. For example, in yaw for a finite track vehicle the expected response is a yaw rate, the value of which is the forward speed multiplied by the steer angle and divided by the wheelbase. This might also be called 'idealized yaw rate'. 'Idealized' does not imply 'ideal' in the sense of most optimum.

The reason for wishing to capture the expected response is to compare it with the actual response. The difference between actual and expected is then logically termed 'unexpected response' and is important in quantifying operator interpretation of the vehicle. One vehicle might display a yaw response which differs from another by only a few per cent, for example; a comparison of the unexpected components of response might show that one has double the unexpected response of the other and explain the strong preference of operators for one over the other even though the objective overall response is very similar.

If the terms expected and unexpected cause consternation then the control theory terms 'reference' (demanded) and 'actual' could be substituted.

Finite element method Simple engineering structures can be represented using a closed-form equation derived using differential calculus. The beam

equation is the most widely used of these forms, being familiar to most engineers. These might be thought of as infinitesimal (infinitely small) element solutions, being derived by considering an infinitesimal slice then summing (integrating) the results.

The derivation of closed-form solutions for more complex structures subject to complex loading patterns rapidly becomes cumbersome and impractical. The finite element (FE) method uses small but not infinitesimal chunks of the structure, each of which has a closed-form solution, and assembles them imposing conditions of force and displacement continuity at the boundaries between elements. The resulting set of simultaneous equations is converted to matrix form and is well suited to being solved using a digital computer.

The finite element method was invented in principle during the latter stages of the Second World War and immediately thereafter, but did not achieve widespread use until the Apollo programme in the 1960s in America. In the last 30 years it has become more and more popular, with FE tools now available for use with home computers.

Forced response Forced response is the response of a system under some external excitation. Excitation is usually time varying; if it isn't then the problem is a static one.

If the input excitation has been established for some time then the behaviour of the system will have achieved 'steady state' (q.v.); the response will be stationary (q.v.) in character. Such solutions can be calculated using the 'harmonic forced response' method. A transfer function is calculated based on the free vibration (natural solution) response of the system then multiplied with the frequency spectrum of the input excitation to provide a response spectrum.

Refinement (q.v.) problems are frequently addressed using the harmonic forced response method.

If the input excitation has not been established for some time, then a solution method is required which can capture the developing phase relationships in the system. This is a 'transient forced response'. There is typically a computational resource penalty of an order of magnitude when switching to transient solution methods from harmonic ones.

Gyroscope, gyroscopic torques Much mystique surrounds gyroscopes and gyroscopic torques. Gyroscopes do not produce forces, only torques (moments). Gyroscopic torques are a logical consequence of Newton's third law in its correct and full form. Sometimes expressed succinctly as 'applied force is equal to rate of change of momentum', if a full 6×6 formulation is pursued then differentiating the product of the inertia tensor and velocity vector yields some off-diagonal terms if the inertia tensor varies with time, as it does with a rotating body which isn't spherical.

Handwheel Handwheel is the preferred term for what is popularly called the steering wheel. The reason for this distinction is that a typical car has three steering wheels – two are roadwheels and the other is the handwheel. Using handwheel avoids ambiguity although it may seem a little cumbersome.

Harmonic Harmonic in dynamic terms means 'consisting of one or more sine waves'.

When the phrase 'assume harmonic solutions' is used, it means 'assume the solution consists of one or more sine waves'. There is no implication of fixed frequency relationships; the term harmonic is sometimes confused in careless usage with 'harmonies' as used in music.

Heave Heave is one of three motions performed by the whole vehicle on its suspension, referred to collectively as 'primary ride'. It is a motion whereby the whole vehicle rises and falls evenly, with no rotation about any axis. The other two ride motions are pitch and roll. For motorcycles the roll motion is not a primary ride motion but the fundamental degree of freedom for the vehicle. Heave is also known as bounce, or jounce.

In reality, ride motions are never pure heave or pitch but always some combination of the two. This fact is a frequent source of confusion between development staff and analysis staff; the two groups use the terms differently. The problem is even more acute when including roll, with confusion around the notion of the 'roll centre' as a motion centre for the vehicle.

Inertial conjugate (centre of percussion) Inertial conjugate is the preferred term for the location at which no translation occurs when a free body with finite mass and inertia properties is loaded in a direction that does not pass through its centre of gravity. No translation occurs at this point during load application, whether or not the load is percussive (an impact).

This phenomenon gives rise to the behaviour of 'rigid' bats in some sports, particularly baseball and the like, that is described as the 'sweet spot'. This is not to be confused with the use of the same term for strung rackets.

The term 'centre of percussion' is not preferred to describe this location since it implies a percussive loading must be present for the concept to be useful.

Jounce Jounce is another term for heave. It is of US origin and in widespread use within Ford.

Kinematics Kinematics is the study of motion. In a mechanism it is the study of the motion of the individual motions of the components and how they relate to and constrain each other.

Modes, modal analysis Modes is shorthand for 'modes of vibration'. See 'eigensolution' for a description. 'Modal' is an adjective meaning 'of or relating to a mode or modes'. Modal analysis is thus a fairly loose term; its preferred use is as part of the expression experimental modal analysis, or better still modal test, in which experimental methods are used to discern the modes of vibration of a structure. Analysis to predictively calculate modal behaviour is distinguished by the expression 'modal solution' (solution being a general word for the submission, retrieval and interpretation of a set of results to a problem using a digital computer).

Multibody system analysis, multibody codes Mechanical systems can be viewed as a connection of separate items, or bodies, connected by various

means. Such a system, comprised of multiple bodies, can be analysed by the application of Newtonian or Lagrangian methods to formulate the equations of motion, which may then be interrogated in a variety of ways – integrated through time, solved for an eigensolution and so on. This is multibody system analysis.

A group of software packages, or codes as they are informally referred to, have emerged which greatly ease the task of formulating and solving the equations of motion. The best known is called MSC.ADAMS – Automated Dynamic Analysis of Mechanical Systems – developed by MSC. Software.

Until recently, an implicit assumption in this type of analysis has been that the elements comprising the system are rigid, but this limitation is being removed by the elegant integration of multibody methods with structural dynamics methods.

No-slip yaw rate No-slip yaw rate is the yaw rate required to support a vehicle travelling in a curved path, allowing it to change heading in order to have the correct orientation when it leaves the corner.

If the vehicle did not yaw when travelling in, say, a 90 degree corner then it would be travelling sideways upon exiting the corner. If it is to be travelling forwards (in a vehicle-centred sense – i.e. as noted by the operator) when it leaves the corner then it must have rotated in plan during the corner.

Consideration of basic physics leads to the observation that no-slip yaw rate is centripetal acceleration divided by forward velocity.

Non-holonomic constraints

> *Non-holonomic constraints involve non-integrable relationships between velocities. In vehicle dynamics they arise typically if wheels are assumed to roll without slip in problems of more than one dimension. Suppose a car is parked in an open, flat, high-friction area and radial line marks are appended to the tyre sidewalls and to the points on the ground nearest to them. The car is then driven slowly, without tyre slip, round the area and eventually returned to the precise location where it started. Although the car body can be re-positioned precisely the tyre marks will not, in general, align now.*

Sharp, R.S. Multibody dynamics applications in vehicle engineering (1998).

NVH See Refinement.

Objective Objective is unfortunately ambiguous. In one sense (as a noun) it is similar to ‘target’ but that is not its preferred usage. The preferred usage is in contrast with ‘subjective’ (q.v.) and is as an adjective. It refers to measurements or conclusions that are independent of the person who observes. The term arises from basic English sentence construction which is ‘subject–verb–object’. If A observes B then B is the object of A’s observation; B is always B whether A or C observes.

Objectivity is essential to dynamic activities; without it work cannot be credible, reproducible or professional. These three are prerequisite for any scientific activity.

Oversteer, understeer Oversteer is strictly the condition in which the slip angle of the rear tyres exceeds that of the front tyres. Understeer is strictly the reverse.

Before debating this matter, a review of Segel and Milliken's papers from 1956 are in order, where all this was laid down as fact with test work and mathematical development. The definitions arrived at in there are applicable in the linear region only. The persistence of their usage for limit behaviour is an extension beyond their validity. Sometimes, drivers may refer to oversteer and mean a yaw overshoot after turn-in, which is somewhat confusingly a consequence of an understeering car. Equally, a car which has genuine oversteer behaviour will have non-oscillatory roots to its characteristic equation, resulting in excessive yaw damping which manifests itself as a reluctance to turn in and is reported as transient understeer.

Some modern cars have steady state oversteer behaviour on low grip surfaces since it dulls response and makes the vehicle manageable, even though it guarantees the need for driver correction.

Preferred alternative forms of reference are such subjective terms as 'push on' or 'loose rear' (that's loose, not lose) or more technical descriptions, such as 'real roots for the characteristic equation', 'rear slip angle exceeds front' and so on.

The importance of both oversteer and understeer as steady state phenomena in road vehicles in the linear region is greatly exaggerated. Its prime effect in the steady state is to encourage the driver to adjust the handwheel slightly, since it results in a path error due to the difference between demanded (idealized, expected (q.v.)) and no-slip yaw rates (q.v.). In normal road driving this is completely trivial; fitting a 'faster' steering rack will mask the perception of path error related to understeer completely.

For transient handling, the development of body slip angle (q.v.) is of much more importance; the yaw rate associated with changes in body slip angle is acutely sensed by the driver and is used to give warning of an impending spin even though it is only a small fraction of the total yaw rate. If the vehicle manages its body slip rate poorly, then it can give the impression of an impending spin even if no such event was likely. Even at low lateral accelerations, body slip rate is a strong modifier on perceived transient performance.

Path error Path error is a preferred term for steady state understeer. When the vehicle 'runs wide' from the driver's intended path, the normal driver response is to add more steer angle. If the lateral acceleration is high and the path error is large, then more steer angle may not help reduce path error. This situation is reported by many drivers as 'pushing on' and is common limit handling behaviour for safe road vehicles.

Path error is strictly the difference between idealized (demanded, expected (q.v.)) yaw rate and no-slip yaw rate (q.v.). It is a numerical quantity suitable for discernment from logged data or mathematical models.

Pitch Pitch is one of three motions performed by the whole vehicle on its suspension, referred to collectively as 'primary ride'. It is a motion whereby the front of the vehicle rises and falls in opposition to the rear of the vehicle, rotating about the lateral axis of the vehicle. The other two ride motions are

heave and roll. For PTWs (Powered Two Wheelers) the roll motion is not a primary ride motion but the fundamental degree of freedom for the vehicle.

Predictive methods Predictive methods is an umbrella term for all forms of mathematical modelling, from statistical to explicit, from numerical to algebraic.

PTW PTW is an acronym for 'Powered Two Wheeler' – a generic term encompassing mopeds, scooters, motorcycles, enclosed motorcycles, feet firsts (FFs), and any other thing which has two wheels and is self-powered.

Rake Rake is the angle between the steering axis and the vertical for an upright motorcycle. Typical values for rake vary from 23 degrees for a sports machine to over 30 degrees for a cruiser. Rake is also known as castor, and is occasionally quoted as an angle from the ground plane.

Rate Rate means, clearly and unambiguously, the first time derivative. It is shorthand for 'rate of change with time'. Using rate for derivatives other than time is not preferred. In particular, using rate as in 'spring rate' is undesirable; 'stiffness' is preferred in this instance, though the authors make this error frequently.

Rebound Rebound is a term used specifically to describe a motion of the suspension arrangement in which the wheel travels away from the body. Its opposite is bump (q.v.).

Refinement Refinement is a general term that refers to the ability of a vehicle to isolate its operator and other occupants from external disturbances and from disturbances generated by the vehicle itself – for example, engine vibration.

Refinement is frequently referred to as 'NVH'. This stands for 'Noise, Vibration and Harshness'. The distinction between the three phenomena is not well defined. It is suggested that noise refers to audible phenomena from 30 Hz upward, vibration to dynamic phenomena below about 10 Hz and harshness to tactile sensations of vibration of intermediate frequency, for example steering column shake at idle.

Segment 'Segment' is industry shorthand for 'market segment' – the term used to define the objectives for the vehicle in terms of who will buy how many copies of it.

Shock absorber See Damper.

Slip, slip angle (of tyres) Slip is perhaps the poorest word possible to describe the behaviour of a tyre under lateral loading. A rolling tyre will not support a lateral load due to the repeated relaxation of the sidewalls just behind the contact patch. This action causes the tyre to 'walk' sideways under an applied lateral load. Combined with the forward motion, this results in an angle between the wheel plane and the direction of motion. That angle is dubbed the 'slip angle'. The presence of a slip angle does not imply sliding friction at the contact patch, despite the linguistic link between slip and slide. This is a frequent source of confusion for newcomers to the field.

To further add confusion, the behaviour of a tyre under a tractive or braking torque is also referred to as slip, and is often quantified in per cent. A free-rolling wheel is at zero slip, a completely locked wheel is at 100% brake slip. One hundred per cent tractive slip is when the wheel is spinning twice as fast as the free-rolling wheel. The presence of tractive/braking slip does not imply sliding friction at the contact patch, though this is the case at high slip percentages (greater than 20%), as it is at high slip angles (greater than about 6 degrees).

Stability Stability means the response to a disturbance is bounded (non-infinite). In practical terms for a motorcycle this would mean it won't fall over if nudged. This is clearly not the case when the machine is at rest but is generally true of the motorcycle/rider combination at all speeds above zero. For running vehicles, the notion of stability is generally associated with the control of body slip angle (q.v.) and hence implicitly the yaw rate behaviour of the vehicle. In practice a response that is simply 'finite' is insufficient to guarantee stability in any useful sense; vehicles are not simply 'stable' or 'instable' but have degrees of stability that are often related to the nature of the non-linearity of the system. For example, the front wheel wobble (q.v.) problem on a motorcycle is unstable on-centre but has a 'bounded instability' in the sense that the increasingly non-linear behaviour of the tyres dissipates more and more energy as the amplitude of the cycle rises. This has the effect of 'containing' the instability in the system within bounded limits.

Figure C.2 shows a comparison between a vehicle that has a passively stable response and another with a less stable response during a chicane manoeuvre. Both vehicles have comparable mass, wheelbase, inertia properties and tyre fitments. The manoeuvre is completed off-throttle and it can be seen that the less stable vehicle produces a very aggressive yaw acceleration at the steer reversal (3.8 seconds) and a high yaw rate persists for some time, resulting in a half spin of the vehicle.

It can be seen for a well-controlled manoeuvre like this one, performed under identical conditions with the same driver, it would be easy to formulate some measure of stability based on area under the yaw rate curve. To compare vehicles on an absolute basis requires a well-controlled test that is

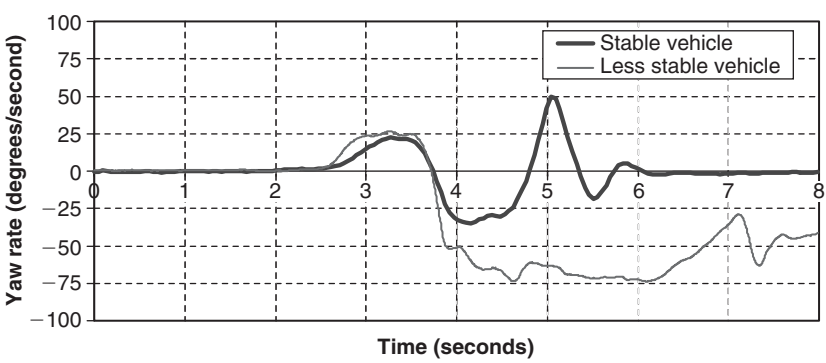

Fig. C.2 Time domain comparison of stable and less stable vehicle during 120 kph entry chicane manoeuvre

tester, venue and weather independent – a more difficult task but addressed in part by the ISO manoeuvres.

Stationary In dynamics, stationary does not mean immobile. It is a property of a time-domain signal and is such that lengthening the observation period does not alter the fundamental characteristics (mean, RMS, standard deviation, etc.) of the signal.

Steady state In general, steady state refers to the condition where phase relationships are fixed and no longer vary with time.

In the sense used in vehicle dynamics work, it is that definition applied to a vehicle cornering. The phase relationship between all motions of the vehicle is fixed; there is neither yaw nor roll acceleration that is anything other than established and harmonic. In the simplest sense the vehicle is travelling steadily on a curved path. Note that steady state does not imply equilibrium.

Steering offset Steering offset is a fairly general term that has specific meanings when considering the steering system of a finite track vehicle. It is the lateral distance between the steer axis and the wheel plane. It can be seen that if the steer axis is inclined when viewed from the front of the vehicle (as is generally the case) then this offset has different values at different heights above ground.

Wherever it is measured, positive steering offset is when the wheel plane is outboard of the steer axis. Negative steering offset is the reverse.

Steering offset is of interest at ground level since it determines steering system loads (and hence handwheel torque) under differential longitudinal loads. Excessive ground level offset promotes nervousness under braking and sensitivity to ABS operation. However, it also assists the driver in retaining control under split mu braking conditions, with or without ABS. Negative ground level offset makes the handwheel and vehicle insensitive to ABS operation.

The steering offset at wheel centre height, usually called 'hub level offset' dominates the sensitivity of the vehicle to tractive effort imbalance – usually called 'torque steer'.

Subjective Subjective is in contrast with 'objective' (q.v.) and is an adjective. It refers to measurements or conclusions that are dependent on the person who observes.

It would be unfair to suggest that subjectivity has no place, but excessive reliance on unreproducible observations is unhelpful, unproductive and unprofessional.

Symbolic codes (multibody system analysis)

> *Conceptually, the simplest approach to solving … [a multibody system problem] is to give the whole set of differential and algebraic equations to a powerful and appropriate solver … Simulations tend to be painfully slow … Symbolic preparation of the problem for numerical solution implies that the symbol manipulations, which are performed only once ahead of numerical processing, can be devoted to making the [later repeated] numerical operations minimal.*

It also implies independence of the symbolic equation building and the numerical solution.

Sharp, R.S. Multi-body dynamics applications in vehicle dynamics (1998).

Traction, tractive Traction for ground vehicles is the process of deploying power via a torque at the roadwheels in order to provide a forward force on the vehicle. Such force is sometimes referred to as 'tractive effort'. Multiplying that force by the vehicle velocity gives 'tractive power'.

Trail Trail is the distance between the point at which the steering axis intercepts the ground plane and the front wheel contact patch centre. Positive trail implies the steering axis intercepts the ground ahead of the front wheel contact patch. Trail can be measured to two different points; the geometric centre of the contact patch and the centre of lateral load of the contact patch. The difference between the two measurements is often referred to as 'pneumatic trail'. The measurement to the geometric centre of the contact patch is then 'mechanical'.

With finite track vehicles, trail is an important contributor to the self-aligning behaviour of the steering system and handwheel efforts.

With motorcycles, negative trail machines existed into the 1920s but the destabilizing effects with speed rendered them impractical for high-speed use. Negative trail occasionally appears on mountain bicycles today and does not guarantee instability of the machine/rider system. At low speeds, high roll angles and significant steer angles, trail is substantially modified by the wheel geometry.

Transient (cornering) In general, transient refers to the condition where phase relationships are not fixed and are varying with time. In the sense used in this work, it is that definition applied to a vehicle cornering. The phase relationship between all motions of the vehicle is developing and changing. Rates of change are generally decaying with time and the transient motion becomes the steady state motion if sufficient time is allowed. For the transient aspects of the motion to decay completely, something around 3 seconds is required for cars and motorcycles. This is rarely achieved in practice and so reality consists of a connected series of transient events.

Understeer See Oversteer and Expected response.

Vehicle dynamics For the purpose of this work, a vehicle is defined as a wheeled device capable of propelling itself over the ground. Dynamics, from the Greek 'dynamos' meaning energy, is the study of time-varying phenomena. Most dynamic phenomena involve the shuffling or transforming of energy between one item in a system and another. The phrase 'vehicle dynamics' is generally used to refer to phenomena of interest to the rider or driver of the vehicle in guiding its path – roll, turn-in, and so on. It includes consideration of elements such as tyres and suspension dampers, and is very much a system level activity.

Vehicle programme 'Vehicle programme' is industry shorthand for 'vehicle design, development and sign-off programme'. It is that defined activity that takes as input a desire to have a vehicle in a certain market segment and produces as output a fully mature design, ready to be mass produced. The

start of vehicle programmes is shrouded in obfuscation in order that each manufacturer can claim their vehicle programmes are shorter than others; the end of the vehicle programme is frequently referred to as 'job 1' or 'launch'.

Weave Weave is one of the lowest fundamental modes of vibration of a motorcycle. It is a combination of roll, yaw and lateral motion that result in the machine following a sinuous path. Modern road machines rarely display weave behaviour poorly damped enough to hinder the rider's control of the machine but even current machines can display a low enough level of weave damping to diminish the rider's confidence, particularly when laden. The highest performance machines typically employ an aluminium beam frame concept and have excellent weave damping, to the point where weave mode cannot readily be discerned with a typical 'rider rock' manoeuvre (a hands-off hip flick) but must instead be found using a swept sine handlebar input.

Wheel hop A description of the system resonance which consists of the unsprung mass (wheel, tyre, brake components, hub, bearings and some proportion of suspension members, springs and dampers) as the dominant kinetic energy storage and the tyre as the dominant strain energy storage, with the tyre providing the dominant energy dissipation route. Typical frequencies are usually around 12 Hz on a finite track vehicle, 15 Hz on a road motorcycle.

Wheel trajectory map A collective name for the characteristics that describe the orientation and location of the wheel plane in relation to the vehicle body. The characteristics are all defined with respect to bump (q.v.) motion. In a finite track vehicle, the wheel trajectory map includes bump steer, bump camber, bump recession and bump track change. The interaction of each of these characteristics with the vehicle is subtle and complicated. For motorcycles it is generally only bump recession, also known as anti-pitch or anti-squat, that is of interest.

Wheelbase Wheelbase is the distance between the front and rear wheel centres of a wheeled vehicle.

Wobble Wobble is a faintly comical term used to describe a distinctly serious trait of motorcycle behaviour. Originally referred to as 'speedman's wobble' this was shortened to just wobble by frequent usage. It describes the mode of vibration of a motorcycle in which the steered mass is in motion more or less independently of the non-steered mass and rider. It is typically around 8 Hz and generally well damped enough that it does not present a problem. However, when ill-damped it can present a terrifying experience whereby the amplitude of the motion set off by some small disturbance grows until it is only restrained by the steered mass colliding with some part of the motorcycle at each extreme. It is also referred to as flutter, shimmy or headshake.

Yaw, yaw rate Yaw is simply rotation when viewed in plan view. Yaw rate is the first time derivative and is often referred to as yaw velocity. Yaw is measured in degrees or radians and yaw rate in degrees/second or radians/second.

References

Allen, R.W., Rosenthal, T.J. and Szostak, H.T. Steady state and transient analysis of ground vehicle handling. SAE Paper 870495, Society of Automotive Engineers, 400 Commonwealth Drive, Warrendale, PA 15096, USA, 1987.

Anderson, R.J. and Hanna, D.M. Comparison of three vehicle simulation methodologies. Proceedings 11th IAVSD Symposium, 1989.

Austin, A. and Hollars, M.G. Concurrent design and analysis of mechanisms. Kinematics and Dynamics of Multi-body Systems Seminar (S057), Institution of Mechanical Engineers, November 1992.

Bakker, E., Nyborg, L. and Pacejka, H.B. Tyre modelling for use in vehicle dynamics studies. SAE paper 870421, Society of Automotive Engineers, 400 Commonwealth Drive, Warrendale, PA 15096, USA, 1986.

Bakker, E., Pacejka, H.B. and Lidner, L. A new tyre model with application in vehicle dynamics studies. SAE Paper 890087, 4th Auto Technologies Conference, Monte Carlo, 1989.

Bartlett, W. Driver abilities in closed course testing. SAE Paper 2000-01-0179, Society of Automotive Engineers, 400 Commonwealth Drive, Warrendale, PA 15096, USA, 2000.

Bayle, P., Forissier, J.F. and Lafon, S. A new tyre model for vehicle dynamic simulations. *Automotive Technology International*, pp. 193–198, 1993.

Blinchikoff and Zverev. *Digital Filtering in the Time and Frequency Domain.* Noble, 2001.

Blundell, M.V. Full vehicle modelling and simulation of a Rolls Royce. Internal consulting report to Rolls Royce Motor Cars Ltd, Tedas Ltd, Coventry, 1990.

Blundell, M.V. Full vehicle modelling and simulation using the ADAMS software system. Institution of Mechanical Engineers Paper C427/16/170, Autotech '91, Birmingham, November 1991.

Blundell, M.V. The modelling and simulation of vehicle handling Part 1: Analysis methods. *Journal of Multi-body Dynamics, Proceedings of the Institution of Mechanical Engineers*, Vol. 213 Part K, pp. 103–118, 1999a.

Blundell, M.V. The modelling and simulation of vehicle handling Part 2: Vehicle modelling. *Journal of Multi-body Dynamics, Proceedings of the Institution of Mechanical Engineers*, Vol. 213 Part K, pp. 119–133, 1999b.

Blundell, M.V. The modelling and simulation of vehicle handling Part 3: Tyre modelling. *Journal of Multi-body Dynamics, Proceedings of the Institution of Mechanical Engineers*, Vol. 214 Part K, pp. 1–32, 2000a.

Blundell, M.V. The modelling and simulation of vehicle handling Part 4: Handling simulation. *Journal of Multi-body Dynamics, Proceedings of the Institution of Mechanical Engineers*, Vol. 214 Part K, pp. 71–94, 2000b.

Blundell, M.V. Computer modelling of tyre behaviour for vehicle dynamics. The 3rd European Conference for Tire Design and Manufacturing Technology, Hamburg, Germany, 2003.

Chace, M.A. A network-variational basis for generalised computer representation of multifreedom, constrained, mechanical systems. Design Automation Conference, Miami, Florida, 1969.

Chace, M.A. and Korybalski, K.E. Computer graphics in the schematic representation of nonlinear, constrained, multifreedom mechanical systems. Computer Graphics 70 Conference, Brunel University, April 1970a.

Chace, M.A. DAMN-A prototype program for the design analysis of mechanical networks. 7th Annual Share Design Automation Workshop, San Francisco, California, June 1970b.

Chace, M.A. and Angel, J.C. Interactive simulation of machinery with friction and impact using DRAM. SAE Paper No. 770050, Society of Automotive Engineers, 400 Commonwealth Drive, Warrendale, PA 15096, USA, February 1977.

Chace, M.A. Modeling of dynamic mechanical systems. CAD/CAM Robotics and Automation Institute, Tucson, Arizona, February 1985.

Cooper, D.W., Bitonti, F., Frayne, D.N. and Hansen, H.H. Kinematic analysis method (KAM). SAE Paper No. SP-272, Society of Automotive Engineers, 400 Commonwealth Drive, Warrendale, PA 15096, USA, May 1965.

Costa, A.N. Application of multibody systems techniques to vehicle modelling. Colloquium Model Building Aids for Dynamic Simulation, IEE Digest No. 1991/196, 1991.

Crolla, D.A., Horton, D. and Firth, G. Applications of multibody systems software to vehicle dynamics problems. Kinematics and Dynamics of Multibody Systems Seminar (S057), Institution of Mechanical Engineers, 1992.

Crolla, D.A., Horton, D.N.L., Brooks, P.C., Firth, G.R., Shuttleworth, D.W. and Yip, C.N. A systematic approach to vehicle design using VDAS (Vehicle Dynamics Analysis Software). SAE Paper 940230, Society of Automotive Engineers, 400 Commonwealth Drive, Warrendale, PA 15096, USA, 1994.

Crolla, D.A. Vehicle dynamics – theory into practice. Automobile Division Chairman's Address, Institution of Mechanical Engineers, 1995.

Davis, D.C. A radial-spring terrain-enveloping tire model. V*ehicle System Dynamics*, 3, pp. 55–69, 1974.

Dixon, J.C. The roll-centre concept in vehicle handling dynamics. *Proceedings of the Institution of Mechanical Engineers*, Vol. 210, No. D1, pp. 69–78, 1987.

Døssing, Brueland Kjaer, Structural Testing Part 2: Model Analysis and Stimulation, 1988.

D'Souza, A.F. and Garg, V.K. *Advanced Dynamics: Modelling and Analysis.* Englewood Cliffs; London: Prentice Hall, ISBN 0130113123, 1984.

Fiala, E. Seitenkrafte am rollenden Luftreifen. *VDI-Zeitschrift 96*, 973, 1954.

Fonda, A.G. Tire tests and interpretation of experimental data. *Proceedings of the Automobile Division, Institution of Mechanical Engineers*, 1956.

Forsythe, G.E., Malcolm, M.A. and Moler, C.B. *Computer Methods for Mathematical Computations.* Englewood Cliffs, N.J., Prentice Hall, Inc., 1977.

French, T. *Tyre Technology.* IOP Publishing, ISBN 0-85274-360-2, 1989.

Garrett, T.K. Automobile dynamic loads: some factors applicable to design. *Automobile Engineer*, February 1953.

Gear, C.W. Simultaneous numerical solution of differential-algebraic equations. *IEEE Transactions on Circuit Theory,* Vol. CT-18, No. 1, pp. 89–95, January 1971.

Gillespie, T.D. *Fundamentals of Vehicle Dynamics.* SAE Publications, Society of Automotive Engineers, 400 Commonwealth Drive, Warrendale, PA 15096, USA, 1992.

Gipser, M. FTire, a new fast tire model for ride comfort simulations. *Proceedings of the 14th European ADAMS Users' Conference*, Berlin, Germany, November 1999.

Hales, F.D. Vehicle dynamics undergraduate course notes. Loughborough University, 1989.

Harty, D. The myth of accuracy. *The Journal of the Engineering Integrity Society*, January 1999.

He, J., Crolla, D.A., Levesley, M.C. and Manning, W.J. Coordinated active rear steering and variable torque distribution control for vehicle stability enhancement. *Proceedings of the Sixteenth International Conference on Systems Engineering (ICSE2003)*, Vol. 1, pp. 243–248, ISBN 0-905949-91-9, Coventry, UK, 9–11 September 2003.

Hogg, S.S., Dickison, J.G., Maddison, S.J. and Yardley, A.J. Design and prediction of vehicle handling and stability. Institution of Mechanical Engineers Paper C389/122, FISITA92, 1992.

Holt, M.J. and Cornish, R.H. Simulation tools for vehicle handling dynamics. Kinematics and Dynamics of Multi-body Systems Seminar (S057), Institution of Mechanical Engineers, November 1992.

Holt, M.J. Simulation tools for vehicle handling dynamics. Multi-body system dynamics codes for vehicle dynamics applications Seminar (S275), Institution of Mechanical Engineers, 1994.

Hucho, W.R. and Ahmed, S.R. *Aerodynamics of Road Vehicles: From Fluid Mechanics to Vehicle Engineering*. 4th Edition, SAE Publications, Society of Automotive Engineers, 400 Commonwealth Drive, Warrendale, PA 15096, USA, ISBN 0768000297, 1998.

Hudi, J. AMIGO – A modular system for generating ADAMS models. *Proceedings of the 5th European ADAMS News Conference*, Tedas GmbH, Marburg, FR Germany, October 1988.

Kaminski, S. WOODS – A worksheet orientated design system. *Proceedings of the 6th European ADAMS News Conference*, Kurhaus Wiesbaden, FR Germany, April 1990.

Kawagoe, K., Sume, K. and Watanabe, M. Evaluation and improvement of vehicle roll behaviour. SAE Paper 970093, Society of Automotive Engineers, 400 Commonwealth Drive, Warrendale, PA 15096, USA, 1997.

Kisielewicz, L.T. and Ando, K. Accurate simulation of road tire vehicle interactions using PAM_CRASH™/ADAMS™ coupled solution. '92 ISID ADAMS Users Conference – Tokyo, November 1992.

Knappe, L.F. A computer-orientated mechanical system. *Mechanical Engineering*, ASME, Vol. 87, No. 5, May 1965.

Kortum, W., Sharp, R.S. and de Pater, A.D. Application of multibody computer codes to vehicle system dynamics. Progress Report to the 12th IAVSD Symposium on a Workshop and Resulting Activities, Lyon, 1991.

Kortum, W. and Sharp, R.S. (eds). Multibody computer codes in vehicle system dynamics. *Supplement to Vehicle System Dynamics*, Vol. 22, 1993.

Lechmer, D and Perrin, C. The actual use of dynamic performance of vehicles. *Proceedings of the Institute of Mechanical Engineers*, Vol. 207, 1993.

Lee, Lee, Ha and Han. Four wheel independent steering system for vehicle handling improvement by active rear toe control. *JSME International Journal*, Vol. 42, No. 4, 1999.

Leva, A., Cox, C. and Ruano, A. Hands-on PID autotuning: a guide to better utilisation. International Federation of Automatic Control, 2002. http://www.oeaw.ac.at/ifac/publications/pbriefs/PB_Final_LevaCoxRuan.pdf

Limpert, R. Brake design and safety. Society of Automotive Engineers, 400 Commonwealth Drive, Warrendale, PA 15096, USA, 1999.

Loeb, J.S., Guenther, D.A., Chen, H.H. and Ellis, J.R. Lateral stiffness, cornering stiffness and relaxation length of the pneumatic tyre. SAE Paper 900129, Society of Automotive Engineers, 400 Commonwealth Drive, Warrendale, PA 15096, USA, 1990.

Makita, M. and Torii, S. An analysis of tire cornering characteristics using a magic formula tire model. JSAE Paper 923063, *Proceedings of the International Symposium on Advanced Vehicle Control 1992 (AVEC 92)*, Yokohama, September 1992.

Milliken, W.F. and Whitcomb, D.W. General introduction to a programme of dynamic research. *Proceedings of Automobile Division, Institution of Mechanical Engineers*, 1956.

Milliken, W.F. and Milliken, D.L. *Race Car Vehicle Dynamics*. SAE Publications, Society of Automotive Engineers, 400 Commonwealth Drive, Warrendale, PA 15096, USA, 1995.

Milliken, W.F. and Milliken, D.L. *Chassis Design – Principles and Analysis*. SAE Publications, Society of Automotive Engineers, 400 Commonwealth Drive, Warrendale, PA 15096, USA, 2001.

Moore, D.F. *The Friction of Pneumatic Tyres*. Elsevier Scientific Publishing Company, ISBN 0-444-41323-5, 1975.

Mousseau, C.W., Sayers, M.W. and Fagan, D.J. Symbolic quasi-static and dynamic analyses of complex automobile models. In *The Dynamics of Vehicles on Roads and on Tracks* (ed. G. Sauvage), *Proceedings of the Twelth IAVSD Symposium*, 1992, pp. 446–459 (Swets and Zeitlinger, Lisse).

Olley, M. Road manners of the modern motor car. *Proceedings of the Institution of Mechanical Engineers*, 1945.

Orlandea, N. Node-analogous, sparsity-orientated methods for simulation of mechanical dynamic systems. PhD Thesis, The University of Michigan, 1973.

Orlandea, N., Chace, M.A. and Calahan, D.A. A sparsity-orientated approach to the dynamic analysis and design of mechanical systems – Part I. Paper No. 76-DET-19, ASME Mechanisms Conference, Montreal, October 1976 (also Trans. *ASME Journal of Engineering for Industry*, 1977a).

Orlandea, N., Chace, M.A. and Calahan, D.A. A sparsity-orientated approach to the dynamic analysis and design of mechanical systems – Part II. Paper No. 76-DET-20, ASME Mechanisms Conference, Montreal, October 1976 (also Trans. *ASME Journal of Engineering for Industry*, 1977b).

Orlandea, N. and Chace, M. Simulation of a vehicle suspension with the ADAMS computer program. SAE Paper 770053, Society of Automotive Engineers, 400 Commonwealth Drive, Warrendale, PA 15096, USA, 1977.

Ozdalyan, B. and Blundell, M.V. Anti-lock braking system simulation and modelling in ADAMS. International Conference on Simulation '98 (IEE), Conference Publication Number 457, pp. 140–144, University of York, UK, 30 September–2 October 1998.

Pacejka, H.B. and Sharp, R.S. Shear force generation by pneumatic tyres in steady state conditions: a review of modelling aspects. *Vehicle System Dynamics*, 20, pp. 121–176, 1991.

Pacejka, H.B. and Bakker, E. The magic formula tyre model, tyre models for vehicle dynamic analysis. *Proceedings of the 1st International Colloquium on Tyre Models for Vehicle Dynamic Analysis*, ed. H.B. Pacejka, Swets & Zeitlinger, Lisse, pp. 1–18, 1993.

Pacejka, H.B. The role of tyre dynamic properties. Seminar on Smart Vehicles, Delft. *Proceedings: Vehicle System Dynamics*, Special Issue, February 1995.

Pacejka, H.B. and Besselink, I.J.M. Magic formula tyre model with transient properties. *Proceedings of the Berlin Tyre Colloquium, Vehicle System Dynamics Supplement* 27, Swets & Zeitlinger, Lisse, pp. 145–155, 1997.

Pacejka, H.B. *Tyre Mechanics and Vehicle Dynamics*. Elsevier Science, 2002.

Palmer, D. Course notes – high performance driving training. Driving Developments, 1999.

Phillips, B.D.A. Chassis engineering. Course notes, Coventry University, 2000.

Pilling, M. *Tyres from the Car's Point of View*. Institute of Materials, Wolverhampton, February 1995.

Rai, N.S. and Soloman, A.R. Computer simulation of suspension abuse tests using ADAMS. SAE Paper 820079, Society of Automotive Engineers, 400 Commonwealth Drive, Warrendale, PA 15096, USA, 1982.

Rice, R.C. (ed.). *SAE Fatigue Design Handbook*. Society of Automotive Engineers, 400 Commonwealth Drive, Warrendale, PA 15096, USA, ISBN 1-56091-917-5, 1997.

Ro and Kim. *Four Wheel Steering for Vehicle Handling Improvement*. Institution of Mechanical Engineers, 1996.

Ross-Martin, T.J., Darling, J. and Woolgar, R. The simulation of vehicle dynamics using the roll centre concept. Institution of Mechanical Engineers Paper C389/047, FISITA92, 1992.

Ryan, R. ADAMS – Multibody systems analysis software. *In Multibody Systems Handbook*/W. Schielen (Editor), Springer-Verlag, Berlin, 1990.

Ryan, R. ADAMS Mechanical systems simulation software. *Multibody Computer Codes in Vehicle Systems Dynamics*. Swets & Zeitlinger B.V., Amsterdam/Lisse, Vol. 22 Supplement, ISBN 90-265-1365-8, 1993.

SAE Publication, *Vehicle Dynamics Terminology, Handbook Supplement*, SAE J670e. Society of Automotive Engineers, 400 Commonwealth Drive, Warrendale, PA 15096, USA, 1976.

Sayers, M.W. Automated formulation of efficient vehicle simulation codes by symbolic computation (AUTOSIM). *Proceedings 11th IAVSD Symposium of Vehicles on Roads and Tracks*, Kingston, Ontario, Swets and Zeitlinger, Lisse, 1990.

Sayers, M.W. Computer modelling and simulation of vehicle dynamics. *UMTRI Research Review*, Vol. 23, No. 1, July 1992.

Scapaticci, D., Coeli, P. and Minen, D. ADAMS implementation of synthetic trajectories of the wheels with respect to the car body for handling manoeuvres simulations. *Proceedings of the 8th European ADAMS News Conference*, Munich, October 1992.

Schielen, W. (ed.). *Multibody Systems Handbook*. Springer-Verlag, Berlin, 1990.

Schuring, D.J., Pelz, W. and Pottinger, M.G. The BNPS model – an automated implementation of the 'Magic Formula' concept. IPC-7 Conference and Exposition, Phoenix, 1993.

Segel, L. Theoretical prediction and experimental substantiation of the response of the automobile to steering control. *Proceedings of Automobile Division, Proceedings of the Institution of Mechanical Engineers*, pp. 310–330, 1956.

Segel, L. An overview of developments in road vehicle dynamics: past, present and future. *Proceedings of the Institution of Mechanical Engineers Conference on 'Vehicle Ride and Handling'*, London, pp. 1–12, 1993.

Sharp, R.S. and El-Nashar, M.A. A generally acceptable digital computer based model for the generation of shear forces by pneumatic tyres. *Vehicle System Dynamics*, 15, pp. 187–209, 1986.

Sharp, R.S. On the accurate representation of tyre shear forces by a multi-radial-spoke model. *Proceedings of the 11th IAVSD Symposium on the Dynamics of Vehicles on Roads and Tracks*, ed. R.J. Anderson, Swets & Zeitlinger, Lisse, pp. 528–541, 1990.

Sharp, R.S. Computer codes for road vehicle dynamic models. Institution of Mechanical Engineers Paper 427/16/064, Autotech '91, Birmingham, November 1991.

Sharp, R.S. Magic formula method for representation of tyre forces and moments. Course notes, Cranfield Institute of Technology, 1992.

Sharp, R.S. Tyre structural mechanics influencing shear force generation: ideas from a multi-radial-spoke model, tyre models for vehicle dynamic analysis: *Proceedings of the 1st International Colloquium on Tyre Models for Vehicle Dynamic Analysis*, ed. H.B. Pacejka, Swets & Zeitlinger, Lisse, pp. 145–155, 1993.

Sharp, R.S. Review of currently available codes – benchmarking attempt. Multi-body System Dynamics Codes for Vehicle Dynamics Applications Seminar (S275), Institution of Mechanical Engineers, 1994.

Sharp, R.S. Use of the symbolic modelling code AUTOSIM for vehicle dynamics. School of Mechanical Engineering, Cranfield University, 1997.

Sharp, R.S. Multi-body dynamics applications in vehicle dynamics. Institution of Mechanical Engineers, International Conference on Multi-body Dynamics (1 86058 152 8), C553/7/045/98, pp. 215–228, December 1998.

Sharp, R.S. Aspects of the lateral and longitudinal control of automobiles. Cranfield University, 2000.

Sitchen, A. Acquisition of transient tire force and moment data for dynamic vehicle handling simulations. SAE Paper 831790, Society of Automotive Engineers, 400 Commonwealth Drive, Warrendale, PA 15096, USA, 1983.

Smiley, R.F. Evaluation and extension of linearized theories for tire motion and wheel shimmy. Technical Report NACA-TM-1299, NASA, 1957.

Smiley, R.F. and Horne, W.B. Mechanical properties of pneumatic tires with special reference to modern aircraft tires. Technical Report NASA-TR-64, Langley Research Center, NASA, 1960.

Tandy, K., Heydinger, G.T., Christos, J.P. and Guenther, D.A. Improving vehicle handling simulation via sensitivity analysis. Institution of Mechanical Engineers Paper C389/396, FISITA92, 1992.

Terlinden, M.W., Langer, W. and Hache, M. MOGESSA – A modular full vehicle simulation system based on ADAMS. *Proceedings of the 4th*

European ADAMS News Conference, Tedas GmbH, Marburg, FR Germany, September 1987.

Trungle, C.V. Engineering a winner at Newman/Hass Racing. *Dynamic Dimensions*, Vol. 2, No. 3, Mechanical Dynamics Inc., 1991.

van der Jagt, P., Pacejka, H.B. and Savkoor, A.R. Influence of tyre and suspension dynamics on the braking performance of an anti-lock system on uneven roads. Institution of Mechanical Engineers, Paper No. C382/047, pp. 453–460, 1989.

van Oosten, J.J.M. and Bakker, E. Determination of magic tyre model parameters, tyre models for vehicle dynamic analysis. *Proceedings of the 1st International Colloquium on Tyre Models for Vehicle Dynamic Analysis*, ed. H.B. Pacejka, Swets & Zeitlinger, Lisse, pp. 19–29, 1993.

van Oosten, J.J.M., Unrau, H.J., Reidal, A. and Bakker, A. Standardization in tire modelling and tire testing – TYDEX Workgroup, TIME Project. *Tire Science and Technology*, TSTCA, Vol. 27, No. 3, pp. 188–202, July–September 1999.

van Oosten, J.J.M. and Jansen, S.T.H. High frequency tyre modelling using SWIFT-Tyre. *Proceedings of the 14th European ADAMS Users' Conference*, Berlin, Germany, November 1999.

Vesimaki, M. 3D contact algorithm for tire–road interaction. *Proceedings of the 12th European ADAMS Users' Conference*, Marburg, Germany, November 1997.

von der Ohe, M. Front and rear suspension of the new Mercedes model W201. SAE Paper No. 831045, 1983.

Wenzel, T.A., Blundell, M.V., Burnham, K.J. and Williams, R.A. Modelling and estimation of automotive vehicle states. *Proceedings of the Sixteenth International Conference on Systems Engineering* (ICSE2003), Vol. 2, pp. 744–749, ISBN 0-905949-91-9, Coventry, UK, 9–11 September 2003.

Whitehead, J. The essential contribution of rig measurement to suspension design and development. Institution of Mechanical Engineers Paper C498/7/061/95, *Proceedings of Autotech* '95, Birmingham, November 1995.

Wielenga, T. Analysis methods and model representation in ADAMS. MDI Technical Paper No. 41, Mechanical Dynamics Inc., 2301 Commonwealth Blvd, Ann Arbor, Michigan, USA, October 1987.

Will, A.B. and Żak, S.H. Modelling and control of an automated vehicle. In P. Lugner and J.K. Hedrick, eds, *Vehicle System Dynamics*, Vol. 27. Lisse: Swets & Zeitlinger, 1997.

Wittenburg, J. and Wolz, U. MESA VERDE: a symbolic program for nonlinear articulated rigid body dynamics. *Proceedings of Tenth ASME Design Engineering Division Conference on Mechanical Vibration and Noise*, Cincinnati, 1985.

Wong, J.Y. *Theory of Ground Vehicles*. New York: John Wiley & Sons, Inc., 3rd edition, 2001.

Wu, Y. and Wu, A. *Taguchi Methods for Robust Design*. ASME Press, New York, 2000.

This page intentionally left blank

Index